Hongxi Yin
David J. Richardson

Optical Code Division Multiple Access Communication Networks

Theory and Applications

TSINGHUA UNIVERSITY PRESS
Springer

Hongxi Yin
David J. Richardson

Optical Code Division Multiple Access Communication Networks
Theory and Applications

Hongxi Yin
David J. Richardson

Optical Code Division Multiple Access Communication Networks

Theory and Applications

With 159 figures

TSINGHUA UNIVERSITY PRESS

Springer

AUTHORS:

Dr. Hongxi Yin
School of Electronics Engineering and
Computer Science
Peking University
100871 Beijing ,China

Prof. David J. Richardson
Optoelectronics Research Centre
University of Southampton
SO17 1BJ Southampton,UK

ISBN 978-7-302-17328-1 **Tsinghua University Press, Beijing**
ISBN 978-3-540-68445-9 **Springer Berlin Heidelberg New York**
e ISBN 978-3-540-68468-8 **Springer Berlin Heidelberg New York**

Library of Congress Control Number: 2008927072

Co-published by Tsinghua University Press, Beijing and Springer-Verlag GmbH Berlin Heidelberg

Springer is a part of Springer Science+Business Media
springer.com

Cover design: Frido Steinen-Broo, EStudio Calamar, Spain
Printed on acid-free paper

Hongxi Yin
David J. Richardson

光码分多址通信网络理论与应用

Optical Code Division Multiple Access Communication Networks

Theory and Applications

TSINGHUA UNIVERSITY PRESS
Springer

图书在版编目(CIP)数据

光码分多址通信网络理论与应用=Optical Code Division Multiple Access Communication Networks: Theory and Applications：英文 /殷洪玺，(英)理查德(Richardson, D. J.)著. —北京：清华大学出版社，2008.6
ISBN 978-7-302-17328-1

Ⅰ.光…　Ⅱ.①殷…　②理…　Ⅲ.码分多址－移动通信－通信网－研究－英文　Ⅳ.TN929.533

中国版本图书馆 CIP 数据核字(2008)第 049955 号

责任编辑：龙启铭
责任校对：王淑云
责任印制：

出版发行：清华大学出版社　　**地　　址**：北京清华大学学研大厦 A 座
http://www.tup.com.cn　　**邮　　编**：100084
社 总 机：010-62770175　　**邮　　购**：010-62786544
投稿与读者服务：010-62776969, c-service@tup.tsinghua.edu.cn
质量反馈：010-62772015, zhiliang@tup.tsinghua.edu.cn

印 刷 者：
装 订 者：
经　　销：全国新华书店
开　　本：153×235　　**印张**：24.75　　**字数**：560 千字
版　　次：2008 年 6 月第 1 版　　**印次**：2008 年 6 月第 1 次印刷
印　　数：1～0000
定　　价：00.00 元

Preface

The customized and service-orientated all-optical network can implement ultrahigh speed transmitting, routing and switching of data in the optical domain, and has the transparency to data formats and protocols which increases network flexibility and functionality such that future network requirements can be met. OCDMA technology is one of the promising technologies to implement all-optical networks, which has the potential to exploit the previously unmined bandwidth of optical fiber and take advantage of the predominance of radio CDMA, such as subscribers' flexible and effective sharing of the spectrum and time and space resources, and resisting jamming and eavesdropping.

OCDMA is a category of multiplexing and internetworking technologies that encodes/decodes signals through employing simple and cost-effective passive optical components (not requiring optical logic components) such that the signal multiplexing, routing and switching can be implemented smoothly. It has many advantages, such as asynchronous random access, simple management, flexible networking, good compatibility with WDM and TDM, suitable for bursty traffic, supporting multiple services and differentiated QoS, while providing some confidentiality of data transmission. It is a very important technology to implement optical access networks, metropolitan area networks and optical signal multiplexing and switching in backbone networks.

OCDMA has a twenty-year history from its first proposal and its first experimental demonstration in principle. However, since the information capacity demands were so much smaller and the development scale of communication networks was so limited in the past, the current higher functionalities of networks were not required. At the same time, WDM technology provided the transmission tunnels and wavelength switching for ultrahigh speed data, which could then meet the earlier demands of optical network functionalities. Therefore, OCDMA has remained outside the mainstream of optical communication research for a long time. However, at present, with the advent of the knowledge economy and the global reach of the Internet, the disharmony between the service provisions of

transport networks and access networks is becoming a serious issue. Meanwhile, there exist many issues in data backbone networks, such as the electronic node bottlenecks, clumsy and low-efficient granularity of traffic, and so on.

To solve these current issues, it seems that the ability of WDM and TDM technologies is inadequate while, the high networking flexibility of OCDMA and the very good complementary properties of OCDMA with WDM and TDM are now recognized. Simultaneously, due to the rapid advancement of optical component technologies, all aspects of OCDMA technologies have become research hotspots, which should boost OCDMA development.

In this book, the first chapter introduces the evolution of optical communication systems and networks, and the status and role of OCDMA in optical communication systems and networks. The history of the main encoding/decoding theories and technologies, the composition and performance analyses of systems, and the network architectures and applications obtained are provided, including the published research results acquired by the research teams of the authors of this book and a number of newly proposed and improved schemes of existing technologies. The reader may wish to validate some of them through experiments.

In terms of the superposition behavior of optical signals, OCDMA can be categorized as either incoherent OCDMA or coherent OCDMA. Furthermore, incoherent OCDMA is mostly divided into one-dimensional temporally encoding OCDMA, spectral amplitude encoding OCDMA and two-dimensional wavelength-hopping/time-spreading encoding OCDMA, etc. The coherent OCDMA is mainly classified into spectral phase encoding OCDMA and temporal phase encoding OCDMA and so on.

In the second and third chapters we introduce the cardinality bounds, various constructions, performances and constructed examples of one- and two-dimensional codes. In the second chapter, we first give the definitions, the bounds on their cardinalities, diverse constructions and performance of the unipolar codes suitable for one-dimensional incoherent OCDMA. These codes include constant-weight symmetric OOCs, constant-weight asymmetric OOCs, variable-weight OOCs, prime codes, extended prime codes and modified prime codes, quadratic congruence codes, extended quadratic congruence codes and synchronous quadratic congruence codes, etc. Then the size, the generating methods and performances of the bipolar codes employed by spectral phase encoding and temporal phase encoding for the coherent OCDMA are discussed in detail. These bipolar codes encompass m-sequences, Gold codes, Walsh-Hadamard codes and the asymptotically optimal 4-phase codes. At the same time, after being modified, these codes can also be applied to the incoherent spectral amplitude OCDMA encoding. In addition, the combinations amongst these codes can be used to construct 2-D WH/TS codes that are well-suited for incoherent 2-D WH/TS OCDMA systems.

The third chapter describes the definition of 2-D WH/TS OCDMA codes, which can be applied to 2-D incoherent OCDMA networks, the constructions of

2-D incoherent OCDMA codes with OOC, PC, EQCC, OCFHC, m-sequence, Walsh-Hadamard codes, CHPC, etc., and the performance analysis of these codes. These two-dimensional WH/TS incoherent OCDMA codes include multiple wavelength optical orthogonal codes, PC/PC codes, PC/EQCC codes, OOC/PC codes, PC/OOC codes, OCFHC/OOC codes, B/U and B/B codes with the differential detection, MLEWHPC codes implementing multiple bit rates, multiple services and multiple QoS and so on.

In the fourth chapter, the operational principle of OCDMA optical encoding and decoding, and a large number of implementing schemes and techniques are illustrated, which include one-dimensional incoherent fixed and tunable optical encoders and decoders with time encoding, two-dimensional incoherent wavelength-hopping/time-spreading fixed and tunable optical encoders and decoders, the spectral-amplitude incoherent optical encoders and decoders, the incoherent 2-D bipolar/unipolar optical en/decoders and the coherent spectral-phase and temporal-phase optical en/decoders, etc.

The fifth chapter presents the existing and representative analysis approaches of system performance with the different receiver models that have been proposed in references, and shows a large number of simulating results on system performance. These systems include one-dimensional incoherent OCDMA systems with the correlation receiver models and the chip-level receiver models, two-dimensional incoherent OOK-OCDMA communication systems, the spectral amplitude encoding incoherent OCDMA system based on fiber-optic Bragg gratings, and the spectral phase encoding and the temporal phase encoding coherent OCDMA systems. These analysis methods are very helpful for the analysis and design of OCDMA systems.

In the last chapter, OCDMA network architecture, primary research results on OCDMA local area network protocols and applications of OCDMA technologies are detailed, focusing on OCDM/WDM hybrid multiplexing, the interconnections of OCDMA networks with OTDM networks and WDM networks, OCDM/WDM hybrid networks, the architectures of OCDMA LANs, the primarily random access protocols of OCDMA LANs, optical packet switching networks with optical code labels, data transmission confidentiality provided by OCDMA networks, and some other applications of OCDMA. This content has very important reference value for OCDMA network design and for further advancement of the research on OCDMA applications.

Many advantages of OCDMA technology and novel demands for coming optical network functionalities make OCDMA technology very promising from an application perspective. After a long period of neglect, OCDMA has become a research hotspot in optical communication technologies in recent years, making great progress. However, in order to push forward the application of OCDMA technology, great efforts are still required by researchers in the OCDMA community. This book systematically presents OCDMA optical coding/decoding theory and implementation techniques, systems and networks, which adequately reflect the

current global research results on OCDMA theory and experiments. It is a valuable textbook or reference book for postgraduates majoring in telecommunication to obtain a well-knit theoretical foundation and for engineering technicians in the fields of R&D and management of optical fiber communications.

The authors regret any omissions or errors, and reader comments or suggestions will be warmly welcomed.

Acknowledgements

Many years ago, my Ph. D. supervisors, Professors Shuwen Yang and Guangzhao Zhang, guided me as a novice in the field of OCDMA. During a period when OCDMA technology was out of favor, I concentrated on WDM optical communication systems and networks. The current requirements for advanced optical networks has revived OCDMA research, which reawakened my research interest in OCDMA. My research has been enabled through the support of the National Natural Science Foundation Council of China. A excellent opportunity for studying and doing research work in a leading institute, the Optoelectronics Research Centre (ORC) of University of Southamptom, UK, has been provided by the China Scholarship Council and School of Electronics Engineering and Computer Science and State Key Laboratory on Advanced Optical Communication Systems & Networks of Peking University. The world-class research personnel and resources of ORC greatly enhanced my research capability. The guidance and support of my ORC supervisor, Professor David J. Richardson, who is also the co-author of this book, has been invaluable in producing this work.

I would like to thank my Ph. D. supervisors, Professors Yang and Zhang, who directed my initial research in OCDMA many years ago. I would also like to express my gratitude to my collaborating supervisor, Professor Deming Wu, when I did my post-doctorial research at Peking University, for his supporting me in furthering my studies of OCDMA while I studied optical WDM systems and networks. I am especially grateful to Professor Richardson, Deputy Director of Optoelectronics Research Centre of University of Southampton for his guidance to me and collaboration. For the valuable suggestions and encouragements, I thank my colleagues, Drs. Z. Zhang, C. Tian, P. Petropoulos and M. Ibsen, for their collaborative research on OCDMA networks in the same research group. Special thanks are due to Dr. Z. Zhang for his reading the manuscript so quickly and providing constructive comments, and my students, Shurong Sun, Wei Liang and Liqiao Qin, for providing several simulation results included in the book.

I would also like to thank the State Scholarship Council for funding my visit to ORC of University of Southampton, and the Council of National Natural Science Foundation of China for continuing supporting to my research team. I am very indebted to the School of Electronics Engineering and Computer Science and State Key Laboratory on Advanced Optical Communication Systems & Networks of Peking University for their support, which enabled the author to study and visit the UK despite of the heavy teaching and research workload. I also want to thank the ORC of University of Southampton for providing very good scientific research conditions, which enabled the completion of this book.

I must acknowledge Editor Qiming Long and association at Springer Press and Tsinghua University Press for their efforts in publishing this book, and the IEEE for provision of the copyright permission on several figures. I also want to thank all authors of cited references in this book for their generous provision.

Finally, I am very indebted to my wife and daughter, Fan Yang and Yue Yin, for their encouragement and support of my research endeavors, especially during my absences in the UK. A special thanks is owned to my father- and mother-in-law Professor Kuanghan Yang and Senior Engineer Bin Liang for their concern and love over many years.

Hongxi Yin

Contents

1 Introduction

1.1 Developments and Applications of Optical Fiber Communication Systems and Networks

1.1.1 Optical Fiber Communication Systems

Optical fiber communication is a communication approach to transport information from one point to another using light as a carrier and optical fibers as transmission media. In ancient times, in order to speed up information transmission, people learned how to use optical signals, such as smoke signals, semaphores, etc., to communicate. However, the utility of these methods was very limited. In the early 1960s, American physicists invented the ruby laser[1], and the proposals for optical communication via dielectric waveguides or glass optical fibers to avoid degradation of the optical signal by the atmosphere were made almost simultaneously in 1966 by Kao and Hockham[2] and Werts[3]. Initially the optical fibers exhibited very high attenuation (i.e., 1000dB/km) and were therefore not competitive with the coaxial cables which they were to replace (i.e., 5 to 10dB/km). In 1970, the Corning Company in America manufactured a fiber-optic with attenuation of 17dB/km, and the optical fiber losses at 1310 nm wavelength were reduced to 0.3dB/km[4] in 1974. In 1977, the field trial of the first commercial use of the multimode fibers between two telephone offices in Chicago 7000 meters distant was made successfully[5].

As the transmission media of communication, optical fibers have many advantages[6].

(1) Enormous communication capacity. In general, the capacity of communication depends on the carrier frequency. The higher the carrier frequency, the larger the available transmission bandwidth and thus the greater information capacity of the communication systems. The optical carrier frequencies in the range of 10^{13} to 10^{16} Hz (generally in the near infrared around 10^{14} Hz or 10^{5} GHz) can yield a far greater potential transmission bandwidth than metallic cable systems (i.e., coaxial cable bandwidth up to around 500 MHz) or even millimeter wave radio systems (i.e., system currently operating with modulation bandwidths of 700 MHz). Furthermore, introducing wavelength division multiplexing (WDM)[7] even more bandwidth in the fiber-optic can be utilized. Thus, many orders of magnitude are gained with optical fibers.

(2) Low transmission loss. The attenuation or transmission losses in optical fibers are very low, in contrast with that in the best metallic cable. Optical fibers have been fabricated with losses as low as 0.2 dB/km. With the advances of technology of fiber-optic manufacturing, optical fibers with lower attenuations will be made and they will facilitate the implementation of communication links with extremely long repeater spacing (long transmission distances without intermediate electronics), thus further reducing both communication system cost and complexity.

(3) Small size and weight. Optical fibers have very small diameters, which are often no greater than the diameter of a human hair. Even when such optical fibers are covered with protective coatings they are far smaller and much lighter than corresponding copper cables. Fiber-optic cables need little layout space and they are very convenient to transport and construct.

(4) Immunity to electromagnetic interference and high signal security in transmission. Optical fibers, which are made of glass, or sometimes of a plastic polymer, are electrical insulators and therefore free from electromagnetic interference (EMI). They can be used in electromagnetic hazardous environments and don't need to be shielded from electromagnetism. Cross interference among several distinct optical signals doesn't occur when they simultaneously transmit in different fibers in the same fiber-optic cable. Furthermore, the optical signals in optical fibers generally don't radiate outside so that it is highly secure for the information to be transmitted in it, except possibly for hostile attack.

(5) Rich resource and potential low cost. The raw material used to manufacture the fiber-optic is silicon dioxide and it is abundant in nature, unlike copper. Moreover, the technology to fabricate optical fibers has matured so that the cost for manufacturing optical fibers has been reduced continuously.

Because optical fibers have so many aforementioned advantages and the technologies of manufacturing optical devices and optical fiber systems have been improved and matured, a flourishing period has come in the development, research and applications of optical fiber communication systems. So far, the developments of optical fiber communication have proceeded through four generations[8]. The first generation optical fiber communication systems used short wavelength at 0.85 μm and multimode fibers which used material based on quartz and whose diameter was 50 μm and whose loss was 4 dB/km. The light source was a light emitting diode (LED) made from Ⅲ-Ⅴs semiconductor compound, alloys of gallium arsenide (AlGaAs), and the optical detector was a p-i-n (PIN) photodiode or Si avalanche photodiode (APD). The first generation optical fiber communication systems were mainly used in the links among central offices and transmitted digital signals with less than third-level (E3) of PCM (pulse code modulation).

The second generation optical fiber communication systems used long wavelength with 1.31 μm single-mode fibers whose loss had been reduced from 4 dB/km to 0.5 dB/km. LEDs made from Ⅲ-Ⅴs semiconductor, the quarternary

alloy InGaAsP, or laser diodes (LD) were used as light sources and InGaAs-PIN/GaAs-FETs were used as optical detectors. The second generation was suitable for being used in the links among central offices with the bit rate of 140 Mb/s or long-haul links with the high bit rate of 400 – 565 Mb/s and distance could achieve 40 km without repeaters.

The third generation optical fiber communication systems uses dispersion-shifted single-mode fibers with wavelength of 1.55 μm, with loss reduced to 0.2 dB/km. They can be used in long-haul telecommunications or submarine long-span telecommunications with a high bit rate of 2.5 Gb/s and a InGaAsP LD light source or a distributed feedback (DFB) LD.

The fourth generation optical fiber communication systems use nonzero-dispersion single-mode fibers with the wavelength of 1.55 μm and WDM, using optical amplifiers such as erbium-doped fiber amplifiers (EDFAs), and Raman amplifiers used to increase the transmission distance. The data rate per wavelength is in the range 2.5 Gb/s to 10 Gb/s.

The scheme of optical fiber communication system is shown in Fig. 1.1. The schematic diagram of a wavelength division multiplexing system is shown in Fig. 1.2.

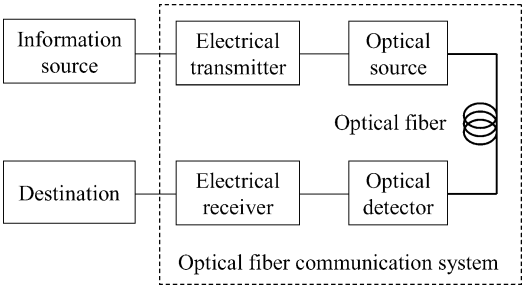

Figure 1.1 Optical fiber communication system

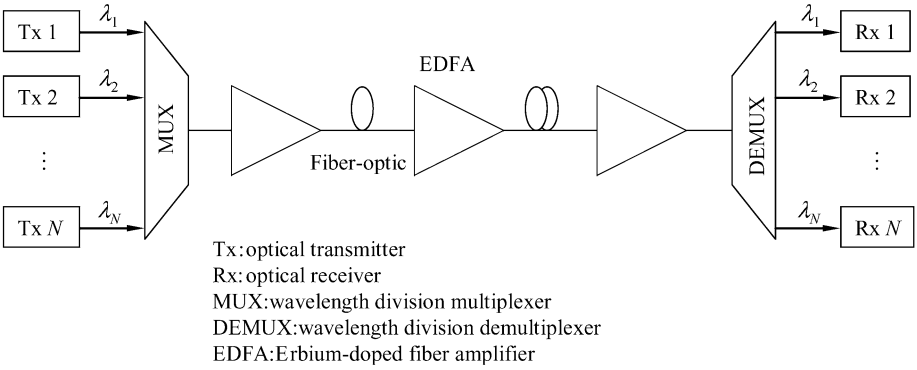

Figure 1.2 Schematic diagram of wavelength division multiplexing system

The research effort on new generation optical fiber communication systems is accelerating. Its trends are to boost the bit rate of a single wavelength channel further, to increase the transmission capacity of the systems, to extend the transmission distance, and to develop ultra-large capacity, ultra-long distance and optical fiber networking, such as a 40 Gb/s system for single wavelength, ultra-wide bandwidth optical fiber amplifier in C, L and S waveband, dynamic dispersion compensation, optical code-division multiple-access, coherent light communication, optical soliton communication and intelligent optical networking, etc. These new technologies for optical fiber communications will lead to improved optical communication systems and networks.

1.1.2 Optical Fiber Communication Networks

1.1.2.1 Optical Transport Networks and Automatically Switched Optical Networks

In 1985, Payne and his colleagues at the University of Southampton first discovered that rare-earth doped fibers could exhibit the phenomena of laser oscillation and amplification, e.g., erbium (Er^{3+})-doped fiber amplifier (EDFA)[9]. With the maturity of EDFA and WDM technologies, optical fiber communication has transferred from point-to-point single wavelength transmission to the point-to-point multi-wavelength WDM transmissions, which greatly increases the system transmission capacity.

With the prevalence of the point-to-point WDM systems and the continuous improvement of system transmission capacity, the electronic digital cross connection (DXC) devices and add/drop multiplexing devices in the network nodes have become increasingly mismatched in bit rates. In other words, the tremendous link transmission rates (capacities) of WDM are seriously mismatched with the low bit rates (capacities) of cross connection devices and add/drop multiplexing devices. Therefore, in order to use WDM wavelength routing and to eliminate the effect of electronic bottleneck in the network nodes, ITU-T (International Telecommunication Union-Telecommunication Standardization Sector) introduced the optical transport network (OTN) concepts in 1998[10]. WDM OTN uses optical add/drop multiplexing (OADM) devices and optical cross-connection (OXC) devices in its nodes, implements the function of optical wavelength add/drop and cross connection in the optical domain, without the optical-to-electrical conversion. In this way, the traffic, blocking probability, network scalability and survivability of WDM network can be optimized and designed based on wavelength routing. Owing to the avoidance of the limitations of the electronic bottleneck, the network transmission capacity and throughput of nodes can be greatly increased. However, the traditional OTN has many shortcomings technically. For example, it cannot react rapidly and exactly to changes of network states because of centralized network management, the

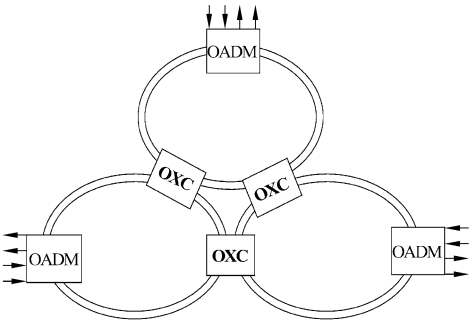

(a) The topological structure of OTN

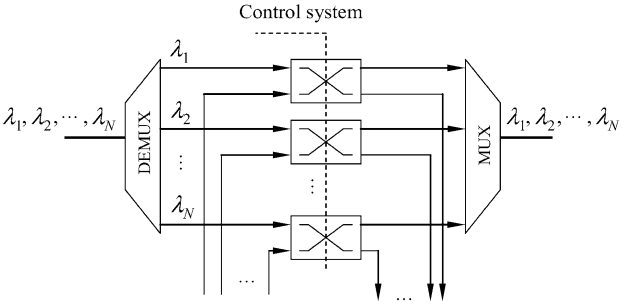

(b) OADM structure

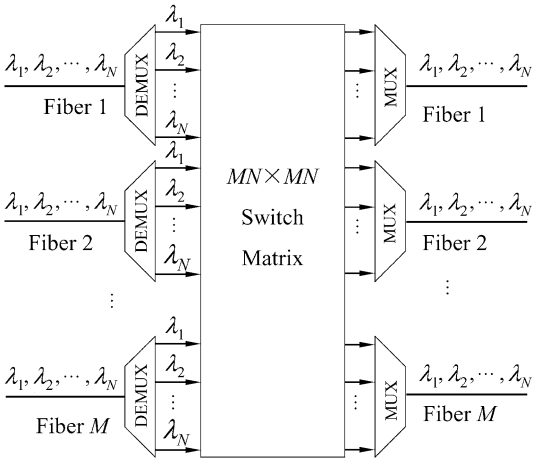

(c) OXC structure

OTN: Optical transport network

OXC: Optical cross connector

OADM: Optical add/drop multiplexer

Figure 1.3 Scheme of OTN topologic structure

configurations of optical channels need manual intervention, and the interoperability of network devices is so poor that the scalability of networks is limited.

To sum up, OTN cannot satisfy the requirements of optical networks. Thus, ITU-T put forward the requirements of automatically switched transport networks (ASTN), G.807 (G.astn)[11] and the architecture for the automatically switched optical network (ASON), G.8080[12] in 2001. G.8080 gave the definition of ASON and introduced the concept of dynamic switching and the cooperation mechanism between the service layer and transport layer. Up to now, optical communication networks are not only an optical transport network but also include the functions of switching and control. The scheme of OTN topologic structure is shown in Fig. 1.3(a). Fig. 1.3(b) and (c) represent the structures of OADM and OXC in OTN, respectively.

ASON is divided into three planes according to its network architecture, which are transport plane (TP), control plane (CP) and management plane (MP). The most basic and core function of ASON is to set up an optical channel to connect two points in terms of the requirement of the request agent. ASON supports three kinds of connections: permanent connections, soft permanent connections and switching connections. These connections include unidirectional point-to-point connections, bi-directional point-to-point connections and bi-directional point-to-multipoint connections. The logic architecture of ASON is shown in Fig. 1.4.

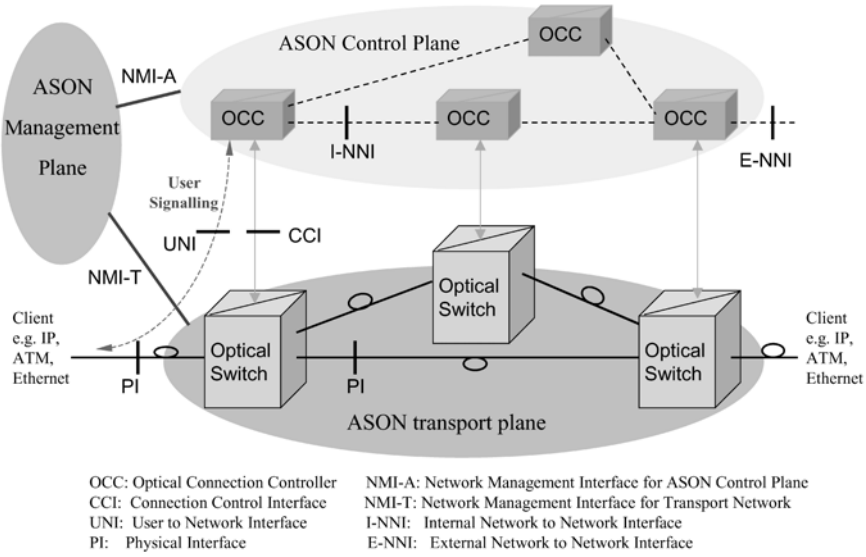

Figure 1.4 Logic architecture of ASON[12]

The main characteristics of ASON are service transparency, being able to provide all kinds of broadband services and applications with high quality for the users rapidly, using quick and effective protection and recovery mechanisms for

performance monitoring and failure recovery over the optical layer, real-time traffic engineering control and bandwidth management over the optical layer, very good device interoperability and network scalability. These merits make ASON the trend of the next generation optical transport network.

1.1.2.2 Optical Access Networks

With the performance of OTN continually being upgraded by using new techniques, the access network, called the last mile (Ethernet community has renamed it to the first mile), has many problems such as narrow bandwidth, high failure rate, and high cost of operation and maintenance. It is not able to support new services and applications, especially multimedia services and new broadband services, because copper wire is still the transmission media in the access network at present. Thus, it has become the bottleneck of communication networks. The bandwidth requirements for new services per user are shown in Fig. 1.5[14].

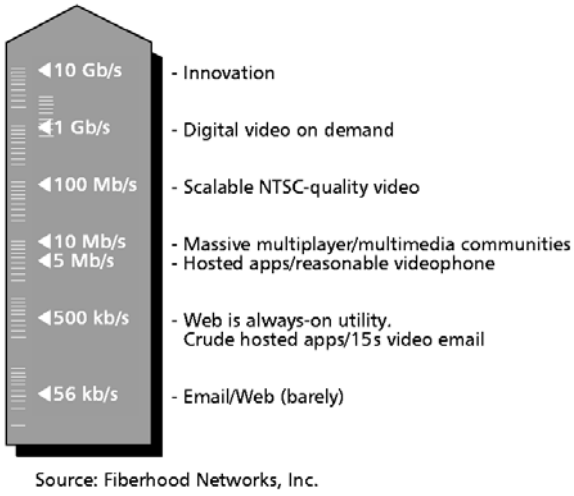

Figure 1.5 Bandwidth requirements for new services per user (Adapted from Ref. [14], with permission from IEEE © 2007)

The extensive employment of the Internet has caused the rapid increase of bandwidth requirements on the access network. Although the current broadband access technologies such as asymmetric digital subscriber line (ADSL) based on telephone lines and cable modem (CM) based on common antenna television (CATV) can meet the needs of some services such as Web surfing, email and so on, it is not able to satisfy the bandwidth requirements of multimedia services and broadband services, for example, the stream media, interactive applications, especially the requirements of three networks merging into one network, namely the telecommunication network, the computer network and the broadcast television network.

ADSL possesses the property of asymmetry between the volume of data flow of uplink and that of downlink, and thus it is basically suitable for applications such as user surfing on the Internet and video on demand (VOD), etc. However, it is not applicable to interconnecting local area networks (LAN). Internet access services are commonly offered by deploying ADSL with ATM/Ethernet. ADSL remote devices are equipped at the customer end and DSLAM (digital subscriber line access multiplexer) is outfitted at the central offices, and they are connected by the common telephone wires. ADSL remote devices provide the Ethernet interface for the user computers, and DSLAM connects with the Internet service provider (ISP) by ATM (asynchronous transfer mode) or fast Ethernet (FE). The subscribers can achieve the Internet access with broadband by using such a network. DSLAM can be put in the room where ISP locates at and connects with ISP by the access network, or it is connected with the ISP access platform by a local area network. VOD services can be provided by the mode of ADSL + ATM.

Cable modem[15] is another broadband technique whose uplink and downlink are asymmetric and is suitable for providing two kinds of services, namely Internet surfing and VOD, where Internet access service can be offered by means of HFC (hybrid fiber coaxial cable) + Cable Modem + Ethernet/ATM. A HFC head device is mounted at the central office, which interconnects with Internet through ATM or fast Ethernet and implements the function of signal modulation and blend. The data signal is transmitted to the subscribers by HFC and the cable modem fulfills the functions of signal decoding and demodulation and transmits the digital signal to a PC (personal computer) via an Ethernet port. In reverse, a cable modem receives the uplink signals transmitted by a PC and sends them to the head end devices by HFC after the signals are encoded and modulated.

Although both ADSL and cable modem can provide many kinds of services by networking they just manage to satisfy the bandwidth requirements of the current broadband services. The bandwidth of ADSL is smaller than that of the cable modem. Nevertheless, there exist many problems such as the stability, reliability, power supply, operation and maintenance when a cable modem and HFC are used to build up a network. Moreover, due to the bandwidth of network links shared by all of users the bandwidth that is assigned to each user is highly limited. Therefore, they can not offer the broadband digital services actually when the number of users increases. Hence, ADSL and cable modem are only the transition techniques of the current access network, and only the optical access network (OAN) represents the trend towards the access network of the future.

Optical access networks can technically be divided into two categories, the active optical network (AON) and the passive optical network (PON). The former uses the electrical demultiplexer and the latter uses the optical demultiplexer. Because PON can avoid the effect of electromagnetic interference and thunder on the outdoor devices, it can reduce the failure probability of lines and outdoor devices and improve the reliability of systems. Meanwhile, it can economize the cost of operation and maintenance and has very good transparency, and it is

suitable for signals with any format and any bit rate. Thus it is a promising technique expected to be utilized by the telecommunication operation and maintenance departments for a long time. The typical PON network architecture is shown in Fig. 1.6[16].

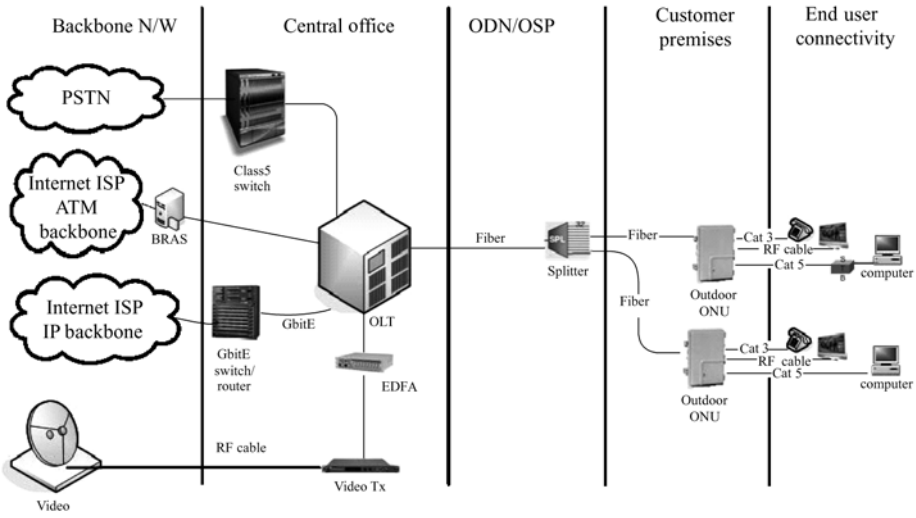

Figure 1.6 Typical PON architecture[16]

PON can also be divided into APON (ATM PON), based on ATM and EPON (Ethernet PON), based on Ethernet, and WDM-PON that combines the technique of WDM with the technique of PON. APON uses the technology of concentration and statistical multiplexing of ATM. However, ATM uses the fixed length cell with 53 Bytes in which there are a cell overhead of 5 Bytes and a payload of 48 Bytes. This means that it is difficult for ATM to carry the services with IP format because IP requires that the data should be segmented into variable length packets with less than 65,535 Bytes. IP packets must be partitioned into 48-Byte segments and an added 5-Byte cell header to each segment in order to form a cell when IP service is carried by APON. This process is very complex and consumes considerable time and increases the additional cost of OLT (optical line terminal) and ONU (optical network unit).

Different transmission techniques are used when EPON transmits the data downstream from OLT to multiple ONUs and the data upstream from multiple ONUs to OLT and therefore these two processes are completely different. According to the IEEE 802.3 protocol, the broadcast technique is employed to transmit the data downstream from OLT to multiple ONUs with variable length packets up to 1518 Bytes. Each packet has one header to uniquely identify its destination, i.e., ONU. In addition, some packets should go to all of ONUs

(broadcast packets) or to a particular group of ONUs (multicast packet). At the splitter, the traffic is divided into several separate signals (the same as the number of ONUs) and each signal carries all packets of ONUs. When the data reach an ONU, it accepts the packets that are intended for it and discards the packets that are intended for other ONUs. Moreover, TDM technology is employed to manage the upstream traffic and the transmission time slots are dedicated to the ONUs in order to realize the synchronization of the time slots. Once the data are coupled into the common fiber, the upstream packets from ONU don't interfere with each other. The principle of EPON is shown in Fig. 1.7. Because Ethernet is dedicated to carrying IP services it reduces the overhead dynamically in comparison with ATM.

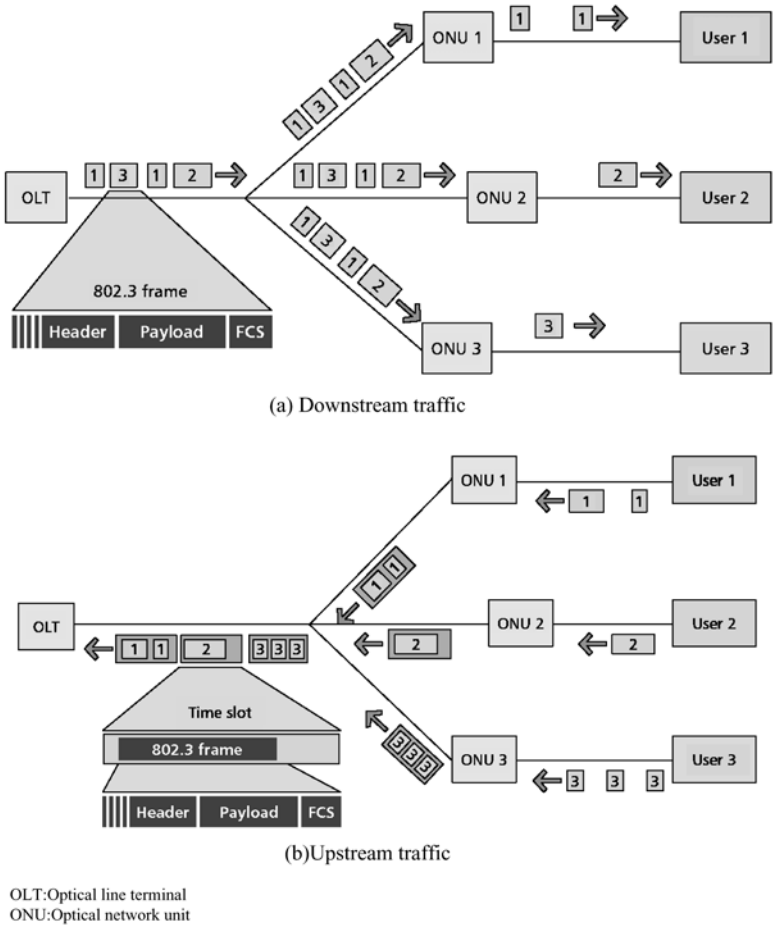

Figure 1.7 The traffic in EPON. (Adapted from Ref. [14], with permission from IEEE © 2007)

Both APON and EPON use TDM (time division multiplexing) technology, thus they belong to TDM PON. The current TDM PON supports data rates from 155 Mb/s to 1Gb/s, which is shared by 8 to 32 users. However, in such a TDM PON, the time-share transmission in the uplink restricts the bandwidth for a single user. In the PON system based on TDMA (time-division multiple access) it is difficult to provide ~Gb/s bandwidth of uplink to all users and furthermore it is also difficult to offer the services with the different bit rates to each user in the uplinks. Therefore, TDM PON is not the systemic solution of FTTH (fiber-to-the-home) to transport the symmetric services with a rate of ~Gb/s.

WDM-PON[19] is the organic combination of WDM technique with PON, which sets up the point-to-point links between OLT and each user through assigning one unique wavelength to each user. The service providers expect to implement the transition from TDM-PON to WDMA smoothly. If it is possible to realize mass production and the specification is widely used, the cost of ONU will be reduced significantly. WDM in which the spacing of wavelength is greater than 20 nm is called coarse WDM (CWDM). ITU G.695 defines the optical interface standards of CWDM and ITU G.694-2 defines the total wavelength range from 1270 nm to 1611 nm, in which the wavelength spacing is 20 nm and the total usable number of channels is 18. The low-water-peak fiber defined by ITU G.652 C&D eliminates the attenuation in the wavelength range from 1370 nm to 1410 nm that exists in ordinary single mode fibers, and it can be used with CWDM to achieve broad spectral range transmission. However, because the dispersion will increase with the increase of wavelength, the transmission distance may be limited due to the signal dispersion when the data rate becomes higher. The main shortcoming of CWDM is the limited number of channels, which makes it difficult for CWDM-PON to be extended. Furthermore, the shorter the wavelength, the greater the channel loss, so the transport distance and the light separation ratio are limited. Simple WDM-PON architecture is shown in Fig. 1.8[19]. Figure 1.9 represents wavelength assignment for CWDM[20].

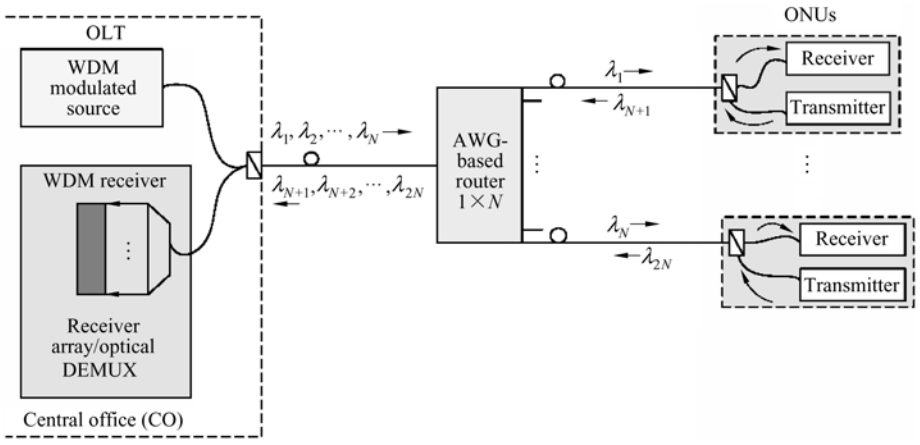

Figure 1.8 Simple WDM-PON architecture (After Ref. [19])

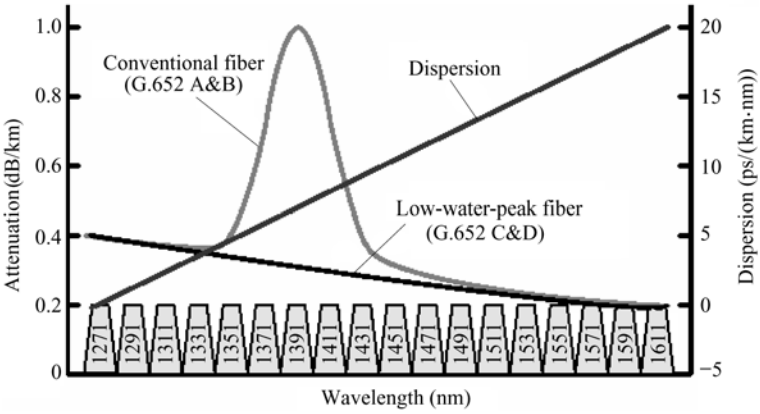

Figure 1.9 Wavelength assignment for CWDM (After Ref. [19])

The wavelength spacing of DWDM is much smaller than that of CWDM, typically 3.2 nm. PON using DWDM can offer sufficient bandwidth to more users. However, the wavelength of each light source and the central wavelength of each WDM filter need to be monitored in order to avoid the cross talk between neighbor channels because the spacing of DWDM is smaller. Since DWDM-PON needs tunable wavelength devices and temperature control, its cost is higher than that of CWDM-PON.

In view of customer demand, the single play will be soon transferred to the triple play, such as on high-speed Internet, IP phone and broadcast video, etc. In the long run, the service demand will further evolve towards high bit rate and user-enabled. That is because a great many of peer-to-peer applications such as the gigabyte files of uncompressed 1.2 Gb/s high-definition class or even 6 Gb/s super-high-definition class digital movies, as well as bi-directional medical applications of telediagnosis and surgery, etc., will be deployed universally[22]. Customized services would be another demand for a wide variety of service options in the bit rate and QoS (quality of service). Without an abundant bandwidth of uplink available either on demand or on an always-on basis, these applications could not be well supported and, consequently, ordinary nonpeer-to-peer users will be put in a disadvantageous position by being forced to share the limited bandwidth with a small number of bandwidth-hungry users. Therefore, in the upgrading scenario of the FTTH in the near future, the downlink not only has high bit-rate, but the uplink must also possess high bit-rate as well in order to meet the subscribers' needs. Thus FTTH should be developed into a novel-system of gigabit-symmetric FTTH from the current FTTH with asymmetry between the uplink and the downlink.

OCDMA (optical code division multiple access) is another solution for multiple access other than TDMA (time division multiple access) and WDMA (wavelength division multiple access), which can implement the multiplexing, switching and add/drop of multi-channel signals over the backbone network and MAN

(metropolitan area network) separately, or in a combination of TDM and WDM through the encoding and decoding of the optical signal directly. OCDMA can realize the multiple-access networking among many users over LAN (local area network) and the access network and it is an ideal technical candidate for the future ~Gb/s symmetric FTTH. The scheme of OCDMA-PON is shown in Fig. 1.10.

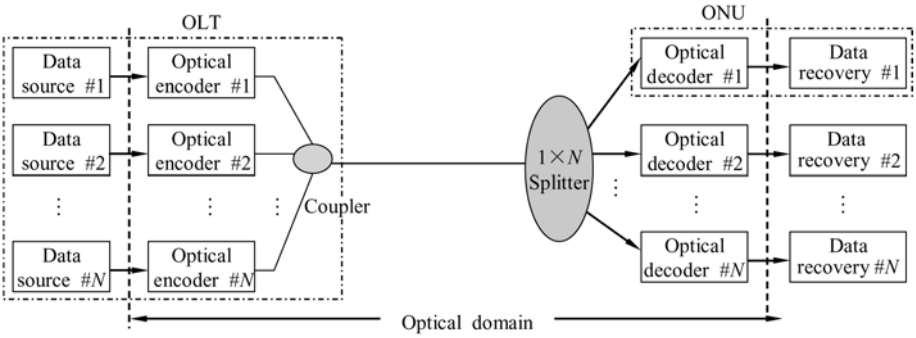

Figure 1.10 OCDMA-PON[22]

1.2 Technology Evolution and Typical Experimental Systems of OCDMA

In the late 1970's, CDMA (code division multiple access) technology was aimed at military communication, which was a spread frequency technique increasing the robust security of information transmission. Spread frequency communication has been used in military communications for a long time in order to resist intended interference and implement low probability of detection. In these days, CDMA has been widely used in the field of wireless communication, especially, the third generation wireless communication systems. OCDMA is a technology to realize multiplexing transmission and multiple access by coding in the optical domain, which supports multiple simultaneous transmissions in the same timeslot and the same frequency. It is another technology of multiplexing and multiple-access besides OTDM and WDM and a potentially promising technique for optical networks in the future, and especially, due to its easy access and flexible network structure, it is very applicable to the access network.

In 1986, Prucnal, Santoro and Fan proposed to realize the fiber-optic LAN by using optical signal processing[23, 24], and used prime codes to carry out the experiment of electronic encoding and fiber-optic delay line decoding, verifying the feasibility to implement incoherent OCDMA system by encoding in the time domain. In 1988, Weiner, Heritage and Salehi[25] demonstrated how to spread the femto-second optical pulse into picosecond-duration pseudonoise bursts. The spread frequency was achieved by encoding the light spectrum into pseudorandom

binary phase and then by decoding the spectrum phase encoded to recover the original pulse. They proposed that the coherent ultra-short pulse coding and decoding could be applied to the fast reconfigurable OCDMA communication networks. Both breakthrough studies were milestones for the development of OCDMA.

Optical encoding and decoding for incoherent OCDMA uses unipolar codes whereas the bipolar codes used in RF CDMA (radio frequency code division multiple access) have poor performance in OCDMA system and can not be used. Therefore, unipolar codes with good system performance need to be developed. Consequently, in the earlier years, the research on incoherent OCDMA focused on looking for and obtaining unipolar codes with good auto-and cross-correlations, such as OOC (optical orthogonal/pseudo-orthogonal codes)[26 – 29], PC (prime codes)[23, 30], QCC (quadratic congruence codes)[31], etc. In order to improve the performances of PC and QCC, EPC (extended prime codes)[32], MPC (modified prime codes)[33] and EQCC (extended quadratic congruence codes)[34] have been proposed again. Among these one-dimensional codes, OOC has the best performance but its construction is complicated, compared with those of other codes. Although one-dimensional OOC possesses the ideal auto- and cross-correlations, and its cardinality, that is, the number of codewords, is the largest, the number of users is inversely proportional to the data rate for single user in one-dimensional incoherent OCDMA systems because the cardinality of codes is proportional to the length of time-spread. Whereas, the data rate for a single user is inversely proportional to the length of the time-spread. Meanwhile, the cardinality of code is approximately inversely proportional to the square of the code-weight. And moreover, the smaller the code-weight becomes, the more the error probability increases. In order to meet the requirement of bit-error-rate, the simultaneous number of active users in the network must be reduced.

Owing to the reasons mentioned above, the application of one-dimensional codes to incoherent OCDMA system is limited. In order to increase the number of users, unipolar codes with larger capacity need to be designed. Therefore, starting around 1990, researchers transferred their interests from the study on one-dimensional codes to 2D (two-dimensional) OOCs[35 – 43], which enormously increases the capacity of the system and improves the performance. Great progress has been made in aspects of the encoding algorithms and the hardware implementations of en/decoders of incoherent OCDMA and the experimental systems and the network protocols of OCDMA, and many OCDMA system and network experiments in the laboratories and in the field have been performed. For instance, a 16-users demonstration experiment[44] with 1.25 Gb/s per user and the FFH-OCDMA signal transporting 80km by using fiber Bragg grating arrays encoding was reported in OFC'2001 and the experiment is shown in Fig. 1.11. An OCDMA network demonstration experiment[45] with star structure done by Princeton University in America was reported in IEEE Photonics Technology Letters 18(7) in 2006. The experiment was operated at 115 Gchip/s. This demonstration used off-the-shelf devices to implement 2-D wavelength-time

incoherent OCDMA encoding, with a single user bit rate of 5 Gb/s and 10^{-13} bit-error-rate or better. The schematic of the experimental setup is shown in Fig. 1.12. In another demonstration, the OCDMA LAN protocol demonstration experiment[46] done by University of Southern California in USA was reported in OFC'2006, which used an OCDMA network with 2-D wavelength-time encoding and supported 6 users and demonstrated a transmission scheduling algorithm to

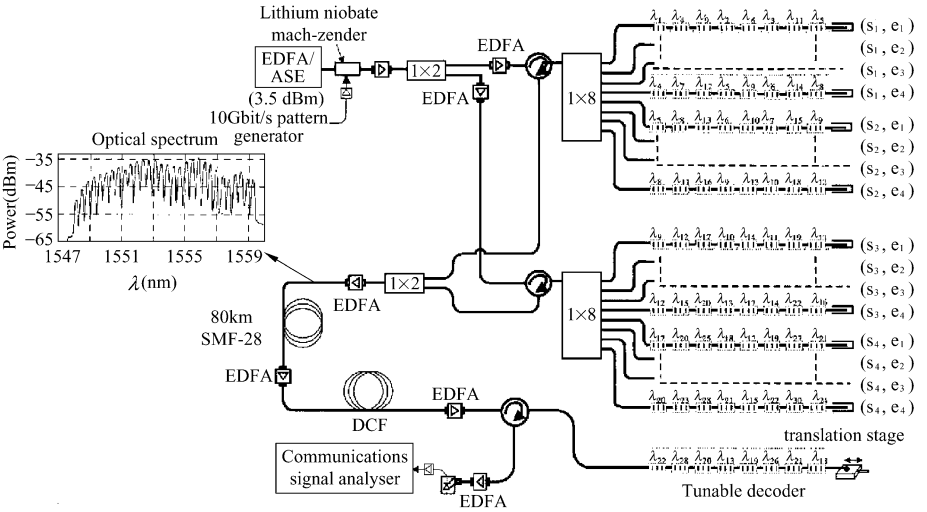

Figure 1.11 Wavelength-time OCDMA system at 1.25 Gbits/s for the transmission of signals from 16 users through 80km of fiber. (Adapted from Ref. [44])

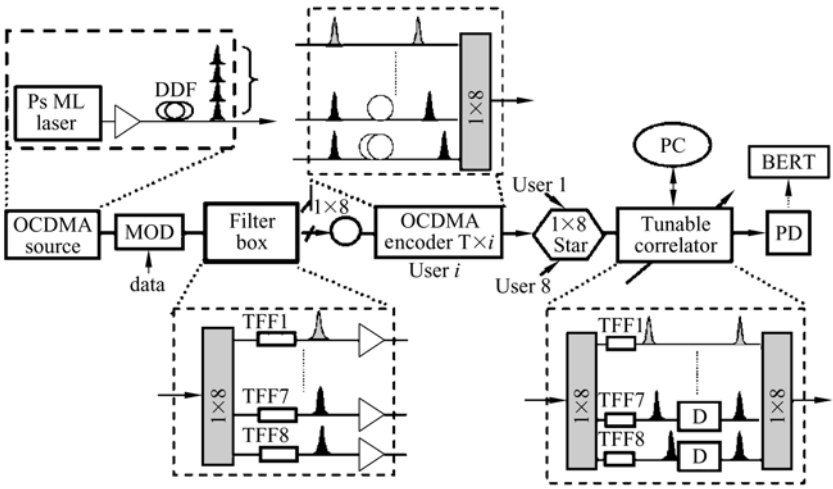

Figure 1.12 Schematic of the experimental setup. (Adapted from Ref. [45], with permission from IEEE © 2007)

avoid OCDMA network "congestion collapse". Results from the measurements showed that transmission scheduling could provide orders of magnitude improvement in bit error rate. The data rate for each subscriber was 625 Mb/s in this experiment. The experimental system is shown in Fig. 1.13. In addition, a number of unipolar implementation schemes of bipolar codes have been proposed, for example, the balanced detection[47, 48] and etc.

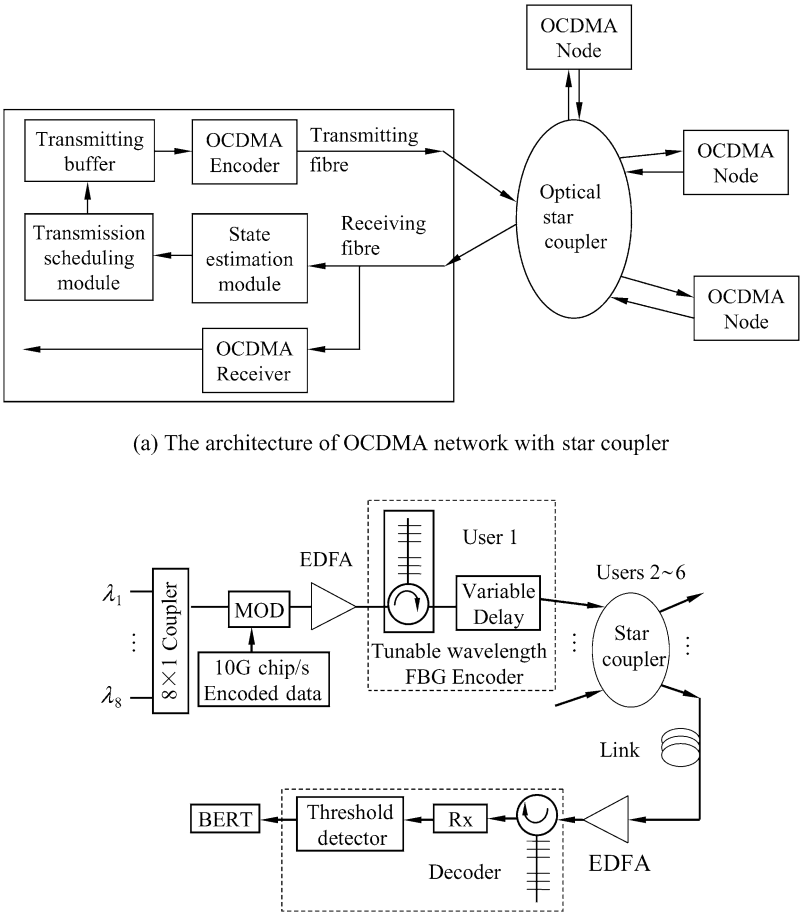

Figure 1.13 OCDMA network structure and its experimental setup (After Ref.[46])

The encoding for the coherent OCDMA system uses binary codes (two-phase codes), such as m-sequences[49], Gold codes[49], Walsh-Hadamard codes[50], etc. Because the coherent OCDMA systems can directly employ the bipolar codes used by RF CDMA communication systems and the encoding and decoding theory of bipolar codes has matured sufficiently, research on coherent OCDMA focuses on

how to implement bipolar encoding and decoding physically and how to analyze and improve the system performance. The coherent OCDMA systems using spectral phase encoding are easily affected by the shortcomings of fiber-optic transmission, such as the nonlinearity and dispersion, etc. Especially, the coherent OCDMA signal would be subject to the effect of the dispersion of optical fiber because its bandwidth is broad[51]. In addition, the spectral phase encoding used bulk optic components in the earlier days. However, the spectral phase en/decoders had many disadvantages such as being massive in terms of size, poor operational stability, easily affected by outside environment, being difficult to be encapsulated and mass produce and high price. With the development of the theory and technology of integrated optics, the spectral phase en/decoders can be implemented in integrated form[52, 53] in the future. In order to overcome the current difficulties of manufacturing the spectral phase en/decoders, temporal phase encoding OCDMA has been proposed and integrated optics or superstructure fiber Bragg grating (SSFBG)[54] can be used to achieve the optical time-phase en/decoders. With the development and gradual maturation of the technology of optical fiber gratings, the fiber-optic grating has been widely used in the optical communication and can also be applied to OCDMA to implement the spectral amplitude encoding, the spectral phase encoding, the temporal phase encoding and the hybrid 2-D wavelength-time encoding[55 – 58].

Similarly, the technology of coherent OCDMA has been investigated thoroughly and deeply since the mid-1980's and enormous advance has been made in the hardware realization of OCDMA en/decoders, the test systems and the network protocols of OCDMA, etc. Many reports about the laboratory experiments and the field trials of OCDMA systems and networks have emerged. The typically experimental system involved a field trial of 111km transmission of 3-WDM × 10-OCDMA × 10.71Gb/s/user demonstrated by Japan National Institute of Information and Communication Technology reported at OFC'2006[59], which used the multi-port optical en/decoders in the central office and the tunable transversal-filter type decoders in the optical network unit, and differential-phase-shift-keying (DPSK) data format. The truly asynchronous WDM/OCDMA access network has been implemented with 10 users per wavelength with bit-error-rate (BER) $<10^{-9}$ without using FEC (forward error correction) or optical threshold devices. The network architecture and the experimental setup are shown in Fig. 1.14 and Fig. 1.15, respectively. SPECTS (spectral phase encoded time spreading) OCDMA LAN experiment with 32 simultaneous users done by University of California (Davis) in America was reported at OFC'2006, in which the data rate for each user was 10 Gb/s. The demonstration employed polarization multiplexing, an NOLM (nonlinear optical loop mirror) time gate as well as a nonlinear thresholder and FEC. The testbed achieved bit-error-rate (BER) $<10^{-11}$ with FEC and BER less than 10^{-9} for up to 28 users without any forward error correction. The schematic block of this experimental network is shown in Fig. 1.16.

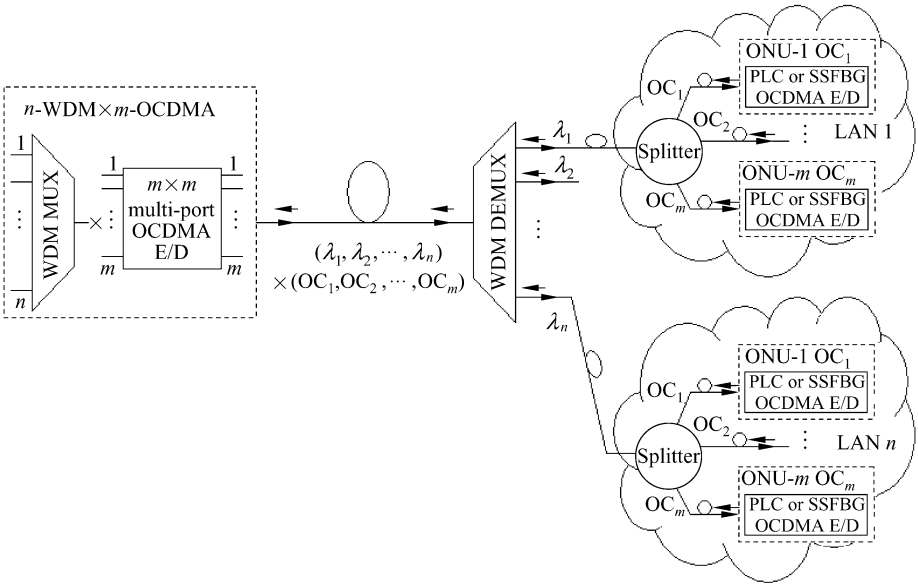

Figure 1.14 WDM/OCDMA network architecture (After Ref.[59])

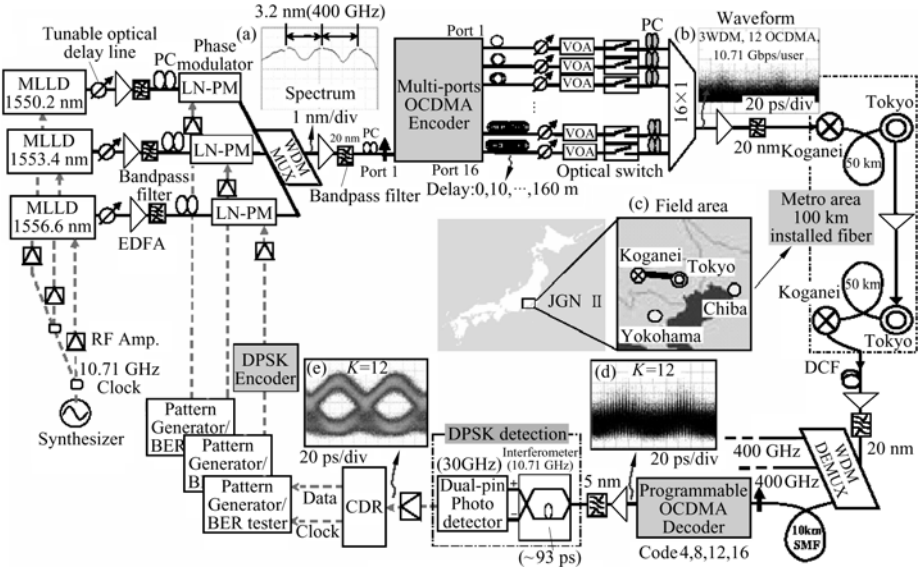

Figure 1.15 Experimental setup (Adapted from Ref.[59])

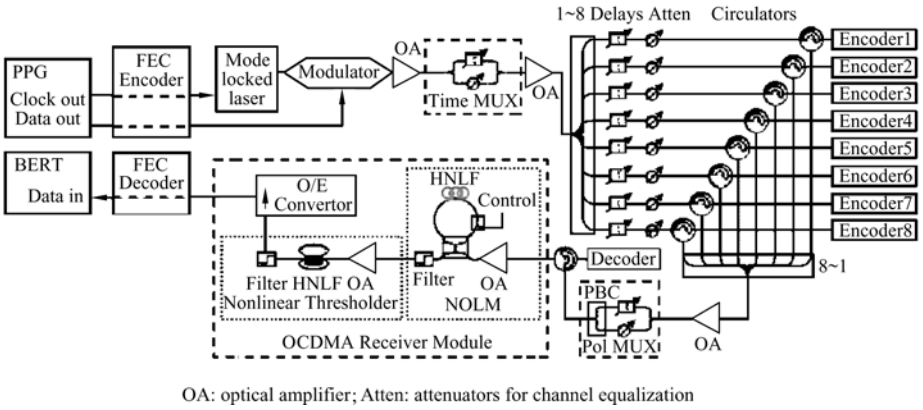

Figure 1.16 The block diagram of SPECTS OCDMA testbed (Adapted from Ref.[60])

Many universities, institutes and companies have made great effort in developing technologies of OCDMA for about two decades, including Princeton University, University of California-Davis (UC Davis), University of California-Los Angeles (UCLA), University of Southern California (USC), School of Optics at the University of Central Florida (CREOL), University of Hofstra, Purdue University, University of California-San Diego, University of Arizona, Lincoln Laboratory of MIT (Massachusetts Institute of Technology), Lawrence Livermore National Laboratory (LLNL), Telcordia Technologies, Essex Corp, Kambrook Technical Associates, Mendez R&D Associates, Alcatel SEL and Bell communication Research (Bellcore) in America, and University of Southampton, University of Strathclyde in UK, and National Institute of Information and Communication Technology (NICT), Osaka University, NTT(Nippon Telegraph and Telephone Corporation) in Japan, and Universite Lavel, McGill University, University of Ottawa, AP Networks in Canada, and ETRI, Korea Telecom, Seowon University, Korea National University in Korea, Deutsche Telecom in Germany, etc. Especially, American DARPA (Defense Advanced Research Projects Agency) has been supporting the OCDMA Program[61] joined by many universities and companies, which has obtained numerous research achievements in many aspects, such as coding algorithms and schemes, advanced encoding and decoding hardware, network architecture, simulation and applications. This program will play an important role in promoting the development of OCDMA technology. It can be seen from the research achievements on OCDMA obtained in recent years that the research schemes of OCDMA have emerged continuously and revealed very good prospects for the optical access network, LAN and MAN. In addition, IP routing and the sensor network can be implemented by using OCDMA technologies, and many new applications such as transmitting multimedia, realizing different QoS, different bit-rate, different data securities, etc., are achieved in the communication networks.

1.3 Technique Characteristics and System Classifications of OCDMA

OCDMA has become a promising technology to implement truly all-optical communication and networking that uses optical signal processing directly, combining the advantages of electrical CDMA with the bandwidth predominance of fiber-optic and optical-signal processing devices. The passive optical-access-networks, LAN and WAN, can be built up by using OCDMA technology. The combination of OCDMA with WDM or/and TDM can enhance signal multiplexing and label switching through the combination of OCDMA with WDM or/and IP over WAN so that the transmission and switching capacity of network can be improved, the flexibility of network can be enhanced and the performance of the communication network can be heightened.

1.3.1 Technique Characteristics of OCDMA

(1) OCDMA can implement high-speed transmission, switching and add/drop of data through using all-optical signal processing and thus it can realize all-optical communication and all-optical networking and overcome the effect of electronic bottleneck, which exists in the electronic node in the traditional network.

(2) Subscribers can access the network at random and the network has soft capacity. Meanwhile, the pattern of networking is very flexible.

(3) OCDMA doesn't need buffering in queue because it uses the tell-to-go protocol.

(4) OCDMA networks can assign the bandwidth dynamically and implement the bandwidth assignment with different granularities deftly, and use optical network bandwidth effectively.

(5) The traffic, protocol and network topology are transparent in the OCDMA network. OCDMA can support variable bit-rate traffic and bursty traffic and implement differential QoS according to demand. OCDMA networks can be readily upgraded and extended.

(6) An OCDMA network is somewhat secure and cryptic for the transmission information.

(7) An OCDMA network needs fewer devices than a WDM network and its equipment is simple, and the implementing cost of OCDMA networks is low. A DWDM network needs accurate wavelength control and conversion. Furthermore, OCDMA is highly compatible with DWDM and TDM.

(8) OCDMA networks employ distributed management, which is simple and it is convenient to locate network failure and protect and recover.

Because of the advantages mentioned above, OCDMA can support multimedia including voice, data, video, including IP traffic, video-on-demand, streaming media,

interactive applications, etc. And it also offers many kinds of QoS and differential degrees of security according to different services and user's requirements. Meanwhile, it can overcome the shortcomings of asymmetric uplink and downlink in current access networks and supports FTTH of the peer-to-peer traffic.

1.3.2 Classifications of OCDMA Systems

Many types of OCDMA systems have been proposed as the result of intensive research on OCDMA in the past 20 years. If we classify them in terms of the nature of the superposition of the optical signal, they can be divided into coherent OCDMA systems and incoherent OCDMA systems. The coherent OCDMA system makes use of the coherent property of light and implements bipolar encoding of the optical signal, i.e., encoding the phase of optical signals, with the phase of light detected at the receiving terminals. The form of signal addition is the superposition of light signal amplitudes. This kind of OCDMA system needs to use ultrashort broadband light pulse sources. The incoherent OCDMA system employs the presence of light signal or absence of light signal to represent the binary "1" and "0" respectively, which is unipolar encoding, where the light signals are detected with the square-law devices at the receiving terminals. This form of signal addition is the superposition of light powers. This kind of OCDMA system may use incoherent light sources, such as amplified spontaneous emission (ASE), light-emitting diode (LED), etc.

If we categorize them depending on the differences of coding approaches for optical signals, there are six kinds of OCDMA systems:

(1) direct-sequence or temporal encoding OCDMA systems, also known as spread-spectrum encoding OCDMA systems;

(2) spectral amplitude encoding OCDMA systems;

(3) spectral phase encoding OCDMA systems;

(4) temporal phase encoding OCDMA systems;

(5) two-dimensional spatial encoding OCDMA systems, also known as spread-space encoding;

(6) hybrid encoding OCDMA systems. This kind of system uses a combination of the encoding approaches mentioned above. We can acquire two-dimensional encoding, for instance, wavelength-hopping/time-spread (WH/TS) encoding, through using the combination of spectrum encoding with temporal encoding. If space-encoding is combined with WH/TS encoding again, space-spread/ wavelength-hopping/time-spreading encoding (SS/WH/TS)[40] can be obtained and the other options may be deduced by analogy.

Options (1), (2) and (5) refer to incoherent OCDMA systems, (3) and (4) are coherent OCDMA systems, and (6) may be either.

If we sort them according to the amount of resources of time, wavelength and space used, they can be divided into one-dimensional systems, two-dimensional

systems and three-dimensional systems. The aforementioned types of (1), (2), (3) and (4) belong to one-dimensional systems, (5) is two-dimensional system, and the systems with greater than two dimensions can be implemented by (6). If the polarization is also taken into account, the four-dimensional systems can be obtained.

References

[1] T. H. Maiman: Stimulated optical radiation in ruby. Nature, London, 1987, 1960, pp493 – 494

[2] K. C. Kao and G. A. Hockham:Dielectric fibre surface waveguides for optical frequencies. *Proc. IEE*, 113(7), 1966, pp1151 – 1158

[3] A. Werts: Propagation de la lumiere coherente dans les fibres optiques. *L'Onde Electrique*, 460, 1966, pp967 – 998

[4] http://www.corning.com

[5] http://www.ofsoptics.com/labs

[6] John M. Senior: Optical fibre communications: principles and practice. -Second Edition, Prentice Hall, 1992

[7] John M. Senior: Wavelength division in optical fibre networks. *Communications Internat*., 15(4), 1988, pp52 – 54

[8] W. Y. Gu: Optical fiber communication system. Gao Deng Jiao Yu Press, China, 2001

[9] R. J. Mears, L. Reekie, I. M. Jauncey, D. N. Payne: Low-noise erbium-doped fibre amplifier operating at 1.54 μm. *IEE Electronics Letters*, Vol.23(19), 1987, pp1026 – 1028

[10] ITU-T G.709/Y.1331: Optical Transport Network (OTN). http://www.itu.int/rec/T-rec -G.709, 2001

[11] ITU Draft Recommendation G.807/Y.1302: Requirements for the Automatic Switched Transport Network(ASTN). July 2001

[12] ITU Draft Recommendation G.8080/Y.1304: Architecture for the Automatic Switched Optical Network. November 2001

[13] ITU Draft Recommendation G.7715/Y.1706: Architecture and Requirements for Routing in automatically Switched Optical Networks. 2002

[14] Glen Kramer and Gerry Pesavento, Alloptic, Inc.: Ethernet passive optical network (EPON): building a next-generation optical access network. *IEEE Communications Magazine*, Feb. 2002, pp66 – 73

[15] http://www.ccidedu.com: The comparison of the advantage and disadvantage between two networking techniques: ADSL and Cable Modem.

[16] Jani Saheb Shaik, N R Patil: FTTH Deployment Options for Telecom Operators. Sterlite Optical Technologies Ltd, http://www.sterliteoptical.com

[17] http://en.wikipedia.org/wiki/Passive_Optical_Network: Passive Optical Network.

[18] http://www.iec.org: Ethernet Passive Optical Networks. The International Engineering Consortium.

[19] Amitabha Banerjee, Youngil Park, Frederick Clarke and Huan Song, Sunhee Yang, Glen Kramer, Kwangjoon Kim, Biswanath Mukherjee: Wavelength-division-multiplexed passive optical network (WDM-PON) technologies for broadband access: a review (Invited), *Journal of Optical Networking*, Vol.4, No.11, November 2005, pp737 – 758

[20] R. Lauder: Technology and economics for coarse wavelength multiplexing workshop. http://ieeexplore.ieee.org (2004)

[21] T. Fujii, K. Shirakawa, M. Nomura, and T. Yamaguchi: Cinema-class digital content distribution via optical networks (Invited). in Proc. OpNeTec, Pisa, Italy, Oct. 2004, pp11 – 18

[22] Ken-ichi Kitayama, Xu Wang, and Naoya Wada: OCDMA over WDM PON—Solution Path to Gigabit-Symmetric FTTH. *IEEE/OSA Journal of Lightwave Technology*, Vol.24, No.4, April 2006, pp1654 – 1662

[23] Prucnal, P. R., Santoro, M. A., Fan, T. R.: Spread Spectrum Fiber-optic Local Area Network Using Optical Processing. *IEEE/OSA Journal of Lightwave Technology*, Vol.4, No.5, May 1986, pp547 – 554

[24] Prucnal, R. P, Santoro, M. A., Sehgal, S. K.: Ultrafast All-Optical Synchronous Multiple Access Fiber Networks. *IEEE Journal on Selected Areas in Communications*, Vol.4, No. 9, 1986, pp1484 – 1494

[25] Weiner, A. M., Heritage, J. P. and Salehi, J. A.: Encoding and decoding of femtosecond pulse. *Optics Letters*, Vol.13, No.4, May 1988, pp300 – 302

[26] Jawad.A.Salehi: Code division multiple-access techniques in optical fiber networks - part I: Fundamental principles. *IEEE Trans. on Communications*, Vol.37, No.8, Aug. 1989, pp824 – 833

[27] Jawad.A. Salehi and C. A. Brackett: Code division multiple-access techniques in optical fiber networks-part II: Systems performance analysis. *IEEE Trans. on Communications*, Vol.37, No.8, Aug. 1989, pp834 – 842

[28] Jawad.A. Salehi, F. R. K. Chung, and V. K. Wei: Optical orthogonal codes: Design, analysis, and applications. *IEEE Trans. on Information Theory*, Vol.35, No.3, May 1989, pp595 – 605

[29] H. Chung and P. Kumar: Optical orthogonal codes—new bounds and an optimal construction. *IEEE Trans. on Information theory*, Vol.36, No.4, July 1990, pp866-873

[30] A. S. Holmes and R. R. Syms: All-optical CDMA using “quasi-prime” codes. *IEEE/OSA Journal of Lightwave Technology*, Vol.10, No.2, Feb. 1992, pp279 – 286

[31] S. V. Maric, Z. I. Kostic, and E. L. Titlebaum: A new family of optical code sequences for use in spread-spectrum fiber-optic local area networks. *IEEE Trans. on Communications*, Vol.41, No.8, Aug. 1993, pp1217 – 1221

[32] G.-C. Yang and Wing. C. Kwong: Performance analysis of optical CDMA with prime codes. *IEE Electronics Letters*, Vol.31, No.7, Mar. 1995, pp569 – 570

[33] Wing. C. Kwong, P. A. Perrier, and P. R. Prucnal: Performance comparison of asynchronous and synchronous code-division multiple-access techniques for fiber-optic local area networks. *IEEE Trans. on Communications*, Vol.39, No.11, Nov. 1991, pp1625 – 1634

[34] S. V. Maric: New family of algebraically designed optical orthogonal codes for use in CDMA fiber-optic networks. *IEE Electronics Letters*, Vol.29, No.6, Feb./Mar./Apr. 1993, pp538 – 539

[35] Eugene Park, Antonio J. Mendez, and Elsa M. Garmire: Temporal/spatial optical CDMA networks-design, demonstration, and comparison with temporal networks. *IEEE Photonics Technology Letters*, Vol. 4, No.10, Oct. 1992, pp1160 – 1162

[36] Tancevski L., Andonovic I.: Wavelength hopping/time spreading code division multiple access systems. *IEE Electronics Letters*, Vol. 30 No. 17, August 1994, pp1388 – 1390

[37] L. Tancevski, I. Andonovic, M. Tur, and J. Budin:Hybrid wavelength hopping/time spreading code division multiple access systems. *IEE Proc.-Optoelectron.*, Vol.143, June 1996, pp161 – 166

[38] L. Tancevski, and I. Andonovic: Hybrid wavelength-hopping/time-spreading schemes for use in massive optical networks with increased security. *IEEE/OSA Journal of Lightwave Technology*, Vol.14, No.12 , Dec. 1996, pp2636 – 2646

[39] G. C. Yang, W. C. Kong: Performance comparison of multiwavelength CDMA and WDMA+CDMA for fiber-optic networks. *IEEE Trans. on Communications* Vol.45, No.11, Nov. 1997, pp1426 – 1434

[40] Sangin. Kim, Kyungsik Yu and Namkyoo Park: A new family of space/wavelength/time spread three-dimensional optical code for OCDMA networks. *IEEE/OSA Journal of Lightwave technology*, vol.18, No.4, April 2000, pp502 – 511

[41] Raymond M. H. Yim, Jan Bajcsy and R. Chen:A new family of 2-D wavelength-time codes for optical CDMA with differential detection. *IEEE Photonics Technology Letters*, Vol.15, No.1, Jan. 2003, pp165 – 167

[42] Svetislav V. Maric, Vincent K. N. Lau: Multirate Fiber-Optic CDMA: System Design and Performance Analysis. *IEEE/OSA Journal of Lightwave Technology*, Vol.16, No. 1, Jan. 1998, pp9 – 17

[43] Naser G. Tarhuni, Timo O. Korhonen, Edward Mutafungwa, Mohammed S. Elmusrati: Multiclass Optical Orthogonal Codes for Multiservice Optical CDMA Networks. *IEEE/OSA Journal of Lightwave Technology*, Vol.24, No.2, Feb. 2006, pp694 – 704

[44] H. Ben Jaafar, S. LaRochelle, P.-Y. Cortes, H. Fathallah: 1.25 Gbit/s transmission of optical FFH-OCDMA signals over 80 km with 16 users. OFC2001, TuV3-1

[45] Camille-Sophie Brès, Ivan Glesk, Paul R. Prucnal: Demonstration of an Eight-User 115-Gchip/s Incoherent OCDMA System Using Supercontinuum Generation and Optical Time Gating. *IEEE Photonics Technology Letters*, Vol.18, No.7, 2006, pp889 – 891

[46] P. Saghari, P. Kamath, V. Arbab, M. Haghi, A. E. Willner, J. A. Bannister, J. D. Touch: Experimental demonstration of an interference-avoidance-based protocol for O-CDMA network. OFC'2006, PDP46

[47] Cedric F. Lam, Dennis T. K. Tong, Ming C. Wu, Eli Yablonovitch: Experimental Demonstration of Bipolar Optical CDMA System Using a Balanced Transmitter and Complementary Spectral Encoding. *IEEE Photonics Technology Letters*, Vol.10, No.10, 1998, pp1504 – 1506

[48] Lim Nguyen, Tasshi Dennis, Behnaam Aazhang, James F. Young: Experimental Demonstration of Bipolar Codes for Optical Spectral Amplitude CDMA Communication. *IEEE/OSA Journal of Lightwave Technology*, Vol.15, No.9, Sept. 1997, pp1647 – 1653

[49] V. K. Bhargava, D. Haccoun, R. Matyas and P. P. Nuspl: Digital communications by satellite – modulation, multiple access and coding. Wiley-Interscience, 1981, pp269 – 292

[50] Yixian Yang, Xuduan Lin:Coding Cryptography. Ren Min You Dian Press, China, 1992

[51] P. R. Prucnal, et. al.: Optical code division multiple access: fundamentals and application. CRC Press, Taylor &Francis Group, 2006, pp56

[52] Naoya Wada, Ken-Ichi Kitayama: A 10 Gb/s Optical Code Division Multiplexing Using 8-Chip Optical Bipolar Code and Coherent Detection. *IEEE/OSA Journal of Lightwave Technology,* Vol.17, No.10, 1999, pp1758 – 1765

[53] Chau-Han Lee, Shan Zhong, Xiao Lin, J.F. Young and, Y.J. Chen: Planar lightwave circuit design for programmable complementary spectral keying encoder and decoder. *IEE Electronics Letters*, Vol.35, No.21, 1999, pp1813 – 1815

[54] P. C. Teh, P. Petropoulos, M. Ibsen, and D. J. Richardson: Phase Encoding and Decoding of Short Pulses at 10 Gb/s Using Superstructured Fiber Bragg Gratings. *IEEE Photonics Technology Letters*, Vol. 13, No. 2, 2001, pp154 – 156

[55] Zou Wei, H. Ghafouri-Shiraz, and H. M. H. Shalaby: A New Code Families for Fiber-Bragg- Grating-Based Spectral-Amplitude-Coding Optical CDMA Systems. *IEEE Photonics Technology Letters*, Vol.13, No.8, 2001, pp890 – 892

[56] A. Grunnet-Jepsen, A.E. Johnson, E.S. Maniloff, T.W. Mossberg, M.J. Munroe and J.N. Sweetser: Fibre Bragg grating based spectral encoder/decoder for lightwave CDMA. *IEE Electronics Letter*s, Vol.35, No.13, 1999, pp1096 – 1097

[57] A. Grunnet-Jepsen, A. E. Johnson, E. S. Maniloff, T. W. Mossberg, M. J. Munroe, and J. N. Sweetser: Demonstration of All-Fiber Sparse Lightwave CDMA Based on Temporal Phase Encoding. *IEEE Photonics Technology Letters*, Vol.11, No.10, 1999, pp1283 – 1285

[58] N. Wada, H. Sotobayashi and K. Kitayama: 2.5Gbit/s time-spread/wavelength-hop optical code division multiplexing using fibre Bragg grating with supercontinuum light source. *IEE Electronics Letters*, Vol.36, No.9, 2000, pp815 – 817

[59] Xu Wang, Naoya Wada, Tessuya Miyazaki, Gabrilla Cincotti and Ken-ich Kitayama: Field Trial of 3-WDM × 10-OCDMA × 10.71Gbps, truly-asynchronous, WDM/DPSK-OCDMA using hybrid E/D without FEC and optical threshold. OFC'2006, PDP44

[60] V. J. Hernandez, W. Cong, R. P. Scott, C. Yang, N. K. Fontaine, B. H. Kolner, J. P. Heritage, S. J. B. Yoo: 320-Gb/s capacity (32users × 10Gb/s SPECTS O-CDMA local area network testbed. OFC'2006, PDP45

[61] Jagdeep Shah: Optical OCDMA. *Optics & Photonics News*, April 2003, pp42 – 47

2 One-dimensional OCDMA Codes

2.1 Introduction

In an OCDMA network, the transmission signal over a fiber-optic channel is formed by the superimposing of pseudorandom OCDMA signals encoded from multiple channels. The signal is broadcast to each node (subscriber) in the network and a receiver in each node decodes the signal. If the output of the decoder in this receiver is an autocorrelation, the node can detect the information sent to it from the aforementioned pseudorandom signals. Alternatively, if the output of the decoder is a cross-correlation function (no apparent peak value), then the node cannot receive the information. Therefore, in order to implement OCDMA communication and networking, address codes with sufficient performance are required. When a set of code parameters is chosen, a code can be constructed that has as many codewords (corresponding to the number of nodes in the network) as necessary and good enough auto- and cross-correlation so that accurate synchronization can be implemented and the interference (called multiple access interference, MAI) from other nodes can be suppressed effectively by decoding the signals. This requires that the address codes satisfy two conditions[1, 2] :

- all address codewords can be easily identified from shifted versions, and
- all address codewords can be easily distinguished from (a possibly shifted version of) every other codeword.

From the viewpoint of coding theory, the address codewords need to satisfy:

- each codeword in a set has a high autocorrelation peak and low autocorrelation sidelobes;
- the cross-correlation function between each codeword and any other codeword in the same set of address codewords is low.

Since the mid-1980s, the encoding theory and encoding technology of OCDMA have been studied and developed thoroughly and many research accomplishments have been made [40]. The encoding approaches of OCDMA can be divided into seven categories based on the choice of different light sources (e.g., coherent vs. incoherent, narrowband vs. broadband), different detection schemes (e.g., coherent vs. incoherent) and encoding approaches (e.g., time vs. wavelength, amplitude vs. phase), which are shown in Table 2.1.

From Table 2.1, it can be seen that according to the light sources used (coherent optical sources or incoherent optical sources) and differing forms of signal superimposing, OCDMA systems can be divided into two broad categories: coherent OCDMA systems and incoherent OCDMA systems. The coherent

Table 2.1 Types and characteristics of OCDMA encoding

Name of encoding	Bipolar/ Unipolar	Number of dimensions	Coherent/ Incoherent	Processing approaches and characteristics of optical signals	Typical codes
Pulse amplitude encoding	Unipolar	One-dimension	Incoherent	Time encoding uses the incoherent light sources and the fiber-optic delay lines to process the incoherent optical signals and the detection is to sum optical intensity at the decoder. It is the simplest implement approach, however, requires the unipolar pseudo-orthogonal codes and its cross-correlation function of code is nonzero. Also, the ultrashort pulse light sources are needed and the systems are subject to the nonlinearity and dispersion.	OOC, PC, QCC, HCC
Pulse phase encoding	Bipolar codes	One-dimension	Coherent	Temporal phase encoding uses the superposition of light fields using fiber-optic delay lines and phase modulators or SSFBG to process the coherent optical signals and the bipolar or multi-polar codes used in the wireless CDMA can be employed and their cross-correlation functions are close-to-zero, and therefore the multi-access interference in the systems can be greatly reduced. Also, the ultrashort pulse light sources are reqired and the systems are subject to the nonlinearity and dispersion.	m-sequences, Gold codes, Walsh-Hadamard codes
Spectral amplitude encoding	Bipolar codes	One-dimension	Incoherent	The encoding is carried out in the wavelength domain. An ultrashort broadband light pulse is firstly scattered in multiple wavelengths by a diffraction grating in free space, spectral coding is performed by passing spectral components of the pulse through a phase or amplitude mask, and the coded spectral components are recombined by another grating to form a code sequence. The length of the code sequence is determined by the solution of the gratings and masks. Bipolar orthogonal codes are employed to minimize MAI.	
Spectral phase encoding	Bipolar codes	One-dimension	Coherent		

Continued

Name of encoding	Bipolar/ Unipolar	Number of dimensions	Coherent/ Incoherent	Processing approaches and characteristics of optical signals	Typical codes
Wavelength-hopping/ time-spreading encoding	Unipolar codes	Two-dimension	Incoherent	The schemes require 2-D optical codes in the wavelength and time domains and can implement lower probability of interception and offer the scalability and flexibility. This characteristic in the physical layer can be useful for time-sensitive secure transmissions, such as in strategic or military systems, where encryption delay is critical. Meanwhile, with 2-D codes, the requirement of ultrashort pulses is significantly reduced and wavelength-time systems are less susceptible to fiber dispersion than coherent-spectral-coding systems, even some sort of fiber-dispersion management strategy may also be utilized.	2-D WH/TS OOCs
Space encoding	Unipolar codes	Two-dimension	Incoherent	The schemes need to use multiple fibers or multiple-core fibers, and deploy 2-D optical codes with time and space. The 2-D codes were originally applied to transmitting 2-D spatial pictures.	2-D Space codes
Three-dimension encoding	Unipolar codes	Three-dimension	Incoherent	The encoding is carried out in space, wavelength and time domains or in polarization, wavelength and time domains. In principle, the scheme can increase the cardinality of codes in comparison with 2-D codes, decrease the code lengths and improve the code performance. However, its implementation is complicated and needs to control many parameters of fibers and devices.	Space/wavelength/time codes or polarization/wavelength/time codes

OCDMA systems make use of coherent property of optical signals and implement bipolar encoding of data by encoding the phases of optical signals. The optical phases are detected at receiving terminals by superimposing of the amplitudes of optical fields. The incoherent OCDMA systems represent the binary "1" and "0" using the presence of light signal or the absence of light signal and implement unipolar encoding data signals. The square-law detectors are employed for detecting optical signals at receiving terminals and the forms of signal superimposing are power superimposing. Because coherent OCDMA systems use bipolar encoding, the bipolar codes from the electrical wireless CDMA can be directly deployed, such as m-sequences, Gold codes, Walsh- Hadamard codes[36 – 38, 40], etc. Due to the presence of negative components in bipolar codes, the cross-correlation functions between any two codewords can be close-to-zero, which makes MAI very small and thus the system performance can be greatly improved and the number of network nodes can be increased. However, pulse-phase encoding with bipolar codes requires ultrashort coherent optical pulse sources, which are susceptible to the nonlinearity and dispersion of fiber-optic. As to the spectral amplitude and phase coding, the number of subscribers in a system and the system performance are confined by the resolutions of optical gratings and masks[40]. Furthermore, spectral amplitude coding also requires a pair of complementary signals at the source ends and differential detections at receiving ends[58].

Because incoherent OCDMA systems use the presence of light signal energy or no light signal energy to represent binary "1" and "0", they can not denote and detect the negative components in bipolar codes. Therefore, the bipolar codes applied to electrical wireless CDMA can not be applied to incoherent OCDMA systems, which can only use unipolar codes. This is the reason why the unipolar codes well-suited for incoherent OCDMA systems need to be developed. These unipolar codes should have very large cardinalities and very good auto- and cross-correlations. In order to guarantee that the systems can be synchronized conveniently when the users access the network, each codeword in a unipolar code must possess autocorrelation peaks as high as possible and autocorrelation sidelobes as low as possible. At the same time, the cross-correlation functions must be as low as possible to reduce MAI. Therefore, the unipolar codes should be the codes of sparse "1", that is, the number of "0" must be far greater than the number of "1" in the codes.

Moreover, unlike bipolar codes whose autocorrelation sidelobes and cross-correlation functions are close-to-zero, for unipolar codes the best autocorrelation sidelobes and cross-correlation functions are 1. Thus, the best unipolar codes can but be quasi-orthogonal, corresponding to positive systems and can not implement true orthogonality. However, we still call such unipolar codes optical orthogonal codes (OOCs), in order to follow the custom in references.

For the sake of implementation of incoherent OCDMA, one-dimensional unipolar codes were deeply studied in the earlier days mostly and one-dimensional codes obtained are mainly OOC[1 – 7, 11 – 18] and algebraic congruence codes. The latter

can also be divided into prime sequence codes (PC, linear congruence codes)[24 – 29], quadratic congruence codes (QCC)[8, 9, 30], cubic congruence codes (CCC)[35], hyperbolic congruence codes (HCC)[31 – 34], and so on. The constructions of algebraic congruence codes are relatively simple but their cardinalities and auto- and cross-correlation properties are not as good as that of OOC. The cardinality of OOC is the greatest in one-dimensional codes but the construction of OOC is relatively complex. In addition, if we generalize the definition of OOC, the algebraic congruence code can also be regarded as one kind of OOCs in the broad sense.

Because the cardinality of one-dimensional codes is proportional to the code length, i.e., the frequency-spreading length, the frequency-spreading length is limited to the optical pulse width and the delay precision of fiber-optic delay lines preconditioned by the users' data rates. Therefore, the cardinality (corresponding to the number of users) of one-dimensional unipolar codes that can be implemented is relatively small based on current state-of-the-art, and thus, unipolar codes with greater cardinalities and better performances are required so that OCDMA networks can support a greater number of simultaneous users. It is noted by a great deal of research effort that one of the possible approaches is the deployment of 2-D optical orthogonal codes. 2-D optical orthogonal codes do not increase the code length (may even reduce the code length) and at the same time enlarge the size of codes without degrading performance. For example, multiple wavelength or multiple optical fibers can be utilized as another encoding dimension to combine with the time dimension to form 2-D codes, such as 2-D wavelength-hopping/time-spreading codes (for short, wavelength-time codes), and 2-D wavelength-hopping/space-spreading codes (wavelength-space codes)[42 – 48]. Other types of codes are 3-D space-spreading/wavelength-hopping/time-spreading codes and 3-D polarization/wavelength-hopping/time-spreading codes, which are obtained by adding another encoding dimension on the basis of 2-D codes[49 – 51].

Although it is difficult to deploy one-dimensional codes to implement high-speed data communications and to put one-dimensional coding systems into practice due to the limitations of current state-of-the-art, the algebra encoding methodology of the constructions of one-dimensional codes, particularly OOC, has provided insight into the investigation of multi-dimensional codes. Many types of multi-dimensional codes that possess greater cardinalities and better performance have been constructed by combining OOC and other encoding patterns. The cardinalities of these multi-dimensional codes have improved significantly compared with one-dimensional OOC and they are suitable for the incoherent OCDMA systems. The transmission of multiple-service and multi-rate can be implemented by using multi-dimensional codes, while the differential QoS and security of services can be provided by such multi-dimensional encoding systems[52 – 57].

Whereas there are too much content about OCDMA encoding, we will discuss them in two chapters. This chapter only presents one-dimension unipolar codes and bipolar codes and two-dimensional codes will be introduced in next chapter.

This chapter is organized as follows. In section 2.2, 2.3, 2.4, we describe constant-weight symmetric OOCs, constant-weight asymmetric OOCs and variable-weight OOCs respectively. We review prime codes, extended prime codes and modified prime codes in section 2.5. The quadratic congruence codes, extended quadratic congruence codes and synchronous quadratic congruence codes are discussed in section 2.6. We introduce bipolar codes in section 2.7, which are applied to the coherent OCDMA systems. Finally, a summary is given in section 2.8.

2.2 Constant-weight Symmetric OOCs

2.2.1 Definition of Constant-weight Symmetric OOCs

An $(n, w, \lambda_a, \lambda_c)$ -optical orthogonal code (OOC) C is a family of (0,1)-sequences of length n and Hamming-weight (the number of "1" in each codeword) w, and the periodic autocorrelation of each codeword $X = (x_0, x_1, \cdots, x_{n-1})$ and the periodic cross-correlation between any two distinct codewords $X = (x_0, x_1, \cdots, x_{n-1})$ and $Y = (y_0, y_1, \cdots, y_{n-1})$ satisfy the following properties respectively[3]:

$$\left.\begin{aligned} \theta_{XX}(\tau) = \sum_{i=0}^{n-1} x_i \cdot x_{i\oplus\tau} = \begin{cases} w & \tau = 0 \\ \leqslant \lambda_a & 1 \leqslant \tau \leqslant n-1 \end{cases} \\ \theta_{XY}(\tau) = \sum_{i=0}^{n-1} x_i \cdot y_{i\oplus\tau} \leqslant \lambda_c \qquad 0 \leqslant \tau \leqslant n-1 \end{aligned}\right\} \tag{2.1}$$

for $x_i, y_i \in \{0,1\}$, all intergers $\tau \neq 0 (\mathrm{mod}\, n)$ and $X \neq Y$, where OOC is defined according to the periodic correlation, and therefore, "$\oplus$" will be employed to denote modulo- n addition.

From the set-theoretical perspective, an $(n, w, \lambda_a, \lambda_c)$ -OOC, C, can be alternatively viewed as a family of w-sets of integers modulo-n[3], in which each w set corresponds to a codeword and the integers within each w set specify the positions of nonzero chips (i.e., "1" chip) of the codeword. Then the correlation properties can be reformulated as follows[3].

① The autocorrelation property:

$$|(a + X) \bigcap (b + X)| \leqslant \lambda_a$$

for any $X \in C$ and any $a \neq b (\mathrm{mod}\, n)$.

② The cross-correlation property:

$$|(a + X) \bigcap (b + Y)| \leqslant \lambda_c$$

for any $X \neq Y \in C$ and any *a*, *b*. Note that $a + X = \{a + x : x \in X\}$ and all integers under consideration are taken modulo-*n*. The set-theoretical perspective offers a convenient notation for OOC when *w* is much smaller than *n*.

From now on, a set notation will be used to denote an $(n, w, \lambda_a, \lambda_c)$-OOC unless otherwise specified.

The number of codewords (i.e., $|C|$) in an $(n, w, \lambda_a, \lambda_c)$-OOC is called the cardinality of the code and the largest possible cardinality is denoted by $\Phi(n, w, \lambda_a, \lambda_c)$, that is, $|C|_{\max} = \Phi(n, w, \lambda_a, \lambda_c)$. An $(n, w, \lambda_a, \lambda_c)$-OOC is called the constant-weight symmetric OOC when $\lambda_a = \lambda_c = \lambda$, and we use the shorthand notations of an (n, w, λ) code and a $\Phi(n, w, \lambda)$ the largest possible cardinality. An $(n, w, \lambda_a, \lambda_c)$-OOC is called the constant-weight asymmetric OOC when $\lambda_a \neq \lambda_c$. Otherwise, an $(n, w, \lambda_a, \lambda_c)$-OOC is said to be the variable-weight OOC when *w* is not a constant.

Example 2.1 $X_1 = \{0101000001000\}$ and $X_2 = \{0010011000000\}$ are two codewords of an $(n, w, \lambda_a, \lambda_c) = (n, w, \lambda) = (13, 3, 1)$ optical orthogonal code. Then, they can be denoted by $X_1 = \{(1, 3, 9) \bmod 13\}$, $X_2 = \{(2, 5, 6) \bmod 13\}$, and $X = \{X_1, X_2\}$ in set notation. The waveforms of these two codewords are shown in Fig. 2.1.

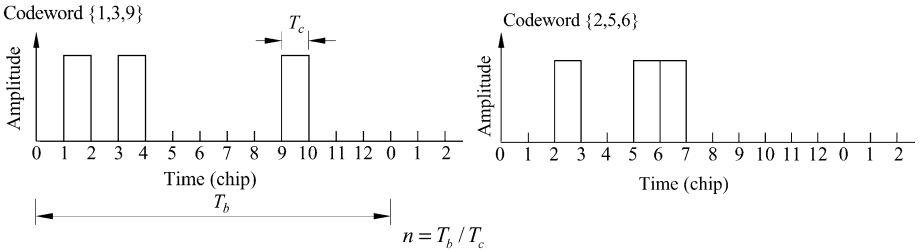

Figure 2.1 The waveforms of two codewords of (13, 3, 1) OOC

2.2.2 Cardinality of Constant-weight Symmetric OOCs

Theorem 2.1[3, 6] A Johnson bound of a constant-weight error-correcting code can be used to derive a general upper bound of the cardinality $|C|$ of an (n, w, λ)-OOC, given by

$$\Phi(n, w, \lambda) \leqslant \left\lfloor \frac{1}{w} \left\lfloor \frac{(n-1)}{(w-1)} \left\lfloor \frac{(n-2)}{(w-2)} \right\rfloor \ldots \left\lfloor \frac{(n-\lambda)}{(w-\lambda)} \right\rfloor \ldots \right\rfloor \right\rfloor \right\rfloor \tag{2.2}$$

Proof: See Ref. [6].

In particular, as to an $(n,w,1)$-optical orthogonal code, we have

$$\Phi(n,w,1) \leqslant \left\lfloor \frac{n-1}{w(w-1)} \right\rfloor \tag{2.3}$$

where $\lfloor x \rfloor$ denotes the largest integer of less than or equal to x.

If $w=3,\lambda=1$,

$$\Phi(n,3,1) \leqslant \left\lfloor \frac{n-1}{6} \right\rfloor \tag{2.4}$$

When n is even, we have the slightly stronger upper bound

$$\Phi(n,w,1) \leqslant \left\lfloor \frac{n-2}{w(w-1)} \right\rfloor \tag{2.5}$$

If the cardinality $|C|$ in an (n,w,λ)-OOC, C, satifies $|C|=\Phi(n,w,\lambda)$, C is said to be OOC-optimized. If $|C|=\left\lfloor \frac{1}{w}\left\lfloor \frac{(n-1)}{(w-1)}\left\lfloor \frac{(n-2)}{(w-2)}\right\rfloor \ldots \left\lfloor \frac{(n-\lambda)}{(w-\lambda)}\right\rfloor \ldots \right\rfloor \right\rfloor \right\rfloor$, C is called an optimal OOC. If $|C|$ is close to $\Phi(n,w,\lambda)$, C is called a quasi-optimal OOC. When $\lambda=1$, the cardinalities of some optimal OOCs are shown in Table 2.2.

Table 2.2 The cardinalities of some optimal OOCs[3]

w	n	$\lvert C\rvert$	w	n	$\lvert C\rvert$	w	n	$\lvert C\rvert$
3	31	5	3	4095	682	5	85	4
3	63	10	4	40	3	5	341	17
3	127	21	4	121	10	5	1365	68
3	255	42	4	364	30	5	5461	273
3	511	85	4	1093	91	6	156	5
3	1023	170	4	3280	273	6	631	21
3	2047	341				6	3156	105

2.2.3 Constructions of Constant-weight Symmetric OOCs

The construction of OOC is equivalent to the design of a codeword block and the construction of a codeword block may use the primary theory of numbers, finite projective geometries, finite fields, algebraic coding theory and various other combinatorial disciplines. The constructions are divided into combinational

constructions[1 – 5], algebraic constructions[3, 5 – 14], constructions of finite projective geometries[3, 15] iterative constructions[3, 5, 16 – 18], and so on.

2.2.3.1 Combinational Contructions[1 – 5]

Optical orthogonal codes can be constructed by various conbinatorial methods. For the case of $\lambda = 1$, the problem of constructing OOCs is equvalent to the problem of packing difference sets.

(1) Constructions of (n,2,1)-OOCs

$\{(0,1),(0,2),\cdots,(0,\phi),\bmod n\}$ is an (n,2,1) optimal OOC. When n is odd, $\phi = \dfrac{n-1}{2}$ and when n is even, $\phi = \dfrac{n}{2} - 1$.

(2) Constructions of (n,3,1) Optimized and Optimal OOCs

Assume $n = 6l + v'$ for $1 \leqslant v' \leqslant 6$.

① $l \equiv 0 \pmod 4$

Assume $l = 4u \geqslant 8$, the following l arrays with 3 elements form an (n,3,1) optimized OOC as:

$\{0, 4u+i, 8u-i\}$ $(1 \leqslant i \leqslant 2u-1)$;

$\{0, 8u-1+i, 12u-i\}$ $(1 \leqslant i \leqslant u)$;

$\{0, 9u+1+i, 11u-i\}$ $(1 \leqslant i \leqslant u-2)$;

and $\{0, 6u, 10u\}, \{0, 9u, 9u+1\}, \{0, 10u+1, 12u\}$.

Example 2.2 Construct an (49,3,1)-OOC.

Assume $l = 8$, $u = 2$ and $n = 6l + v' = 48 + v'$ for $1 \leqslant v' \leqslant 6$, we can obtain an optical orthogonal code as follows: (0,9,15), (0,10,14), (0,11,13), (0,16,23), (0,17,22) and (0,12,20), (0,18,19), (0,21,24) and $|C|$=8.

② $l \equiv 1 \pmod 4$

Assume $l = 4u + 1 \geqslant 9$, an (n,3,1) optimized optical orthogonal code can be constructed by l arrays with 3 elements as follows:

$\{0, l+i, 2l+1-i\}$ $(1 \leqslant i \leqslant 2u)$;

$\{0, 2l+i, 3l-i\}$ $(1 \leqslant i \leqslant u)$;

$\{0, 2l+u+2+i, 3l-u-i\}$ $(1 \leqslant i \leqslant u-2)$;

and $\{0, l+2u+1, 2l+2u+1\}, \{0, 2l+u+1, 2l+u+2\}, \{0, 2l+2u+2, 3l\}$.

Example 2.3 Construct an (55,3,1)-OOC.

Assume $l = 9$, $u = 2$, $n = 6l + v' = 54 + v'$ for $1 \leqslant v' \leqslant 6$, we can get an (55,3,1)-OOC as follows: (0,10,18), (0,11,17), (0,12,16), (0,13,15), (0,19,26), (0,20,25) and (0,14,23), (0,21,22), (0,24,27) and $|C|$= 9.

③ $l \equiv 2 \pmod 4$

Assume $l = 4u + 2 \geqslant 6$, then the following 3-element arrays form an (n,3,1) optimized OOC:

$\{0, l+i, 2l-i\} \quad \left(1 \leqslant i \leqslant \frac{l}{2}-1\right)$;

$\{0, 2l-1+i, 3l-i\} \quad (1 \leqslant i \leqslant u)$;

$\{0, 2l+u+1+i, 3l-u-i\} \quad (1 \leqslant i \leqslant u-1)$;

and $\left\{0, \frac{3}{2}l, \frac{5}{2}l\right\}, \{0, 2l+u, 2l+u+1\}, \left\{0, \frac{5}{2}l+1, 3l+1\right\}$.

Notice that this method can not construct an $(n,3,1)$ -OOC when $n = 6l+2$.

Example 2.4 Construct an (37,3,1)-optical orthogonal code.

Assume $l = 6$, $u = 1$, $n = 6l + v' = 36 + v'$ for $1 \leqslant v' \leqslant 6$, the obtained OOC is as follows:

(0,7,11), (0,8,10), (0,12,17) and (0,9,15), (0,13,14), (0,16,19), and $|C| = 6$.

④ $l \equiv 3 (\mathrm{mod}\, 4)$

Assume $l = 4u+3 \geqslant 7$, then when $n \neq 2 (\mathrm{mod}\, 6)$, the following 3-element arrays form an $(n,3,1)$ optimized OOC as

$\{0, l+i, 2l+1-i\} \quad (1 \leqslant i \leqslant 2u+1)$;

$\{0, 2l+i, 3l+1-i\} \quad (1 \leqslant i \leqslant u+1)$;

$\{0, 2l+u+3+i, 3l-u-1-i\} \quad (1 \leqslant i \leqslant u-2)$;

and $\{0, l+2u+2, 2l+2u+2\}, \{0, 2l+u+2, 3l+3\}, \{0, 2l+2u+3, 3l+1\}$.

Example 2.5 Construct an (43,3,1)-OOC.

Assume $l = 7$, $u = 1$, $n = 6l + v' = 42 + v'$ for $1 \leqslant v' \leqslant 6$, we can find the OOC as follows:

(0,8,14), (0,9,13), (0,10,12), (0,15,20), (0,16,19) and (0,11,18), (0,19,22), and the cardinality of the OOC is $|C| = 7$.

(3) Constructions of $(n,4,1)$-OOCs

Assume $n = 12l+1$, $l = 6u$, then the folowing 4-element arrays form an $(n,4,1)$ -OOC[5] that includes $l-2$ codewords, but its cardinality is not optimal.

$\{0, a_1u+d_1+i, b_1u+e_1+2i, c_1u+f_1+3i\} \quad L_1 \leqslant i \leqslant U_1$

$\{0, a_2u+d_2+i, b_2u+e_2+2i, c_2u+f_2+3i\} \quad L_2 \leqslant i \leqslant U_2$

$\{0, a_3u+d_3+i, b_3u+e_3+2i, c_3u+f_3+3i\} \quad L_3 \leqslant i \leqslant U_3$

$\{0, a_4u+d_4+i, b_4u+e_4+2i, c_4u+f_4+3i\} \quad L_4 \leqslant i \leqslant U_4$

$\{0, a_5u+d_5+i, b_5u+e_5+2i, c_5u+f_5+3i\} \quad L_5 \leqslant i \leqslant U_5$

$\{0, a_6u+d_6+i, b_6u+e_6+2i, c_6u+f_6+3i\} \quad L_6 \leqslant i \leqslant U_6$

There are a number of parameters a_j, b_j, c_j, d_j, e_j, f_j, L_j and U_j $(1 \leqslant j \leqslant 6)$, in this construction that must be determined. A general method to find them requires additional reaserch. However, the parameters shown in Table 2.3, are suitible for this construction[5].

Table 2.3 Parameters a_j, b_j, c_j, d_j, e_j, f_j, L_j, and U_j are awaiting to be determined [5]

j	a_j	b_j	c_j	d_j	e_j	f_j	L_j	U_j
1	35	5	0	0	0	1	0	$u-1$
2	21	13	0	0	0	0	1	$u-1$
3	47	19	0	1	1	2	0	$u-1$
4	23	5	8	0	1	1	0	$u-1$
5	41	25	8	0	0	0	1	$u-1$
6	43	31	8	0	1	2	0	$u-1$

Example 2.6 Construct an (217,4,1)-OOC.

Using the construction of the $(n,4,1)$-OOC, assume $n=12l+1$, $l=6u=18$ for $u=3$, we can construct an (217,4,1)-OOC as follows: (0,1,15,105), (0,4,17,106), (0,7,19,107), (0,3,41,64), (0,6,43,65), (0,2,58,142), (0,5,60,143), (0,8,62,144), (0,16,25,69), (0,18,28,70), (0,20,31,71), (0,27,77,124), (0,30,79,125), (0,26,94,129), (0,29,96,130), (0,32,98,131), and $|C|=16$.

Some construction results of $(n,w,1)$-OOCs obtained with combinatorial methods are shown in Table 2.4. The autocorrelation function curve of codeword (1,34,50,56,60) and the cross-correlation function curve between it and codeword (9,32,39,93,129) in (137,5,1)-OOC are shown in Fig. 2.2.

Table 2.4 Some construction results of $(n,w,1)$-OOCs obtained with combinatorial methods

n	w	Codewords of (n,w,1)-OOC	$\|C\|$
7	3	(0,1,3)	1
13	3	(0,1,4),(0,2,7)	2
19	3	(0,1,5),(0,2,8),(0,3,10)	3
25	3	(0,1,6),(0,2,9),(0,3,11),(0,4,13)	4
31	3	(0,1,7),(0,2,11),(0,3,15),(0,4,14),(0,5,13)	5
37	3	(0,7,11),(0,8,10),(0,9,15),(0,12,17),(0,13,14),(0,16,19)	6
43	3	(0,8,14),(0,9,13),(0,10,12),(0,11,18),(0,15,20),(0,16,19), (0,9,22)	7
49	3	(0,9,15),(0,10,14),(0,11,13),(0,12,20),(0,16,23),(0,17,22),(0,18,19), (0,21,24)	8
55	3	(0,10,18),(0,11,17),(0,12,16),(0,13,15),(0,14,23),(0,19,26),(0,20,25), (0,21,22),(0,24,27)	9
217	4	(0,1,15,105),(0,2,58,142),(0,3,41,64),(0,4,17,106),(0,5,60,143), (0,6,43,65),(0,7,19,107),(0,8,62,144),(0,16,25,69),(0,18,28,70), (0,20,31,71),(0,26,94,129),(0,27,77,124),(0,29,96,130),(0,30,79,125), (0,32,98,131)	16

Continued

n	w	Codewords of (n,w,1)-OOC	$\lvert C \rvert$
341	5	(0,1,85,21,5),(0,2,170,10,42),(0,3,111,104,53),(0,6,222,106,208), (0,9,268,151,105),(0,11,45,76,198),(0,12,103,75,212),(0,13,35,227,43), (0,15,107,146,164),(0,17,264,203,165),(0,19,88,267,220),(0,22,90,55,152), (0,23,293,252,118),(0,24,206,83,150),(0,25,54,169,221), (0,26,269,86,113),(0,37,147,217,81)	17
181	6	(0,1,42,59,125,135),(0,5,29,82,114,132),(0,7,40,51,113,151), (0,8,95,110,155,175),(0,36,64,133,154,156),(0,107,146,150,159,162)	6

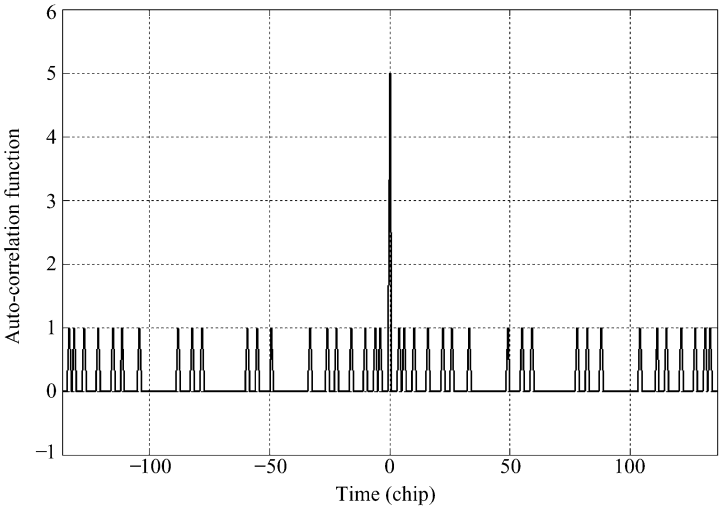

(a) Auto-correlation function of codeword (1,34,50,56,60)

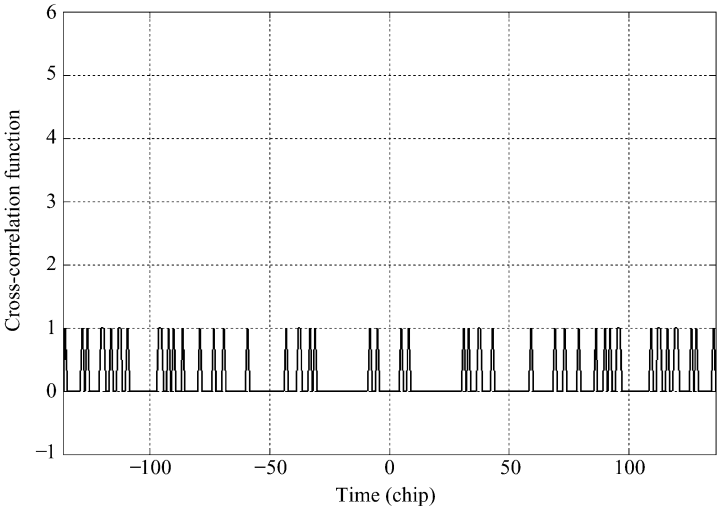

(b) Cross-correlation function between codewords (1,34,50,56,60) and (9,32,39,93,129)

Figure 2.2 The correlation functions of (137,5,1)-OOC

2.2.3.2 Algebraic Constructions

(1) Algebraic Construction 1

Assume that α is a primitive element of a finite field $GF(p^{2m})$, p is any prime number and m is an integer that is greater than or equal to 1. Set $q = p^m + 1$ and let $\beta = \alpha^q$. Let f be the logarithmic map from $GF(p^{2m}) \setminus \{0\}$ to the integer set $\{0,1,\cdots, p^{2m}-1\}$, that is,

$$f(\alpha^t) = t \tag{2.6}$$

If the characteristic functions of the subsets S_i $(1 \leqslant i \leqslant p^m - 2)$, in $\{0,1,\cdots, p^{2m}-1\}$, may be taken as the codewords of an OOC we can obtain an $(p^{2m}-1, p^m+1, 2)$ optimal OOC[5, 6]. Then the subsets, S_i, are given by

$$S_i = \{f(x) \mid (x-1)^{p^m+1} = \beta^i\}, \quad 1 \leqslant i \leqslant p^m - 2 \tag{2.7}$$

Otherwise, the characteristic functions of S_i drive at a map $g(x)$ from $\{0,1,\cdots, p^{2m}-1\}$ to $\{0,1\}$, given by

$$g(x) = \begin{cases} 1 & \text{if } x \in S_i \\ 0 & \text{if } x \in \{0,1,\cdots, p^{2m}-1\} \setminus S_i \end{cases} \tag{2.8}$$

The $p^m - 2$ codewords can be obtained with this method, which satisfy the equal sign of (2.2), and therefore, the constructed OOC is an optimal OOC.

Proof: See Ref.[6].

Example 2.7 Construct an $(63,9,2) = (2^6-1, 2^3+1, 2)$ optimal optical orthogonal code.

We can get $m = 3$, $p = 2$ and $p^m - 2 = 6$. α is an primitive element of the finite field $GF(p^{2m}) = GF(2^6)$ and $\beta = \alpha^{p^m+1}$. Let's choose an irreducible polynomial of degree 6, $x^6 + x + 1$, over $GF(p) = GF(2)$ and from the irreducible polynomial, the element table of $GF(2^6)$ modulo-$(x^6 + x + 1)$ can be obtained as follows:

$\alpha^0 \equiv 1$	$\alpha^7 \equiv \alpha^2 + \alpha$	$\alpha^{14} \equiv \alpha^4 + \alpha^2$
$\alpha^1 \equiv \alpha$	$\alpha^8 \equiv \alpha^3 + \alpha^2$	$\alpha^{15} \equiv \alpha^5 + \alpha^3$
$\alpha^2 \equiv \alpha^2$	$\alpha^9 \equiv \alpha^4 + \alpha^3$	$\alpha^{16} \equiv \alpha^4 + \alpha + 1$
$\alpha^3 \equiv \alpha^3$	$\alpha^{10} \equiv \alpha^5 + \alpha^4$	$\alpha^{17} \equiv \alpha^5 + \alpha^2 + \alpha$
$\alpha^4 \equiv \alpha^4$	$\alpha^{11} \equiv \alpha^5 + \alpha + 1$	$\alpha^{18} \equiv \alpha^3 + \alpha^2 + \alpha + 1$
$\alpha^5 \equiv \alpha^5$	$\alpha^{12} \equiv \alpha^2 + 1$	$\alpha^{19} \equiv \alpha^4 + \alpha^3 + \alpha^2 + \alpha$
$\alpha^6 \equiv \alpha + 1$	$\alpha^{13} \equiv \alpha^3 + \alpha$	$\alpha^{20} \equiv \alpha^5 + \alpha^4 + \alpha^3 + \alpha^2$

Continued

$\alpha^{21} \equiv \alpha^5 + \alpha^4 + \alpha^3 + \alpha + 1$	$\alpha^{36} \equiv \alpha^4 + \alpha^2 + \alpha$	$\alpha^{50} \equiv \alpha^5 + \alpha^4 + \alpha^2$
$\alpha^{22} \equiv \alpha^5 + \alpha^4 + \alpha^2 + 1$	$\alpha^{37} \equiv \alpha^5 + \alpha^3 + \alpha^2$	$\alpha^{51} \equiv \alpha^5 + \alpha^3 + \alpha + 1$
$\alpha^{23} \equiv \alpha^5 + \alpha^3 + 1$	$\alpha^{38} \equiv \alpha^4 + \alpha^3 + \alpha + 1$	$\alpha^{52} \equiv \alpha^4 + \alpha^2 + 1$
$\alpha^{24} \equiv \alpha^4 + 1$	$\alpha^{39} \equiv \alpha^5 + \alpha^4 + \alpha^2 + \alpha$	$\alpha^{53} \equiv \alpha^5 + \alpha^3 + \alpha$
$\alpha^{25} \equiv \alpha^5 + \alpha$	$\alpha^{40} \equiv \alpha^5 + \alpha^3 + \alpha^2 + \alpha + 1$	$\alpha^{54} \equiv \alpha^4 + \alpha^2 + \alpha + 1$
$\alpha^{26} \equiv \alpha^2 + \alpha + 1$	$\alpha^{41} \equiv \alpha^4 + \alpha^3 + \alpha^2 + 1$	$\alpha^{55} \equiv \alpha^5 + \alpha^3 + \alpha^2 + \alpha$
$\alpha^{27} \equiv \alpha^3 + \alpha^2 + \alpha$	$\alpha^{42} \equiv \alpha^5 + \alpha^4 + \alpha^3 + \alpha$	$\alpha^{56} \equiv \alpha^4 + \alpha^3 + \alpha^2 + \alpha + 1$
$\alpha^{28} \equiv \alpha^4 + \alpha^3 + \alpha^2$	$\alpha^{43} \equiv \alpha^5 + \alpha^4 + \alpha^2 + \alpha + 1$	$\alpha^{57} \equiv \alpha^5 + \alpha^4 + \alpha^3 + \alpha^2 + \alpha$
$\alpha^{29} \equiv \alpha^5 + \alpha^4 + \alpha^3$	$\alpha^{44} \equiv \alpha^5 + \alpha^3 + \alpha^2 + 1$	$\alpha^{58} \equiv \alpha^5 + \alpha^4 + \alpha^3 + \alpha^2 + \alpha + 1$
$\alpha^{30} \equiv \alpha^5 + \alpha^4 + \alpha + 1$	$\alpha^{45} \equiv \alpha^4 + \alpha^3 + 1$	$\alpha^{59} \equiv \alpha^5 + \alpha^4 + \alpha^3 + \alpha^2 + 1$
$\alpha^{31} \equiv \alpha^5 + \alpha^2 + 1$	$\alpha^{46} \equiv \alpha^5 + \alpha^4 + \alpha$	$\alpha^{60} \equiv \alpha^5 + \alpha^4 + \alpha^3 + 1$
$\alpha^{32} \equiv \alpha^3 + 1$	$\alpha^{47} \equiv \alpha^5 + \alpha^2 + \alpha + 1$	$\alpha^{61} \equiv \alpha^5 + \alpha^4 + 1$
$\alpha^{33} \equiv \alpha^4 + \alpha$	$\alpha^{48} \equiv \alpha^3 + \alpha^2 + 1$	$\alpha^{62} \equiv \alpha^5 + 1$
$\alpha^{34} \equiv \alpha^5 + \alpha^2$	$\alpha^{49} \equiv \alpha^4 + \alpha^3 + \alpha$	$\alpha^{63} \equiv 1$
$\alpha^{35} \equiv \alpha^3 + \alpha + 1$		

According to this table, equation $S_i = \{f(x) : (x-1)^{p^m+1} = \beta^i, 1 \leqslant i \leqslant p^m - 2\}$ can be transformed into equation $(\alpha^y + 1)^9 = \alpha^{9i}$, $1 \leqslant i \leqslant 6$, where the values of y satisfy $1 \leqslant y \leqslant p^{2m} - 1$ and thus y has five values for each value of i. For example, in order to solve the equation $(\alpha^y + 1)^9 = \alpha^9$ when $i = 1$, we use $y = 6$ to make a trial. We can obtain $\alpha^y + 1 = \alpha^6 + 1$ and $\alpha^6 \equiv \alpha + 1$ can be derived from the table. Then, $\alpha^6 + 1 = \alpha + 1 + 1 = \alpha$ is obtained and therefore $(\alpha^6 + 1)^9 = \alpha^9$, that is equal to the right side of aforementioned equation. Hence, $y = 6$ is a solution of the equation $(\alpha^y + 1)^9 = \alpha^9$. We can find eight other solutions using a similar method and finally obtain the block of an optical orthogonal codeword as $S_1 = \{6, 22, 23, 39, 48, 50, 54, 58, 60\}$.

Similarly, we can get $S_2 = \{12, 15, 33, 37, 44, 45, 46, 53, 57\}$ for $i = 2$ by solving the equation $(\alpha^y + 1)^9 = \alpha^{18}$, $S_3 = \{4, 9, 14, 20, 32, 34, 47, 49, 61\}$ for $i = 3$ by solving $(\alpha^y + 1)^9 = \alpha^{27}$, $S_4 = \{3, 11, 24, 25, 27, 29, 30, 43, 51\}$ for $i = 4$ by solving $(\alpha^y + 1)^9 = \alpha^{36}$, $S_5 = \{2, 7, 10, 16, 17, 36, 55, 56, 62\}$ for $i = 5$ by solving $(\alpha^y + 1)^9 = \alpha^{45}$, $S_6 = \{1, 5, 8, 18, 28, 31, 35, 40, 59\}$ for $i = 6$, by solving $(\alpha^y + 1)^9 = \alpha^{54}$. In this way, all codewords of the (63,9,2)-OOC have been constructed.

The construction results of some $(n, w, 2)$-OOCs are shown in Table 2.5. (Because there are so many data, the codewords of only three OOCs are given in Table 2.5.)

Table 2.5 Codewords of three $(n,w,2)$-OOCs constructed by Algebraic Construction 1

n	w	$(n,w,2)$ optical orthogonal code	$\|C\|$
15	5	(1,4,5,6,9),(2,3,8,10,12)	2
63	9	(1,5,8,18,28,31,35,40,59),(2,7,10,16,17,36,55,56,62), (3,11,24,25,27,29,30,43,51), (4,9,14,20,32,34,47,49,61),(6,22,23,39,48,50,54,58,60), (12,15,33,37,44,45,46,53,57)	6
255	17	(23,25,29,34,43,45,113,114,137,145,152,171,178,186,209,210) (19,35,46,49,50,58,68,78,86,87,90,101,117,163,165,226,228) (5,15,26,55,77,80,115,119,123,158,161,183,212,223,233,240,253) (38,70,71,75,92,98,100,116,136,156,172,174,180,197,201,202,234) (2,8,11,32,42,44,85,126,128,138,159,162,168,176,194,231,249) (10,30,52,61,67,110,111,154,160,169,191,211,225,230,238,246,251) (7,12,41,59,94,112,141,146,173,179,190,192,204,216,218,229,235) (17,57,76,89,93,105,139,140,142,147,149,150,184,196,200,213,232) (13,40,79,106,120,130,135,155,166,185,187,189,208,219,239,244,254) (1,4,16,21,22,63,64,69,81,84,88,97,133,170,207,243,252) (6,47,56,73,95,96,102,108,109,131,148,157,198,214,217,242,245) (20,53,60,65,83,104,122,127,134,167,195,205,210,221,222,237,247) (3,28,48,51,54,74,99,107,121,151,164,175,182,193,206,236,250) (14,24,27,37,82,91,103,118,125,129,153,177,181,188,203,215,224)	14

(2) Algebraic Construction 2[5,6,19,20]

Assume $w=2m+1$, $n=w(w-1)r+1$. Let m and r be integers so that n is a prime number. Again let α be any primitive root modulo-n and set $c=(w-1)r$. For $1\leqslant i\leqslant c-1$, let S_i denote the set

$$S_i=\{\alpha^{i+jc}\mid 0\leqslant j\leqslant w-1\} \tag{2.9}$$

i is the index of the set S_i and let $i=i_k$ for each k, $1\leqslant k\leqslant m$. If and only if $(\alpha^{kc}-1)\in S_i$, then the characteristic functions of the subsets $S_0,S_m,S_{2m},\cdots,S_{(r-1)m}$ may be taken as codewords of an optimal $(n,w,1)$-OOC if the subscripts $i_1,i_2,\cdots,i_m$ are all distinct modulo-m. All the arithmetic is modulo-n.

Example 2.8 Construct an $(n,w,1)=(61,5,1)$ optimal OOC.

$n=61$ is a prime number and thus $m=2$, $r=3$, $c=12$. Choose $\alpha=2$ as a primitive root of $GF(61)$. We can obtain the subsets:

$S_0=\{1,9,20,58,34\}$

$S_2=\{4,36,19,49,14\}$

$S_4=\{16,22,15,13,56\}$

which are all codewords of $(n,w,1)=(61,5,1)$-OOC. Note that all the arithmetic above is modulo-61.

Some results of $(n,2m+1,1)$ optical orthogonal codes that are constructed by using the algebraic construction 2 are shown in Table 2.6.

Table 2.6 Some $(n,2m+1,1)$ -OOCs constructed by Algebraic Construction 2[6]

m	w	α	n	C	$\lvert C\rvert$
2	5	2	61	$S_i=\{2^{2i+12k}\mid 0\leqslant k\leqslant 4\}\quad 0\leqslant i\leqslant 2$	3
		2	101	$S_i=\{2^{2i+20k}\mid 0\leqslant k\leqslant 4\}\quad 0\leqslant i\leqslant 4$	5
		7	241	$S_i=\{7^{2i+48k}\mid 0\leqslant k\leqslant 4\}\quad 0\leqslant i\leqslant 11$	12
		3	281	$S_i=\{3^{2i+56k}\mid 0\leqslant k\leqslant 4\}\quad 0\leqslant i\leqslant 13$	14
		2	421	$S_i=\{2^{2i+84k}\mid 0\leqslant k\leqslant 4\}\quad 0\leqslant i\leqslant 20$	21
		7	601	$S_i=\{7^{2i+120k}\mid 0\leqslant k\leqslant 4\}\quad 0\leqslant i\leqslant 29$	30
		7	3541	$S_i=\{7^{2i+708k}\mid 0\leqslant k\leqslant 4\}\quad 0\leqslant i\leqslant 176$	177
3	7	10	337	$S_i=\{10^{3i+48k}\mid 0\leqslant k\leqslant 6\}\quad 0\leqslant i\leqslant 7$	8
		2	421	$S_i=\{2^{3i+60k}\mid 0\leqslant k\leqslant 6\}\quad 0\leqslant i\leqslant 9$	10
		3	463	$S_i=\{3^{3i+66k}\mid 0\leqslant k\leqslant 6\}\quad 0\leqslant i\leqslant 10$	11
		2	883	$S_i=\{2^{3i+126k}\mid 0\leqslant k\leqslant 6\}\quad 0\leqslant i\leqslant 20$	21
		2	3571	$S_i=\{2^{3i+510k}\mid 0\leqslant k\leqslant 6\}\quad 0\leqslant i\leqslant 84$	85
4	9	5	1153	$S_i=\{5^{4i+128k}\mid 0\leqslant k\leqslant 8\}\quad 0\leqslant i\leqslant 15$	16
		10	1873	$S_i=\{10^{4i+208k}\mid 0\leqslant k\leqslant 8\}\quad 0\leqslant i\leqslant 25$	26
		5	2017	$S_i=\{5^{4i+224k}\mid 0\leqslant k\leqslant 8\}\quad 0\leqslant i\leqslant 27$	28
		5	3673	$S_i=\{5^{4i+408k}\mid 0\leqslant k\leqslant 8\}\quad 0\leqslant i\leqslant 50$	51

(3) Algebraic Construction 3[5,6,19,20]

Assume $w=2m$, $n=w(w-1)r+1$ and let m and r be integers so that n is a prime number. Again suppose β to be a primitive root modulo-n of $GF(n)$ and set $c=wr$. For $0\leqslant i\leqslant c-1$, let T_i denote the set

$$T_i=\{\beta^{i+jc}:0\leqslant j\leqslant w-2\}\bigcup\{0\} \tag{2.10}$$

where i is the subscript of T_i and then, $i_0,i_1,i_2,\cdots,i_{m-1}$ are the subscripts of T_i that include 1, β^c-1, $\beta^{2c}-1,\cdots,\beta^{(m-1)c}-1$, respectively. If $i_0,i_1,i_2,\cdots,i_{m-1}$ are all distinct modulo-m, then the characteristic functions of the subsets T_0,T_m, $T_{2m},\cdots,T_{(r-1)m}$ may be taken as codewords of an optimal $(n,w,1)$ -OOC. All the arithmetic is modulo-n.

Example 2.9 Construct an $(n,w,1)=(181,6,1)$ optical orthogonal code.

Assume that $m=3$, $r=6$ and $c=36$ from $n=181$ and $w=6$. Choose $\beta=2$ as the primitive root modulo-181 of $GF(181)$. We can find the subsets

$T_0 = \{0,1,42,59,125,135\}$

$T_3 = \{0,8,95,110,155,175\}$

$T_6 = \{0,36,64,133,154,156\}$

$T_9 = \{0,107,146,150,159,162\}$

$T_{12} = \{0,5,29,82,114,132\}$

$T_{15} = \{0,7,40,51,113,151\}$

which are all codewords of $(n,w,1) = (181,6,1)$-OOC. All the arithmetic is modulo-181.

Some results of $(n,2m,1)$ optical orthogonal code constructed by Algebraic Construction 3 are shown in Table 2.7.

Table 2.7 Some results of $(n,2m,1)$-OOC constructed by Algebraic Construction 3[6]

m	*w*	β	*n*	*C*
2	4	5	73	$T_i = \{0\} \bigcup \{5^{2i+24k} \mid 0 \leqslant k \leqslant 2\} \quad 0 \leqslant i \leqslant 5$
		5	97	$T_i = \{0\} \bigcup \{5^{2i+32k} \mid 0 \leqslant k \leqslant 2\} \quad 0 \leqslant i \leqslant 7$
		2	181	$T_i = \{0\} \bigcup \{2^{2i+60k} \mid 0 \leqslant k \leqslant 2\} \quad 0 \leqslant i \leqslant 14$
		6	229	$T_i = \{0\} \bigcup \{6^{2i+76k} \mid 0 \leqslant k \leqslant 2\} \quad 0 \leqslant i \leqslant 18$
		5	277	$T_i = \{0\} \bigcup \{5^{2i+92k} \mid 0 \leqslant k \leqslant 2\} \quad 0 \leqslant i \leqslant 22$
		2	3613	$T_i = \{0\} \bigcup \{2^{2i+1204k} \mid 0 \leqslant k \leqslant 2\} \quad 0 \leqslant i \leqslant 300$
3	6	2	181	$T_i = \{0\} \bigcup \{2^{3i+36k} \mid 0 \leqslant k \leqslant 4\} \quad 0 \leqslant i \leqslant 5$
		2	211	$T_i = \{0\} \bigcup \{2^{3i+42k} \mid 0 \leqslant k \leqslant 4\} \quad 0 \leqslant i \leqslant 6$
		7	241	$T_i = \{0\} \bigcup \{7^{3i+48k} \mid 0 \leqslant k \leqslant 4\} \quad 0 \leqslant i \leqslant 7$
		3	631	$T_i = \{0\} \bigcup \{3^{3i+126k} \mid 0 \leqslant k \leqslant 4\} \quad 0 \leqslant i \leqslant 20$
		6	3301	$T_i = \{0\} \bigcup \{6^{3i+660k} \mid 0 \leqslant k \leqslant 4\} \quad 0 \leqslant i \leqslant 109$
4	8	11	1009	$T_i = \{0\} \bigcup \{11^{4i+144k} \mid 0 \leqslant k \leqslant 6\} \quad 0 \leqslant i \leqslant 17$
		3	3137	$T_i = \{0\} \bigcup \{3^{4i+448k} \mid 0 \leqslant k \leqslant 6\} \quad 0 \leqslant i \leqslant 55$
		5	3697	$T_i = \{0\} \bigcup \{5^{4i+528k} \mid 0 \leqslant k \leqslant 6\} \quad 0 \leqslant i \leqslant 65$

2.2.3.3 Constructions of Finite Projective Geometry[3, 15]

A finite vector space $V(d+1,q)$ is composed of $d+1$ dimensional vectors with coordinates from the finite field $GF(q)$, where q is a prime power. Points in the projective geometry $PG(d,q)$ correspond to lines through the origin in $V(d+1,q)$ while s-space in $PG(d,q)$ corresponds to $(s+1)$-dimensional subspaces through the origin in $V(d+1,q)$.

In $V(d+1,q)$, there are q vectors on a line and therefore, $q-1$ nonzero vectors are on a line through the origin. Two lines through the origin do not share any nonzero vectors. There are $q^{d+1}-1$ nonzero vectors all together. Hence, there are $(q^{d+1}-1)/(q-1)$ different lines through the origin in $V(d+1,q)$. Furthermore, there are q^2-1 nonzero vectors on a plane through the origin and they can be partitioned into $q+1$ lines, in which each line consists of $q-1$ vectors. Thus there are $q+1$ points on a line in $PG(d,q)$. Similarly, it can be shown that there are $(q^{d+1}-1)/(q-1)$ points in $PG(d,q)$.

A vector β in the space $V(d+1,q)$ has $d+1$ coordinates with values from the finite field $GF(q)$, or alternatively, it can be viewed as an element β of the extension field $GF(q^{d+1})$. Assuming α to be a primitive element of $GF(q^{d+1})$, then the nonzero elements of $GF(q^{d+1})$ are the 0^{th} through the $(q^{d+1}-2)^{\text{th}}$ power of α. If $\alpha^{\gamma}=\beta$, then $\log_{\alpha}\beta=\gamma$ is obtained as the discrete logarithm. Therefore, the discrete logarithm establishes one-to-one correspondence between the nonzero vectors in $V(d+1,q)$ and the integers $\{0,1,\cdots,q^{d+1}-2\}$. The nonzero vectors on a line through the origin are the $i^{\text{th}},(i+n)^{\text{th}},\cdots,(i+(q-2)n)^{\text{th}}$ powers of the primitive element for some values of *i*, where $n=(q^{d+1}-1)/(q-1)$ is the size of $PG(d,q)$. For an arbitrary point *p* in $PG(d,q)$, let $\log p$ be the discrete logarithm of any vector on the line corresponding to *p* modulo *n* in $V(d+1,q)$. Then, log(·) is a one-to-one mapping between the points of the projective geometry $PG(d,q)$ and the integers modulo *n*. Each line in the projective geometry corresponds to a subset of integers modulo *n*.

In addition, assuming the cyclic shift of a line *L* in $PG(d,q)$ to be the set of points $\{p\colon \log p=1+\log p'(\bmod n)$ for some point p' on $L\}$, then the cyclic shift of a line is still a line in $PG(d,q)$. An orbit is a set of lines in $PG(d,q)$ that are cyclic shifts of one another. The number of lines in an orbit is its size, which is necessarily a divisor of *n*. An orbit is full if its size is *n* and otherwise it is incomplete.

Now, let us construct $(n,w,1)$-OOC from the finite projective geometry $PG(d,q)$, where $n=(q^{d+1}-1)/(q-1)$ and $w=q+1$. Suppose there are *m* full orbits in $PG(d,q)$. Take one representative line from each full orbit and map each line into a set of integers modulo *n* under log(·). The resulting *m* sets with *w* elements form an OOC with the described parameters and desired correlation properties. Two lines intersect at no more than one point, and therefore two different shifts of a codeword set intersect at most once, and arbitrary shifts of two codeword sets intersect at most once. In the following, we show the construction procedure with an example.

Example 2.10 Construct (7,3,1)-OOC from the projective plane $PG(2,2)$ and the extension Galois field $GF^*(2^{2+1})$.

First of all, it is necessary that all nonzero vectors and their discrete logarithms in $GF^*(2^{2+1})$ are found. Choose a primitive irreducible polynomial of degree 3 over $GF(2)$, $f(x)=x^3+x+1$, and let α be a primitive element. Then, the individual powers of α are $\alpha^0=(0,0,1)$, $\alpha^1=(0,1,0)$, $\alpha^2=(1,0,0)$, $\alpha^3=(0,1,1)$, $\alpha^4=(1,1,0)$, $\alpha^5=(1,1,1)$, $\alpha^6=(1,0,1)$ respectively.

The corresponding relationships between the discrete logarithms and the vectors are $0\to(0,0,1)$, $1\to(0,1,0)$, $2\to(1,0,0)$, $3\to(0,1,1)$, $4\to(1,1,0)$, $5\to(1,1,1)$, $6\to(1,0,1)$ respectively.

From the dual relationship between the projective planes and lines in the projective geometry, the dual equation is obtained as:

$$X_2x_2+X_1x_1+X_0x_0=0$$

The seven vectors (corresponding to point coordinates) mentioned above are regarded as the coefficients of the equation respectively. Then, the equations for the seven lines are:

$0\to(0,0,1)\to l_0:\ x_0=0\to(0,0,1),(0,1,0),(0,1,1)$ on the line l_0, whose serial number is (0,1,3);

$1\to(0,1,0)\to l_1:\ x_1=0\to(0,0,1),(1,0,0),(1,0,1)$ on the line l_1, whose serial number is (0,2,6);

$2\to(1,0,0)\to l_2:\ x_2=0\to(0,1,0),(1,0,0),(1,1,0)$ on the line l_2, whose serial number is (1,2,4);

$3\to(0,1,1)\to l_3:\ x_1+x_0=0\to(0,0,1),(1,1,0),(1,1,1)$ on the line l_3, whose serial number is (0,4,5);

$4\to(1,1,0)\to l_4:\ x_2+x_1=0\to(1,0,0),(0,1,1),(1,1,1)$ on the line l_4, whose serial number is (2,3,5);

$5\to(1,1,1)\to l_5:\ x_2+x_1+x_0=0\to(0,1,1),(1,1,0),(1,0,1)$ on the line l_5, whose serial number is (3,4,6);

$6\to(1,0,1)\to l_6:\ x_2+x_0=0\to(0,1,0),(1,1,1),(1,0,1)$ on the line l_6, whose serial number is (1,5,6).

These seven lines correspond to seven codewords of an (7,3,1)-OOC, which are (0,1,3),(0,2,6),(1,2,4),(0,4,5),(2,3,5),(3,4,6),(1,5,6). However, since they include six cyclic shifts of a codeword, there is only $7/7=1$ codeword in an (7,3,1)-OOC. Therefore, anyone chosen from them is the constructed codeword of an (7,3,1)-OOC.

With a similar approach, the $(n,w,1)=((q^{d+1}-1)/(q-1),q+1,1)$-OOC with arbitrary values can be constructed in the projective space $PG(d,q)$ over Galois field. For instance, seventeen codewords can be obtained for an (341,5,1)-OOC using $PG(4,4)$, which are shown in Table 2.8. Table 2.9 shows the cardinalities of some $(n,w,1)$-OOC's and the parameters employed, q and d.

Table 2.8 All codeword sets of an optimal (341, 5, 1)-OOC

s_1 = {0,1,85,21,5}	s_7 = {0,12,103,75,212}	s_{13} = {0,23,293,252,118}
s_2 = {0,2,170,10,42}	s_8 = {0,13,305,227,43}	s_{14} = {0,24,206,83,150}
s_3 = {0,3,111,104,53}	s_9 = {0,15,107,146,164}	s_{15} = {0,25,54,169,221}
s_4 = {0,6,222,106,208}	s_{10} = {0,17,264,203,165}	s_{16} = {0,26,269,86,113}
s_5 = {0,9,268,151,105}	s_{11} = {0,19,88,267,220}	s_{17} = {0,37,147,217,81}
s_6 = {0,11,45,76,198}	s_{12} = {0,22,90,55,152}	

Table 2.9 $(n,w,1)$-OOC from finite projective geometry $PG(d,q)$

n	w	$\lvert C \rvert$	d	q	n	w	$\lvert C \rvert$	d	q
31	3	5	4	2	364	4	30	5	3
63	3	10	5	2	1093	4	91	6	3
127	3	21	6	2	3280	4	273	7	3
255	3	42	7	2	85	5	4	3	4
511	3	85	8	2	341	5	17	4	4
1023	3	170	9	2	1365	5	68	5	4
2047	3	341	10	2	5461	5	273	6	4
4095	3	682	11	2	156	6	5	3	5
40	4	3	3	3	631	6	21	4	5
121	4	10	4	3	3156	6	105	5	5

The number of lines in the projective geometry $PG(d,q)$ is

$$\frac{(q^{d+1}-1)(q^{d+1}-q)}{(q^2-1)(q^2-q)} = \frac{(q^{d-1}-1)n}{q^2-1} = \frac{n(n-1)}{w(w-1)} \tag{2.11}$$

When d is even, q^2-1 divides $q^{d-1}-1$ without remainder. Moreover, all orbits are full and the resulting OOC's are optimal. When d is odd, q^2-1 can not divide $q^{d-1}-1$ exactly and there exists only one incomplete orbit, and the other orbits are full. Then, the number of complete orbits is $\lfloor (n-1)/w(w-1) \rfloor = (q^d-q)/(q^2-1)$ which satisfies the upper bound of Equation (2.2). Thus, the OOC obtained is also optimal.

Similarly, when $s>1$, an s-dimensional space in projective geometry can be employed to construct an OOC with $\lambda>1$. An s-dimensional space consists of $(q^{s+1}-1)/(q-1)$ points and the intersection of two s spaces is at most $s-1$ spaces, which are composed of $(q^s-1)/(q-1)$ points. The cyclic shift of an s space is also an s space. Now, we generalize the definition of an orbit as a set of s spaces that are cyclic shifts of each other. The number of dimensions of an orbit must be divided by n. The construction of an OOC with the codelength

$n=(q^{d+1}-1)/(q-1)$, code-weight $w=(q^{s+1}-1)/(q-1)$, and auto-and cross-correlation constraint $\lambda=(q^{s}-1)/(q-1)$ is as follows:

1) Take one representative from each orbit with *n* member first.

2) The discrete logarithm of the points in each representative *s* space forms a codeword.

The codewords form an (n,w,λ)-OOC with the prescribed parameters.

2.2.3.4 Recursive Constructions[5, 3, 16 – 18, 22]

Another $(v_1v_2,k,1)$ -OOC, *C*, can be constructed by employing an $(v_1,k,1)$-OOC, C_1, and an $(v_2,k,1)$ -OOC, C_2, and C is also an optimal OOC if C_1 and C_2 are optimal OOC.

Definition 2.1 A difference array $DA(s,n)$ is defined as an $s\times n$ dimension matrix $\boldsymbol{M}=[m_{ij}]$ such that $m_{ij}\in\{0,1,2,\cdots,n-1\}$, and for any two rows M_u and M_w of $\boldsymbol{M}$ and any integer *i*, there exists only one column to satisfy

$$m_{uj}-m_{wj}\equiv i(\mathrm{mod}\,n).$$

Let $C_1=\{(a_{i0},a_{i1},\cdots,a_{ik-1}):1\leqslant i\leqslant l_1\}$ be an $(v_1,k,1)$ -OOC, which contains l_1 codewords and $C_2=\{(b_{i0},b_{i1},\cdots,b_{ik-1}):1\leqslant i\leqslant l_2\}$ be an $(v_2,k,1)$ -OOC, which contains l_2 codewords. Again, assume that $\boldsymbol{M}=DA(k,v_2)$ is a difference array of $k\times v_2$ dimensions. Then, the following family of *k* -element subsets forms an $(v_1v_2,k,1)$ -OOC [5], which has $l_2+v_2l_1$ codewords.

Type Ⅰ: $\{v_1m_{0i}+a_{j0},v_1m_{1i}+a_{j1},...,v_1m_{(k-1)i}+a_{j(k-1)}\}$, $1\leqslant i\leqslant v_2$, $1\leqslant j\leqslant l_1$;

Type Ⅱ: $\{v_1b_{i0},v_1b_{i1},...,v_1b_{i(k-1)}\}$, $1\leqslant i\leqslant l_2$.

In order to prove the correctness of aforementioned recursion constructions, we only need to prove that there are no repeating differences in the codewords. We take into account a difference $d \bmod (v_1v_2)$. If $d\equiv 0 \bmod v_1$, d can but be generated by a codeword in Type Ⅱ. Assume $d'\equiv d/v_1$, then C_2 generates at most once of d'. Thus, a certain codeword of Type Ⅱ in *C* produces at most once of *d*. If $d\neq 0 \bmod v_1$, then, assuming $d=v_1x+y$ for $0\leqslant y<v_1$, the difference $y\,(\mathrm{mod}\,v_1)$ is produced at most once by C_1. On the assumption that $a_{jw}-a_{ju}\equiv y\,(\mathrm{mod}\,v_1)$, $1\leqslant j\leqslant l_1$, $0\leqslant w\neq u<k$, then the difference $x\,(\mathrm{mod}\,v_2)$ is uniquely generated by a certain column *i* of the difference array $\boldsymbol{M}$ in the way of $m_{wi}-m_{ui}$. Hence, *C* produces at most once $d \bmod (v_1v_2)$.

If C_1 and C_2 are optimal, and there exists a difference array $DA(k, v_2)$, then C is also an optimal OOC. C_1 and C_2 can be exchanged with each other in the recursion constructions mentioned above. Because the construction of difference array plays an important role in the recursion construction of OOC, we introduce two methods of generating difference array.

Construction 1 (mutually prime method):

When each number among $1, 2, \cdots, k-1$ is prime with n, then the matrix $\boldsymbol{M} = (m_{ij})$ of $k \times n$ dimensions is a difference array $DA(k, n)$, where $m_{ij} = ij \pmod{n}$, $0 \leqslant i \leqslant k-1$, $0 \leqslant j \leqslant n-1$.

When $k = 2, 3, 4, 6$ and C_2 is an optimal OOC, then $v_2 = n_1 + l_2 k(k-1)$ is prime with each number among $1, 2, \cdots, k-1$ and there exists the difference array $DA(k, v_2)$. If C_1 is optimal, then C is also an optimal OOC.

Example 2.11 Let $C_1 = C_2 = \{(0,1,3) \bmod 7\}$ and

$$\boldsymbol{M} = \begin{bmatrix} 0 & 0 & 0 & 0 & 0 & 0 & 0 \\ 0 & 1 & 2 & 3 & 4 & 5 & 6 \\ 0 & 2 & 4 & 6 & 1 & 3 & 5 \end{bmatrix}$$

Then, based on the recursive construction mentioned above we can construct a new OOC as follows:

$C = \{(0,1,3), (0,8,17), (0,15,31), (0,22,45), (0,29,10), (0,36,24), (0,43,38), (0,7, 21) \pmod{49}\}$ and C, C_1 and C_2 are optical OOC.

Example 2.12 Making use of $(v_1, k, 1) = (7,3,1) : C_1 = \{(0,1,3) \bmod 7\}$ as well as $(v_2 k, 1) = (13,3,1) :\ C_2 = \{(0,1,4), (0,2,7) \bmod 13\}$ and constructed difference array

$$\boldsymbol{M} = DA(k, v_2) = \begin{bmatrix} 0 & 0 & 0 & 0 & 0 & 0 & 0 & 0 & 0 & 0 & 0 & 0 & 0 \\ 0 & 1 & 2 & 3 & 4 & 5 & 6 & 7 & 8 & 9 & 10 & 11 & 12 \\ 0 & 2 & 4 & 6 & 8 & 10 & 12 & 1 & 3 & 5 & 7 & 9 & 11 \end{bmatrix} (\text{mod} 13)$$

An (91,3,1)-OOC can be generated, which is

$C = \{(0,1,3), (0,8,17), (0,15,31), (0,22,45), (0,29,59), (0,36,73), (0,43,87), (0,50,10), (0,57,24), (0,64,38), (0,71,52), (0,78,66), (0,85,80), (0,7,28), (0,14,49) \bmod 91\}$

Its cardinality is $|C| = 15$.

Construction 2 (orthogonal array method):

Difference arrays can also be obtained by using orthogonal arrays or orthogonal Latin squares. An orthogonal array $OA(n, s)$ is an $s \times n^2$ matrix, whose elements are taken from $Z_n = \{0, 1, \cdots, n-1\}$ and any ordinal array (i, j) doesn't repeat in any two rows. When $s \geqslant 2$, each ordinal pair happens to appear once in any two chosed rows.

Given an orthogonal array $A=[a(i,j)]$ of $OA(k,k)$ and an $(v,k,1)$-OOC with l codewords, the method to obtain a difference array $B=DA(k,v)$ is as follows.

Assume that the codewords of C are denoted as $\{C_{i0},C_{i1},\cdots,C_{i(k-1)}\}(\mathrm{mod}\,v)$, $1\leqslant i\leqslant l$.

Then, each column of the difference array B can be represented as

$$<C_{sa(0,j)},C_{sa(1,j)},\cdots,C_{sa(k-1,j)}>,\ 1\leqslant s\leqslant l,\ 0\leqslant j\leqslant k(k-1)$$

In addition, an all-zero column should be added in B so that the total number of coloumns in B is $1+l(k-1)k=v$.

In order to prove that B is a difference array $DA(k,v)$ indeed, let's choose any two rows x and y from B. We only need to prove that there exists uniquely one column corresponding to (s,j), $1\leqslant s\leqslant l$, $0\leqslant j\leqslant k(k-1)$ for each integer $i\neq 0(\mathrm{mod}\,v)$, such that $C_{sa(y,j)}\equiv i(\mathrm{mod}\,v)$. This is equivalent to $a(x,j)=\hat{x}$, $a(y,j)=\hat{y}$, and furthermore s is only a codeword in C to satisfy $C_{s\hat{x}}-C_{s\hat{y}}\equiv i(\mathrm{mod}\,v)$. There is uniquely one column j in the two chosen columns and x and y of A such that $a(x,j)=\hat{x}$, and $a(y,j)=\hat{y}$. Therefore, each difference is uniquely produced and then B is a difference array $DA(k,v)$.

If $k=p^{\alpha}$ is a prime power, then we can construct the ortogonal arrays $OA(k,k+1)$ and $OA(k,k)$ through the parallel lines in the finite projective geometry. The orthogonal arrays correspond to the orthogonal Latin squares[22].

Example 2.13 Let $C_1=C_2=\{(0,1,3)\,\mathrm{mod}\,7\}$ and

$$\boldsymbol{A}=\begin{bmatrix}0&1&2&0&1&2\\2&0&1&1&2&0\\1&2&0&2&0&1\end{bmatrix}$$

From $C_1(c_{10}=0,c_{11}=1,c_{12}=3)$ and $\boldsymbol{A}$, we can firstly construct

$$\boldsymbol{B}=\begin{bmatrix}0&1&3&0&1&3&0\\3&0&1&1&3&0&0\\1&3&0&3&0&1&0\end{bmatrix}$$

Then, from C_1, C_2 and $\boldsymbol{B}$ we get an $(49,3,1)$-OOC as follows:

$C=\{(0,10,22),(1,7,24),(3,8,21),(0,8,24),(3,7,22),(1,10,21),(0,1,3),$
$(0,7,21)(\mathrm{mod}\,49)\}$.

The cardinality of the OOC is $|C|=8$.

It can be seen that the recursion construction is valid for $k=2,3,4,5,6,7,8,9$ if

we combine the two methods mentioned above. For $k=10$, $v=91,$ the difference set $\{0,1,3,9,27,49,56,61,77,81\}(\text{mod } 91)$ is an $(91,10,1)$-OOC.

The constructions of the constant-weight symmetric OOCs include the combinatorial constructions, the algebraic constructions, the recursion constructions, etc. The combinatorial constructions employ the relationship between OOCs and the difference families. An $(n,w,1)$ difference family is exactly an $(n,w,1)$ -OOC, and therefore, the combinatorial constructions are only suitable for constructing the $(n,w,1)$ -OOCs. When $w\leqslant 3$ the optical orthogonal code with optimal cardinality can be easily constructed. Although the optical orthogonal code can be constructed for $w=4$, its cardinality is not optimal and the construction process is complicated. When $w\geqslant 5$, it is difficult to construct the $(n,w,1)$ -OOCs. Because the performance (BER, bit error rate) of OCDMA systems decline dramatically as w is reduced, the number of simultaneous users is very limited in a practical network.

The algebraic construction uses the finite field theory to construct OOC. In principle, it is suitable for constructing any kind of OOCs but its constructing process is relatively complicated. So far, the existing constructions can be used to construct some constant-weight symmetric OOC with given codelength and code-weight. The more general algebraic constructions of OOCs are still to be investigated.

The constructions of projective geometry construct OOC based on finite projective geometry. The lines in a finite projective geometry correspond to OOC codewords with weight *w.* This is because any two lines in a projective geometry intersect at most one point. Therefore, OOC with autocorrelation $\lambda_a=1$ and cross-correlation $\lambda_c=1$ can be obtained.

The recursion constructions use difference arrays to construct OOC. For example, an $(n_1n_2,w,1)$-OOC, C, can be constructed by using an existing $(n_1,w,1)$ -OOC, C_1 , with cardinality $|C_1|$ and an $(n_2,w,1)$ -OOC, C_2 , with cardinality $|C_2|$. If the cardinalities of C_1 and C_2 are optimal then C is also optimal and its cardinality is $|C_2|+n_2|C_1|$. When we construct C we firstly need to construct a difference array and then design C using C_1, C_2 and the difference array. This kind of construction is only suitable for constructing the constant-weight symmetric OOC.

One of the reasons why the cardinality of constant-weight symmetric OOCs is confined is that the autocorrelation constraint and cross-correlation constraint are the same. In fact, because their impacts on the system performance are different, in order to increase the capacity of the system, i.e., the number of users, the autocorrelation constraint of OOC can be relaxed. This will result in the constant-weight asymmetric OOC that we will introduce in the next section.

2.3 Constant-weight Asymmetric Optical Orthogonal Codes

The autocorrelation constraint of OOC acts as a guarantee that each signature sequence is different from its cyclic shift and this property enables the receiver to implement synchronization, i.e., to find the beginning of its message and locate the boundaries of the codeword. The cross-correlation acts as a guarantee that each signature sequence is different from cyclic shifts of other signature sequences and this property enables the receiver to identify its message in the presence of interference from other subscribers. Thus, the cross-correlation is very helpful for the receiver to achieve synchronization in the presence of multiple subscribers and track its message after synchronization. Therefore, the autocorrelation constraint only contributes to synchronization, while the cross-correlation affects synchronization and operation as well[11]. If the autocorrelation constraint is properly relaxed under the premise of satisfying the requirements of system performance, that is, let the autocorrelation constraint λ_a be greater than the cross-correlation constraints λ_c, the cardinality of OOC will be increased greatly. We will introduce the OOC with $\lambda_a > \lambda_c$, i.e., the constant-weight asymmetric OOC as follows.

2.3.1 Definition of Constant-weight Asymmetric OOCs

When $\lambda_a \neq \lambda_c$, $\lambda_c = 1$, $\lambda_a > 1$, an $(n, w, \lambda_a, \lambda_c)$-OOC, C, can be called an $(n, w, \lambda_a, \lambda_c)$ constant-weight asymmetric $(n, w, \lambda_a, \lambda_c)$-OOC, C[11]. It is easily seen that the constant-weight symmetric OOC is only an extraordinary case of the constant-weight asymmetric $(n, w, \lambda_a, \lambda_c)$-OOC.

$\Phi(n, w, \lambda_a, \lambda_c)$ is the cardinality of an optimal $(n, w, \lambda_a, \lambda_c)$-OOC with the given parameters, i.e., $\Phi(n, w, \lambda_a, \lambda_c) \equiv \max\{|C|: C \text{ is an } (n, w, \lambda_a, \lambda_c)\text{-OOC}\}$.

2.3.2 Cardinality Upper and Lower Bounds on Constant-weight Asymmetric OOCs

The theorem on the cardinality upper bound on the constant-weight asymmetric OOC is as follows.

Theorem 2.2[11] Assuming that C is an $(n, w, \lambda_a, \lambda)$ optimal OOC, then the upper bound of the constant-weight asymmetric OOC is

$$\Phi(n, w, \lambda_a, \lambda) \leqslant \frac{(n-1)(n-2)\cdots(n-\lambda)\lambda_a}{w(w-1)(w-2)\cdots(w-\lambda)} \tag{2.12}$$

Let $\lambda = 1$ and $\lambda_a = \lambda$ in (2.12). Then we have

$$\Phi(n,w,\lambda,1) = \lambda\Phi(n,w,1,1) = \lambda\Phi(n,w,1) \tag{2.13}$$

It can be seen that the cardinality of an $(n,w,\lambda,1)$ asymmetric optimal OOC is λ times greater than that of an $(n,w,1)$ symmetric optimal OOC.

With regard to the lower bound, there is Theorem 2.3:

Theorem 2.3[11]:
$$\Phi(n,w,\lambda_a,\lambda_c) \geqslant \frac{\binom{n}{w} - A}{B} \tag{2.14}$$

where

$$A = \sum_{\substack{\delta=1 \\ \delta \mid n}}^{\lfloor n/2 \rfloor} \sum_{N=0}^{\lfloor w\delta/n \rfloor} \left[\Delta(N - w\delta/n) \binom{\delta}{N} + \sum_{c=\lfloor w\delta/n \rfloor}^{w-\lambda_a+N-1} \binom{c}{N} \binom{w - Nn/\delta - 1}{c - N - 1} \binom{\delta}{N} \binom{n - Nn/\delta}{c - N} \right]$$
$$+ |\{\delta : 1 \leqslant \delta \leqslant \lfloor n/2 \rfloor, \delta \nmid n\}| \sum_{c=1}^{w-\lambda_a-1} \binom{w-1}{c-1} \binom{n}{c}$$

$\lfloor x \rfloor$ denotes the biggest integer smaller than or equal to x.

$$\Delta(y) = \begin{cases} 1 & \text{if } y = 0 \\ 0 & \text{otherwise} \end{cases}$$

and

$$B = n \sum_{i > \lambda_c} \binom{n-w}{w-i} \binom{w}{i}$$

The proof of Theorem 2.2 and Theorem 2.3 can be found in Reference [11].

2.3.3 Constructions of Constant-weight Asymmetric (*n*,*w*,2,1)-OOCs

Two $(n,w,2,1)$-OOCs constructions will be introduced in this section, which are based on a balanced incomplete block design (BIBD). A BIBD is a structure equivalent to an $(n,w,1,1)$-OOC. The following two methods to construct $(n,w,2,1)$-OOCs we will introduce loosen the autocorrelation constraints from 1 to 2 and result in the decrease of block-length in comparison with the associated $(n,w,1,1)$ code.

2.3.3.1 Construction 1[11]

① When w is even let $w = 2m$ and choose n to be a prime number such that

$n = w^2 t/2 + 1$ for an integer t. Let α be a primitive element of $GF(n)$ such that $\{\log_\alpha[\alpha^{kmt} - 1] : 1 \leqslant k \leqslant m\} \bmod m$ are all distinct modulo-m and nonzero modulo-m. Then the following blocks:

$$\{[\alpha^{mi}, \alpha^{m(i+t)}, \alpha^{m(i+2t)}, \cdots, \alpha^{m(i+(2m-1)t)}] : i = 0,1,\cdots,t-1\} \tag{2.15}$$

form a constant-weight asymmetric $(n,w,2,1)$-OOCs with $w = 2m$ and its cardinality is $|C| = t = \dfrac{2(n-1)}{w^2} \approx 2\Phi(n,w,1,1)$.

② When w is odd, assume $w = 2m+1$ and choose n to be a prime number such that $n = (w^2-1)t/2 + 1$ for an integer t. Let α be a primitive element of $GF(n)$ such that $\{\log_\alpha[\alpha^{k(m+1)t} - 1] : 1 \leqslant k \leqslant m\} \bmod (m+1)$ are all distinct modulo-m and nonzero modulo-m. Then the following blocks:

$$\{[0, \alpha^{(m+1)i}, \alpha^{(m+1)(i+t)}, \alpha^{(m+1)(i+2t)}, \cdots, \alpha^{(m+1)(i+(2m-1)t)}] : i = 0,1,\cdots,t-1\} \tag{2.16}$$

form a constant-weight asymmetric $(n,w,2,1)$-OOCs with $w = 2m+1$ and its cardinality is

$$|C| = t = \frac{2(n-1)}{w^2 - 1} \approx 2\Phi(n,w,1,1).$$

Example 2.14 Construct a constant-weight asymmetric (37,5,2,1)-OOCs.

It can be seen that n is a prime number equal to 37. From $w = 2m+1 = 5$ and $n = (w^2-1)t/2 + 1 = 37$, we can obtain $m = 2$ and $t = 3$. Choose $\alpha = 2$ as the primitive element of $GF(37)$. From

$$\{[0, \alpha^{3i}, \alpha^{3(i+3)}, \alpha^{3(i+6)}, \alpha^{3(i+9)}] (\bmod 37) : i = 0,1,2\},$$

and $2^6 = 27 \bmod 37$, $2^9 = 31 \bmod 37$, $2^{18} = 36 \bmod 37$ and $2^{27} = 6 \bmod 37$, the code consisting of the blocks is as follows:

$$(0,1,31,36,6),(0,8,26,29,11),(0,27,23,10,14).$$

The cardinalities of some constant-weight asymmetric (n,w,2,1)-OOCs constructed by using Construction 1 are shown in Table 2.10[11].

2.3.3.2 Construction 2[11]

① Construction of an $(n,w,2,1)$-OOCs with $w = 4m$. Let $n = w^2 t/2 + 1$ be a prime number, where $w = 4m$. Assume that α is a primitive element of $GF(n)$. The following equations:

$\alpha^{k4mt+y} - 1 = \alpha^{i_k}$, for $k = 0,1,\cdots,m-1$

$\alpha^{k4mt} - \alpha^{y} = \alpha^{j_k}$, for $k = 1,2,\cdots,m$

Table 2.10 Cardinalities of $(n,w,2,1)$-OOCs constructed using Construction 1

n	w	$\|C\|$	Bound from Thm.2.2	n	w	$\|C\|$	Bound from Thm.2.2
5	3	1	1	13	5	1	1
13	3	3	4	37	5	3	3
29	3	7	9	61	5	5	6
37	3	9	12	73	5	6	7
53	3	13	17	97	5	8	9
61	3	15	20	181	5	15	18
101	3	25	33	193	5	16	19
109	3	27	36	241	5	20	24
149	3	37	49	313	5	26	31
157	3	39	52	337	5	28	33
173	3	43	57	349	5	29	34
181	3	45	60	373	5	31	37
197	3	49	65	409	5	34	40
17	4	2	2	421	5	35	42
73	4	9	12	541	5	45	54
89	4	11	14	577	5	48	57
97	4	12	16	19	6	1	1
193	4	24	32	199	6	11	13
233	4	29	38	487	6	27	32
241	4	30	40	829	6	46	55
281	4	35	46	883	6	49	58
401	4	50	66				

$\alpha^{k4mt}-1=\alpha^{r_k}$, for $k=1,2,\cdots,m$

$\alpha^{y}(\alpha^{k4mt}-1)=\alpha^{s_k}$, for $k=1,2,\cdots,m$

hold for some integer y, $1\leqslant y\leqslant 4mt-1$, where the integers $i_0,i_1,\cdots,i_{m-1},j_1,\cdots,j_m,r_1,\cdots,r_m$ and $s_1,\cdots,s_m$ are all distinct modulo-$4m$. Then the blocks

$$\{[\alpha^{4mi},\alpha^{y+4mi},\alpha^{4mt+4mi},\alpha^{4mt+y+4mi},\cdots,\alpha^{4m(2m-1)t+4mi},\alpha^{4m(2m-1)t+y+4mi}]:i=0,1,\cdots,t-1\} \tag{2.17}$$

form the codewords of an $(n,w,2,1)$-OOCs with $w=4m$ and the cardinality of the code is $|C|=t=\dfrac{2(n-1)}{w^2}\approx 2\Phi(n,w,1,1)$.

Example 2.15 Construct an (41,4,2,1)-OOCs.

$n=41$ is a prime number. We have $m=1$ from $w=4m=4$ and $t=5$ to be an integer from $n=w^2t/2+1=41$. Choose $y=3$ and $\alpha=6$ as the primitive element

of $GF(41)$. Therefore, $6^y-1=10=6^8$, $6^{20}-6^y=29=6^7$, $6^{20}-1=39=6^6$ and $6^y(6^{20}-1)=19=6^9$, that is, $i_0=8$, $j_1=7$, $r_1=6$ and $s_1=9$. Hence, i_0, j_1, r_1, s_1 are all distinct modulo-4. Then, from

$$\{[\alpha^{4i},\alpha^{3+4i},\alpha^{20+4i},\alpha^{20+3+4i}](\mathrm{mod}\,41):i=0,1,2,3,4\},$$

and $6^3=11 \bmod 41$, $6^4=25 \bmod 41$, $6^{20}=40 \bmod 41$, $6^{23}=30 \bmod 41$, we can obtain the blocks of codewords as follows: (1,11,40,30), (25,29,16,12), (10,28,31,13), (4,3,37,38), (18,34,23,7).

Its cardinality is $|C|=5>\Phi(41,4,1)=3$. However, due to $|C|=5<\Phi(41,4,2,1)=6$, the code is not optimal.

② Construction of an $(n,w,2,1)$-OOCs for $w=4m+1$. Let $n=(w^2-1)t/2+1$ is a prime number, where $w=4m+1$. And assume that α is a primitive element of $GF(n)$. The following equations:

$\alpha^{k(4m+2)t+y}-1=\alpha^{i_k}$, for $k=0,1,\cdots,m-1$

$\alpha^{k(4m+2)t}-\alpha^{y}=\alpha^{j_k}$, for $k=1,2,\cdots,m$

$\alpha^{k(4m+2)t}-1=\alpha^{r_k}$, for $k=1,2,\cdots,m$

$\alpha^{y}(\alpha^{k(4m+2)t}-1)=\alpha^{s_k}$, for $k=1,2,\cdots,m$

hold for some integer y, $1\leqslant y\leqslant(4m+2)t-1$, where y, $i_0,i_1,\cdots,i_{m-1}$, $j_1,\cdots,j_m$, $r_1,\cdots,r_m$ and $s_1,\cdots,s_m$ are all distinct modulo-$(4m+2)$ and nonzero modulo-$(4m+2)$. Then, the following blocks:

$$\{[0,\ \alpha^{(4m+2)i},\alpha^{y+(4m+2)i},\alpha^{(4m+2)t+(4m+2)i},\alpha^{(4m+2)t+y+(4m+2)i},\cdots,$$
$$\alpha^{(4m+2)(2m-1)t+(4m+2)i},\alpha^{(4m+2)(2m-1)t+y+(4m+2)i}]:i=0,1,\cdots,t-1\} \tag{2.18}$$

form an $(n,w,2,1)$-OOC with $w=4m+1$. Its cardinality is $|C|=t=\dfrac{2(n-1)}{w^2-1}\approx 2\Phi(n,w,1,1)$.

Example 2.16 Construct an (61,5,2,1)-OOCs.

$n=61$ is a prime number. $m=1$ and $t=5$ can be obtained from $w=4m+1=5$ and $n=(w^2-1)t/2+1=61$ respectively. Choose $\alpha=2$ as the primitive element of $GF(n)$. When we choose $y=9$, $2^y-1=23=2^{57}$, $2^{30}-2^y=36=2^{14}$, $2^{30}-1=59=2^{31}$ and $2^y(2^{30}-1)=13=2^{40}$, i.e., $i_0=57(\mathrm{mod}\,6)=3$, $j_1=14(\mathrm{mod}\,6)=2$, $r_1=31(\mathrm{mod}\,6)=1$ and $s_1=40(\mathrm{mod}\,6)=4$. Furthermore, i_0, j_1, r_1 and s_1 are nonzero modulo-6 and all distinct modulo-6. Then, from

$$\{[0,\alpha^{6i},\alpha^{9+6i},\alpha^{30+6i},\alpha^{30+9+6i}](\mathrm{mod}\,61):i=0,1,2,3,4\}$$

and $2^6=3 \bmod 61$, $2^9=24 \bmod 61$, $2^{30}=60 \bmod 61$, $2^{39}=37 \bmod 61$, we obtain

the code consisting of the blocks: (0,1,24,60,37), (0,3,11,58,50), (0,9,33,52,28), (0,27,38,34,23), (0,20,53,41,8). Its cardinality is $\Phi(61,5,2,1) = 5 > \Phi(61,5,1) = 3$.

The cardinalities of $(n,w,2,1)$-OOCs constructed by using Construction 2 are shown in Table 2.11. Some parameters of the $(n,w,2,1)$-OOCs that can be constructed using the approaches described above are given in Table 2.10 and Table 2.11 where we include the upper bound on $\Phi(n,w,2,1)$ derived from Theorem 2.2. From Theorem 2.2, it can be seen that it is impossible to construct an $(n,w,2,1)$-OOC with more than $2(n-1)/w(w-1)$ codewords. When w is even, an OOC with $2(n-1)/w^2$ codewords can be constructed. When w is odd, an OOC with $2(n-1)/(w^2-1)$ codewords can be constructed.

Table 2.11 The Cardinality of $(n,w,2,1)$-OOCs constructed using Construction 2

n	w	$\lvert C \rvert$	Bound from Thm.2.2	n	w	$\lvert C \rvert$	Bound from Thm.2.2
41	4	5	6	277	5	23	27
73	4	9	12	313	5	26	31
89	4	11	14	337	5	28	33
97	4	12	16	349	5	29	34
113	4	14	18	373	5	31	37
137	4	17	22	397	5	33	39
193	4	24	32	409	5	34	40
233	4	29	38	421	5	35	42
241	4	30	40	541	5	45	54
257	4	32	42	641	8	20	22
281	4	35	46	929	8	29	33
313	4	39	52	1217	8	38	43
337	4	42	56	1409	8	44	50
353	4	44	58	1601	8	50	57
401	4	50	66	281	9	7	7
13	5	1	1	401	9	10	11
37	5	3	3	521	9	13	14
61	5	5	6	601	9	15	16
73	5	6	7	761	9	19	21
97	5	8	9	881	9	22	24
109	5	9	10	1201	9	30	33
157	5	13	15	1361	9	34	37
181	5	15	18	1481	9	37	41
193	5	16	19	1601	9	40	44
229	5	19	22	1721	9	43	47
241	5	20	24	1801	9	45	50

2.4 Variable-weight Optical Orthogonal Codes

Previous work on OOC in the previous sections has assumed that the weight of each codeword is the same, that is, a constant-weight OOC. In this section, we study another family of OOC, in which the weight of each codeword is not exactly the same, i.e., the variable-weight optical orthogonal code. If the codewords in such an OOC are classified in terms of the size of the weight, they can be divided into a number of subsets. When such a codeword is assigned to a subscriber in an OCDMA network as its own address code, the quality of transmission service of the user using a codeword with larger weight is higher, and the quality of transmission service of a user using a codeword with smaller weight is lower. Thus, multiple performance requirements from different users and different services can be satisfied such that an OCDMA network can offer flexible and diversified services to many kinds of users and multiple transmission media.

2.4.1 Definition of Variable-weight OOCs[13]

An (n,W,L,λ_c,Q) variable-weight OOC, C, is a binary n-chip set, which satisfies three properties:

Weight Distribution: Each n-chip in C has a Hamming weight contained in the set W and furthermore, there are exactly $q_i|C|$ codewords of weight w_i, that is, q_i denotes the fraction of codewords of weight w_i.

Autocorrelation Constraints: For any codeword $X=(x_0,x_1,\cdots,x_{n-1})\in C$ with Hamming weight $w_i\in W$ and any integer τ, $1\leqslant\tau\leqslant n-1$,

$$\sum_{i=0}^{n-1}x_i x_{i\oplus\tau}\leqslant\lambda_a^i$$

Cross-correlation Constraints: For any two codewords $X=(x_0,x_1,\cdots,x_{n-1})\in C$ and $Y=(y_0,y_1,\cdots,y_{n-1})\in C$, $X\neq Y$ and any integer τ, $0\leqslant\tau\leqslant n-1$,

$$\sum_{i=0}^{n-1}x_i y_{i\oplus\tau}\leqslant\lambda_c$$

where "$\oplus$" in the subscripts above denotes the addition modulo-n. W, L and Q represent the sets $\{w_0,w_1,\cdots,w_p\}$, $\{\lambda_a^0,\lambda_a^1,\cdots,\lambda_a^p\}$ and $\{q_0,q_1,\cdots,q_p\}$ respectively. Therefore, it can be seen that the variable-weight optical orthogonal code is the generalization of the constant-weight OOC.

2.4.2 Upper and Lower Bounds on Cardinality of Variable-weight OOCs

Define $\Phi(n,W,L,\lambda_c,Q)$ as the cardinality of an optimal variable-weight optical orthogonal code with the given parameters, i.e.,

$$\Phi(n,W,L,\lambda_c,Q) \equiv \max\{|C|: C \text{ is an } (n,W,L,\lambda_c,Q) \text{ variable-weight OOC}\}.$$

The upper and lower bounds on cardinality of an (n,W,L,λ_c,Q) variable-weight optical orthogonal code are given by Theorem 2.4 and Theorem 2.5 [13].

Theorem 2.4[13] Let $\lambda_a^i \geqslant \lambda_c (\lambda_a^i \in L)$. Then an upper bound on the cardinality of an (n,W,L,λ_c,Q) variable-weight OOC is

$$\Phi(n,W,L,\lambda_c,Q) \leqslant \frac{(n-1)(n-2)\cdots(n-\lambda_c)}{\sum_{i=0}^{p} q_i w_i (w_i-1)(w_i-2)\cdots(w_i-\lambda_c)/\lambda_a^i} \tag{2.19}$$

Theorem 2.5[13] An lower bound on the cardinality of an (n,W,L,λ_c,Q) variable-weight optical orthogonal code is

$$\Phi(n,W,L,\lambda_c,Q) \geqslant \frac{\sum_{i=0}^{p}\left[\binom{n}{w_i} - F\right]}{G} \tag{2.20}$$

where:

$$F = \sum_{\substack{\delta=1 \\ \delta|n}}^{\lfloor n/2 \rfloor} \sum_{N=0}^{\lfloor w_i\delta/n \rfloor} \left[\Delta(N - w_i\delta/n)\binom{\delta}{N} + \sum_{c=\lceil w_i\delta/n \rceil}^{w_i-\lambda_a^i+N-1} \binom{c}{N}\binom{w_i - Nn/\delta - 1}{c-N-1}\binom{\delta}{N}\binom{n-Nn/\delta}{c-N} \right]$$

$$+ |\{\delta : 1 \leqslant \delta \leqslant \lfloor n/2 \rfloor, \delta \nmid n\}| \sum_{c=1}^{w_i-\lambda_a^i-1} \binom{w_i-1}{c-1}\binom{n}{c}$$

$$\Delta(x) = \begin{cases} 1 & \text{if } x = 0 \\ 0 & \text{otherwise} \end{cases}$$

and $G = n\sum_{i=0}^{p} \sum_{j=\lambda_c+1}^{w_i} q_i \binom{n-w_i}{w_i-j}\binom{w_i}{j}$. $\cdot\lfloor x \rfloor$ denotes an integer smaller than or equal to *x,* and $\lceil y \rceil$ represents to take an integer greater than or equal to *y*.

The proof of Theorem 2.4 and 2.5 are omitted here. If the reader is interested in its details, please read Reference [13].

2.4.3 Constructions of Variable-weight OOCs[13]

A balanced incomplete block design (BIBD), $B[v,b,r,k,\lambda]$, is a family consisting of b different k-elements subsets (or called blocks), which are taken from v distinct objects. The family also needs to satisfy the following two requirements:

- each object occurs in exactly r different blocks;
- each 2-element subset in the object set occurs in exactly λ blocks and the five parameters for a block design satisfy the elementary relations as follows:

$$bk = vr$$

$$r(k-1) = \lambda(v-1)$$

In Reference [3], the $(n,w,1,1)$ constant-weight OOC with $\lambda = 1$ was constructed by using the techniques of BIBD. Reference [5] constructed the $(n,w,2,1)$ constant-weight OOC through the modified techniques of BIBD. An $(n,W,L,1,Q)$ variable-weight OOC is constructed by generalizing the techniques to construct $(n,w,1,1)$ and $(n,w,2,1)$ constant-weight OOCs.

2.4.3.1 Constructions of $(n,\{w+1,w\},\{1,1\},1,\{t_0/(t_0+t_1),t_1/(t_0+t_1)\})$ Variable-weight Symmetric OOCs

In order to construct an $(n,\{w+1,w\},\{1,1\},1,\{t_0/(t_0+t_1),t_1/(t_0+t_1)\})$ variable-weight symmetric OOC, we combine the optimal construction of an $(n,w,1,1)$ -OOC and that of $(n,w+1,1,1)$-OOC. Because the cardinality of the variable-weight OOC constructed by this technique achieves the upper bound in Theorem 2.4, it is an optimal construction. The detailed construction is as follows.

Let $w = 2m+1$ and choose $n = (w+1)wt_0 + w(w-1)t_1 + 1$ to be a prime number. If r denotes the greatest common divisor of t_0 and t_1, assume that α is a primitive element of the Galois field $GF(n)$ such that

$$\{\log_\alpha[\alpha^{x_j}(\alpha^{[(w+1)t_0+(w-1)t_1]k}-1)]:1\leqslant k\leqslant m, j=0,1,\cdots,(t_1/r)-1\}$$

$$\{\log_\alpha[\alpha^{z_l}(\alpha^{[(w+1)t_0+(w-1)t_1]k}-1)]:1\leqslant k\leqslant m, l=0,1,\cdots,(t_0/r)-1\}$$

are all distinct modulo-$((m+1)t_0+mt_1)/r$, where x_j and z_l are integers between 0 and $(m+1)t_0+mt_1-1$. Then the following blocks

$$\{[0,\alpha^{[(m+1)t_0+mt_1]i/r+z_l},\alpha^{[(m+1)t_0+mt_1]i/r+z_l+(2m+2)t_0+2mt_1},\cdots,\alpha^{[(m+1)t_0+mt_1]i/r+z_l+(2m+2)2mt_0+4m^2t_1}]:$$

$$i=0,1,\cdots,r-1, l=0,1,\cdots,(t_0/r)-1\} \tag{2.21}$$

and

$$\{[\alpha^{[(m+1)t_0+mt_1]i/r+x_j}, \alpha^{[(m+1)t_0+mt_1]i/r+x_j+(2m+2)t_0+2mt_1}, \cdots, \alpha^{[(m+1)t_0+mt_1]i/r+x_j+(2m+2)2mt_0+4m^2t_1}]: i=0,1,\cdots,r-1, l=0,1,\cdots,(t_1/r)-1\} \quad (2.22)$$

produce an $(n,\{w+1,w\},\{1,1\},1,\{t_0/(t_0+t_1),t_1/(t_0+t_1)\})$-OOCs. Its cardinality is $|C|=t_0+t_1$, which reaches the upper bound of Theorem 2.4. Thus, it is an optimal variable-weight OOC. Table 2.12 shows the cardinalities of a variable-weight OOC constructed by this technique and some of its construction parameters. Some constructed results of the $(n,\{w+1,w\},\{1,1\},1,\{t_0/(t_0+t_1),$ $t_1/(t_0+t_1)\})$ OOC are shown in Table 2.13.

Example 2.17 Construct an $(37,\{4,3\},\{1,1\},1,\{1/2,1/2\})$-OOCs.

$n=37$ is a prime number and $w=3$, $\lambda_a^0=1$, $\lambda_a^1=1$, $\lambda_c=1$, $q_0=\frac{1}{2}$, $q_1=\frac{1}{2}$.

We can get $m=1$ from $w=2m+1=3$. Again, $t_0=t_1=2$ can be obtained by $n=(w+1)wt_0+w(w-1)t_1+1$. $r=2$ is the greatest common divisor of t_0 and t_1.

Choose $\alpha=2$ as a primitive root of $GF(37)$. Picking $z_0=0$ and $x_0=1$, and using (2.21) and (2.22), we can get the blocks to indicate the positions of 1's in the codewords as follows: (0,1,10,26), (0,6,8,23) and (2,15,20), (9,12,16).

Table 2.12 Cardinalities and Construction Parameters of Codes $(n,\{w+1,w\},$ $\{1,1\},1,\{t_0/(t_0+t_1),t_1/(t_0+t_1)\})$ Constructed by this Technique

Code	t_0	t_1	Primitive α	x_0	x_1	z_0
(19,{4,3},{1,1},1,{1/2,1/2})	1	1	2	2	–	0
(37,{4,3},{1,1},1,{1/2,1/2})	2	2	2	1	–	0
(109,{4,3},{1,1},1,{1/2,1/2})	6	6	6	2	–	0
(127,{4,3},{1,1},1,{1/2,1/2})	7	7	3	2	–	0
(163,{4,3},{1,1},1,{1/2,1/2})	9	9	2	1	–	0
(181,{4,3},{1,1},1,{1/2,1/2})	10	10	2	1	–	0
(199,{4,3},{1,1},1,{1/2,1/2})	11	11	3	2	–	0
(73,{4,3},{1,1},1,{1/3,2/3})	3	6	5	1	2	0
(193,{4,3},{1,1},1,{1/3,2/3})	8	16	5	1	3	0
(101,{6,5},{1,1},1,{1/2,1/2})	2	2	2	3	–	0
(151,{6,5},{1,1},1,{1/2,1/2})	3	3	6	4	–	0
(701,{6,5},{1,1},1,{1/2,1/2})	14	14	2	1	–	0
(751,{6,5},{1,1},1,{1/2,1/2})	15	15	3	2	–	0
(71,{6,5},{1,1},1,{1/3,2/3})	2	2	7	1	6	0

Table 2.13 Some Results Constructed of $(n,\{w+1,w\},\{1,1\},1,\{t_0/(t_0+t_1),t_1/(t_0+t_1)\})$-OOCs

$(n,\{w+1,w\},\{1,1\},1,\{q_0,q_1\})$	t_0	t_1	α	x_0	z_0	t_0	C
(19,{4,3},{1,1},1,{1/2,1/2})	1	1	2	2	–	0	$\{0\}\bigcup\{2^{3i+6k}\mid 0\leqslant k\leqslant 2\}$, $\{2^{3i+2+6k}\mid 0\leqslant k\leqslant 2\}, i=0$
(37,{4,3},{1,1},1,{1/2,1/2})	2	2	2	1	–	0	$\{0\}\bigcup\{2^{3i+12k}\mid 0\leqslant k\leqslant 2\}$, $\{2^{3i+1+12k}\mid 0\leqslant k\leqslant 2\}, 0\leqslant i\leqslant 1$
(109,{4,3},{1,1},1,{1/2,1/2})	6	6	6	2	–	0	$\{0\}\bigcup\{6^{3i+36k}\mid 0\leqslant k\leqslant 2\}$, $\{6^{3i+2+36k}\mid 0\leqslant k\leqslant 2\}, 0\leqslant i\leqslant 5$
(127,{4,3},{1,1},1,{1/2,1/2})	7	7	3	2	–	0	$\{0\}\bigcup\{3^{3i+42k}\mid 0\leqslant k\leqslant 2\}$, $\{3^{3i+2+42k}\mid 0\leqslant k\leqslant 2\}, 0\leqslant i\leqslant 6$
(163,{4,3},{1,1},1,{1/2,1/2})	9	9	2	1	–	0	$\{0\}\bigcup\{2^{3i+54k}\mid 0\leqslant k\leqslant 2\}$, $\{2^{3i+1+54k}\mid 0\leqslant k\leqslant 2\}, 0\leqslant i\leqslant 8$
(181,{4,3},{1,1},1,{1/2,1/2})	10	10	2	1	–	0	$\{0\}\bigcup\{2^{3i+60k}\mid 0\leqslant k\leqslant 2\}$, $\{2^{3i+1+60k}\mid 0\leqslant k\leqslant 2\}, 0\leqslant i\leqslant 9$
(199,{4,3},{1,1},1,{1/2,1/2})	11	11	3	2	–	0	$\{0\}\bigcup\{3^{3i+66k}\mid 0\leqslant k\leqslant 2\}$, $\{3^{3i+2+66k}\mid 0\leqslant k\leqslant 2\}, 0\leqslant i\leqslant 10$
(73,{4,3},{1,1},1,{1/3,2/3})	3	6	5	1	2	0	$\{0\}\bigcup\{5^{4i+24k}\mid 0\leqslant k\leqslant 2\}$, $\{5^{4i+1+24k}\mid 0\leqslant k\leqslant 2\}, 0\leqslant i\leqslant 2$ $\{5^{4i+2+24k}\mid 0\leqslant k\leqslant 2\}, 0\leqslant i\leqslant 2$
(193,{4,3},{1,1},1,{1/3,2/3})	8	16	5	1	3	0	$\{0\}\bigcup\{5^{4i+64k}\mid 0\leqslant k\leqslant 2\}$, $\{5^{4i+1+64k}\mid 0\leqslant k\leqslant 2\}, 0\leqslant i\leqslant 7$ $\{5^{4i+3+64k}\mid 0\leqslant k\leqslant 2\}, 0\leqslant i\leqslant 7$
(101,{6,5},{1,1},1,{1/2,1/2})	2	2	2	3	–	0	$\{0\}\bigcup\{2^{5i+20k}\mid 0\leqslant k\leqslant 4\}$, $\{2^{5i+3+20k}\mid 0\leqslant k\leqslant 4\}, 0\leqslant i\leqslant 1$
(151,{6,5},{1,1},1,{1/2,1/2})	3	3	6	4	–	0	$\{0\}\bigcup\{6^{5i+30k}\mid 0\leqslant k\leqslant 4\}$, $\{6^{5i+4+30k}\mid 0\leqslant k\leqslant 4\}, 0\leqslant i\leqslant 2$
(701,{6,5},{1,1},1,{1/2,1/2})	14	14	2	1	–	0	$\{0\}\bigcup\{2^{5i+140k}\mid 0\leqslant k\leqslant 4\}$, $\{2^{5i+1+140k}\mid 0\leqslant k\leqslant 4\}, 0\leqslant i\leqslant 13$
(751,{6,5},{1,1},1,{1/2,1/2})	15	15	3	2	–	0	$\{0\}\bigcup\{3^{5i+150k}\mid 0\leqslant k\leqslant 4\}$, $\{3^{5i+2+150k}\mid 0\leqslant k\leqslant 4\}, 0\leqslant i\leqslant 14$
(71,{6,5},{1,1},1,{1/3,2/3})	1	2	7	1	6	0	$\{0\}\bigcup\{7^{7i+14k}\mid 0\leqslant k\leqslant 4\}$, $\{7^{7i+1+14k}\mid 0\leqslant k\leqslant 4\}$, $\{7^{7i+6+14k}\mid 0\leqslant k\leqslant 4\}, i=0$

2.4.3.2 Constructions of Variable-weight Asymmetric OOCs

(1) Construction of $(n,\{w+1,w\},\{2,2\},1,\{t_0/(t_0+t_1),t_1/(t_0+t_1)\})$-OOCs

Let $w=2m$ and choose n to be a prime number such that $n=[(w+1)^2-1]/$

$2t_0 + w^2/2t_1 + 1$. If r denotes the greatest common divisor of t_0 and t_1, and α is a primitive element of $GF(n)$ such that

$$\{\log_\alpha[\alpha^{x_j}(\alpha^{[(m+1)t_0+mt_1]k}-1)]:1\leqslant k\leqslant m, j=0,1,\cdots,(t_1/r)-1\},$$

$$\{\log_\alpha[\alpha^{z_l}(\alpha^{[(m+1)t_0+mt_1]k}-1)]:1\leqslant k\leqslant m, l=0,1,\cdots,(t_0/r)-1\},$$

are all distinct modulo-$((m+1)t_0+mt_1)/r$, where x_j and z_l are integers between 0 and $(m+1)t_0+mt_1-1$, then the following blocks

$$\{[0,\alpha^{[(m+1)t_0+mt_1]i/r+z_l},\alpha^{[(m+1)t_0+mt_1]i/r+z_l+(m+1)t_0+mt_1},\cdots,\alpha^{[(m+1)t_0+mt_1]i/r+z_l+(m+1)(2m-1)t_0+m(2m-1)t_1}]:$$
$$i=0,1,\cdots,r-1,l=0,1,\cdots,(t_0/r)-1\} \tag{2.23}$$

and

$$\{[\alpha^{[(m+1)t_0+mt_1]i/r+x_j},\alpha^{[(m+1)t_0+mt_1]i/r+x_j+(m+1)t_0+mt_1},\cdots,\alpha^{[(m+1)t_0+mt_1]i/r+x_j+(m+1)(2m-1)t_0+m(2m-1)t_1}]:$$
$$i=0,1,\cdots,r-1,j=0,1,\cdots,(t_1/r)-1\} \tag{2.24}$$

form an $(n,\{w+1,w\},\{2,2\},1,\{t_0/(t_0+t_1),t_1/(t_0+t_1)\})$-OOC. Its cardinality is $|C|=t_0+t_1$, which does not reach the upper bound of Theorem 2.4. Thus, it is only close to an optimal code. Table 2.14 shows the cardinalities of OOCs constructed by this method and some parameters used to construct the OOCs. Some results of $(n,\{w+1,w\},\{2,2\},1,\{t_0/(t_0+t_1),t_1/(t_0+t_1)\})$-OOCs constructed are shown in Table 2.15.

Table 2.14 Cardinalities and construction parameters of codes $(n,\{w+1,w\},\{2,2\},1,\{t_0/(t_0+t_1),t_1/(t_0+t_1)\})$ constructed by this technique

Code	t_0	t_1	Primitive α	x_0	z_0
(41,{5,4},{2,2},1,{1/2,1/2})	2	2	6	1	0
(61,{5,4},{2,2},1,{1/2,1/2})	3	3	2	1	0
(101,{5,4},{2,2},1,{1/2,1/2})	5	5	2	1	0
(181,{5,4},{2,2},1,{1/2,1/2})	9	9	2	1	0
(281,{5,4},{2,2},1,{1/2,1/2})	14	14	3	4	0

Table 2.15 Some results constructed of $(n,\{w+1,w\},\{2,2\},1,\{t_0/(t_0+t_1),t_1/(t_0+t_1)\})$-OOCs

$(n,\{w+1,w\},\{2,2\},1,\{q_0,q_1\})$	t_0	t_1	α	x_0	z_0	C
(41,{5,4},{2,2},1,{1/2,1/2})	2	2	6	1	0	$\{0\}\bigcup\{6^{5i+10k}\mid 0\leqslant k\leqslant 3\}$, $\{6^{5i+1+10k}\mid 0\leqslant k\leqslant 3\}, 0\leqslant i\leqslant 1$

Continued

$(n,\{w+1,w\},\{2,2\},1,\{q_0,q_1\})$	t_0	t_1	α	x_0	z_0	C
(61,{5,4},{2,2},1,{1/2,1/2})	3	3	2	1	0	$\{0\}\bigcup\{2^{5i+15k} \mid 0\leqslant k\leqslant 3\}$, $\{2^{5i+1+15k} \mid 0\leqslant k\leqslant 3\}, 0\leqslant i\leqslant 2$
(101,{5,4},{2,2},1,{1/2,1/2})	5	5	2	1	0	$\{0\}\bigcup\{2^{5i+25k} \mid 0\leqslant k\leqslant 3\}$, $\{2^{5i+1+25k} \mid 0\leqslant k\leqslant 3\}, 0\leqslant i\leqslant 4$
(181,{5,4},{2,2},1,{1/2,1/2})	9	9	2	1	0	$\{0\}\bigcup\{2^{5i+45k} \mid 0\leqslant k\leqslant 3\}$, $\{2^{5i+1+45k} \mid 0\leqslant k\leqslant 3\}, 0\leqslant i\leqslant 8$
(281,{5,4},{2,2},1,{1/2,1/2})	14	14	3	4	0	$\{0\}\bigcup\{3^{5i+70k} \mid 0\leqslant k\leqslant 3\}$, $\{3^{5i+4+70k} \mid 0\leqslant k\leqslant 3\}, 0\leqslant i\leqslant 13$

(2) Construction of $(n,\{2w,w\},\{2,2\},1,\{t_0/(t_0+2t_1),2t_0/(t_0+2t_1)\})$-OOCs

Let $w=2m$ and choose n to be a prime number such that $n=2w^2t_0+w^2t_1+1$. If r indicates the greatest common divisor of t_0 and t_1, and α is a primitive element of $GF(n)$ such that

$$\{\log_\alpha[\alpha^{x_j}(\alpha^{[2mt_0+mt_1]k}-1)]:1\leqslant k\leqslant m, j=0,\cdots,(t_1/r)-1\},$$

$$\{\log_\alpha[\alpha^{z_l}(\alpha^{[2mt_0+mt_1]k}-1)]:1\leqslant k\leqslant 2m, l=0,\cdots,(t_0/r)-1\},$$

are all distinct modulo-$(2mt_0+mt_1)/r$, where x_j and z_l are integers between 0 and $2mt_0+mt_1-1$, then, the following blocks

$$\{[\alpha^{[2mt_0+mt_1]i/r+z_l},\alpha^{[2mt_0+mt_1]i/r+z_l+2mt_0+mt_1},\cdots,\alpha^{[2mt_0+mt_1]i/r+z_l+2m(4m-1)t_0+m(4m-1)t_1}]: i=0,1,\cdots,r-1, l=0,1,\cdots,(t_0/r)-1\} \tag{2.25}$$

$$\{[\alpha^{[2mt_0+mt_1]i/r+x_j},\alpha^{[2mt_0+mt_1]i/r+x_j+4mt_0+2mt_1},\cdots,\alpha^{[2mt_0+mt_1]i/r+x_j+2m(4m-2)t_0+m(4m-2)t_1}]: i=0,1,\cdots,r-1, j=0,1,\cdots,(t_1/r)-1\} \tag{2.26}$$

and

$$\{[\alpha^{[2mt_0+mt_1]i/r+x_j+2mt_0+mt_1},\alpha^{[2mt_0+mt_1]i/r+x_j+6mt_0+3mt_1},\cdots,\alpha^{[2mt_0+mt_1]i/r+x_j+2m(4m-1)t_0+m(4m-1)t_1}]: i=0,1\cdots,r-1, j=0,1,\cdots,(t_1/r)-1\} \tag{2.27}$$

form an $(n,\{2w,w\},\{2,2\},1,\{t_0/(t_0+2t_1),2t_1/(t_0+2t_1)\})$ OOC. Its cardinality is $|C|=t_0+2t_1$, which fails to achieve the upper bound of Theorem 2.4. Therefore, the OOC is only close to an optimal code. The cardinality and parameters of codes constructed by this technique are shown in Table 2.16.

Table 2.16 Cardinality of constructed $(n,\{2w,w\},\{2,2\},1,\{t_0/(t_0+2t_1),2t_1/(t_0+2t_1)\})$-OOCs

Code	t_0	t_1	Primitive α	x_0	z_0
$(2017,\{8,4\},\{2,2\},1,\{1/3,2/3\})$	42	84	5	2	0
$(2593,\{8,4\},\{2,2\},1,\{1/3,2/3\})$	54	108	7	4	0

2.4.3.3 Constructions of $(n,\{2w,w\},\{2,1\},1,\{t_0/(t_0+t_1),t_1/(t_0+t_1)\})$ Variable-weight OOCs with Non-equal Autocorrelation Constraints

The technique to construct an $(n,\{2w,w\},\{2,1\},1,\{t_0/(t_0+t_1),t_1/(t_0+t_1)\})$ OOC is detailed as follows.

Let $w=2m+1$ and choose n to be a prime number such that $n=2w^2t_0+w(w-1)t_1+1$. If r denotes the greatest common divisor of t_0 and t_1, and α is a primitive element of $GF(n)$ such that

$$\{\log_\alpha[\alpha^{x_j}(\alpha^{[(2m+1)t_0+mt_1]k}-1)]:1\leqslant k\leqslant m, j=0,\cdots,(t_1/r)-1\},$$

$$\{\log_\alpha[\alpha^{z_l}(\alpha^{[(2m+1)t_0+mt_1]k}-1)]:1\leqslant k\leqslant 2m+1, l=0,\cdots,(t_0/r)-1\},$$

are all distinct modulo-$((2m+1)t_0+mt_1)/r$, where x_j and z_l are integers between 0 and $(2m+1)t_0+mt_1-1$. Then the following blocks

$$\{[\alpha^{[(2m+1)t_0+mt_1]i/r+z_l},\alpha^{[(2m+1)t_0+mt_1]i/r+z_l+(2m+1)t_0+mt_1},\cdots,\alpha^{[(2m+1)t_0+mt_1]i/r+z_l+(2m+1)(4m+1)t_0+m(4m+1)t_1}]:$$

$$i=0,1,\cdots,r-1,l=0,1,\cdots,(t_0/r)-1\} \tag{2.28}$$

and

$$\{[\alpha^{[(2m+1)t_0+mt_1]i/r+x_j},\alpha^{[(2m+1)t_0+mt_1]i/r+x_j+2(2m+1)t_0+2mt_1},\cdots,\alpha^{[(2m+1)t_0+mt_1]i/r+x_j+(2m+1)(4m+1)t_0+m(4m+1)t_1}]:$$

$$i=0,1,\cdots,r-1,j=0,1,\cdots,(t_1/r)-1\} \tag{2.29}$$

form an $(n,\{2w,w\},\{2,1\},1,\{t_0/(t_0+t_1),t_1/(t_0+t_1)\})$-OOC. The cardinality of the constructed code is $|C|=t_0+t_1$, which does not achieve the upper bound of Theorem 2.4. Therefore, it is only close to an optimal OOC. The cardinalities and the constructing parameters of $(n,\{2w,w\},\{2,1\},1,\{t_0/(t_0+t_1),t_1/(t_0+t_1)\})$-OOCs are shown in Table 2.17.

Table 2.17 Cardinality and Constructing Parameters of Some $(n,\{2w,w\},\{2,1\},1,\{t_0/(t_0+t_1),t_1/(t_0+t_1)\})$-OOCs

Code	t_0	t_1	Primitive α	x_0	z_0
(97,{6,3},{2,1},1,{1/2,1/2})	4	4	5	1	0
(241,{6,3},{2,1},1,{1/2,1/2})	10	10	7	1	0
(409,{6,3},{2,1},1,{1/2,1/2})	17	17	21	3	0
(457,{6,3},{2,1},1,{1/2,1/2})	19	19	13	1	0
(211,{10,5},{2,1},1,{1/2,1/2})	3	3	2	1	0

2.5 Prime Codes

We will introduce how to construct unipolar codes using the congruence techniques in this section and the coming up two sections. The congruence techniques make use of the congruence operations in the finite field to construct the optical address codes for users. The congruence techniques have strong regularity and are simple in comparison with the constructions of OOC. However, the correlation properties of the congruence codes are not as good as those of OOC. Therefore, it is not useful for one-dimensional codes to be applied to OCDMA networking as the address codes of subscribers. Nevertheless, combining with OOC, one-coincidence frequency-hopping code (OCFHC) etc., one-dimensional congruence codes can be employed to construct two-dimension optical orthogonal codes with larger sizes and good correlation properties. In terms of the different congruence operations, the congruence codes can be classified into linear congruence codes (LCC), quadratic congruence codes (QCC), cubical congruence codes (CCC), hyperbolic congruence code (HCC) and so on.

The basic idea of constructing the congruence codes is as follows. Firstly, choose a prime number p and produce a group of sequences $y_i(j)$, $0 \leqslant i \leqslant p-1$, $0 \leqslant j \leqslant p-1$, using congruence operation over Galois Field $GF(p)=\{0,1,2,\cdots,p-1\}$. Then, according to a certain algorithm, map this group of sequences into a group of binary sequences and $y_i(j)$ corresponds to the 1's position of jth chip (called the slot) of ith codeword. When a different congruence operation is deployed, a different congruence code can be obtained. The congruence operations in common use are as follows:

Linear congruence operator

$$y_i(j;a,b)=\{i\cdot(a\cdot j+b)\} \bmod p \tag{2.30}$$

where a and b are constants. When $a=1$ and $b=0$, it can generate the prime sequences[24, 25].

Quadratic congruence operator

$$y_i(j;a,b,c) = \{i \cdot (a \cdot j^2 + b \cdot j + c)\} \bmod p \tag{2.31}$$

where a, b and c are constants. When $a = b = \frac{1}{2}$ and $c = 0$, it can produce the quadratic congruence sequences[8,9,30].

Cubical congruence operator

$$y_i(j;a,b) = (i(j+a)^3 + b) \bmod p \tag{2.32}$$

where a and b are constants. When $a = b = 0$, it can generate the cubical congruence sequences[35].

Hyperbolic congruence operator

$$y_i(j) = (a \cdot \frac{i}{j} + b) \bmod p \tag{2.33}$$

where a and b are constants. When $a = 1$, it can produce the hyperbolic congruence sequences[31 – 34]. $i, j, a, b \in GF(p) = \{0,1,\cdots,p-1\}$ in the aforementioned four equations.

2.5.1 Basic Prime Codes

The prime code (PC) is a typical linear congruence code. The construction of a PC is as follows[25].

Firstly, choose p as a prime number and based on Galois field $GF(p)$, construct a prime sequence:

$$S_i = (s_{i,0}, s_{i,1}, \cdots, s_{i,j}, \cdots, s_{i,(p-1)}),\ i = 0,1,\cdots,p-1 \tag{2.34}$$

where the element in this prime sequence is

$$s_{i,j} = \{i \cdot j\} (\bmod p) \tag{2.35}$$

$s_{i,j}$, i and j are the elements over the Galois field $GF(p) = \{0,1,\cdots,p-1\}$.

Then, with the prime sequence S_i and the following map:

$$c_{i,k} = \begin{cases} 1 & \text{if } k = s_{i,j} + j \cdot p, \text{for } j = \{0,1,2,\cdots,p-1\} \\ 0 & \text{elsewhere} \end{cases} \tag{2.36}$$

a binary prime code can be obtained as follows:

$$C_i = (c_{i,0}, c_{i,1}, \cdots, c_{i,k}, \cdots, c_{i(n-1)}),\ \ i = 0,1,\cdots,p-1,\ n = p^2 \tag{2.37}$$

The codelength and codeweight of the prime code are $n = p^2$ and $w = p$ respectively. Maximum autocorrelation sidelobe and maximum cross-correlation function are $\lambda_a = p-1$ and $\lambda_c = 2$ respectively. The cardinality of PC is $|C| = p$. According to the definition of optical orthogonal code, PC is a quasi-OOC with the parameters $(n, w, \lambda_a, \lambda_c) = (p^2, p, p-1, 2)$.

Example 2.18 Assuming $p = 5$, the prime sequence S_i and the prime code C_i constructed are shown in Table 2.18 and Table 2.19.

Table 2.18 Prime sequences S_i constructed for $p = 5$

Elements of $GF(5)$	0	1	2	3	4
S_0	0	0	0	0	0
S_1	0	1	2	3	4
S_2	0	2	4	1	3
S_3	0	3	1	4	2
S_4	0	4	3	2	1

Table 2.19 Prime codes C_i constructed for $p = 5$

Prime sequence S_i	Prime code C_i
$S_0 = (00000)$	10000 10000 10000 10000 10000
$S_1 = (01234)$	10000 01000 00100 00010 00001
$S_2 = (02413)$	10000 00100 00001 01000 00010
$S_3 = (03142)$	10000 00010 01000 00001 00100
$S_4 = (04321)$	10000 00001 00010 00100 01000

From Table 2.19, it can be seen that each codeword in a prime code can be divided into p subsets with the length p for each subset. There is exactly one "1" in each subset and the position of this "1" is determined by the element in the corresponding prime sequence. The advantage of the prime code is that its generation algorithm is very simple and the shortcomings are that it has larger autocorrelation sidelobes equal to $p-1$, its cross-correlation is not equal to 1 and the cardinality of the prime code is only equal to its weight. Figure 2.3 takes the $(p^2, p, p-1, 2) = (11^2, 11, 10, 2)$ prime code as an example and shows the curves of its correlation functions.

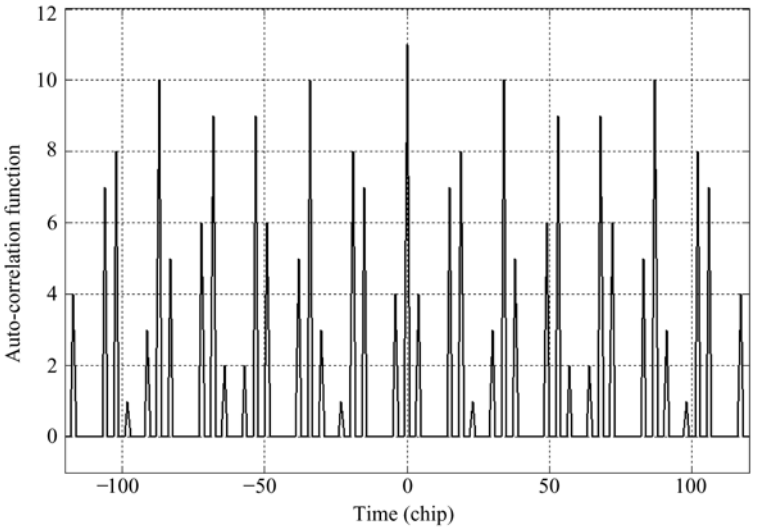

(a) Autocorrelation function of the codeword (0,4,8,1,5,9,2,6,10,3,7)

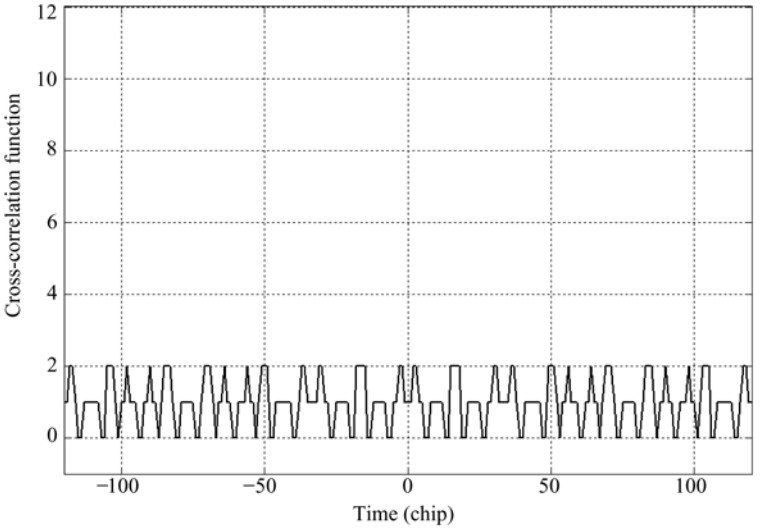

(b) Cross-correlation function of between the codewords (0,2,4,6,8,10,1,3,5,7,9) and (0,4,8,1,5,9,2,6,10,3,7)

Figure 2.3 Correlation functions of $(p^2, p, p-1, 2) = (11^2, 11, 10, 2)$ prime code

2.5.2 Extended Prime Codes

In order to reduce the cross-correlation of the prime code to 1, the extended prime code (EPC) has been proposed[25, 26]. Its construction is as follows. Firstly, construct a prime code. Then, $(p-1)$ (or more) "0" are patched to each subsequence of each

prime codeword. Therefore, the extended prime code can be constructed by using the prime code and the map of equation (2.38).

$$c_{i,k} = \begin{cases} 1 & \text{if } k = s_{i,j} + j(2p-1), \text{for } j = \{0, \cdots, p-1\} \\ 0 & \text{otherwise} \end{cases} \tag{2.38}$$

The codelength and the codeweight of the extended prime code are $n = p(2p-1)$ and $w = p$ respectively. Its maximum autocorrelation sidelobe and cross-correlation are $\lambda_a = p-1$ and $\lambda_c = 1$ respectively. The cardinality of EPC is $|C| = p$. EPC is a quasi-OOC with the parameters $(n, w, \lambda_a, \lambda_c) = (p(2p-1), p, p-1, 1)$ so the cross-correlation property of EPC is better than that of PC at the expense of increasing the codelength.

Example 2.19 When $p = 5$, the extended prime code C_i constructed is shown in Table 2.20, based on the prime sequence S_i constructed in Example 2.18 and the map of equation (2.38).

Table 2.20 Extended prime codes C_i constructed for $p = 5$

Prime sequence S_i	Extended prime code C_i
$S_0 = (00000)$	10000**0000** 10000**0000** 10000**0000** 10000**0000** 10000**0000**
$S_1 = (01234)$	10000**0000** 01000**0000** 00100**0000** 00010**0000** 00001**0000**
$S_2 = (02413)$	10000**0000** 00100**0000** 00001**0000** 01000**0000** 00010**0000**
$S_3 = (03142)$	10000**0000** 00010**0000** 01000**0000** 00001**0000** 00100**0000**
$S_4 = (04321)$	10000**0000** 00001**0000** 00010**0000** 00100**0000** 01000**0000**

2.5.3 Modified Prime Codes

2.5.3.1 Asynchronous Modified Prime Codes

Because the cardinality of PC corresponds to the largest number of users, *M*, in an OCDMA network, which is equal to the weight of PC, w, and furthermore w equals a prime number *p*, we must increase *p*, i.e., the larger the weight *w* is required, in order to increase the number of users in a network. When *w* becomes very large, the resulting cost and optical power losses of OCDMA encoder/decoder can be very high. In order to overcome this difficulty, it is expected that when the largest number of users increases, the code-weight must retain a suitable size. The modified prime code (MPC)[27] can be obtained through removing some 'redundant' pulses from the original prime code with *p* pulses under the premise of guaranteeing the requirement of bit-error-rate (BER) such as 10^{-9} and the number of users.

Therefore, the weight of MPC is smaller than that of PC, i.e., $w<p$.

The construction of MPC is as follows. Firstly, generate a prime code with p codewords. Then, arbitrary $p-w$ 1's are removed from this prime code and the remaining 1's form a new code C' with constant weight w. The resulting C' still has p distinct codewords C'_i and its length n is bounded by

$$\min\{p^2; 2wp-2\} \leqslant n \leqslant p^2 \tag{2.39}$$

The codewords of an MPC are derived from a set of modified prime sequences

$$S'_i = (s_{i,a_0}, \cdots, s_{i,a_l}, \cdots, s_{i,a_{(w-1)}})$$

where $i \in GF(p)$. w components of the modified prime sequences, s_{i,a_l}, can be denoted by

$$s_{i,a_l} = \{i \cdot a_l\} (\text{mod } p) \tag{2.40}$$

where $l = 0,1,\cdots,w-1$, $a_l \in GF(p)$ and $a_0 < a_1 < \cdots < a_l < \cdots < a_{(w-1)}$.

The ith codeword of MPC, C'_i, is represented by

$$C'_i = (c'_{i,0}, \cdots, c'_{i,k}, \cdots, c'_{i,(n-1)}), \text{ for } i \in GF(p) \tag{2.41}$$

where

$$c'_{i,k} = \begin{cases} 1, & \text{for } k = s_{i,a_l} + a_l \cdot p; l = \{0,1,\cdots,w-1\} \\ 0, & \text{otherwise} \end{cases} \tag{2.42}$$

All the w 1's of C'_i are assigned to the w individual subsequences of equal length p and the a_l th 1 is located in the s_{i,a_l} th position of the a_l th subsequence. The length and the weight of MPC are n and $w(<p)$ respectively. MPC has the same periodic cross-correlation λ_c as original prime code, being equal to 2 and its maximum autocorrelation sidelobe is $\lambda_a \leqslant w-1$. The cardinality of MPC is $|C| = p$. If some 1's in some positions of an MPC are removed carefully, the highest sidelobe of an autocorrelation, λ_a, may be reduced. In doing so, the number of codewords not only increases without the increasing of code-weight but the autocorrelation property can also be improved. That is helpful for system synchronization. Because this modified prime code is only applicable to asynchronous OCDMA communication systems, it is called asynchronous modified prime code.

Example 2.20 When $p=5$ and $w=4$, construct a modified prime code with the codelength $n = p^2 = 25$.

Firstly, construct the modified prime sequence with $p=5$, shown in Table 2.21. Then, construct the modified prime code using the map given by equation 2.42, which is shown in Table 2.22.

Table 2.21 Modified prime codes S_i' constructed for $p=5$ and $w=4$

i \ a_k	a_0	a_1	a_2	a_3	Modified prime sequence
	0	**1**	**2**	**3**	
0	0	0	0	0	S_0'
1	0	1	2	3	S_1'
2	0	2	4	1	S_2'
3	0	3	1	4	S_3'
4	0	4	3	2	S_4'

Table 2.22 Modified prime codes C_i' constructed for codelength $n=p^2=25$, $p=5$ and $w=4$

i	a_0	a_1	a_2	a_3	Modified prime sequence	Modified prime code C_i'
	0	**1**	**2**	**3**		
0	0	0	0	0	S_0'	10000 10000 10000 10000 00000
1	0	1	2	3	S_1'	10000 01000 00100 00010 00000
2	0	2	4	1	S_2'	10000 00100 00001 01000 00000
3	0	3	1	4	S_3'	10000 00010 01000 00001 00000
4	0	4	3	2	S_4'	10000 00001 00010 00100 00000

2.5.3.2 Synchronous Modified Prime Codes

Synchronous modified prime code (SMPC)[25, 28, 29] can be obtained through shifting a prime sequence p times in time and then mapping the prime sequence into a binary sequence. In this way, the number of available codewords of SMPC increases p times that of the cardinality of prime code, i.e., $|C|=p^2$, such that the number of subscribers in a network increases significantly. However, SMPC can only be applied to synchronous OCDMA system, that is, the network must provide a synchronous signal. Thus, SMPC augments its cardinality at the expense of sacrificing asynchronous network access.

The construction of SMPC is as follows. Firstly, generate a time-shifting sequence with a prime sequence

$$S_{i,l} = (s_{i,l,0}, s_{i,l,1}, \cdots, s_{i,l,j}, \cdots, s_{i,l,p-1}) \tag{2.43}$$

The element of this sequence is given by

$$s_{i,l,j} = (i \otimes j) \oplus l \tag{2.44}$$

where $i, j, l \in GF(p) = \{0,1,\cdots, p-1\}$ and "$\otimes$" denotes multiplication modulo-p, and "$\oplus$" represents modulo-p addition.

Then, map the time-shifting sequence $S_{i,l}$ into a binary (0,1) sequence

$$C_{i,l} = (c_{i,l,0}, c_{i,l,1}, \cdots, c_{i,l,k}, \cdots, c_{i,l,p^2-1}) \tag{2.45}$$

where

$$c_{i,l,k} = \begin{cases} 1 & \text{if } k = s_{i,l,j} + jp \ \text{ for } j = \{0,1,\cdots, p-1\} \\ 0 & \text{otherwise} \end{cases} \tag{2.46}$$

The codelength and the codeweight of SMPC are $n = p^2$ and $w = p$ respectively. The maximum value of its autocorrelation sidelobes is $\lambda_a = p$ and its cardinality is $|C| = p^2$. These p^2 codewords can be divided into p groups with p codewords each in terms of the original prime code. The first sequence in every group is the original prime sequence that acts as a seed to generate other sequences in this group and shifts circularly in time to produce other sequences.

In the synchronous modified prime code, the peaks of the cross-correlation functions between the time-shifted versions of any two code sequences can be as high as the autocorrelation peak, however, the peaks always delay from the autocorrelation-peak position. The synchronous receiver is deployed so that it always makes decisions at the expected autocorrelation-peak position, i.e., the last chip position of the code sequence. Therefore, the receiver can ward off the adjacent cross-correlation peaks and distinguish the autocorrelation peak correctly.

From Reference [25], it can be seen that the cross-correlation function at the last chip position is zero if the two code sequences originate from the same group, i.e., have the same i value, but at most one if they originated from different groups, i.e., have different i value. However, the cross-correlation function at other chip positions can be as high as p if the two code sequences are from the same group, but at most two if they originated from different groups. The autocorrelation peak of SMPC is always equal to its weight, p.

Example 2.21 When $p = 5$, the synchronous modified prime code constructed by using the construction described above is shown in Table 2.23.

Table 2.23 Synchronous modified prime codes $C_{i,l}$ for $p = 5$

i	l	Synchronous Modified Prime Sequence $S_{i,l}$	Synchronous Modified Prime Code $C_{i,l}$
0	0	$S_{0,0}$ = 0 0 0 0 0	$C_{0,0}$ = 10000 10000 10000 10000 10000
	1	$S_{0,1}$ = 1 1 1 1 1	$C_{0,1}$ = 01000 01000 01000 01000 01000
	2	$S_{0,2}$ = 2 2 2 2 2	$C_{0,2}$ = 00100 00100 00100 00100 00100
	3	$S_{0,3}$ = 3 3 3 3 3	$C_{0,3}$ = 00010 00010 00010 00010 00010
	4	$S_{0,4}$ = 4 4 4 4 4	$C_{0,4}$ = 00001 00001 00001 00001 00001
1	0	$S_{1,0}$ = 0 1 2 3 4	$C_{1,0}$ = 10000 01000 00100 00010 00001
	1	$S_{1,1}$ = 1 2 3 4 0	$C_{1,1}$ = 01000 00100 00010 00001 10000
	2	$S_{1,2}$ = 2 3 4 0 1	$C_{1,2}$ = 00100 00010 00001 10000 01000
	3	$S_{1,3}$ = 3 4 0 1 2	$C_{1,3}$ = 00010 00001 10000 01000 00100
	4	$S_{1,4}$ = 4 0 1 2 3	$C_{1,4}$ = 00001 10000 01000 00100 00010
2	0	$S_{2,0}$ = 0 2 4 1 3	$C_{2,0}$ = 10000 00100 00001 01000 00010
	1	$S_{2,1}$ = 1 3 0 4 2	$C_{2,1}$ = 01000 00010 10000 00001 00100
	2	$S_{2,2}$ = 2 4 1 3 0	$C_{2,2}$ = 00100 00001 01000 00010 10000
	3	$S_{2,3}$ = 3 0 2 4 1	$C_{2,3}$ = 00010 10000 00100 00001 10000
	4	$S_{2,4}$ = 4 1 3 0 2	$C_{2,4}$ = 00001 01000 00010 10000 00100
3	0	$S_{3,0}$ = 0 3 1 4 2	$C_{3,0}$ = 10000 00010 01000 00001 00100
	1	$S_{3,1}$ = 1 4 2 0 3	$C_{3,1}$ = 01000 00001 00100 10000 00010
	2	$S_{3,2}$ = 2 0 3 1 4	$C_{3,2}$ = 00100 10000 00010 01000 00001
	3	$S_{3,3}$ = 3 1 4 2 0	$C_{3,3}$ = 00010 01000 00001 00100 10000
	4	$S_{3,4}$ = 4 2 0 3 1	$C_{3,4}$ = 00001 00100 10000 00010 01000
4	0	$S_{4,0}$ = 0 4 3 2 1	$C_{4,0}$ = 10000 00001 00010 00100 01000
	1	$S_{4,1}$ = 1 0 4 3 2	$C_{4,1}$ = 01000 10000 00001 00010 00100
	2	$S_{4,2}$ = 2 1 0 4 3	$C_{4,2}$ = 00100 01000 10000 00001 00010
	3	$S_{4,3}$ = 3 2 1 0 4	$C_{4,3}$ = 00010 00100 01000 10000 00001
	4	$S_{4,4}$ = 4 3 2 1 0	$C_{4,4}$ = 00001 00010 00100 01000 10000

2.6 Quadratic Congruence Codes

2.6.1 Basic Quadratic Congruence Codes

The construction of the quadratic congruence code (QCC)[8] is as follows. Firstly, choose a prime number, p. Based on the Galois field, construct a quadratic

congruence sequence

$$S_i = (s_{i,0}, s_{i,1}, \cdots, s_{i,j}, \cdots, s_{i,(p-1)}),\ i = 1,2,\cdots,p-1 \tag{2.47}$$

The elements of the quadratic congruence sequence are given by

$$s_{i,j} = \left\{ i \cdot \frac{j(j+1)}{2} \right\} (\text{mod } p),\ 1 \leqslant i \leqslant p-1,\ 0 \leqslant j \leqslant p-1 \tag{2.48}$$

where $s_{i,j} \in GF(p) = \{0,1,\cdots,p-1\}$.

Then, from the quadratic congruence sequence S_i, we can construct a binary $\{0,1\}$ sequence, i.e., a quadratic congruence code

$$C_i = (c_{i,0}, c_{i,1}, \cdots, c_{i,k}, \cdots, c_{i,(n-1)}),\ i = 1,2,\cdots,p-1 \tag{2.49}$$

by the map

$$c_{i,k} = \begin{cases} 1 & \text{if } k = s_{i,j} + j \cdot p \text{ for } i = 0,1,\cdots,p-1 \text{ and } j = \left\lfloor \frac{k}{p} \right\rfloor, \text{ for } k = 0,1,\cdots,p^2-1 \\ 0 & \text{otherwise} \end{cases} \tag{2.50}$$

where $\lfloor x \rfloor$ denotes an integer smaller than or equal to x.

The length and the weight of the quadratic congruence code are $n = p^2$ and $w = p$ respectively. Its cardinality is $|C| = p-1$. The maximum sidelobe of autocorrelation and the maximum cross-correlation function are $\lambda_a = 2$ and $\lambda_c = 4$ respectively. In terms of the definition of OOC, the quadratic congruence code is a quasi-OOC with the parameters $(n, w, \lambda_a, \lambda_c) = (p^2, p, 2, 4)$. It can be seen that the maximum sidelobe of autocorrelation of QCC has been improved greatly compared with that of the prime code, which is $\lambda_a = p-1$. However, its cross-correlation function is too large and the property of its autocorrelation is still not ideal. (the ideal maximum value of the autocorrelation sidelobe is 1.)

Example 2.22 Construct a quadratic congruence code with $p = 7$.

Firstly, construct a quadratic congruence sequence S_i, $1 \leqslant i \leqslant 6$, by using the quadratic congruence operator

$$s_{i,j} = \left\{ i \cdot \frac{j(j+1)}{2} \right\} (\text{mod } 7),\ 1 \leqslant i \leqslant 6,\ 0 \leqslant j \leqslant 6$$

which is shown in the left-hand side of Table 2.24. By using the map of equation (2.50), the resulting quadratic congruence code is shown in the right-hand side of Table 2.24.

Table 2.24 Quadratic Congruence Sequences and Quadratic Congruence Codes for $p=7$

i	Quadratic Congruence Sequence S_i	Quadratic Congruence Code C_i
1	$S_1 = 0\ 1\ 3\ 6\ 3\ 1\ 0$	$C_1 = 1000000\ 0100000\ 0001000\ 0000001\ 0001000\ 0100000\ 1000000$
2	$S_2 = 0\ 2\ 6\ 5\ 6\ 2\ 0$	$C_2 = 1000000\ 0010000\ 0000001\ 0000010\ 0000001\ 0010000\ 1000000$
3	$S_3 = 0\ 3\ 2\ 4\ 2\ 3\ 0$	$C_3 = 1000000\ 0001000\ 0010000\ 0000100\ 0010000\ 0001000\ 1000000$
4	$S_4 = 0\ 4\ 5\ 3\ 5\ 4\ 0$	$C_4 = 1000000\ 0000100\ 0000010\ 0001000\ 0000010\ 0000100\ 1000000$
5	$S_5 = 0\ 5\ 1\ 2\ 1\ 5\ 0$	$C_5 = 1000000\ 0000010\ 0100000\ 0010000\ 0100000\ 0000010\ 1000000$
6	$S_6 = 0\ 6\ 4\ 1\ 4\ 6\ 0$	$C_6 = 1000000\ 0000001\ 0000100\ 0100000\ 0000100\ 0000001\ 1000000$

2.6.2 Extended Quadratic Congruence Codes

In order to improve the properties of auto- and cross-correlation of the quadratic congruence code, the extended quadratic congruence code (EQCC) is proposed[9]. The construction of EQCC is basically the same as that of QCC. In addition, choose p as a prime number first and then construct a quadratic congruence sequence S_i based on the Galois field. However, when the quadratic congruence sequence S_i is mapped into a binary $\{0,1\}$ sequence, the mapping equation used in EQCC is different from that in QCC. The map in EQCC is as follows:

$$c_{i,k} = \begin{cases} 1 & \text{if } k = s_{i,j} + j(2p-1) \text{ for } i = 0,1,\cdots,p-1 \\ & \text{and } j = \left\lfloor \frac{k}{2p-1} \right\rfloor, \text{for } k = 0,1,\cdots,p(2p-1)-1 \\ 0 & \text{otherwise} \end{cases} \tag{2.51}$$

where $\lfloor x \rfloor$ denotes an integer smaller than or equal to x.

The extended quadratic congruence code constructed is given by

$$C_i = (c_{i,0}, c_{i,1}, \cdots, c_{i,k}, \cdots, c_{i,(n-1)}), \quad i = 1,2,\cdots,p-1 \tag{2.52}$$

where $n = p(2p-1)$.

The codelength and the code-weight of EQCC are $n = p(2p-1)$ and $w = p$ respectively. The maximum value of the autocorrelation sidelobe λ_a and the maximum cross-correlation function λ_c of EQCC are 1 and 2 respectively and the cardinality of EQCC is $|C| = p-1$. According to the definition of OOC, EQCC is a quasi-OOC with the parameters $(n, w, \lambda_a, \lambda_c) = (p(2p-1), p, 1, 2)$. It can be seen that the correlation properties of EQCC have been improved greatly,

but the improvement is obtained at the expense of increasing the codelength nearly twice.

Example 2.23 Construct an extended quadratic congruence code with $p=5$.

Firstly, construct a quadratic congruence sequence S_i, $1 \leqslant i \leqslant 4$, using the quadratic congruence operator

$$s_{i,j} = \left\{ i \cdot \frac{j(j+1)}{2} \right\} (\mathrm{mod}\, 5),\ 1 \leqslant i \leqslant 4,\ 0 \leqslant j \leqslant 4$$

which is shown in the left-hand side of Table 2.25. Then, the extended quadratic congruence code constructed is shown in the right-hand side of Table 2.25 through making use of the map of equation (2.51).

Table 2.25 Quadratic congruences sequences and extended quadratic congruence codes for $p=5$

i	Quadratic congruence sequence S_i	extended quadratic congruence code C_i
1	$S_1 = 0\ 1\ 2\ 1\ 0$	$C_1 = 100000000\ 010000000\ 001000000\ 010000000\ 100000000$
2	$S_2 = 0\ 2\ 1\ 2\ 0$	$C_2 = 100000000\ 001000000\ 010000000\ 001000000\ 100000000$
3	$S_3 = 0\ 3\ 4\ 3\ 0$	$C_3 = 100000000\ 000100000\ 000010000\ 000100000\ 100000000$
4	$S_4 = 0\ 4\ 2\ 4\ 0$	$C_4 = 100000000\ 000010000\ 001000000\ 000010000\ 100000000$

From Table 2.25, it can be seen that each codeword of EQCC can also be divided into p subsequences and there is only one 1 in every subset as in QCC. However, the length of each subsequence in every codeword of EQCC is $2p-1$ rather than p.

2.6.3 Synchronous Quadratic Congruence Codes

The construction of the synchronous quadratic congruence code (SQCC)[30] is as follows. Firstly, choose p as a prime number and based on the Galois field, design a quadratic congruence sequence

$$S_{a,\alpha,\beta} = (s_{a,\alpha,\beta}(0), s_{a,\alpha,\beta}(1), \cdots, s_{a,\alpha,\beta}(k), \cdots, s_{a,\alpha,\beta}(p-1)) \tag{2.53}$$

where $a \in GF(p) \setminus 0 = \{1,2,\cdots,p-1\}$, $\alpha, \beta \in GF(p) = \{0,1,\cdots,p-1\}$.

The elements of this quadratic congruence sequence are given by

$$s_{a,\alpha,\beta}(k) = \{a(k+\alpha)^2 + \beta\} (\text{mod } p),\ k = 0,1,\cdots, p-1 \tag{2.54}$$

where $a \in \{1,2,\cdots, p-1\}$, $\alpha, \beta \in GF(p) = \{0, 1, \cdots, p-1\}$. By varying the parameters a, α and β, $(p-1) \times p \times p = p^3 - p^2$ different sequences can be generated from $S_{a,\alpha,\beta}$.

Then, a binary $\{0,1\}$ sequence, i.e., the synchronous quadratic congruence code can be constructed by

$$C_{a,\alpha,\beta} = (c_{a,\alpha,\beta}(0), c_{a,\alpha,\beta}(1), \cdots, c_{a,\alpha,\beta}(i), \cdots, c_{a,\alpha,\beta}(p^2-1)) \tag{2.55}$$

using the map

$$c_{a,\alpha,\beta}(i) = \begin{cases} 1 & \text{iff } kp + s_{a,\alpha,\beta}(k) = i; i = 0,1,\cdots, p^2-1; k = \left\lfloor \frac{i}{p} \right\rfloor \\ 0 & \text{otherwise} \end{cases} \tag{2.56}$$

from $S_{a,\alpha,\beta}$, where $a \in \{1,2,\cdots, p-1\}$, $\alpha, \beta \in GF(p) = \{0,1,\cdots, p-1\}$. $\lfloor x \rfloor$ denotes the largest integer smaller than or equal to x. The binary sequence $C_{a,\alpha,\beta}$ can be divided into p subsequences where the length of each subsequence is p. $s_{a,\alpha,\beta}(k)$ represents the position where the k^{th} 1 in the binary sequence $C_{a,\alpha,\beta}$ is located in the k^{th} subsequence.

For a given value of a, p^2 code sequences can be designed and the process of construction is shown in Table 2.26. Because a takes p values from 1 to $p-1$, $p^2(p-1)$ code sequences can be designed. And when $a = 0$, only p code sequences that are all distinct can be generated. Therefore, The cardinality of the synchronous quadratic congruence code that can be constructed is $p^2(p-1) + p = p^3 - p^2 + p$.

Table 2.26 $S_{1,\alpha,\beta}$ and $C_{1,\alpha,\beta}$ sequences for $p = 5$ and $a = 1$

α	β	$S_{1,\alpha,\beta}$	$C_{1,\alpha,\beta}$
0	0	(0,1,4,4,1)	10000 01000 00001 00001 01000
	1	(1,2,0,0,4)	01000 00100 10000 10000 00001
	2	(2,3,1,1,3)	00100 00010 01000 01000 00010
	3	(3,4,2,2,4)	00010 00001 00100 00100 00001
	4	(4,0,3,3,0)	00001 10000 00010 00010 10000
1	0	(1,4,4,1,0)	01000 00001 00001 01000 10000
	1	(2,0,0,2,1)	00100 10000 10000 00100 01000
	2	(3,1,1,3,2)	00010 01000 01000 00010 00100
	3	(4,2,2,4,3)	00001 00100 00100 00001 00010
	4	(0,3,3,0,4)	10000 00010 00010 10000 00001

Continued

α	β	$S_{1,\alpha,\beta}$	$C_{1,\alpha,\beta}$
2	0	(4,4,1,0,1)	00001 00001 01000 10000 01000
	1	(0,0,2,1,2)	10000 10000 00100 01000 00100
	2	(1,1,3,2,1)	01000 01000 00010 00100 01000
	3	(2,2,4,3,2)	00100 00100 00001 00010 00100
	4	(3,3,0,4,3)	00010 00010 10000 00001 00010
3	0	(4,1,0,1,4)	00001 01000 10000 01000 00001
	1	(0,2,1,2,0)	10000 00100 01000 00100 10000
	2	(1,3,2,3,1)	01000 00010 00100 00010 01000
	3	(2,4,3,4,2)	00100 00001 00010 00001 00100
	4	(3,0,4,0,3)	00010 10000 00001 10000 00010
4	0	(1,0,1,4,4)	01000 10000 01000 00001 00001
	1	(2,1,2,0,0)	00100 01000 00100 10000 10000
	2	(3,2,3,1,1)	00010 00100 00010 01000 01000
	3	(4,3,4,2,2)	00001 00010 00001 00100 00100
	4	(0,4,0,3,3)	10000 00001 10000 00010 00010

Theorem 2.6[30] If $a_1 \neq a_2$, then the congruence equation (2.57) has at most two non-congruence solutions.

$$s_{a_1,\alpha_1,\beta_1}(k) = s_{a_2,\alpha_2,\beta_2}(k) (\mathrm{mod}\, p), k = 0,1,\cdots,p-1 \tag{2.57}$$

When $a_1 = a_2$, equation (2.57) has at most one non-congruence solution, except if $\alpha_1 = \alpha_2$ and $\beta_1 = \beta_2$ when there are p non-congruence solutions in equation (2.57).

Proof: See Ref.[30].

Based on Theorem 2.6, we can obtain the properties[30] of the binary sequence $s^{QC}_{a,\alpha,\beta}(i)$ as follows:

(1) For the same a and all the combinations of $\alpha_1, \alpha_2, \beta_1, \beta_2$ except when $\alpha_1 = \alpha_2$ and $\beta_1 = \beta_2$, there exists

$$\sum_{i=0}^{p^2-1} \left[c_{a,\alpha_1,\beta_1}(i) \times c_{a,\alpha_2,\beta_2}(i) \right] \leqslant 1 \tag{2.58}$$

(2) When ($\alpha_1 = \alpha_2$ and $\beta_1 = \beta_2$), then

$$\sum_{i=0}^{p^2-1} \left[c_{a,\alpha_1,\beta_1}(i) \times c_{a,\alpha_2,\beta_2}(i) \right] = p \tag{2.59}$$

(3) For an arbitrary combination of $a_1, a_2, \alpha_1, \alpha_2, \beta_1, \beta_2$ except when ($a_1 = a_2$

and $\alpha_1 = \alpha_2$ and $\beta_1 = \beta_2$) simultaneously, there exists

$$\sum_{i=0}^{p^2-1}\left[c_{a_1,\alpha_1,\beta_1}(i)\times c_{a_2,\alpha_2,\beta_2}(i)\right] \leqslant 2 \tag{2.60}$$

Therefore, the binary sequence $C_{a,\alpha,\beta}$ can be used as the subscriber address codes in a synchronous OCDMA system, and its length and weight are p^2 and p respectively. The autocorrelation peak of each codeword of SQCC is p. If the value of the cross-correlation function between the codewords at the time when the peak of autocorrelation occurs is required to be smaller than or equal to 1, p^2 codewords can be constructed choosing any value of a between 1 and $p-1$. When these codewords are assigned to p^2 subscribers the maximum number of simultaneous users with errorless communication is $p-1$. If the value of cross-correlation function between the codewords at the time when the peak of autocorrelation occurs is required to be smaller than or equal to 2, $p^3 - p^2 + p$ codewords can be constructed by $a = 0,1,\cdots,p-1$. Although there can exist at most p^3-p^2+p subscribers in a network, the number of simultaneous subscribers with errorless communication is only $(p-1)/2$.

Because the space in this book is limited, we no longer introduce the hyperbolic congruence codes[31 – 34] and the cubical congruence codes[35]. Interested readers can look up the associated references.

Table 2.27 shows the performance comparison of several congruence codes. From the table, it can be seen that the correlation properties of the congruence codes are not optimal and neither are their cardinalities. Furthermore, once the length of a congruence code is given, then its weight is also determined. However,

Table 2.27 Performance comparison of congruence codes

Code	Length	Weight	Peak of Auto-Correlation Sidelobe	Peak of Cross-correlation Function	Cardinality
PC	p^2	p	$p-1$	2	p
EPC	$p(2p-1)$	p	$p-1$	1	p
AMPC	n $\min\{p^2;2wp-2\} \leqslant n \leqslant p^2$	$w < p$	$w-1$	2	p
QCC	p^2	p	2	4	$p-1$
EQCC	$p(2p-1)$	p	1	2	$p-1$

the construction algorithm of the congruence code is very simple and has strong regularity. Therefore, two-dimensional OCDMA codes with good performance can be constructed by combining the congruence codes with OOC or just among themselves.

2.7 Bipolar Codes

In this section we will introduce the bipolar codes that can be applied to the coherent OCDMA system and the incoherent OCDMA system using differential detection, i.e., balanced detection. We are primarily concerned with the maximal-length sequences (called m-sequences in short), Gold sequences, 4-phase sequences with near-optimum correlation and Walsh-Hadamard codes. Because there exist negative components in the codewords of the bipolar codes, the properties of the bipolar codes are better than those of the unipolar codes.

2.7.1 m-Sequence

The m-sequence[36] is a pseudorandom sequence in the most common use, which can be generated by the feedback-shift-registers and has the maximal period. Therefore, it is called the maximal linear feedback-shift-register sequence. The period of an m-sequence is not only associated with the number of stages of shift-registers, but is also related to the linear feedback logic. When an r-stage shift-register is employed, the period of the m-sequence generated is $n = 2^r - 1$. The linear feedback logic is determined by a primitive polynomial of degree r, equation (2.61).

$$f(x) = \sum_{i=0}^{r} c_i x^i \tag{2.61}$$

A primitive polynomials of degree r, $f(x)$, must satisfy the following three conditions:

(1) $f(x)$ is an irreducible polynomial, that is, it can no longer be decomposed into smaller factors.

(2) $x^n + 1$ can be exactly divided by $f(x)$, where $n = 2^r - 1$.

(3) $x^q + 1$ cannot be exactly divided by $f(x)$, where $q < n$.

Example 2.24 Find all primitive polynomials of degree $r = 4$.

Due to $r = 4$, the period of the m-sequence generated by a 4-stage shift-register is $n = 2^r - 1 = 2^4 - 1 = 15$. By factoring the polynomial $x^{15} + 1$, we can obtain

$$x^{15} + 1 = (x^4 + x^3 + x^2 + x + 1)(x^4 + x + 1)(x^4 + x^3 + 1)(x^2 + x + 1)(x + 1)$$

where the factors x^2+x+1 and $x+1$ are not the polynomials of degree 4, therefore, they are not the primitive polynomial. Furthermore, because $x^4+x^3+x^2+x+1$ can divide into x^5+1, it is also not a primitive polynomial. The remaining x^4+x^3+1 and x^4+x+1 satisfy the three conditions above. Therefore, they are primitive.

In general, an *r*-stage linear feedback shift-register is shown in Fig. 2.4, in which a_{r-i} denotes the state of the $(r-i)^{\text{th}}$ stage shift-register and $c_i(i=0,1,\cdots,r)$ indicates the link state of the feedback line in the shift-register, where $c_i=1$ represents the line connected, and otherwise $c_i=0$ represents the line disconnected. The expression of the linear feedback logic is

$$a_r = c_1 a_{r-1} \oplus c_2 a_{r-2} \oplus c_3 a_{r-3} \oplus \cdots \oplus c_r a_0 \tag{2.62}$$

If we move the a_r left of the equal sign to the right-hand and substitute $a_r = c_0 a_r (c_0=1)$ into equation (2.62), then equation (2.62) can be rewritten as

$$0 = \sum_{i=0}^{r} c_i a_{r-i} \tag{2.63}$$

where the coefficient $c_i(i=0,1,\cdots,r)$ is the coefficient of the primitive polynomial (2.61). After substituting c_i into equation (2.62) we can obtain the linear feedback logic. The m-sequence can be generated by the r-stage linear feedback shift-register obtained.

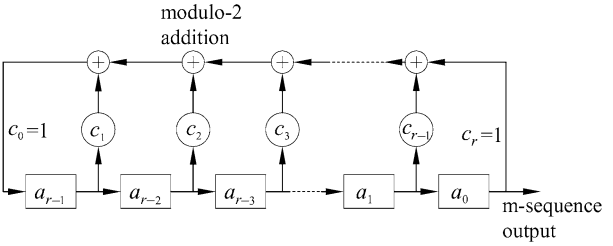

Figure 2.4 r-stage linear feedback shift-register

Example 2.25 Generate an m-sequence with the period $n=2^4-1=15$ by the primitive polynomial x^4+x+1 of degree $r=4$.

From the primitive polynomial x^4+x+1, $c_4=c_1=c_0=1$ and $c_3=c_2=0$ can be obtained. Thus, the linear feedback logic is

$$a_4 = a_3 \oplus a_0$$

The resulting 4-stage maximal-length linear feedback shift-register is shown in Fig. 2.5.

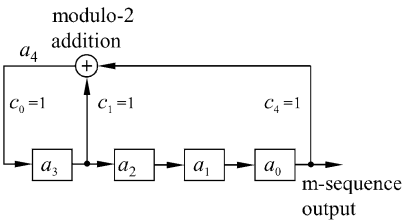

Figure 2.5 4-stage maximal-length linear feedback shift-register

Suppose that the initial state of the shift-register is 1000. Then, under the action of shift-clock, after 15 clock times the shift-register can produce the maximal-length linear shift-register sequence with the period of 15 at its output, 111101011001000.

From the argument above, it is known that we can build an m-sequence generator as long as a primitive polynomial is found. The number of m-sequences with the period of $n=2^r-1$ is the same as the number of the r -stage primitive polynomials. The number of the r -stage primitive polynomials[37] is

$$|C|=\frac{\phi(2^r-1)}{r} \tag{2.64}$$

where $\phi(2^r-1)$ is an Euler number, i.e., the number of positive integers including 1 that are relatively prime to and less than 2^r-1, which is

$$\phi(2^r-1)=\begin{cases}2^r-2 & \text{if } 2^r-1 \text{ is a prime number}\\ (p_1-1)(p_2-2) & \text{if } 2^r-1=p_1p_2, \text{for } p_1,\ p_2 \text{ are prime numbers}\end{cases} \tag{2.65}$$

Example 2.26 Find the number of the primitive polynomials for $r=5$.

Because of $2^r-1=2^5-1=31$ being a prime number, the number of positive integers including 1 that are relatively prime to and less than 31 is

$$\phi(2^5-1)=2^5-2=30$$

Thus, the number of primitive polynomials is

$$|C|=\frac{\phi(2^r-1)}{r}=\frac{30}{5}=6$$

that is, the number of m-sequences with length 31 is 6.

Many primitive polynomials have been obtained by computation and Table 2.28 shows some primitive polynomials. Note that the inverse polynomials of the

primitive polynomials given in Table 2.28, i.e., $x^r \cdot f(x^{-1})$ are also primitive polynomials that can generate maximal-length linear shift-register sequences.

Table 2.28 Parameters of some m-sequences and some coefficients of primitive polynomials generating m-sequences

Number of stages r	Sequence length $n = 2^r - 1$	Number of m-sequence	Primitive polynomials
2	3	1	[1,2]
3	7	2	[1,3]
4	15	2	[1,4]
5	31	6	[2,5],[2,3,4,5],[1,2,4,5]
6	63	6	[1,6],[1,2,5,6],[2,3,5,6]
7	127	18	[1,2,3,7],[2,3,4,7],[1,2,4,5,6,7],[2,5,6,7],[2,4,6,7], [1,3,6,7],[1,2,3,4,5,7],[3,7],[1,7]
8	255	16	[2,3,4,8],[3,5,6,8],[1,2,5,6,7,8],[1,3,5,8] ,[2,5,6,8], [1,5,6,8],[1,2,3,4,6,8],[1,6,7,8]
9	511	48	[4,9],[3,4,6,9],[4,5,8,9],[1,4,8,9],[2,3,5,9],[5,6,8,9], [2,7,8,9],[1,2,4,5,6,9],[1,3,4,6,7,9],[3,5,6,7,8,9]
10	1023	60	[3,10],[2,3,8,10],[1,3,4,10],[1,5,8,10],[4,5,8,10], [1,4,9,10],[3,4,8,10],[2,3,5,10],[1,2,5,10],[2,4,9,10]
11	2047	176	[1,11],[2,5,8,11],[2,3,7,11],[2,3,5,11],[2,3,10,11], [1,5,6,11],[1,3,5,11],[1,4,9,11],[2,6,8,11] [3,8,9,11]
12	4095	144	[1,4,6,12],[2,3,9,12],[1,2,5,10,11,12],[1,2,4,6,11,12], [5,6,7,9,11,12],[1,3,5,9,11,12],[4,7,8,9,11,12], [5,6,7,9,11,12],[1,2,3,8,9,12],[2,6,8,9,10,12]

Example 2.27 Find the m-sequences for $r = 4$.

Because $2^r - 1 = 2^4 - 1 = 15 = 3 \times 5$, and 3 and 5 are all prime, then

$$\phi(2^4 - 1) = (3-1)(5-1) = 8$$

Thus, the number of the primitive polynomials is

$$|C| = \frac{\phi(2^r - 1)}{r} = \frac{8}{4} = 2$$

namely, the number of m-sequences with length 15 is 2. We have found a 4-stage primitive polynomial in Example 2.25, $f(x) = x^4 + x + 1$, and its inverse polynomial

$$x^4 \cdot f(x^{-1}) = x^4(x^{-4} + x^{-1} + 1) = x^4 + x^3 + 1$$

is another primitive polynomial. The primitive polynomial corresponds to the linear feedback logic $a_4 = a_1 \oplus a_0$. The m-sequence generated by its corresponding 4-stage linear feedback shift-register is 000100110101111. The number of m-sequences for $r = 4$ is two in total and another m-sequence we have found in Example 2.25 is 111101011001000.

Four properties of m-sequences are as follows[36].

① The period of the m-sequence generated by an *r*-stage shift-register is $2^r - 1$.

② The probability of appearance of "1" and "0" in an m-sequence is approximately the same and the number of 1s is only one more than the number of 0s in an m-sequence.

③ Generally, a subsequence of 1s or 0s in an m-sequence is called a run. There are totally $2^r - 1$ runs in an m-sequence, where the number of runs for length 1 is 1/2 of the total runs and the number of runs for length 2 is 1/4, the number of runs for length 3 is 1/8, etc. Finally, there exist a consecutive "1" run for length r and a consecutive "0" run for length $r - 1$.

④ When 0 and 1 in an m-sequence take the values of "1" and "-1" respectively, the cyclic autocorrelation function of the m-sequence is

$$R_{XX}(\tau) = \sum_{i=0}^{n-1} x_i x_{i\oplus\tau} = \begin{cases} 2^r - 1 & \tau = 0 \\ -1 & 0 < \tau \leqslant n-1 \end{cases} \tag{2.66}$$

where $X = (x_0, x_1, \cdots, x_i, \cdots, x_{n-1})$ is any codeword of m-sequence and $n = 2^r - 1$. It means that the autocorrelation function of an m-sequence takes only two values, namely, the autocorrelation function peak at zero-shift is $n = 2^r - 1$ and the autocorrelation sidelobe at nonzero shift is -1.

Let the cross-correlation function of any two m-sequences $X = (x_0, x_1, \cdots, x_i, \cdots, x_{n-1})$ and $Y = (y_0, y_1, \cdots, y_i, \cdots, y_{n-1})$ be

$$R_{XY}(\tau) = \sum_{i=0}^{n-1} x_i y_{i\oplus\tau}, \ 0 \leqslant \tau \leqslant n-1 \tag{2.67}$$

Although m-sequences have ideal the autocorrelation property, it is difficult to find a general method to predict their cross-correlation functions. It has been shown[37] by investigation that only very small sets of m-sequences can have good cross-correlation properties and large sets of m-sequences generally have quite poor cross-correlation properties. Figure 2.6 and Fig. 2.7 show the curves of the autocorrelation function of the m-sequence (1,–1,–1,–1,1,–1,–1,1,1,–1,1,–1,1,1,1,1) and the cross-correlation function between it and (1,–1,–1,–1,1,1,1,1,–1,1,–1,1,1,–1,–1). The ratio of the maximum cross-correlation value versus the peak of autocorrelation is 7/16 = 44%.

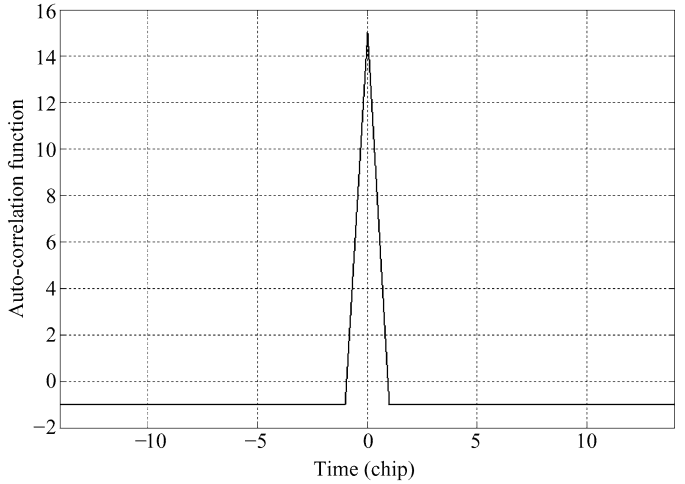

Figure 2.6 Autocorrelation function of m-sequence (1,–1,–1,–1,1,–1,–1,1,1,–1,1, –1,1,1,1)

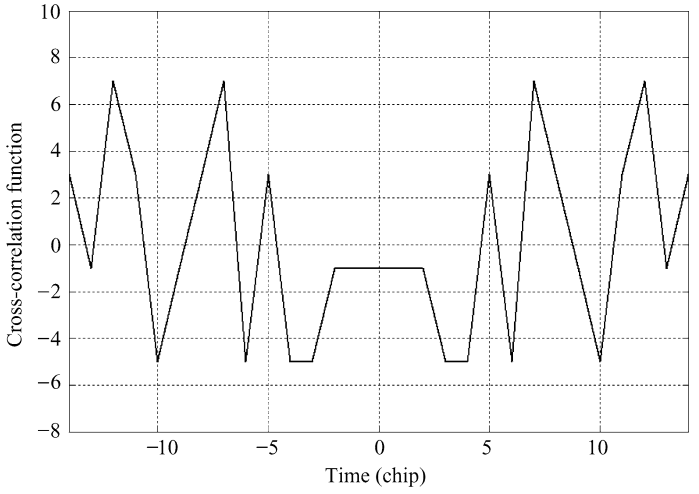

Figure 2.7 Cross-correlation function of m-sequences (1,–1,–1,–1,1,–1,–1,1,1,–1,1, –1,1,1,1) and (1,–1,–1,–1,1,1,1,1,–1,1,–1,1,1,–1,–1)

2.7.2 Gold Codes

Gold code[37, 38, 40] is a combination code of m-sequences that can be generated by the bit-by-bit modulo-2 addition of two m-sequences under the control of a synchronizing clock. Its scheme is shown in Fig. 2.8. These two generators of m-sequences have the same period and rate. The period of combination code

produced by the generator of Gold code is the same as that of these two subsequences. Although the Gold code is obtained by the modulo-2 addition of two m-sequences, it is a non-maximal linear shift-register sequence.

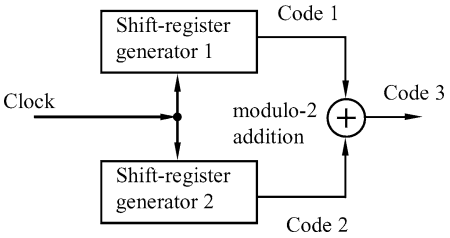

Figure 2.8 Generator of Gold code

2^r-1 Gold codewords can be generated by varying the relative shifts of two preferred m-sequences with the period $n=2^r-1$. Taking account of the two original m-sequences, the cardinality of Gold codes with the period n is

$$|C|=2^r-1+2=2^r+1 \tag{2.68}$$

For example, using two m-sequences with the period $n=2^r-1=2^5-1$, $|C|=2^r+1=2^5+1=33$ Gold codewords can be produced.

Assume that $X=(x_0,x_1,\cdots,x_i,\cdots,x_{n-1})$ and $Y=(y_0,y_1,\cdots,y_i,\cdots,y_{n-1})$ are two m-sequences with the period $n=2^r-1$, then the resulting Gold codewords are as follows:

$$X, Y, X\oplus Y, X\oplus Y^{(-1)}, X\oplus Y^{(-2)},\cdots, X\oplus Y^{(-i)},\cdots, X\oplus Y^{(-(n-1))},$$

where $Y^{(-i)}=(y_i,y_{i+1},\cdots,y_{n-1},y_0,y_1,\cdots,y_{i-1})$ is the ith cyclic left-shift of $Y=(y_0,y_1,\cdots,y_i,\cdots,y_{n-1})$, $y_i=\{+1,-1\}$, $x_i=\{+1,-1\}$. "$\oplus$" denotes exclusive-OR operation, i.e., $+1\oplus+1=-1\oplus-1=+1$, $+1\oplus-1=-1\oplus+1=-1$.

Gold code not only has many more codewords than m-sequence but its cross-correlation property is also improved greatly by picking two preferred m-sequences to generate Gold code. Gold codes have three-valued autocorrelation and cross-correlation function $\theta_{XY}(\tau)$ with values $\{-t_r-1,-1,t_r-1\}$, where $t_r=2^{\lfloor (r+2)/2-1\rfloor}$. $\lfloor x\rfloor$ denotes the largest integer of less than or equal to x.

The cross-correlation function values of Gold codes do not exceed the maximal value of the cross-correlation function between the two preferred m-sequences that generate the Gold codes. However, autocorrelation functions of Gold codes are slightly worse than those of m-sequences.

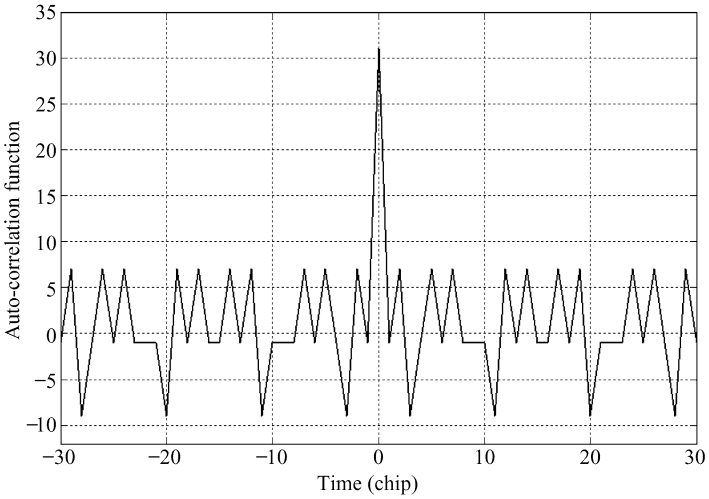

Figure 2.9 Autocorrelation function of Gold code $X = (-1,-1,-1,-1,1,-1,1,-1,1,-1,1,1,1,1,-1,-1,-1,-1,1,-1,1,-1,-1,-1,-1,1,1,-1,-1,-1,1)$

Figure 2.9 and Fig. 2.10 show the curves of autocorrelation function of Gold code $X = (-1,-1,-1,-1,-1,-1,-1,1,1,1,1,-1,1,1,-1,1,1,1,1,1,1,-1,1,1,1,-1,1,-1,-1,1,-1)$ and cross-correlation function between it and $Y = (-1,-1,-1,-1,1,-1,1,-1,1,-1,1,1,1,1,1,-1,-1,-1,-1,1,-1,1,-1,-1,-1,-1,1,1,-1,-1,-1,1)$. The ratio of the maximum cross-correlation value versus the peak of autocorrelation is 9/31 = 29%.

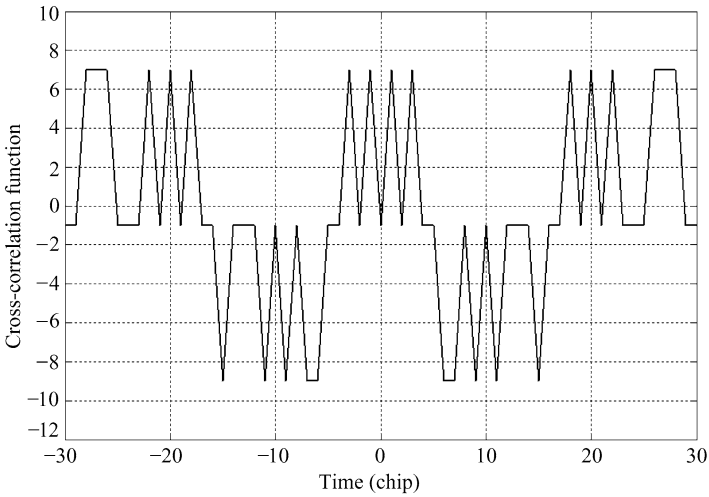

Figure 2.10 Cross-correlation function between two Gold codes $X = (-1,-1,-1,-1,-1,-1,-1,1,-1,1,-1,1,-1,1,1,1,1,1,-1,-1,-1,-1,1,-1,1,-1,1,-1,-1,-1,-1,1,1,1,-1,-1,-1,1)$ and $Y = (-1,-1,-1,-1,-1,-1,-1,-1,1,1,1,1,1,-1,1,1,1,-1,1,1,1,1,1,1,1,-1,1,1,1,1,-1,1,-1,-1,-1,1,-1)$

Example 2.28 Find Gold sequences with length 7 and the values of their cross-correlation function.

From the primitive polynomials of degree $r=3$, $f(x)=x^3+x+1$ and $x^{-3}f(x^{-1})=x^3(x^{-3}+x^{-1}+1)=x^3+x^2+1$, we can obtain the preferred pair of two m-sequences, which are $X=(+1,+1,-1,-1,-1,+1,-1)$ and $Y=(+1,+1,-1,+1,-1,-1,-1)$. Then 9 Gold sequences: X, Y, $X\oplus Y=(+1,+1,+1,-1,+1,-1,+1)$, $X\oplus Y^{-1}=(+1,-1,-1,+1,+1,-1,-1)$, $X\oplus Y^{-2}=(-1,+1,+1,+1,+1,+1,-1)$, $X\oplus Y^{-3}=(+1,-1,+1,+1,-1,+1,+1)$, $X\oplus Y^{-4}=(-1,-1,+1,-1,-1,-1,-1)$, $X\oplus Y^{-5}=(-1,-1,-1,-1,+1,+1,+1)$, $X\oplus Y^{-6}=(-1,+1,-1,+1,-1,-1,+1)$ can be generated. Their cross-correlation functions have three values: –5, –1 and +3.

2.7.3 Walsh-Hadamard Codes

Walsh-Hadamard code[5] consists of the row vectors of a Walsh code matrix arranged according to the order of Hadamard. It is also called Walsh code. The elements of this Walsh matrix are ± 1, which can be rapidly generated from the following recursion relation:

$$\boldsymbol{H}(i+1)=\begin{bmatrix}\boldsymbol{H}(i) & \boldsymbol{H}(i)\\ \boldsymbol{H}(i) & -\boldsymbol{H}(i)\end{bmatrix} \tag{2.69}$$

where $i=0,1,2,\cdots,\boldsymbol{H}(0)=+1$. Using this recursion expression, we can deduce

$$\boldsymbol{H}(1)=\begin{bmatrix}+1 & +1\\ +1 & -1\end{bmatrix}\begin{matrix}\text{---}\ \boldsymbol{H}(1)_0\\ \text{---}\ \boldsymbol{H}(1)_1\end{matrix}$$

$$\boldsymbol{H}(2)=\begin{bmatrix}+1 & +1 & +1 & +1\\ +1 & -1 & +1 & -1\\ +1 & +1 & -1 & -1\\ +1 & -1 & -1 & +1\end{bmatrix}\begin{matrix}\text{---}\boldsymbol{H}(2)_0\\ \text{---}\boldsymbol{H}(2)_1\\ \text{---}\boldsymbol{H}(2)_2\\ \text{---}\boldsymbol{H}(2)_3\end{matrix}$$

$$\boldsymbol{H}(3)=\begin{bmatrix}+1 & +1 & +1 & +1 & +1 & +1 & +1 & +1\\ +1 & -1 & +1 & -1 & +1 & -1 & +1 & -1\\ +1 & +1 & -1 & -1 & +1 & +1 & -1 & -1\\ +1 & -1 & -1 & +1 & +1 & -1 & -1 & +1\\ +1 & +1 & +1 & +1 & -1 & -1 & -1 & -1\\ +1 & -1 & +1 & -1 & -1 & +1 & -1 & +1\\ +1 & +1 & -1 & -1 & -1 & -1 & +1 & +1\\ +1 & -1 & -1 & +1 & -1 & +1 & +1 & -1\end{bmatrix}\begin{matrix}\text{---}\boldsymbol{H}(3)_0\\ \text{---}\boldsymbol{H}(3)_1\\ \text{---}\boldsymbol{H}(3)_2\\ \text{---}\boldsymbol{H}(3)_3\\ \text{---}\boldsymbol{H}(3)_4\\ \text{---}\boldsymbol{H}(3)_5\\ \text{---}\boldsymbol{H}(3)_6\\ \text{---}\boldsymbol{H}(3)_7\end{matrix}$$

$$\cdots$$

It can be seen that $\boldsymbol{H}(i)$ is a $2^i \times 2^i$ square matrix consisting of the elements +1 and –1. Because it is the same as $\boldsymbol{H}_{2^i}$ that is $\boldsymbol{H}$ matrix of $2^i \times 2^i$ dimensions, $i = 2,3,\cdots$, and is constructed by Hadamard matrix (in short, called $\boldsymbol{H}$ matrix) of 2×2 dimensions:

$$\boldsymbol{H}_2 = \begin{bmatrix} +1 & +1 \\ +1 & -1 \end{bmatrix}, \text{ i.e.,}$$

$$\boldsymbol{H}_{2^i} = \underbrace{\boldsymbol{H}_2 \otimes \boldsymbol{H}_2 \otimes \cdots \otimes \boldsymbol{H}_2}_{i\text{'s}}$$

Therefore, $\boldsymbol{H}(i)$ is also called a Hadamard matrix. The code consisting of each row of the matrix is referred to as Hadamard code. In view of the two persons' contribution to this code, we call it Walsh-Hadamard code. "$\otimes$" denotes Kronecker product of two matrices (also known as the direct produce or the tensor product), which is defined as:

With $\boldsymbol{A} = \begin{bmatrix} a_{11} & a_{12} & \cdots & a_{1n} \\ a_{21} & a_{22} & \cdots & a_{2n} \\ \cdots & \cdots & \cdots & \cdots \\ a_{m1} & a_{m2} & \cdots & a_{mn} \end{bmatrix}$ and $\boldsymbol{B} = \begin{bmatrix} b_{11} & b_{12} & \cdots & b_{1l} \\ b_{21} & b_{22} & \cdots & a_{2l} \\ \cdots & \cdots & \cdots & \cdots \\ a_{k1} & a_{k2} & \cdots & a_{kl} \end{bmatrix}$, then

$$\boldsymbol{A} \otimes \boldsymbol{B} = \begin{bmatrix} a_{11}\boldsymbol{B} & a_{12}\boldsymbol{B} & \cdots & a_{1n}\boldsymbol{B} \\ a_{21}\boldsymbol{B} & a_{22}\boldsymbol{B} & \cdots & a_{2n}\boldsymbol{B} \\ \cdots & \cdots & \cdots & \cdots \\ a_{m1}\boldsymbol{B} & a_{m2}\boldsymbol{B} & \cdots & a_{mn}\boldsymbol{B} \end{bmatrix} \text{ and } \boldsymbol{B} \otimes \boldsymbol{A} = \begin{bmatrix} \boldsymbol{A}b_{11} & \boldsymbol{A}b_{12} & \cdots & \boldsymbol{A}b_{1l} \\ \boldsymbol{A}b_{21} & \boldsymbol{A}b_{22} & \cdots & \boldsymbol{A}a_{2l} \\ \cdots & \cdots & \cdots & \cdots \\ \boldsymbol{A}a_{k1} & \boldsymbol{A}a_{k2} & \cdots & \boldsymbol{A}a_{kl} \end{bmatrix}$$

$\boldsymbol{A} \otimes \boldsymbol{B}$ or $\boldsymbol{B} \otimes \boldsymbol{A}$ are all matrices of $(mk) \times (nl)$ dimensions.

In the pattern of synchronous communication, the autocorrelation function value of a Walsh-Hadamard code obtained by a Walsh matrix of $n \times n = 2^i \times 2^i$ dimensions is equal to $n = 2^i$ and its cross-correlation function value equals 0, namely,

$$\boldsymbol{H}(i)_j (\boldsymbol{H}(i)_k)^{\mathrm{T}} = \begin{cases} 2^i & j = k \\ 0 & j \neq k \end{cases} \tag{2.70}$$

For example, $\boldsymbol{H}(2)_1 = \begin{bmatrix} +1 & -1 & +1 & -1 \end{bmatrix}$, $\boldsymbol{H}(2)_2 = \begin{bmatrix} +1 & +1 & -1 & -1 \end{bmatrix}$, then

$$\boldsymbol{H}(2)_1 (\boldsymbol{H}(2)_1)^{\mathrm{T}} = \begin{bmatrix} +1 & -1 & +1 & -1 \end{bmatrix} \begin{bmatrix} +1 \\ -1 \\ +1 \\ -1 \end{bmatrix} = 4$$

$$\boldsymbol{H}(2)_1(\boldsymbol{H}(2)_2)^{\mathrm{T}} = \begin{bmatrix} +1 & -1 & +1 & -1 \end{bmatrix} \begin{bmatrix} +1 \\ +1 \\ -1 \\ -1 \end{bmatrix} = 0$$

2.7.4 Maximal-length 4-phase Codes over Galois Ring *GR*(4,*r*)

We will introduce the construction of the maximal-length 4-phase codes[39] over a Galois ring $GR(4,r)$ in this subsection. This code has the same period and the cardinality as the binary Gold code, $n = 2^r - 1$ and $|C| = n + 2 = 2^r + 1$ respectively. However, its maximal value of cross-correlation is $\sqrt{2}$ times smaller than that of a Gold sequence. Therefore, it is a near-optimum code[39]. When this code is applied to OCDMA systems, it can improve the performance.

The construction of 4-phase code with the period $n = 2^r - 1$ is as follows. Firstly, find a primitive irreducible polynomial of degree r over $Z_4[x]$, which is divided into $x^{2^r-1} - 1$. Its modulo-2 map is a primitive irreducible polynomial over $Z_2[x]$. Assume that we find a primitive irreducible polynomial of degree r over $Z_4[x]$, which is

$$f(x) = x^r + c_{r-1}x^{r-1} + \cdots + c_1 x + c_0 \tag{2.71}$$

From equation (2.71), we can obtain the coefficients of the polynomial: c_0, c_1, c_2, $\cdots$, c_{r-2} and c_{r-1}, $c_i \in \{0,1,2,3\}$, $0 \leqslant i \leqslant r-1$. Table 2.29 shows the coefficients of the polynomials over $Z_4[x]$ with degree up to 10. Any polynomial of degree r in the table can generate this near-optimum 4-phase code.

Thus, the feedback logic of the linear feedback shift-register of degree r can be obtained from the coefficients c_0, c_1, c_2, $\cdots$, c_{r-2}, c_{r-1}, that is, by the following equation

$$\begin{aligned} a_r &= -c_{r-1}a_{r-1} - c_{r-2}a_{r-2} - \cdots - c_0 a_0 \\ &= [(-c_{r-1}) \bmod r]a_{r-1} + [(-c_{r-2}) \bmod r]a_{r-2} + \cdots \\ &\quad + [(-c_1) \bmod r]a_1 + [(-c_0) \bmod r]a_0 \\ &= c'_{r-1}a_{r-1} + c'_{r-2}a_{r-2} + \cdots + c'_0 a_0 \end{aligned} \tag{2.72}$$

we can get c'_0, c'_1, c'_2, $\cdots$, c'_{r-2}, c'_{r-1} and then construct the linear feedback shift-register of degree r, which is shown in Fig. 2.11.

The linear feedback shift-register of degree r can generate a 4-phase sequence. When the shift-register is set in different initial states (except the all-0 state) and

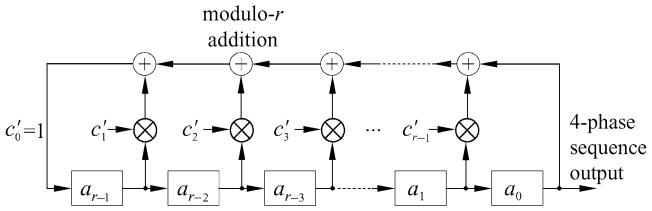

Figure 2.11 4-phase linear feedback shift-register of degree r

shifts periodically, different sequences can be generated. Note that any repetitions of sequences produced by cyclic-shift must be removed.

Example 2.29 Generate a 4-phase code with the period length 7 from $f(x) = x^3 + 2x^2 + x + 3$.

From $f(x) = x^3 + c_2x^2 + c_1x + c_0 = x^3 + 2x^2 + x + 3$, we can obtain $c_0 = 3$, $c_1 = 1$ and $c_2 = 2$. Furthermore, we have

$c'_0 = (-c_0) \bmod r = (-3) \bmod 4 = 1$, $c'_1 = (-c_1) \bmod r = (-1) \bmod 4 = 3$ and $c'_2 = (-c_2) \bmod r = (-2) \bmod 4 = 2$.

The resulting 3-stage linear feedback shift-register is shown in Fig. 2.12.

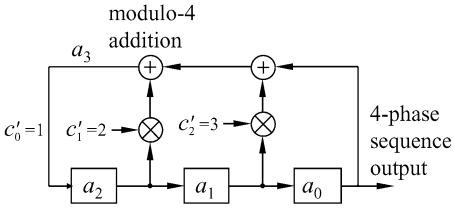

Figure 2.12 Linear feedback shift-register producing 4-phase near-optimum code with length 7

Under the cyclic shift, this shift-register can generate 9 4-phase codes as follows: 2002022, 3221211, 1223233, 1013102, 1100123, 2010333, 1112030, 2133003 and 2303130, shown in table 2.29.

Table 2.29 Coefficients of characteristic polynomials[39]

Number of Stages r	Sequence Length $n = 2^r - 1$	Number of Sequences $\lvert C \rvert = 2^r + 1$	Coefficient of Characteristic Polynomial
3	7	9	1213, 1323
4	15	17	10231, 13201
5	31	33	100323, 113013, 113123, 121003, 123133, 130133

Continued

Number of Stages r	Sequence Length $n=2^r-1$	Number of Sequences $\|C\|=2^r+1$	Coefficient of Characteristic Polynomial
6	63	65	1002031, 1110231, 1211031, 1301121, 1302001, 1320111
7	127	129	10020013, 10030203, 10201003, 10221133, 10233123, 11122323, 11321133, 11332133, 11332203, 12303213, 12311203, 12331333, 13002003, 13212213, 13223213, 11131123, 12122333, 13210123
8	255	257	100103121, 100301231, 102231321, 111310321, 111002031, 111021311, 121320031, 113120111, 121102121, 121201121, 121301001, 132103001, 123013111, 123132201, 130023121, 130200111
9	511	513	1000030203, 1001011333, 1001233203, 1002231013, 1020100003, 1020332213, 1021123003, 1021301133, 1021331123, 1022121323, 1023112133, 1110220323, 1111300013, 1111311013, 1112201133, 1113303003, 1130312123, 1131003213, 1131003323, 1131030123, 1132331203, 1133013203, 1133022333, 1210032123, 1210220333, 1211003133, 1211213013, 1213232203, 1230103133, 1230313123, 1231310123, 1232100323, 1232310133, 1232322013, 1233113203, 1300013333, 1301110213, 1301301213, 1301323323, 1302210213, 1302212123, 1303122003, 1303313333, 1320322013, 1320333013, 1321003133, 1322110203, 1323013013
10	1023	1025	10000203001, 10002102111, 10002123121, 10020213031, 10030023231, 10030200001, 10203103311, 10203122121, 10211131111, 10213010311, 10213330231, 10231100111, 10233222121, 11100113201, 11111110231, 11113111201, 11120120001, 11120232311, 11122031321, 11131011031, 11301031201, 11301210321, 11301320031, 11312010231, 11321001121, 11323133321, 11323202111, 11330130201, 11330223121, 12100122031, 12102023121, 12110012311, 12120311321, 12122130201, 12122233201, 12132020121, 12132120001, 12132203311, 12301210311, 12311302121, 12313022111, 12321103231, 12321222031, 12331133031, 12333132311, 13002310311, 13011013111, 13011232231, 13020010231, 13022100121, 13022212321, 13031202001, 13033113321, 13201002031, 13201021311, 13201111111, 13203331201, 13223211031, 13230112321, 13232003001

Notice: for example, when the degree is 3, the coefficients 1213 correspond to the polynomial $f(x)=x^3+2x^2+x+3$.

2.8 Summary

We have introduced systematically the constructions, the cardinalities and the properties of auto- and cross-correlation of one-dimensional incoherent OCDMA codes, such as optical orthogonal codes, prime codes and quadratic congruence codes, as well as the bipolar codes, such as m-sequences, Gold codes and Walsh-Hadamard codes. In addition, we have also studied near-optimum 4-phase sequences. One-dimensional incoherent OCDMA codes are applicable to one-dimensional incoherent OCDMA networks as the address codes for subscribers. The bipolar codes and the near-optimum 4-phase sequences are suitable for the coherent OCDMA networks as subscribers' address codes.

The incoherent OCDMA adopts incoherent detection. What is measured is the energy of the optical signal. Because there is no negative component in such a system, the incoherent OCDMA code is a unipolar code. Therefore, the orthogonality between any two codewords is difficult, even impossible, to implement. Because only quasi-orthogonality can be realized, the correlation properties and the cardinalities are confined. In one-dimensional incoherent OCDMA codes, although the constructions of the algebraic congruence codes are simple and easily realized in hardware, they have poor correlation properties and small cardinalities. Meanwhile their cardinalities are confined to prime numbers and their flexibility is poor when they are used. Despite a lot of effort, their performances still cannot satisfy practical requirements. The correlation properties and the cardinality of optical orthogonal codes are the best among one-dimensional incoherent OCDMA codes. However, their constructions are relatively complicated and confined by many factors.

The biggest limitation of one-dimensional incoherent OCDMA codes is that the code-cardinality is proportional to the length of frequency-spreading. Due to the limitation of current technology, it is difficult to make the width of chip optical pulses narrower than the order of magnitude of ps (pico-second) from the practical point of view in optical fiber communication systems. Furthermore, even if we can make an optical pulse narrower, it is difficult for it to be transmitted a long distance because of existing limitations in the fiber-optic, such as nonlinearity, dispersion, etc.

Due to the aforementioned reasons, there is an impact between the data rate for a single user and the number of users in a network such that the practical application of one-dimensional OCDMA systems is limited. However, because of the easy implementation of incoherent OCDMA systems, the coding theories for one-dimensional incoherent OCDMA codes establish the basis for the implementation of two-dimensional incoherent OCDMA coding and networks, which are promising for future practical applications. The constructions of two-dimensional codes are mostly based on the constructions of one-dimensional codes introduced in this chapter. Therefore, it is very important from the

theoretical and practical point of view for the readers to learn the coding theories of one-dimensional incoherent OCDMA codes.

The coherent OCDMA network deploys bipolar codes that are widely applied to electrical CDMA systems. Because the negative components exist in the bipolar codes, they have ideal correlation properties and large cardinalities. Furthermore, existing systematic coding theory is of use for reference. However, the technologies for the implementation of the coherent OCDMA system are relatively complicated and difficult to be realized. The practical application of the coherent OCDMA system depends on the progress of technologies of coherent OCDMA. In addition, the bipolar codes are also applicable to the incoherent OCDMA systems using differential detection.

Although much effort has been expended for many years and great progress has been made in the coding theories for OCDMA systems, there are still some theoretical issues to be studied deeply, such as the constructions of OOC with better performance, larger capacity and more flexible set of parameters, the constructions of optimal multiple-phase codes, the theoretical analytical methods for system performance, etc.

References

[1] Jawad.A.Salehi: Code division multiple-access techniques in optical fiber networks -part I: Fundamental principles. *IEEE Trans. on Communications*, Vol.37, No.8, Aug. 1989, pp824 – 833

[2] Jawad.A.Salehi and C. A. Brackett: Code division multiple-access techniques in optical fiber networks-part II: Systems performance analysis. *IEEE Trans. on Communications*, Vol.37, No.8, Aug. 1989, pp834 – 842

[3] Jawad. A. Salehi, F. R. K. Chung, and V. K. Wei: Optical orthogonal codes: Design, analysis, and applications. *IEEE Trans. on Information theory*, Vol.35, Nol.3, May 1989, pp595 – 605

[4] Chang Y. X., Ryoh F. H., Mao Y.: Combinational constructions of optical orthogonal codes with weight 4. *IEEE Trans. on Information Theory*, Vol.49, No.5, 2003, pp1283 – 1292

[5] Yixian Yang, Xuduan Lin: Coding Cryptography. Ren Min You Dian Press, China, 1992

[6] H. Chung and P. Kumar: Optical orthogonal codes-new bounds and an optimal construction. *IEEE Trans. on Information theory*, Vol.36, No.4, July 1990, pp866 – 873

[7] R.Petrovic: Orthogonal codes for CDMA optical fiber LAN's with variable bit interval. *IEE Electronics Letters*, Vol.26, No.10, 1990, pp662 – 664

[8] S. V. Maric: A new family of optical code sequences for use in spread-spectrum fiber-optic local area networks. *IEEE Transactions on Communications*, Vol.41, No.8, 1993, pp1217 – 1221

[9] S. V. Maric. New family of algebraically designed optical orthogonal codes for use in CDMA fiber-optic networks. *IEE Electronics Letters*, Vol.29, No.6, 1993, pp538 – 539

[10] Gun-Chang Yang: On the construction of 2^n codes for optical code-division multiple-access. *IEEE Trans. on Communications*, Vol.43, No.2/3/4, 1995, pp495 – 502

[11] Guu-Chang Yang: Optical orthogonal codes with unequal auto- and cross-correlation constraints. *IEEE Trans. on Information Theory*, Vol.41, No.1, 1995, pp96 – 106

[12] S. V. Marec, Mark D. Hahm, Edward L. Titlebaum: Construction and performance analysis of a new family of optical orthogonal codes for CDMA fiber-optic networks. *IEEE Trans. on Communications*, Vol.43,No.2/3/4, 1995, pp485 – 489

[13] G C. Yang: Variable-weight optical orthogonal codes for CDMA networks with multiple performance requirements. *IEEE Trans. on Communications*, Vol.44, No.1, 1996, pp47 – 55

[14] Y. X. Chang, J. Yin: Further results on optimal optical orthogonal codes with weight 4. *Discrete Mathematics*, Vol.279, No.1, 2004, pp135 – 153

[15] N. Miyamoto, Mizuno H., Shinohara S.: Optical orthogonal codes obtained from conics on finite projective planes. *Finite Fields & Their Applications*, Vol. 10, No.3, 2004, pp405 – 411

[16] Chen Zhi, Fan Pingzhi, and Jin Fan: Disjoint deference sets, difference triangle sets, and related codes. *IEEE Trans. on Information Theory*, Vol.38, No.2, 1992, pp518 – 521

[17] Abel R., Julian R., Buratti M.: Some progress on (v, 4,1) difference families and optical orthogonal codes. Journal of Combinational Theory- Series A, Vol.106, no.1, 2004, pp59 – 75

[18] Chu Wen S., Colomb S. W.: A new recursive construction for optical orthogonal codes. *IEEE Trans. on Information Theory*, Vol.49, No.11, 2003, pp3072 – 3076

[19] R. C. Bose: On the construction of balanced incomplete block designs. Ann. Eugenics, Vol. 9, 1993, pp353 – 399

[20] R. M. Wilson: Cyclotomy and difference families in elementary Abelian groups. Journal of Number Theory, Vol. 4, 1972, pp17 – 47

[21] F. Khansefid: Sets of (0, l)-sequences with application to optical-fibre networks. Ph.D. dissertation, University of Southern California, Aug. 1988

[22] Hall M.: Combinational Theory. 2nd Edition, John Wiley, 1986

[23] Hanani H.: The existence and constructions of balanced incomplete block design. *Ann. Math. Statist*., Vol.32, 1961, pp361 – 386

[24] Prucnal, P. R.: Santoro, M. A., Fan, T. R.: Spread Spectrum Fiber-optic Local Area Network Using Optical Processing. *IEEE/OSA Journal of Lightwave Technology*, Vol. 4, No. 5, May 1986, pp547 – 554

[25] G. -C. Yang and W. C. Kwong: Prime Codes with Applications to CDMA Optical and Wireless Networks. Norwood: Artech House, 2002

[26] G. -C. Yang and Wing. C. Kwong: Performance analysis of optical CDMA with prime codes. *IEE Electronics Letters*, Vol.31, No.7, Mar. 1995, pp569 – 570

[27] J. -G. Zhang and W. C. Kwong: Effective design of optical code-division multiple access networks by using the modified prime code. *IEE Electronics Letters*, Vol.33, No.3, 1997, pp229 – 230

[28] Wing. C. Kwong, P. A. Perrier, and P. R. Prucnal: Performance comparison of asynchronous and synchronous code-division multiple-access techniques for fiber-optic local area networks. *IEEE Trans. on Communications*, Vol.39, No.11, Nov. 1991, pp1625 – 1634

[29] H. M. H. Shalaby: Synchronous fiber-optic CDMA systems with interference estimators. *IEEE/OSA Journal of Lightwave Technology*, Vol.17, No.11, Nov. 1999, pp2268 – 2275

[30] Z. Kostic: The design and performance analysis for several new classes of codes for optical synchronous CDMA and for arbitrary-medium time-hopping synchronous CDMA systems. *IEEE Trans. on Communications*, Vol.42, No.8, 1994, pp2608 – 2617

[31] Svetislav V. Marie, and Edward L. Titlebaum: A Class of Frequency Hop Codes with Nearly Ideal Characteristics for Use in Multiple-Access Spread-Spectrum Communications and Radar and Sonar Systems. *IEEE Trans. on Communications*, Vol.40, No. 9, September 1992, pp1442 – 1447

[32] Menghui Zheng and Alexander Albicki: A Modified Hyperbolic Congruential Frequency Hop Codes for Asynchronous Event Signaling. IEEE, 1995, pp666 – 670

[33] Leszek D. Wronski. Razak Hossain, and Alexander Albicki: Extended Hyperbolic Congruential Frequency Hop Code: Generation and Bounds for Cross- and Auto-Ambiguity Function. *IEEE Trans. on Communications*, Vol. 44, No. 3, March 1996, pp301 – 305

[34] Razak Hossain, Leszek D. Wronski and Alexander Albicki: Signal Generation for Extended Hyperbolic Congruential Frequency Hop Codes. *IEEE Trans. on Cricuits and Systems-II*: *Analog and Digital Signal Processing*, Vol. 41, No. 1, January 1994, pp33 – 39

[35] Svetislav V. Maric, Edward L. Titlebaum: Frequency hop multiple access codes based upon the theory of cubic congruence. *IEEE Trans. on Aerospace and Electronic System*s, Vol.26, No.6, 1990, pp1035 – 1039

[36] Zhigang Cao, Yasheng Qian: The principle of modern telecommunication. Tsinghua University Press, 1992

[37] R. C. Dixon: Spread spectrum system. A Wiley-Interscience Publication, 1976, pp53 – 92

[38] V. K. Bhargava, D. Haccoun, R. Matyas and P. P. Nuspl: Digital communications by satellite-modulation, multiple access and coding. A Wiley-Interscience Publication, 1981, pp269 – 292

[39] Serdar Boztas, Roger Hammons and P Vijay Kumar: 4-phase sequences with near-optimum correlation properties. *IEEE Trans. on Information Theory*, Vol.38, No.3, May 1992, pp1101 – 1113

[40] P. R. Prucnal, et. al.: Optical code division multiple access: fundamentals and application. CRC Press, Taylor &Francis Group, 2006, pp55

[41] Sangin Kim, Kyungsik Yu, and Namkyoo Park: A New Family of Space/Wavelength/Time Spread Three-Dimensional Optical Code for OCDMA Networks. *IEEE/OSA Journal of Lightwave Technology*, Vol. 18, No. 4, April 2000, pp502 – 511

[42] L. Tancevski and I. Andonovic: Wavelength hopping/time spreading code division multiple access systems. *IEE Electronics Letters*, Vol.30, No.17, 1994, pp1388 – 1390

[43] G. -C. Yang and Wing C. Kwong: Performance Comparison of Multiwavelength CDMA and WDMA + CDMA for Fiber-Optic Networks. *IEEE Trans. on Communications*, Vol.45, No.11, November 1997, pp1426 – 1434

[44] W. C. Kwong, G.-C. Yang, V. Baba, C.-S. Bres, P. R. Prucnal: Multiple-wavlength optical orthogonal codes under prime-sequence permutations for optical CDMA. *IEEE Trans. on Communications*, Vol.53, No.1, Jan. 2005, pp117 – 123

[45] S. P. Wan and Y. Hu: Two-dimensional optical system with prime/OOC codes. *IEEE Photonics Technology Letters*, Vol.13, No.13, Dec. 2001, pp1373 – 1375

[46] L. Tancevski, Ivan Andonovic: Hybrid wavelength hopping/time spreading schemes for use in massive optical networks with increased security. *IEEE/OSA Journal of Lightwave Technology*, Vol.4, No.12, Dec. 1996, pp2636 – 2647

[47] L. Tancevski and I. Andonovic, M. Tur and J. Budin: Massive optical LANs using wavelength hopping/time spreading with increased security. *IEEE Photonics Technology Letters*, Vol.8, No.13, Jul. 1996, pp935 – 937

[48] Shurong Sun, Hongxi Yin, Ziyu Wang, Anshi Xu: A New Family of 2-D Optical Orthogonal Codes and Analysis of its Performance in Optical CDMA Access Networks. *IEEE/OSA Journal of Lightwave Technology*, Vol.24, No.4, 2006,pp1646 – 1653

[49] Rogério N. Nogueira, Antonio L. J. Teixeira, João L. Pinto, José F. Rocha: Polarization-Assisted OCDMA Using Fiber Bragg Gratings Written in Highly Birefringent Fibers. *IEEE Photonics Technology Letters*, Vol.18, No.7, 2006, pp841 – 843

[50] Y. Frignac, G. Charlet, W. Idler, R. Dischler, P. Tran, S. Lanne, S. Borne, C. Martinelli, G. Veith, A. Jourdan, J.-P. Hamaide, and S. Bigo: Transmission of 256 wavelength-division and polarization-division multiplexed channels at 42.7 Gb/s (10.2 Tb/s capacity) over 3×100 km of TeraLight fiber. OFC'2002, pp FC5-1 – FC5-3

[51] John E. McGeehan, S. M. R. Motaghian Nezam, P. Saghari, Alan E. Willner, Reza Omrani, P. Vijay Kumar: Experimental Demonstration of OCDMA Transmission Using a Three-Dimensional (Time-Wavelength-Polarization) Codeset. *IEEE/OSA Journal of Lightwave Technology*, Vol. 23, No. 10, 2005, pp3282 – 3286

[52] Svetislav V. Maric, Oscar Moreno, Carlos J. Corrada: Multimedia Transmission in Fiber-optic LAN's Using Optical CDMA. *IEEE/OSA Journal of Lightwave Technology*, Vol. 14, No. 10**,** 1996, pp2149 – 2153

[53] Wing C. Kwong, and Guu-Chang Yang: Multiple-Length Extended Carrier-Hopping Prime Codes for Optical CDMA Systems Supporting Multirate Multimedia Services. *IEEE/OSA Journal of Lightwave Technology*, Vol.23, No.11, 2005, pp3653 – 3662

[54] Naser G. Tarhuni, Timo O. Korhonen, Edward Mutafungwa, Mohammed S. Elmusrati: Multiclass Optical Orthogonal Codes for Multiservice Optical CDMA Networks. *IEEE/OSA Journal of Lightwave Technology*, Vol.24, No.2, 2006, pp694 – 704

[55] D.E. Leaird, Z. Jiang and A.M. Weiner: Experimental investigation of security issues in OCDMA: a code-switching scheme. *IEE Electronics Letters*, Vol.41 No.14, 2005, pp817 – 819

[56] Thomas H. Shake*:* Security Performance of Optical CDMA against Eavesdropping. *IEEE/OSA Journal of Lightwave Technology*, Vol. 23, No. 2, 2005, pp655 – 670

[57] Thomas H. Shake: Confidentiality Performance of Spectral-Phase-Encoded Optical CDMA. *IEEE/OSA Journal of Lightwave Technology*, Vol.23, No.4, April 2005, pp1652 – 1663

[58] Cedric F. Lam, Dennis T. K. Tong, Ming C. Wu, Eli Yablonovitch: Experimental Demonstration of Bipolar Optical CDMA System Using a Balanced Transmitter and Complementary Spectral Encoding. *IEEE Photonics Technology Letters*, Vol.10, No.10, 1998, pp1504 – 1506

3 Two-Dimensional OCDMA Codes

3.1 Introduction

The number of users in a OCDMA network using one-dimensional (1-D) incoherent time-domain encoding is very limited. This is because the number of subscribers is proportional to the length of frequency-spreading, whereas the data rate of a single user is inversely proportional to the length of frequency-spreading. Because the length of frequency-spreading is constrained by the current state-of-the-art, the larger the number of subscribers in a network, the more serious is the multiple access interference (MAI), or called multiple user interference (MUI). The bit error rate of the system increases and the number of subscribers that can communicate with each other simultaneously is small in practice. Aimed at the shortcoming of one-dimensional incoherent OCDMA codes, two-dimensional (2-D) wavelength-hopping/time-spreading incoherent OCDMA was proposed. It has been shown[1] that 2-D wavelength-hopping/time-spreading (WH/TS) encoding incoherent OCDMA systems, in general, perform better than OCDMA+WDMA (wavelength-division multiple-access) hybrid systems[32]. Even under the best scenario that a central controller is deployed to uniformly distribute all available wavelength to simultaneous subscribers in the hybrid scheme, the 2-D WH/TS scheme performs better if the traffic load is medium. Furthermore, when the traffic is heavy, the performance is much better. Therefore, in comparison with 1-D incoherent OCDMA systems, the incoherent OCDMA systems using 2-D WH/TS encoding not only allow increased number of users and simultaneous communication subscribers in a network, improving the performance of the network, but also simplify the network control and management, reducing processing time and alleviating the complexity and cost of hardware implementation.

This chapter introduces the definition of 2-D OCDMA codes that can be applied to 2-D incoherent OCDMA networks and the constructions of 2-D incoherent OCDMA codes with OOC, PC, EQCC, OCFHC (one-coincidence frequency-hopping code), m-sequence, Walsh-Hadamard code, CHPC (carrier-hopping prime code), etc. So far, 2-D incoherent OCDMA codes proposed in the references are mainly multiple-wavelength optical orthogonal codes (MWOOC)[1], PC/PC codes (prime codes for both wavelength-hopping and time-spreading)[7], PC/EQCC codes (prime codes for wavelength-hopping and extended quadratic congruence codes for time-spreading)[8, 9], OOC/PC codes (optical orthogonal codes for wavelength-hopping and prime codes for time-spreading)[10], PC/OOC codes (prime codes for wavelength-hopping and optical orthogonal codes for

time-spreading)[11, 12], OCFHC/OOC codes (one-coincidence frequency-hopping codes for wavelength-hopping and optical orthogonal codes for time-spreading)[14], B/U codes (one kind of bipolar code for wavelength-hopping and one kind of unipolar code for time-spreading)[16] and B/B[19] code (one kind of bipolar code for wavelength-hopping and another kind of bipolar code for time-spreading) using the differential detection, multiple-length extended wavelength-hopping prime codes (MLEWHPC)[27 – 30] for implementing multiple bit rate, multiple services and multiple quality-of-services (QoS), and so on. We will describe them one by one. Finally, we will analyze and compare the performances of these incoherent OCDMA codes.

A 2-D $(m \times n, w, \lambda_a, \lambda_c)$ wavelength-hopping/time-spreading (WH/TS) incoherent OCDMA code, or so-called multi-wavelength optical orthogonal code[1], C, is a set of binary $\{0,1\}$ $m \times n$ matrices, each Hamming weight being w. Each $m \times n$ matrix represents a codeword, which consists of m rows and n columns, where m is related to the number of available wavelengths and n is the code length, i.e., the number of time chips. The code length is determined by the bit period T and each bit period corresponds to n chips, or time slots. Each subscriber in a network is assigned a matrix as its own address signature. In the on-off keying OCDMA communication pattern, when a user wishes to convey a data bit "1", it transmits a sequence of pulses, in terms of the address matrix of its intended receiving node. The binary "1" in the i^{th} row will be sent with the i^{th} wavelength, $i \in [0, m-1]$. However, nothing will be sent for a data bit "0". Meanwhile, the 2-D $(m \times n, w, \lambda_a, \lambda_c)$ WH/TS codes also need to satisfy the following properties[1].

Autocorrelation Constraint. For any 2-D incoherent OCDMA codeword $X \in C$ and any integer τ $(0 < \tau < n)$, the binary discrete 2-D autocorrelation sidelobe of X is not larger than a nonnegative integer λ_a such that

$$\sum_{i=0}^{m-1} \sum_{j=0}^{n-1} x_{i,j} x_{i,j \oplus \tau} \leqslant \lambda_a \tag{3.1}$$

where $x_{i,j} \in \{0,1\}$ denotes an element of X at the i^{th} row and the j^{th} column, and "$\oplus$" represents modulo-n addition.

Cross-correlation constraint. For any two distinct 2-D incoherent OCDMA codewords $X, Y \in C$ $(X \neq Y)$ and any integer τ $(0 \leqslant \tau < n)$, the binary discrete 2-D cross-correlation of X and Y is not greater than a nonnegative integer λ_c such that

$$\sum_{i=0}^{m-1} \sum_{j=0}^{n-1} x_{i,j} y_{i,j \oplus \tau} \leqslant \lambda_c \tag{3.2}$$

where $y_{i,j} \in \{0,1\}$ denotes an element of Y at the i^{th} row and the j^{th} column.

There is at most one "1" in every column of each codeword of most 2-D WH/TS codes, such as multiple wavelength optical orthogonal codes, PC/PC codes, PC/OOC codes, OOC/PC codes, PC/EQCC codes, OCFHC/OOC codes, etc. There are multiple "1" in every column of each codeword of other 2-D WH/TS codes, for instance, 2-D bipolar/unipolar codes, 2-D bipolar/bipolar codes and so on. The schematic diagrams of codeword matrices of 2-D WH/TS codes are shown in Fig. 3.1.

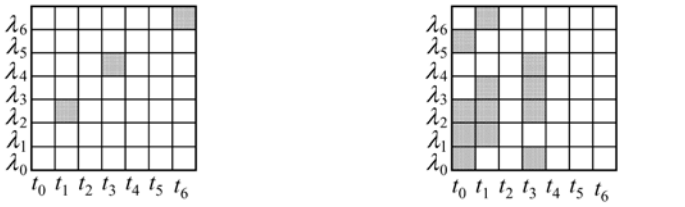

(a) {(2,1),(4,3),(6,6)}MWOOC

(b) $(C_0C_1 0C_2 000)$B/U 2-D W-T OC
C_0=(0,1,2,5) C_1=(1,2,3,6) C_2=(0,2,3,4)

Figure 3.1 Schematic diagrams of codeword matrices of 2-D WH/TS codes

Let $\Phi(m\times n, w, \lambda_a, \lambda_c) \equiv \max\{|C|, C \text{ is an } (m\times n, w, \lambda_a, \lambda_c) \text{ 2-D OCDMA code}\}$ be the upper bound on the cardinality of a 2-D OCDMA code, where $|C|$ denotes the cardinality of a 2-D OCDMA code. When $|C| = \Phi(m\times n, w, \lambda_a, \lambda_c)$, the 2-D OCDMA code is optimal. When $|C|$ is near $\Phi(m\times n, w, \lambda_a, \lambda_c)$, it is called asymptotically optimal 2-D OCDMA code.

When the autocorrelation constraint is equal to the cross-correlation constraint, i.e., $\lambda_a = \lambda_c = \lambda$, the upper bound[1] on the cardinality of a constant-weight symmetric 2-D OCDMA code obtained by the Johnson bound[2] of 1-D code is

$$\Phi(m\times n, w, \lambda, \lambda) \leqslant \frac{m(mn-1)(mn-2)\cdots(mn-\lambda)}{w(w-1)\cdots(w-\lambda)} \tag{3.3}$$

When the autocorrelation constraint does not equal the cross-correlation constraint, i.e., $\lambda_a > \lambda_c$, $\lambda_a = \lambda + k$ and $\lambda_c = \lambda$, the upper bound on the cardinality of a constant-weight asymmetric 2-D OCDMA code[1] is

$$\Phi(m\times n, w, \lambda + k, \lambda) \leqslant \frac{m(mn-1)(mn-2)\cdots(mn-\lambda)(\lambda+k)}{w(w-1)\cdots(w-\lambda)} \tag{3.4}$$

where k is any positive integer.

3.2 Multi-wavelength Optical Orthogonal Codes

We describe three constructions of MWOOC[1] in this section. One construction among them is an optimal construction of MWOOC based on that of the conventional 1-D OOC and the cardinality of MWOOC constructed by this method achieves the theoretical upper bound of equation (3.3). The other two constructions are based on the construction of the traditional frequency-hopping sequences. One is based on the prime sequences (PS) and another is based on Reed-Solomon codes (RS codes). The cardinalities of MWOOC obtained by these two constructions are near the theoretical upper bound of equation (3.3) and therefore, these MWOOCs are asymptotically optimal.

3.2.1 Constructions of MWOOCs Based on Constructions of 1-D OOCs

The construction of MWOOC based on the construction of 1-D OOC is as follows[1].

First of all, let n be a prime number such that $n = w(w-1)t+1$ for any given integer w and some integer t. The position blocks of any $(n,w,1,1)$-OOC[2–4] constructed are:

$$\{[a_{i,0}, a_{i,1}, a_{i,2}, \cdots, a_{i,j}, \cdots, a_{i,w-1}] : i \in [0, t-1]\} \tag{3.5}$$

where the element $a_{i,j}$ in the i^{th} block represents the displacement of the j^{th} pulse (i.e., a binary "1") in the i^{th} codeword.

After modifying these t position blocks of 1-D OOC, the following 2-D position blocks can be obtained:

$$\begin{aligned}&\{[(a_{i,0}+k(\bmod n), ja_{i,0}(\bmod n)), (a_{i,1}+k(\bmod n), ja_{i,1}(\bmod n)), (a_{i,2}+k(\bmod n),\\ &ja_{i,2}(\bmod n)), \cdots, (a_{i,j}+k(\bmod n), ja_{i,j}(\bmod n)), \cdots, (a_{i,w-1}+k(\bmod n),\\ &ja_{i,w-1}(\bmod n))] : i \in [0,t-1], j \in [0,n-1], k \in [0,n-1]\}\end{aligned} \tag{3.6}$$

and thus an $(n \times n, w, 1, 1)$-MWOOC is formed, where an ordered pair (v,h) denotes the vertical (v) and horizontal (h) displacements of a pulse from the bottom-leftmost corner of a matrix (namely, v represents the wavelength of the pulse and h represents the pulse position in time slot). Therefore, $n^2 t$ distinct codewords can be obtained.

Including the block

$$\{[(l, a_{i,0}), (l, a_{i,1}), (l, a_{i,2}), \cdots, (l, a_{i,j}), \cdots, (l, a_{i,w-1})] : i \in [0, t-1], l \in [0, n-1]\} \tag{3.7}$$

corresponding to the codewords, the cardinality of this $(n\times n,w,1,1)$-MWOOC is $n^2t+nt=n(n+1)t$.

Proof: See Ref.[1].

Since $|C|=n(n+1)t=\dfrac{n(n^2-1)}{w(w-1)}\geqslant \Phi(n\times n,w,1,1)\leqslant \dfrac{w(wn-1)}{w(w-1)}$, the cardinality of MWOOC constructed by this construction achieves the theoretical upper bound. Therefore, it is an optimal 2-D WH/TS OOC.

Assume that there is an $(n,w,1,1)$ OOC with the cardinality *t* and *n* wavelengths are employed such that the total cardinality is only *nt*. The cardinality of an $(n\times n,w,1,1)$-MWOOC is $(n+1)$ times as large as that of the WDMA+CDMA hybrid scheme of $(n,w,1,1)$-OOC + *w* wavelengths.

Example 3.1 Let $w=3$, $t=2$ and $n=13$. For the primitive element $\alpha=2$, we can get two codeword blocks [1,3,9] and [2,5,6] from an (13,3,1,1)-OOC. 364 codewords of an optimal $(13\times13,3,1,1)$-MWOOC can be constructed by using the construction whose position blocks of 2-D are as follows:

$$[(k,1),(k,3),(k,9)],\ [(k,2),(k,5),(k,6)],\ [(1+k,j),(3+k,3j),(9+k,9j)]$$

and $[(2+k,2j),(5+k,5j),(6+k,6j)]$, where $k\in[0,12]$ and $j\in[0,12]$.

3.2.2 2-D Constructions of MWOOCs

2-D approaches[1] use the modified frequency-hopping sequences such as the prime codes and RS (Reed-Solomon) codes to construct MWOOC. The 2-D WH/TS codes constructed with these two methods are called the generalized multi-wavelength prime codes (GMWPC) and the generalized multi-wavelength Reed-Solomon codes (GMWRSC).

3.2.2.1 Construction of GMWPC with $p_1p_2\cdots p_k$ Codewords[1]

Given an integer *c* and a set of prime numbers $p_k,p_{k-1},\cdots,p_1$ such that $p_k\geqslant p_{k-1}\geqslant\cdots\geqslant p_1\geqslant c$, then, the following 2-D blocks

$$\begin{aligned}&\{[(0,0),(1,i_1+i_2p_1+\cdots+i_kp_1p_2\cdots p_{k-1}),(2,2\otimes_{p_1}i_1+(2\otimes_{p_2}i_2)p_1+\cdots\\&+(2\otimes_{p_k}i_k)p_1p_2\cdots p_{k-1}),\cdots,(c-1,(c-1)\otimes_{p_1}i_1+((c-1)\otimes_{p_2}i_2)p_1,+\cdots\\&+((c-1)\otimes_{p_k}i_k)p_1p_2\cdots p_{k-1})]:i_1\in[0,p_1-1],i_2\in[0,p_2-1],\cdots,i_k\in[0,p_k-1]\}\end{aligned}\tag{3.8}$$

form an $(c\times p_1p_2\cdots p_k,c,0,1)$ GMWPC, *C*, with the cardinality $p_1p_2\cdots p_k$, where "$\otimes_{p_k}$" denotes modulo-p_k multiplication. Its autocorrelation sidelobe is zero and

its maximal value of cross-correlation function is 1.

Proof: See Ref. [1].

For the code with $m = c$, $n = p_1 p_2 \cdots p_k$, $w = c$ and $\lambda_a = \lambda_c = \lambda = 1$, from equation (3.3) we can obtain the upper bound on the cardinality

$$\begin{aligned}\Phi(c \times p_1 p_2 \cdots p_k, c, 1, 1) &\leqslant c(c \times p_1 p_2 \cdots p_k - 1)/c(c-1) \\ &= p_1 p_2 \cdots p_k + (p_1 p_2 \cdots p_k - 1)/(c-1).\end{aligned}$$

Compared with the cardinality of the $(c \times p_1 p_2 \cdots p_k, c, 0, 1)$-GMWPC, the upper bound is greater by a factor of $1/[1 + 1/(c-1) - 1/(c-1)p_1 p_2 \cdots p_k]$. When c becomes big enough, the factor is nearly equal to 1. Hence, this code is an asymptotically optimal code.

Example 3.2 Let $c = p_1 = p_2 = p_3 = 5$. This GMWPC has 125 codewords, X_{i_1, i_2, i_3}, which are denoted by the following blocks

$$\begin{aligned}&\{[(0,0),(1, i_1 + 5i_2 + 25i_3),(2, 2 \otimes_5 i_1 + (2 \otimes_5 i_2)5 + (2 \otimes_5 i_3)25), \\ &\quad (3,(3 \otimes_5 i_1 + (3 \otimes_5 i_2)5 + (3 \otimes_5 i_3)25)),(4, 4 \otimes_5 i_1 + (4 \otimes_5 i_2)5 + (4 \otimes_5 i_3)25)]: \\ &\quad i_1 \in [0,4], i_2 \in [0,4], i_3 \in [0,4]\}.\end{aligned}$$

For example, $X_{3,1,1}$ is a 5×125 matrix, which corresponds to the block [(0,0), (1,33),(2,61),(3,94),(4,122)].

3.2.2.2 Construction of GMWRSC with $p_1 p_2 \cdots p_k$ Codewords[1]

A Reed-Solomon (RS) code with the length $N = p - 1$ over a Galois field $GF(p)$ of a prime number p is a cyclic code with a generator polynomial

$$g(x) = (x - \alpha^b)(x - \alpha^{b+1}) \cdots (x - \alpha^{b+\delta-2}) \tag{3.9}$$

where α is a primitive element of $GF(p)$, δ is the minimum distance, and the integer b (with a typical value of 1) determine the starting terms of $g(x)$ [5, 6]. A codeword of such a $[N, K, \delta]$ RS code, $c = (c_0, c_1, \cdots, c_j, \cdots, c_{p-2})$, is usually denoted in a polynomial form, that is, $c(x) = c_0 + c_1 x + \cdots + c_j x^j + \cdots + c_{p-2} x^{p-2}$, where $c_j \in GF(p)$ is the polynomial coefficient and $K = N - \delta + 1$ is the code dimension. The code cardinality Φ is usually associated with the dimension K, namely, $\Phi = p^K$. Moreover, the codeword can also be represented as $c(x) = z(x)g(x)$, where $z(x)$ is the information polynomial of c.

For example, suppose $\delta = N - 1$ (i.e., $K = 2$) and $b = 1$, then we have $g(x) = (x - \alpha)(x - \alpha^2) \cdots (x - \alpha^{p-3})$. The codeword with $z(x) = 1$ is represented by $\overline{a}_0 = (a_0, a_1, \cdots, a_j, \cdots, a_{p-2})$, where $a_j \in GF(p)$. We obtain p codewords as $\overline{a}_i = (a_{i,0}, a_{i,1}, \cdots, a_{i,j}, \cdots, a_{i,p-2})$ with $i = \{0, 1, \cdots, p-1\}$, where $a_{i,j} = a_j \oplus_p i$ and

"$\oplus_p$" denotes modulo-p addition[6]. All these codewords are the qualified candidates for the construction of GMWRSC.

Now that we have reviewed this background of RS codes, we proceed to study the construction of GMWRSC.

Assume a set of prime numbers $p_1, p_2, \cdots, p_k$ such that $p_k \geqslant p_{k-1} \geqslant \cdots \geqslant p_1$. After the codewords of a 1-D RS code $\overline{a}_i$ for $i \in [0, p_1 - 1]$ are modified, we can obtain the following 2-D blocks

$$[(a_{i,0}, 0), (a_{i,1}, 1), \cdots, (a_{i,j}, j), \cdots, (a_{i,p_1-2}, p_1 - 2)] \tag{3.10}$$

which are the bases of the generalized code. Then, the blocks

$$\begin{aligned}
&\{[(a_{i,0} \oplus l, ((a_{i,0} \oplus l) \otimes_{p_2} i_2)(p_1 - 1) + \cdots + ((a_{i,0} \oplus l) \otimes_{p_k} i_k)(p_1 - 1)p_2 \cdots p_{k-1}),\\
&(a_{i,1} \oplus l, 1 + ((a_{i,1} \oplus l) \otimes_{p_2} i_2)(p_1 - 1) + \cdots + ((a_{i,1} \oplus l) \otimes_{p_k} i_k)(p_1 - 1)p_2 \cdots p_{k-1}), \cdots,\\
&(a_{i,p_1-2} \oplus l, (p_1 - 2) + ((a_{i,p_1-2} \oplus l) \otimes_{p_2} i_2)(p_1 - 1) + \cdots + ((a_{i,p_1-2} \oplus l) \otimes_{p_k} i_k)\\
&(p_1 - 1)p_2 \cdots p_{k-1})] : l = \{0, 1, 2, \cdots, p_1 - 1\}, i_2 \in \{0, 1, 2, \cdots, p_2 - 1\}, \cdots,\\
&i_k \in \{0, 1, 2, \cdots, p_k - 1\}\}
\end{aligned} \tag{3.11}$$

form an $(p_1 \times (p_1 - 1)p_2 \cdots p_k, p_1 - 1, 0, 1)$-GMWRSC with the cardinality $p_1 p_2 \cdots p_k$. Its autocorrelation sidelobe is zero and the value of its cross-correlation function is at most 1. "$\oplus$" denotes modulo-p_1 addition and "$\otimes_{p_k}$" indicates modulo-p_k multiplication.

Proof: See Ref. [1].

For a GMWRSC with $m = p_1$, $n = (p_1 - 1)p_2 \cdots p_k$, $w = p_1 - 1$ and $\lambda_a = \lambda_c = \lambda = 1$, from equation (3.3), we can obtain the upper bound

$$\begin{aligned}
\Phi(p_1 \times (p_1 - 1)p_2 \cdots p_k, p_1 - 1, 1, 1) &\leqslant p_1(p_1(p_1 - 1)p_2 \cdots p_k - 1)/(p_1 - 1)(p_1 - 2)\\
&= p_1 p_2 \cdots p_k + (2p_1(p_1 - 1)p_2 \cdots p_k - p_1)/(p_1 - 1)(p_1 - 2).
\end{aligned}$$

In comparison with the cardinality of $(p_1 \times (p_1 - 1)p_2 \cdots p_k, p_1 - 1, 0, 1)$ GMWRSC, the upper bound is greater by a factor of $1/[1 + 2/(p_1 - 2) - 1/(p_1 - 1)(p_1 - 2)p_2 \cdots p_k]$. When p_1 is large enough, the factor is nearly equal to 1. Hence, this code is asymptotically optimal.

Example 3.3 Let $p_1 = 5$. The generator polynomial is $g(x) = (x - \alpha)(x - \alpha^2)$. Thus, we get the codewords: $\overline{a}_0$ =(0,1,4,3), $\overline{a}_1$ = (1,2,0,4), $\overline{a}_2$ = (2,3,1,0), $\overline{a}_3$ = (3,4,2,1) and $\overline{a}_4$ = (4,0,3,2). The corresponding two-dimensional blocks: [(0,0), (1,1),(4,2),(3,3)], [(1,0),(2,1),(0,2),(4,3)], [(2,0),(3,1),(1,2),(0,3)], [(3,0),(4,1), (2,2),(1,3)] and [(4,0),(0,1),(3,2),(2,3)] are the basis to generate the GMWRSC.

Assuming $p_2 = 7$, the resulting $(5 \times 28, 4, 0, 1)$ GMWRSC have $p_1 \times p_2 = 5 \times 7 = 35$ codewords, which are denoted by the following 2-D clocks

$$\{[(l, (l \otimes_7 i_2)4), (1 \oplus l, 1 + ((1 \oplus l) \otimes_7 i_2)4), (4 \oplus l, 2 + ((4 \oplus l) \otimes_7 i_2)4), \\ (3 \oplus l, 3 + ((3 \oplus l) \otimes_7 i_2)4)] : l \in [0, 4], i_2 \in [0, 6]\}$$

where " $\oplus$ " represents modulo-5 addition and " $\otimes_7$ " indicates modulo-7 multiplication.

3.2.3 Performance Analysis of BER of MWOOCs

In order to focus on the performance comparison of three MWOOCs, only the impact of multiple access interferences on the performance of OCDMA system using MWOOC is taken into account and the influences of thermal noise and shot noise in the photo-detector are neglected. Meanwhile, for the sake of mathematical convenience, chip synchronization is also assumed, which corresponds to the worst scenario, i.e., the upper bound of BER. Because the thermal noise and shot noise are not considered here, an error bit occurs only when the accumulative multiple access interference at a particular subscriber, which is receiving a bit "0", reaches an amount that exceeds the decision threshold. In this case, BER of the multi-wavelength system[1] with $(n \times n, w, 1, 1)$ MWOOC is

$$P_{\mathrm{b}} = \frac{1}{2} \sum_{i=Th}^{N-1} \binom{N-1}{i} \left(\frac{w^2}{2n^2} \right) \left(1 - \frac{w^2}{2n^2} \right)^{N-1-i} \tag{3.12}$$

where *Th* denotes the decision threshold of a receiver. For the optimal decision, *Th* is usually set to the code weight. *N* indicates the number of users in a system.

Supposing p to be a prime number, BER of an OCDMA system using an $(p \times p^2, p, 0, 1)$ GMWPC[1] is

$$P_{\mathrm{b}} = \frac{1}{2} \sum_{i=Th}^{N-1} \binom{N-1}{i} \left(\frac{p}{2p^2} \right)^i \left(1 - \frac{p}{2p^2} \right)^{N-1-i} \tag{3.13}$$

where *Th* is set to the code weight p.

BER of an OCDMA system using a $(p \times (p-1)p, p-1, 0, 1)$ GMWRSC[1] is

$$P_{\mathrm{b}} = \frac{1}{2} \sum_{i=Th}^{N-1} \binom{N-1}{i} \left(\frac{p-1}{2p^2} \right)^i \left(1 - \frac{p-1}{2p^2} \right)^{N-1-i} \tag{3.14}$$

where *Th* is set to the code weight $p-1$.

Assume that a central controller is deployed in the hybrid scheme. BER versus the number of simultaneous subscribers for GMWRSC system and WDMA+CDMA hybrid system with OOCs for various values of a prime number p is shown in Fig. 3.2[1]. Under the scenario of medium traffic load, it can be seen that the multi-wavelength scheme has more users and has better performance compared with the WDMA+CDMA hybrid scheme, which uses a central controller to uniformly distribute all available wavelengths to N simultaneous subscribers. Especially, if the traffic load is heavy, the former performs better than the latter. In addition, the network management, control and communication protocol will become complicated and the processing time delay and cost will increase in the hybrid scheme.

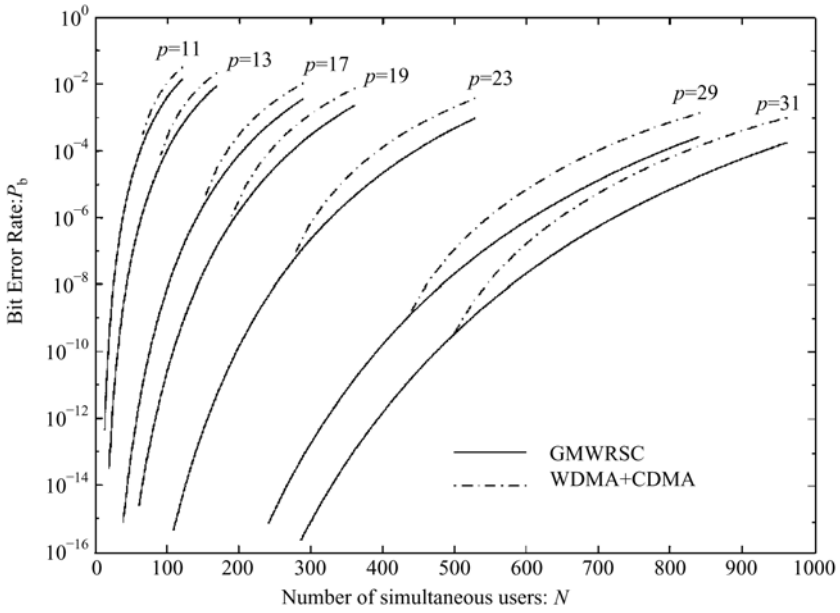

Figure 3.2 Curves of bit-error-rate versus the number of simultaneous subscribers for GMWRSC system and hybrid system with OOCs for various values of a prime number p (Adapted from Ref.[1], with permission from IEEE © 2007)

3.3 2-D PC/PC Codes

2-D PC/PC codes[7] can be obtained by using prime codes (PC) for both wavelength-hopping and time-spreading. We illustrate the construction of 2-D PC/PC codes with an example.

Example 3.4 Let a prime number $p = 5$. We can obtain the prime sequences and the prime code shown in Table 3.1. These prime sequences are respectively

$s_0 = (0\ 0\ 0\ 0\ 0)$, $s_1 = (0\ 1\ 2\ 3\ 4)$, $s_2 = (0\ 2\ 4\ 1\ 3)$, $s_3 = (0\ 3\ 1\ 4\ 2)$ and $s_4 = (0\ 4\ 3\ 2\ 1)$. Furthermore, let $H_1 = (0\ 1\ 2\ 3\ 4)$, $H_2 = (0\ 2\ 4\ 1\ 3)$, $H_3 = (0\ 3\ 1\ 4\ 2)$ and $H_4 = (0\ 4\ 3\ 2\ 1)$. $s_i (i = 0,1,\cdots, p-1)$ is employed as time-spreading and $H_i (i = 1,\cdots, p-1)$ is deployed to determine wavelength-hopping. Because the wavelength-hopping pattern obtained for $i = 0$ is meaningless, there is no H_0.

Table 3.1 Prime codes obtained for the prime number $p = 5$

i \ j	0	1	2	3	4		Prime codes corresponding to s_i
0	(s_0)	0	0	0	0	0	10000 10000 10000 10000 10000
1	(s_1)	0	1	2	3	4 (H_1)	10000 01000 00100 00010 00001
2	(s_2)	0	2	4	1	3 (H_2)	10000 00100 00001 01000 00010
3	(s_3)	0	3	1	4	2 (H_3)	10000 00010 01000 00001 00100
4	(s_4)	0	4	3	2	1 (H_4)	10000 00001 00010 00100 01000

Every "1" pulse of each codeword corresponds to a different wavelength for the prime code in Table 3.1 and the choice of wavelengths is determined by H_i. Hence, The codewords of 2-D PC/PC WH/TS codes constructed are shown in Table 3.2.

From Table 3.2, it can be seen that any two codewords either have different wavelength-hopping or possess different time-spreading. For instance, although the codewords $s_0 H_1$ and $s_0 H_2$ have the same time-spreading, they possess different wavelength-hopping. Whereas, while the wavelength-hopping of $s_0 H_1$ and $s_1 H_1$ is the same, their time-spreadings are different. Therefore, the maximal value of cross-correlation function of the 2-D PC/PC code is one and the sidelobes of its autocorrelation are zero.

The code length of 2-D PC/PC code, i.e., the number of time slots (chips), is $n = p^2$. The number of available wavelengths and the code weight are $m = p$ and $w = p$ respectively. The constraints of autocorrelation and cross-correlation are $\lambda_a = 0$ and $\lambda_c = 1$ respectively. Hence, the parameters of this code is $(m \times n, w, \lambda_a, \lambda_c) = (p \times p^2, p, 0, 1)$. The peak value of autocorrelation is equal to the code weight p and the cardinality is $|C|_{\text{PC/PC}} = p(p-1)$. Although its cardinality is smaller than the cardinality of 1-D OCDMA+WDMA hybrid system (namely, p^2) using one-dimensional PC, the properties of autocorrelation and cross-correlation of this code have been considerably improved. (The original 1-D OCDMA system has $\lambda_a = p - 1$ and $\lambda_c = 2$.) Thus, the real asynchronous OCDMA communication can be implemented.

Table 3.2 2-D PC/PC Codes

	2-D PC/PC codewords				
$s_0\ H_1$	$\lambda_0\ 0000$	$\lambda_1\ 0000$	$\lambda_2\ 0000$	$\lambda_3\ 0000$	$\lambda_4\ 0000$
$s_0\ H_2$	$\lambda_0\ 0000$	$\lambda_2\ 0000$	$\lambda_4\ 0000$	$\lambda_1\ 0000$	$\lambda_3\ 0000$
$s_0\ H_3$	$\lambda_0\ 0000$	$\lambda_3\ 0000$	$\lambda_1\ 0000$	$\lambda_4\ 0000$	$\lambda_2\ 0000$
$s_0\ H_4$	$\lambda_0\ 0000$	$\lambda_4\ 0000$	$\lambda_3\ 0000$	$\lambda_2\ 0000$	$\lambda_1\ 0000$
$s_1\ H_1$	$\lambda_0\ 0000$	$0\ \lambda_1\ 000$	$00\ \lambda_2\ 00$	$000\ \lambda_3\ 0$	$0000\ \lambda_4$
$s_1\ H_2$	$\lambda_0\ 0000$	$0\ \lambda_2\ 000$	$00\ \lambda_4\ 00$	$000\ \lambda_1\ 0$	$0000\ \lambda_3$
$s_1\ H_3$	$\lambda_0\ 0000$	$0\ \lambda_3\ 000$	$00\ \lambda_1\ 00$	$000\ \lambda_4\ 0$	$0000\ \lambda_2$
$s_1\ H_4$	$\lambda_0\ 0000$	$0\ \lambda_4\ 000$	$00\ \lambda_3\ 00$	$000\ \lambda_2\ 0$	$0000\ \lambda_1$
$s_2\ H_1$	$\lambda_0\ 0000$	$00\ \lambda_1\ 00$	$0000\ \lambda_2$	$0\ \lambda_3\ 000$	$000\ \lambda_4\ 0$
$s_2\ H_2$	$\lambda_0\ 0000$	$00\ \lambda_2\ 00$	$0000\ \lambda_4$	$0\ \lambda_1\ 000$	$000\ \lambda_3\ 0$
$s_2\ H_3$	$\lambda_0\ 0000$	$00\ \lambda_3\ 00$	$0000\ \lambda_1$	$0\ \lambda_4\ 000$	$000\ \lambda_2\ 0$
$s_2\ H_4$	$\lambda_0\ 0000$	$00\ \lambda_4\ 00$	$0000\ \lambda_3$	$0\ \lambda_2\ 000$	$000\ \lambda_1\ 0$
$s_3\ H_1$	$\lambda_0\ 0000$	$000\ \lambda_1\ 0$	$0\ \lambda_2\ 000$	$0000\ \lambda_3$	$00\ \lambda_4\ 00$
$s_3\ H_2$	$\lambda_0\ 0000$	$000\ \lambda_2\ 0$	$0\ \lambda_4\ 000$	$0000\ \lambda_1$	$00\ \lambda_3\ 00$
$s_3\ H_3$	$\lambda_0\ 0000$	$000\ \lambda_3\ 0$	$0\ \lambda_1\ 000$	$0000\ \lambda_4$	$00\ \lambda_2\ 00$
$s_3\ H_4$	$\lambda_0\ 0000$	$000\ \lambda_4\ 0$	$0\ \lambda_3\ 000$	$0000\ \lambda_2$	$00\ \lambda_1\ 00$
$s_4\ H_1$	$\lambda_0\ 0000$	$0000\ \lambda_1$	$000\ \lambda_2\ 0$	$00\ \lambda_3\ 00$	$0\ \lambda_4\ 000$
$s_4\ H_2$	$\lambda_0\ 0000$	$0000\ \lambda_2$	$000\ \lambda_4\ 0$	$00\ \lambda_1\ 00$	$0\ \lambda_3\ 000$
$s_4\ H_3$	$\lambda_0\ 0000$	$0000\ \lambda_3$	$000\ \lambda_1\ 0$	$00\ \lambda_4\ 00$	$0\ \lambda_2\ 000$
$s_4\ H_4$	$\lambda_0\ 0000$	$0000\ \lambda_4$	$000\ \lambda_3\ 0$	$00\ \lambda_2\ 00$	$0\ \lambda_1\ 000$

From equation (3.3), we can obtain the upper bound on the cardinality of $(m \times n, w, \lambda_a, \lambda_c) = (p \times p^2, p, 1, 1)$ code as

$$\Phi(p \times p^2, p, 1, 1) \leqslant \frac{p(p^3 - 1)}{p(p-1)} = p^2 + p + 1$$

It can be seen that the cardinality of 2-D PC/PC code does not reach the theoretical upper bound. The main advantage of 2-D PC/PC code is that its construction is simple.

3.4 2-D PC/EQCC Codes

2-D PC/EQCC code[8, 9] is constructed by using prime codes and their cyclic shifts for wavelength-hopping and extended quadratic congruence codes for time-spreading. The construction of 2-D PC/EQCC code is as follows.

(1) Choose a prime number p and construct $(p-1)$ codewords of EQCC using the construction of EQCC described in section 2.6.2.

(2) Based on the prime number p, construct a shifted prime sequence

$$S_i(k) = (s_{i,0}(k), s_{i,1}(k), \cdots, s_{i,j}(k), \cdots, s_{i,p-1}(k))$$
$$i = 1,2,\cdots,p-1, \quad j = 0,1,\cdots,p-1, \quad k = 0,1,\cdots,p-1 \tag{3.15}$$

where $S_i(k)$ represents the cyclic shift of the prime sequence S_i. The element in the sequence is

$$s_{i,j}(k) = [i \cdot j - k + p](\text{mod } p)$$
$$i = 1,2,\cdots,p-1, \quad j = 0,1,\cdots,p-1, \quad k = 0,1,\cdots,p-1 \tag{3.16}$$

It can be seen that $S_i(0),\ i = 1,2,\cdots,p-1,$ is a prime sequence for $k = 0$, which has $p-1$ non-all-zero elements. This is because the prime sequence with all-zero elements is meaningless when it is mapped into a wavelength sequence and therefore, it is not taken into account. Again let k range between 1 and $p-1$, that is, $S_i(0)$ is circularly shifted by $(p-1)$ times. $(p-1)$ shifting sequences can be obtained and $(p-1)\times(p-1)$ cyclic shift sequences can be acquired totally. Including $(p-1)$ sequences from $S_i(0)$, $p(p-1)$ sequences can be produced in all.

(3) Let the elements in the $p(p-1)$ sequences be the numbers of wavelength we can obtain $p(p-1)$ sequences consisting of wavelengths $W_i(k)$ as follows:

$$W_i(k) = (\lambda_{s_{i,0}(k)}, \lambda_{s_{i,1}(k)}, \cdots, \lambda_{s_{i,j}(k)}, \cdots, \lambda_{s_{i,p-1}(k)})$$
$$i = 1,2,\cdots,p-1, \quad j = 0,1,\cdots,p-1, \quad k = 0,1,\cdots,p-1 \tag{3.17}$$

(4) The $p(p-1)$ wavelength sequences are mapped into $p-1$ code sequences of EQCC and then $p(p-1)^2$ codewords of the 2-D PC/EQCC code can be obtained.

2-D PC/EQCC code has the parameter of $(m \times n, w, \lambda_a, \lambda_c) = (p \times p(2p-1), p, 0, 2)$, which employs p wavelengths and $p(2p-1)$ time slots (chips), i.e., the code length. Because every "1" pulse in each codeword uses a different wavelength, the constraint of its autocorrelation is zero, i.e., $\lambda_a = 0$. Since the maximal value of cross-correlation function for EQCC is equal to 2, the cross-correlation constraint of 2-D PC/EQCC code is $\lambda_c = 2$. Its cardinality is $|C| = p(p-1)^2$, which is much less than the theoretical upper bound on the cardinality of equation (3.3).

Example 3.5 Assuming $p = 5$, an EQCC code constructed is shown in Table 3.3. When $p = 5$, non-all-zero prime sequences and their cyclic shift sequences $S_i(k),\ i = 1,2,3,4,\ k = 0,1,2,3,4,$ are shown in Table 3.4. Furthermore, $S_i(k)$ are

mapped into the wavelength sequences $W_i(k)$, $i=1,2,3,4$ and $k=0,1,2,3,4$, which are shown in Table 3.5.

Table 3.3 Extended Quadratic Congruence Codes for $p=5$

QC sequence	EQCC code				
0 1 3 1 0	100000000	010000000	000100000	010000000	100000000
0 2 1 2 0	100000000	001000000	010000000	001000000	100000000
0 3 4 3 0	100000000	000100000	000010000	000100000	100000000
0 4 2 4 0	100000000	000010000	001000000	000010000	100000000

Table 3.4 Prime sequences and their cyclic shift sequences $S_i(k)$

i	$S_i(0)$	$S_i(1)$	$S_i(2)$	$S_i(3)$	$S_i(4)$
1	01234	40123	34012	23401	12340
2	02413	41302	30241	24130	13024
3	03142	42031	31420	20314	14203
4	04321	43210	32104	21043	10432

Table 3.5 Wavelength Sequences $W_i(k)$ corresponding to $S_i(k)$

$W_i(0)$	$W_i(1)$	$W_i(2)$	$W_i(3)$	$W_i(4)$
$\lambda_0\ \lambda_1\ \lambda_2\ \lambda_3\ \lambda_4$	$\lambda_4\ \lambda_0\ \lambda_1\ \lambda_2\ \lambda_3$	$\lambda_3\ \lambda_4\ \lambda_0\ \lambda_1\ \lambda_2$	$\lambda_2\ \lambda_3\ \lambda_4\ \lambda_0\ \lambda_1$	$\lambda_1\ \lambda_2\ \lambda_3\ \lambda_4\ \lambda_0$
$\lambda_0\ \lambda_2\ \lambda_4\ \lambda_1\ \lambda_3$	$\lambda_4\ \lambda_1\ \lambda_3\ \lambda_0\ \lambda_2$	$\lambda_3\ \lambda_0\ \lambda_2\ \lambda_4\ \lambda_1$	$\lambda_2\ \lambda_4\ \lambda_1\ \lambda_3\ \lambda_0$	$\lambda_1\ \lambda_3\ \lambda_0\ \lambda_2\ \lambda_4$
$\lambda_0\ \lambda_3\ \lambda_1\ \lambda_4\ \lambda_2$	$\lambda_4\ \lambda_2\ \lambda_0\ \lambda_3\ \lambda_1$	$\lambda_3\ \lambda_1\ \lambda_4\ \lambda_2\ \lambda_0$	$\lambda_2\ \lambda_0\ \lambda_3\ \lambda_1\ \lambda_4$	$\lambda_1\ \lambda_4\ \lambda_2\ \lambda_0\ \lambda_3$
$\lambda_0\ \lambda_4\ \lambda_3\ \lambda_2\ \lambda_1$	$\lambda_4\ \lambda_3\ \lambda_2\ \lambda_1\ \lambda_0$	$\lambda_3\ \lambda_2\ \lambda_1\ \lambda_0\ \lambda_4$	$\lambda_2\ \lambda_1\ \lambda_0\ \lambda_4\ \lambda_3$	$\lambda_1\ \lambda_0\ \lambda_4\ \lambda_3\ \lambda_2$

Afterwards, the wavelength of the wavelength sequences in Table 3.5 are orderly filled to the position of "1" in each EQCC codeword in Table 3.3. In doing so, a 2-D PC/EQCC codes obtained are shown in Table 3.6. The total number of codewords is $p(p-1)^2=5\times(5-1)^2=80$.

Using similar approach, a 2-D QCC/PC code with the parameters $(m\times n, w, \lambda_a, \lambda_c) = (p\times p^2, p, 0, 2)$ can also be constructed. The cardinality of this code is $|C|=p^2(p-1)$. We only give one example of constructing a 2-D QCC/PC code.

Example 3.6 Assuming $p=5$, a prime code constructed is shown in Table 3.7. From $p=5$, the quadratic congruence sequences and their cyclic shift versions $S_i(k)$ for $i=1,2,3,4$ and $k=0,1,2,3,4$, are shown in Table 3.8. Furthermore, $S_i(k)$ are mapped into the wavelength sequences $W_i(k)$, $i=1,2,3,4$ and $k=0,1,2,3,4$, are shown in Table 3.9.

Table 3.6 2-D PC/EQCC codes for $p = 5$

1：	λ_0 00000000	0 λ_1 0000000	000 λ_2 00000	0 λ_3 0000000	λ_4 00000000
			……		
20：	λ_1 00000000	0 λ_0 0000000	000 λ_4 00000	0 λ_3 0000000	λ_2 00000000
21：	λ_0 00000000	00 λ_1 000000	0 λ_2 0000000	00 λ_3 000000	λ_4 00000000
			……		
40：	λ_1 00000000	00 λ_0 000000	0 λ_4 0000000	00 λ_3 000000	λ_2 00000000
41：	λ_0 00000000	000 λ_1 00000	0000 λ_2 0000	000 λ_3 00000	λ_4 00000000
			……		
60：	λ_1 00000000	000 λ_0 00000	0000 λ_4 0000	000 λ_3 00000	λ_2 00000000
61：	λ_0 00000000	0000 λ_1 0000	00 λ_2 000000	0000 λ_3 0000	λ_4 00000000
			……		
80：	λ_1 00000000	0000 λ_0 0000	00 λ_4 000000	0000 λ_3 0000	λ_2 00000000

Table 3.7 Prime Codes for $p = 5$

Prime sequence	Prime code				
00000	10000	10000	10000	10000	10000
01234	10000	01000	00100	00010	00001
02413	10000	00100	00001	01000	00010
03142	10000	00010	01000	00001	00100
04321	10000	00001	00010	00100	01000

Table 3.8 Quadratic congruence sequences and their cyclic shift versions $S_i(k)$

i	$S_i(0)$	$S_i(1)$	$S_i(2)$	$S_i(3)$	$S_i(4)$
1	01310	40204	34143	23032	12421
2	02120	41014	30403	24342	13231
3	03430	42324	31213	20102	14041
4	04240	43134	32023	21412	10301

Table 3.9 Wavelength sequences $W_i(k)$ corresponding to $S_i(k)$

$W_i(0)$	$W_i(1)$	$W_i(2)$	$W_i(3)$	$W_i(4)$
$\lambda_0\ \lambda_1\ \lambda_3\ \lambda_1\ \lambda_0$	$\lambda_4\ \lambda_0\ \lambda_2\ \lambda_0\ \lambda_4$	$\lambda_3\ \lambda_4\ \lambda_1\ \lambda_4\ \lambda_3$	$\lambda_2\ \lambda_3\ \lambda_0\ \lambda_3\ \lambda_2$	$\lambda_1\ \lambda_2\ \lambda_4\ \lambda_2\ \lambda_1$
$\lambda_0\ \lambda_2\ \lambda_1\ \lambda_2\ \lambda_0$	$\lambda_4\ \lambda_1\ \lambda_0\ \lambda_1\ \lambda_4$	$\lambda_3\ \lambda_0\ \lambda_4\ \lambda_0\ \lambda_3$	$\lambda_2\ \lambda_4\ \lambda_3\ \lambda_4\ \lambda_2$	$\lambda_1\ \lambda_3\ \lambda_2\ \lambda_3\ \lambda_1$
$\lambda_0\ \lambda_3\ \lambda_4\ \lambda_3\ \lambda_0$	$\lambda_4\ \lambda_2\ \lambda_3\ \lambda_2\ \lambda_4$	$\lambda_3\ \lambda_1\ \lambda_2\ \lambda_1\ \lambda_3$	$\lambda_2\ \lambda_0\ \lambda_1\ \lambda_0\ \lambda_2$	$\lambda_1\ \lambda_4\ \lambda_0\ \lambda_4\ \lambda_1$
$\lambda_0\ \lambda_4\ \lambda_2\ \lambda_4\ \lambda_0$	$\lambda_4\ \lambda_3\ \lambda_1\ \lambda_3\ \lambda_4$	$\lambda_3\ \lambda_2\ \lambda_0\ \lambda_2\ \lambda_3$	$\lambda_2\ \lambda_1\ \lambda_4\ \lambda_1\ \lambda_2$	$\lambda_1\ \lambda_0\ \lambda_3\ \lambda_0\ \lambda_1$

Afterwards, the wavelengths in the wavelength sequences in Table 3.9 are orderly filled to the positions of 1's in each codeword of PC in Table 3.7. Then, the resulting 2-D QCC/PC code is shown in Table 3.10. The total number of codewords is $p^2(p-1)=5^2\times(5-1)=100$.

Table 3.10 2-D QCC/PC Codes for $p=5$

1:	λ_0 0000	λ_1 0000	λ_3 0000	λ_1 0000	λ_0 0000
			……		
20:	λ_1 0000	λ_0 0000	λ_3 0000	λ_0 0000	λ_1 0000
21:	λ_0 0000	0 λ_1 000	00 λ_3 00	000 λ_1 0	0000 λ_0
			……		
40:	λ_1 0000	0 λ_0 000	00 λ_3 00	000 λ_0 0	0000 λ_1
41:	λ_0 0000	00 λ_1 00	0000 λ_3	0 λ_1 000	000 λ_0 0
			……		
60:	λ_1 0000	00 λ_0 00	0000 λ_3	0 λ_0 000	000 λ_1 0
61:	λ_0 0000	000 λ_1 0	0 λ_3 000	0000 λ_1	00 λ_0 00
			……		
80:	λ_1 0000	000 λ_0 0	0 λ_3 000	0000 λ_0	00 λ_1 00
81:	λ_0 0000	0000 λ_1	000 λ_3 0	00 λ_1 00	0 λ_0 000
			……		
100:	λ_1 0000	0000 λ_0	000 λ_3 0	00 λ_0 00	0 λ_1 000

3.5 2-D OOC/PC Codes

A 2-D OOC/PC code[10] is constructed by using one-dimensional OOC for wavelength-hopping and prime code for time-spreading. Its construction is as follows:

(1) First of all, an $(n,w,\lambda)=(n_{\mathrm{OOC}},p,1)$ OOC with the cardinality $|C|_{\mathrm{OOC}}$ is constructed by the constructions introduced in Chapter 2, whose codewords are

$$\begin{aligned} &C_i=(i_0^{(i)},i_1^{(i)},\cdots,i_k^{(i)},\cdots,i_{w-1}^{(i)}),\quad 0\leqslant i_k^{(i)}\leqslant n-1,\quad k=0,1,\cdots,w-1\\ &i=0,1,\cdots,|C|_{\mathrm{OOC}}-1 \end{aligned} \tag{3.18}$$

(2) Map C_i to the wavelength sequence $H_{i,j}$

$$\begin{aligned} &H_{i,j}=(\lambda_{i_0^{(i)}\oplus j},\lambda_{i_1^{(i)}\oplus j},\cdots,\lambda_{i_k^{(i)}\oplus j},\cdots,\lambda_{i_{w-1}^{(i)}\oplus j}),\quad 0\leqslant i_k^{(i)}\leqslant n-1,\quad k=0,1,\cdots,w-1\\ &i=0,1,\cdots,|C|_{\mathrm{OOC}}-1,\quad j=0,1,\cdots,n_{\mathrm{OOC}}-1 \end{aligned} \tag{3.19}$$

(3) Construct a prime code for a prime number p. Then, $H_{i,j}$ is mapped to the position of "1" in the prime code D_k, $k = 0,1,\cdots,p-1$, one by one.

An $(m \times n, w, \lambda_a, \lambda_c)$ OCDMA code can be constructed by using this approach and the number of available wavelengths, m, corresponds to the code length of one-dimensional OOC, n_{OOC}, i.e., $m = n_{\text{OOC}}$. The number of time slots, i.e., the code length of the two-dimensional OCDMA code is equal to the length of prime code, p^2, and the code weight is $w = p$. Because there is no repeated wavelength in any codeword, the maximal autocorrelation sidelobe and the maximal value of cross-correlation function of 2-D OOC/PC are $\lambda_a = \lambda_c = 1$. Hence, the parameter of 2-D OOC/PC code is $(m \times n, w, \lambda_a, \lambda_c) = (n_{\text{OOC}} \times p^2, p, 1, 1)$ and its cardinality in all is $|C| = n_{\text{OOC}} \cdot |C|_{\text{OOC}} \cdot p$. Since the cardinality of one-dimensional OOC is $|C|_{\text{OOC}} \approx \frac{n_{\text{OOC}} - 1}{w(w-1)} = \frac{n_{\text{OOC}} - 1}{p(p-1)}$, then $|C| = n_{\text{OOC}} \cdot |C|_{\text{OOC}} \cdot p = \frac{n_{\text{OOC}}(n_{\text{OOC}} - 1)}{p-1}$. Moreover, the theoretical upper bound of the cardinality of an $(n_{\text{OOC}} \times p^2, p, 1, 1)$ code obtained from equation (3.3) is

$$\Phi(n_{\text{OOC}} \times p^2, p, 1, 1) = \frac{n_{\text{OOC}}(n_{\text{OOC}} p^2 - 1)}{p(p-1)} \approx \frac{n_{\text{OOC}}^2 p}{p-1}$$

It can be seen that the cardinality of 2-D OOC/PC code is nearly p times smaller than the theoretical upper bound.

Example 3.7 Let $p = 3$. The prime sequences S_k and the corresponding code sequences D_k constructed are shown in Table 3.11.

Table 3.11 S_k and D_k for $p = 3$

Prime Sequences S_k	Prime Codes D_k
$S_0 = (000)$	100 100 100
$S_1 = (012)$	100 010 001
$S_2 = (021)$	100 001 010

Using the constructions of one-dimensional OOC, we can construct two codewords, (0,1,4) and (1,3,8), of an (13,3,1)-OOC.

Employing prime code for time-spreading and two codewords of this OOC and their cyclic shifts modulo-13 for wavelength-hopping, we can construct $n_{\text{OOC}} \cdot \Phi_{\text{OOC}} \cdot p = 13 \times 2 \times 3 = 78$ codewords of 2-D OOC/PC code, which are shown in Table 3.12, where $i = 0, 1$ and "$\oplus$" denotes modulo-13 addition.

Table 3.12 2-D OOC/PC Codes

Map from $H_{i,j}$ to D_k for $j=0,1,\cdots,12$	2-D OOC/PC Codes for $j=0,1,\cdots,12$
$H_{0,j}D_0$	$\lambda_{0\oplus j}\ 00\quad \lambda_{1\oplus j}\ 00\quad \lambda_{4\oplus j}\ 00$
$H_{0,j}D_1$	$\lambda_{0\oplus j}\ 00\quad 0\ \lambda_{1\oplus j}\ 0\quad 00\ \lambda_{4\oplus j}$
$H_{0,j}D_2$	$\lambda_{0\oplus j}\ 00\quad 00\ \lambda_{1\oplus j}\quad 0\ \lambda_{4\oplus j}\ 0$
$H_{1,j}D_0$	$\lambda_{1\oplus j}\ 00\quad \lambda_{3\oplus j}\ 00\quad \lambda_{8\oplus j}\ 00$
$H_{1,j}D_1$	$\lambda_{1\oplus j}\ 00\quad 0\ \lambda_{3\oplus j}\ 0\quad 00\ \lambda_{8\oplus j}$
$H_{1,j}D_2$	$\lambda_{1\oplus j}\ 00\quad 00\ \lambda_{3\oplus j}\quad 0\ \lambda_{8\oplus j}\ 0$

3.6 2-D PC/OOC Codes

A 2-D PC/OOC code[11, 12] is a kind of two-dimensional wavelength-hopping/time-spreading codes, which can be constructed by using prime code for wavelength-hopping and optical orthogonal code for time-spreading. This code allows the number of wavelengths and code length to be chosen independently and the code cardinality to be quadratic function of the number of wavelengths. Meanwhile, it keeps the property of $\lambda_c = 1$ and is suitable for the applications of high bit-rate OCDMA systems.

The construction of an $(m \times n_{\mathrm{OOC}}, w, 1, 1)$ 2-D PC/OOC code is as follows.

(1) First of all, construct an $(n_{\mathrm{OOC}}, w, 1, 1)$ OOC, C, using the constructions described in Chapter 2, which can be expressed as

$$\{[c_{i,0}, c_{i,1}, \cdots, c_{i,j}, \cdots, c_{i,w-1}] : i \in [0, t_1 - 1], \quad j \in [0, w-1]\} \tag{3.20}$$

where $n_{\mathrm{OOC}} \geqslant w(w-1)\Phi_{\mathrm{OOC}} + 1$. Φ_{OOC} denotes the cardinality of C, which is given by

$$\Phi_{\mathrm{OOC}} = \left\lfloor \frac{n_{\mathrm{OOC}} - 1}{w(w-1)} \right\rfloor \tag{3.21}$$

(2) Let p be a prime number and there exists $p \geqslant w$. The p prime sequences constructed are

$$\{[s_{i,0}, s_{i,1}, \cdots, s_{i,j}, \cdots, s_{i,p-1}] : i \in [0, p-1], \quad j \in [0, p-1]\} \tag{3.22}$$

where $s_{i,j} = \{i \cdot j\} \bmod p$.

(3) From each prime sequence (except for the all-zero sequence) constructed in Step (2), we choose w elements cyclically each time such that the truncated prime sequence is

$$\{[s_{i,\tau}, s_{i,1\oplus\tau}, \cdots, s_{i,j\oplus\tau}, \cdots, s_{i,(w-1)\oplus\tau}]: \\ i \in [1, p-1], \quad j \in [0, w-1], \quad \tau \in [0, p-1]\} \tag{3.23}$$

where "$\oplus$" denotes modulo-p addition.

Afterwards, the elements in these truncated sequences are regarded as the number of the wavelength such that we can obtain $p-1$ groups (group 1 to group $p-1$) with p prime sequences each. In all $(p-1)p$ truncated prime wavelength-hopping sequences can be produced.

(4) The truncated prime wavelength-hopping sequences obtained from Step (3) are mapped to the position of 1's in the OOC codewords constructed in Step (1). In this way, $\Phi_{\text{OOC}}(p-1)p$ codewords of a 2-D PC/OOC code can be obtained. It must be noted that the prime sequence of $i=0$ can not be directly mapped into the codewords of OOC as the number of the wavelength because only one codeword with λ_0 in all of pulse 1 is generated in doing so, which is meaningless. However, because there are p available wavelengths in a 2-D PC/OOC code, we can replace "1" in each codeword of OOC by the same wavelength and p wavelengths exactly produce p codewords of 2-D PC/OOC code, which are regarded as the 0^{th} group codewords of 2-D PC/OOC code. Thus, the cardinality in all is[11]

$$\Phi_{\text{PC/OOC}} = \Phi_{\text{OOC}}[(p-1)p + p] = \Phi_{\text{OOC}} p^2 \tag{3.24}$$

Example 3.8 Let $p=7$. The derived prime sequences over Galois field $GF(7)$ for $p=7$ are shown in Table 3.13. From the construction of 1-D OOC, only one codeword of an (7,3,1,1)-OOC, 0110100, is constructed, whose codeword block is (1,2,4). Meanwhile, the code weight is 3, which satisfies the requirement of no greater than $p=7$. Then, the 2-D PC/OOC code matrices can be derived by using $p=7$ wavelengths, $\{\lambda_0, \lambda_1, \lambda_2, \cdots, \lambda_6\}$, and the codeword of the (7,3,1,1)-OOC, 0110100.

First of all, choose three elements from each prime sequence in order, which are regarded as the number of the wavelength. Then, these three wavelengths are mapped into the positions of 1's pulses of 0110100 in order. In doing so, a 2-D PC/OOC codeword can be derived. In this way, from $p-1=6$ non-all-zero prime sequences, $p-1$ groups with p code matrices of 2-D PC/OOC in each group can be obtained. In addition, every "1" in the codeword 0110100 is mapped into the same wavelength. Because there are $p=7$ wavelengths in all, $p=7$ codewords in the 0^{th} group can be obtained. Therefore, the overall number of code matrices derived is $\Phi_{\text{OOC}}\Phi_{\text{group}}p = \Phi_{\text{OOC}}p^2 = 1\times 7^2 = 49$. The resulting overall codewords are shown in Table 3.14.

Table 3.13 Prime sequences of $GF(7)$

i	S_i						
0	0	0	0	0	0	0	0
1	0	1	2	3	4	5	6
2	0	2	4	6	1	3	5
3	0	3	6	2	5	1	4
4	0	4	1	5	2	6	3
5	0	5	3	1	6	4	2
6	0	6	5	4	3	2	1
	$w=3$						
	$w=5$						

Table 3.14 Codewords (or matrices) of 2-D PC/OOC code based on $GF(7)$, 7 wavelengths and the codeword 0110100 from the (7,3,1,1)-OOC

group 0	group 1	group 2	⋯	group 6
$0:0\lambda_0\lambda_0 0\lambda_0 00$	$7:0\lambda_0\lambda_1 0\lambda_2 00$	$14:0\lambda_0\lambda_2 0\lambda_4 00$	…	$42:0\lambda_0\lambda_6 0\lambda_5 00$
$1:0\lambda_1\lambda_1 0\lambda_1 00$	$8:0\lambda_1\lambda_2 0\lambda_3 00$	$15:0\lambda_2\lambda_4 0\lambda_6 00$	…	$43:0\lambda_6\lambda_5 0\lambda_4 00$
$2:0\lambda_2\lambda_2 0\lambda_2 00$	$9:0\lambda_2\lambda_3 0\lambda_4 00$	$16:0\lambda_4\lambda_6 0\lambda_1 00$	…	$44:0\lambda_5\lambda_4 0\lambda_3 00$
$3:0\lambda_3\lambda_3 0\lambda_3 00$	$10:0\lambda_3\lambda_4 0\lambda_5 00$	$17:0\lambda_6\lambda_1 0\lambda_3 00$	…	$45:0\lambda_4\lambda_3 0\lambda_2 00$
$4:0\lambda_4\lambda_4 0\lambda_4 00$	$11:0\lambda_4\lambda_5 0\lambda_6 00$	$18:0\lambda_1\lambda_3 0\lambda_5 00$	…	$46:0\lambda_3\lambda_2 0\lambda_1 00$
$5:0\lambda_5\lambda_5 0\lambda_5 00$	$12:0\lambda_5\lambda_6 0\lambda_0 00$	$19:0\lambda_3\lambda_5 0\lambda_0 00$	…	$47:0\lambda_2\lambda_1 0\lambda_0 00$
$6:0\lambda_6\lambda_6 0\lambda_6 00$	$13:0\lambda_6\lambda_0 0\lambda_1 00$	$20:0\lambda_5\lambda_0 0\lambda_2 00$	…	$48:0\lambda_1\lambda_0 0\lambda_6 00$

This construction is not only used to construct the 2-D PC/OOC code with the code weight $w \leqslant p$ (p is a prime number to represent the number of available wavelengths) and the maximal cardinality $\Phi_{\text{PC/OOC}} = \Phi_{\text{OOC}} p^2$ over Galois field $GF(p)$, but also will be employed to derive the 2-D PC/OOC code with the maximal cardinality $\Phi_{\text{PC/OOC}} = \Phi_{\text{OOC}} p'^2$ over the nonprime integer Galois field $GF(p')$ (p' is a nonprime integer to indicate the number of available wavelengths.) as long as the code weight is no greater than the smallest prime factor of the nonprime integer, i.e., $w \leqslant p_1$ ($p' = p_1 p_2 \cdots p_k$, $p_1 \leqslant p_2 \leqslant \cdots \leqslant p_k$, k is a positive integer.)

For example, assuming $p' = 9 = 3 \times 3$, as long as $w \leqslant 3$, an asymptotically optimal $(m \times n, w, 1, 1)$ 2-D PC/OOC code with the cardinality $\Phi_{\text{PC/OOC}} = \Phi_{\text{OOC}} p'^2$ can be constructed. However, if $w > 3$, then the cardinality of the 2-D code constructed is very small and the auto- and cross-correlation constraints of the

code cannot be met. If the number of available wavelengths is a positive integer $p' = p_1 p_2 \cdots p_k$ and the code weight $w > p_1$, then we should deploy the largest prime number p, which is less than or equal to p' such that $p \geqslant w > p_1$ and $\Phi_{\text{PC/OOC}} = \Phi_{\text{OOC}} p^2$, where $p_1 \leqslant p_2 \leqslant \cdots \leqslant p_k$ and they are prime for a positive integer k. The derived nonprime sequences of Galois field $GF(9)$ for $p' = 9$ are shown in Table 3.15.

Lemma 3.1[11]: The autocorrelation sidelobes and cross-correlation functions of 2-D PC/OOC code are at most 1 only if one-dimensional optical codes employed in the time domain have both values no greater than 1.

Proof: See Ref. [11].

Table 3.15 Nonprime Sequences of $GF(9)$

i	S_i								
0	0	0	0	0	0	0	0	0	0
1	0	1	2	3	4	5	6	7	8
2	0	2	4	6	8	1	3	5	7
3	0	3	6	0	3	6	0	3	6
4	0	4	8	3	7	2	6	1	5
5	0	5	1	6	2	7	3	8	4
6	0	6	3	0	6	3	0	6	3
7	0	7	5	3	1	8	6	4	2
8	0	8	7	6	5	4	3	2	1
	$w=3$								
	$w=5$								

From equation (3.3), the theoretical upper bound on the cardinality of an $(p \times n_{\text{OOC}}, w, 1, 1)$ 2-D PC/OOC code is given by[11]

$$\begin{aligned} \Phi_{\text{PC/OOC}} &\leqslant \Phi(p \times n_{\text{OOC}}, w, 1, 1) \leqslant \frac{p(pn_{\text{OOC}} - 1)}{w(w-1)} \\ &= \Phi_{\text{OOC}} p^2 + \frac{p^2 - p}{w(w-1)} \end{aligned} \tag{3.25}$$

where $n_{\text{OOC}} = w(w-1)\Phi_{\text{OOC}} + 1$. Comparing equation (3.25) with equation (3.24), it can be found that the actual cardinality of the 2-D PC/OOC code is very near to the theoretical upper bound of (3.24) when w is large. Therefore, the 2-D PC/OOC code is asymptotically optimal. Table 3.16 shows the cardinalities of some 2-D PC/OOC codes.

Table 3.16 Cardinality of some 2-D PC/OOC codes

$n = n_{OOC}$	w	Φ_{OOC}	Number of Wavelengths	p or p'	$\Phi_{PC/OOC}$
7	3	1	3	3	9
7	3	1	7	7	49
13	3	2	3	3	18
13	3	2	5	5	50
19	3	3	5	5	75
31	3	5	4	3	45
31	4	2	7	7	98
31	5	1	13	13	169
37	3	6	3	3	54
37	4	3	5	5	75
37	4	3	7	7	147
41	3	6	8	7	294
41	4	3	15	13	507
41	5	2	16	13	338

3.7 2-D OCFHC/OOC Codes

2-D OCFHC/OOC codes[14] are constructed by deploying one-coincidence frequency-hopping code (OCFHC) for wavelength-hopping and OOC for time-spreading. Because the prime code is an exclusive case of OCFHC for $k = 1$, 2-D OCFHC/OOC doesn't have the restriction that the number of wavelengths must be a prime number. Hence, 2-D OCFHC/OOC codes can achieve more flexible choice of the number of wavelengths, have good correlation properties and their cardinalities are asymptotically optimal.

Next, we introduce the constructions of 2-D OCFHC/OOC code and their performance. As preliminary knowledge, we first review the construction of OCFHC.

3.7.1 Constructions of 2-D OCFHC/OOC Codes

3.7.1.1 Construction of OCFHC

Frequency-hopping code (FHC) is a collection of codewords to determine where to place different carrier frequencies (expressed as wavelengths in the optical domain) in different time slots. There are four parameters with regard to FHC's design, which are the number of frequencies Q, the code length L, the code cardinality N, and the maximum value of correlation between any two codewords, H_{max}.

Let A be a set of Q frequencies

$$A = \{f_0, f_1, \cdots, f_{Q-1}\} \tag{3.26}$$

Suppose that S is an FHC with the code length L, then S can be expressed as

$$S = \{S_0, S_1, \cdots, S_{N-1}\} \tag{3.27}$$

where S_v, $0 \leqslant v \leqslant N-1$, is an FHC code, represented as

$$S_v = \{s_v(0), s_v(1), \cdots, s_v(j), \cdots, s_v(L-1)\}, \quad s_v(j) \in A \tag{3.28}$$

The definition of the correlation between any two distinct codewords, X and Y in S, is given by

$$H_{XY}(\tau) = \sum_{j=0}^{L-1} h[x(j), y(j \oplus_L \tau)], \qquad 0 \leqslant \tau \leqslant L-1 \tag{3.29}$$

where $x(j), y(j \oplus_L \tau) \in A$ and "$\oplus_L$" denotes modulo-L addition, and

$$h[x(j), y(j \oplus_L \tau)] = \begin{cases} 1, & \text{if } x(j) = y(j \oplus_L \tau) \\ 0, & \text{if } x(j) \neq y(j \oplus_L \tau) \end{cases} \tag{3.30}$$

$H_{\max}$ denotes the maximum value of $H_{XY}(\tau)$, i.e.,

$$H_{\max} = \max\{H_{XY}(\tau)\} \tag{3.31}$$

When each frequency only occurs one time in each codeword, $H_{\max}$ of the code is equal to one. This code is called the one-coincidence frequency-hopping code (OCFHC), which satisfies

$$N \leqslant \frac{Q(Q-1)}{L} \tag{3.32}$$

If the equation (3.32) becomes an equality, then OCFHC is an optimal code, that is, the number of codewords of OCFHC is maximal. An OCFHC with the number of available frequencies Q, the code length L and the maximum correlation value $H_{\max}$ is called an $(L, Q, H_{\max})$-OCFHC. Based on Galois field $GF(p^k)$, an OCFHC with the code length $L = p^k - 1$ can be constructed, which has $N = p^k$ codewords. The detailed steps[15] of the construction are as follows:

(1) First of all, choose a prime number p and then select a primitive polynomial of degree n over Galois field $GF(p)$.

(2) Let α be a primitive element of Galois field $GF(p^k)$ and the nonzero

elements over $GF(p^k)$ are expressed as powers of α,

$$G = \{\alpha^0, \alpha^1, \alpha^2, \cdots, \alpha^{p^k-2}\} \tag{3.33}$$

(3) Add an element β_v over $GF(p^k)$ to every element of G, and a codeword of OCFHC can be generated, that is,

$$S_v = \{s_v(0), s_v(1), \cdots, s_v(p^k-2)\}, \quad v = 0,1,\cdots,N-1 \tag{3.34}$$

where $s_v(j) = \alpha^j \oplus_p \beta_v$, $j = 0,1,\cdots,p^k-2$, "$\oplus_p$" denotes modulo-p addition and $\beta_v = (v_0 v_1 \cdots v_{k-1}) \in GF(p^k)$.

(4) Adding different elements of $GF(p^k)$, then p^k non-repeated codewords of OCFHC can be obtained in all.

Example 3.9 Construct an $(L,Q,H_{\max}) = (p^k-1, p^k, 1)$ OCFHC using $Q = p^k = 8$ wavelengths.

From $Q = p^k = 8$, we have $p = 2$ and $k = 3$. The code length of OCFHC is $L = p^k - 1 = 2^3 - 1 = 7$. The overall number of codewords constructed is $N = p^k = 2^3$. The construction steps are as follows:

(1) Choose a primitive polynomial of degree 3 over $GF(2)$: $f(x) = x^3 + x + 1$.

(2) Select a primitive element α over $GF(2^3)$, then there exists $\alpha^3 + \alpha + 1 = 0$.

(3) The nonzero elements over $GF(2^3)$ are expressed as powers of α,

$$G = \{1, \alpha, \alpha^2, \alpha+1, \alpha^2+\alpha, \alpha^2+\alpha+1, \alpha^2+1\}.$$

G can also be expressed by as a decimal number as $G = \{1,2,4,3,6,7,5\}$.

(4) Add an element β_v of $GF(2^3)$ to each element of G to yield non-repeated codewords of OCFHC.

(5) $p^k = 2^3$ non-repeated codewords of an OCFHC code can be acquired by adding different elements to G, as shown in Table 3.17. Expressed in decimal numbers, the result is shown in Table 3.18.

3.7.1.2 Construction of 2-D OCFHC/OOC Codes

Employing OCFHC for wavelength-hopping and OOC for time-spreading, a 2-D $(p^k \times n_{\text{OOC}}, w, \lambda_a, \lambda_c)$ OCFHC/OOC code consisting of 0 and 1 can be constructed, where p^k represents the number of available wavelengths, w is the code weight and n_{OOC} denotes the code length of 1-D OOC, which is also the code length of the new 2-D OCFHC/OOC code constructed. When the 1-D OOC used is an $(n_{\text{OOC}}, w, 1, 1)$ OOC, the 2-D OCFHC/OOC code constructed has the autocorrelation sidelobe of at most $\lambda_a = 1$ and the cross-correlation function of at most $\lambda_c = 1$,

Table 3.17 $(L,Q,H_{\max})=(2^3-1,2^3,1)$ OCFHC code represented by binary numbers

G	α^0	α^1	α^2	α^3	α^4	α^5	α^6
	001	**010**	**100**	**011**	**110**	**111**	**101**
$S_0 = G + 000$	001	010	100	011	110	111	101
$S_1 = G + 001$	000	011	101	010	111	110	100
$S_2 = G + 010$	011	000	110	001	100	101	111
$S_3 = G + 100$	101	110	000	111	010	011	001
$S_4 = G + 011$	010	001	111	000	101	100	110
$S_5 = G + 110$	111	100	010	101	000	001	011
$S_6 = G + 111$	110	101	011	100	001	000	010
$S_7 = G + 101$	100	111	001	110	011	010	000

Table 3.18 $(L,Q,H_{\max})=(2^3-1,2^3,1)$ OCFHC code indicated in decimal numbers

G	α^0	α^1	α^2	α^3	α^4	α^5	α^6
	1	**2**	**4**	**3**	**6**	**7**	**5**
$S_0 = G + 0$	1	2	4	3	6	7	5
$S_1 = G + \alpha^0$	0	3	5	2	7	6	4
$S_2 = G + \alpha^1$	3	0	6	1	4	5	7
$S_3 = G + \alpha^2$	5	6	0	7	2	3	1
$S_4 = G + \alpha^3$	2	1	7	0	5	4	6
$S_5 = G + \alpha^4$	7	4	2	5	0	1	3
$S_6 = G + \alpha^5$	6	5	3	4	1	0	2
$S_7 = G + \alpha^6$	4	7	1	6	3	2	0

which is a 2-D $(p^k \times n_{\text{OOC}}, w, 1, 1)$ OCFHC/OOC code. Its construction is as follows:

(1) Firstly, choose a prime number p and the number of available wavelengths p^k, and construct an $(L,Q,1)$ OCFHC in terms of abovementioned construction.

(2) Using the construction of 1-D OOC, construct Φ_{OOC} codewords of an $(n_{\text{OOC}}, w, 1)$ OOC. Note the requirement of the code weight $w \leqslant p^k - 1$.

(3) Each codeword (i.e., each row) of OCFHC is regarded as a seed. According to the code weight w of the OOC constructed, w elements as a group are selected orderly and circularly from each codeword of the OCFHC. Therefore, each codeword of OCFHC can generate $p^k - 1$ groups with w elements each. Because there are p^k codewords in an OCFHC, $p^k(p^k - 1)$ groups with w elements each can be produced in all.

(4) Each element in every group with w elements obtained by Step (3) is regarded as the number of the wavelength to yield $p^k(p^k-1)$ wavelength sequences. Then, these wavelengths are mapped into the positions of 1s in each codeword of the OOC one by one. In this way, $\Phi_{\mathrm{OOC}}p^k(p^k-1)$ codewords of 2-D OCFHC/OOC can be generated, which are expressed as C_1 in short, where Φ_{OOC} denotes the cardinality of 1-D OOC, given by $\Phi_{\mathrm{OOC}}=\left\lfloor \frac{n_{\mathrm{OOC}}-1}{w(w-1)} \right\rfloor$.

(5) Using OOC for time-spreading, all "1" pulses in each codeword of OOC are replaced by the same wavelength. In doing so, $\Phi_{\mathrm{OOC}}p^k$ codewords of 2-D OCFHC/OOC can be acquired, which are written down as C_2.

The overall cardinality of a 2-D OCFHC/OOC code, C, is given by

$$\begin{aligned}\Phi_{\mathrm{OCFHC/OOC}} &= \Phi_{C_1}+\Phi_{C_2}=\left[p^k(p^k-1)+p^k\right]\Phi_{\mathrm{OOC}} \\ &= p^{2k}\Phi_{\mathrm{OOC}}=p^{2k}\left\lfloor \frac{n_{\mathrm{OOC}}-1}{w(w-1)} \right\rfloor \end{aligned} \tag{3.35}$$

From equation (3.3), we can obtain the theoretical upper bound on the cardinality of a 2-D $(p^k\times n_{\mathrm{OOC}},w,1,1)$ OCFHC/OOC code:

$$\Phi_{\mathrm{OCFHC/OOC}} \leqslant \frac{p^k(p^k n_{\mathrm{OOC}}-1)}{w(w-1)} \tag{3.36}$$

Comparing (3.35) with (3.36), it can be seen that when w is large enough the cardinality of the 2-D OCFHC/OOC code is close to the upper bound in theory. Thus, it is asymptotically optimal.

Example 3.10 Construct a 2-D $(2^3\times 7,3,1,1)$ OCFHC/OOC code

Firstly, we need to construct a $(L,Q,H_{\max})=(p^k-1,p^k,1)=(2^3-1,2^3,1)$ OCFHC. Because it has been obtained in Example 3.9, we redraw the result in Table 3.19 and express two scenarios in the table, which take on the code weights $w=3$ and $w=5$ of the 2-D OCFHC/OOC code. We take $w=3$ in this example.

Then, we construct a 1-D OOC. For the sake of mathematical convenience, let's deploy the $(7,3,1,1)$ OOC, which only has one codeword (0110100). Its code weight is $w=3\leqslant p^3-1=2^3-1$.

Following the steps from (3) to (5), we obtain the 2-D $(2^3\times 7,3,1,1)$ OCFHC/OOC code, C, which is shown in Table 3.20. Its overall cardinality is

$$\Phi_{\mathrm{PC/OOC}}=p^{2k}\left\lfloor \frac{n_{\mathrm{OOC}}-1}{w(w-1)} \right\rfloor=2^6\left\lfloor \frac{7-1}{3(2-1)} \right\rfloor=64$$

Table 3.19 $(2^3,7,1)$ OCFHC

i	S_i						
0	1	2	4	3	6	7	5
1	0	3	5	2	7	6	4
2	3	0	6	1	4	5	7
3	5	6	0	7	2	3	1
4	2	1	7	0	5	4	6
5	7	4	2	5	0	1	3
6	6	5	3	4	1	0	2
7	4	7	1	6	3	2	0

$w = 3$

$w = 5$

Table 3.20 2-D $(2^3 \times 7,3,1,1)$ OCFHC/OOC Code

C_1				C_2
group 0	**group 1**	**…**	**group 7**	**group 8**
$0:0\lambda_1\lambda_2 0\lambda_4 00$	$7:0\lambda_0\lambda_3 0\lambda_5 00$	…	$49:0\lambda_4\lambda_7 0\lambda_1 00$	$56:0\lambda_0\lambda_0 0\lambda_0 00$
$1:0\lambda_2\lambda_4 0\lambda_3 00$	$8:0\lambda_3\lambda_5 0\lambda_2 00$	…	$50:0\lambda_7\lambda_1 0\lambda_6 00$	$57:0\lambda_1\lambda_1 0\lambda_1 00$
$2:0\lambda_4\lambda_3 0\lambda_6 00$	$9:0\lambda_5\lambda_2 0\lambda_7 00$	…	$51:0\lambda_1\lambda_6 0\lambda_3 00$	$58:0\lambda_2\lambda_2 0\lambda_2 00$
$3:0\lambda_3\lambda_6 0\lambda_7 00$	$10:0\lambda_2\lambda_7 0\lambda_6 00$	…	$52:0\lambda_6\lambda_3 0\lambda_2 00$	$59:0\lambda_3\lambda_3 0\lambda_3 00$
$4:0\lambda_6\lambda_7 0\lambda_5 00$	$11:0\lambda_7\lambda_6 0\lambda_4 00$	…	$53:0\lambda_3\lambda_2 0\lambda_1 00$	$60:0\lambda_4\lambda_4 0\lambda_4 00$
$5:0\lambda_7\lambda_5 0\lambda_1 00$	$12:0\lambda_6\lambda_4 0\lambda_0 00$	…	$54:0\lambda_3\lambda_2 0\lambda_0 00$	$61:0\lambda_5\lambda_5 0\lambda_5 00$
$6:0\lambda_5\lambda_1 0\lambda_2 00$	$13:0\lambda_4\lambda_0 0\lambda_3 00$	…	$55:0\lambda_2\lambda_0 0\lambda_4 00$	$62:0\lambda_6\lambda_6 0\lambda_6 00$
				$63:0\lambda_7\lambda_7 0\lambda_7 00$

3.7.2 Performance of 2-D OCFHC/OOC Codes

3.7.2.1 Correlation Properties of 2-D OCFHC/OOC Codes

From the process of generating 2-D OCFHC/OOC code, we know that every 1's pulse of each codeword in C_1 possesses a different wavelength. Therefore, the autocorrelation sidelobe of each codeword in C_1 is zero. Although every 1's pulse of each codeword in C_2 has the same wavelength, its autocorrelation sidelobe is at most 1 because the construction of C_2 employs the $(n_{\text{OOC}},w,1,1)$ OOC for time-spreading. Hence, the autocorrelation sidelobe of 2-D OCFHC/OOC is at most 1.

As for C_1, because we use OCFHC for wavelength-hopping and OOC with $\lambda = 1$ for time-spreading, the cross-correlation between any two codewords is at most 1. For C_2, although all pulses in each codeword deploy the same wavelength, the cross-correlation between any two codewords is also at most 1, due the use of the OOC with $\lambda = 1$ for time-spreading. For any two codewords in C_1 and C_2 respectively, with C_1 constructed by using each codeword of OCFHC as a seed and each wavelength in each codeword of OCFHC occuring at most once, each wavelength in every codeword of C_1 also appears at most once. On the other hand, each codeword of C_2 only contains one wavelength. Thus, the cross-correlation between any two codewords in C_1 and C_2 respectively is at most 1. Therefore, the maximal value of cross-correlation of a 2-D OCFHC/OOC is at most one.

3.7.2.2 BER of OCDMA Systems with 2-D OCFHC/OOC Codes

Letting q_i denote the average number of "hits" between a codeword from C_i ($i = 1, 2$) and another codeword from C ($C = C_1 + C_2$), we obtain

$$q_1 = \frac{\frac{w}{2n_{\mathrm{OOC}}} \cdot wt_1 + \frac{1}{2n_{\mathrm{OOC}}}[w^2(p^k - 1)t_1 - w]}{\Phi_c - 1} = \frac{\frac{w^2}{2n_{\mathrm{OOC}}}(p^k t_1 + t_2) - \frac{w}{2n_{\mathrm{OOC}}}}{\Phi_c - 1} \tag{3.37}$$

$$q_2 = \frac{\frac{w^2}{2n_{\mathrm{OOC}}}(t_1 - 1) + \frac{w}{2n_{\mathrm{OOC}}} \cdot w(p^k - 1)t_1}{\Phi_c - 1} = \frac{\frac{w^2}{2n_{\mathrm{OOC}}}(p^k t_1 - 1)}{\Phi_c - 1} \tag{3.38}$$

where t_1 and t_2 indicate the cardinalities of the $(n_{\mathrm{OOC}}, w, 1, 1)$ OOC and the $(p^k, w, 1, 1)$ OOC respectively, which are given by

$$t_1 = \left\lfloor \frac{n_{\mathrm{OOC}} - 1}{w(w-1)} \right\rfloor, \quad t_2 = \left\lfloor \frac{p^k - 1}{w(w-1)} \right\rfloor$$

Let q indicate the average number of "hits" between any two codewords in C, which then can be expressed as

$$q = \frac{\Phi_{c_1}}{\Phi_c} \cdot q_1 + \frac{\Phi_{c_2}}{\Phi_c} \cdot q_2 \tag{3.39}$$

When the multiple subscribers' interferences (MUI) are taken into account, but the thermal and shot noise in photo-detection are neglected, for the number of active users K and the decision threshold Th equal to w, the bit-error-rate (BER) is given by

$$P_{\mathrm{b}} = \frac{1}{2} \sum_{i=Th}^{K-1} \binom{K-1}{i} q^i (1-q)^{K-1-i} \tag{3.40}$$

Figure 3.3 shows the curves of BER versus the number of simultaneous subscribers for different codes with different preferences shown in the figure. It can be seen that OCFHC/OOC outperforms PC/PC.

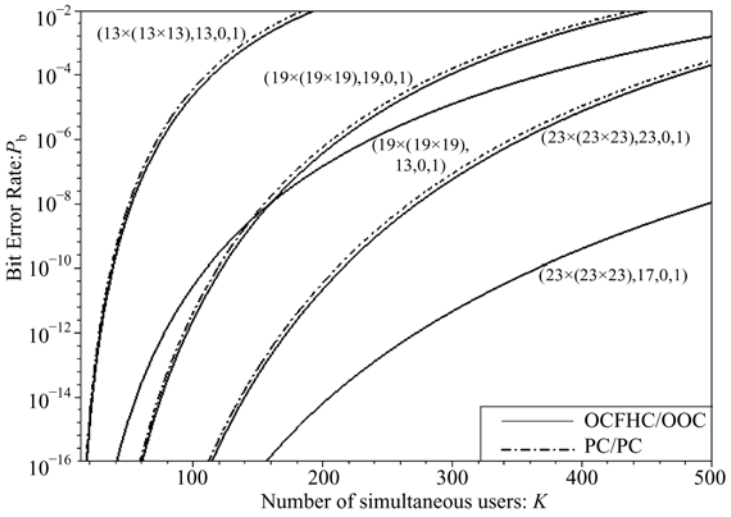

Figure 3.3 BER versus the number of simultaneous subscribers for different codes with different preferences

3.8 2-D B/U OCDMA Codes

There is at most one pulse (i.e., one wavelength) on every column (corresponding to one time slot) in the $m \times n$ wavelength-time matrix of 2-D OCDMA codes described in above, where m represents the number of rows, related to the number of available wavelengths, and n indicates the number of columns, related to the number of time slots (so-called chips, i.e., the code length). In this section, we will introduce another kind of 2-D OCDMA code, the 2-D bipolar/unipolar (B/U) OCDMA code[16], which employs the unipolar version of bipolar

codes for wavelength-hopping and optical unipolar codes for time-spreading. There can be multiple pulses (i.e., multiple wavelengths) on every column (i.e., each time slot) of its code matrix, and multiple wavelengths determined by the unipolar version of bipolar codes. This kind of code can increase the numbers of subscribers and simultaneous users in a network without sacrificing performance. Utilizing programmable arrayed waveguide gratings (AWGs), tunable fiber Bragg gratings (FBGs) or thin-film filters, etc., fast, programmable and integrated hardware encoder/decoders can be implemented[16].

Because the numbers of wavelengths and time slots of 2-D B/U codes are not restricted by the prime numbers, there is flexibility in choosing the numbers of wavelengths and time slots. Although 2-D B/U codes employ bipolar codes for wavelength-hopping, only the "+1" elements of the binary codes are transmitted and nothing is transported for the "−1" elements (namely, the unipolar version of the bipolar code). The "−1" elements are simulated by using balanced photodetectors in the systems in References [17] and [18]. However, the systems using 2-D B/U codes differ in that they do not require transmitting the complement of the unipolar version of the bipolar codes. Further details about OCDMA systems using 2-D B/U codes will be discussed in Chapter 4.

The construction of 2-D B/U codes is similar to that of 2-D PC/OOC codes. The only difference is that each "1" in a codeword of an OOC is mapped into a wavelength according to a certain algorithm when a 2-D PC/OOC code is constructed. However, every "1" in a codeword of an OOC is mapped into a multi-wavelength code obtained by a bipolar code using an algorithm similar to the process of the constructed 2-D B/U codes. In order to reduce the multiple access interference (MAI) as much as possible, we employ the 1-D OOC with $\lambda_a = \lambda_c = 1$ for time-spreading. The specific construction of 2-D B/U code is as follows:

Step 1: Construct all multi-wavelength codewords using a binary code with good correlation properties, such as m-sequences, Walsh-Hadamard codes, etc.

The approach to construct all multi-wavelength codewords is simple. Each "+1" element in a bipolar code corresponds to a wavelength and the number of each wavelength depends on the position of "+1" element in the bipolar codeword. For example, in bipolar sequences, the "+1" at the first position corresponds to the wavelength λ_0, the "+1" at the second position corresponds to the wavelength λ_1, and the rest may be deduced by analogy. The "−1" elements in the sequences are changed into "0"s. Thus the multi-wavelength codewords are acquired.

Example 3.11 Construct the multi-wavelength codes using an m-sequence and Walsh-Hadamard code.

(1) Construct a multi-wavelength code using an m-sequence.

For the sake of mathematical convenience, assume that the length of an

m-sequence selected is $n=7$, yielding (+1 +1 +1 –1 +1 –1 –1). Then, the m-sequence is shifted cyclically six times and a cyclic shift sequence can be produced from every cyclic shift. Therefore, we can obtain six cyclic shift sequences in all. Including the original sequence, seven m-sequences can be derived in all. Then, these sequences are mapped as the multi-wavelength codewords. For example, the 0^{th} codeword in the m-sequences (+1 +1 +1 –1 +1 –1 –1) corresponds to the multi-wavelength codeword C_0, which is $\lambda_0\lambda_1\lambda_2\lambda_4$. The resulting multi-wavelength codewords of the m-sequences are shown in Table 3.21.

Table 3.21 Multi-wavelength codewords generated by m-sequence with length 7, (+1 +1 +1 –1 +1 –1 –1), and its cyclic shift sequences

sequences		wavelengths	sequences		wavelengths
$+1+1+1-1+1-1-1$	C_0	$\lambda_0\lambda_1\lambda_2\lambda_4$	$-1+1-1-1+1+1+1$	C_4	$\lambda_1\lambda_4\lambda_5\lambda_6$
$-1+1+1+1-1+1-1$	C_1	$\lambda_1\lambda_2\lambda_3\lambda_5$	$+1-1+1-1-1+1+1$	C_5	$\lambda_0\lambda_2\lambda_5\lambda_6$
$-1-1+1+1+1-1+1$	C_2	$\lambda_2\lambda_3\lambda_4\lambda_6$	$+1+1-1+1-1-1+1$	C_6	$\lambda_0\lambda_1\lambda_3\lambda_6$
$+1-1-1+1+1+1-1$	C_3	$\lambda_0\lambda_3\lambda_4\lambda_5$			

(2) Construct multi-wavelength codewords by employing Walsh-Hadamard code.

Firstly, we construct all codewords of a Walsh-Hadamard code for length $n=8$. Then, we obtain the multi-wavelength codewords by employing the map relation from the bipolar code to the multi-wavelength code. The construction procedure and the results are shown in Table 3.22. Eight multi-wavelength codewords are produced, $\{C_0, C_1, \cdots, C_7\}$.

Table 3.22 Multi-wavelength codewords produced by Walsh-Hadamard code with length 8[16]

sequences		wavelengths	sequences		wavelengths
$+1-1+1-1+1-1+1-1$	C_0	$\lambda_0\lambda_2\lambda_4\lambda_6$	$+1-1+1-1-1+1-1+1$	C_4	$\lambda_0\lambda_2\lambda_5\lambda_7$
$+1+1-1-1+1+1-1-1$	C_1	$\lambda_0\lambda_1\lambda_4\lambda_5$	$+1+1-1-1-1-1+1+1$	C_5	$\lambda_0\lambda_1\lambda_6\lambda_7$
$+1-1-1+1+1-1-1+1$	C_2	$\lambda_0\lambda_3\lambda_4\lambda_7$	$+1-1-1+1-1+1+1-1$	C_6	$\lambda_0\lambda_3\lambda_5\lambda_6$
$+1+1+1+1-1-1-1-1$	C_3	$\lambda_0\lambda_1\lambda_2\lambda_3$	$+1+1+1+1+1+1+1+1$	C_7	$\lambda_0 \sim \lambda_7$

Step 2: Construct the prime sequences of a prime number p, which is greater than or equal to the code weight w of a time-spreading unipolar code, i.e., $w \leqslant p$.

Example 3.12 Let $p=7$. The prime sequences over Galois field $GF(7)$ are constructed, as shown in Table 3.23.

Table 3.23 Prime sequences over $GF(7)$

i	S_i						
0	0	0	0	0	0	0	0
1	0	1	2	3	4	5	6
2	0	2	4	6	1	3	5
3	0	3	6	2	5	1	4
4	0	4	1	5	2	6	3
5	0	5	3	1	6	4	2
6	0	6	5	4	3	2	1
	$w=3$						
	$w=5$						

Step 3: Construct a unipolar code for the time-spreading sequences.

In order to reduce MAI as much as possible, the time-spreading unipolar code that has the autocorrelation sidelobe and cross-correlation function of at most 1 in the time domain is required. We choose the OOC for the time-spreading sequences here. For the sake of simplification, we select the (7,3,1,1)-OOC, which only has one codeword (0110100) and satisfies $w=3 \leqslant p=7$.

Step 4: Map the multi-wavelength codewords obtained onto the "1" time slots of the time-spreading unipolar code such that a 2-D B/U code is obtained.

The mapping method is the same as the technique that is used to map the wavelengths to the "1" time slots of the OOC, which has been introduced in the construction of 2-D PC/OOC in Section 3.6. Hence, we do not repeat the details here.

In this way, the overall cardinality of the 2-D B/U code obtained is given by[16]

$$\Phi_{\mathrm{B/U}} = \Phi_{\mathrm{bipolar}} \Phi_{\mathrm{group}} \Phi_{\mathrm{unipolar}} \tag{3.41}$$

where Φ_{bipolar} denotes the cardinality of a bipolar code. For an m-sequence or a Walsh-Hadamard code, it can be expressed as

$$\Phi_{\mathrm{bipolar}} = n_{\mathrm{bipolar}} = \text{ number of wavelengths} \tag{3.42}$$

where n_{bipolar} indicates the code length of a bipolar code. Φ_{group} represents the number of groups obtained when the multi-wavelength code is mapped into an unipolar code. When the mapping of the prime sequence is employed, $\Phi_{\mathrm{group}} = p$, where p is a prime number. Φ_{unipolar} denotes the cardinality of the unipolar code used for time-spreading. When an $(n_{\mathrm{OOC}}, w, 1, 1)$ - OOC is utilized, it is given by

$$\Phi_{\mathrm{unipolar}} = \Phi_{\mathrm{OOC}} \leqslant \frac{n_{\mathrm{OOC}} - 1}{w(w-1)} \tag{3.43}$$

where n_{OOC} is the code length of the OOC and w is the code weight of the OOC. At the same time, $w \leqslant p$ is required.

When $\Phi_{\mathrm{group}} = \Phi_{\mathrm{bipolar}} = p$, the cardinality of the 2-D B/U code, $\Phi_{\mathrm{B/U}}$, reaches optimal, which is

$$\Phi_{\mathrm{B/U}} = \Phi_{\mathrm{bipolar}} \Phi_{\mathrm{group}} \Phi_{\mathrm{OOC}} = p^2 \left\lfloor \frac{n_{\mathrm{OOC}} - 1}{w(w-1)} \right\rfloor \tag{3.44}$$

where p is a prime number.

Note that although this approach can be deployed to construct 2-D B/U code in the nonprime Galois field, the code cardinality may decrease in some cases. This is because the nonprime field can produce some repeated elements, which can not be employed as the seed for a permuting multi-wavelength code. This issue is left for the readers to consider. Table 3.24 shows the cardinality of some 2-D B/U codes.

Table 3.24 Cardinality of some 2-D B/U codes

$n = n_{\mathrm{OOC}}$	w	Φ_{OOC}	Φ_{bipolar}	Φ_{group}	$\Phi_{\mathrm{B/U}}$
7	3	1	4	3	12
7	3	1	7	7	49
13	3	2	7	7	98
19	3	3	7	7	147
31	4	2	7	7	98
37	4	3	7	7	147
41	3	6	7	7	294
41	4	3	15	13	507
73	4	6	4	3	72
73	4	6	7	7	294
73	4	6	8	7	336
73	4	6	15	13	1170

Example 3.13 Based on the prime sequences of $GF(7)$, seven multi-wavelength codewords constructed by the m-sequences and the time-spreading codeword 0110100 of the (7,3,1,1)-OOC result in the 2-D B/U code shown in Table 3.25.

The resulting overall cardinality is

$$\Phi_{\mathrm{B/U}} = p^2 \left\lfloor \frac{n_{\mathrm{OOC}} - 1}{w(w-1)} \right\rfloor = 7^2 \times 1 = 49$$

As for the correlation properties of the 2-D B/U code, see Theorem 3.2. Figure 3.4 shows a schematic diagram of a codewords of the 2-D B/U code.

Table 3.25 2-D B/U code based on $GF(7)$, seven multi-wavelength codewords $C_0 \sim C_6$ and the time-spreading codewords 0110100 of the (7,3,1,1)-OOC

group 0	group 1	group 2	…	group 6
$0:0C_0C_00C_00$	$7:0C_0C_10C_20$	$14:0C_0C_20C_40$	…	$42:0C_0C_60C_50$
$1:0C_1C_10C_10$	$8:0C_1C_20C_30$	$15:0C_2C_40C_60$	…	$43:0C_6C_50C_40$
$2:0C_2C_20C_20$	$9:0C_2C_30C_40$	$16:0C_4C_60C_10$	…	$44:0C_5C_40C_30$
$3:0C_3C_30C_30$	$10:0C_3C_40C_50$	$17:0C_6C_10C_30$	…	$45:0C_4C_30C_20$
$4:0C_4C_40C_40$	$11:0C_4C_50C_60$	$18:0C_1C_30C_50$	…	$46:0C_3C_20C_10$
$5:0C_5C_50C_50$	$12:0C_5C_60C_00$	$19:0C_3C_50C_00$	…	$47:0C_2C_10C_00$
$6:0C_6C_60C_60$	$13:0C_6C_00C_10$	$20:0C_5C_00C_20$	…	$48:0C_1C_00C_60$

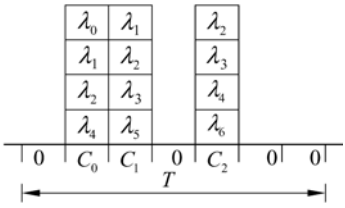

Figure 3.4 Scheme of the code matrix $0C_0C_10C_200$ of the 2-D B/U code

Theorem 3.2[16] The autocorrelation sidelobes and cross-correlation functions of the 2-D B/U code are both at most 1 only if the autocorrelation sidelobes and cross-correlation functions of the time-spreading unipolar codes deployed are both no greater than 1.

Proof: See Ref. [16].

3.9 2-D B/B OCDMA Codes

The 2-D bipolar/bipolar (B/B) OCDMA codes[19] are constructed by using one type of bipolar codes for wavelength-hopping and another type of bipolar codes for time-spreading. In conventional OCDMA communication systems, even in OCDMA systems with 2-D B/U codes, it is assumed that the codewords (matrices) are transmitted only on data bit 1's but nothing on data bit 0's. When the 2-D B/B codes that are introduced in this section are applied to OCDMA communication systems, the 2-D B/B code matrices are sent on data bit 1's and the complements on data bit 0's. For example, assume that a subscriber deploys the codeword $C_0C_1C_2\overline{C}_3\overline{C}_4C_5\overline{C}_6$ to transmit data bit 1's such that the complement wavelength matrix $\overline{C}_0\overline{C}_1\overline{C}_2C_3C_4\overline{C}_5C_6$ is employed to send data bit 0's. According to classical communication theory, a 3-dB improvement in the signal-to-interference ratio (SIR) can be acquired in a system using positive and negative

components to transmit data bit 1's and 0's respectively. Therefore, by employing the bipolar codes for time-spreading and the signal transmission of data bit 0's, the system performance can be substantially improved, and at the same time, the security and confidentiality of information transmission can be enhanced. The encoders and decoders of 2-D B/B codes can be implemented by utilizing the rapidly programmable and integrated hardware based on WDM devices such as AWGs or thin-film filters.

3.9.1 Construction of 2-D B/B Codes

The construction of 2-D B/B codes resembles the construction of 2-D B/U codes. The difference between these two approaches is that 2-D B/U employs the unipolar codes for time-spreading, whereas 2-D B/B codes deploys the bipolar codes for time-spreading. Their similarity is that in both of them there exists a multi-wavelength codeword in the "1" time slot and neither restrict the number of wavelengths on each column of a code matrix. The construction of 2-D B/B codes is as follows:

Step 1: Construct the multi-wavelength codewords and their complement codewords.

(1) Construct the modified m-sequences and their cyclic shift versions or use directly Walsh-Hadamard code.

In order to guarantee the orthogonality between the multi-wavelength bipolar codewords (i.e., the cross-correlation values are zero.) the number of 0's must be equal to the number of 1's in each codeword of the bipolar code chosen for wavelength-hopping. However, the number of 1's is one more than the number of 0's in an m-sequence and its cyclic shift versions. Hence, the m-sequence and its cyclic shifts must be modified. The method of modification is to patch one "zero" following the m-sequence and its cyclic shift versions such that the number of 0's is equal to the number of 1's in these sequences. The m-sequence 1110100 of length 7 and its six cyclic shift versions modified are shown in the left-hand side of Table 3.26. As for Walsh-Hadamard code, the cyclic shift and modification are not necessary. What we need to do is to eliminate the codeword of all "1". When $m = 8$, Walsh-Hadamard code obtained is shown in the right-hand side of Table 3.26.

(2) The positions of "1"s in each sequence obtained by Step (1) are regarded as the number of the wavelength such that we can acquire the multi-wavelength codeword, $C_i (i = 0,1,\cdots,\Phi_{\mathrm{MWC}} - 1)$, and its complement codeword of multi-wavelength, $\overline{C}_i (i = 0,1,\cdots,\Phi_{\mathrm{MWC}} - 1)$. $\overline{C}_i$ consists of the remaining wavelengths except for the wavelengths that are contained by C_i. For example, C_0 is

$\lambda_0\lambda_1\lambda_2\lambda_4$ such that $\overline{C}_0$ is $\lambda_3\lambda_5\lambda_6\lambda_7$. For both cases of m-sequence and Walsh-Hadamard, $m=8$ wavelengths $\{\lambda_0,\lambda_1,\lambda_2,\cdots,\lambda_7\}$ are required. The numbers of multi-wavelength codewords and their complements obtained are $\Phi_{MWC}=7$.

In general, the lengths of modified m-sequences and Walsh-Hadamard codes are both 2^k, where k is a positive integer.

Table 3.26 Multi-wavelength bipolar codewords based on the modified m-sequences and Walsh-Hadamard code with length 8[19]

Modified m-sequences		wavelengths		wavelengths	Walsh code		wavelengths		wavelengths
11101000	C_0	$\lambda_0\lambda_1\lambda_2\lambda_4$	$\overline{C}_0$	$\lambda_3\lambda_5\lambda_6\lambda_7$	10101010	C_0	$\lambda_0\lambda_2\lambda_4\lambda_6$	$\overline{C}_0$	$\lambda_1\lambda_3\lambda_5\lambda_7$
01110100	C_1	$\lambda_1\lambda_2\lambda_3\lambda_5$	$\overline{C}_1$	$\lambda_0\lambda_4\lambda_6\lambda_7$	11001100	C_1	$\lambda_0\lambda_1\lambda_4\lambda_5$	$\overline{C}_1$	$\lambda_2\lambda_3\lambda_6\lambda_7$
00111010	C_2	$\lambda_2\lambda_3\lambda_4\lambda_6$	$\overline{C}_2$	$\lambda_0\lambda_1\lambda_5\lambda_7$	10011001	C_2	$\lambda_0\lambda_3\lambda_4\lambda_7$	$\overline{C}_2$	$\lambda_1\lambda_2\lambda_5\lambda_6$
10011100	C_3	$\lambda_0\lambda_3\lambda_4\lambda_5$	$\overline{C}_3$	$\lambda_1\lambda_2\lambda_6\lambda_7$	11110000	C_3	$\lambda_0\lambda_1\lambda_2\lambda_3$	$\overline{C}_3$	$\lambda_4\lambda_5\lambda_6\lambda_7$
01001110	C_4	$\lambda_1\lambda_4\lambda_5\lambda_6$	$\overline{C}_4$	$\lambda_0\lambda_2\lambda_3\lambda_7$	10100101	C_4	$\lambda_0\lambda_2\lambda_5\lambda_7$	$\overline{C}_4$	$\lambda_1\lambda_3\lambda_4\lambda_6$
10100110	C_5	$\lambda_0\lambda_2\lambda_5\lambda_6$	$\overline{C}_5$	$\lambda_1\lambda_3\lambda_4\lambda_7$	11000011	C_5	$\lambda_0\lambda_1\lambda_6\lambda_7$	$\overline{C}_5$	$\lambda_2\lambda_3\lambda_4\lambda_5$
11010010	C_6	$\lambda_0\lambda_1\lambda_3\lambda_6$	$\overline{C}_6$	$\lambda_2\lambda_4\lambda_5\lambda_7$	10010110	C_6	$\lambda_0\lambda_3\lambda_5\lambda_6$	$\overline{C}_6$	$\lambda_1\lambda_2\lambda_4\lambda_7$

Step 2: Construct the prime sequences over Galois field $GF(p)$ of a prime number p, where $p \geqslant w$ and w denotes the number of "1" in a codeword of time-spreading bipolar code.

For example, when $p=7$, the prime sequences over $GF(7)$ are shown in Table 3.27. Then, every not-all-zero prime sequence as a seed is shifted circularly such that $p-1$ cyclic shift sequences can be obtained. For instance, through the left-cyclic shifts of the sequence 0123456, we can get six cyclic shift sequences: 1234560, 2345601, 3456012, 4560123, 5601234, 6012345. As for the all-zero prime sequence, we change it into the sequences of all-1, all-2,$\cdots$, all-$(p-1)$ rather than shift it circularly. In this way, p sequences are also acquired.

Step 3: Construct the time-spreading bipolar Barker sequences.

In order to implement 3dB SIR improvement of system performance, the "even" and "odd" correlation functions of the chosen bipolar code for time-spreading are required to be taken into account. The definitions of "even" and "odd" correlation functions are based on the patterns of two continuous data bits. The former denotes the circumstance of a data bit "1" followed by another "1" or a data bit "0" followed by another "0" and the later is for the case of a data bit "1" followed by a data bit "0" or vice versa. In order to guarantee the maximal autocorrelation sidelobe of the bipolar/bipolar codes no greater than one, the best candidate that can be applied to the bipolar/bipolar coding scheme as the time-spreading bipolar code is the family of Barker sequences[20]. Barker sequences are binary sequences that possess the even and odd "non-periodical"

autocorrelation sidelobes of at most 1. Their lengths are 2, 3, 4, 5, 7, 11 and 13 respectively, where the even and odd "periodical" autocorrelation sidelobes of Barker sequences with the length 3, 5, 7, 11 and 13 are also at most 1[19]. These sequences are +1+1−1, +1+1+1−1+1, +1+1+1−1−1+1−1, +1+1+1−1−1−1+1−1−1 +1−1 and +1+1+1+1+1−1−1+1+1−1+1−1+1.

Because there exists only one Barker sequence employed as the time-spread bipolar codeword for a given length, the Barker sequence's cross-correlation property is inconsequential[19]. The cross-correlation functions of the bipolar/ bipolar codes are always at most 1 because the maximum cross-correlation function of the prime sequences employed for the permutations is 1 and the autocorrelation sidelobes of the time-spreading bipolar codes are also bounded by 1. Therefore, as a matter of fact, any bipolar codes with good autocorrelation properties can be employed as the time-spreading codes for 2-D B/B codes.

Table 3.27 Prime sequences over $GF(7)$

(a) Prime sequences over $GF(7)$

i	S_i						
0	0	0	0	0	0	0	0
1	0	1	2	3	4	5	6
2	0	2	4	6	1	3	5
3	0	3	6	2	5	1	4
4	0	4	1	5	2	6	3
5	0	5	3	1	6	4	2
6	0	6	5	4	3	2	1
	← $n = 7$ →						

(b) Prime sequences over $GF(7)$ and their cyclic shift versions

group 0	group 1	group 2	⋯	group 6
0:0000000	7:0123456	14:0246135	⋯	42:0654321
1:1111111	8:1234560	15:2461350	⋯	43:6543210
2:2222222	9:2345601	16:4613502	⋯	44:5432106
3:3333333	10:3456012	17:6135024	⋯	45:4321065
4:4444444	11:4560123	18:1350246	⋯	46:3210654
5:5555555	12:5601234	19:3502461	⋯	47:2106543
6:6666666	13:6012345	20:5024613	⋯	48:1065432

Lemma 3.3[19]: The absolute values of autocorrelation sidelobes and cross-correlation functions of the bipolar/bipolar codes are at most 1 only if the even and odd periodical autocorrelation sidelobes of the bipolar codes used in the time domain are at most 1.

Proof: See Ref.[19].

Step 4: Generate 2-D B/B codes through mapping based on the Barker sequence, the prime sequences and versions of their cyclic shifts, the multi-wavelength codewords and their complements obtained from the above steps.

The multi-wavelength codewords are generated by mapping the elements of the prime sequences and the versions of their cyclic shifts into the number of the wavelength. The elements in the Barker sequence determine either the multi-wavelength code matrices or the complement multi-wavelength matrices used. When an element in Barker is +1, it is replaced by a multi-wavelength codeword at the corresponding position. When an element in Barker is −1, it is replaced by a complement multi-wavelength codeword at the corresponding position. For

instance, we choose $n = p = \Phi_{\mathrm{MWC}} = 7$ and employ the Barker sequence +1+1+1−1−1+1−1 with the length 7 such that the 2-D B/B codewords obtained are shown in Table 3.28.

Note that the bipolar/bipolar code matrices in Table 3.28 are used to transmit the data bit 1. When the data bit 0 is transmitted, the corresponding complement of multi-wavelength is deployed. For example, it is assumed that we utilize the codeword of number 7, $C_0C_1C_2\overline{C}_3\overline{C}_4C_5\overline{C}_6$, to send the data bit "1" such that its multi-wavelength complement codeword, $\overline{C}_0\overline{C}_1\overline{C}_2C_3C_4\overline{C}_5C_6$, is employed to transmit the data bit "0".

Table 3.28 Bipolar/Bipolar codewords with length $n = 7$ based on $GF(7)$, seven multi-wavelength bipolar codewords in Table 3.26 and the time-spreading Barker-sequence 1110010[19]

group 0	group 1	group 2	⋯	group 6
$0: C_0C_0C_0\overline{C}_0\overline{C}_0C_0\overline{C}_0$	$7: C_0C_1C_2\overline{C}_3\overline{C}_4C_5\overline{C}_6$	$14: C_0C_2C_4\overline{C}_6\overline{C}_1C_3\overline{C}_5$	⋯	$42: C_0C_6C_5\overline{C}_4\overline{C}_3C_2\overline{C}_1$
$1: C_1C_1C_1\overline{C}_1\overline{C}_1C_1\overline{C}_1$	$8: C_1C_2C_3\overline{C}_4\overline{C}_5C_6\overline{C}_0$	$15: C_2C_4C_6\overline{C}_1\overline{C}_3C_5\overline{C}_0$	⋯	$43: C_6C_5C_4\overline{C}_3\overline{C}_2C_1\overline{C}_0$
$2: C_2C_2C_2\overline{C}_2\overline{C}_2C_2\overline{C}_2$	$9: C_2C_3C_4\overline{C}_5\overline{C}_6C_0\overline{C}_1$	$16: C_4C_6C_1\overline{C}_3\overline{C}_5C_0\overline{C}_2$	⋯	$44: C_5C_4C_3\overline{C}_2\overline{C}_1C_0\overline{C}_6$
$3: C_3C_3C_3\overline{C}_3\overline{C}_3C_3\overline{C}_3$	$10: C_3C_4C_5\overline{C}_6\overline{C}_0C_1\overline{C}_2$	$17: C_6C_1C_3\overline{C}_5\overline{C}_0C_2\overline{C}_4$	⋯	$45: C_4C_3C_2\overline{C}_1\overline{C}_0C_6\overline{C}_5$
$4: C_4C_4C_4\overline{C}_4\overline{C}_4C_4\overline{C}_4$	$11: C_4C_5C_6\overline{C}_0\overline{C}_1C_2\overline{C}_3$	$18: C_1C_3C_5\overline{C}_0\overline{C}_2C_4\overline{C}_6$	⋯	$46: C_3C_2C_1\overline{C}_0\overline{C}_6C_5\overline{C}_4$
$5: C_5C_5C_5\overline{C}_5\overline{C}_5C_5\overline{C}_5$	$12: C_5C_6C_0\overline{C}_1\overline{C}_2C_3\overline{C}_4$	$19: C_3C_5C_0\overline{C}_2\overline{C}_4C_6\overline{C}_1$	⋯	$47: C_2C_1C_0\overline{C}_6\overline{C}_5C_4\overline{C}_3$
$6: C_6C_6C_6\overline{C}_6\overline{C}_6C_6\overline{C}_6$	$13: C_6C_0C_1\overline{C}_2\overline{C}_3C_4\overline{C}_5$	$20: C_5C_0C_2\overline{C}_4\overline{C}_6C_1\overline{C}_3$	⋯	$48: C_1C_0C_6\overline{C}_5\overline{C}_4C_3\overline{C}_2$

3.9.2 Cardinalities of 2-D B/B Codes[19]

The cardinality of a chosen bipolar code in the wavelength domain depends on the number of wavelengths used. If we deploy the modified m-sequences or Walsh-Hadamard code then the cardinality of both is

$$\Phi_{\mathrm{MWC}} = \text{Number of wavelengths} - 1 \tag{3.45}$$

where $\Phi_{\mathrm{MWC}} = p$. The number of available prime sequences $\Phi_{\mathrm{group}} = p$ over $GF(p)$ is determined by the length n of the chosen bipolar code in the time domain, i.e., $n = p$. Thus, the cardinality of a 2-D B/B code is

$$\Phi_{\mathrm{B/B}} = p^2 \tag{3.46}$$

Note that when $\Phi_{\mathrm{MWC}} \neq n$, the resulting cardinality of 2-D B/B code is non-optimal. For example, we suppose that for $n = p = 13$ we can obtain 13 multi-wavelength bipolar codewords and their complements ($\Phi_{\mathrm{MWC}} = 15$) from

the m-sequences and Walsh-Hadamard code of length 13, which are expressed as C_i and $\overline{C}_i$ ($i \in [0,12]$). Afterwards, based on the length $n=13$ determined by the prime sequences over $GF(13)$ (as shown in Table 3.29) we choose the time-spreading Barker sequence: +1+1+1+1+1−1−1+1+1−1+1−1+1. According to the aforementioned construction, the resulting overall codewords of the 2-D B/B code with the cardinality $\Phi_{B/B} = p^2 = 169 < 15^2 = 225$, are shown in Table 3.30. Table 3.31 shows the cardinalities of some 2-D B/B codes.

Table 3.29 Prime sequences over $GF(13)$

i	S_i												
0	0	0	0	0	0	0	0	0	0	0	0	0	0
1	0	1	2	3	4	5	6	7	8	9	10	11	12
2	0	2	4	6	8	10	12	1	3	5	7	9	11
3	0	3	6	9	12	2	5	8	11	1	4	7	10
4	0	4	8	12	3	7	11	2	6	10	1	5	9
5	0	5	10	2	7	12	4	9	1	6	11	3	8
6	0	6	12	5	11	4	10	3	9	2	8	1	7
7	0	7	1	8	2	9	3	10	4	11	5	12	6
8	0	8	3	11	6	1	9	4	12	7	2	10	5
9	0	9	5	1	10	6	2	11	7	3	12	8	4
10	0	10	7	4	1	11	8	5	2	12	9	6	3
11	0	11	9	7	5	3	1	12	10	8	6	4	2
12	0	12	11	10	9	8	7	6	5	4	3	2	1

Table 3.30 2-D B/B code matrices[19] of length 13 constructed based on $GF(7)$, 13 multi-wavelength bipolar codewords and the time-spreading Barker 1111100110101

group 0	**group 1**
$0: C_0C_0C_0C_0C_0\overline{C}_0\overline{C}_0C_0C_0\overline{C}_0C_0\overline{C}_0C_0$	$13: C_0C_1C_2C_3C_4\overline{C}_5\overline{C}_6C_7C_8\overline{C}_9C_{10}\overline{C}_{11}C_{12}$
$1: C_1C_1C_1C_1C_1\overline{C}_1\overline{C}_1C_1C_1\overline{C}_1C_1\overline{C}_1C_1$	$14: C_1C_2C_3C_4C_5\overline{C}_6\overline{C}_7C_8C_9\overline{C}_{10}C_{11}\overline{C}_{12}C_0$
$2: C_2C_2C_2C_2C_2\overline{C}_2\overline{C}_2C_2C_2\overline{C}_2C_2\overline{C}_2C_2$	$15: C_2C_3C_4C_5C_6\overline{C}_7\overline{C}_8C_9C_{10}\overline{C}_{11}C_{12}\overline{C}_0C_1$
⋮ ⋮	⋮ ⋮
$12: C_{12}C_{12}C_{12}C_{12}C_{12}\overline{C}_{12}\overline{C}_{12}C_{12}C_{12}\overline{C}_{12}C_{12}\overline{C}_{12}C_{12}$	$25: C_{12}C_0C_1C_2C_3\overline{C}_4\overline{C}_5C_6C_7\overline{C}_8C_9\overline{C}_{10}C_{11}$
…	**group 6**
…	$156: C_0C_{12}C_{11}C_{10}C_9\overline{C}_8\overline{C}_7C_6C_5\overline{C}_4C_3\overline{C}_2C_1$
…	$157: C_{12}C_{11}C_{10}C_9C_8\overline{C}_7\overline{C}_6C_5C_4\overline{C}_3C_2\overline{C}_1C_0$
…	$158: C_{11}C_{10}C_9C_8C_7\overline{C}_6\overline{C}_5C_4C_3\overline{C}_2C_1\overline{C}_0C_{12}$
⋮	⋮ ⋮
…	$168: C_1C_0C_{12}C_{11}C_{10}\overline{C}_9\overline{C}_8C_7C_6\overline{C}_5C_4\overline{C}_3C_2$

Table 3.31 Cardinalities of some 2-D B/B codes[19]

$n=p$	Φ_{group}	Φ_{MWC}	Number of wavelengths	$\Phi_{\text{B/B}}$
3	3	3	4	9
5	5	7	8	25
7	7	7	8	49
11	11	15	16	121
13	13	15	16	169
31	31	31	32	961

3.10 2-D Wavelength-hopping Prime Codes and Extended Wavelength-hopping Prime Codes for OCDMA

We introduce 2-D wavelength-hopping prime codes (WHPC)[13, 21] and extended wavelength-hopping prime codes (EWHPC)[13, 21 – 23] in this section. WHPC has only one pulse per row in its code matrix and EWHPC is an extension of WHPC that removes the restriction of only one pulse per row in its code matrix. Therefore, EWHPC is very applicable to high-speed OOCDMA systems with limited time slots.

3.10.1 2-D WHPCs

For the given integers w, k and a set of prime numbers $\{p_1, p_2, \cdots, p_k\}$, 2-D $(w \times p_1 p_2 \cdots p_k, w, 0, 1)$-WHPC is a collection of binary $\{0,1\}$ $w \times p_1 p_2 \cdots p_k$ matrices with code length $p_1 p_2 \cdots p_k$, code weight w and cardinality $p_1 p_2 \cdots p_k$, where $p_k \geqslant p_{k-1} \geqslant \cdots \geqslant p_2 \geqslant p_1 \geqslant w.$ w represents the number of rows of the matrix (related to the number of available wavelengths) and $p_1 p_2 \cdots p_k$ denotes the number of columns of the matrix (related to the number of time slots, i.e., the number of chips). Because there is only one pulse (namely, one binary 1) in every row of each matrix and each pulse of the matrix is assigned to a distinct wavelength, the autocorrelation sidelobes of WHPC are zero ($\lambda_a = 0$) and its maximum cross-correlation function is one ($\lambda_c = 1$). It can be seen that the prime code is a special case of WHPC with $k = 1$ and $w = p_1$, which uses only one wavelength and has only p_1 single-wavelength codewords (Note that the prime code has $\lambda_a = p_1 - 1$ and $\lambda_c = 2$). The 2-D PC/PC code is a subset of WHPC with $k = 2$ and $w = p_1 = p_2$, which has $p_1(p_1 - 1)$ code matrices. Strictly speaking, a 2-D PC/PC code is the scenario of WHPC with $k = 2$ subtracting WHPC with $k = 1$, that is, under the same parameters, WHPC has p_1 code matrices more than the 2-D PC/PC code.

3.10.1.1 Construction of 2-D WHPCs[13]

Given two positive integers w and k, and a set of prime integers $\{p_1, p_2, \cdots, p_k\}$ such that $p_k \geqslant p_{k-1} \geqslant \cdots \geqslant p_2 \geqslant p_1 \geqslant w$, then the code matrices, $\boldsymbol{X}_{i_1,i_2,\cdots,i_k}$, with the ordered pairs

$$\begin{aligned}&\{[(0,0),(1,i_1+i_2p_1+\cdots+i_kp_1p_2\cdots p_{k-1}),(2,2\otimes_{p_1} i_1+(2\otimes_{p_2} i_2)p_1+\cdots+(2\otimes_{p_k} i_k)p_1p_2\cdots p_{k-1}),\\&\cdots,(w-1,(w-1)\otimes_{p_1} i_1+((w-1)\otimes_{p_2} i_2)p_1+\cdots+((w-1)\otimes_{p_k} i_k)p_1p_2\cdots p_{k-1})]:\\&i_1=\{0,1,\cdots,p_1-1\},i_2=\{0,1,\cdots,p_2-1\},\cdots,i_k=\{0,1,\cdots,p_{k-1}\}\}\end{aligned} \tag{3.47}$$

form a 2-D $(w\times p_1p_2\cdots p_k, w, 0, 1)$ -WHPC, which has the code length of $p_1p_2\cdots p_k$ and the code weight of w and the cardinality of $|C|=p_1p_2\cdots p_k$, where "$\otimes_{p_j}$" expresses a modulo-p_j multiplication and $j=\{1,2,3,\cdots,k\}$. (For the ease of representation, each matrix can equivalently be written as a set of ordered pairs of w ones, i.e., one ordered pair for every binary one, where each ordered pair (λ_v, t_h) represents the vertical (v) and horizontal (h) displacements of a binary one from the bottom-leftmost corner of a matrix. In other words, λ_v denotes the transmitting wavelength and t_h indicates the time position of a binary one in the matrix.)

Example 3.14 Let $k=3$ and $w=p_1=p_2=p_3=5$. Then, the code matrices, $\boldsymbol{X}_{i_1,i_2,i_3}$, with the ordered pairs

$$\begin{aligned}&\{[(0,0),(1,i_1+5i_2+25i_3),(2,2\otimes_5 i_1+(2\otimes_5 i_2)5+(2\otimes_5 i_3)25),\\&(3,3\otimes_5 i_1+(3\otimes_5 i_2)5+(3\otimes_5 i_3)25),(4,4\otimes_5 i_1+(4\otimes_5 i_2)5+(4\otimes_5 i_3)25)]:\\&i_1\in[0,4],i_2\in[0,4],i_3\in[0,4]\}\end{aligned}$$

form a 2-D $(5\times125,5,0,1)$ WHPC, which has the code length $p_1p_2p_3=125$, code weight 5 and cardinality $|C|=p_1p_2p_3=125$. For example $\boldsymbol{X}_{1,2,3}=[(0,0),(1,86),(2,47),(3,108),(4,69)]$.

3.10.1.2 Correlation Properties of 2-D WHPCs

Theorem 3.4[13] The autocorrelation sidelobe of any matrix in an 2-D $(w\times p_1p_2\cdots p_k, w, 0, 1)$ WHPC is zero and the cross-correlation function between any two distinct matrices in this code is at most one.

Proof: See Ref.[13].

3.10.1.3 Cardinality of 2-D WHPCs

Based on equation (3.3), let $m=w$, $n=p_1p_2\cdots p_k$, $\lambda_a=0$ and $\lambda_c=1$. Then, we can obtain the upper bound on the cardinality of the 2-D $(w\times p_1p_2\cdots p_k, w, 0, 1)$ WHPC

$$\Phi(w\times p_1p_2\cdots p_k,w,0,1)\leqslant\Phi(w\times p_1p_2\cdots p_k,w,1,1)$$
$$\leqslant\frac{w(w\times p_1p_2\cdots p_k-1)}{w(w-1)}=p_1p_2\cdots p_k+\frac{p_1p_2\cdots p_k-1}{(w-1)} \tag{3.48}$$

However, the actual cardinality of 2-D $(w\times p_1p_2\cdots p_k,w,0,1)$ WHPC is $p_1p_2\cdots p_k$, which is smaller than the upper bound of the cardinality of 2-D $(w\times p_1p_2\cdots p_k,w,1,1)$-OOC. It is near to the upper bound when w is large. Thus, it is asymptotically optimal.

3.10.2 2-D EWHPCs

3.10.2.1 2-D $(wp'\times p_1p_2\cdots p_k,w,0,1)$ EWHPCs[13, 21]

2-D WHPC is restricted to only one pulse in every row of its code matrices and the number of available wavelengths is equal to the code weight. This limits the cardinality of 2-D WHPC. When the number of available wavelengths is greater than the actual number of wavelengths required, we can obtain the extended wavelength-hopping prime codes (EWHPC) by eliminating the one-pulse-per-row restriction and modifying WHPC. EWHPC can support more flexible code design and increase substantially its own cardinality (as much as w times the cardinality of WHPC) while maintaining ideal correlation properties.

Of course, for the scenarios where the number of available wavelengths is greater than the actual number of wavelengths required, $m=wp'$ available wavelengths can also be divided into p' (p' is a prime number.) groups with w wavelengths each. Each group employs the same $p_1p_2\cdots p_k$ codeword matrices of WHPC such that $p'p_1p_2\cdots p_k$ code matrices can be obtained. However, in doing so, except when the cardinality is relatively quite small (when EWHPC has $(w+1)p'p_1p_2\cdots p_k$ code matrices), a central controller is also required to control the on-line probability of each wavelength uniformly. Unfortunately, the cost of network utilization and the additional overhead of network management will be increased substantially.

(1) Construction of 2-D EWHPCs

Step 1: Let $w=p_1$. Given a positive integer k, construct an $(p_1\times p_1p_2\cdots p_k,p_1,0,1)$ WHPC with the code weight p_1, the code length $p_1p_2\cdots p_k$ and the $p_1p_2\cdots p_k$ codewords by using the construction of WHPC. The ordered pairs of the code matrices $\boldsymbol{X}_{i_1,i_2,\cdots,i_k}$ are

$$\{[(0,0),(1,i_1+i_2p_1+\cdots+i_kp_1p_2\cdots p_{k-1}),(2,2\otimes_{p_1}i_1+(2\otimes_{p_2}i_2)p_1+\cdots$$
$$+(2\otimes_{p_k}i_k)p_1p_2\cdots p_{k-1}),\cdots,(p_1-1,(p_1-1)\otimes_{p_1}i_1+((p_1-1)\otimes_{p_2}i_2)p_1+\cdots$$
$$+((p_1-1)\otimes_{p_k}i_k)p_1p_2\cdots p_{k-1})]:i_1=\{0,1,\cdots,p_1-1\},i_2=\{0,1,\cdots,p_2-1\},$$
$$\cdots,i_k=\{0,1,\cdots,p_{k-1}\}\} \tag{3.49}$$

where "$\otimes_{p_j}$" represents modulo-p_j multiplication for $j=[1,k]$, $p_k \geqslant p_{k-1} \geqslant \cdots \geqslant p_2 \geqslant p_1 \geqslant w$.

Step 2: Given the positive integer w and prime number p' such that $p' \geqslant w$ and $p_1 \geqslant wp'$,

$$\{[l_1,(l_1 \oplus_w l_2)+w,(l_1 \oplus_w (2 \otimes_{p'} l_2))+2w,\cdots,(l_1 \oplus_w ((w-1) \otimes_{p'} l_2)+(w-1)w]: l_1=\{0,1,\cdots,w-1\}, l_2=\{0,1,\cdots,w-1\}\} \quad (3.50)$$

and $$\{[l_2 w, l_2 w+1,\cdots,l_2 w+(w-1)]: l_2=\{0,1,\cdots,p'-1\}\} \quad (3.51)$$

where "$\otimes_{p'}$" and "$\oplus_w$" represent modulo-p' multiplication and modulo-w addition respectively. The first component of each ordered pair of EWHPC is generated from equation (3.50) and equation (3.51). Then, based on the first components, we choose w ordered pairs from the code matrices $\boldsymbol{X}_{i_1,i_2,\cdots,i_k}$ obtained from equation (3.49) forming the new code matrices $\boldsymbol{X}_{i_1,i_2,\cdots,i_k,l_1,l_2}$ and $\boldsymbol{X}_{i_1,i_2,\cdots,i_k,l_2}$. In other words, we obtain an $(wp' \times p_1 p_2 \cdots p_k, w, 0, 1)$ -EWHPC with code length $p_1 p_2 \cdots p_k$, code weight w (the number of available wavelengths, wp') and cardinality $(w^2+p')p_1 p_2 \cdots p_k$. (Because the w^2 first components of the ordered pairs are produced from equation (3.50) and p' first components of the ordered pairs are produced from the equation (3.51), and since there are $p_1 p_2 \cdots p_k$ second components of the ordered pairs, therefore the cardinality is $(w^2+p')p_1 p_2 \cdots p_k$).

Example 3.15 Let $w=p'=3$ and $p_1=p_2=11$ such that $k=2$. From equation (3.49), we obtain $p_1 p_2 = 11 \times 11 = 121$ code matrices of WHPC, $\boldsymbol{X}_{i_1,i_2}$, with the ordered pairs

$$\{[(0,0),(1,i_1+11i_2),(2,2 \otimes_{11} i_1+(2 \otimes_{11} i_2)11),\cdots,(10,10 \otimes_{11} i_1+(10 \otimes_{11} i_2)11)]: i_1 \in [0,10], i_2 \in [0,10]\}.$$

For example, when $i_1=2$ and $i_2=5$, we get $\boldsymbol{X}_{2,5}=[(0,0),(1,57),(2,114),(3,50),(4,107),(5,43),(6,89),(7,25),(8,82),(9,18),(10,75)]$.

Then, from equation (3.50) and equation (3.51) respectively, we obtain

$$\{[l_1,(l_1 \oplus_3 l_2)+3,(l_1 \oplus_3 (2 \otimes_3 l_2))+6]: l_1=\{0,1,2\}, l_2=\{0,1,2\}\}$$
$$\{[3l_2,3l_2+1,3l_2+2]: l_2=\{0,1,2\}\}$$

For instance, when $l_1=1, l_2=1,$ we acquire two groups of first components: [1,5,6] and [3,4,5]. In terms of the first components, we choose the ordered pairs from

$\boldsymbol{X}_{2,5}$ and then obtain $\boldsymbol{X}_{2,5,1,1}=[(1,57),(5,43),(6,89)]$, $\boldsymbol{X}_{2,5,1}=[(3,50),(4,107),(5,43)]$. By the same argument, when $l_1=1$, $l_2=2$, two groups of the first components [1,3,8] and [6,7,8] are obtained and we choose the ordered pairs from $\boldsymbol{X}_{2,5}$. Thus, the codeword matrices $\boldsymbol{X}_{2,5,1,2}=[(1,57),(3,50),(8,82)]$ and $\boldsymbol{X}_{2,5,2}=[(6,89),(7,25),(8,82)]$ are obtained.

Similarly, when $l_1=2$ and $l_2=2$, a group of the first components [2,4,6] is found. We obtain $\boldsymbol{X}_{2,5,2,2}=[(2,114),(4,107),(6,89)]$ by picking the ordered pairs from $\boldsymbol{X}_{2,5}$. In this way, an $(9\times121,3,0,1)$-EWHPC with the code weight 3 and the code length 121 can be produced, which has $(w^2+p')p_1p_2=(3^2+3)\times11\times11=1452$ code matrices divided into $w^2+p'=3^2+3=12$ groups. On the other hand, if $wp'=9$ wavelengths are divided into 3 groups such that each group has 3 wavelengths, we can only obtain $p'p_1p_2=3\times11\times11=363$ code matrices of WHPC with code length 121 and code weight 3. It is obvious that the cardinality of EWHPC increases substantially in comparison with WHPC.

(2) Cardinality of 2-D EWHPCs

Let $m=wp'$, $n=p_1p_2\cdots p_k$, $\lambda_a=0$ and $\lambda_c=1$. Based on equation (3.3), the upper bound on the cardinality of a 2-D $(wp'\times p_1p_2\cdots p_k,w,0,1)$ EWHPC is[13]

$$\begin{aligned}&\Phi(wp'\times p_1p_2\cdots p_k,w,0,1)\leqslant\Phi(wp'\times p_1p_2\cdots p_k,w,1,1)\\&\leqslant\frac{wp'(wp'p_1p_2\cdots p_k-1)}{w(w-1)}=p'^2p_1p_2\cdots p_k+\frac{p'^2p_1p_2\cdots p_k-p'}{(w-1)}\end{aligned}\tag{3.52}$$

The actual cardinality of the $(wp'\times p_1p_2\cdots p_k,w,0,1)$-EWHPC is $(w^2+p')p_1p_2\cdots p_k$. Thus, the cardinality of EWHPC does not achieve the theoretical upper bound of equation (3.52). If $p'=w$, then the upper bound of equation (3.52) becomes

$$\Phi(w^2\times p_1p_2\cdots p_k,w,0,1)\leqslant w^2p_1p_2\cdots p_k+\frac{w^2p_1p_2\cdots p_k-w}{(w-1)}\tag{3.53}$$

which is a factor $1+1/[w^2-1+(w-1)/(p_1p_2\cdots p_k-1)]$ more than the actual cardinality. It can be seen that when w is large, the factor is close to one and therefore, the $(wp'\times p_1p_2\cdots p_k,w,0,1)$-EWHPC is asymptotically optimal.

(3) Performance of 2-D EWHPCs

Theorem 3.5[21] The autocorrelation sidelobes of any code matrix in the $(wp'\times p_1p_2\cdots p_k,w,0,1)$-EWHPC are zero and the maximum value of cross-correlation functions between any two distinct code matrices in the code set is one. There are $w\times p_1p_2\cdots p_k$ subsets of w matrices each from (3.50) and $p_1p_2\cdots p_k$

subsets of p' matrices each from (3.51) such that the cross-correlation values of all matrices within a subset are zero.

Proof: See Ref.[21].

In order to analyze the performance of the $(wp' \times p_1 p_2 \cdots p_k, w, 0, 1)$ -EWHPC, we need to know the probability that one of pulses (i.e., a binary one) in a signature matrix to "hit" with a pulse in a received matrix, given by[22]

$$q = \frac{1}{2} \cdot \frac{w}{n} \cdot \frac{w}{m} \times R = \frac{w}{2 \cdot p' \cdot p_1 p_2 \cdots p_k} \times R \tag{3.54}$$

where 1/2 comes from the assumption that the transmissions of 0 and 1 data bits are equiprobable, w/n is the collision probability due to the horizontal alignment of the w pulse in n time slots, and w/m is the collision probability due to the vertical alignment of the w pulse in m wavelengths, R indicates the ratio of the number of matrices contributing one collision (to the cross-correlation function) to the total number of interfering matrices, w is the code weight, $n = p_1 p_2 \cdots p_k$ is the code length, and $m = wp'$ is the number of available wavelengths. Since EWHPC does not employ repeated wavelengths in each matrix and R is deployed to account for the matrices with zero cross-correlation property,

$$\begin{aligned} R = & \sum_{\text{all subsets}} P(\text{a matrix causes a hit} | \text{the matrix is from a subset}) \times \\ & P'(\text{the subset is chosen from the code set } \Phi) \\ = & \frac{\Phi - 1 - (w-1) p_1 p_2 \cdots p_k}{\Phi - 1} \cdot \frac{w^2}{w^2 + p'} + \frac{\Phi - 1 - (p'-1) p_1 p_2 \cdots p_k}{\Phi - 1} \cdot \frac{p'}{w^2 + p'} \\ = & 1 - \frac{(w^3 - w^2 + p'^2 - p') p_1 p_2 \cdots p_k}{(\Phi - 1)(w^2 + p')} \end{aligned} \tag{3.55}$$

where $\Phi = (w^2 + p') p_1 p_2 \cdots p_k$ is the code cardinality, and $\Phi - 1$ denotes the overall number of possible interfering matrices. The first term in R reflects that there are $w \times p_1 p_2 \cdots p_k$ subsets of w matrices each from (3.50) such that the cross-correlation values between all matrices within a subset are zero. Thus, there are in total $(w-1) p_1 p_2 \cdots p_k$ matrices that will not employ the same wavelengths as the desired matrix, out of $\Phi - 1$ possible interferers. There are in all w^2 such subsets, out of $w^2 + p'$ subsets. The second term in R comes from the fact that there are $p_1 p_2 \cdots p_k$ subsets of p' matrices each from (3.51), such that the cross-correlation values of all matrices within the subset. Similarly, there are in all $(p'-1) p_1 p_2 \cdots p_k$ matrices that will not deploy the same wavelengths

as the desired matrix, out of $\Phi - 1$ possible interferers. There are totally p' such subsets, out of $w^2 + p'$ subsets.

When $w = p'$, (3.55) is simplified into[22]

$$R = 1 - \frac{(w-1)p_1 p_2 \cdots p_k}{\Phi - 1} \approx 1 - \frac{w-1}{w^2 + w} \tag{3.56}$$

It can be seen that R has little effect on the collision probability q in (3.54), especially when w is large.

Consider the case of chip synchronization with the bit error rate (BER) of the system employing EWHPC for the cross-correlation functions of at most one given by[22]

$$P_{\mathrm{b}} = \frac{1}{2}\sum_{i=Th}^{K-1}\binom{K-1}{i} q^i (1-q)^{K-1-i} \tag{3.57}$$

where Th represents the decision threshold of the receiver and K indicates the total number of simultaneous subscribers. In general, Th is set to w for optimal decision.

For the chip-asynchronous case, by utilizing the Gaussian approximation the BER $P_{\mathrm{b|G}}$ of EWHPC for the cross-correlation functions of at most one can be obtained[22], such that

$$P_{\mathrm{b|G}} = \Theta\left(\frac{-w}{\sqrt{4(K-1)\sigma^2}}\right) \tag{3.58}$$

where K is the total number of simultaneous subscribers, $\Theta = \left(\frac{1}{\sqrt{2\pi}}\right)\int_{-\infty}^{x} \exp(-y^2/2)\mathrm{d}y$ is the unit-normal cumulative distribution function. $\sigma^2 = \sigma_{\mathrm{syn}}^2 = (1-q)q$ for the chip-synchronous case and $\sigma^2 = \sigma_{\mathrm{syn}}^2 = (2q/3) - q^2$ for the chip-asynchronous case are obtained respectively. From Fig. 3.5, it can be seen that the performance of the chip-asynchronous case is superior to the chip-synchronous case. In fact, the former is close to the real situation. The purpose of presenting the chip-synchronous case to analyze the BER is for ease of computation. In doing so, we get an upper bound on the BER, i.e., the worst case. For example, for 100 simultaneous subscribers with $w = 3$, $p' = 5$, $k = 2$ and $n = p_1 p_2 = 17 \times 19 = 323$, $P_{\mathrm{b|G}} = 1.7 \times 10^{-8}$ for the chip-synchronous case and $P_{\mathrm{b|G}} = 7.3 \times 10^{-12}$ for the chip-asynchronous case. It can be seen that the latter is more than three orders of magnitude better than the former in the BER. In addition, the difference in the BER between the two cases increases as w, p' and n increase.

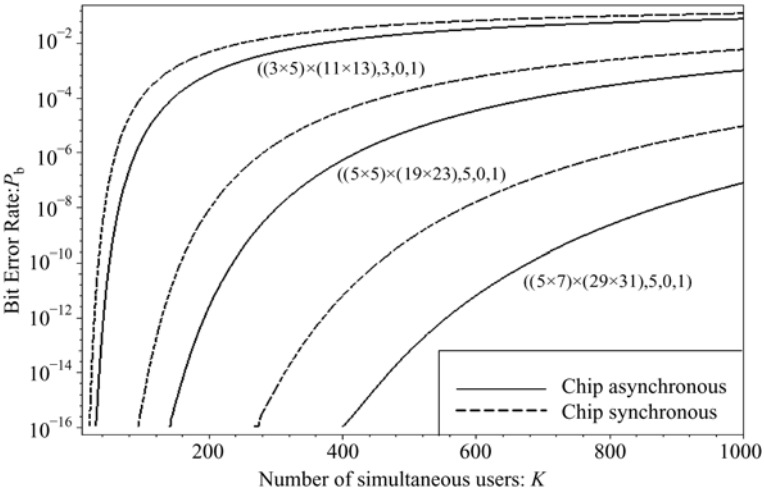

Figure 3.5 BER versus the number of simultaneous users K for an OCDMA system with the $(wp' \times p_1 p_2, w, 0, 1)$ -EWHPC, for $k = 2$, with and without the chip-synchronous assumption

3.10.2.2 2-D $(p_1 p_2 \cdots p_k \times p_1, w, 0, 1)$ EWHPCs

We assumed that the number of time slots was always greater than the number of available wavelengths when we introduced 2-D OCDMA codes in the above sections. However, the assumption may not be always true in high bit-rate systems. For example, with the present optical time-division multiplexing (OTDM) technology[23, 24], 10-plus Gb/s OCDMA systems can support about 30 chips in the time domain[25]. Such a small number of chips can accommodate only a very limited numbers of subscribers and simultaneous users, even in 2-D OCDMA networks. However, this limitation can be compensated for and even improved in the wavelength-hopping/time-spreading coding scheme by increasing the number of available wavelengths when using lasers with broadened super-continuum spectra. Such 2-D $(p_1 p_2 \cdots p_k \times p_1, w, 0, 1)$ extended wavelength-hopping/time-spreading codes (EWHPC)[25] that have more wavelengths than time slots are introduced in this section. The cardinality of these EWHPCs is enlarged quadratically and the ideal correlation properties (the autocorrelation sidelobes are zero and the cross-correlation functions are at most one) are preserved. Meanwhile, this kind of code also has a special wavelength-shift property to support flexible implementation of programmable hardware based on AWGs and FBGs[25].

(1) Construction of 2-D EWHPCs[25]

Given a positive integer k and a set of prime numbers $\{p_1, p_2, \cdots, p_k\}$ such that $p_k \geqslant p_{k-1} \geqslant \cdots \geqslant p_2 \geqslant p_1 \geqslant w$, the matrices $\boldsymbol{X}_{i_1, i_2, \cdots, i_k, l_1, l_2, \cdots, l_k}$ with the ordered pairs

$$
\begin{aligned}
&\{[(l_1 + l_2 p_1 + l_3 p_1 p_2 + \cdots + l_k p_1 p_2 \cdots p_{k-1}, 0),\\
&((i_1 \oplus_{p_1} l_1) + (i_2 \oplus_{p_1} l_2) p_1 + (i_3 \oplus_{p_1} l_3) p_1 p_2 + \cdots + (i_k \oplus_{p_1} l_k) p_1 p_2 \cdots p_{k-1}, 1),\\
&(((2 \otimes_{p_1} i_1) \oplus_{p_1} l_1) + ((2 \otimes_{p_2} i_2) \oplus_{p_1} l_2) p_1 + ((2 \otimes_{p_3} i_3) \oplus_{p_1} l_3) p_1 p_2 + \cdots\\
&\qquad + ((2 \otimes_{p_k} i_k) \oplus_{p_1} l_k) p_1 p_2 \cdots p_{k-1}, 2), \cdots,\\
&((((w-1) \otimes_{p_1} i_1) \oplus_{p_1} l_1) + (((w-1) \otimes_{p_2} i_2) \oplus_{p_1} l_2) p_1 + (((w-1) \otimes_{p_3} i_3) \oplus_{p_1} l_3) p_1 p_2 +\\
&\qquad \cdots + (((w-1) \otimes_{p_k} i_k) \oplus_{p_1} l_k) p_1 p_2 \cdots p_{k-1}, w-1)]:\\
&\text{group } 1: i_1 \in [0, p_1 - 1],\ i_2 \in [0, p_2 - 1],\ \cdots,\ i_{k-1} \in [0, p_{k-1} - 1],\ i_k \in [1, p_k - 1],\\
&\qquad l_1 \in [0, p_1 - 1],\ l_2 \in [0, p_2 - 1],\ \cdots,\ l_{k-1} \in [0, p_{k-1} - 1],\ l_k = 0\\
&\text{group } 2: i_1 \in [0, p_1 - 1],\ i_2 \in [0, p_2 - 1],\ \cdots,\ i_{k-2} \in [0, p_{k-2} - 1],\ i_{k-1} \in [1, p_{k-1} - 1],\\
&\qquad i_k = 0,\\
&\qquad l_1 \in [0, p_1 - 1],\ l_2 \in [0, p_2 - 1], \cdots,\ l_{k-2} \in [0, p_{k-2} - 1],\ l_{k-1} = 0,\\
&\qquad l_k \in [0, p_k - 1]\\
&\qquad\qquad \vdots\\
&\text{group } k-1: i_1 \in [0, p_1 - 1],\ i_2 \in [1, p_2 - 1],\ i_3 = i_4 = \cdots = i_k = 0,\\
&\qquad l_1 \in [0, p_1 - 1],\ l_2 = 0,\ l_3 \in [0, p_3 - 1], \cdots,\ l_k \in [0, p_k - 1]\\
&\text{group } k: \quad i_1 \in [1, p_1 - 1],\ i_2 = i_3 = i_4 = \cdots = i_k = 0,\\
&\qquad l_1 = 0,\ l_2 \in [0, p_2 - 1], \cdots,\ l_k \in [0, p_k - 1]\}
\end{aligned}
\tag{3.59}
$$

$$
\begin{aligned}
&\{[(l_1 + l_2 p_1 + l_3 p_1 p_2 + \cdots + l_k p_1 p_2 \cdots p_{k-1}, 0),\\
&((i_1 \oplus_{p_1} l_1) + (i_2 \oplus_{p_1} l_2) p_1 + (i_3 \oplus_{p_1} l_3) p_1 p_2 + \cdots + (i_k \oplus_{p_1} l_k) p_1 p_2 \cdots p_{k-1}, 0),\\
&(((2 \otimes_{p_1} i_1) \oplus_{p_1} l_1) + ((2 \otimes_{p_2} i_2) \oplus_{p_1} l_2) p_1 + ((2 \otimes_{p_3} i_3) \oplus_{p_1} l_3) p_1 p_2 + \cdots\\
&\qquad + ((2 \otimes_{p_k} i_k) \oplus_{p_1} l_k) p_1 p_2 \cdots p_{k-1}, 0), \cdots,\\
&((((w-1) \otimes_{p_1} i_1) \oplus_{p_1} l_1) + (((w-1) \otimes_{p_2} i_2) \oplus_{p_1} l_2) p_1 + (((w-1) \otimes_{p_3} i_3) \oplus_{p_1} l_3) p_1 p_2\\
&\qquad + \cdots + (((w-1) \otimes_{p_k} i_k) \oplus_{p_1} l_k) p_1 p_2 \cdots p_{k-1}, 0)]:\\
&\text{group } 1: i_1 \in [0, p_1 - 1],\ i_2 \in [0, p_2 - 1], \cdots,\ i_{k-1} \in [0, p_{k-1} - 1],\ i_k = 1,\\
&\qquad l_1 \in [0, p_1 - 1],\ l_2 \in [0, p_2 - 1], \cdots,\ l_{k-1} \in [0, p_{k-1} - 1],\ l_k = 0\\
&\text{group } 2: i_1 \in [0, p_1 - 1],\ i_2 \in [0, p_2 - 1], \cdots,\ i_{k-2} \in [0, p_{k-2} - 1],\ i_{k-1} = 1,\ i_k = 0\\
&\qquad l_1 \in [0, p_1 - 1],\ l_2 \in [0, p_2 - 1], \cdots,\ l_{k-2} \in [0, p_{k-2} - 1],\ l_{k-1} = 0,\\
&\qquad l_k \in [0, p_k - 1]\\
&\qquad\qquad \vdots\\
&\text{group } k-1: i_1 \in [0, p_1 - 1],\ i_2 = 1,\ i_3 = i_4 = \cdots = i_k = 0,\\
&\qquad l_1 \in [0, p_1 - 1],\ l_2 = 0,\ l_3 \in [0, p_3 - 1], \cdots,\ l_k \in [0, p_k - 1]\\
&\text{group } k: i_1 = 1,\ i_2 = i_3 = i_4 = \cdots = i_k = 0,\\
&\qquad l_1 = 0,\ l_2 \in [0, p_2 - 1], \cdots,\ l_k \in [0, p_k - 1]\}
\end{aligned}
\tag{3.60}
$$

form a $(p_1p_2\cdots p_k \times p_1, w, 0, 1)$ EWHPC with code length p_1 code weight w, with the number of possible wavelengths $p_1p_2p_3\cdots p_k$. Its overall cardinality is

$$|C| = (p_1p_2\cdots p_{k-1})^2 p_k + (p_1p_2\cdots p_{k-2})^2 p_{k-1}p_k + (p_1p_2\cdots p_{k-3})^2 p_{k-2}p_{k-1}p_k + \cdots + p_1^2 p_2p_3\cdots p_k + p_1p_2p_3\cdots p_k \quad (3.61)$$

In this expression of cardinality, the first term represents the number of code matrices in group 1, the second term indicates the number of code matrices in group $2, \cdots$, and the k^{th} term expresses the number of code matrices in group k.

This kind of code shows the wavelength-shift property. The groups in (3.59) and (3.60) can be divided into a number of subgroups and the matrices are the wavelength-shifted versions of each other within each subgroup. The general expressions for the number of subgroups and the number of wavelength-shifted matrices per subgroup are shown in Table 3.32.

Table 3.32 General equations for the number of subgroups and the number of wavelength-shifted matrices per subgroup in the $(p_1p_2\cdots p_k \times p_1, w, 0, 1)$ wavelength-hopping prime code[25]

groups	number of subgroups	number of matrix/subgroups
1	p_k	$p_1p_2\cdots p_{k-1}$
	$(p_{k-1}-1)p_{k-1}p_k$	$p_1p_2\cdots p_{k-2}$
	$(p_{k-2}-1)(p_{k-1}-1)p_{k-2}p_{k-1}p_k$	$p_1p_2\cdots p_{k-3}$
	$\vdots$	$\vdots$
	$(p_2-1)(p_3-1)\cdots(p_{k-1}-1)p_2p_3\cdots p_k$	p_1
2	p_{k-1}	$p_1p_2\cdots p_{k-2}p_k$
	$(p_{k-2}-1)p_{k-2}p_{k-1}$	$p_1p_2\cdots p_{k-3}p_k$
	$(p_{k-3}-1)(p_{k-2}-1)p_{k-3}p_{k-2}p_{k-1}$	$p_1p_2\cdots p_{k-4}p_k$
	$\vdots$	$\vdots$
	$(p_2-1)(p_3-1)\cdots(p_{k-2}-1)p_2p_3\cdots p_{k-1}$	p_1p_k
3	p_{k-2}	$p_1p_2\cdots p_{k-3}p_{k-1}p_k$
	$(p_{k-3}-1)p_{k-3}p_{k-2}$	$p_1p_2\cdots p_{k-4}p_{k-1}p_k$
	$(p_{k-4}-1)(p_{k-3}-1)p_{k-4}p_{k-3}p_{k-2}$	$p_1p_2\cdots p_{k-5}p_{k-1}p_k$
	$\vdots$	$\vdots$
	$(p_2-1)(p_3-1)\cdots(p_{k-3}-1)p_2p_3\cdots p_{k-2}$	$p_1p_{k-1}p_k$
$\vdots$	$\vdots$	$\vdots$
$k-1$	p_2	$p_1p_3p_4\cdots p_k$
k	p_1	$p_2p_3\cdots p_k$

Example 3.16 Let $k=2$, $p_2=5$ and $p_1=w=3$. The matrices $\boldsymbol{X}_{i_1,i_2,l_1,l_2}$ with the ordered pairs

$$\{[(l_1+3l_2,0),(i_1\oplus_3 l_1+(i_2\oplus_3 l_2)3,1),((2\otimes_3 i_1)\oplus_3 l_1+((2\otimes_5 i_2)\oplus_3 l_2)3,2)]:$$

group 1: $i_1\in[0,2]$, $i_2\in[1,4]$ group 2: $i_1\in[1,2]$, $i_2=0$
$l_1\in[0,2]$, $l_2=0$ $l_1=0$, $l_2\in[0,4]\}$

$$\{[(l_1+3l_2,0),(i_1\oplus_3 l_1+(i_2\oplus_3 l_2)3,0),((2\otimes_3 i_1)\oplus_3 l_1+((2\otimes_5 i_2)\oplus_3 l_2)3,0)]:$$

group 1: $i_1\in[0,2]$, $i_2=1$ group 2: $i_1=1$, $i_2=0$
$l_1\in[0,2]$, $l_2=0$ $l_1=0$, $l_2\in[0,4]\}$

There are $36+9=45$ matrices in group 1 and group 2 has $10+5=15$ matrices. Therefore, the cardinality of the $(15\times3,3,0,1)$-EWHPC is $p_1^2p_2+p_1p_2=3^2\times5+3\times5=60$. All codeword matrices are shown in Table 3.33. By close inspection, we can find that there are $p_2=5$ subgroups in group 1 and each subgroup has $p_1=3$ wavelength-shifted matrices. There are $p_1=3$ subgroups of $p_2=5$ wavelength-shifted matrices for each subgroup.

Table 3.33 $(15\times3,3,0,1)$ wavelength-hopping prime code[25]

group 1

(i_1,i_2,l_1,l_2)	sequences	(i_1,i_2,l_1,l_2)	sequences	(i_1,i_2,l_1,l_2)	sequences	(i_1,i_2,l_1,l_2)	sequences
$(0,1,0,0)$	$(\lambda_0,\lambda_3,\lambda_6)$ & $(\lambda_0+\lambda_3+\lambda_6,0,0)$	$(0,2,0,0)$	$(\lambda_0,\lambda_6,\lambda_{12})$	$(0,3,0,0)$	$(\lambda_0,\lambda_9,\lambda_3)$	$(0,4,0,0)$	$(\lambda_0,\lambda_{12},\lambda_9)$
$(1,1,0,0)$	$(\lambda_0,\lambda_4,\lambda_8)$ & $(\lambda_0+\lambda_4+\lambda_8,0,0)$	$(1,2,0,0)$	$(\lambda_0,\lambda_7,\lambda_4)$	$(1,3,0,0)$	$(\lambda_0,\lambda_{10},\lambda_5)$	$(1,4,0,0)$	$(\lambda_0,\lambda_{13},\lambda_{11})$
$(2,1,0,0)$	$(\lambda_0,\lambda_5,\lambda_7)$ & $(\lambda_0+\lambda_5+\lambda_7,0,0)$	$(2,2,0,0)$	$(\lambda_0,\lambda_8,\lambda_{13})$	$(2,3,0,0)$	$(\lambda_0,\lambda_{11},\lambda_4)$	$(2,4,0,0)$	$(\lambda_0,\lambda_{14},\lambda_{10})$
$(0,1,1,0)$	$(\lambda_1,\lambda_4,\lambda_7)$ & $(\lambda_1+\lambda_4+\lambda_7,0,0)$	$(0,2,1,0)$	$(\lambda_1,\lambda_7,\lambda_{13})$	$(0,3,1,0)$	$(\lambda_1,\lambda_{10},\lambda_4)$	$(0,4,1,0)$	$(\lambda_1,\lambda_{13},\lambda_{10})$
$(1,1,1,0)$	$(\lambda_1,\lambda_5,\lambda_6)$ & $(\lambda_1+\lambda_5+\lambda_6,0,0)$	$(1,2,1,0)$	$(\lambda_1,\lambda_8,\lambda_{12})$	$(1,3,1,0)$	$(\lambda_1,\lambda_{11},\lambda_3)$	$(1,4,1,0)$	$(\lambda_1,\lambda_{14},\lambda_9)$
$(2,1,1,0)$	$(\lambda_1,\lambda_3,\lambda_8)$ & $(\lambda_1+\lambda_3+\lambda_8,0,0)$	$(2,2,1,0)$	$(\lambda_1,\lambda_6,\lambda_{14})$	$(2,3,1,0)$	$(\lambda_1,\lambda_9,\lambda_5)$	$(2,4,1,0)$	$(\lambda_1,\lambda_{12},\lambda_{11})$
$(0,1,2,0)$	$(\lambda_2,\lambda_5,\lambda_8)$ & $(\lambda_2+\lambda_5+\lambda_8,0,0)$	$(0,2,2,0)$	$(\lambda_2,\lambda_8,\lambda_{14})$	$(0,3,2,0)$	$(\lambda_2,\lambda_{11},\lambda_5)$	$(0,4,2,0)$	$(\lambda_2,\lambda_{14},\lambda_{11})$
$(1,1,2,0)$	$(\lambda_2,\lambda_3,\lambda_7)$ & $(\lambda_2+\lambda_3+\lambda_7,0,0)$	$(1,2,2,0)$	$(\lambda_2,\lambda_6,\lambda_{13})$	$(1,3,2,0)$	$(\lambda_2,\lambda_9,\lambda_4)$	$(1,4,2,0)$	$(\lambda_2,\lambda_{12},\lambda_{10})$
$(2,1,2,0)$	$(\lambda_2,\lambda_4,\lambda_6)$ & $(\lambda_2+\lambda_4+\lambda_6,0,0)$	$(2,2,2,0)$	$(\lambda_2,\lambda_7,\lambda_{12})$	$(2,3,2,0)$	$(\lambda_2,\lambda_{10},\lambda_3)$	$(2,4,2,0)$	$(\lambda_2,\lambda_{13},\lambda_9)$

group 2

(i_1,i_2,l_1,l_2)	sequences	(i_1,i_2,l_1,l_2)	sequences
$(1,0,0,0)$	$(\lambda_0,\lambda_1,\lambda_2)$ & $(\lambda_0+\lambda_1+\lambda_2,0,0)$	$(1,0,0,3)$	$(\lambda_9,\lambda_{10},\lambda_{11})$ & $(\lambda_9+\lambda_{10}+\lambda_{11},0,0)$
$(2,0,0,0)$	$(\lambda_0,\lambda_2,\lambda_1)$	$(2,0,0,3)$	$(\lambda_9,\lambda_{11},\lambda_{10})$
$(1,0,0,1)$	$(\lambda_3,\lambda_4,\lambda_5)$ & $(\lambda_3+\lambda_4+\lambda_5,0,0)$	$(1,0,0,4)$	$(\lambda_{12},\lambda_{13},\lambda_{14})$ & $(\lambda_{12}+\lambda_{13}+\lambda_{14},0,0)$
$(2,0,0,1)$	$(\lambda_3,\lambda_5,\lambda_4)$	$(2,0,0,4)$	$(\lambda_{12},\lambda_{14},\lambda_{13})$
$(1,0,0,2)$	$(\lambda_6,\lambda_7,\lambda_8)$ & $(\lambda_6+\lambda_7+\lambda_8,0,0)$		
$(2,0,0,2)$	$(\lambda_6,\lambda_8,\lambda_7)$		

(2) Cardinality of 2-D WHPCs

From (3.3), we can obtain the upper bound on the cardinality of the $(p_1 p_2 \cdots p_k \times p_1, w, 0, 1)$-EWHPC[25]

$$\Phi(p_1 p_2 \cdots p_k \times p_1, w, 0, 1) \leqslant \frac{p_1 p_2 \cdots p_k (p_1 p_2 \cdots p_k p_1 - 1)}{w(w-1)} = \frac{p_1^3 (p_2 \cdots p_k)^2}{w(w-1)} - \frac{p_1 p_2 \cdots p_k}{w(w-1)} \tag{3.62}$$

In Comparison with the actual cardinality of the $(p_1 p_2 \cdots p_k \times p_1, w, 0, 1)$-EWHPC, (3.62) is larger by a factor of approximately $1 - w(w-1)p_1^{-1}[p_k^{-1} + (p_{k-1}p_k)^{-1} + \cdots + (p_1 p_2 \cdots p_k)^{-1}]$. Furthermore, if $p_1 = p_2 = \cdots = p_k = p = w$, the upper bound in (3.61) becomes

$$\Phi(p^k \times p, p, 0, 1) \leqslant p^{2k-1} + p^{2k-2} + \cdots + p^k + p^{k-1} \tag{3.63}$$

and the actual cardinality of the $(p_1 p_2 \cdots p_k \times p_1, w, 0, 1)$-EWHPC becomes $p^{2k-1} + p^{2k-2} + \cdots + p^k$. Hence, the upper bound is greater by a factor of $(p-1)/(p^{k+1}-1)$ than the actual cardinality. The factor is nearly equal to zero for a large p or k. Therefore, the $(p_1 p_2 \cdots p_k \times p_1, w, 0, 1)$-EWHPC is asymptotically optimal.

(3) Performance of 2-D EWHPCs

Theorem 3.6[25] The autocorrelation sidelobes of any code matrices in the $(p_1 p_2 \cdots p_k \times p_1, w, 0, 1)$-EWHPC are zero and the maximum cross-correlation function between any two distinct code matrices in the code set is one.

Theorem 3.7[25] The maximal number of wavelength-shifted matrices that can be produced by a given matrix $\boldsymbol{X}_{i_1, i_2, \cdots, i_k, l_1, l_2, \cdots, l_k}$ in the $(p_1 p_2 \cdots p_k \times p_1, w, 0, 1)$-EWHPC is equal to

$$(p_1 - j_1)(p_2 - j_2) \cdots (p_k - j_k)$$

where $i_m \in [0, p_m - 1]$, $l_m \in [0, p_m - 1]$, and $j_m = \max\{q_m \otimes_{p_m} i_m : q_m \in [0, w-1]\}$ for all $m = \{1, 2, \cdots, k\}$.

The proof of Theorem 3.6 and 3.7 can be found in Reference [25].

In order to analyze the performance of the $(p_1 p_2 \cdots p_k \times p_1, w, 0, 1)$-EWHPC, we need to know the collision probability between one of the pulses (namely, one binary one) in a signature matrix and a pulse in a received matrix. The wavelength-shifted property of EWHPC can be employed to improve the collision probability since the code contains no common wavelengths and hence, have cross-correlation value equal to zero, if these matrices all come from the

same group. Considering this unique property of EWHPC, we get the "average" probability of one collision

$$q = \frac{w^2}{2nm} \times R = \frac{w^2}{2p_1 \cdot p_1 p_2 \cdots p_k} \times R \tag{3.64}$$

where 1/2 is due to the assumption that the transmission of data bit of "0" and "1" is equiprobable, w is the code weight, n denotes the code length, m is the number of wavelengths and R represents the ratio of the number of matrices contributing to one collision (to the cross-correlation function) to the total number of interfering matrices.

In terms of the pattern of "subgroup" partitions mentioned above, we have[25]

$$R = \sum_{\text{all subgroups}} P(\text{a matrix causes a hit}|\text{the matrix is from a subgroup}) \times P'(\text{the subgroup is chosen from the code set } \Phi)$$

The general form of R would be a long expression because the number of subgroups increases with increasing k. For example, when $k = 2$ group 1 gives p_2 subgroups of p_1 matrices each and group 2 gives p_1 subgroups of p_2 matrices each. Thus, we have

$$R_2 = \frac{\Phi_2 - p_1}{\Phi_2 - 1} \cdot \frac{p_1}{\Phi_2} \cdot p_2 + \frac{\Phi_2 - p_2}{\Phi_2 - 1} \cdot \frac{p_2}{\Phi_2} \cdot p_1 + \frac{\Phi_2 - 1}{\Phi_2 - 1} \cdot \frac{\Phi_2 - 2p_1 p_2}{\Phi_2 - 1} \cdot 1 \tag{3.65}$$

where $\Phi_2 = p_1^2 p_2 + p_1 p_2$ is the code cardinality and $\Phi_2 - 1$ represents the total number of interfering matrices. For $k = 3$, group 1 gives p_3 subgroups of $p_1 p_2$ matrices each and $(p_2 - 1)p_2 p_3$ subgroups of p_1 matrices each, group 2 gives p_2 subgroups of $p_1 p_3$ matrices each, and group 3 gives p_1 subgroups of $p_2 p_3$ matrices each. Thus, we have

$$\begin{aligned} R_3 = {} & \frac{\Phi_3 - p_1 p_2}{\Phi_3 - 1} \cdot \frac{p_1 p_2}{\Phi_3} \cdot p_3 + \frac{\Phi_3 - p_1}{\Phi_3 - 1} \cdot \frac{p_1}{\Phi_3} \cdot (p_2 - 1) p_2 p_3 + \frac{\Phi_3 - p_1 p_3}{\Phi_3 - 1} \cdot \frac{p_1 p_3}{\Phi_3} \cdot p_2 \\ & + \frac{\Phi_3 - p_2 p_3}{\Phi_3 - 1} \cdot \frac{p_2 p_3}{\Phi_3} \cdot p_1 + \frac{\Phi_3 - 1}{\Phi_3 - 1} \cdot \frac{\Phi_3 - p_1 p_2^2 p_3 - 2p_1 p_2 p_3}{\Phi_3} \cdot 1 \end{aligned} \tag{3.66}$$

where $\Phi_3 = (p_1 p_2)^2 p_3 + p_1^2 p_2 p_3 + p_1 p_2 p_3$ is the code cardinality.

The bit error rate of EWHPC[25] is

$$P_b = \frac{1}{2} \sum_{i=Th}^{K-1} \binom{K-1}{i} q^i (1-q)^{K-1-i} \tag{3.67}$$

where Th and K express the decision threshold of a receiver and the total number of simultaneous subscribers respectively. For the optimal decision, we set $Th = w$.

Figure 3.6 shows the curves of bit error rate (BER) P_b versus the number of simultaneous users K for 2-D wavelength-hopping/time-spreading OCDMA system with $(p_1 p_2 \cdots p_k \times p_1, w, 0, 1)$- EWHPC. It can be seen from the diagram that the BER performance degrades as the number of simultaneous users K increases, but improves with more wavelengths and/or chips.

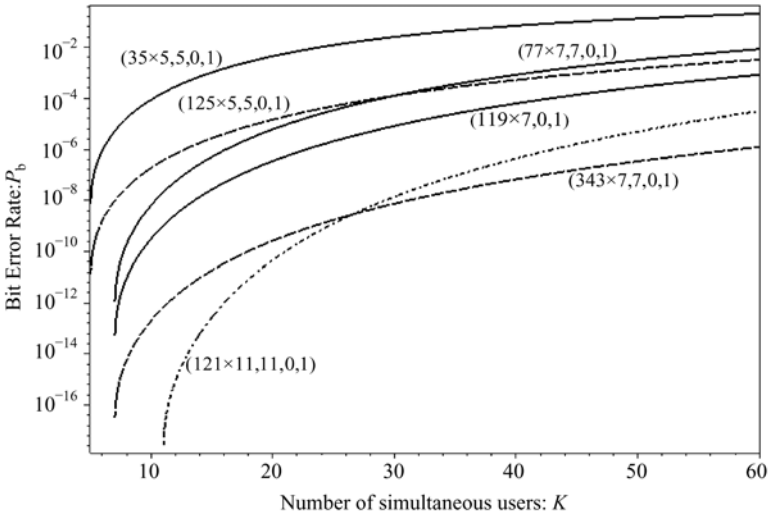

Figure 3.6 Bit Error Rate P_b versus the number of simultaneous users K for 2-D WH/TS OCDMA system with $(p_1 p_2 \cdots p_k \times p_1, w, 0, 1)$- EWHPC[25]

3.11 Multiple-length Extended Wavelength-hopping Prime Codes for OCDMA

When 2-D wavelength-hopping/time-spreading OCDMA codes were introduced in the above sections it was assumed that there was only one type of medium in an OCDMA network and the bit rates among subscribers were the same. However, in practice, it is expected that future communication networks, especially access networks, will support a large variety of multimedia services, such as data, voice, image and video, and accommodate simultaneously all kinds of subscribers with very different bit-rates and quality-of-service (QoS). Therefore, the use of single-length wavelength-time codes alone will not be able to serve these multi-rate and multimedia systems efficiently. In order to be able to support multimedia services with different bit-rate requirements, we now

introduce a new family of 2-D multiple-length constant-weight EWHPCs with ideal correlation properties, i.e., the multiple-length extended wavelength-hopping prime code (MLEWHPC)[27 – 30], which can be obtained by extending wavelength-hopping prime codes with single length. The resulting MLEWHPCs will have identical autocorrelation peaks and the cross-correlation of at most one. As distinct from conventional single-length codes, the performance of MLEWHPCs becomes better as the code length decreases, i.e., the high-bit-rate media, such as video, will have better performance than lower-bit-rate media, for instance, voice. Hence, these codes can be applied to OCDMA networks to support the prioritization of services of different media, which is very important for a network to guarantee the QoS for those media (namely, video) that require high bit rate and real-time support. In an OCDMA network using multi-length 2-D wavelength-hopping/time-spreading code, the QoS can be dynamically matched with the requirement of subscribers by allocating different length codeword matrices to different subscribers.

3.11.1 Definition of Multiple-length Constant-weight Wavelength-time Codes[27, 28]

An $(m \times N, w, A, B, D)$ multiple-length constant-weight wavelength-time code, C, is a collection of binary {0,1} code matrices with a set of code lengths $N = \{n_0, n_1, \cdots, n_i, \cdots, n_{k-1}\}$, the number of available wavelengths m, a code weight w, a set of autocorrelation constraints $A = \{\lambda_a^{(0)}, \lambda_a^{(1)}, \cdots, \lambda_a^{(i)}, \cdots, \lambda_a^{(k-1)}\}$, a set of cross-correlation constraints $B = \{\lambda_c^{(0)}, \lambda_c^{(1)}, \cdots, \lambda_c^{(i)}, \cdots, \lambda_c^{(k-1)}, \lambda\}$, and a set of matrix-cardinality distributions $D = \{d_0, d_1, \cdots, d_i, \cdots, d_{k-1}\}$, where k denotes the number of different code lengths in C such that.

Length distribution: The length of each code matrix n_i in C is an element of the length set. There are $d_i \cdot |C|$ code matrices with the length n_i, where d_i represents the ratio of the number of code matrices of the length n_i in C to the total code cardinality of C, $|C|$.

Autocorrelation constraint: For any code matrix $\boldsymbol{X} \in C$ with the length n_i, the constraint of its autocorrelation sidelobes is $\lambda_a^{(i)}$ such that

$$\sum_{s=0}^{m-1} \sum_{t=0}^{n_i-1} x_{s,t} x_{s,t \oplus_{n_i} \tau} \leqslant \lambda_a^{(i)}, \quad \tau \in (0, n_i)$$

where $x_{s,t} \in \{0,1\}$ is an element in $\boldsymbol{X}$, "$\oplus_{n_i}$" indicates modulo-n_i addition and τ is the delay of any integer multiples of a chip.

Intra-cross-correlation constraint: For any two distinct code matrices $\boldsymbol{X} \in C$ and $\boldsymbol{Y} \in C$ with the same length n_i, their cross-correlation functions are at most $\lambda_c^{(i)}$ such that

$$\sum_{s=0}^{m-1}\sum_{t=0}^{n_i-1} x_{s,t} y_{s,t\oplus_{n_i}\tau} \leqslant \lambda_c^{(i)}, \quad \tau \in [0, n_i)$$

where $y_{s,t} \in \{0,1\}$ is an element in $\boldsymbol{Y}$.

Inter-cross-correlation constraint: For any two distinct code matrices $\boldsymbol{X} \in C$ and $\boldsymbol{Y} \in C$ with the lengths n_i and n_j respectively, their cross-correlation functions are at most λ such that

$$\sum_{s=0}^{m-1}\sum_{t=0}^{n_i-1} x_{s,t} y_{s,t\oplus_{n_j}\tau} \leqslant \lambda, \quad \tau \in [0, n_j)$$

$$\sum_{s=0}^{m-1}\sum_{t=0}^{n_j-1} x_{s,t\oplus_{n_i}\tau} y_{s,t} \leqslant \lambda, \quad \tau \in [0, n_i)$$

where "$\oplus_{n_j}$" denotes modulo-n_j addition and $n_i \neq n_j$.

3.11.2 Construction of MLWHPCs

We first introduce the construction of multiple-length wavelength-hopping prime code (MLWHPC) since MLWHPC is employed as a seed to generate the multiple-length extended wavelength-hopping prime code (MLEWHPC)[13, 27]. Each code matrix of MLWHPC consists of an $m \times n_i$ 2-D $\{0,1\}$ pattern with code weight *w*, i.e., it contains *w* ones in *m* rows (related to the number of available wavelengths) and n_i columns (related to the number of time slots). The autocorrelation sidelobes of MLWHPC are zero and its cross-correlation functions are at most one. MLWHPC is generated by introducing a set of integers $\{t_1, t_2, \cdots, t_{k-1}\}$ and controlling the number of matrices with each length out of k different lengths in the code set.

Given a set of prime numbers $\{p_1, p_2, \cdots, p_k\}$ such that $p_k \geqslant p_{k-1} \geqslant \cdots \geqslant p_2 \geqslant p_1$ and $p_1 \geqslant t_1 \geqslant t_2 \geqslant \cdots \geqslant t_{k-1} \geqslant 0$, the code matrices $\boldsymbol{X}_{i_1}$ with the ordered pairs[13]

$$\{[(0,0),(1,i_1),(2,2\otimes_{p_1} i_1),\cdots,(p_1-1,(p_1-1)\otimes_{p_1} i_1)] : i_1 \in [t_1, p_1-1]\} \qquad (3.68)$$

matrices $\boldsymbol{X}_{i_1,i_2}$ with the ordered pairs

$$\{[(0,0),(1,i_1+i_2p_1),(2,2\otimes_{p_1} i_1+(2\otimes_{p_2} i_2)p_1),\cdots,$$
$$(p_1-1,(p_1-1)\otimes_{p_1} i_1+((p_1-1)\otimes_{p_2} i_2)p_1)]: i_1\in[t_2,t_1-1], i_2=[0,p_2-1]\} \tag{3.69}$$

…

and matrices $\boldsymbol{X}_{i_1,i_2,\cdots,i_k}$ with the ordered pairs

$$\{[(0,0),(1,i_1+i_2p_1+\cdots+i_kp_1p_2\cdots p_{k-1}),(2,2\otimes_{p_1} i_1+(2\otimes_{p_2} i_2)p_1+\cdots$$
$$+(2\otimes_{p_k} i_k)p_1p_2\cdots p_{k-1}),\cdots,(p_1-1,(p_1-1)\otimes_{p_1} i_1+((p_1-1)\otimes_{p_2} i_2)p_1+\cdots$$
$$+((p_1-1)\otimes_{p_k} i_k)p_1p_2\cdots p_{k-1})]: i_1\in[0,t_{k-1}-1], i_2\in[0,p_2-1],\cdots,i_k\in[0,p_k-1]\} \tag{3.70}$$

form an MLWHPC with the code weight $w=p_1$, which has $\gamma_1=p_1-t_1$ code matrices of length p_1, $\gamma_2=(t_1-t_2)p_2$ code matrices of length p_1p_2, $\gamma_3=(t_2-t_3)p_2p_3$ code matrices of length $p_1p_2p_3,\cdots,\gamma_{k-1}=(t_{k-2}-t_{k-1})p_2p_3\cdots p_{k-1}$ code matrices of length $p_1p_2\cdots p_{k-1}$, and $\gamma_k=t_{k-1}p_2p_3\cdots p_k$ code matrices of length $p_1p_2\cdots p_{k-1}p_k$, where " $\otimes_{p_j}$ " indicates modulo-p_j multiplication for $j=\{1,2,\cdots,k\}$.

Example 3.17 Let $k=2$, $p_1=p_2=11$, $t_1=6$ and construct an MLWHPC.

We have $w=p_1=11$. From (3.68), we obtain the matrices $\boldsymbol{X}_{i_1}$ with the ordered pairs

$$\{[(0,0),(1,i_1),(2,2\otimes_{11} i_1),\cdots,(10,10\otimes_{11} i_1)]: i_1=\{6,7,\cdots,10\}\},$$

that is, there are $\gamma_1=p_1-t_1=11-6=5$ code matrices of length $p_1=11$.

Also, from (3.69), we find the matrices $\boldsymbol{X}_{i_1,i_2}$ with the ordered pairs

$$\{[(0,0),(1,i_1+11i_2),(2,2\otimes_{11} i_1+(2\otimes_{11} i_2)11),\cdots,(10,10\otimes_{11} i_1+(10\otimes_{11} i_2)11)]:$$
$$i_1=\{0,1,\cdots,5\}, i_2=\{0,1,\cdots,10\}\}$$

namely, there are $\gamma_2=(t_1-t_2)p_2=(6-0)\times 11=66$ code matrices of length $p_1p_2=11\times 11=121$.

3.11.3 Construction of MLEWHPCs[27, 28]

MLWHPC has a stringent restriction, namely that all wavelengths are employed in each code matrix, i.e., $w=m$. However, if a multimedia OCDMA system can achieve the performance required with a lower code weight, this limitation means that the number of available wavelengths in the code matrices is greater than the

number of actual needed wavelengths and so we can improve the code cardinality by utilizing the extra wavelengths efficiently without deterioration of the code performance.

If the number of available wavelengths m is greater than the code weight w, i.e. $m = wp'$, where p' is a prime number, we can construct a family of MLEWHPCs, which permits the utilization of the extra wavelengths efficiently without sacrificing the original correlation properties, and at the same time, realizes larger cardinality than the original MLWHPC. Generally speaking, each of the original MLWHPC matrices expressed as $\boldsymbol{X}_{i_1,i_2,\cdots,i_j}$ (with $i_1 = [t_1, p_1 - 1]$ (or $i_1 = [t_i, t_{i-1} - 1]$, or $i_1 = [0, t_{k-1} - 1]$), $i_2 = [0, p_2 - 1]$, $\cdots, i_j = [0, p_j - 1]; j \in [2, k]$) is taken as a seed to generate $w^2 + p'$ groups of new matrices[21]. These new matrices have the cross-correlation functions of at most one, and we even achieve zero cross-correlation function values of some new matrices, improving the new code over the original.

Given prime numbers p' and w such that $p' \geqslant w$ and $p_1 \geqslant wp'$, we can obtain the w ordered pairs of new code matrices $\boldsymbol{X}_{i_1,i_2,\cdots,i_k,l_1,l_2}$ and $\boldsymbol{X}_{i_1,i_2,\cdots,i_k,l_2}$ through picking the ordered pairs from the code matrices $\boldsymbol{X}_{i_1,i_2,\cdots,i_k}$ with the first component of each ordered pair in (3.68) – (3.70) given by

$$\{[(l_1, (l_1 \oplus_w l_2)) + w, (l_1 \oplus_w (2 \otimes_{p'} l_2)) + 2w, \cdots, (l_1 \oplus_w ((w-1) \otimes_{p'} l_2)) + (w-1)w] : \\ l_1 \in [0, w-1], l_2 \in [0, w-1]\} \tag{3.71}$$

and

$$\{[l_2 w, l_2 w + 1, \cdots, l_2 w + w - 1] : l_2 \in [0, p' - 1]\} \tag{3.72}$$

respectively. The resulting MLEWHPC with the number of available wavelengths $m = wp'$ and the code weight w has $\phi_1 = (w^2 + p')(p_1 - t_1)$ code matrices of length p_1, $\phi_2 = (w^2 + p')(t_1 - t_2)p_2$ code matrices of length $p_1 p_2$, $\phi_3 = (w^2 + p')(t_2 - t_3)p_2 p_3$ code matrices of length $p_1 p_2 p_3, \cdots$, $\phi_{k-1} = (w^2 + p') \cdot (t_{k-2} - t_{k-1}) p_2 p_3 \cdots p_{k-1}$ code matrices of length $p_1 p_2 \cdots p_{k-1}$, and $\phi_k = (w^2 + p') t_{k-1} p_2 p_3 \cdots p_k$ code matrices of length $p_1 p_2 \cdots p_k$, where $\otimes_{p'}$ indicates modulo- p' multiplication and $\oplus_w$ represents modulo- w addition.

Example 3.18 Let $k = 2$, $w = p' = 3$, $p_1 = p_2 = 11$ and $t_1 = 6$. From (3.71) and (3.72), we obtain

$$\{[(l_1, (l_1 \oplus_3 l_2)) + 3, (l_1 \oplus_3 (2 \otimes_3 l_2)) + 6] : l_1 \in [0, 2], i_2 \in [0, 2]\}, \\ \{[3l_2, 3l_2 + 1, 3l_2 + 2] : i_2 \in [0, 2]\}.$$

Then, from each original matrix obtained in Example 3.17, $w^2+p'=12$ new matrix groups can be generated, i.e., form the double-length EWHPC code matrices, where we obtain in total $(w^2+p')(p_1-t_1)=12\times5=60$ code matrices of $\boldsymbol{X}_{i_1,l_1,l_2}$ and $\boldsymbol{X}_{i_1,l_2}$, ($i_1\in[6,10], l_1\in[0,2]$, $l_2\in[0,2]$) with the length $p_1=11$ by choosing three ordered pairs among the ordered pairs of the original matrices $\boldsymbol{X}_{i_1}$, $(w^2+p')t_1p_2=792$ code matrices of $\boldsymbol{X}_{i_1,i_2,l_1,l_2}$ and $\boldsymbol{X}_{i_1,i_2,l_2}$, ($i_1\in[0,5]$, $i_2\in[0,10], l_1\in[0,2], l_2\in[0,2]$) with the length $p_1p_2=121$ by choosing three ordered pairs among the ordered pairs of the original matrices $\boldsymbol{X}_{i_1,i_2}$. For example, $\boldsymbol{X}_{i_1,i_2,l_2}=\boldsymbol{X}_{6,1,2}$ is a 9×11 matrix, whose ordered pairs are [(1,6),(3,7),(8,4)]; $\boldsymbol{X}_{i_1,i_2,l_1,l_2}=\boldsymbol{X}_{2,6,2,2}$ is a 9×121 matrix, whose ordered pairs are [(2,15),(4,30),(6,34)]. This MLEWHPC has the code weight 3. Table 3.34 shows some examples of MLEWHPCs[27].

Table 3.34 Examples of MLEWHPCs, where k is the number of different lengths in the code set[27]

$(w,p',p_1,p_2,\cdots,p_k)$	$(t_1,t_2,\cdots,t_{k-1})$	k	(code length, cardinality) of each services	Total cardinality
(3,3,11,11)	(6)	2	(11,60),(121,792)	852
(3,3,13,13)	(7)	2	(13,72),(169,1092)	1164
(3,3,11,11,13)	(6,3)	3	(11,60),(121,396),(1573,5148)	5604
(5,7,37,37)	(11)	2	(37,832),(1369,13024)	13856

3.11.4 Cardinality of MLEWHPCs

By modifying the upper bound on cardinality of single length EWHPC[13, Th.2.10], the upper bound on cardinality of MLEWHPC is given by[27]

$$\Phi\leqslant\frac{p'\left(wp'\prod_{j=1}^{k}p_j-1\right)}{\sum_{i=1}^{k}d_i\left(\prod_{j=i+1}^{k}p_jw-1\right)} \tag{3.73}$$

where p' is a prime number, d_i denotes the ratio of the number of matrices of length n_i to the total number of matrices in the code set. The total number of matrices in MLEWHPC is

$$\Phi_{\text{MLEWHPC}}=(w^2+p')[(p_1-t_1)+(t_1-t_2)p_2+\cdots+(t_{k-2}-t_{k-1})p_2\cdots p_{k-1}+t_{k-1}p_2\cdots p_k]$$

and the rations are

$$d_1 = \frac{(w^2 + p')(p_1 - t_1)}{\Phi_{\text{MLEWHPC}}}$$
$$d_2 = \frac{(w^2 + p')(t_1 - t_2)p_2}{\Phi_{\text{MLEWHPC}}}$$
$$\cdots$$
$$d_{k-1} = \frac{(w^2 + p')(t_{k-2} - t_{k-1})p_2 \cdots p_{k-1}}{\Phi_{\text{MLEWHPC}}}$$
$$d_k = \frac{(w^2 + p')t_{k-1}p_2 \cdots p_k}{\Phi_{\text{MLEWHPC}}}.$$

Through some mathematical manipulations, we have[27]

$$\frac{\Phi_{\text{MLEWHPC}}}{\Phi} \approx \frac{(w^2 + p')(p_1 - t_1)}{p'^2 p_1}\left(1 - \frac{1}{wp_2p_3 \cdots p_k}\right) + \frac{(w^2 + p')(t_1 - t_2)}{p'^2 p_1}$$
$$\times\left(1 - \frac{1}{wp_3p_4 \cdots p_k}\right) + \cdots + \frac{(w^2 + p')(t_{k-2} - t_{k-1})}{p'^2 p_1}\left(1 - \frac{1}{wp_k}\right) + \frac{(w^2 + p')t_{k-1}}{p'^2 p_1}\left(1 - \frac{1}{w}\right) \tag{3.74}$$

The value of this expression is close to one for large w and p' nearly w. Therefore, MLEWHPC is asymptotically optimal.

3.11.5 Performance of MLEWHPCs

Generally speaking, the performance of single length EWHPCs[21] depends on their cross-correlation functions, which depend upon the code weight, the code length and the number of available wavelengths. The identical performance of each subscriber in the OCDMA network transmitting the same medium needs to be taken into account. However, when MLEWHPC is applied to a network, the performance of a subscriber relies on not only the length of its address matrix, but also the length of the received address matrix. In other words, the multiple access interference (MAI) received by a subscriber is composed of the cross-correlation functions, which are obtained by correlating the user's address matrix and the received interfering matrices with shorter, identical and longer lengths. If the address matrix of a subscriber is shorter than the arriving matrices, the performance analysis resembles that of the same length matrices[13, 15, 20] and can be carried out by using conventional methods for single length codes, since the cross-correlation property of MLEWHPC still accords with the rule for single

length codes. However, it is more complicated to compute MAI at a subscriber when the address matrix of the user is longer than the arriving address matrices (say the length of the former, n_l, is r multiple of the latter length, i.e., $n_l = rn_s$). The complete inter-cross-correlation process will involve $r+1$ copies of the arriving short matrix, producing $r+1$ successive cross-correlation functions (in order to distinguish, we call the cross-correlation functions between any two matrices with the same length and different lengths the intra- and inter-cross-correlation functions respectively). It is noted that the inter-cross-correlation functions may be as large as the autocorrelation peak (i.e., the code weight), if the matrices are not constructed carefully.

In order to minimize MAI, the MLEWHPC must be constructed in the following manner[27].

(1) The intra-cross-correlation function between any two matrices with the same length in the code set is at most one.

(2) The inter-cross-correlation function between one short address matrix and one arriving long address matrix in the code set is at most one.

(3) The inter-cross-correlation function between one long address matrix (e.g., $\boldsymbol{X}_{i_1,i_2,\cdots i_k,l_1,l_2}$) and the $p_{g+1}p_{g+2}\cdots p_k$ copies of a short address matrix (e.g., $\boldsymbol{X}_{i_1',i_2',\cdots,i_g',l_1',l_2'}$) is at most one, where $i_1 \neq i_1'$ and $g < k$. Since all of the cross-correlation functions are at most one, the process of performance analysis of MLEWHPC can be simplified.

Theorem 3.8[27] The autocorrelation sidelobes of any matrix in MLEWHPC are all zero and the intra- and inter-cross-correlation functions between any two distinct matrices in the code set are both at most one. We have $w(p_1 - t_1), w(t_1 - t_2)p_2, \cdots$, and $wt_{k-1}p_2p_3\cdots p_k$ subsets of w matrices each from (3.71), and $p_1 - t_1$, $(t_1 - t_2)p_2, \cdots$, and $t_{k-1}p_2p_3\cdots p_k$ subsets of p' matrices each from (3.72), such that the cross-correlation functions of all matrices within one subset are all zero.

Proof: See Ref.[27].

Assume that each matrix has w pulses (i.e., the code weight) and $m = wp'$ available wavelengths. Let γ_i and ϕ_i represent the numbers of MLWHPC and MLEWHPC with the length n_i respectively for $i \in [1,k]$, where k is the number of distinct lengths in the code set. From the constructions of these two codes, we have $\phi_i = (w^2 + p')\gamma_i$, such that the probability of one-coincidence between two code matrices with the same length n_i in MLEWHPC is given by[22]

$$q_i = \frac{w^2}{2mn_i}\cdot R_i = \frac{w^2}{2mn_i}\left[\frac{\phi_i - (w-1)\gamma_i}{\phi_i - 1}\cdot\frac{w^2}{w^2+p'} + \frac{\phi_i - (p'-1)\gamma_i}{\phi_i - 1}\cdot\frac{p'}{w^2+p'}\right]$$
$$= \frac{w}{2p'n_i}\left[1 - \frac{(w^3 - w^2 + p'^2 - p')\gamma_i}{(\phi_i - 1)(w^2+p')}\right] \tag{3.75}$$

where the factor 1/2 comes from the equiprobable data bits of 0 and 1, R_i expresses the ratio of the number matrices contributing to one coincidence (in the cross-correlation function) to the total number of interfering matrices with the length n_i. In order to obtain R_i, there are $w^2/(w^2+p')$ opportunities to choose the EWHPC matrices in the w^2 new matrices generated by (3.71), for each matrix of length n_i originated from the group of γ_i matrices. There are $p'/(w^2+p')$ chances to choose the EWHPC matrices in the p' matrices originated from (3.72). For each matrix from (3.71), there are $(w-1)$ new matrices that have no wavelength overlap, namely, the cross-correlation value is zero. For each matrix obtained from (3.72), there are p' new matrices that have no wavelength overlap.

From the argument for the correlation properties of the code it is known that the number of coincidences between any two matrices of distinct lengths is always less than or equal to one. Hence, the probability of one coincidence between one address matrix of length n_i and one arriving address matrix of length n_j, for $i \neq j$, is given by[27]

$$q_{i,j} = \frac{w^2}{2mn_j} \cdot R_j = \frac{w}{2p'n_j}\left[1 - \frac{(w^3 - w^2 + p'^2 - p')\gamma_j}{(\phi_j - 1)(w^2 + p')}\right] \tag{3.76}$$

where R_j denotes the ratio of the number of matrices contributing to one coincidence (to the cross-correlation function) to the total number of interfering matrices of length n_j. The resulting R_j is the same as (3.76) if only the subscript i in (3.76) is changed into the subscript j.

Modifying the BER formula[33, eq.(4)], we can obtain the BER $P_{\mathrm{b},i}$ of subscribers with the address matrices of length n_i as[27]

$$P_{\mathrm{b},i} = \frac{1}{2}\sum_{\sum_{i=1}^{k} l_i = w}^{K-1}\left[\binom{K_i - 1}{l_i} q_i^{l_i}(1-q_i)^{K_i - 1 - l_i} \cdot \prod_{j=1, j\neq i}^{k}\binom{K_j}{l_j} q_{i,j}^{l_j}(1-q_{i,j})^{K_j - l_j}\right] \tag{3.77}$$

where $K = \sum_{j=1}^{k} K_j$ represents the total number of simultaneous subscribers, K_j denotes the number of simultaneous subscribers employing the matrices of length n_j, the product terms with l_i expresses MAI contributed by arriving matrices of the same lengths n_i, and the product terms with l_j denotes MAI contributed by arriving matrices of different lengths n_j, $j \neq i$.

For two media services (i.e., $k = 2$), the probability of one coincidence between two matrices with the same lengths can be obtained by modifying (3.75),

yielding[27]

$$q_s = \frac{w}{2p'n_s}\left[1 - \frac{(w^3 - w^2 + p'^2 - p')(p_1 - t_1)}{(\phi_s - 1)(w^2 + p')}\right] \tag{3.78}$$

and

$$q_l = \frac{w}{2p'n_l}\left[1 - \frac{(w^3 - w^2 + p'^2 - p')t_1 p_2}{(\phi_l - 1)(w^2 + p')}\right] \tag{3.79}$$

for the short matrices of lengths $n_s = p_1$ and the long matrices of lengths $n_l = rn_s = p_2 p_1$ respectively, where $r = p_2$ and the cardinalities of matrices with these two lengths are $\phi_s = (w^2 + p')(p_1 - t_1)$ and $\phi_l = (w^2 + p')t_1 p_2$ respectively. Because the number of coincidences between one long matrix and $r+1$ copies of one short arriving matrix is at most one, the probability of one coincidence between one long address matrix and one short arriving address matrix can be obtained by modifying (3.76)[27],

$$q_{l,s} = \frac{w}{2p'n_s}\left[1 - \frac{(w^3 - w^2 + p'^2 - p')(p_1 - t_1)}{(\phi_s - 1)(w^2 + p')}\right] \tag{3.80}$$

Similarly, the probability of one coincidence between one short address matrix and one long arriving matrix is given by[27]

$$q_{s,l} = \frac{w}{2p'n_l}\left[1 - \frac{(w^3 - w^2 + p'^2 - p')t_1 p_2}{(\phi_l - 1)(w^2 + p')}\right] \tag{3.81}$$

From (3.77), the bit error rate of subscribers employing the address matrices with the lengths n_s and n_l are[27]

$$P_{\mathrm{b},s} = \frac{1}{2}\sum_{l_s + l_l = w}^{K_l + K_s - 1}\left[\binom{K_s - 1}{l_s} q_s^{l_s}(1 - q_s)^{K_s - 1 - l_s} \times \binom{K_l}{l_l} q_{s,l}^{l_l}(1 - q_{s,l})^{K_l - l_l}\right] \tag{3.82}$$

and

$$P_{\mathrm{b},l} = \frac{1}{2}\sum_{l_s + l_l = w}^{K_l + K_s - 1}\left[\binom{K_l - 1}{l_l} q_l^{l_l}(1 - q_l)^{K_l - 1 - l_l} \times \binom{K_s}{l_s} q_{l,s}^{l_s}(1 - q_{l,s})^{K_s - l_s}\right] \tag{3.83}$$

respectively, where K_s and K_l represent the numbers of simultaneous subscribers with the address matrices of lengths n_s and n_l.

For three media services ($k = 3$), the probabilities of one coincidence between two matrices of the same lengths are obtained by modifying (3.75)[27],

$$q_l = \frac{w}{2p'n_l}\left[1 - \frac{(w^3 - w^2 + p'^2 - p')t_2 p_2 p_3}{(\phi_l - 1)(w^2 + p')}\right] \tag{3.84}$$

$$q_m = \frac{w}{2p'n_m}\left[1 - \frac{(w^3 - w^2 + p'^2 - p')(t_1 - t_2)p_2}{(\phi_m - 1)(w^2 + p')}\right] \tag{3.85}$$

and

$$q_s = \frac{w}{2p'n_s}\left[1 - \frac{(w^3 - w^2 + p'^2 - p')(p_1 - t_1)}{(\phi_s - 1)(w^2 + p')}\right] \tag{3.86}$$

for the short matrix of length $n_s = p_1$, the medium matrix of length $n_m = rn_s = p_2 p_1$ and the long matrix of length $n_l = r'n_m = r'rn_s = p_3 p_2 p_1$ respectively, where $r = p_2$ and $r' = p_3$. The cardinalities of matrices with these three lengths are $\phi_s = (w^2 + p')(p_1 - t_1)$, $\phi_m = (w^2 + p')(t_1 - t_2)p_2$ and $\phi_l = (w^2 + p')t_2 p_2 p_3$ respectively. Because the number of coincidences between one long matrix and $r' + 1$ copies of one medium matrix is at most one, the probability of one coincidence between one long matrix and one medium arriving matrix can be obtained by modifying (3.76)[27],

$$q_{l,m} = \frac{w}{2p'n_m}\left[1 - \frac{(w^3 - w^2 + p'^2 - p')(t_1 - t_2)p_2}{(\phi_m - 1)(w^2 + p')}\right] \tag{3.87}$$

Since the number of coincidences between one long address matrix and $rr' + 1$ copies of one short arriving matrix is at most one, the probability of one coincidence between one long address matrix and one short arriving matrix can be obtained by modifying (3.76)[27],

$$q_{l,s} = \frac{w}{2p'n_s}\left[1 - \frac{(w^3 - w^2 + p'^2 - p')(p_1 - t_1)}{(\phi_s - 1)(w^2 + p')}\right] \tag{3.88}$$

Because the maximum number of coincidences between one medium matrix and $r + 1$ copies of one short matrix is one, the probability of one coincidence between one medium matrix and one short arriving matrix can be obtained by modifying (3.76)[27],

$$q_{m,s} = \frac{w}{2p'n_s}\left[1 - \frac{(w^3 - w^2 + p'^2 - p')(p_1 - t_1)}{(\phi_s - 1)(w^2 + p')}\right] \tag{3.89}$$

Because the maximum number of coincidences between one medium matrix and one long arriving matrix is one, the probability of one coincidence for this case is[27]

$$q_{m,l} = \frac{w}{2p'n_l}\left[1 - \frac{(w^3 - w^2 + p'^2 - p')t_2 p_2 p_3}{(\phi_l - 1)(w^2 + p')}\right] \tag{3.90}$$

Because the maximum number of coincidences between one short address matrix and one long arriving address matrix is one, the probability of one coincidence for this circumstance is[27]

$$q_{s,l} = \frac{w}{2p'n_l}\left[1 - \frac{(w^3 - w^2 + p'^2 - p')t_2 p_2 p_3}{(\phi_l - 1)(w^2 + p')}\right] \tag{3.91}$$

Because the maximum number of coincidences between one short address matrix and one medium arriving matrix is one, the probability of one coincidence can be obtained as[27]

$$q_{s,m} = \frac{w}{2p'n_m}\left[1 - \frac{(w^3 - w^2 + p'^2 - p')(t_1 - t_2)p_2}{(\phi_m - 1)(w^2 + p')}\right] \tag{3.92}$$

From (3.77), the bit error rate $P_{\mathrm{b},s}$, $P_{\mathrm{b},m}$ and $P_{\mathrm{b},l}$ of subscribers employing the matrices with the lengths n_s, n_m and n_l respectively, are given by[27]

$$P_{\mathrm{b},s} = \frac{1}{2}\sum_{l_s+l_m+l_l=w}^{K_l+K_m+K_s-1}\binom{K_s-1}{l_s}q_s^{l_s}(1-q_s)^{K_s-1-l_s} \times \binom{K_m}{l_m}q_{s,m}^{l_m}(1-q_{s,m})^{K_m-l_m} \times \binom{K_l}{l_l}q_{s,l}^{l_l}(1-q_{s,l})^{K_l-l_l} \tag{3.93}$$

$$P_{\mathrm{b},m} = \frac{1}{2}\sum_{l_s+l_m+l_l=w}^{K_l+K_m+K_s-1}\binom{K_m-1}{l_m}q_m^{l_m}(1-q_m)^{K_m-1-l_m} \times \binom{K_l}{l_l}q_{m,l}^{l_l}(1-q_{m,l})^{K_l-l_l} \times \binom{K_s}{l_s}q_{m,s}^{l_s}(1-q_{m,s})^{K_s-l_s} \tag{3.94}$$

and

$$P_{\mathrm{b},l} = \frac{1}{2}\sum_{l_s+l_m+l_l=w}^{K_l+K_m+K_s-1}\binom{K_l-1}{l_l}q_l^{l_l}(1-q_l)^{K_l-1-l_l} \times \binom{K_s}{l_s}q_{l,s}^{l_s}(1-q_{l,s})^{K_s-l_s} \times \binom{K_m}{l_m}q_{l,m}^{l_m}(1-q_{l,m})^{K_m-l_m} \tag{3.95}$$

where K_s, K_m and K_l denote the numbers of simultaneous subscribers employing the matrices with the lengths n_s, n_m and n_l respectively.

In order to verify the validity of this analysis, substituting $K_j = 0$ into (3.77) and letting $P_{i,j} = 0$ for all $j \neq i$, reduces $P_{\mathrm{b},i}$ to[27]

$$P_{\mathrm{b},i} = \frac{1}{2}\sum_{l_i=w}^{K_i-1}\binom{K_i-1}{l_i} q_i^{l_i}(1-q_i)^{K_i-1-l_i} \tag{3.96}$$

It can be seen that this result is identical to the bit error rate formula of single length EWHPC.

An $(9\times\{11,121,1331\}, 3, \{1,1,1\}, \{1,1,1,1\}, \{60/4812, 396/4812, 4356/4812\})$ triple-length EWHPC[27] is employed as an example, where $k=3$, $r=r'=p_3=p_2=p_1=11$, $w=p'=3$, $t_2=3$ and $t_1=6$. Figure 3.7 shows the BERs versus the numbers of simultaneous subscribers K_l employing long matrices and K_m utilizing medium matrices for the fixed number of subscribers $K_s=5$ using short matrices. The topmost, middle, and lowest curved surfaces in Fig. 3.7 represent the performance of subscribers employing the long, medium and short address matrices, that is, $P_{\mathrm{b},l}$, $P_{\mathrm{b},m}$ and $P_{\mathrm{b},s}$ respectively. It can be seen that the performance usually becomes worse as the total number of simultaneous subscribers, $K_l+K_m+K_s$, increases, and the performance of subscribers employing the shortest matrices is always the best. This is because the multiple copies of the shortest matrices produce strong MAI in the process of inter-cross-correlation. However, the performance differences of subscribers with the medium and long matrices are smaller since the medium and long matrices encounter the same number of short matrices.

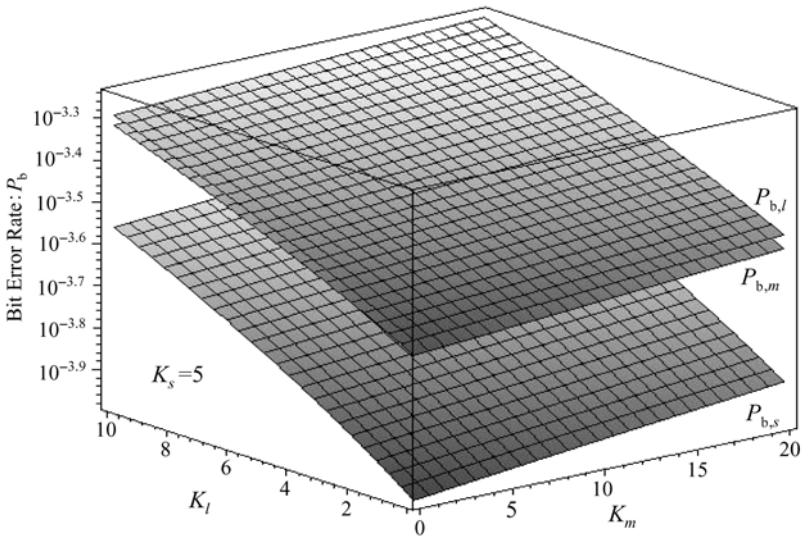

Figure 3.7 BERs versus the numbers of simultaneous users K_l and K_m for the $(9\times\{11,121,1331\}, 3,\{1,1,1\},\{1,1,1,1\}, \{60/4812,396/4812,4356/4812\})$ triple-length EWHPC with $K_s=5$ [27]

3.11.6 Illustration of Implementing Multimedia Traffic Integration Using MLEWHPCs in an OCDMA System

MLEWHPC can be applied to an OCDMA system to implement multimedia service integration[28]. As an example, consider three media transmitted in an OCDMA system: digitized voice, data and digitized video, as shown in Fig. 3.8. The real-time video transmission is a consecutive traffic model, which needs the highest priority and bit rate. We assume that the bit-rate of video, $1/T_v$, is an integral multiple of the data bit-rate, $1/T_d$, i.e., $1/T_v = p_2/T_d$, and the bit-rate of data traffic $1/T_d$ is an integral multiple of the bit-rate of voice, namely, $1/T_d = p_3/T_s = 1/(p_2T_v)$, where p_2 and p_3 are the extended factors of the MLEWHPC constructed. In this case, the bit-rate of video traffic is the highest. Assuming that for video traffic the length of the code is p_1, then we have

$T_v = p_1T_c$ (the bit-period of video traffic)
$T_d = p_2p_1T_c$ (the bit-period of data traffic)
$T_s = p_3p_2p_1T_c$ (the bit-period of voice traffic)

where T_c is the width of time slot. In other words, for data traffic the length of the code employed is p_1p_2 and for voice traffic the length of the code used is $p_1p_2p_3$.

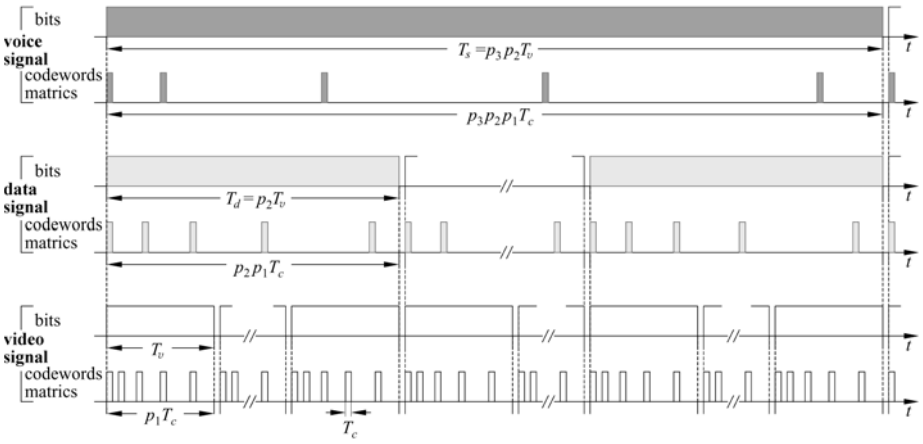

Figure 3.8 Relationship between the bit duration of digitized voice, data and digitized video traffic, and the code length[28]

Example 3.19 Let $k = 3$, $w = p' = 3$, $p_1 = p_2 = p_3 = 11$, $t_1 = 3$ and $t_2 = 1$ such that we obtain matrices with three lengths, among which there are $(w^2 + p') \times (p_1 - t_1) = 12 \times 8 = 96$ code matrices with the length p_1=11, $(w^2 + p')(t_1 - t_2) \times$

$p_2 = 264$ code matrices with the length $p_1 p_2$ =121, and $(w^2 + p')t_1 p_2 p_3 = 4356$ code matrices with the length $p_1 p_2 p_3 = 1331$. Assuming $T_c = 9$ps, then the data rate is about 10Gb/s when the code of length 11 is used to transmit the video traffic. The data rate is about 1Gb/s when the code of length 121 is employed to transmit the data traffic. The data rate is about 100Mb/s if the code of length 1331 is utilized to transmit the voice traffic. Since the performance of the traffic transmitted by the shortest code is the best, QoS of video traffic can be guaranteed.

3.12 Summary

In this chapter, we have introduced fourteen types of 2-D unipolar codes for wavelength-hopping/time-spreading OCDMA and one type of bipolar code. Among the 2-D codes, two types of multi-length codes are presented and the others are the single-length codes. The performance comparison of 2-D single-length codes is shown in Table 3.35 and the performance comparison of multi-length codes is shown in Table 3.36. For 2-D unipolar and single-length codes, from the point of view of the complexity of code constructions, the flexibility of wavelength and code length chosen, the code cardinality and the correlation property, the PC/OOC, OCFHC/OOC, WHPC and EWHPC are superior to other codes and more applicable to the OCDMA networks. Since the PC/OOC requires the number of wavelengths to be prime and the number of available wavelengths of OCFHC/OOC is the power of a prime number, PC/OOC is a special example of OCFHC/OOC. Therefore, OCFHC/OOC is more convenient in practice.

Since EWHPC is obtained by extending WHPC, its performance is superior to that of WHPC. Especially, for the $(wp' \times p_1 p_2 \cdots p_k, w, 0, 1)$ EWHPC, it results in flexibility of system design because the number of available wavelengths need not equal the code weight. Under the ideal correlation property, the cardinality of EWHPC is w-multiple of that of WHPC. What is more, another EWHPC, i.e., the $(p_1 p_2 \cdots p_k \times p_1, w, 0, 1)$ code, allows the number of wavelengths to be greater than the number of code lengths. This is very helpful in applications in high bit-rate systems. From the point of view of cardinality, OCFHC/OOC is slightly superior to EWHPC. Thus, as a whole, the performance of OCFHC/OOC and EWHPC is the best. However, since 2-D unipolar codes, which can be constructed by the existing constructions up to now, belong to the codes with special length, wavelength and weight, the employed codes must be chosen by the analysis and optimization of the network, the resources offered and the performance of code required by the network in the practical applications.

Although 2-D bipolar/unipolar and bipolar/bipolar codes can improve performance, they have high requirements for encoder and decoder hardware,

increasing the complexity and cost of implementation. Future applications of these two types of codes depends on the progress of optical component technology and electronic device technology.

The future network should be able to offer different services to different subscribers on demand. Therefore, the network should be able to utilize the integration of different services and provide different quality of services. MLWHPC and MLEWHPC can be useful in such networks. There are still many issues about multi-length wavelength-hopping/time-spreading codes that need to be investigated, such as the constructions of codes with flexible choice of code parameters.

Table 3.35 Performance comparison of some typical wavelength-hopping/time-spreading codes

2-D wavelength-hopping/time-spreading	Parameters of $(m \times n, w, \lambda_a, \lambda_c)$ Code	Number of available wavelengths	Code length	Cardinality	λ_c
PC/PC	$(p \times p^2, p, 0, 1)$	p	p^2	$p(p-1)$	1
PC/EQCC	$(p \times p(2p-1), p, 0, 2)$	p	$p(2p-1)$	$p(p-1)^2$	2
QCC/PC	$(p \times p^2, p, 0, 2)$	p	p^2	$p^2(p-1)$	2
OOC/PC	$(n_{\mathrm{OOC}} \times p^2, p, 1, 1)$	n_{OOC}	p^2	$\dfrac{n_{\mathrm{OOC}}(n_{\mathrm{OOC}}-1)}{p-1}$	1
PC/OOC	$(p \times n_{\mathrm{OOC}}, w, 1, 1)$	p	n_{OOC}	$\Phi_{\mathrm{OOC}} \cdot p^2$	1
OCFHC/OOC	$(p^k \times n_{\mathrm{OOC}}, w, 1, 1)$	p^k	n_{OOC}	$\dfrac{p^{2k}(n_{\mathrm{OOC}}-1)}{w(w-1)}$	1
Bipolar/ Unipolar	$(\Phi_{\mathrm{bipolar}} \times n_{\mathrm{OOC}}, w, 1, 1)$	Φ_{bipolar}	n_{OOC}	$p^2\left\lfloor \dfrac{n_{\mathrm{OOC}}-1}{w(w-1)} \right\rfloor$	1
WHPC	$(w \times p_1 p_2 \cdots p_k, w, 0, 1)$	w	$p_1 p_2 \cdots p_k$	$p_1 p_2 \cdots p_k$	1
EWHPC	$(wp' \times p_1 p_2 \cdots p_k, w, 0, 1)$ $p_k \geqslant p_{k-1} \geqslant \cdots \geqslant p_1$	wp'	$p_1 p_2 \cdots p_k$	$(w+1)p' p_1 p_2 \cdots p_k$	1
	$(p_1 p_2 \cdots p_k \times p_1, w, 0, 1)$ $p_k \geqslant p_{k-1} \geqslant \cdots \geqslant p_1 \geqslant w$	$p_1 p_2 \cdots p_k$	w	Eq. 3.80	1
MWOOC based on 1-D OOC	$(n \times n, w, 1, 1)$	n	n	$\dfrac{n(n^2-1)}{w(w-1)}$	1
GMWPC	$(c \times p_1 p_2 \cdots p_k, c, 0, 1)$	c	$p_1 p_2 \cdots p_k$	$p_1 p_2 \cdots p_k$	1
GMWRSC	$(p_1 \times (p_1 - 1) p_2 \cdots p_k,$ $p_1 - 1, 0, 1)$	p_1	$(p_1 - 1) p_2 \cdots p_k$	$p_1 p_2 \cdots p_k$	1

Table 3.36 Performance of MLWHPC and MLEWHPC

ML 2-D WH/TS Code	MLWHPC	MLEWHPC
Parameters of $(m\times N, w, A, B, D)$ Code	$(p_1\times N, p_1, A, B, D)$	$(wp'\times N, w, A, B, D)$
Number of wavelengths used	p_1	wp'
Code length distribution	$N=\{p_1, p_1p_2, \cdots, p_1p_2\cdots p_k\}$	$N=\{p_1, p_1p_2, \cdots, p_1p_2\cdots p_k\}$
Autocorrelation constraint	$\lambda_a^{(i)}=0\ ,\ 0\leqslant i\leqslant k-1$	$\lambda_a^{(i)}=0,\ \ 0\leqslant i\leqslant k-1$
Intra- and inter-cross-correlation constraints	$\lambda_c^{(i)}=1\ , 0\leqslant i\leqslant k-1\ ;\ \lambda=1$	$\lambda_c^{(i)}=1,\ \ 0\leqslant i\leqslant k-1;\ \lambda=1$
Cardinality Distribution	$\lvert C\rvert_{\text{MLWHPC}}\ D=$ $\{p_1-t_1, (t_1-t_2)p_2, \cdots,$ $(t_{k-2}-t_{k-1})p_2p_3\cdots p_{k-1},$ $t_{k-1}p_2p_3\cdots p_k\}$	$\lvert C\rvert_{\text{MLEWHPC}}\ D=$ $(w^2+p')\{p_1-t_1, (t_1-t_2)p_2, \cdots,$ $(t_{k-2}-t_{k-1})p_2p_3\cdots p_{k-1},$ $t_{k-1}p_2p_3\cdots p_k\}$
Total Cardinality	$\lvert C\rvert_{\text{MLWHPC}}$	$\lvert C\rvert_{\text{MLEWHPC}}$

Table 3.37 shows the characteristic comparison of several codes introduced in this chapter, from the viewpoint of the flexibility of choosing wavelengths and code lengths, the code cardinality of being a function of wavelength, and the cross-correlation properties.

Table 3.37 Characteristics of Several Codes in Table 3.35

2-D Wavelength-Hopping/ Time-Spreading Codes	Are the numbers of wavelengths and code lengths chosen independently?	Is the code cardinality quadratic function of the number of wavelengths?	Is the maximum value of cross-correlation functions equal to one?
PC/PC	×	√	√
PC/EQCC	×	√	×
QCC/PC	×	√	×
OOC/PC	√	×	√
PC/OOC	√	√	√
OCFHC/OOC	√	√	√
B/U	√	√	√
MWOOC based on 1-D OOC	×	×	√
GMWPC	×	×	√
GMWRSC	×	×	√
WHPC	√	×	√
EWHPC	√	×	√
MLWHPC	√	×	√
MLEWHPC	√	×	√

References

[1] G.-C. Yang and Wing C. Kwong: Performance Comparison of Multiwavelength CDMA and WDMA+CDMA for Fiber-Optic Networks. *IEEE Trans. on Communications*, Vol.45, No.11, 1997, pp1426 – 1434

[2] F. R. K. Chung, J. A. Salehi, and V. K. Wei: Optical orthogonal codes: Design, analysis, and applications. *IEEE Trans. on Information Theory*, Vol.35, No.3, May 1989, pp595 – 604

[3] H. Chung, and P. V. Kumar: Optical orthogonal codes—new bounds and an optimal construction. *IEEE Trans. on Information Theory*, Vol. 36, No.4, July 1990, pp866 – 872

[4] G. C. Yang and T. Fuja: Optical orthogonal codes with unequal auto- and cross-correlation constraints. *IEEE Trans. on Information Theory*, Vol.41, No.1, Jan. 1995, pp96 – 106

[5] F. J. MacWilliams and N. J. A. Sloane. The Theory of Error-Correcting Codes. Amsterdam, The Netherlands: North-Holland, 1986

[6] G.-C. Yang and J.-Y. Jaw: Performance analysis and sequence designs of synchronous code-division multiple access systems with multi-media services. Proc. Inst. Elect. Eng.—Communications, 1994, Vol.141, No.6, pp371 – 378

[7] L. Tancevski, I. Andonovic: Wavelength hopping/time spreading code division multiple access systems. *IEE Electronics Letters*, Vol.30, No.17, 1994, pp1388 – 1390

[8] L. Tancevski, Ivan Andonovic: Hybrid wavelength hopping/time spreading schemes for use in massive optical networks with increased security. *IEEE/OSA Journal of Lightwave Technology*, Vol.4, No.12, Dec. 1996, pp2636 – 2647

[9] L. Tancevski, I. Andonovic, M. Tur, J. Budin: Massive optical LANs using wavelength hopping/time spreading with increased security. *IEEE Photonics Technology Letters*, Vol.8, No.13, Jul. 1996, pp935 – 937

[10] S. P. Wan, Y. Hu: Two-dimensional optical system with prime/OOC codes. *IEEE Photonics Technology Letters*, Vol.13, No.13, 2001, pp1373 – 1375

[11] W. C. Kwong, G.-C. Yang, V. Baba, C.-S. Bres, P. R. Prucnal: Multiple-wavlength optical orthogonal codes under prime-sequence permutations for optical CDMA. *IEEE Trans. on Communications,* Vol.53, No.1, Jan. 2005, pp117 – 123

[12] Shurong Sun, Hongxi Yin, Anshi Xu: A New Family of 2-D Optical Orthogonal Codes for Optical CDMA Access Networks. The 11th Asia-Pacific Conference on Communications, October 2005, Perth, Western Australia, 1A3

[13] G.-C. Yang and W. C. Kwong: Prime Codes with Applications to CDMA Optical and Wireless Networks. Boston, MA: Artech House, 2002

[14] Shurong Sun, Hongxi Yin, Ziyu Wang, Anshi Xu: A New Family of 2-D Optical Orthogonal Codes and Analysis of its Performance in Optical CDMA Access Networks. *IEEE/OSA Journal of Lightwave Technology*, Vol.24, No.4, 2006, pp1646 – 1653

[15] Wenhua Mei, Yixian Yang: The theory of address coding for frequency-hopping communications. National Defense Industry Press, China, 1996, pp82 – 95

[16] W. C. Kwong, G.-C. Yang, and Y.-C. Liu: A new family of wavelength time optical CDMA codes utilizing programmable arrayed waveguide gratings. *IEEE Journal Selected Areas on Communications*, Vol.23, No.8, August 2005, pp1564 – 1571

[17] L. Nguyen, T. Dennis, B. Aazhang, and J. F. Young: Optical spectral amplitude CDMA communication. *IEEE/OSA Journal of Lightwave Technology*, Vol.15, No.9, Sep. 1997, pp1647 – 1653

[18] J.-F. Huang and D.-Z. Hsu: Fiber-grating-based optical CDMA spectral coding with nearly orthogonal m-sequence codes. *IEEE Photonics Technology Letters*, Vol.12, No.9, Sep. 2000, pp1252 – 1254

[19] Wing C. Kwong, Guu-Chang Yang and Cheng-Yuan Chang: Wavelength-hopping Time-Spreading Optical CDMA with Bipolar Codes. *IEEE/OSA Journal of Lightwave Technology*, Vol. 23, No. 1, Jan. 2005, pp260 – 267

[20] A. W. Lam and S. Tantaratana, Theory and Application of Spread Spectrum Systems. Piscataway, NJ: IEEE, 1994

[21] G.-C. Yang and W. C. Kwong: A new class of carrier-hopping codes for code-division multiple-access optical and wireless systems. *IEEE Communications Letters*, Vol. 8, No. 1, Jan. 2004, pp51 – 53

[22] G.-C. Yang and W. C. Kwong: Performance analysis of extended carrier-hopping prime codes for optical CDMA. *IEEE Trans. on Communications*, Vol. 53, No. 5, May 2005, pp876 – 881

[23] L. R. Chen, S. D. Benjamin, P.W. E. Smith, and J. E. Sipe: Applications of ultrashort pulse propagation in Bragg gratings for wavelength-division multiplexing and code-division multiple access. *IEEE Journal of Quantum Electronics*, Vol. 34, 1998, pp2117 – 2129

[24] K.-L. Deng, R. J. Runser, P. Toliver, I. Glesk, and P. R. Prucnal: A highly scalable, rapidly reconfigurable, multicasting-capable, 100Gb/s photonic switched interconnect based upon OTDM technology. *IEEE/OSA Journal Lightwave Technology*, Vol. 18, No.7, 2000, pp1892 – 1904

[25] Wing C. Kwong, Guu-Chang Yang: Extended Carrier-Hopping Prime Codes for Wavelength-Time Optical Code-Division Multiple Access. *IEEE Trans. on Communications*, Vol.52, No.7, 2004, pp1084 – 1091

[26] Sangin. Kim, Kyungsik Yu and Namkyoo Park: A new family of space/wavelength/time spread three-dimensional optical code for OCDMA networks. *IEEE/OSA Journal of Lightwave Technology*, Vol.18, No.4, April 2000, pp502 – 511

[27] Wing C. Kwong, and Guu-Chang Yang: Multiple-length Extended Carrier-Hopping Prime Codes for Optical CDMA Systems Supporting Multirate Multimedia Services. *IEEE/OSA Journal of Lightwave Technology*, Vol. 23, No. 12, Nov. 2005, pp3653 – 366

[28] Paul R. Prucnal, et al: Optical Code Division Multiple Access—Fundamental and Applications. CRC Press, Taylor & Francis, 2006

[29] G. -C. Yang and W. C. Kwong: Design of multilength optical orthogonal codes for optical code-division multiple-access multimedia networks. *IEEE Trans. on Communications*, Vol. 50, No. 8, Aug. 2002, pp1258 – 1265

[30] Wing C. Kwong and Guu-Chang Yang: Multiple-length Multiple-wavelength Optical Orthogonal Codes for Optical CDMA Systems Supporting Multirate Multimedia Services. *IEEE Journal on Selected Areas in Communications*, Vol. 22, No. 9, 2004, pp1640 – 1647

[31] Wing C. Kwong and Guu-Chang Yang: Frequency-hopping Codes for Multimedia Services in Mobile Telecommunications. *IEEE Trans. on Vehicular Technology*, Vol.48, No. 6, 1999, pp1906 – 1915

[32] P. A. Perrier and P. R. Prucnal: Wavelength-division integration of services in fiber-optic networks. *Int. J. Digital Analog Cabled Syst*., Vol. 1, 1988, pp149 – 157

[33] G.-C. Yang: Variable-weight optical orthogonal codes for CDMA networks with multiple performance requirements. *IEEE Trans. on Communications*, Vol.44, No.1, 1996, pp47 – 55

4 Optical Encoders and Decoders for OCDMA

4.1 Introduction

The typical network architecture for OCDMA with broadcast star is shown in Fig. 4.1. It can be seen that one of the key issues to implement OCDMA networking and communication is how to encode and decode the user's data such that the optical channel can be shared, that is, we need to develop the practical encoding and decoding techniques that can be exploited to generate and recognize appropriate code sequences reliably. Therefore, The OCDMA encoders and decoders are the key components to implement OCDMA systems. In order to actualize the data communications among multiple users based on OCDMA communication technology, one unique codeword-waveform is assigned to each subscriber in an OCDMA network, which is chosen from specific OCDMA address codes, and therefore, different users employ different address codeword-waveforms. In an OCDMA network using on-off keying pattern, the user's data is transmitted by each information bit "1" which is encoded into desired address codeword. However, the transmitter does not produce any optical pulses when the information bit "0" is sent. Figure 4.2 gives the schematic diagrams of waveforms employed to transmit data of three subscribers in an OCDMA network.

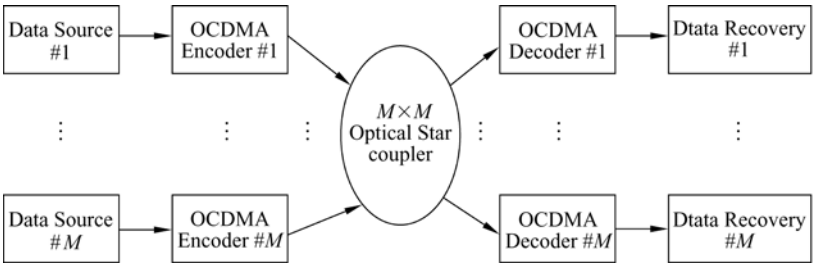

Figure 4.1 Schematic diagram of an OCDMA system

In terms of the difference of signal modulation and detection pattern, OCDMA encoders/decoders are roughly classified into coherent optical en/decoders and incoherent optical en/decoders. The incoherent optical en/decoders employ simple intensity-modulation/direct-detection technology and the coherent optical en/decoders are based on the modulation and detection of optical signal phase. The commonly used optical en/decoders in the incoherent OCDMA are based on time-spreading encoding (sometimes, called time encoding), spectral amplitude

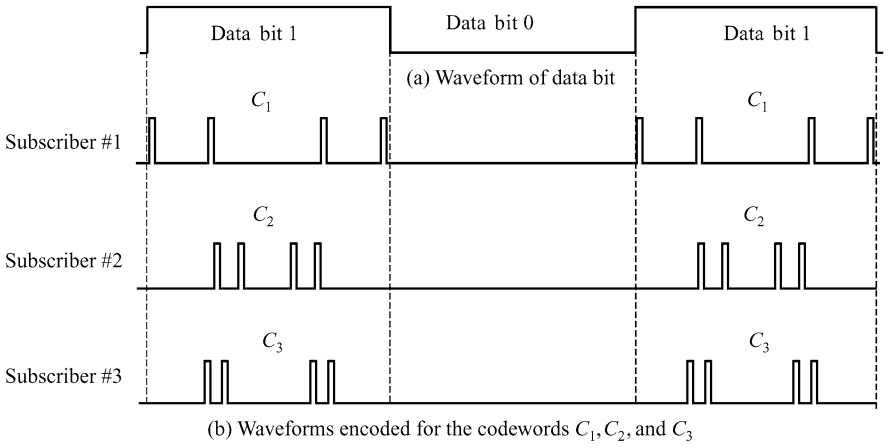

Figure 4.2 Waveforms encoded for OCDMA

encoding, spatial encoding, two-dimensional wavelength-hopping/time-spreading, and complementary spectrum transmission/balanced (differential) detection encoding as well. The coherent optical en/coders in common use are spectral phase time-spreading en/decoders and temporal phase en/decoders. When an optical en/decoder can only en/decode one subscriber's data, it is called a fixed optical en/decoder. Because one user requires communicating with different subscribers during different period of time in an OCDMA network, therefore, it needs to encode the data differently so that it can be transmitted to different subscribers. Similarly, each user intends to receive information from different subscribers in different time, and thus it requires a tunable optical-decoder such that it can detect and receive the data message from the network. This type of optical encoders and decoders is called the tunable optical en/decoders.

This chapter is organized as follows. One-dimensional incoherent fixed and tunable optical encoders and decoders with time encoding are introduced in section 4.2. Two-dimensional incoherent wavelength-hopping/time-spreading fixed and tunable optical encoders and decoders are described in section 4.3. The spectral-amplitude incoherent optical encoders and decoders are discussed in section 4.4. The incoherent 2-D bipolar/unipolar optical en/decoders are given in section 4.5. The coherent spectral-phase optical en/decoders and temporal-phase optical en/decoders are presented in section 4.6. At last, the summary of this chapter is given in section 4.7.

4.2 One-dimensional Incoherent Optical Encoders and Decoders

From Chapter 2, it is known that although there are many types of one-dimensional unipolar optical codes (which takes the value {0,1}), each codeword

in arbitrary optical code can always be represented as a corresponding codeword block, where each element in every block indicates the position of "1" in the codeword. Therefore, the structures and operational principles of any one-dimensional incoherent optical en/decoders are similar with each other. For the sake of convenient description and considering that optical orthogonal codes (OOCs) have the best correlation performance among one-dimensional optical codes, we will take one-dimensional OOC as an example to describe the structure and principle of its optical encoder/decoder.

Each codeword in a one-dimensional $(n, w, \lambda_a, \lambda_c)$ OOC corresponds to a 1-D codeword block $\{i_1, i_2, \cdots, i_j, \cdots, i_w\}$, where i_j represents the position of the j^{th} "1" of a codeword, $0 \leqslant i_j \leqslant n-1$. Thus, a fixed and tunable one-dimensional incoherent optical encoder and decoder can be composed of an optical power splitter, a number of fixed or tunable fiber-optic delay lines and an optical power combiner[1 – 3].

4.2.1 Fixed Optical Encoder and Decoder

A fixed optical encoder of incoherent OCDMA for a 1-D $(n, w, \lambda_a, \lambda_c)$ OOC is shown in Fig. 4.3 (a), which consists of a $1 \times w$ optical power splitter, w fiber-optic delay lines and a $w \times 1$ optical power combiner. The delay of the j^{th} fiber-optic delay line is $i_j \tau$, $0 \leqslant i_j \leqslant n-1$, where n is the code length of the optical orthogonal code, w is the code weight, and τ is the width of a chip, i.e., the time-width of an optical pulse. At the beginning of a data bit cycle of a user, the light source sends an optical pulse with time-width τ into the optical modulator. For the on-off keying communication pattern, the optical modulator outputs an optical pulse when the data bit is "1" and the optical modulator outputs nothing when the data bit is "0". Then, the optical pulse corresponding to the data bit "1" is encoded by an optical encoder whose output is an optical pulse-signal waveform corresponding to an optical orthogonal codeword. Because there is no optical signal to be input into the optical encoder for a data bit "0", nothing is output from the optical encoder. A fixed optical decoder is shown in Fig. 4.3(b), whose structure is the same as its corresponding encoder except that the delay of its j^{th} fiber-optic delay line is changed into $(n-1-i_j)\tau$, $0 \leqslant i_j \leqslant n-1$. When the input of the decoder is the output signal from its corresponding encoder, its output is an autocorrelation function of its corresponding OOC codeword. Finally, the data bit will be restored after the optical-to-electrical conversion and threshold decision. If the decoder input is an encoded waveform from other OOC codeword, its output is a cross-correlation function. Since an autocorrelation peak does not occur there is no data output.

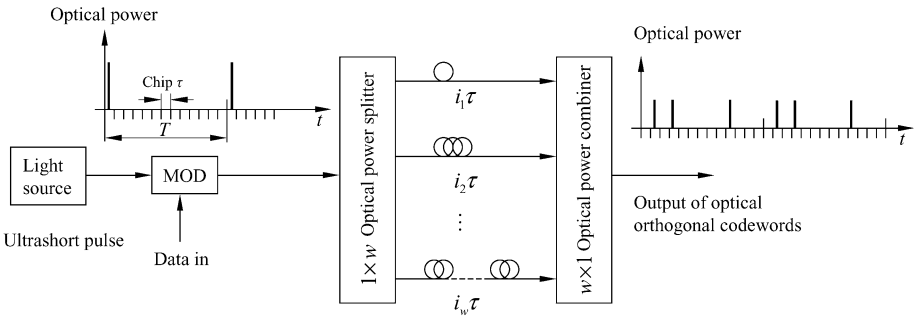

(a) All-optical encoder (Scenario of input 11)

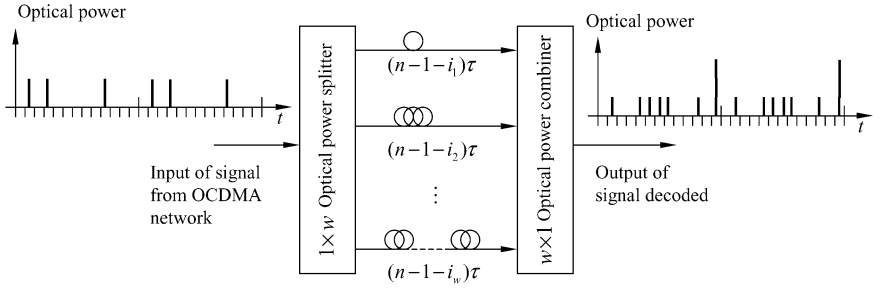

(b) All-optical decoder

Figure 4.3 Schematic diagrams of all-optical encoder and decoder for OCDMA system

Example 4.1 An $(n, w, \lambda) = (13,3,1)$ OOC has two codewords that corresponds to the codeword blocks (1,3,9) and (2,5,6). If a subscriber needs to implement encoding of codeword (2,5,6), then there are three fiber-optic delay lines in its encoder and decoder respectively. The delays of three fiber-optic delay lines in its encoder are $i_1\tau = 2\tau$, $i_2\tau = 5\tau$ and $i_3\tau = 6\tau$ respectively, and the delays of three optical fiber delay lines in its decoder are $(n-1-i_1)\tau = 10\tau$, $(n-1-i_2)\tau = 7\tau$ and $(n-1-i_3)\tau = 6\tau$ respectively. The input and output optical signal waveforms of the codeword (2,5,6) corresponding optical encoder is shown in Fig. 4.4(a) and (b). The discrete autocorrelation function output by the (2,5,6) optical decoder is shown in Fig. 4.4(c) and the cross-correlation between the codewords (2,5,6) and (1,3,9) is shown in Fig. 4.4(d). Note that the output of (2,5,6) optical decoder is the superposition of them both.

4.2.2 Tunable OOC Encoder and Decoder

Since a user needs to communicate with different subscribers during different time, each subscriber in a network has at least one of optical encoder and decoder

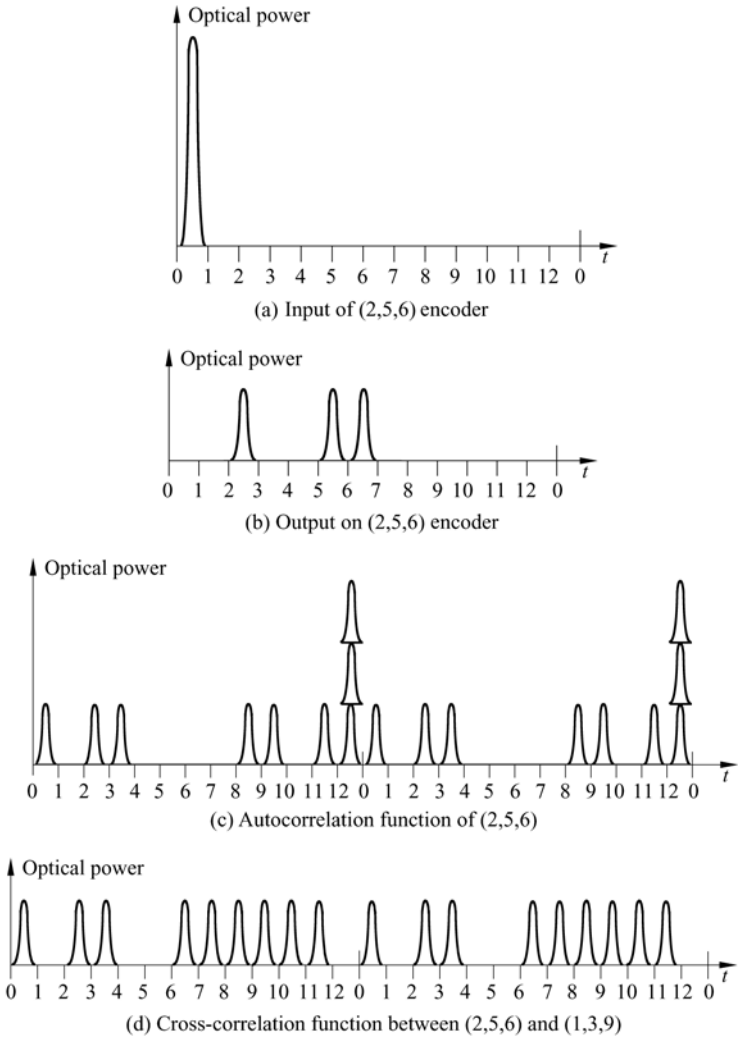

Figure 4.4 Inputs and Outputs of Optical Encoder and Decoder

tunable in order to implement the point-to-point, point-to-multipoint, multipoint-to-multipoint and broadcast communications.

A tunable OOC encoder is shown in Fig. 4.5, which consists of a $1 \times w$ optical power splitter, w tunable optical fiber delay lines, a $w \times 1$ optical power combiner and a delay selection controller. The range of tunable delay of each tunable optical fiber delay line is from 0 to $(n-1)\tau$, where n is the code length of an OOC, w is the code weight of the OOC and τ is the width of a chip optical pulse. Each tunable optical fiber delay line has the same architecture, shown in Fig. 4.6, which is composed of $m+1$ stages of 2×2 optical switches and optical fiber delay lines, where m satisfies $2^{m-1} < n \leqslant 2^m$. The delay of the

k^{th} stage of the tunable delay line is $2^{k-1}\tau$, $1 < k \leqslant m$. When a control signal $a_k^j = 0$, the k^{th} stage switch is set to cross-state, and when the control signal $a_k^j = 1$, it is set to bar-state. The state of each optical switch is changed by the delay control logic in the delay controller such that the delay of the j^{th} tunable delay line becomes $i_j \cdot \tau$. The control logic is stored in a ROM (read-only memory) beforehand and the delay controller employs "look-up-table" approach to set the delay of the j^{th} tunable delay line $i_j \cdot \tau$.

Before starting the data transmission a subscriber sends firstly an address, i.e., a codeword block $\{i_1, i_2, \cdots, i_j, \cdots, i_w\}$, to its delay controller. Then, the delay controller chooses w control sequences $(a_1^j \cdots a_m^j)$ from the delay control look-up table for the states of all switches, where $1 \leqslant j \leqslant w$. Therefore, when a short optical pulse corresponding to a data bit '1" is sent to the optical encoder, its output is an optical pulse sequence of C_i, which is determined by the codeword block $\{i_1, i_2, \cdots, i_j, \cdots, i_w\}$, where C_i is a codeword of an OOC. However, since a data bit is "0", the absence of short optical pulse is sent to the encoder, and thus the encoder outputs all "0".

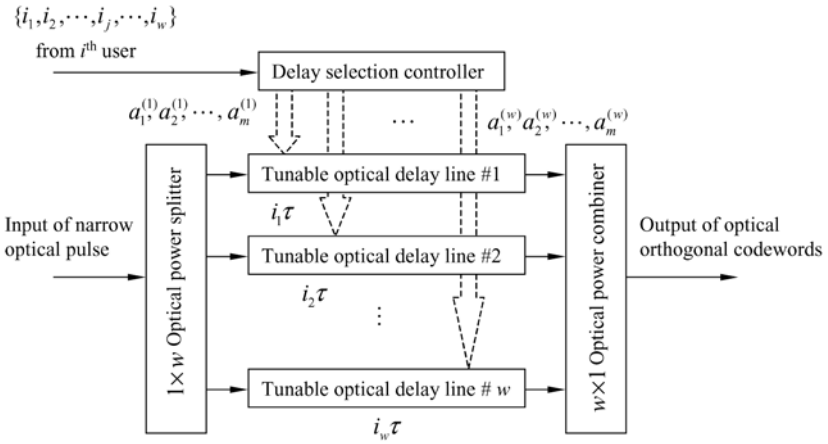

Figure 4.5 Schematic diagram of tunable OOC optical encoder

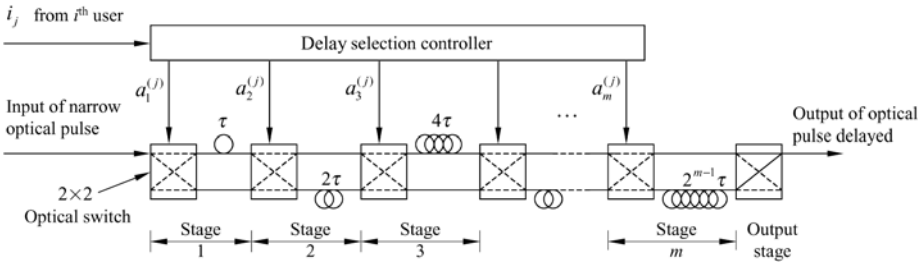

Figure 4.6 Block diagram of tunable optical fiber delay line

The structure of a tunable optical decoder is the same as an optical encoder except that the input of the delay controller of the tunable delay line is changed into $\{n-1-i_1, n-1-i_2, \cdots, n-1-i_j, \cdots, n-1-i_w\}$, in order to guarantee that the output pulse sequence C_i^l is the desired time-reversed sequence C_i and the optical decoder can perform the correlation operation on demand. If the input pulse sequence matches to C_i corresponding to the decoder the output is an autocorrelation function, otherwise the output is a cross-correlation function of the two codewords.

Example 4.2 The tunable optical encoder in an OCDMA network employing an $(n, w, \lambda_a, \lambda_c) = (41,4,2,1)$ OOC as subscribers' address code, is composed of an 1×4 optical power splitter, four tunable fiber-optic delay lines and a 4×1 optical power combiner. The OOC has five codewords, whose codeword blocks are (1,11,30,40), (3,4,37,38), (7,18,23,34), (10,13,28,31), (12,16,25,29). Each codeword is employed to control the states of 2×2 optical switches such that the optical encoder performs encoding of the short optical pulse transmitted when an input data bit is "1".

Since the delay value of the j^{th} tunable fiber-optic delay line is $i_j \cdot \tau$, $0 \leqslant i_j \leqslant n-1$, $2^{m-1} < n \leqslant 2^m$, $j = 1,2,3,4$. From $n = 41$, we can obtain $m = 6$. The resulting delay control logic is illustrated in Table 4.1, which can implement the delay of pulse in any codeword of arbitrary OOC with the codelength less than or equeal to 64. The control sequences of four tunable fiber-optic delay lines which constitute the encoder corresponding the codewords aforementioned are illustrated in Table 4.2. The corresponding tunable optical decoder is the same as the encoder, what we only need to do is that the delay value of the j^{th} tunable fiber-optic delay line is changed into $(n-1-i_j \cdot \tau)$, $0 \leqslant i_j \leqslant n-1$, $2^{m-1} < n \leqslant 2^m$, $j = 1,2,3,4$.

Table 4.1 Delay-controlled logic table for delay lines of tunable optical encoder

Delay (multiple of τ)	$a_6^j a_5^j a_4^j a_3^j a_2^j a_1^j$	Delay (multiple of τ)	$a_6^j a_5^j a_4^j a_3^j a_2^j a_1^j$	Delay (multiple of τ)	$a_6^j a_5^j a_4^j a_3^j a_2^j a_1^j$
0	000000	9	011011	18	110110
1	000011	10	011110	19	110101
2	000110	11	011101	20	111100
3	000101	12	010100	21	111111
4	001100	13	010111	22	111010
5	001111	14	010010	23	111001
6	001010	15	010001	24	101000
7	001001	16	110000	25	101011
8	011000	17	110011	26	101110

Continued

Delay (multiple of τ)	$a_6^j a_5^j a_4^j a_3^j a_2^j a_1^j$	Delay (multiple of τ)	$a_6^j a_5^j a_4^j a_3^j a_2^j a_1^j$	Delay (multiple of τ)	$a_6^j a_5^j a_4^j a_3^j a_2^j a_1^j$
27	101101	40	111000	53	011111
28	100100	41	111011	54	011010
29	100111	42	111110	55	011001
30	100010	43	111101	56	001000
31	100001	44	110100	57	001011
32	100000	45	110111	58	001110
33	100011	46	110010	59	001101
34	100110	47	110001	60	000100
35	100101	48	010000	61	000111
36	101100	49	010011	62	000010
37	101111	50	010110	63	000001
38	101010	51	010101		
39	101001	52	011100		

Table 4.2 Control sequence table for four tunable delay lines of tunable optical encoder ($j = 1,2,3,4$)

Codeword No.	Codeword Block	$a_6^1 a_5^1 a_4^1 a_3^1 a_2^1 a_1^1$	$a_6^2 a_5^2 a_4^2 a_3^2 a_2^2 a_1^2$	$a_6^3 a_5^3 a_4^3 a_3^3 a_2^3 a_1^3$	$a_6^4 a_5^4 a_4^4 a_3^4 a_2^4 a_1^4$
1	(1,11,30,40)	000011	011101	100010	111000
2	(3,4,37,38)	000101	001100	101111	101010
3	(7,18,23,34)	001001	110110	111001	100110
4	(10,13,28,31)	011110	010111	100100	100001
5	(12,16,25,29)	010100	110000	101011	100111

The architectures and principle of optical encoders and decoders corresponding to other one-dimensional incoherent (unipolar) optical codes are very similar to those of OOC encoders and decoders. We will not describe them one by one here. With regard to optical encoder and decoder of the prime code (PC), since each codeword in a prime code can be divided into p subsequences and there is neither more nor less than one "1" in each subsequence, each fiber-optic delay line to be employed to implement PC tunable encoder/decoder consists of a tunable delay line followed a fixed delay line. Note that the 0^{th} reference path acts only as the compensating delay since the first "1" in each codeword of PC is at the position of the 0^{th} chip without exception. Since the delay range of arbitrary tunable delay line is merely between 0 and $(p-1)\tau$, the PC tunable optical encoder/decoder can reduce the number of 2×2 optical switches employed, optical power loss is decreased and the implementation cost is debased. Interested readers can

refer to Reference [2]. However, PC has poor correlation properties and its cardinality is less than that of OOC relatively.

One-dimensional incoherent time encoding is the first OCDMA encoding/decoding approach[1] implemented in history. However, it has been limited in its practical implementation because of its requirement of short optical pulses and long code length for good correlation properties, and large loss of optical power.

4.3 Two-Dimensional Incoherent WH/TS Optical Encoders and Decoders

The wavelength-hopping/time-spreading OCDMA is a type of 2-D encoding to perform the frequency spreading in time domain and wavelength domain simultaneously, which not only increases the flexibility of code design, but improves the properties of codes dramatically. If there does not exist wavelength-reuse in each codeword of a 2-D code constructed, its autocorrelation sidelobes can achieve zero. Meanwhile, the cross-correlation function values of 2-D codes are lower than those of OCDMA codes with time encoding. The biggest merits of 2-D codes are the significant increase of the cardinalities, which makes the numbers of users and simultaneous subscribers in a network increase enormously, and the reduction of the code length, which results in the data rate of single user to boost largely.

For a 2-D $(m \times n, w, \lambda_a, \lambda_c)$ OOC with the number of available wavelengths m, the number of slots, i.e., code length n, code weight w, the auto- and cross-correlation constraints of λ_a and λ_c respectively, its corresponding 2-D codeword blocks are $\{(i_1, j_1),(i_2, j_2),\cdots,(i_v, j_h),\cdots,(i_w, j_w)\}$, $0 \leqslant i_v \leqslant m-1$, $0 \leqslant j_h \leqslant n-1$, $1 \leqslant v, h \leqslant w$, where i_v represents the wavelength number of a pulse in the code, j_h represents the slot number of the pulse to locate.

4.3.1 Fixed 2-D Incoherent WH/TS Optical Encoders and Decoders

A broadband light source or a multi-wavelength light source outputs short pulse trains with the repetition rate $1/T$ and the width τ, which are modulated by the input data in an optical modulator. For the on-off keying mode, the modulator outputs an optical pulse when a transmitted data bit is "1", otherwise it outputs the absence of optical signal if the transmitted data bit is "0". Then, the narrow optical pulse corresponding to the data bit "1" is fed into a 2-D incoherent WH/TS optical encoder to perform encoding.

The fixed 2-D incoherent WH/TS optical encoder is shown in Fig. 4.7(a), which consists of an $1 \times w$ wavelength-division demultiplexer, w fixed fiber-optic

delay lines and an $w\times 1$ wavelength-division multiplexer. The short optical pulse corresponding to data bit "1" is firstly separated into w optical pulses with the wavelengths $\lambda_{i_1},\lambda_{i_2},\cdots,\lambda_{i_w}$, $(0\leqslant i_1,i_2,\cdots,i_w\leqslant m-1)$, respectively by the wavelength-division demultiplexer. These w optical pulses are again delayed $j_1\tau,j_2\tau,\cdots,j_w\tau$ respectively, where $0\leqslant j_1,j_2,\cdots,j_w\leqslant n-1$, τ is the time width of an optical pulse. Finally, they are combined and output by the wavelength division multiplxer. In doing so, the 2-D WH/TS optical encoding of input data is achieved.

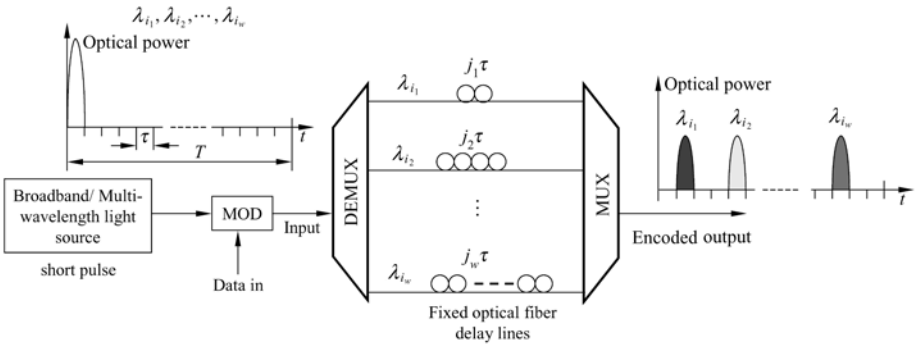

(a) Fixed 2-D incoherent WH/TS optical encoder

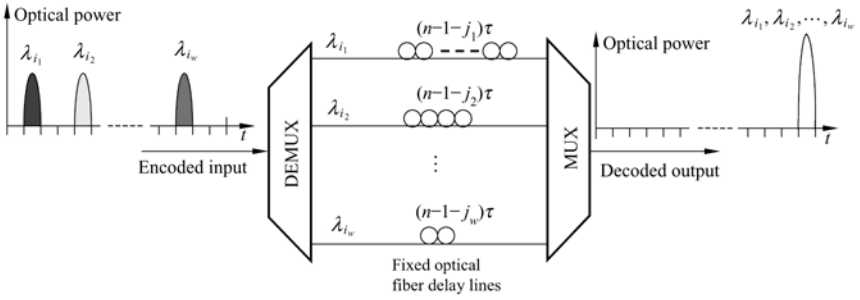

(b) Fixed 2-D incoherent WH/TS optical decoder

MOD: modulator; MUX: multiplexer; DEMUX: demultiplexer

Figure 4.7 Fixed 2-D incoherent WH/TS optical encoder/decoder for OCDMA

The architecture of a 2-D WH/TS decoder, as illustrated in Fig. 4.7(b), is very similar to that of the 2-D WH/TS encoder. What is needed to be changed is only that the delays of the fiber-optic delay lines corresponding to those in the encoder are changed into $(n-1-j_1)\tau$, $(n-1-j_2)\tau,\cdots,(n-1-j_w)\tau$, in order to shift the output autocorrelation peak to the last slot (chip) position in a corresponding data bit period after the encoded signal is decoded. When the input of the decoder is the corresponding optical encoder output, the decoder outputs an autocorrelation function. The data bit is restored after optical-to-electrical conversion and threshold

decision at the time of the occurrence of autocorrelation peak through an electronic circuit. If an input of the optical decoder is not the output of the corresponding optical encoder, the output of the decoder is a cross-correlation function. At last, after a certain processing of electronic circuit, there is no data output in the receiving end. In this way, the optical decoding and data recovery are implemented.

Example 4.3 The $(m \times n, w, \lambda_a, \lambda_c) = (13 \times 13, 3, 1, 1)$ multi-wavelength OOC has 364 codewords. Two of them are [(2,2),(4,6),(10,5)] and [(2,4),(5,10),(6,12)] respectively. 2-D optical encoder and decoder for this multi-wavelength OOC are all composed of one 1×3 wavelength division demultiplexer, one 3×1 multiplexer and three fixed fiber-optic delay lines. From the codeword [(2,2), (4,6),(10,5)], the obtained delays of three fiber-optic delay lines corresponding to the wavelengths λ_2, λ_4 and λ_{10} in the optical encoder are $j_1\tau = 2\tau$, $j_2\tau = 6\tau$ and $j_3\tau = 5\tau$ respectively, and the delays of three delay lines in the optical decoder are $(n-1-j_1)\tau = 10\tau$, $(n-1-j_2)\tau = 6\tau$ and $(n-1-j_3)\tau = 7\tau$ respectively. The input and output optical pulse signal waveforms of the optical encoder corresponding to the codeword [(2,2),(4,6),(10,5)] is illustrated in Fig. 4.8(a) and (b). The discrete autocorrelation function output by the [(2,2), (4,6),(10,5)] optical decoder is shown in Fig. 4.8(c). The cross-correlation function between the codewords [(2,2),(4,6),(10,5)] and [(2,4),(5,10),(6,12)] is shown in Fig. 4.8(d). The output of the [(2,2),(4,6),(10,5)] decoder is the superposition of them.

4.3.2 Tunable 2-D Incoherent WH/TS Optical Encoder and Decoder

A WH/TS optical code is a two-dimensional code, which has two freedoms. Therefore, the tunable 2-D incoherent WH/TS optical encoder and decoder can be tuned in two freedoms. For example, each codeword in MWOOC, OOC/PC code, PC/OOC code, OCFHC/OOC code and EWHPC code, includes only a part of available wavelengths and therefore, two freedoms of corresponding optical encoder and decoder need to be tuned. The tunable 2-D incoherent WH/TS optical encoder/decoder are shown in Fig. 4.9, which consists of a $1 \times m$ wavelength division demultiplexer, two $m \times w$ optical switches, w tunable optical delay lines, a $m \times 1$ wavelength division multiplexer, and a wavelength and delay control selector. The wavelength and delay control selector receives a user's instruction and sends the controlling signals to control the selections of wavelengths and delays of every pulse in the codewords. The pulse signal from a broadband light source is modulated by data, which is fed into the optical encoder. It is decomposed into m pulses corresponding to wavelengths $\lambda_0, \lambda_1, \cdots, \lambda_{m-1}$ respectively by the $1 \times m$ wavelength division demultiplexer. Then, when these m pulses pass the $m \times w$ optical switch, the wavelength selection controller

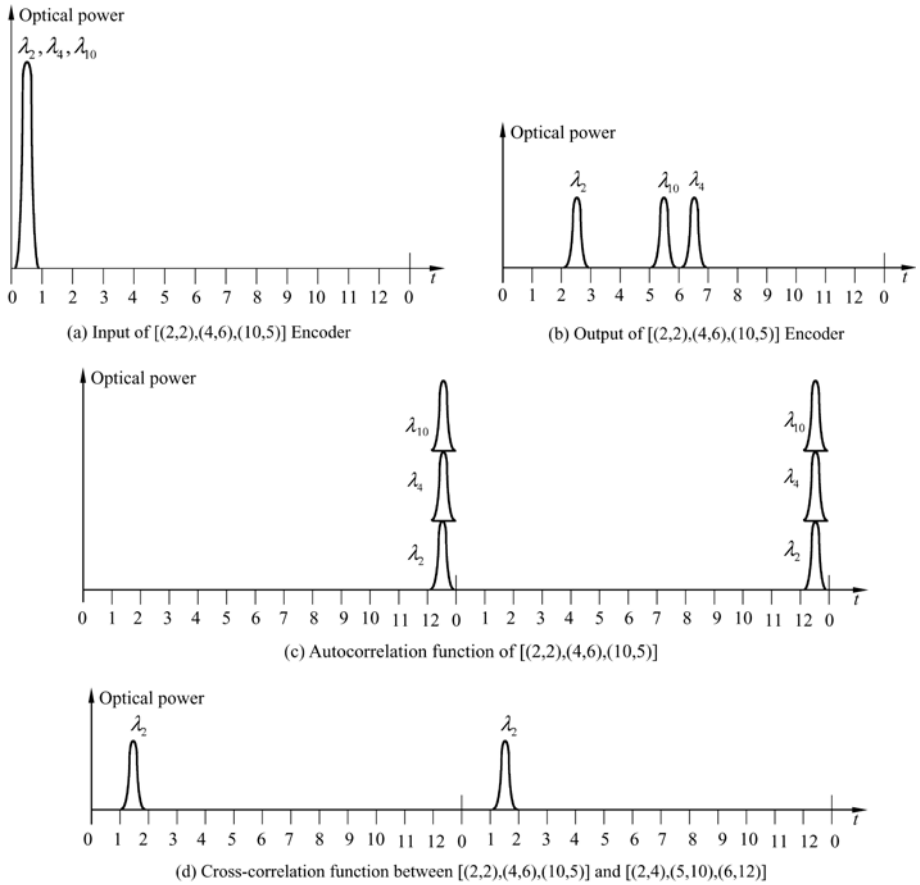

Figure 4.8 Inputs and Outputs of Optical Encoder and Decoder

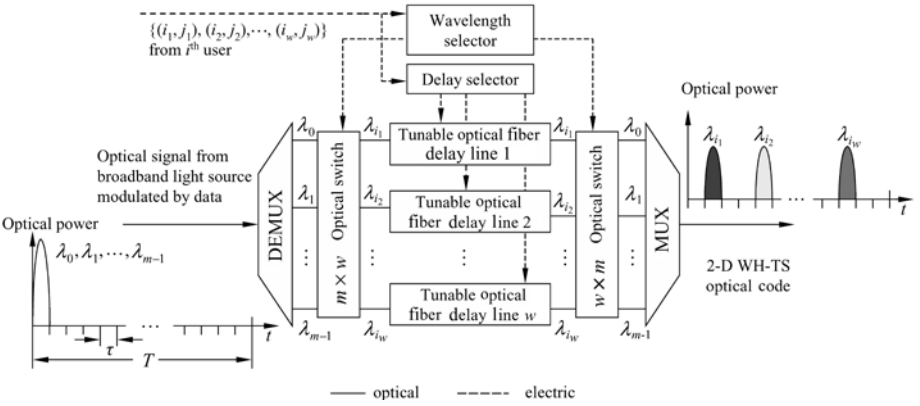

Figure 4.9 Tunable 2-D WH/TS optical encoder/decoder for OCDMA

chooses w pulses corresponding to wavelengths $\lambda_{i_1}, \lambda_{i_2}, \cdots, \lambda_{i_w}$ from a codeword by controlling the state of the $m \times w$ optical switch. Again, when these w pulses go across w tunable fiber-optic delay lines, the delays required by the codeword can be implemented under the controlling of the delay controller. Afterwards, these w optical pulses with delays on demand are fed into the $m \times 1$ wavelength division multiplexer by the $w \times m$ optical switch. The output of the wavelength division multiplexer is the encoding corresponding to the codeword as desired. In this way, the encoding corresponding to arbitrary codeword in the selected 2-D address code in the construction of an OCDMA network can be implemented. Since the architecture and operational principle of tunable delay lines have been introduced in Section 4.2.2 we no longer give unnecessary details here.

However, in some other codes, such as PC/PC code, PC/EQCC code, WHPC code, etc., each codeword contains all of available wavelengths, i.e., $m = w$. For this scenario, the wavelength dimension does not need to be tuned. When the encoding corresponding to different codewords is implemented, the different delays for every pulse need simply to be tunable. Therefore, the tunable 2-D optical encoder/decoder only needs one-dimensional tuning. This simplifies the structure of tunable 2-D optical encoder/decoder. Such a one-dimensional tunable WH/TS optical encoder/decoder with slots tuned only is shown in Fig. 4.10, which only implements the required delays of the pulses with different wavelengths under the controlling of the delay selector, based on the user's signaling.

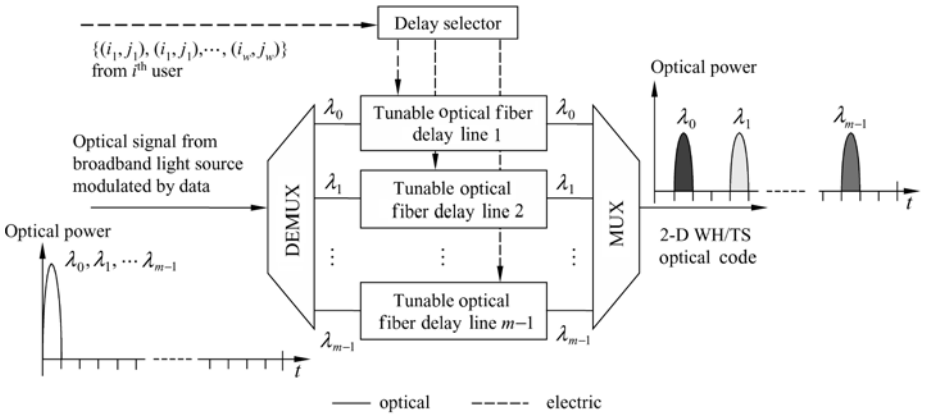

Figure 4.10 One-dimensional tunable 2-D WH/TS optical encoder/decoder for OCDMA

The architecture and operational principle of tunable 2-D incoherent WH/TS decoder is very similar to its corresponding encoder. The only difference is that the delay of the h^{th} optical fiber-optic delay line is changed into $(n-1-j_h)\tau$, $1 \leqslant h \leqslant w$. (Note that the delay of the h^{th} fiber-optic delay line in the tunable optical encoder is $j_h\tau$, $1 \leqslant h \leqslant w$.)

4.3.3 2-D Incoherent WH/TS Optical Encoder and Decoder Using FBGs

2-D incoherent WH/TS optical encoder and decoder can be comprised by using fiber Bragg gratings (FBGs) to reflect the optical signals with different wavelengths, which adopts a series[4] or a parallel structure[5]. The fixed optical encoder and decoder using a series structure are shown in Fig. 4.11. The optical encoder consists of an optical circulator with three ports, w FBGs and w fiber-optic delay lines. A short optical pulse coming from a broadband light source is firstly modulated by data in a modulator and then the modulated narrow optical pulse is fed into port 1 of the optical circulator. The optical signals output from port 2 of the circulator are reflected back by FBGs with different wavelengths. Meanwhile, two adjacent FBGs are connected with the delay lines with different lengths in order to implement the desired delays in terms of the requirement of a 2-D WH/TS codeword. The returning optical pulse signals with different wavelengths and different delays for port 2 are output from port 3. Then, 2-D WH/TS incoherent optical encoding is implemented.

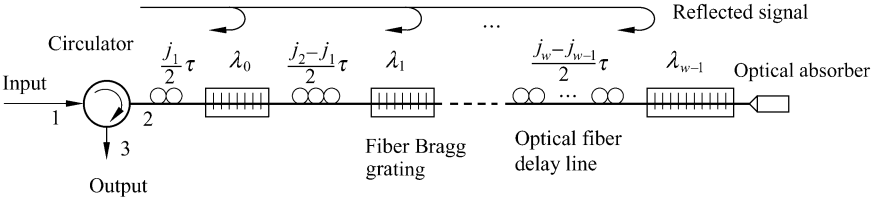

(a) Fixed 2-D WH/TS optical encoder

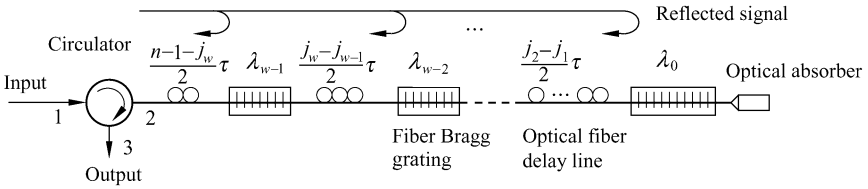

(b) Fixed 2-D WH/TS optical decoder

Figure 4.11 Fixed 2-D WH/TS optical encoder/decoder based on serial FBGs

The structure and operational principle of the optical decoder is similar to its corresponding encoder. The necessary variations are to put these FBGs in reverse-order and to change the delays of fiber-optic delay lines between two adjacent FBGs in order to make their delay values be complementary values of those in its corresponding encoder. The concrete delay parameters have been labeled in Fig. 4.11(b). The structure of 2-D WH/TS tunable optical encoder/ decoder using serial FBGs are the same as that of its fixed encoder/decoder except that the fixed delay lines are changed into tunable delay lines. However, this would result in large

optical power loss. Hence, such a structure is only suitable for the implementation of fixed encoder/decoder. Of course, although the encoder/decoder may be tuned by the piezoelectricity components to strain the fiber Bragg gratings and fiber-optic delay lines to control the reflected wavelengths and delays theoretically, the tuned range is severely limited as a matter of fact.

The fixed 2-D WH/TS optical encoder and decoder using parallel FBGs is shown in Fig. 4.12, which consists of a circulator with three ports, an AWG (arrayed waveguide grating) wavelength-division demultiplexer, w FBGs and w fiber-optic delay lines. After the short optical pulse from a broadband light source is modulated by data, it is fed into port 1 of a circulator. The optical signal output from port 2 is decomposed into w parallel output pulses with wavelengths $\lambda_0, \lambda_1, \cdots, \lambda_{w-1}$ by the AWG. They pass through the fiber-optic delay lines with different lengths and are reflected by FBGs with different wavelengths, and return into the AWG again. The resulting optical pulse trains multiplexed by the AWG enter the optical circulator from its port 2 and then output from port 3 of the circulator. In doing so, 2-D WH/TS incoherent optical encoding is implemented. Since the operational principle of an optical decoder using parallel FBGs is very similar to its corresponding encoder we no longer repeat it. The relationship between the parameters of 2-D WH/TS codes and components in a decoder is shown in Fig. 4.12.

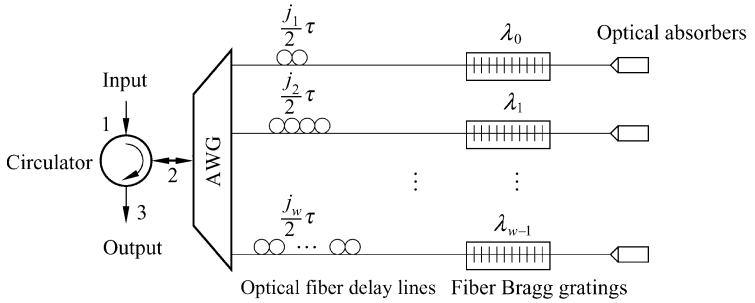

(a) Fixed 2-D WH/TS optical encoder based on parallel FBGs

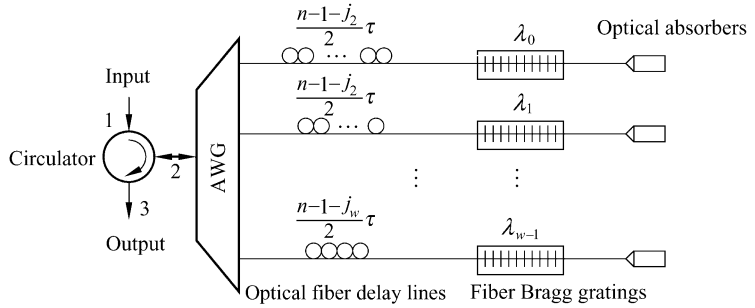

(b) Fixed 2-D WH/TS optical decoder based on parallel FBGs

Figure 4.12 Fixed 2-D WH/TS encoder/decoder based on parallel FBGs

A tunable optical encoder/decoder with this structure is shown in Fig. 4.13, whose difference from the fixed optical encoder/decoder is that the delay lines in the fixed encode/decoder are changed into the tunable delay lines that implement the required delays determined by the codewords under the control of user's signaling in order to realize 2-D WH/TS optical encoding/decoding. The encoder/decoder in such a structure can tune the pulses in the codewords to different slot-displaces, however, it is difficult for the encoder/decoder to implement wavelength-dimension tunable. If the tunable wavelength-dimension needs to be realized we need to add an $m \times w$ optical switch between the tunable delay lines and the AWG and to exchange the $1 \times w$ AWG for an $1 \times m$ AWG. At the same time, the numbers of optical fiber delay lines and FBGs are changed from w to m, where w is a code weight and m is the number of available wavelengths.

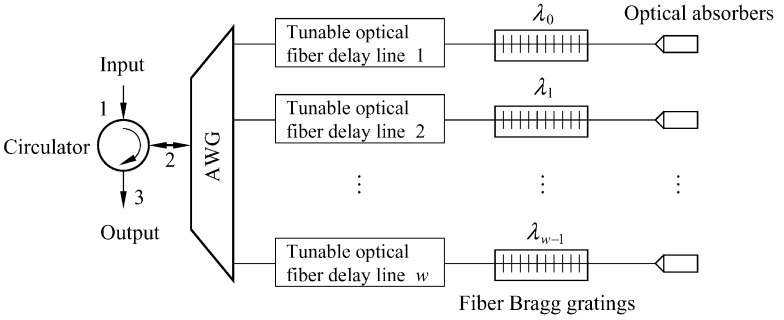

Figure 4.13 Tunable 2-D WH/TS encoder/decoder based on parallel FBGs

A tunable 2-D $m \times n$ WH/TS optical encoder/decoder based on an array of FBGs has been proposed in Reference [6], shown in Fig. 4.14(a). It consists of an optical circulator, an $1 \times \overline{w}$ optical power splitter/combiner and an array of $\overline{w} \times n$ FBGs, which comprises $\overline{w}$ linear arrays of n FBGs, where n indicates the number of slots in each codeword, $\overline{w}$ represents the largest number of wavelengths onto each slot that is less than the code weight w, i.e., $\overline{w} \leqslant w$. The length between the midpoints of two adjacent FBGs is a constant L_{sep} and the chip (slot) length of a codeword is $\tau = \dfrac{2L_{\text{sep}}}{c/n_{\text{eff}}} = \dfrac{2L_{\text{sep}}n_{\text{eff}}}{c}$, where n_{eff} is the effective refractive index of this segment of optical fiber and FBG, c is the speed of light in vacuum, equal to 3×10^{10} cm. If we assume that $L_{\text{sep}} = 1.8$cm and $n_{\text{eff}} = 1.45$, then $\tau = 174$ ps. Again, assume that $n = 9$, an OCDMA system can achieve the data rate of 622.08Mb/s. When $n = 36$, a data rate to be implemented is 155.52Mb/s. (Note that the pulse width from a broadband light source must be less than the chip width τ.) All of FBGs have the same initial wavelength λ_{r}, $\lambda_{\text{r}} \notin [\lambda_{\min}, \lambda_{\max}]$, where $\lambda_{\min}$ and $\lambda_{\max}$ are the minimum and maximum

wavelengths in a 2-D WH/TS code to be implemented. In other words, the initial wavelength of each FBG is outside of the wavelengths that belong to a 2-D WH/TS code to be encoded. In order to tune the wavelengths at random, all FBGs can be tuned as necessary, for example, by applying a segmented piezoelectric stack to strain, or tungsten wire electrified to heat, in order to reflect the required wavelengths defined by a 2-D WH/TS code. When a short broadband optical pulse modulated by data is input from port 1 of the circulator, it is output from port 2 of the circulator and enters $1\times\overline{w}$ optical power splitter and then is split into $\overline{w}$ broadband optical pulses. Each of them is reflected by a linear array of n FBGs, whose central wavelengths are tuned to the wavelengths required by a codeword, and becomes n short pulses with different wavelengths. The n short pulses enter into the $\overline{w}\times 1$ optical combiner again. (In this case, an optical power splitter acts as an optical power combiner.)

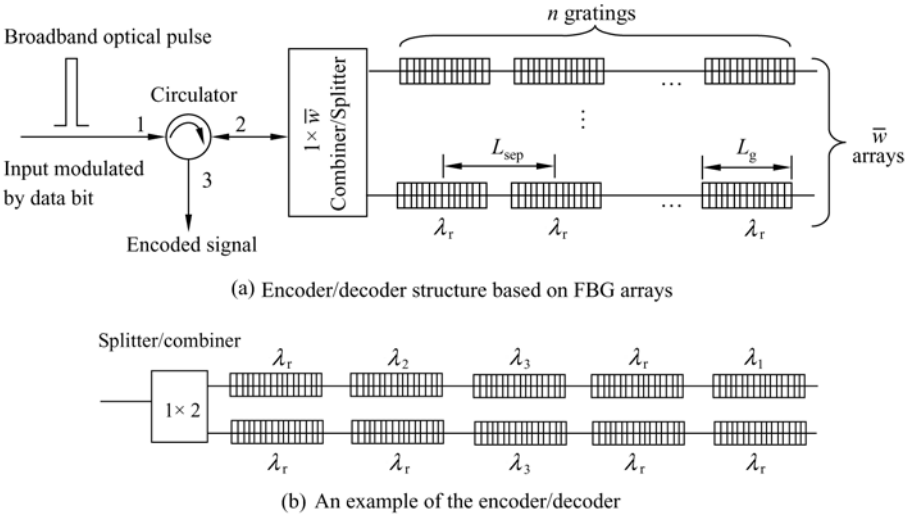

Figure 4.14 Tunable 2-D WH/TS encoder/decoder based on a linear array of n FBGs (After Ref. [6])

The output of the combiner goes into port 2 of the circulator and is output from port 3. The encoding process of a 2-D WH/TS code is achieved. When a 2-D WH/TS code with at most one wavelength onto one slot is encoded only a linear array of n FBGs is required. The reason of employing $\overline{w}$ linear arrays of n FBGs is to implement the codes with multi-wavelengths onto a slot. Note that if the optical pulses emitted by a broadband light source contain the wavelength λ_r the encoder output will include multiple optical pulses with wavelength λ_r bisides the pulses with the required wavelengths of codewords, which will result in interfering of signal. It would be better if an optical filter is added to eliminate

the wavelength λ_r. Fig. 4.14(b) gives an example of such an encoder, whose encoding waveform is illustrated in Fig. 4.15.

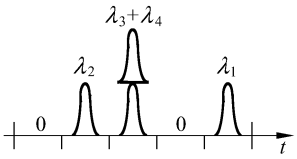

Figure 4.15 Encoding waveform of a 2-D WH/TS codeword

Since the operational principle of a decoder is very similar to that of the encoder, we will not say more than is needed. The advantage of this type of optical encoder/decoder is that it is capable of tuning, which makes it possible to generate many types of 2-D WH/TS codes, including the variable-weight optical codes, the wavelength-reuse codes (i.e., they allow that a couple of pulses onto different chips in a codeword have the same wavelength) and the slot-reuse codes (i.e., they allow that an optical pulse onto a chip in a codeword has multiple different wavelengths.). The shortcoming is that the number of FBGs on each linear array of FBGs is equal to the number of slots. When the number of subscribers in a constructed OCDMA network is large the number of slots of a 2-D WH/TS code becomes big. In this scenario, the required number of FBGs will be large and the volume of an encoder/decoder will be big. Hence, this structure of encoder/decoder is only suitable for tunable encoding of the code with a small number of slots. In addition, it is complicated to be tuned and difficult to control the wavelengths accurately.

4.3.4 GMWRSC Optical Encoder and Decoder with Shared AWG

A GMWRSC (generalized multi-wavelength Reed-Solomon code) optical encoder/decoder[7] based on a shared AWG router makes use of the cyclic properties of AWG router and GMWRSC, which is able to encode/decode multiple codewords of GMWRSC simultaneously and implement multi-users sharing an AWG. Thus, this makes an OCDMA network cheap and compact.

From the construction of the $(p_1 \times (p_1 - 1)p_2 \cdots p_k, p_1 - 1, 0, 1)$ GMWRSC with the cardinality of $p_1 p_2 \cdots p_k$ introduced in Subsection 3.2.2.2, when $k = 1$ and $p_1 = 7$, seven codewords of the $(7 \times 6, 6, 0, 1)$ GMWRSC can be obtained, which are shown in Table 4.3[7]. An ordered pair (ν, h) of a GMWRSC denotes an optical pulse with a wavelength λ_ν at the position of a time chip t_h. In terms of the construction of a GMWRSC, it is known that the codeword $C_{i\oplus 1}$ is a cyclic shift of C_i, where $0 \leqslant i \leqslant 6$ and "$\oplus$" denotes modulo-7 addition. In other

words, the wavelength of optical pulse in each time chip reveals cyclic shift of different codewords.

Table 4.3 RS code for $p_1 = 7$ and $(7 \times 6, 6, 0, 1)$ 2-D GMWRSC[7]

Codewords of Reed-Solomon code	Codewords of $(7 \times 6, 6, 0, 1)$ GMWRSC
$\overline{a_0} = (0,1,4,6,5,2)$	$C_0 = \{(0,0),(1,1),(4,2),(6,3),(5,4),(2,5)\}$
$\overline{a_1} = (1,2,5,0,6,3)$	$C_1 = \{(1,0),(2,1),(5,2),(0,3),(6,4),(3,5)\}$
$\overline{a_2} = (2,3,6,1,0,4)$	$C_2 = \{(2,0),(3,1),(6,2),(1,3),(0,4),(4,5)\}$
$\overline{a_3} = (3,4,0,2,1,5)$	$C_3 = \{(3,0),(4,1),(0,2),(2,3),(1,4),(5,5)\}$
$\overline{a_4} = (4,5,1,2,3,6)$	$C_4 = \{(4,0),(5,1),(1,2),(3,3),(2,4),(6,5)\}$
$\overline{a_5} = (5,6,2,4,3,0)$	$C_5 = \{(5,0),(6,1),(2,2),(4,3),(3,4),(0,5)\}$
$\overline{a_6} = (6,0,3,5,4,1)$	$C_6 = \{(6,0),(0,1),(3,2),(5,3),(4,4),(1,5)\}$

Assuming that a relationship between the in-out ports of a 7×7 cyclic AWG and their corresponding wavelengths is shown in Table 4.4, then the resulting GMWRSC OCDMA encoder and decoder based on the cyclic shift properties of the wavelengths of GMWRSC and AWG are shown in Fig. 4.16(a) and (b) respectively. In the following, we take the encoding process of C_0 as an example to introduce the operational principle of the encoder. First of all, after a broadband light pulse emitted by a broadband light source LED1 is modulated by data, it is incident into port 1 of a circulator. Then, it is output from port 2 of the circulator and enters port 0 of an 7×7 AWG. The optical pulses with wavelengths $\lambda_0 - \lambda_6$ are output from the egresses $0 - 6$ on the left of the AWG respectively. From the codeword C_0, it is known that the optical pulse with wavelength λ_0 should be at the 0^{th} time chip such that it does not need to be delayed. The optical pulse with wavelength λ_1 should be shifted onto the 1^{th} time chip. However, due to the reflected optical pulse traveling through a fiber-optic delay line twice, a fiber-optic delay line with delay $\tau/2$ is connected to the 1^{th} egress of the AWG. In order to shift the optical pulse with wavelength λ_4 onto the 2^{nd} chip, a fiber-optic delay line with delay τ is required in the 4^{th} egress of the AWG. Similarly, The fiber-optic delay lines with delay $3\tau/2$, 2τ and $5\tau/2$ need to be connected to the egress 6, 5 and 2 of the AWG respectively. These optical pulses are reflected back to the incident port traveling through the different delay lines and coupled into the outgoing fiber through the circulator. The encoding of C_0 is achieved. Since C_0 does not contain a pulse of wavelength λ_3, the 3^{rd} port on the left of the AWG does not need any reflector and fiber-optic delay line. The reflector may be implemented by coating the end facet of the fiber delay line with metal. The LED may be

directly or externally modulated relying on transmission speed[7]. The encoded signal is fed into a network.

Table 4.4 Relationship between the in-out ports of a cyclic 7×7 AWG and wavelengths

Input \ Output	0	1	2	3	4	5	6
0	λ_0	λ_1	λ_2	λ_3	λ_4	λ_5	λ_6
1	λ_1	λ_2	λ_3	λ_4	λ_5	λ_6	λ_0
2	λ_2	λ_3	λ_4	λ_5	λ_6	λ_0	λ_1
3	λ_3	λ_4	λ_5	λ_6	λ_0	λ_1	λ_2
4	λ_4	λ_5	λ_6	λ_0	λ_1	λ_2	λ_3
5	λ_5	λ_6	λ_0	λ_1	λ_2	λ_3	λ_4
6	λ_6	λ_0	λ_1	λ_2	λ_3	λ_4	λ_5

Because of the cyclic shift property of GMWRSC, the encoding of other codewords only needs to add the broadband light sources LEDs to their corresponding ingresses of the AWG. We no longer give unnecessary details here.

The GMWSRC decoder is similar to its encoder. However, the delay of every delay line in the decoder must be complementary of that in its corresponding encoder such that all of optical pulses are removed onto the last time chip of a codeword. The concrete parameters have been labeled in Fig. 4.16(b). The schematic diagram of OCDMA network based on GMWRSC is shown in Fig. 4.17.

For the general $(p_1\times(p_1-1)p_2\cdots p_k, p_1-1, 0, 1)$ GMWRSC, the optical encoder/decoder needs to be modified by adding another AWG multiplexer/demultiplexer[7]. The encoder/decoder can still encode p_1 orthogonal codewords simultaneously, and in the OCDMA network, $p_2p_3\cdots p_k$ encoder/decoder will be shared by p_1 subscribers rather than $p_1p_2p_3\cdots p_k$.

In addition, a 2-D WH/TS encoder/decoder with feedback structure using AWG and fiber-optic delay lines has been proposed in References[8] and [9]. Its advantage is that the encoder and decoder can be shared so that a special decoder is not needed. Therefore, the hardware and cost of encoder/decoder can be economized. However, an $m\times m$ AWG can only be employed to a 2-D WH/TS code with $m-1$ available wavelengths. If a light source output contains m wavelengths the unused wavelength needs to be eliminated by a notch filter. For instance, in order to encode/decode the codeword $C_1=\{(0,3),(1,0),(2,1),(3,5),(5,2),(6,4)\}$, because the codeword does not contain the wavelength λ_7, the port corresponding to λ_7 of an 8×8 AWG can be regarded as the input and output ports of the encoder and decoder. (Note that the optical pulse emitted by

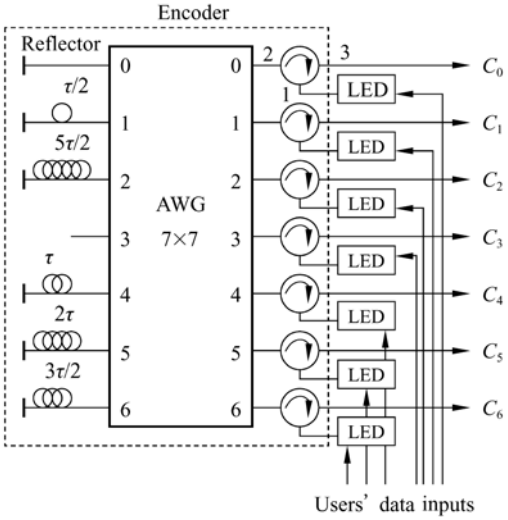

(a) AWG-based optical encoder shared by multiple users

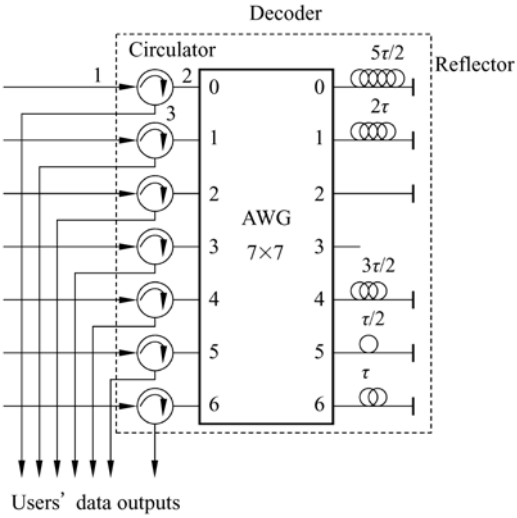

(b) AWG-based optical decoder shared by multiple users

Figure 4.16 AWG-based optical encoder/decoder shared by multiple users of GMWRSC[7]

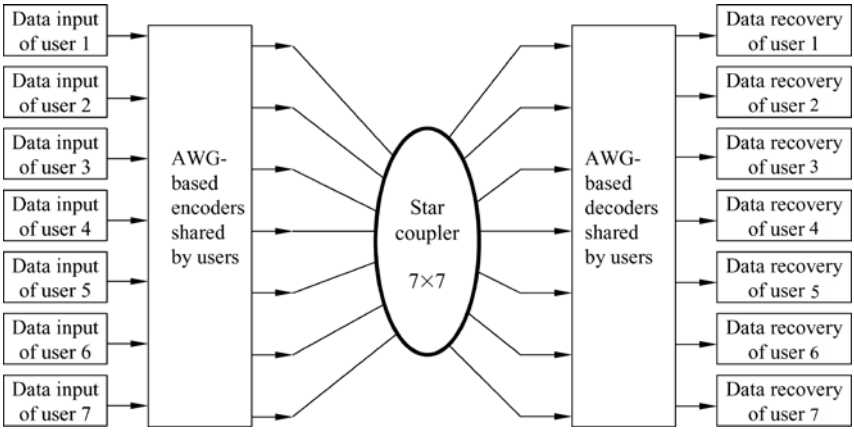

Figure 4.17 Schematic diagram of OCDMA network based on GMWRSC

the light source should not include the wavelength λ_7, otherwise a filter would be required.) The $\{(0,3),(1,0),(2,1),(3,5),(5,2),(6,4)\}$ optical encoder/decoder with such an architecture is shown in Fig. 4.18.

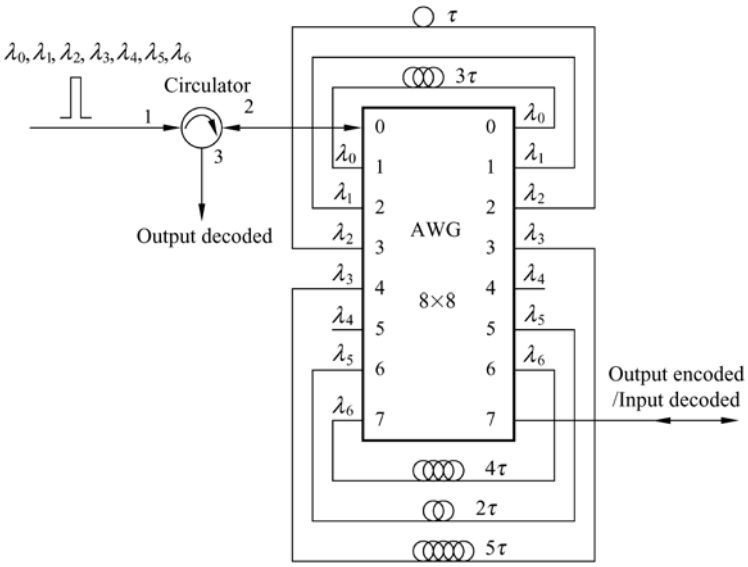

Figure 4.18 2-D WH/TS optical encoder with the feedback structure

For a tunable encoder/decoder, if it only needs to be tuned in time domain the fixed fiber-optic delay lines can be changed into the tunable fiber-optic delay lines. If it still needs to be tuned in wavelength domain it can be implemented by adding an $m \times w$ optical switch on the left of the fiber-optic delay lines and an $w \times m$ optical switch on the right of the fiber-optic delay lines.

4.4 Spectral-Amplitude Incoherent Optical Encoder and Decoder

4.4.1 Spectral-amplitude Incoherent Optical Encoder and Decoder Employing Bulk-optic Components

Spectral-amplitude optical encoder for the incoherent OCDMA is shown in the dashed block of Fig. 4.19[10, 11], which consists of a pair of uniform diffraction gratings, a pair of lenses and a spectral amplitude mask (4*f* system). After an optical pulse from a broadband light source is modulated by data, the first diffraction grating spatially decomposes its spectral components with a certain resolution. The first lens makes these spectral components implement maximal spatial separation and the spectral amplitude mask (corresponding to a user address codeword) filters these spectral components and passes the required spectral components (determined by the chosen user's address codeword). After the mask, the remaining spectral components are reassembled by the second lens and second diffraction grating into a single optical beam to be sent to a network. In doing so, the spectral amplitude incoherent encoding is achieved. The typical

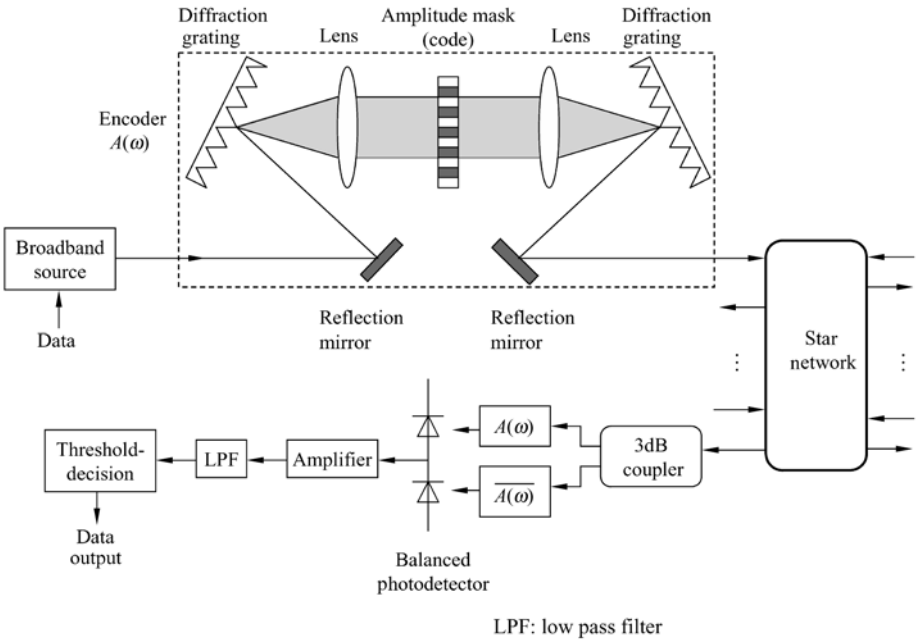

Figure 4.19 Block diagram of spectral-amplitude encoding OCDMA system (After Ref.[10])

incoherent light sources employed by such an encoding approach include Edge-Emitting LED's (EE-LED), Super-luminescent Diodes (SLD), Amplified Spontaneous Emission of Erbium-Doped Fiber Amplifier (EDFA-ASE), etc. In an OCDMA network, each transmitter employs a unique spectral-amplitude-mask, in order to guarantee the orthogonality between any two address codewords corresponding to the spectral-amplitude-masks. The encoded signal is broadcast to all receivers in the network such that all subscribers can share the optical channels.

At the receiving end, the signal is actually decoded by a hybrid optical-electrical decoder, which is composed of a 3dB coupler, two spectral amplitude filters and two differential photodetectors in a differential or balanced configuration. We assume that the spectral function of the spectral amplitude encoder is $A(\omega)$, such that one of the filters in the decoder has the same spectral response, $A(\omega)$, and another filter, i.e. complementary filter, has the complementary response, $\overline{A(\omega)}$. For example, suppose that the encoding employs fifteen wavelengths between λ_1 and λ_{15}, if $A(\omega)$ corresponds to wavelengths $\lambda_1, \lambda_2, \lambda_3, \lambda_4, \lambda_6, \lambda_8, \lambda_9, \lambda_{12}$, and then $\overline{A(\omega)}$ corresponds to wavelengths $\lambda_5, \lambda_7, \lambda_{10}, \lambda_{11}, \lambda_{13}, \lambda_{14}, \lambda_{15}$. In this way, two optical decoding apparatuses are required. Another way[11], which uses only one encoding apparatus, is to replace the spherical lenses by cylindrical lenses and to employ a two-dimensional mask, where one dimension is still utilized for the wavelength while the other is deployed to place the two complementary amplitude patterns. In a practical OCDMA network, if the receiver is fixed, the transmitter must be tunable. This issue can be resolved by employing a tunable spectral amplitude mask, such as spatial-light-modulators (SLM) based on liquid-crystal-display (LCD) technology[11]. The intention of using differential detection is to cancel the multi-user interference from the network in conjunction with the code designed. The permutation of the elements of a spectral amplitude mask, which represents a user address code, employs the bipolar codes with good correlation, such as m-sequences, Walsh-Hadamard codes, etc.

Let $X = (x_0, x_1, \cdots, x_{n-1})$ and $Y = (y_0, y_1, \cdots, y_{n-1})$ be two binary {0,1} sequences such that their periodic cross-correlation is

$$R_{XY}(\tau) = \sum_{i=0}^{n-1} x_i y_{i \oplus \tau} \tag{4.1}$$

Define the complement of sequence X to be $\overline{X} = (\overline{x_0}, \overline{x_1}, \cdots, \overline{x_{n-1}})$ [11], where $\overline{x_i} = 1 - \overline{x_i}$. The periodic cross-correlation sequence between $\overline{X}$ and Y is

$$R_{\overline{X}Y}(\tau) = \sum_{i=0}^{n-1} \overline{x_i} y_{i \oplus \tau} \tag{4.2}$$

where "$\oplus$" represents modulo-n addition.

Since $R_{XY}(\tau) = R_{\overline{X}Y}(\tau)$, a receiver will reject the interference from a user with the address code Y through computing $R_{XY}(\tau) - R_{\overline{X}Y}(\tau)$.

Firstly, a unipolar m-sequence $X = (x_0, x_1, \cdots, x_{n-1})$ with the period n is obtained from the bipolar version by replacing each binary 1 by a 1 and each –1 by a 0. Since the sequence Y is a sequence of cyclical left-sifts of X, i.e., $Y = T^{\tau}X = (X)^{\tau}$, where T is the operator that shifts vectors cyclically to the left by one place and τ represents the number of times of cyclic shifts, namely, $TX = (x_{n-1}, x_0, x_1, \cdots, x_{n-2})$, its discrete autocorrelation function is[11]

$$R_{XY}(\tau) = \sum_{i=0}^{n-1} x_i x_{i\oplus\tau} = \begin{cases} (n+1)/2 & \tau = 0 \\ (n+1)/4 & 1 \leqslant \tau \leqslant n-1 \end{cases} \tag{4.3}$$

where "$\oplus$" indicates modulo-n addition. These results come from the shift-and-add property of an m-sequence, that is, the modulo-2 addition of an m-sequence and any cyclic shift of the same m-sequence is another cyclic shift of the same sequence. In other words, half the 1's in $(X)^{\tau}$ coincide with the 1's of X while the other half the 1's in $(X)^{\tau}$ coincide with the 0's of X. A receiver will reject the signal coming from the interfering subscriber with the address code $(X)^{\tau}$ through computing[10]

$$\begin{aligned} Z &= R_{XY}(\tau) - R_{\overline{X}Y}(\tau) = \sum_{i=0}^{n-1} x_i x_{i\oplus\tau} - \sum_{i=0}^{n-1} (1 - x_i) x_{i\oplus\tau} \\ &= 2R_{XY}(\tau) - R_{XY}(0) = 2 \times \frac{n+1}{4} - \frac{n+1}{2} = 0 \end{aligned}$$

Based on this idea, n cyclic-shift sequences of an m-sequence can be assigned to n subscribers as their address sequences such that such a network can support n simultaneous users without any interference, that is, all subscriber address codewords can implement completely mutual orthogonality in theory.

Example 4.4 The resulting spectral amplitude code based on an m-sequence of length $n = 15$, $X = (1,0,0,0,1,0,0,1,1,0,1,0,1,1,1)$, and its cyclic-shift versions, are shown in Table 4.5. Every "1" in the table corresponds to a wavelength, whose number represents the number of the position of the "1" in the m-sequence while every "0" does not correspond to any wavelength.

The number of frequency bins that can be differentiated by the encoder will determine the code length and the number of subscribers in a system. The largest number of users is approximately given by[10]

$$M \approx 0.5 \frac{\Delta\lambda}{\lambda} \frac{\pi r}{d \cdot \cos(\theta)} \tag{4.4}$$

where λ is the central wavelength of the light source, $\Delta\lambda$ represents the spectral width encoded, r indicates the input beam radius, d is the grating period and θ

Table 4.5 All resulting spectral amplitude codewords from the m-sequence $X = (1,0,0,0,1,0,0,1,1,0,1,0,1,1,1)$ and its cyclic-shift sequences

Number	m-sequence and its cyclic-shift sequences	Spectral amplitude codewords
1	1 0 0 0 1 0 0 1 1 0 1 0 1 1 1	$\lambda_1,\lambda_5,\lambda_8,\lambda_9,\lambda_{11},\lambda_{13},\lambda_{14},\lambda_{15}$
2	1 1 0 0 0 1 0 0 1 1 0 1 0 1 1	$\lambda_1,\lambda_2,\lambda_6,\lambda_9,\lambda_{10},\lambda_{12},\lambda_{14},\lambda_{15}$
3	1 1 1 0 0 0 1 0 0 1 1 0 1 0 1	$\lambda_1,\lambda_2,\lambda_3,\lambda_7,\lambda_{10},\lambda_{11},\lambda_{13},\lambda_{15}$
4	1 1 1 1 0 0 0 1 0 0 1 1 0 1 0	$\lambda_1,\lambda_2,\lambda_3,\lambda_4,\lambda_8,\lambda_{11},\lambda_{12},\lambda_{14}$
5	0 1 1 1 1 0 0 0 1 0 0 1 1 0 1	$\lambda_2,\lambda_3,\lambda_4,\lambda_5,\lambda_9,\lambda_{12},\lambda_{13},\lambda_{15}$
6	1 0 1 1 1 1 0 0 0 1 0 0 1 1 0	$\lambda_1,\lambda_3,\lambda_4,\lambda_5,\lambda_6,\lambda_{10},\lambda_{13},\lambda_{14}$
7	0 1 0 1 1 1 1 0 0 0 1 0 0 1 1	$\lambda_2,\lambda_4,\lambda_5,\lambda_6,\lambda_7,\lambda_{11},\lambda_{14},\lambda_{15}$
8	1 0 1 0 1 1 1 1 0 0 0 1 0 0 1	$\lambda_1,\lambda_3,\lambda_5,\lambda_6,\lambda_7,\lambda_8,\lambda_{12},\lambda_{15}$
9	1 1 0 1 0 1 1 1 1 0 0 0 1 0 0	$\lambda_1,\lambda_2,\lambda_4,\lambda_6,\lambda_7,\lambda_8,\lambda_9,\lambda_{13}$
10	0 1 1 0 1 0 1 1 1 1 0 0 0 1 0	$\lambda_2,\lambda_3,\lambda_5,\lambda_7,\lambda_8,\lambda_9,\lambda_{10},\lambda_{14}$
11	0 0 1 1 0 1 0 1 1 1 1 0 0 0 1	$\lambda_3,\lambda_4,\lambda_6,\lambda_8,\lambda_9,\lambda_{10},\lambda_{11},\lambda_{15}$
12	1 0 0 1 1 0 1 0 1 1 1 1 0 0 0	$\lambda_1,\lambda_4,\lambda_5,\lambda_7,\lambda_9,\lambda_{10},\lambda_{11},\lambda_{12}$
13	0 1 0 0 1 1 0 1 0 1 1 1 1 0 0	$\lambda_2,\lambda_5,\lambda_6,\lambda_8,\lambda_{10},\lambda_{11},\lambda_{12},\lambda_{13}$
14	0 0 1 0 0 1 1 0 1 0 1 1 1 1 0	$\lambda_3,\lambda_6,\lambda_7,\lambda_9,\lambda_{11},\lambda_{12},\lambda_{13},\lambda_{14}$
15	0 0 0 1 0 0 1 1 0 1 0 1 1 1 1	$\lambda_4,\lambda_7,\lambda_8,\lambda_{10},\lambda_{12},\lambda_{13},\lambda_{14},\lambda_{15}$

is the diffraction angle of the central wavelength. Assuming that $\Delta\lambda = 50$ nm, $\lambda = 1550$ nm, $r = 2$mm, $1/d = 1200$ lines/mm grating and $\theta = 68^\circ$ (for Littrow configuration), the number of subscribers is probably $M \approx 325$ [10]. (Note that this is the number of subscribers rather than the number of simultaneous users that can be achieved in the system. The number of simultaneous subscribers still relies on the bit error rate allowed by the system.)

The advantages of spectral amplitude incoherent OCDMA encoding are as follows. The light source with the low price, stable performance and simple drive circuit, such as LED, and the direct detection can be employed. The implementation cost is low and the wavelength control is not required. Furthermore, a frequency-spreading gain is totally independent of the modulation bandwidth (corresponding to the bit rate). The disadvantages are that the code length of address code and the number of users that can be supported in the system are constrained by the resolution of the diffraction grating and mask. In addition, the encoder and decoder using the bulk-optic components have a big volume and it is difficult to be mounted and packaged. At the same time, they have the poor operation stability.

4.4.2 Spectral Amplitude Incoherent Optical Encoder/Decoder Using FBGs

With the development and maturation of FBGs, they can be employed as the

choosing wavelength filters to implement the spectral amplitude encoding (SAE) such that the disadvantages of the bulk-optic spectral amplitude encoder/decoder can be overcome. The SAE OCDMA employing the FBGs in series or the linear array of FBGs, and the superposition FBGs, is extensively investigated and demonstrated[12].

The spectral amplitude encoding OCDMA based on FBGs is shown in Fig. 4.20(a)[12], whose principle is the same as that of Fig. 4.19. The only difference is that the spectral components are chosen by employing the FBGs here rather than by using the diffraction gratings and the spectral amplitude masks in the above subsection. The purpose of using a $1:\alpha$ coupler in Fig. 4.20(a) is to make MUI (multiple user interference) received by PD_1 be equal to MUI received by PD_2, so that they counteract with each other. The spectral function of FBGs is illustrated in Fig. 4.20(b), where $A(\omega)$ represents the reflection spectrum of FBGs and $\overline{A(\omega)}$ is the transmission spectrum of FBGs. The spectral amplitude encoder based on the array of FBGs is shown in Fig. 4.21(a). A broadband optical pulse inputs from port 1 of the circulator and outputs from port 2, and then enters the first array of FBGs. The spectral components corresponding to $A(\omega)$ are reflected back and output from port 3, and then enter the second optical circulator. After reflected by the second array of FBGs, they output from port 6 of the second optical circulator at last. In doing so, the spectral amplitude encoding based on FBGs is achieved. The order of wavelengths reflected by the second array of FBGs is just opposite to that of wavelengths reflected by the first array of FBGs in order to compensate the delay

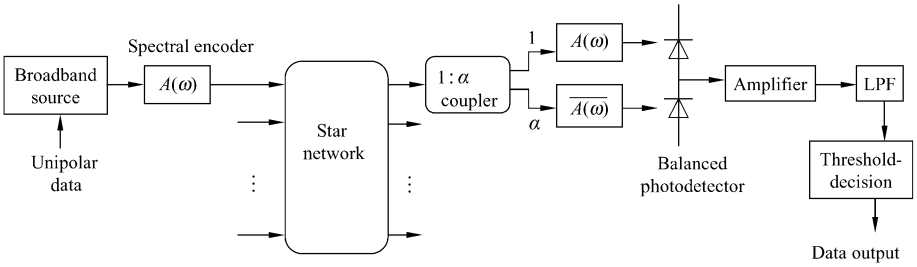

(a) OCDMA system of spectral amplitude encoding

LPF: low pass filter

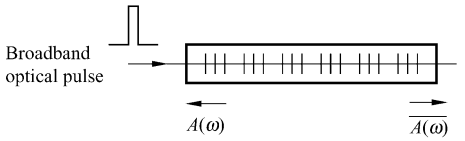

(b) Schematic diagram of the spectral distribution function of FBGs

Figure 4.20 Block diagram of OCDMA system of spectral amplitude encoding with FBGs[12]

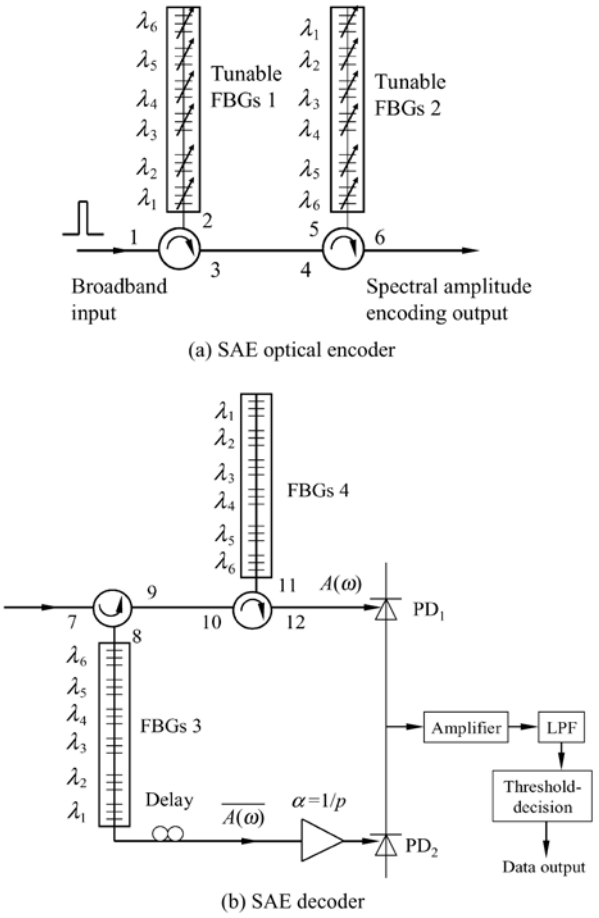

Figure 4.21 Encoder and decoder using a linear array of FBGs for SAE OCDMA (After Ref.[12])

differences caused by the different times of different wavelengths reflected by the first array of FBGs. In this way, the encoded optical pulses of all wavelengths reflected can be guaranteed to reassemble into a bigger optical pulse onto the same slot. In order that any users can communicate with any other subscribers at any time, the FBGs in the encoder should be tunable, that is, the center wavelength of reflected spectrum of each FBG should be able to be tuned. Such a tunable FBG can be implemented by employing a piezoelectricity device to strain the FBG or by using a heater to adjust the temperature of the FBG.

The spectral amplitude decoder is shown in Fig. 4.21(b). Since the optical encoder is tunable the decoder can be fixed. The MUI can be counteracted by employing the transmission spectrum of the first FBG and the balanced detection. In this spectral amplitude encoding OCDMA system based on the en/decoder of the arrays of FBGs, the data rate is no longer limited by the length of the array of

FBGs because the delay of each spectral component is the same after the delay is compensated. Therefore, the bit rate is mainly confined by the maximal modulation rate of the broadband light source and the bandwidth of photodetector applied to the balanced detection.

4.4.3 Incoherent Bipolar Optical Encoder and Decoder Employing Complementary Spectral Encoding

The bipolar complementary spectral optical encoder is shown in Fig. 4.22(a)[13], which consists of two broadband light sources in series, two $1\times n$ wavelength-division demultiplexers, n 2×2 optical switches and a $n\times 1$ wavelength-division multiplexer. The broadband light source can employ the super-luminescent light-emitting diode (SLED) or spontaneous emission output from erbium-doped fibers pumped into super-luminescent mode. Also, the multi-wavelength light source can be employed to replace the broadband light source. Meanwhile, two wavelength-division multiplexers in the optical encoder can be saved when the multi-wavelength light source is utilized. However, the cost of the multi-wavelength light source is higher than that of the broadband light source, such as LED. When the output of data source is "+1", LED1 does not output any optical signal. Thus, there is no optical signal output from DEMUX1. However, LED2 sends out an optical signal and then DEMUX2 outputs n optical pulses with wavelengths $\lambda_1,\lambda_2,\cdots,\lambda_n$. Under the control of the user's balanced address codeword $\{b_1,b_2,\cdots,b_n\}$, n 2×2 optical switches choose the optical pulses with the required wavelengths from them. Finally, the chosen optical pulses are multiplexed and output by a $n\times 1$ wavelength-division multiplexer. Similarly, when the output of data source is "–1", LED2 does not output any optical signal. LED1 sends an optical signal and then DEMUX1 outputs n optical pulses with wavelengths $\lambda_1,\lambda_2,\cdots,\lambda_n$. Under the control of the same user's balanced address codeword $\{b_1,b_2,\cdots,b_n\}$, n 2×2 optical switches choose the optical pulses with the complement wavelengths corresponding to the data bit "+1". At last, the chosen optical pulses are multiplexed and output by a $n\times 1$ wavelength-division multiplexer. In this way, the bipolar complementary spectral optical encoding is achieved and the encoded signal is transmitted into a star network.

The bipolar complementary spectral optical decoder is shown in Fig. 4.22(b), which is composed of a $1\times n$ wavelength-division demultiplexer, n 2×2 optical switches, two $n\times 1$ wavelength-division multiplexers and two photodetectors in series. When the spectral components corresponding to data bit "1" are received, only the MUX3 has output. The output data bit is "+1" after the optical-to-electrical (O/E) conversion of PD_2, the filtering of LPF and the threshold decision. When the spectrum corresponding to data "–1" is received, only MUX2 has output. After O/E conversion of PD_1, "1" is finally output. When the received

signal contains the multiple access interference (MAI) from other subscribers PD1 and PD2 have outputs simultaneously. However, the differential signals output by them in series can counteract MAI. Note that the balanced address codes are required in such a configuration, namely, the numbers of "0" and "1" in every address codeword must be equal, such as in Walsh-Hadamard codes (excluding the codeword consisting of all "1"), modified m-sequence and its cyclic-shift versions and so on, which we have introduced in Section 3.9.

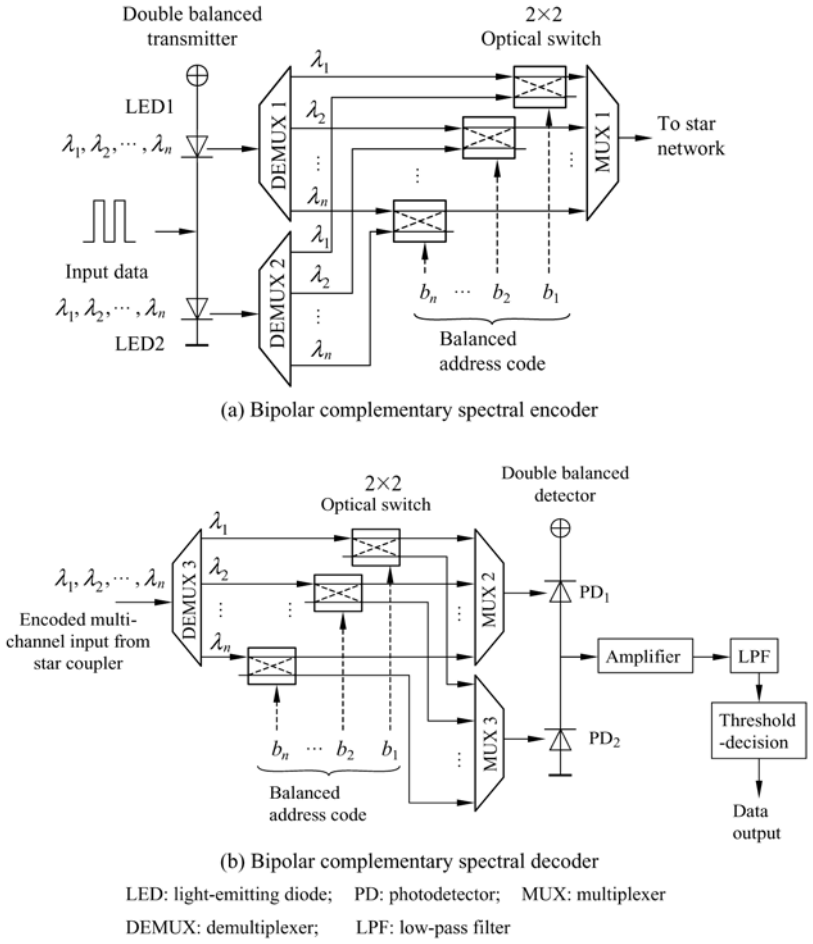

Figure 4.22 Bipolar complementary spectral encoder and decoder (After Ref.[13])

The OCDMA system employing the incoherent bipolar complementary spectrally optical encoder and decoder is shown in Fig. 4.23. Since this type of system employs the bipolar encoding, i.e., each transmitter sends energy for both "0" and "1" bit, an eavesdropper can not demodulate the information by simple amplitude detection. Consequently, the security of transmitted information is

enhanced. Meanwhile, this system does not need the ultrashort coherent optical pulse source, and the system performance is less vulnerable to dispersion issues since the encoder and decoder are only required to possess the function of filtering. In addition, the bipolar signaling has a 3-dB signal-to-noise ratio (SNR) advantage over the on-off keying system. However, because of high cost of multi-wavelength optical source at present, if the LED is employed as the light source of this system, the high data rate can not be achieved. Hence, this system is suitable for the local area network and access network with medium data rate.

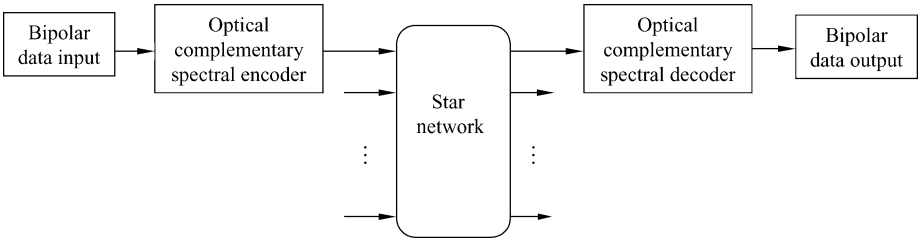

Figure 4.23 Schematic diagram of bipolar spectrally encoding OCDMA network

4.4.4 Spectral Amplitude Optical Encoder and Decoder Using AWG and m-sequence

This type of spectral amplitude encoder/decoder makes use of the cyclic-shift properties of m-sequence and arrayed waveguide grating (AWG), and can encode/decode multiple codewords simultaneously. Therefore, multiple subscribers can share the same hardware, which saves the fiber-optic delay lines and reduces the complexity of the system and the volume of its equipment, and abases the cost. At the same time, it keeps the capability of suppressing MAI. This system works based on on-off keying pattern and encodes the modulated optical signal by employing the inexpensive incoherent light source and controlling the spectrum of the incoherent light source through AWG. Its disadvantages are that there are fewer users in this type of network because the number of subscribers must be equal to the number of wavelengths and the data rate achieved is not high enough due to employing LED as the light source. In addition, since the encoded optical pulses for each user's data reach a receiving end from different fiber-optic lines the lengths of optical fibers between any pair of transmitter-receiver must be exactly equal, which is very difficult to be implemented in practical.

A spectral amplitude encoding OCDMA using m-sequence and AWG router is shown in Fig. 4.24[14], which can implement M subscribers to communicate. Its optical encoder only needs an $M \times M$ AWG. A pair of $M \times M$ AWGs and a pair of balanced differential photodetectors are required in its optical decoder.

The optical encoder is shown in the left of Fig. 4.24. After the optical signal emitted from a broadband light source is modulated by data, it enters the different inputs of the AWG. It is demultiplexed into different wavelength components at the AWG outputs. Since the signals with the same wavelength enter the different inputs of the AWG, they output from different outputs in the cyclic manner. The encoding the different user data can be implemented.

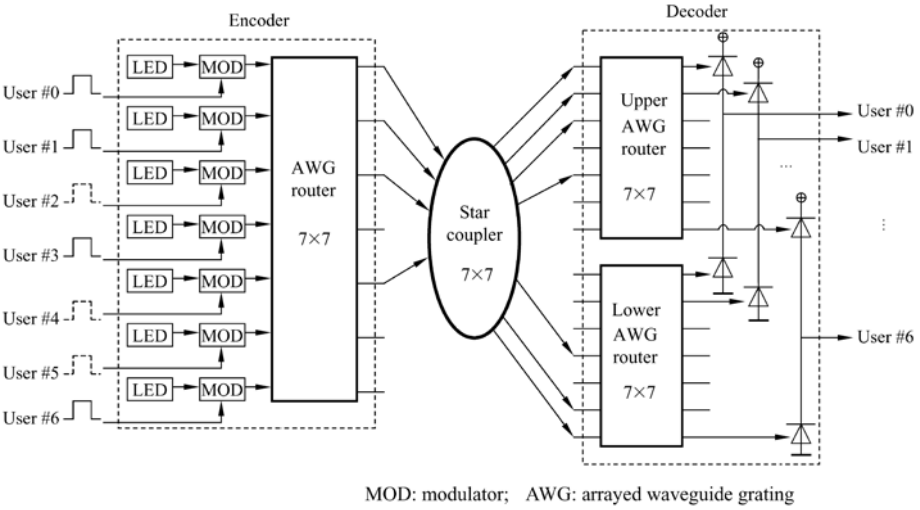

Figure 4.24 Schematic diagram of SAE OCDMA system using AWG router and m-sequence (After Ref.[14])

Let $X=(x_0,x_1,\cdots,x_{n-1})$ be an unipolar m-sequence, i.e., the sequence obtained by the "+1" in the original m-sequence changed into 1 and the "–1" into 0, where n represents the length of the m-sequence. $X_k=T^kX=(x_{k,0},x_{k,1},\cdots,x_{k,n-1})$ indicates the k^{th} cyclic-shift of X, where $k=1,2,\cdots,n-1$ and T is an operator of cyclic shift. In doing so, an m-sequence and $n-1$ cyclic-shift versions of the m-sequence comprise together n sequences, which can be assigned to n subscribers as their address signatures. The left side of Table 4.6 shows an m-sequence 1110100 and its cyclic-shift sequences with length $n=7$, and the circumstance of allocating them to 7 subscribers as their address signatures. The right side of the table gives all corresponding spectral amplitude codewords after encoded by AWG. The position of "1" in the m-sequence corresponds to the number of wavelength. Note that $x_{k,i}=1$ represents the i^{th} input port of the AWG connecting to the star network while $x_{k,i}=0$ indicates that it does not connect to the star network, where $i=0,1,\cdots,n-1$. In addition, the subscript of λ expresses the number of wavelength and the superscript indicates the number of input port of AWG where the pulse with the wavelength comes from. Because of using

on-off keying, only if a data bit sent by a user is "1", the encoded signal is transmitted to the network. Otherwise, when the data bit is "0", nothing is sent to the network. Therefore, the encoded outputs in the 3rd, 5th and 6th row are all "0" due to the data bits being 0's transmitted by the users. There are three pulses with wavelength λ_1, three pulses with wavelength λ_2, two pulses with wavelength λ_3, three pulses with wavelength λ_4, two pulses with wavelength λ_5, two pulses with wavelength λ_6 and one pulse of λ_7 among all pulses sent to the network. For the sake of simple writing, we only show the numbers of pulses in the columns corresponding to wavelengths rather than the wavelengths in Table 4.7. In addition, the digital superscript representing the number of pulses in the table indicates the number of input port where the pulse comes from.

Table 4.6 m-sequence and codewords of length 7 for optical spectral amplitude encoding

User number	Signature sequence	Data bit	Transmitted signals in output ports						
			#0	#1	#2	#3	#4	#5	#6
#0	1 1 1 0 1 0 0	1	$\lambda_1^{(0)}$	$\lambda_2^{(0)}$	$\lambda_3^{(0)}$	0	$\lambda_5^{(0)}$	0	0
#1	0 1 1 1 0 1 0	1	$\lambda_2^{(1)}$	$\lambda_3^{(1)}$	$\lambda_4^{(1)}$	0	$\lambda_6^{(1)}$	0	0
#2	0 0 1 1 1 0 1	0	0	0	0	0	0	0	0
#3	1 0 0 1 1 1 0	1	$\lambda_4^{(3)}$	$\lambda_5^{(3)}$	$\lambda_6^{(3)}$	0	$\lambda_1^{(3)}$	0	0
#4	0 1 0 0 1 1 1	0	0	0	0	0	0	0	0
#5	1 0 1 0 0 1 1	0	0	0	0	0	0	0	0
#6	1 1 0 1 0 0 1	1	$\lambda_7^{(6)}$	$\lambda_1^{(6)}$	$\lambda_2^{(6)}$	0	$\lambda_4^{(6)}$	0	0

Note: The superscript denotes the input port number of AWG router and the subscript represents the wavelength number.

Because of using the star network architecture, all signals in the network can reach any input of entire receiving AWGs connecting to the network, shown in Table 4.7. The spectral decoder is shown in the right side of Fig. 4.24, which comprises two $M \times M$ AWG routers and a pair of balanced differential photodetectors. The connections from the star coupler to the upper AWG are the same as the connections from the encoder router to the star coupler, otherwise the connections from the star coupler to the lower AWG are opposite to the connections from the encoder router to the star coupler (i.e., complementary connections) such that the MAI from other users can be eliminated by the balanced detection. Table 4.7(a) and (b) show the details of the receiving signals at their input ports and the transmitting signals at their output ports of two AWGs, where the figures represent the number of optical pulse corresponding to the wavelength and the superscripts indicate the numbers of the AWG input ports where these pulses come from. The output signal intensity of each balanced photodetector is equal to the difference of the numbers of output optical pulses

from the same number of two AWGs in the decoder. For instance, the 0^{th} user output is the difference of the numbers of output optical pulses from the 0^{th} output port of the upper AWG and the lower AWG, which is $10-6=4$. The data bit 1 is output after the differential signal is amplified by an electric amplifier, filtered by a low pass filter (LPF) and decided by a threshold device. Again, for the second user, two numbers of output optical pulses perform the subtraction operation to obtain $8-8=0$ and at last, the data bit is decided as 0. In this way, the optical decoding is achieved and at the same time, the MAI coming from the network is eliminated. The aforementioned is the ideal case, in which the optical power spectrum output by any broadband light source is very flat. Otherwise, the MAI may not be eliminated completely, and therefore, the optical power spectral equilibrium of each broadband light source output may be required in practical. In addition, since the spectral width of a broadband light source is limited each spectral bin has to be decomposed thinner, in order to make a network support more subscribers. This will make the implementation of such an optical encoding/decoding approach difficult.

Table 4.7 Wavelength distribution in AWG router based decoder

(a) For upper AWG router

#i/p port \ λ	λ_1	λ_2	λ_3	λ_4	λ_5	λ_6	λ_7	#o/p port \ λ	λ_1	λ_2	λ_3	λ_4	λ_5	λ_6	λ_7	Power
#0	3	3	2	3	2	2	1	#0	$3^{(0)}$	$3^{(1)}$	$2^{(2)}$	0	$2^{(4)}$	0	0	10
#1	3	3	2	3	2	2	1	#1	0	$3^{(0)}$	$2^{(1)}$	$3^{(2)}$	0	$2^{(4)}$	0	10
#2	3	3	2	3	2	2	1	#2	0	0	$2^{(0)}$	$3^{(1)}$	$2^{(2)}$	0	$1^{(4)}$	8
#3	0	0	0	0	0	0	0	#3	$3^{(4)}$	0	0	$3^{(0)}$	$2^{(1)}$	$2^{(2)}$	0	10
#4	3	3	2	3	2	2	1	#4	0	$3^{(4)}$	0	0	$2^{(0)}$	$2^{(1)}$	$1^{(2)}$	8
#5	0	0	0	0	0	0	0	#5	$3^{(2)}$	0	$2^{(4)}$	0	0	$2^{(0)}$	$1^{(0)}$	8
#6	0	0	0	0	0	0	0	#6	$3^{(1)}$	$3^{(2)}$	0	$3^{(4)}$	0	0	$1^{(0)}$	10

(b) For lower AWG router

#i/p port \ λ	λ_1	λ_2	λ_3	λ_4	λ_5	λ_6	λ_7	#o/p port \ λ	λ_1	λ_2	λ_3	λ_4	λ_5	λ_6	λ_7	Power
#0	0	0	0	0	0	0	0	#0	0	0	0	$3^{(3)}$	0	$2^{(5)}$	$1^{(6)}$	6
#1	0	0	0	0	0	0	0	#1	$3^{(6)}$	0	0	0	$2^{(3)}$	0	$1^{(5)}$	6
#2	0	0	0	0	0	0	0	#2	$3^{(5)}$	$3^{(6)}$	0	0	0	$2^{(3)}$	0	8
#3	3	3	2	3	2	2	1	#3	0	$3^{(5)}$	$2^{(6)}$	0	0	0	$1^{(3)}$	6
#4	0	0	0	0	0	0	0	#4	$3^{(3)}$	0	$2^{(5)}$	$3^{(6)}$	0	0	0	8
#5	3	3	2	3	2	2	1	#5	0	$3^{(3)}$	0	$3^{(5)}$	$2^{(6)}$	0	0	8
#6	3	3	2	3	2	2	1	#6	0	0	$2^{(3)}$	0	$2^{(5)}$	$2^{(6)}$	0	6

4.5 2-D Incoherent B/U Wavelength/Time Optical Encoder/Decoder

The bipolar/unipolar (B/U) code can be obtained by employing the unipolar version of bipolar codes as wavelength-hopping and the optical uinpolar codes as time-spreading, whose codewords are $m \times n$ wavelength-time matrices, where m is the number of rows, related to the number of available wavelengths, n is the number of columns, related to the number of time slots (i.e., chips). Being different from the conventional wavelength-hopping/time-spreading codes, there are either multiple pulses with different wavelengths determined by the bipolar codes or nothing in every slot of the B/U code matrices. Although the B/U codes employ the bipolar codes as wavelength-hopping the "+1" elements correspond to the optical pulses and the positions of "+1" elements correspond to the numbers of wavelengths. The "–1" elements are emulated by employing the balanced differential photodetectors, which does not need to transmit the complement of the unipolar versions of the bipolar codes. The constructions of the B/U codes have been introduced in Section 3.8. For example, a codeword of a B/U code that is constructed by using Walsh-Hadamard code of length 8 for wavelength-hopping and a (7,3,1,1) OOC for time-spreading is $(C_0 C_1 0 C_2 000)$, where $C_0 = (\lambda_0 \lambda_2 \lambda_4 \lambda_6)$, $C_1 = (\lambda_0 \lambda_1 \lambda_4 \lambda_5)$, $C_2 = (\lambda_0 \lambda_3 \lambda_4 \lambda_7)$. C_i is called a multi-wavelength codeword. Therefore, the multi-wavelength codewords must be generated firstly in order to perform the B/U code encoding and then the required multi-wavelength codewords are arranged into the nonzero slots of the chosen optical unipolar codeword. The schematic diagram of a B/U codeword is shown in Fig. 4.25.

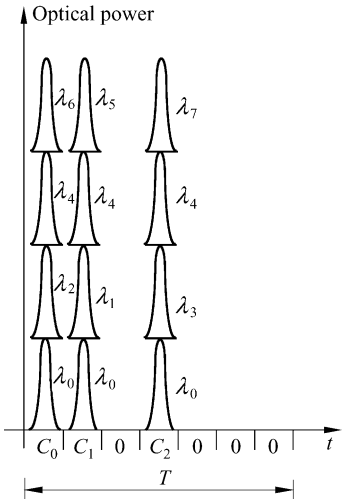

Figure 4.25 Schematic diagram of a bipolar/unipolar codeword based on the multiwavelength codewords of Walsh-Hadamard for length 8 and the codeword 1101000 of the (7,3,1) OOC

The resulting tunable optical encoder for the B/U code based on the B/U code construction is shown in Fig. 4.26[15], which consists of an $1\times w$ optical power splitter, w tunable multi-wavelength codeword generators, w tunable fiber-optic delay lines and an $w\times 1$ optical power combiner. A short optical pulse from a broadband light source is modulated by a user data. When a data bit is "1", the broadband light pulse is sent to $1\times w$ optical power splitter and it is split into w pulses, which enter w multi-wavelength codeword generators. The generated w multi-wavelength codewords are placed into the positions of "1" chips of the chosen time-spreading optical unipolar codeword orderly according to their numbers after they are delayed by w tunable fiber-optic delay lines. Finally, they are reassembled and output by the $w\times 1$ optical combiner. In this way, the optical encoding for the B/U code is achieved. Note that for the data bit "0", the encoder outputs nothing because of none output from the modulator.

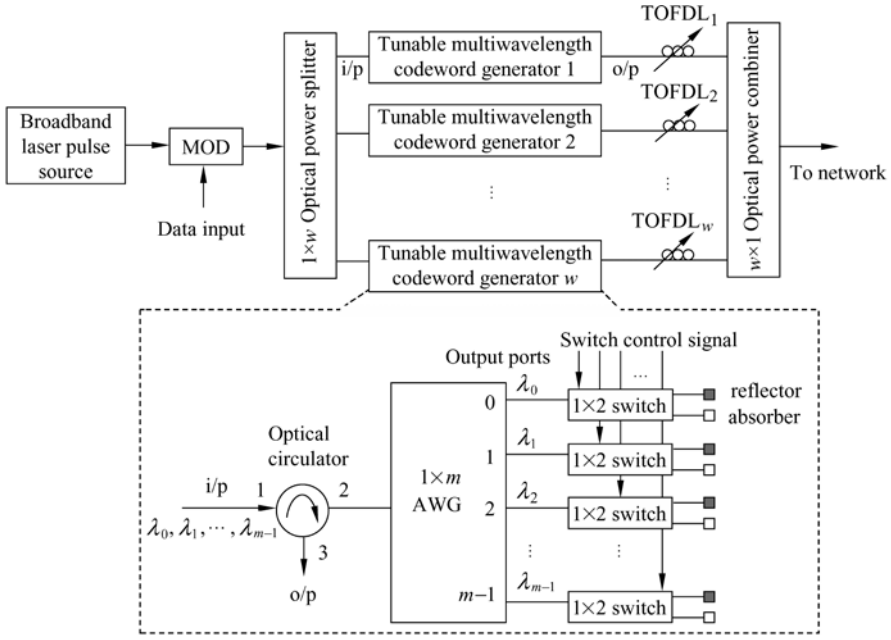

Figure 4.26 Block diagram of tunable optical-encoder for the bipolar/unipolar code[15, 19], where w is the code weight of the optical unipolar code employed in the time-spreading, m is the number of available wavelengths; TOFDL: tunable optical fiber delay lines; i/p: input port; o/p: output port

The tunable multi-wavelength codeword generator comprises an optical circulator, an $1\times m$ AWG, m 1×2 optical switches, m reflectors and m absorbers. An ultrashort broadband optical pulse from the $1\times w$ optical splitter enters port 1 of the circulator and outputs from port 2. Then, it is decomposed into m optical pulses with different wavelengths by the $1\times m$ AWG. When the

required multi-wavelength codeword contains the wavelength λ_j ($j \in [0, m-1]$), the 1×2 optical switch connects the reflector under the controlling of a control signal. Afterwards, the optical pulse is reflected back to the AWG by the reflector. It enters port 2 of the circulator and outputs from port 3. If the required multi-wavelength codeword does not contain the wavelength λ_j, the 1×2 optical switch connects the absorber, none optical pulse outputs from port 3. In doing so, a required multi-wavelength codeword is generated. All multi-wavelength codeword generators have the same architecture, and however they produce different multi-wavelength codewords under the controlling of the control signals. Since the architecture and operational principle of the tunable fiber-optic delay lines are the same as what we have introduced in Section 4.2, we no longer give unnecessary details here.

Assuming that when the value of the control signal is 1 the 1×2 optical switch is connected to the reflector and when the value of the control signal is 0 it is connected to the absorber, the control logic is shown in Table 4.8, which is required to generate eight multi-wavelength codewords based on Walsh-Hadamard code with length 8.

Table 4.8 Control logics corresponding to multi-wavelength codewords

Multi-wavelength codewords	Control logic of 1×2 optical switch (from top to bottom)
$C_0 = (\lambda_0 \lambda_2 \lambda_4 \lambda_6)$	10101010
$C_1 = (\lambda_0 \lambda_1 \lambda_4 \lambda_5)$	11001100
$C_2 = (\lambda_0 \lambda_3 \lambda_4 \lambda_7)$	10011001
$C_3 = (\lambda_0 \lambda_1 \lambda_2 \lambda_3)$	11110000
$C_4 = (\lambda_0 \lambda_2 \lambda_5 \lambda_7)$	10100101
$C_5 = (\lambda_0 \lambda_1 \lambda_6 \lambda_7)$	11000011
$C_6 = (\lambda_0 \lambda_3 \lambda_5 \lambda_6)$	10010110
$C_7 = (\lambda_0 - \lambda_7)$	11111111

The delays of three fiber-optic delay lines in the encoder of the B/U code using the codeword 1101000 of the (7,3,1,1) OOC as time-spreading are 0, τ and 3τ respectively. It can be seen that the fiber-optic delay lines in the encoder of any B/U codeword originated from one optical unipolar codeword do not require to be tuned, which can be implemented by the fixed fiber-optic delay lines. Only the delays of the fiber-optic delay lines in the encoders of the B/U codewords originated from different optical unipolar codewords are different, which need to be tuned.

The cyclic-shift properties of m-sequences and the "wavelength periodicity" of AWGs can be utilized when m-sequences are employed as the wavelength-hopping bipolar codes to generate the multi-wavelength codewords. Because the exit

wavelengths at the output ports are rotatable the exit wavelength number at output port j can be expressed as a modulo-m addition of j and the input port i that is injected with a broadband optical pulse, that is, $\lambda_{(i+j) \bmod m}$, where $i, j \in [0, m-1]$. Through connecting the appropriate output ports to the optical combiner and tuning the optical switches to the desired input ports, the multi-wavelength codewords can be generated by fast programming. In this way, the architecture of tunable multi-wavelength codeword generator can be simplified and the controlling signal becomes simple. Shown in Fig. 4.27[15], the tunable multi-wavelength codeword generator consists of an $1 \times m$ optical switch, an $m \times m$ AWG and a $\left(\frac{m+1}{2}\right) \times 1$ combiner, where m represents the period length of the chosen m-sequence with $m = 7$ in Fig. 4.27. For example, in order to generate the multi-wavelength codeword $C_2 = (\lambda_0 \lambda_2 \lambda_3 \lambda_4)$, the optical switch is connected to port 2 of the AWG. Then, the optical pulses with wavelengths λ_2, λ_3, λ_4, λ_5, λ_6, λ_0 and λ_1 are output from output ports 0 to 6 of the AWG. However, since only the AWG output port 0, 1, 2 and 5 are connected to the optical combiner the optical pulses with wavelengths λ_2, λ_3, λ_4 and λ_0 are chosen, that is, C_2 is generated. Due to the cyclic-shift properties of m-sequences, when the i^{th} multi-wavelength codeword needs to be generated, the optical switch is merely required to be connected to the i^{th} input port of the AWG.

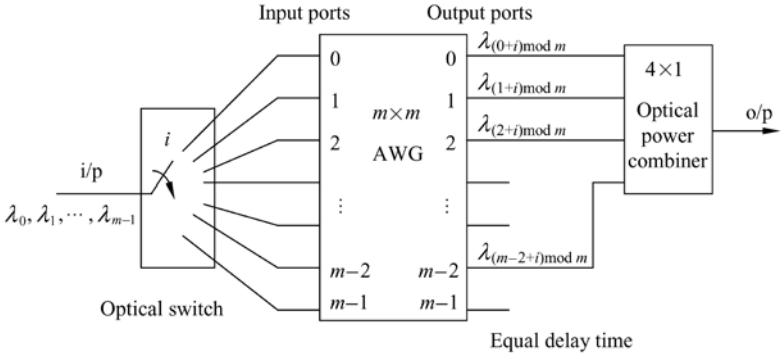

Figure 4.27 Multiwavlength codeword generator of m-sequence for $m = 7$ (Revised from Ref. [15])

The architecture of the B/U code optical decoder is shown in Fig. 4.28[15], which is composed of an $1 \times w$ optical power splitter, w tunable fiber-optic delay lines, w tunable multi-wavelength balanced encoders, an electronic summer, an electronic sampler, an electronic thresholder, a data recovery circuit and an electronic timing controller. An incoming optical B/U codeword is firstly split into w signals by the $1 \times w$ optical power splitter, and the w tunable fiber-optic delay lines shift all multi-wavelength codewords onto the last slot of the

corresponding B/U codeword. For example, for the B/U codeword obtained from the codeword 1101000 of the (7,3,1,1) OOC, its decoder has three tunable delay lines, whose delays are tuned to 6τ, 5τ and 3τ respectively. Then, the balanced multi-wavelength decoders choose the wavelengths and the optical-to-electrical conversions are performed, and the MAIs are counteracted. After these resulting signals are summed, sampled, threshold-decided and recovered under the control of the electronic timing circuit, the signal decoding is finally accomplished.

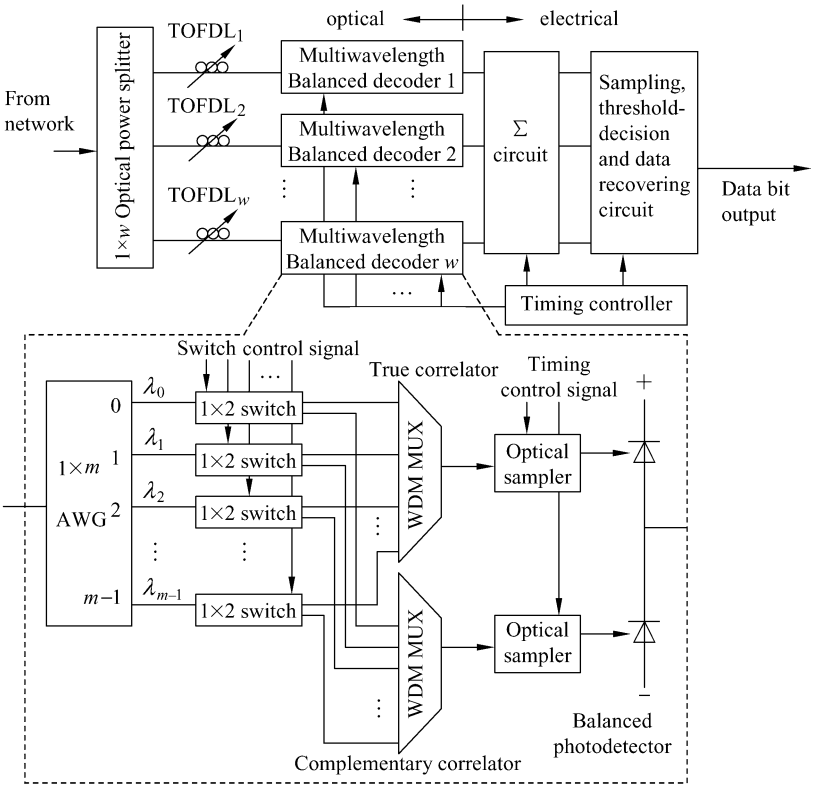

Figure 4.28 Structure of the decoder of bipolar/unipolar code (Revised from Ref. [15])

The tunable multi-wavelength balanced decoder consists of an $1\times m$ AWG, m 1×2 optical switches, two $m\times 1$ WDM multiplexers, two optical samplers and a pair of balanced photodetectors. The coming optical signal from the $1\times w$ optical splitter is split by the $1\times m$ AWG according to different wavelengths. If the decoded multi-wavelength codeword contains the wavelength the 1×2 optical switch corresponding to the wavelength is switched to the upper side, otherwise it is switched to lower side. Consequently, the reciprocally complementary outputs are generated by two $m\times 1$ WDM multiplxers such that the undesired

MAIs from other users can be counteracted through the balanced differential detection. For example, when the multi-wavelength codeword $C_0 = (\lambda_0 \lambda_2 \lambda_4 \lambda_6)$ is decoded, the 0^{th}, 2^{nd}, 4^{th} and 6^{th} optical switches are switched to the upper sides and the 1^{st}, 3^{rd}, 5^{th}, 7^{th} are switched to the lower sides. Then, the wavelengths of optical pulses at the exit of the true correlator are λ_0, λ_2, λ_4 and λ_6, and the wavelengths of optical pulses at the exit of the complementary correlator are λ_1, λ_3, λ_5 and λ_7. Considering the worst scenario, in which eight multi-wavelength codewords $C_0 - C_7$ arrive simultaneously at the multi-wavelength decoder, then the numbers of optical pulses with all kinds of wavelengths arriving at the multi-wavelength decoder are $8\lambda_0$, $4\lambda_1$, $4\lambda_2$, $4\lambda_3$, $4\lambda_4$, $4\lambda_5$, $4\lambda_6$ and $4\lambda_7$. Since the decoder has been tuned to C_0, the number of pulses detected by the upper photodetector is 20 (i.e., $8\lambda_0 + 4\lambda_2 + 4\lambda_4 + 4\lambda_6$), otherwise the number of pulses detected by the lower photodetector is 16(i.e., $4\lambda_1 + 4\lambda_3 + 4\lambda_5 + 4\lambda_7$). Then, the balanced photodetectors give an autocorrelation peak of $20 - 16 = 4$ units of electrical current. Now, assuming the decoder has been tuned to $C_0 = (\lambda_0 \lambda_2 \lambda_5 \lambda_7)$, because the multi-wavelength codewords transmitted from the network are $C_1 - C_7$ the number of pulses detected by the upper photodetector is 16(i.e., $7\lambda_0 + 3\lambda_2 + 3\lambda_5 + 3\lambda_7$) and the number of pulses detected by the lower photodetector is also 16(i.e., $4\lambda_1 + 4\lambda_3 + 4\lambda_4 + 4\lambda_6$). Then, the balanced photodetectors give the $16 - 16 = 0$ unit of electrical current, i.e., zero cross-correlation value.

Due to the cyclic-shift property of m-sequence, the optical encoder corresponding to m-sequence is shown in Fig. 4.29[15], which shows the circumstance of $m = 7$. For other cases, the principle of multi-wavelength optical decoder is the same except that the connections of the AWG exits to the input ports of the true correlator and the complementary correlator and the numbers of the AWG exits are different. Hence, we no longer give unnecessary details here.

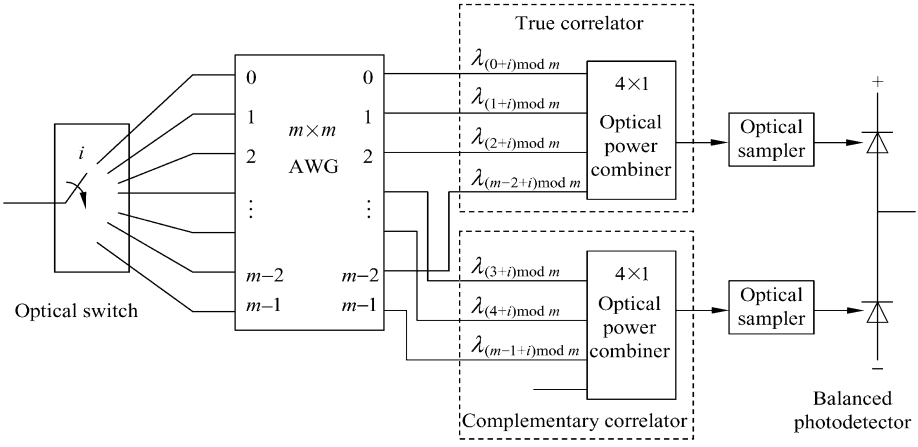

Figure 4.29 Multi-wavelength-codeword decoder of m-sequence for $m = 7$ (After Ref.[15])

The tunable function of a general multi-wavelength code optical encoder/decoder is implemented by employing the tunable fiber-optic delay lines and the 1×2 switches for routing the appropriate wavelengths within one time slot to the true and complementary correlators. Optical samplers, based on optical interferometric devices, such as terahertz optical asymmetric devices and nonlinear optical loop mirror[16, 17], are used in each decoder in order to gate the correlation results from the true and complementary correlators in a specific time slot determined by the optical unipolar codeword used in the subscriber address signature.

It seems that the architecture of this B/U code optical encoder/decoder is very complex. However, it can be implemented by using waveguide integration to reduce its size and cost. The architecture and operational principle of the bipolar/bipolar (B/B) code optical encoder and decoder are similar to those of the B/U code optical encoder and decoder. We don't give their details here. Interested readers can look up Reference [19].

4.6 Coherent Optical Encoder and Decoder

In a coherent OCDMA system, a given user address code is generally applied to encode the phases of optical signal field, which needs a high coherent light source, such as a mode-locked laser. At the receiving end, the coherent OCDMA system relies on the coherent reconstruction of optical signal field to retrieve the encoded user data.

In terms of the manner of the coherent phase encoding applied to the optical signal field, the coherent OCDMA systems are classified into the spectral phase encoding OCDMA and the temporal phase encoding OCDMA. The former manipulates the phase of optical signal in the spectral domain and the latter processes the phase of optical signal in the time domain.

4.6.1 Spectral Phase Encoder and Decoder

The coherent OCDMA spectral phase encoder using the spatial phase modulator (SPM) is shown in Fig. 4.30(a)[20], which comprises a pair of diffraction gratings placed at the focal planes of a unit magnification, confocal lens pair and a multi-element phase modulator. During the duration of T_b corresponding to the data bit "1", an ultrashort coherent optical pulse with the duration of T_c is fed into the optical encoder. The first grating spatially decomposes (with a certain resolution) the spectral components of the input ultrashort pulse. A pseudorandom, spatially patterned phase mask (corresponding to a user address codeword) is inserted midway between the lenses at the point where the optical spectral components experience maximum spatial separation. Thus, the mask introduces

pseudorandom phase shifts among the different spectral components. Then, these spectral components experiencing the required phase shifts are reassembled by the second lens and second grating into a single optical beam. The encoding process has been accomplished. In an OCDMA network, each transmitter employs a different phase mask (corresponding to the subscriber address codewords being mutually orthogonal) and broadcasts its encoded signals to all those receivers that share the same optical channel.

The coherent OCDMA spectral phase optical decoder is shown in Fig. 4.30(b)[20], which is similar to the optical encoder except that its phase mask is the conjugate of the encoding mask. The spectral phase shifts are removed and the original coherent ultrashort pulse is reconstructed when the encoding and decoding masks are a complex conjugate pair. However, when the encoding and decoding masks do not match, the spectral phase shifts can not be removed, and the optical signal

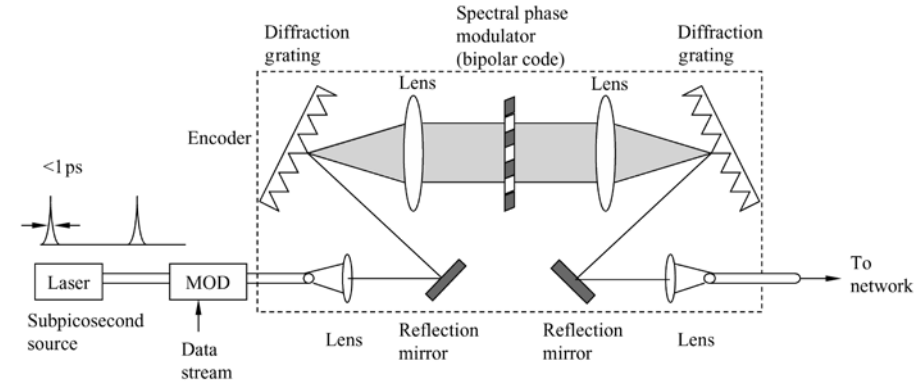

(a) Spectral phase encoder of ultrashort light pulse

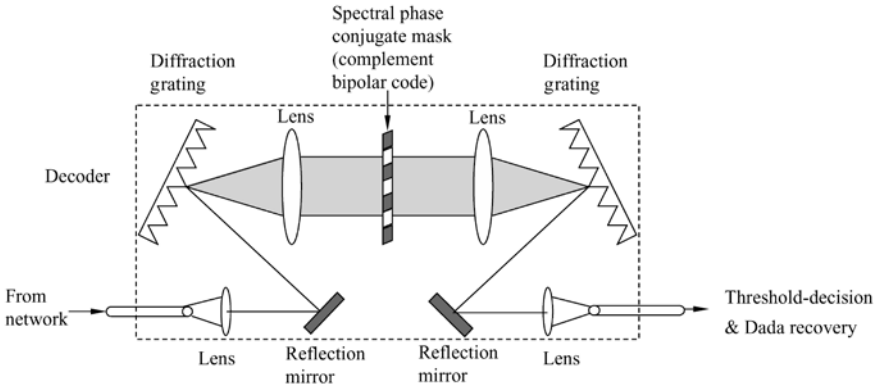

(b) Spectral phase decoder of ultrashort light pulse

Figure 4.30 Encoder and decoder based upon spectral-phase encoding and decoding of ultrashort light pulse[20]

at the output of the decoder remains a low intensity pseudonoise burst. After the photodetection and threshold decision, the desired data bit is restored. Since the multi-element phase mask is fixed, the fixed coherent OCDMA spectral phase optical encoder/decoder can only be implemented. If the electrically controllable phase mask, such as a multi-element liquid crystal phase mask is employed, the tunable coherent spectral phase encoder and decoder can be implemented. For the binary spectral phase codes, the bipolar encoding can be utilized by assigning the phase shifts of $\{0, \pi\}$ corresponding to the code elements $\{+1,-1\}$ of an orthogonal binary address codes. For the quaternary spectral phase encoding, the phase shifts $[0, \pi/2, \pi, 3\pi/2]$ can be allocated to the code elements [+1, j, −1, −j] of an orthogonal quaternary address codes.

A mode-locked laser (MLL) operates with a broad spectrum of wavelengths, each corresponding to a different laser cavity mode. The width of the spectrum is defined both by the bandwidth of the laser gain medium as well as any wideband filtering that may be present inside the laser cavity. By modulating the round trip gain or loss of the laser cavity with a periodic signal, it is possible to lock all of the cavity modes so that they maintain a well-defined phase relationship with each other. The equivalent time domain signal can be determined by taking the Fourier transform of this phase-locked, multi-wavelength comb, as shown in Fig. 4.31[21].

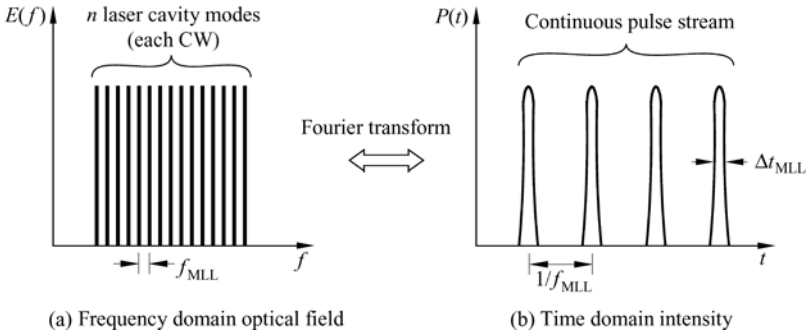

Figure 4.31 Representation of the output signal from a mode-locked laser[21]

The temporal electric field of the mode-locked laser signal is a pulse train with the time spacing $1/f_{\mathrm{MLL}}$, which can be expressed as[21]

$$E(t) = \frac{1}{n} e^{j2\pi f_0 t} \cdot \sum_{i=1}^{n} e^{j2\pi i f_{\mathrm{MLL}} t} \tag{4.5}$$

and the its corresponding optical intensity can be expressed as

$$P(t) \propto |E(t)|^2 \tag{4.6}$$

where f_{MLL} is the pulse repetition frequency, i.e., the frequency spacing between

the MLL lines on the order of 5 – 10 GHz approximately, f_0 is the optical carrier frequency on the order of 10^{14} Hz and the term in the summation represents the envelope of the pulse train. The pulse repetition rate is equal to $1/f_{\mathrm{MLL}}$ and the pulse width, Δt_{MLL}, is equal to $1/(n \cdot f_{\mathrm{MLL}})$, where n is the number of laser cavity modes available. There exists $|E(t)|=1$ at the integer multiples of the period $T=1/f_{\mathrm{MLL}}$.

The pulse train is "spectrally phase encoded" by applying a spectral phase mask $\Phi_{i,\mathrm{code}}$ that multiplies frequency i by a phase term corresponding to a given codeword (in some cases, the amplitude of the spectral phase component also changes, but in the normal case the phase function is of unit amplitude). In the absence of data modulating, the effect of encoding the MLL signal with codeword E and decoding with codeword D can be expressed as[21]

$$E(t)=\frac{1}{n}\mathrm{e}^{\mathrm{j}2\pi f_0 t}\cdot\sum_{i=1}^{n}\Phi_{i,D}\Phi_{i,E}\mathrm{e}^{\mathrm{j}2\pi i f_{\mathrm{MLL}} t} \tag{4.7}$$

The technical difficulties to implement the aforementioned scheme of the coherent OCDMA spectral phase en/decoding are as follows:

(1) obtaining the coherent ultrashort optical pulse sources;

(2) requiring the accurately spatial alignment of bulk-optic components because of the demand of the phase conjugate between the masks in the optical encoder and decoder, especially for the electric controllable phase masks;

(3) optical encoding signals (ultrashort optical pulses trains) being vulnerable to the transmission dispersion and nonlinearity and being difficult to maintain the invariable phase spectrum of the input ultrashort optical pulses;

(4) optical en/decoding limited by the resolution of diffracted gratings and masks;

(5) employing the large free-space bulk-optics which is not compatible with the robust compact packaging requirements of the telecommunications industry.

From the viewpoint of cost, technology and system performance, the coherent OCDMA spectral phase encoding using the bulk-optics is still difficult to be employed practically in the near future. Because of this reason, the coherent OCDMA spectral phase encoding/decoding subsystem integration has been considerably evolved by the effort of collaboration of University of California, Davis, Lawrence Livermore National Laboratory and Royal Institute of Technology, Sweden, supported by DARPA, America[22, 23]. The monolithic and miniaturization OCDMA encoder and decoder consist of InP-based integrated AWGs and spectral phase modulators. The electro-optic phase shifter array is electrically programmable such that the integrated optical encoder and decoder are tunable. This chips utilizes BH waveguides fabricated through a deep dry etching and a HVPE (Hybrid Vapor Phase Epitaxy) single step lateral regrowth process for sidewall passivation and surface planarization, which has implemented the spectral phase en/decoding with 8-chip Hadamard-Walsh code, where "0"

and "1" of Hadamard-Walsh codewords correspond to the phases of π and 0 respectively. The schematic diagram of the integrated optical encoder and decoder is shown in Fig. 4.32. Dry etching and HVPE lateral regrowth in addition to standard wet etching and MOCVD (metal organic chemical vapor deposition) growths achieved active and passive device integration with excellent planarity. Although the monolithic transceiver occupies an extremely small footprint of 4×1 cm, as a matter of fact, it is an integrated micro-system, where a colliding pulse mode (CPM) locked laser and a electro-absorptive modulator at transmitting end, and a Mach-Zehnder interferometer (MZI)-based threshold detector at receiving end are integrated on the chip. The entire chip is implemented in the InP-InGaAsP material system with the operation wavelength of 1550nm. At the same time, the power consumption is very small (~mW).

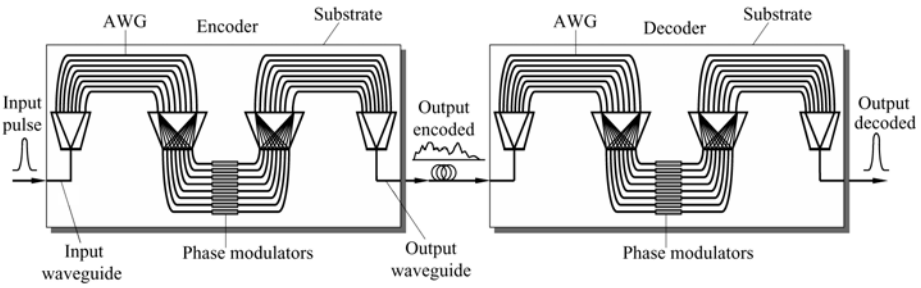

Figure 4.32 OCDMA encoder and decoder based on monolithic AWG-phase modulator-AWG semiconductor chips (After Ref.[22])

In addition, with the development of optical fiber grating technology, the implementing spectral phase encoding and decoding using the FBG devices instead of the bulk-optic system has been proposed[24]. If the reader is interested in its details please look up the associated references.

4.6.2 Temporal Phase Encoder and Decoder

4.6.2.1 Temporal Phase Encoder and Decoder with Parallel Architecture

The temporal phase encoding OCDMA is to manipulate the phase of optical signal in the time domain. The coherent OCDMA system of the temporal phase encoding with parallel processing structure is shown in Fig. 4.33[25]. The schematic waveforms at point a, b, c, d, e and f have been given in Fig. 4.34[21]. The temporal phase encoding OCDMA system is similar to the spectral phase encoding OCDMA to some extent. However, the spectral phase encoding OCDMA is implemented by decomposing firstly the ultrashort optical pulse emitted by the broadband light source, such as a mode-locked laser, into multiple optical pulses

in terms of the different spectral components (or called wavelengths) and then imposing the different phase-shifts to the different spectral components. The temporal phase encoding OCDMA system is actualized by disassembling firstly the ultrashort optical pulse from a mode-locked laser into multiple optical pulses through the differently temporal-delays and then imprinting the different phase shifts to these optical pulses through using multiple different phase shifters. Whereas, because the temporal phase encoding does not partition the optical pulse according to the spectral components, it does not require the broadband light source with very flat spectrum. After the optical pulse from a mode-locked laser is modulated by a user data, the temporal phase-encoding is performed by employing the temporal phase encoder. Firstly, the optical pulse modulated is split into n ultrashort optical pulses and then each optical pulse is delayed by traversing the fiber-optic delay lines with different lengths so that they lie on an equally spaced time chip. Afterwards, each pulse achieves the required phase shift in terms of the subscriber assigned address codeword. Similarly, each phase component corresponds to a phase 0 or π for the binary encoding (corresponding to 1 and -1 of a binary code) and to a phase 0, $\pi/2$, $3\pi/2$ or π for the quaternary encoding (corresponding to 1, j, -1 and $-$j of a quaternary code), etc., where j is a unit of imaginary number, equal to $\sqrt{-1}$. Finally, they are reassembled by an optical combiner and the temporal phase encoding is accomplished. The output signal is transmitted to a network.

In an OCDMA network, a receiver can receive the signals from all subscribers within the network. In order to retrieve the data stream from a specific subscriber, the optical temporal-phase decoder is required to match with its corresponding encoder. The architecture of a temporal phase decoder is the same as that of the encoder except that the phase-shift elements in the decoder must be set to the conjugate elements corresponding to the optical encoder (time-reversal order) in order to perform the correlation operation of the signal received. For example, if the binary phase code $\Phi_{\mathrm{E}} = (\phi_{\mathrm{E1}}, \phi_{\mathrm{E2}}, \phi_{\mathrm{E3}}, \phi_{\mathrm{E4}}, \phi_{\mathrm{E5}}, \phi_{\mathrm{E6}}, \phi_{\mathrm{E7}}) = (\pi, \pi, \pi, 0, 0, \pi, 0)$ is employed to encode, which corresponds to the bipolar code (–1, –1, –1,1,1, –1,1) of length 7, the phase-shifts in its corresponding decoder should be $\Phi_{\mathrm{D}} = (\phi_{\mathrm{D1}}, \phi_{\mathrm{D2}}, \phi_{\mathrm{D3}}, \phi_{\mathrm{D4}}, \phi_{\mathrm{D5}}, \phi_{\mathrm{D6}}, \phi_{\mathrm{D7}}) = (0, \pi, 0, 0, \pi, \pi, \pi)$. In this case, a strong autocorrelation peak can be seen in the output of the decoder. If the decoder does not match with the encoder, the autocorrelation peak can not been seen at the output of the decoder and the decoder output is still kept like a noise. After decoded by a matching decoder, the MAIs from the other undesired subscribers are removed and the correct data output is obtained through the optical-to-electrical conversion, threshold decision and data recovery. For the sake of suppressing MAI effectively and improving the system performance, the techniques, such as the optical time gating and optical thresholding[16], etc. can be employed.

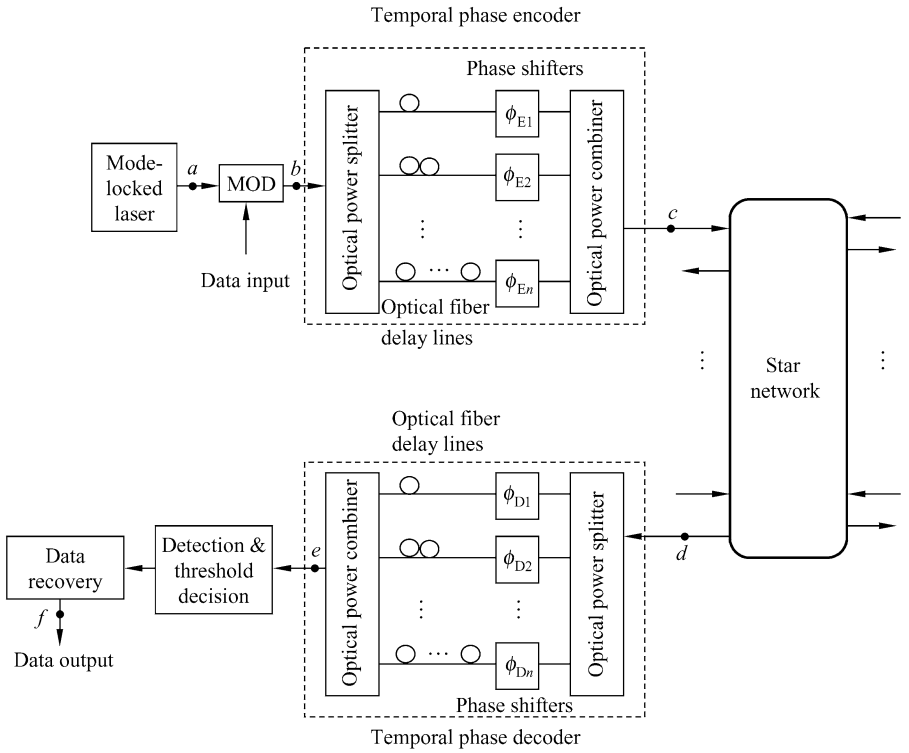

Figure 4.33 Schematic diagram of the temporal phase coded OCDMA (TPC-OCDMA) system architecture[21, 25]

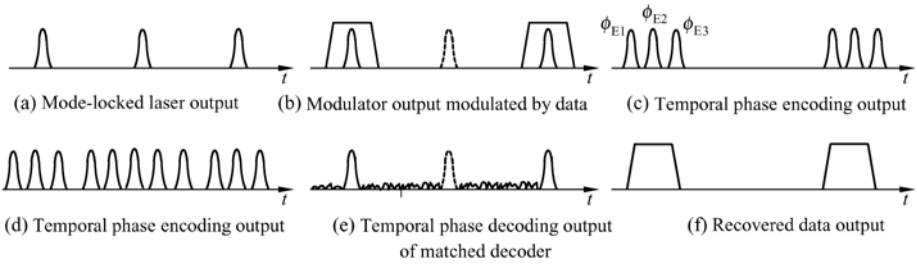

Figure 4.34 Time-domain representations of signals at various stages of the temporal phase coded OCDMA system[21]

The experimental schematic diagram of the tunable temporal phase en/decoder with the parallel structure employing optical waveguide integration proposed in Reference [26] is shown in Fig. 4.35. The waveguide optical encoder and decoder comprise tunable taps, optical phase shifters, delay lines, and a combiner. These are monolithically integrated on Si-substrate by planar lightwave circuit (PLC) fabrication method and are installed in a temperature-controlled box. In encoder, taps are connected via delay lines whose delay time corresponds to the time

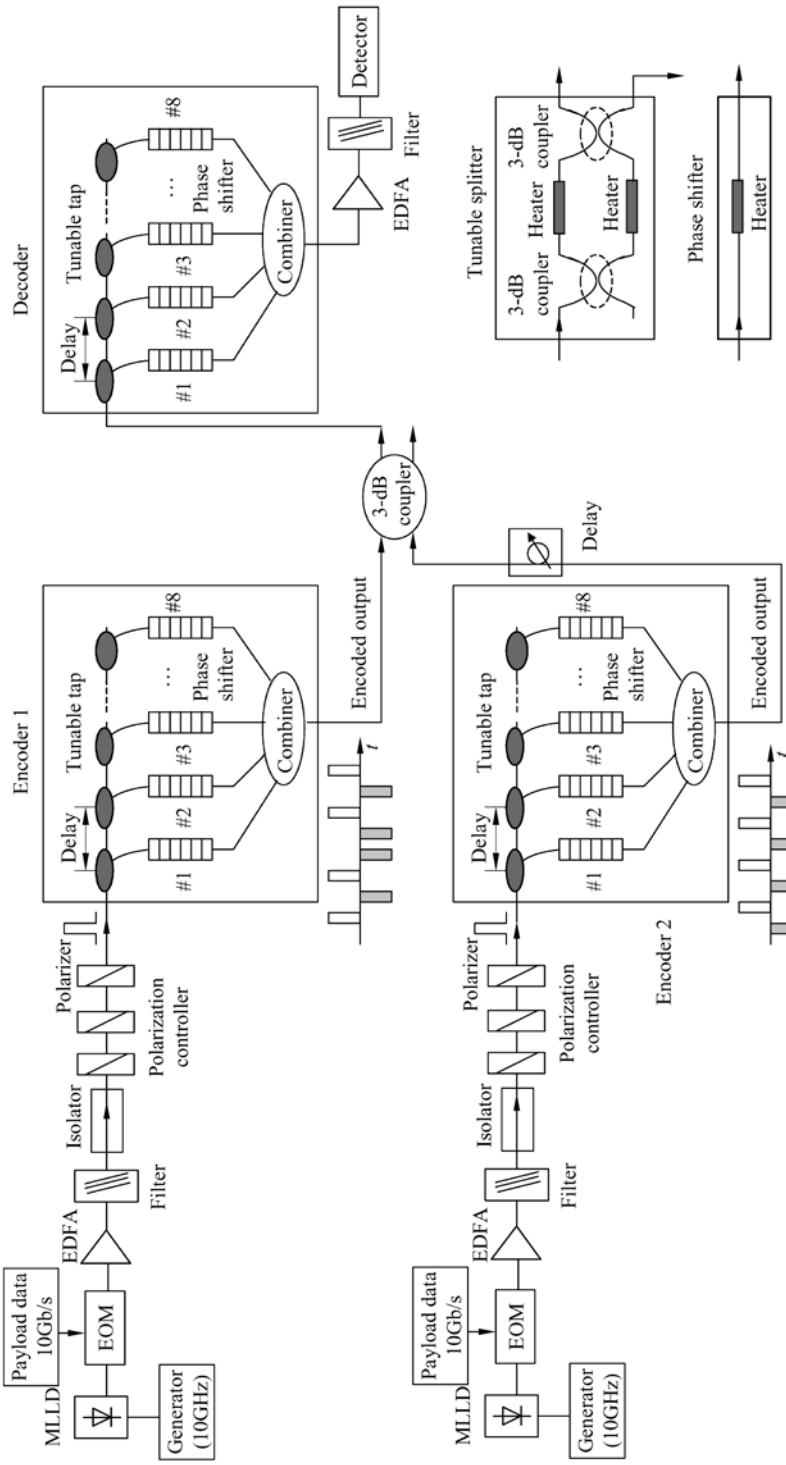

Figure 4.35 Experimental setup diagram of the parallel temporal-phase encoding and decoding for OCDMA (After Ref. [26])

interval between chip pulses. For 10Gb/s 8-chip bipolar code the delay time is set to 5ps. The tunable tap is a Mach-Zehnder interferometer (MZI) being composed of two 3-dB couplers and two optical phase shifters, shown in the inset of top right corner of Fig. 4.35. The optical phase shifter is an optical waveguide partly covered with a heater electrode. The optical carrier phase can be varied by changing the refraction index of the waveguide that is altered by the variation of its temperature. In this experiment, 8-chip pulses with same amplitude are generated by tuning taps. The phases of each chip pulse are shifted by either 0 or π radian, and then the chip pulses are combined by the optical combiner to form a bipolar signature sequence. The decoder has the same structure with the encoder so that the time-reversal operation to the encoded signals received can be done by it.

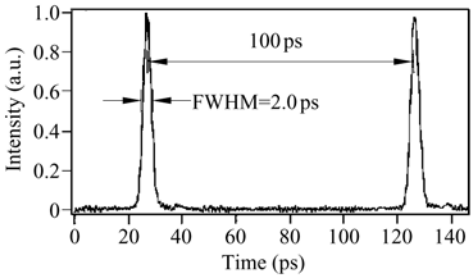

(a) 10 GHz optical pulse stream generated by the mode-locked laser diode

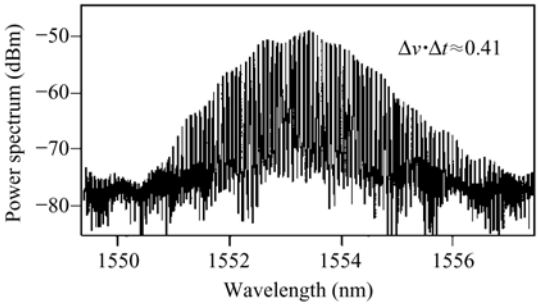

(b) Power spectrum of 10 GHz optical pulse stream

Figure 4.36 Waveform of 10 GHz optical pulse stream and its power spectrum (Adapted from Ref. [26], with permission from IEEE © 2007)

Figure 4.36(a) shows the temporal waveform of 10 GHz optical pulse stream generated by the mode-locked laser diode (MLLD) employed in the experiment, which has the full width at half maximum (FWHM) of approximate 2 ps and the jitter of 0.5 ps. The power spectrum of the optical pulse stream is shown in Fig. 4.36(b). The central wavelength and the time bandwidth product are approximately 1553.3nm and $\Delta\nu \cdot \Delta t \approx 0.41$ respectively. The intensity distribution of the generated 8-chip bipolar codeword $(0, \pi, 0, \pi, 0, \pi, 0, \pi)$ is shown in Fig. 4.37

and the time interval between each chip pulse is 5 ps. The measured intensity distributions of autocorrelation signal corresponding to the codeword $(0,\pi,0,\pi,0,\pi,0,\pi)$ and cross-correlation signal between the codewords $(0,\pi,0,\pi,0,\pi,0,\pi)$ and $(0,\pi,0,\pi,\pi,0,\pi,0)$ are shown in Fig. 4.38(a) and (b) respectively, which are basically consistent with their theoretical results, where the theoretical values of the relative intensity distribution of the autocorrelation of the codeword

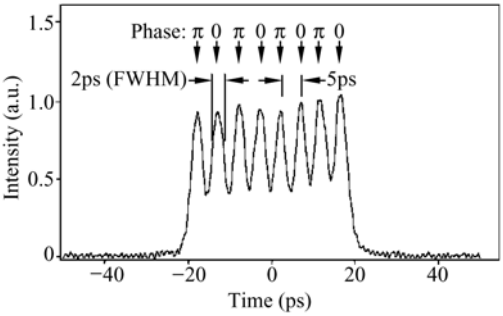

Figure 4.37 Intensity distribution of the generated 8-chip optical bipolar code $(0,\pi,0,\pi,0,\pi,0,\pi)$ (Adapted from Ref.[26], with permission from IEEE © 2007)

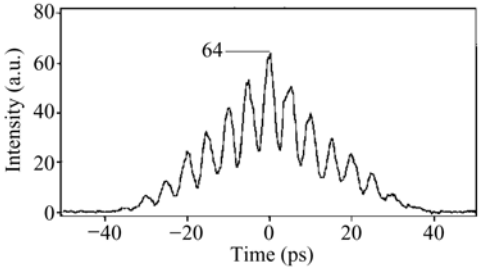

(a) Autocorrelation function of the bipolar codeword $(0,\pi,0,\pi,0,\pi,0,\pi)$

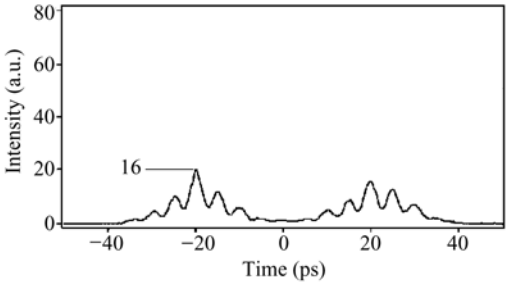

(b) Cross-correlation function between $(0,\pi,0,\pi,0,\pi,0,\pi)$ and $(0,\pi,0,\pi,\pi,0,\pi,0)$

Figure 4.38 Intensity distributions of correlation signals of 8-chip optical bipolar codes (Adapted from Ref. [26], with permission from IEEE © 2007)

$(0,\pi,0,\pi,0,\pi,0,\pi)$ are (1,4,9,16,25,36,49,64, 49,36,25,16,9,4,1) with the peak 64 and the cross-correlation between these codewords takes the values of (0,1,4, 9,16,9,4,1,0,1,4,9,16,9,4,1) with the peak 16 and the ratio of two peaks is $16/64 = 25\%$. Note that the non-periodical correlation is deployed because the adjacent two optical pulses emitted by the light sources in the duration of two adjacent "1" bits are not coherent pulses.

In order to reduce multiple access interference noise and incoherent noise, a coherent detection with sidelobe suppression is employed in this experiment such that the system performance has been improved.

The temporal phase en/decoder implemented by PLC has small size and reliable performance. However, PLC can not be easily employed to generate the temporal phase code in the orders of a hundred-chips order long[27], due to the physical constraint of the silica substrate and design complexity. Therefore, only the limited number of codewords can be produced by using PLC such that the system scalability using PLC en/decoders is poor. Fortunately, the temporal phase en/decoder using the superstructured fiber Bragg grating can generate very long bipolar or multi-polar codes such that the system with a large number of subscribers can be implemented.

[Note that because Gold code is generated by the modulo-2 addition of two preferred m-sequences with the same length the code length should be $2^n - 1$. Two codewords $w_2 = (1,-1,1,-1,1,-1,1,-1)$ and $w_6 = (1,-1,1,-1,-1,1,-1,1)$ of Hadamard-Walsh code with the length 8 were employed in the experiment as a matter of fact.]

4.6.2.2 Temporal Phase Optical Encoder and Decoder Based on SSFBGs

The superstructured fiber Bragg grating (SSFBG)[28, 29] is a type of fiber Bragg gratings, which can be employed to implement more sophisticated functions. Since SSFBGs can be used to implement the filtering of almost arbitrary spectral responses they can be applied to precisely control the temporal and spectral characteristics of optical waveforms. SSFBGs can be obtained by imposing a relatively slowly varying modulation envelope upon the rapidly varying refractive index modulation with uniform amplitude and pitch along the grating length such that a temporal code can be imprinted on the spatial structure of a fiber Bragg grating. When a phase-shifted keying code is utilized, a phase modulation profile can be obtained. The SSFBGs are fabricated using the "continuous grating writing" technique, which effectively writes gratings on a grating plane based on grating plane principle and allows for the fabrication of gratings with truly complex refractive index profiles. The technique uses a simple phase mask with uniform pitch and relies upon precise control of the positioning of the fiber relative to the mask and controlled exposure to the index modifying ultraviolet light used to write the grating, which is highly flexible such that it does not depend on the complex phase mask when the complex SSFBG structure is fabricated. The temporal phase en/decoder for OCDMA can be

implemented by employing SSFBG technology, which offer many advantages in terms of compactness, scalability, integrability, cost and ease of manufacture and compatibility with WDM system, and support a system with a large number of subscribers. Especially, when the code implemented is very long the MAI can be suppressed and the beat noise can be mitigated.

In the weak SSFBG grating limit (The typical reflectivity is less than 20%. However, it is found that the SSFBGs perform well when the reflectivity reaches 50% in many experiments.), that is, where the grating strength is such that the light penetrates the full grating length and the individual elements of the grating contribute more or less equally to the reflected response, the wavevector response $F(\kappa)$ can be simply expressed as the Fourier transform of the spatial superstructure refractive index modulation profile $A(x)$ employed to write the grating[29, 30], namely,

$$F(\kappa) = \frac{1}{2\pi} \int_{-\infty}^{+\infty} A(x) \mathrm{e}^{\mathrm{j}\kappa x} \mathrm{d}x \tag{4.8}$$

The uniform rapid refractive index modulation simply defines the central wavelength. Similarly, the impulse response of a fiber grating, $h(t)$, can be expressed as the inverse Fourier transform of its frequency response $H(\omega)$

$$h(t) = \int_{-\infty}^{+\infty} H(\omega) \mathrm{e}^{-\mathrm{j}\omega t} \mathrm{d}\omega \tag{4.9}$$

From the aforementioned equations and the fact that the wavevector κ is proportional to the optical angle frequency ω, it is obvious that the impulse response of a weak grating has a temporal profile that is given by the complex form of the refractive index superstructured modulation profile of the grating.

When a short and limited bandwidth pulse (i.e., not a unit impulse response) is encoded by the reflection of SSFBG, it is transformed into a temporal waveform expressed by the convolution between the input pulse and the impulse response of the grating, namely,

$$y(t) = x(t) * h(t) \tag{4.10}$$

The corresponding expression in frequency domain is

$$Y(\omega) = X(\omega) H(\omega) \tag{4.11}$$

This means that the Fourier transform $Y(\omega)$ of the output $y(t)$ reflected by the SSFBG is the product of the Fourier transform $X(\omega)$ of the input signal $x(t)$ and the frequency response of the grating frequency response $H(\omega)$. The symbol "$*$" represents a convolution operation. The extension factor of the output waveform is appropriately $\tau = 2n_{\mathrm{eff}} L / c$, where n_{eff} represents the effective

refractive index of the grating, L indicates the length of the grating, c denotes the light speed in vacuum. The factor 2 comes from the fact that the light signal travels twice of the length of the grating because of the round-trip reflected by the grating.

For example, a binary phase code $(0,\pi,0,0,\pi,\pi,\pi)$ (upper trace) and its corresponding refractive index modulation profile along the SSFBG structure (lower trace) are shown in Fig. 4.39, which correspond to the m-sequence (1,–1,1,1, –1, –1, –1) of length 7. The SSFBG has a uniform amplitude refractive index level along its length, but the discrete phase transitions, $\{0,\pi\}$, are written into the grating at the boundaries of adjacent spatial chips, subject to the m-sequence.

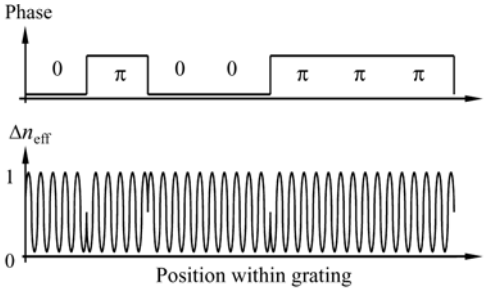

Figure 4.39 Schematic example of corresponding temporal code (upper traces) and corresponding refractive index modulation profiles along the SSFBG structures (lower traces) of an m-sequence bipolar codeword (1,–1,1,1, –1, –1, –1)[30]

Figure 4.40(a) shows the theoretical reflectivity spectrum (solid line) and spectral response to 2.5ps soliton pulses (dashed line) for the bipolar grating $(0,\pi,0,0,\pi,\pi,\pi)$. The impulse response (solid line) and temporal response to 2.5ps soliton pulses (dashed line) for this bipolar grating are shown in Fig. 4.40(b)[30].

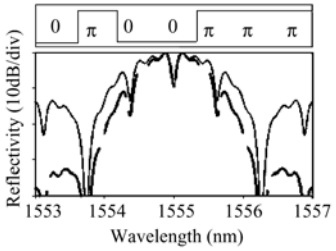

(a) Reflectivity spectrum (solid line) and spectral response to 2.5 ps soliton pulses (dashed line) for the bipolar grating $(0,\pi,0,0,\pi,\pi,\pi)$

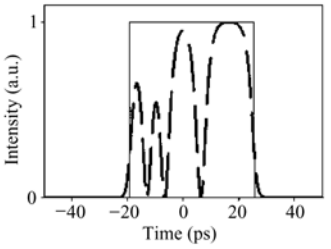

(b) Its impulse response (solid line) and temporal response to 2.5 ps soliton pulses (dashed line)

Figure 4.40 (Adapted from Ref.[30], with permission from IEEE © 2007)

In order to decode the temporal phase encoded signal using the SSFBG, the encoded signal is reflected from the SSFBG decoder with the frequency response $G(\omega)$ such that the frequency response of the decoder output, $R(\omega)$, is given by[30]

$$R(\omega) = Y(\omega)G(\omega) \tag{4.12}$$

If we let $G(\omega) = H^*(\omega)$, there exists in the time domain

$$g(t) = h^*(-t)$$

where the superscript "$*$" denotes the complex conjugate.

The output of the decoder in the time domain, corresponding to equation (4.12), is

$$r(t) = y(t) * h^*(-t) \tag{4.13}$$

Substituting (4.10) into (4.13), we can obtain

$$r(t) = x(t) * h(t) * h^*(-t) = x(t) * [h(t) * h^*(-t)]$$

where $g(t)$ is the inverse Fourier transform of $G(\omega)$, $r(t)$ denotes the inverse Fourier transform of $R(\omega)$ and $h(t) * h^*(-t)$ represents the autocorrelation function of the impulse response of a encoder. When the term $h(t) * h^*(-t)$ is equal to the Dirac's delta function $\delta(t)$, the output of the decoder is the input of its corresponding encoder, namely, the original input signal is retrieved completely. This is the most ideal case that is impossible in practice. However, we can make it approach to $\delta(t)$. In this case, the frequency response of the decoder is

$$G(\omega) = H^*(\omega) \tag{4.14}$$

Its corresponding impulse response in time domain is given by

$$g(t) = h^*(-t) \tag{4.15}$$

Physically, (4.15) means that the superstructured function of the decoder grating is required to be the spatially time-reversed and conjugate form employed to write the encoder grating. For instance, if a bipolar encoding grating corresponds to the binary phase code $(0, \pi, 0, 0, \pi, \pi, \pi)$, then its corresponding decoder is $(\pi, \pi, \pi, 0, 0, \pi, 0)$. Also, for a quaternary phase code $(3\pi/2, 0, 0, \pi/2, \pi, 0, 0, 3\pi/2, \pi/2, 3\pi/2, \pi/2, 0, \pi/2, \pi, 3\pi/2)$, its corresponding decoder is $(\pi/2, \pi, 3\pi/2, 0, 3\pi/2, \pi/2, 3\pi/2, \pi/2, 0, 0, \pi, 3\pi/2, 0, 0, \pi/2)$. As a matter of fact, the temporal phase SSFBG decoder is a matched filter corresponding to the encoder. Figure 4.41 shows the intensity SHG (second harmonic generation) autocorrelation traces[30] of the signals after the decoding

of the $(\pi,\pi,\pi,0,0,\pi,0)$ grating for 2.5ps soliton input pulses encoded by the $(0,\pi,0,0,\pi,\pi,\pi)$ grating. The solid line represents the experimental measurement, whereas the dashed line indicates the theoretical plot. They are basically consistent.

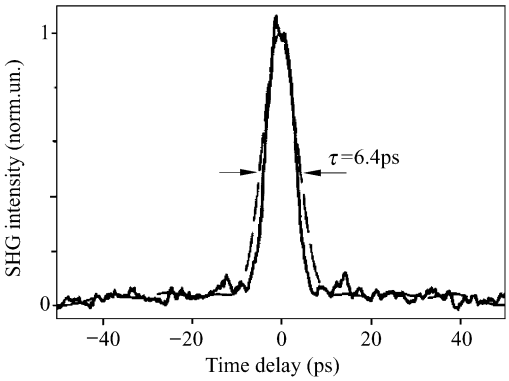

Figure 4.41 Intensity SHG autocorrelation traces of the signals after the decoding of the $(\pi,\pi,\pi,0,0,\pi,0)$ grating for 2.5 ps soliton input pulses encoded by the $(0,\pi,0,0,\pi,\pi,\pi)$ grating. The solid line represents the experimental measurement, whereas dashed line indicates the theoretical plot. (Adapted from Ref. [30], with permission from IEEE © 2007)

If the frequency response of the decoder is not the complex conjugate of the encoder, i.e., $G(\omega) \neq H^*(\omega)$, the output of the decoder is a cross-correlation function of the superstructured profiles (two different codewords) of two different gratings. Note that the overall time length of $r(t)$ is twice of the code length.

An encoding and decoding experimental system of two subscribers each using Gold bipolar code with the code length 63 is shown in Fig. 4.42[30]. The theoretical superstrucured profiles of these two-subscriber encoders and their corresponding measured reflectivity spectra are also given in this figure. Many peaked reflectivity profiles in the reflectivity spectra result from the numerous discrete phase transitions. After these two-user signals were multiplexed and then amplified by EDFA they transmitted 25 km in the standard SMF-28 grade fiber. At the receiving end, the high dispersion of this fiber (~20ps/(nm · km)) was compensated employing a chirped fiber grating. After decoded by the tunable optical decoder the signal output was tested by Bit-Error-Rate Analyzer. The measured results are shown in Fig. 4.43[30], where Fig. 4.43(a) and (b) represent the resulting autocorrelation function traces of the encoder 1: decoder 1 and the encoder 2: decoder 2 respectively and Fig. 4.43 (c) and (d) are their cross-correlation function traces.

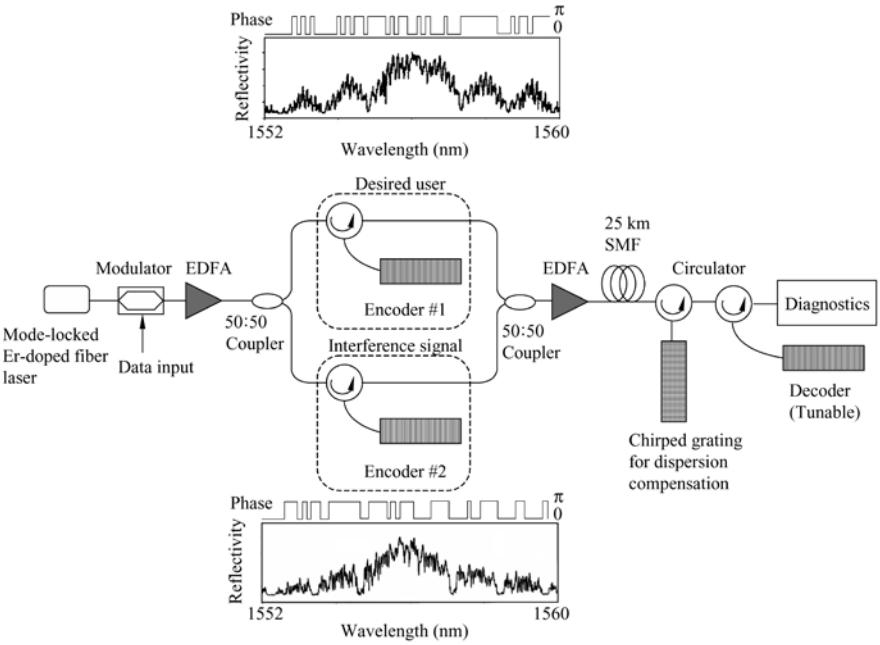

Figure 4.42 Experimental system of two-codewords multiplexing[30] (EDFA: erbium-doped fiber amplifier)

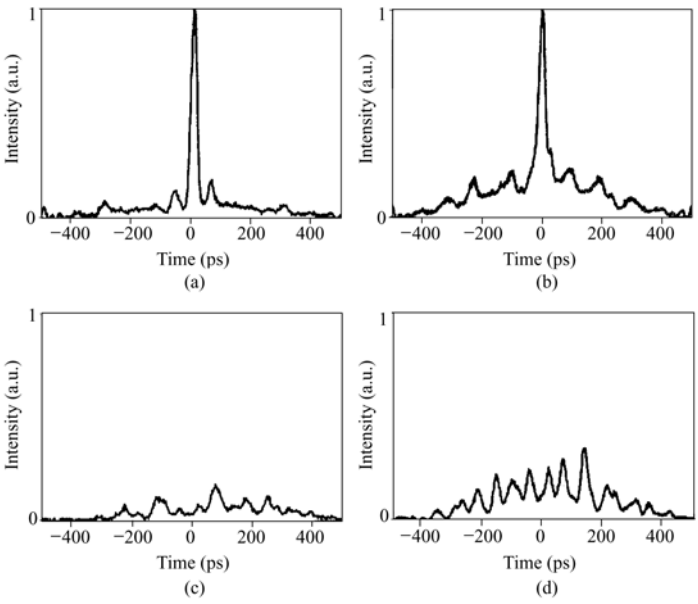

Figure 4.43 Experimental traces of the signals after the coding and decoding process for 2.5 ps soliton input pulses, for the combinations of grating encoder and decoder: (a) $Q_1 * Q_1^*$, (b) $Q_2 * Q_2^*$, (c) $Q_2 * Q_1^*$, and (d) $Q_1 * Q_2^*$. The detection bandwidth was ~20GHz. (Adapted from Ref.[30], with permission from IEEE © 2007)

Reference [33] reported in the first time that the quaternary phase coding grating with the chip-length 255 and the chip rate 320 Gchip/s was implemented in the experiment. Its phase modulation profile, the theoretical and experimental results of spectral reflectivity profiles are shown in Fig. 4.44. It can be seen that the theoretical result is well consistent with the experimental result. With regard to the quaternary phase codes, we have discussed in Subsection 2.7.4.

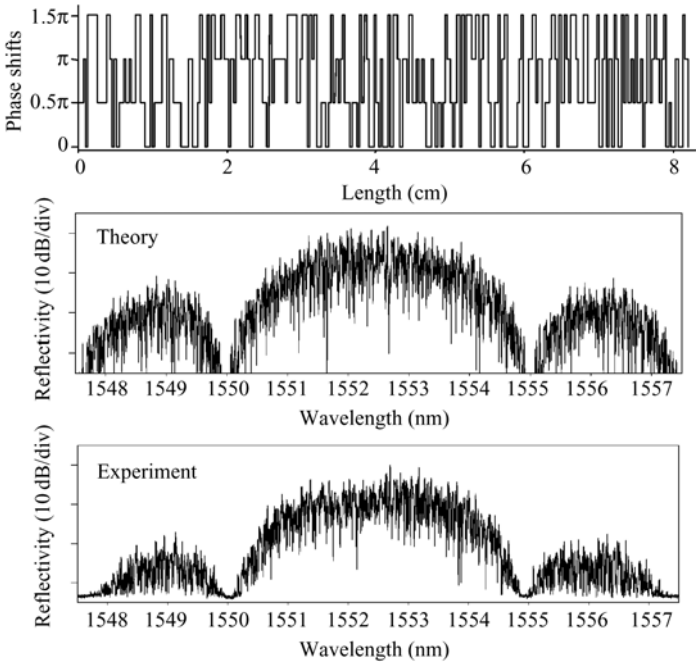

Figure 4.44 Phase modulation profile, and spectral reflectivity profiles (theory and experiment) for a 255-chip 320 Gchip/s quarternary sequences SSFBG (Q_1). The grating has a peak reflectivity of ~25% and is 8.44 cm long. (Adapted from Ref. [33], with permission from IEEE © 2007)

The output waveforms decoded are shown in Fig. 4.45[41], where Q_1 and Q_2 denote two encoders corresponding to two quaternary phase codes with the length 255, Q_1^* represents the decoder corresponding to Q_1, $Q_1 * Q_1^*$ indicates the autocorrelation function curve of Q_1 and $Q_2 * Q_1^*$ expresses the cross-correlation function curve between Q_2 and Q_1. The inset shows theoretical (dashed line) and experimental (solid line) SHG intensity autocorrelation traces of Q_1 and the correctly decoded pulse width was ~3.2 ps.

Reference [34] reported that the temporal phase encoding and decoding of a record-length 511-chip BPSK Gold code was experimentally demonstrated using

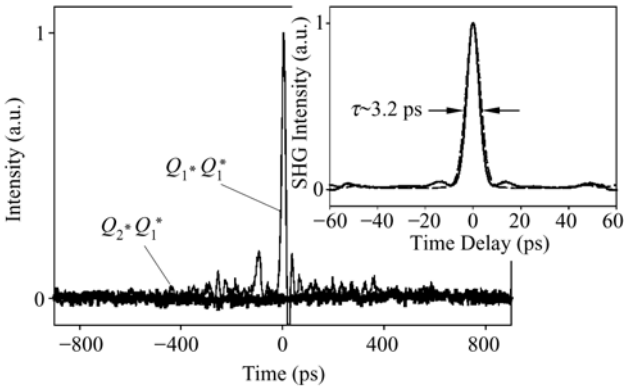

Figure 4.45 Output waveforms obtained after decoding. $Q_1 * Q_1^*$ represents the trace of autocorrelation of the codeword Q_1, $Q_2 * Q_1^*$ indicates the trace of cross-correlation between the codewords Q_1 and Q_2. (After Ref.[41])

the SSFBG with a chip rate of 640 Gship/s. The long optical address-code with the uniform cross-correlation not only makes a system be able to support a larger number of subscribers, but also suppresses MAI and reduces the signal-interference (SI) beat noise through debasing the cross-correlation. The high peak reflectivity 92% was achieved by employing the apodized SSFBG such that the system performance was significantly improved.

In order to implement the communications between any subscribers and the function of signal dynamic add/drop, cross-connection and network reconfiguration, etc., the tunable optical encoder/decoder are required. The tunable optical encoders and decoders with 7-chip bipolar-code[35] and 15-chip quaternary-phase-code[36, 37] based on SSFBG have been implemented by the researchers in University of Southampton, UK.

For an uniform pitch grating, its Bragg central wavelength λ_B can be changed by straining and adjusting its temperature. The variation of its Bragg central wavelength, $\Delta\lambda_B$, can be expressed as[38]

$$\Delta\lambda_B = 2\left(\Lambda\frac{\delta n_{eff}}{\delta l} + n_{eff}\frac{\delta\Lambda}{\delta l}\right)\Delta l + 2\left(\Lambda\frac{\delta n_{eff}}{\delta T} + n_{eff}\frac{\delta\Lambda}{\delta T}\right)\Delta T \tag{4.16}$$

where n_{eff} is the effective refractive index of the fiber core, Λ is the grating period, Δl is the grating variation strained, ΔT is the temperature variation of the grating. The first term in equation (4.16) represents the strain effect on an optical fiber and the second term represents the effect of temperature on an optical fiber. For the phase encoding SSFBG with multiple chips, it is difficult to dynamically modify the phase of every chip through straining the grating. Hence, we focus on the second term of the equation. It is clear that thermal expansion

shifts the Bragg wavelength by changing the grating period as well as the index of refraction. However, the thermo-optic coefficient for silica is higher than the thermal expansion coefficient. Thus, the index change dominates the overall effect. A fine heating element wrapped around the fiber grating can be employed to control this effect such that its Bragg wavelength is changed. The corresponding accumulated phase shift $\Delta\phi$ related to each Bragg wavelength variation at the chip boundary can be given by[36]

$$\Delta\phi \approx \frac{4\pi n_{\text{eff}}}{\lambda_{\text{B}}^2} \int_{-\Delta z/2}^{\Delta z/2} \Delta\lambda_{\text{B}}(T(z))\mathrm{d}z \tag{4.17}$$

where λ_{B} represents the grating initial Bragg wavelength, Δz denotes the length of the heated segment, $T(z)$ is the temperature shift at position z relative to the overall temperature of the uniform grating.

The schematic diagram of tunable 15 chip temporal phase encoder of SSFBG based on the aforementioned principle is shown in Fig. 4.46[36], which comprises a uniform fiber Bragg grating written using the continuous grating writing technique. It is mounted on a stretcher to allow flexible tuning of the overall grating initial center wavelength by hand, where one end is fixed and another end is movable. 16 parallel tungsten wires (18μm diameter) are positioned at equal spacing along the fiber-grating length. Thin wolfram wires are wrapped around the grating to ensure a uniform contact in a small confined area. Each tungsten wire connects a variable potentiometer in series. After a certain voltage is added by the circuit in series each grating segment is locally heated by altering the current in the wolfram wire such that the phase of each chip is changed and thus the SSFBG temporal phase encoder is tunable.

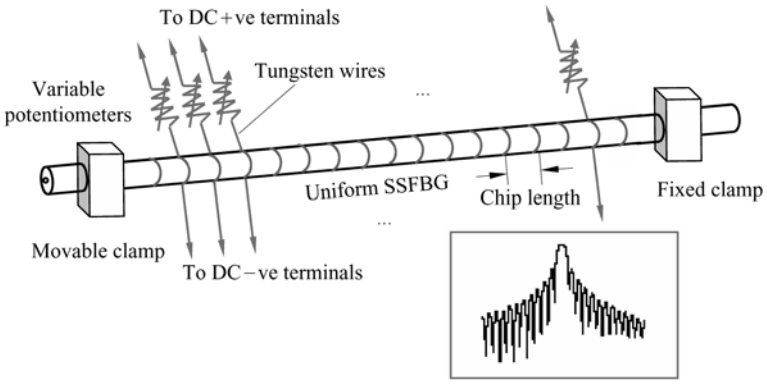

Figure 4.46 Schematic structure of tunable temporal-phase encoder based on SSFBG[36]

The required current values to alter the phase of back reflection light are determined beforehand by measuring the dynamic spectral performance of the grating during heating the core of the grating. It is found in the experiment that when the variations of phases are $\pi/2$, π and $3\pi/2$ respectively, the required current values are 30mA, 60mA and 90mA respectively. The measured function curve of the electric current in the tungsten wire versus the phase shifts in the experiment is shown in Fig. 4.47[35], where the error due to the resolution of the spectrum analyzer and the ammeter are also considered. However, the effects due to small misplacement of the wires from the appropriate positions along the fiber grating length can be considered negligible, as implied by the fact that their spectral profiles remain considerably constant for misplacement of up to 0.2mm.

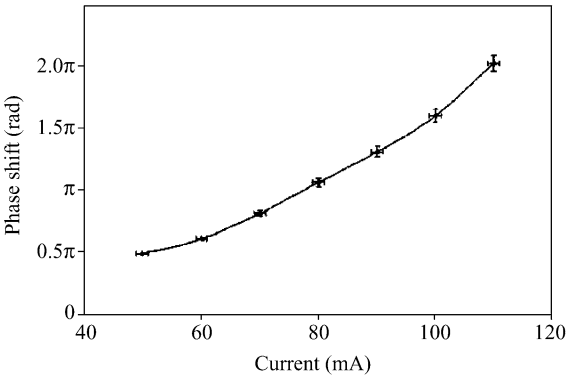

Figure 4.47 Phase shift as a function of electrical current (Current error bars correspond to the current source accuracy of ±0.5 mA; Phase shift error bars correspond to potential Bragg wavelength shifts due to change in the surrounding air temperature) (After Ref.[35])

The proposed and deep-investigated different types of encoding/decoding SSFBGs reported in the references in recent years are shown in Table 4.9. So far, the longest fixed optical encoder and decoder implemented by SSFBG are of 511-chip and the longest tunable encoder and decoder are of 15-chip.

Table 4.9 Different type of encoding/decoding SSFBGs employed in the experiments

Type of code	Type of encoder/ decoder	Code sequence	Code length (chip)	Chip length (mm)	Grating length (mm)	Chip duration (ps)	Temporal code duration (ps)	Peak reflectivity	Published in
Unipolar	Fixed	m-sequence	7	26.9	188.3	260	1820	8%	H. Geiger, et al, ECOC98, TuD10
Bipolar	Fixed	m-sequence	7	0.66	4.62	6.4	44.8	50%	A. Grunnet-Jepsen, et al, IEEE Photon. Tech Letts. 11,1283 (1999)

Continued

Type of code	Type of encoder/ decoder	Code sequence	Code length (chip)	Chip length (mm)	Grating length (mm)	Chip duration (ps)	Temporal code duration (ps)	Peak reflectivity	Published in
Bipolar	Tunable	m-sequence	7	5	35	50	350	75%	M. R. Mokhtar, et al, OFC'2002, ThGG54
Quaternary	Fixed	QPSK	15	5	75	50	750	57%	M. R. Mokhtar, et al, OECC'2002, PD-2-2
Quaternary	Tunable	QPSK	15	5	75	50	750	57%	M. R. Mokhtar, et al, OECC'2002, PD-2-2
Bipolar	Fixed	Gold code	63	0.66	41.58	6.4	403.2	20%	P. C. Teh, et al, OFC'2000, ThHH4-1
Quaternary	Fixed	QPSK	63	0.66	42.2	6.4	403.2	20%	P. C. Teh, et al, OFC'2001, PD37-1
Bipolar	Fixed	Gold code	127	0.64	83	6.4	812.8	79% (AP)	Xu Wang, et al, Optics Express, Vol.12, No.22, 2004, 5457 – 5468
Quaternary	Fixed	QPSK	255	0.33	84.4	3.2	816	25%	P. C. Teh, et al, OFC'2001, PD37-1
Bipolar	Fixed	Gold code	511	0.156	88	1.5	~800	92%	Xu Wang, et al, Optics Lett., 30, 355 – 357 (2005)

QPSK: quaternary-phase shift-keying; AP: apodized SSFBG

4.7 Summary

Optical encoding/decoding technology and optical encoder/decoder for OCDMA are the key technology and components to implement OCDMA communication and networking. In terms of operational principle, OCDMA encoding can be roughly categorized as incoherent encoding and coherent encoding. The incoherent coding is based on optical power intensity. Its typical schemes are the schemes of 2-D wavelength-hopping/time-spreading (WH/TS) encoding, 2-D bipolar/unipolar wavelength-time encoding, 2-D bipolar/bipolar encoding and 1-D spectral amplitude encoding, etc. 2-D WH/TS encoding is to perform simultaneously frequency-spreading in the time-domain and the wavelength-domain, which overcomes the disadvantages of the small numbers of users and simultaneous subscribers and the low dada bit rate that 1-D time-spreading encoding possesses. 2-D WH/TS encoding augments the code cardinality and reduces the code length significantly at the expense of increasing wavelength resources, which results in the enormous increasing of the numbers of users and simultaneous subscribers in a network, and the considerable enhancement of the data rate for each user. Meanwhile, when a network is designed, the compromise among the number of subscribers, the data bit rates of users and the network

resources (such as wavelength) can be made by utilizing two freedoms to design the users' address codes flexibly, in order to improve the efficiency of network resources, which conduces to much convenience for network design. 2-D bipolar/unipolar (B/U) wavelength-time encoding and bipolar/bipolar (B/B) wavelength-time encoding do not have the limitation of at most one-wavelength pulse onto one chip like 2-D WH/TS encoding such that their number of users and simultaneous subscribers can be further improved. Especially, for 2-D B/B wavelength-time encoding, a multi-wavelength codeword is also transmitted when a data bit is "0", which enhances the signal-interference ratio and improves the system performance, and furthermore, reinforces the security of transmitted information. However, the implementation of its optical encoder and decoder is complicated and the cost is relatively high at present. Thus, its practical application awaits for the progress of optoelectronic integrated technology and the drop of its cost. 2-D incoherent OCDMA system is well-suited for the applications of medium- and high-speed optical access network and local area network (LAN).

1-D spectral amplitude encoding (SAE) performs encoding by employing the bipolar code with good auto- and cross-correlation, such as m-sequences, Gold codes, Walsh-Hadamard codes, etc. At the receiving end, the balanced detection is employed to eliminate multiple-user interference. Particularly, 1-D SAE does not require the coherent optical source and only needs the incoherent-broadband optical source, such as light emitted diode (LED) so that the implementation cost is low. Therefore, 1-D SAE is well-suited for optical access network and local area network with medium data rate and low cost. With the progress of optical device and integrated technology, especially the increasing output optical power of the broadband LED, OCDMA with 1-D ASE will become one of practical schemes to realize optical access network and local area network with medium data rate.

The coherent encoding and decoding are based on optical field amplitude and a specific user's codeword is generally employed to encode the phase of optical signal, such as the spectral phase-encoded time-spreading using spatial light phase modulator (SLPM) and the temporal phase encoding with planar lightwave circuit (PLC) and superstructured fiber Bragg grating (SSFBG). With the advancement of techniques of light source, optical integration and FBG manufacturing, in recent years, the coherent encoding OCDMA has been receiving increasing attention from a large number of researchers and has made great progress. For example, 320 Gb/s capacity (32 Users×10 Gb/s) SPECTS (spectral phase-encoded time-spreading) OCDMA local area network testbed[39] using bulk optics implemented by University of California (Davis) was reported on OFC'2006, which was supported by DARPA. 8-chip spectral phase encoding/decoding subsystem[23] using Hadamard-Walsh code implemented by the integrated AWGs and phase-shifters was reported on ECOC'2005, which was accomplished by University of California, Davis, Lawrence Livermore National Laboratory and Royal Institute of Technology, Sweden. The experimental system[39] employing

511-chip SSFBG temporal-phase encoder and decoder implemented by National Institute of Information and Communications Technology(NICT) and Osaka University and Oki Electric Industry Co. of Japan was reported on OFC'2005, which implemented 10 asynchronous users with the data rate 1.25 Gb/s each user and the signal was transmitted over 50km-SMF. The experimental system[33] of temporal-phase encoding and decoding employing 255-chip and quarternary-phase code and the experimental system[37] of optical packet switching based on the OCDMA reconfigurable SSFBG encoder and decoder were implemented by University of Southampton, UK. It can be seen that the coherent OCDMA can realize transmission with high data rate. However, the implementation cost of coherent OCDMA is high because the coherent encoding requires the high-coherent, high-speed and ultrashort pulse light source, such as mode-locked laser, what is more, the spectral-phase time-spreading encoding/decoding also needs the light source with broadband so that the spectrum partition is carried out by encoding. Therefore, the cost of coherent OCDMA is still high so that the common family users in the subscriber access network can not afford it at present. It is relatively suitable for high-speed private network, such as military communication network. Also it can be employed to increase a multiplexing dimension or to implement optical code label switching in a core network. In other words, the coherent OCDMA has a promising application prospect for improving the network function in the private network, the high-speed metropolitan area network and the backbone network through combining with WDM and OTDM.

In addition, the optical encoder/decoder and subsystem with bulk-optic components not only have big size and high implementation cost but their performances are unstable. Thus, it is difficult for them to be widely employed in the future optical network. However, with the progress of technologies of planar light circuit (PLC) and fiber Bragg grating (FBG), it is possible that the practical, performance-reliable and small-size devices and systems can be implemented. Hence, the optical encoders/decoders and subsystems based on photonic-integrated and FBG represent the developing trends of OCDMA components and systems for the future.

In this chapter, the typical schemes, operational principles and recent research advances of optical encoding and decoding proposed in a large volume of literatures have been introduced systematically, which have come forth during the past approximate 20 years research course. At the same time, their advantages and disadvantages have been compared. It can be seen by our analysis and comparison that the 2-D wavelength-hopping/time-spreading en/decoding system and the bipolar spectral-amplitude en/decoding system with the balanced detection for the incoherent OCDMA, and the spectral-phase encoding time-spreading system and the temporal-phase encoding system for the coherent OCDMA are superior to other encoding/decoding schemes, and therefore, it is most possible for them to be used in practical applications.

References

[1] Paul R. Prucnal, Mario A. Santoro, and Ting Rui Fan：Spread Spectrum Fiber-optic Local Area Network Using Optical Processing. *IEEE/OSA Journal of Lightwave Technology*, Vol.4, No.5, May 1986, pp547 – 554

[2] J.-G. Zhang and G. Picchi: Tunable prime-code encoder/decoder for all-optical CDMA applications. *IEE Electronics Letters*, Vol. 29, No. 13, June 1993, pp1211 – 1212

[3] Hongxi Yin, Guangzhao Zhang, Shuwen Yang: Research of tunable optical orthogonal encoder/decoder for optical code-division multiplexing communications. *Journal of China Institute of Communications*, Vol.19, No.3, March 1998, pp85 – 90

[4] C-.K. Lee, J. Kim, and S-.W. Seo: Generation and performance analysis of the frequency-hopping optical orthogonal codes with arbitrary time blank patterns. in *Proceedings of IEEE International Conference on Communications*, 2001, pp.1275 – 1279

[5] Kyoungsik Yu, Jongyoon Shin, and Namkyoo Park: Wavelength-Time Spreading Optical CDMA System Using Wavelength Multiplexers and Mirrored Fiber Delay Lines. *IEEE Photonics Technology Letters,* Vol.12, No.9, 2000, pp1278 – 1280

[6] Lawrence R. Chen: Flexible Fiber Bragg Grating Encoder/Decoder for Hybrid Wavelength-Time Optical CDMA. *IEEE Photonics Technology Letters*, Vol.13, No.11, November 2001, pp1233 – 1235

[7] Sangin Kim: Cyclic Optical Encoders/Decoders for Compact Optical CDMA Networks. *IEEE Photonics Technology Letters*, Vol.12, No.4, 2000, pp428 – 430

[8] S. Yegnanarayanan, P. D. Trinh, and B. Jalali: Recirculating photonic filter: a wavelength-selective time delay for phased-array antennas and wavelength code-division multiple access. *Optics Letters*, Vol.21, No.10, May 1996, pp740 – 742

[9] Sangin Kim, Minjeong Kang, Soojin Park, Youngbok Choi, and Sangpil Han: Incoherent Bidirectional Fiber-Optic Code Division Multiple Access Networks. *IEEE Photonics Technology Letters*, Vol.12, No.7, July 2000, pp921 – 923

[10] D. Zaccarin, and M. Kavehrad: An Optical CDMA System Based on Spectral Encoding of LED. *IEEE Photonics Technology Letters*, Vol.4, No.4, April 1993, pp479 – 428

[11] M. Kavehrad, and D. Zaccarh: Optical Code-Division-Multiplexed Systems Based on Spectral Encoding of Noncoherent Sources. *IEEE/OSA Journal of Lightwave Technology*, Vol. 13, No. 3, March 1995, pp534 – 545

[12] Zou Wei, H. M. H. Shalaby, and H. Ghafouri-Shiraz: Modified Quadratic Congruence Codes for Fiber Bragg-Grating-Based Spectral-Amplitude-Coding Optical CDMA Systems. *IEEE/OSA Journal of Lightwave Technology*, Vol. 19, No. 9, September 2001, pp1274 – 1281

[13] Cedric F. Lam, Dennis T. K. Tong, Ming C. Wu, Eli Yablonovitch: Experimental Demonstration of Bipolar Optical CDMA System Using a Balanced Transmitter and Complementary Spectral Encoding. *IEEE Photonics Technology Letters*, Vol.10, No.10, October 1998, pp1504 – 1506

[14] Chao-Chin Yang, Jen-Fa Huang, Shin-Pin Tseng: Optical CDMA Network Codecs Structured With m-sequence Codes Over Waveguide-Grating Routers. *IEEE Photonics Technology Letters*, Vol.16, No.2, Feb. 2004, pp641 – 643

[15] Wing C. Kwong, Guu-Chang Yang, Yu-Chih Liu: A New Family of Wavelength-Time Optical CDMA Codes Utilizing Programmable Arrayed Waveguide Gratings. *IEEE Journal on Selected Areas in Communications*, Vol.23, No.8, August 2005, pp1564 – 1571

[16] I. Glesk, J. P. Sokoloff, and P. R. Prucnal: Demonstration of all-optical demultiplexing of TDM data at 250 Gb/s. *IEE Electronics Letters*, Vol. 30, No. 4, Feb. 1994, pp339 – 341

[17] J. H. Lee, P. C. Teh, P. Petropoulos, M. Ibsen, and D. Richardson: A grating-based OCDMA coding-decoding system incorporating a nonlinear optical loop mirror for improved code recognition and noise reduction. *IEEE/OSA Journal of Lightwave Technology*, Vol.20, No.1, Jan. 2002, pp36 – 46

[18] J. G. Proakis, Digital Communications, 3rd edition. New York: McGraw-Hill, 1995

[19] Wing C. Kwong, Guu-Chang Yang, Cheng-Yuan Chang: Wavelength-Hopping Time-Spreading Optical CDMA With Bipolar Codes. *IEEE/OSA Journal of Lightwave of Technology*, Vol.23, No.1, Jan 2005, pp260 – 267

[20] Jawad A. Salehi, Andrew M. Weiner, Jonathan P. Heritage: Coherent Ultrashort Light Pulse Code-Division Multiple Access Communication Systems. *IEEE/OSA Journal of Lightwave Technology*, Vol.8, No.3, Mar. 1990, pp478 – 491

[21] P. R. Prucnal, et. al.: Optical code division multiple access: fundamentala and applications. CRC Press, Taylao & Francis Group, 2006

[22] Chen Ji, R. G. Broeke, Y. Du, Jing Cao, N. Chubun, P. Bjeletich, F. Olsson, S. Lourdudoss, R. Welty, C. Reinhardt, P. L. Stephan, and S. J. B. Yoo: Monolithically Integrated InP-Based Photonic Chip Development for O-CDMA Systems. *IEEE Journal of Selected Topics in Quantum Electronics*, Vol.11, No.1, January/February 2005, pp66 – 77

[23] Jing Cao, R. G. Broeke, Chen Ji, Y. Du, N. Chubun, P. Bjeletich, T. Tekin, P. L. Stephan, F. Olsson, S. Lourdudoss, and S. J. B. Yoo: Spectral encoding and decoding of monolithic InP OCDMA encoder. ECOC'2005, pp501 – 502

[24] A. Grunnet-Jepsen, A.E. Johnson, E.S. Maniloff, T.W. Mossberg, M.J. Munroe and J.N. Sweetser: Fibre Bragg grating based spectral encoder/decoder for lightwave CDMA. *IEE Electronics Letters*, Vol.35, No.13, June 1999, pp1096 – 1097

[25] Wei Huang, Mohamed H. M. Nizam, Ivan Andonovic, Moshe Tur: Coherent Optical CDMA (OCDMA) Systems Used for High-Capacity Optical Fiber Networks-System Description, OTDMA Comparison, and OCDMA/WDMA Networking. *IEEE/OSA Journal of Lightwave Technology*, Vol. 18, No. 6, June 2000, pp765 – 778

[26] Naoya Wada, and Ken-Ichi Kitayama: A 10 Gb/s Optical Code Division Multiplexing Using 8-chip Optical Bipolar Code and Coherent Detection. *IEEE/OSA Journal of Lightwave Technology*, Vol.17, No.10, October 1999, pp1758 – 1765

[27] Xu Wang, Koji, Matsushima, Akihiko Nishiki, Naoya, Wada, and Ken-ichi Kitayama: High reflectivity superstructures FBG for coherent optical ode generation and recognition. *Optics Express*, Vol.12, No.22, 2004, pp5457 – 5468

[28] M. Ibsen, M. K. Durkin, M. J. Cole, M. N. Zervas, and R. I. Laming: Recent Advances in Long Dispersion Compensating Fiber Bragg Gratings. London, U.K: IEE, 1999

[29] M. Ibsen, M. K. Durkin, M. J. Cole, and R. I. Laming: Sinc-sampled fiber Bragg gratings for identical multiple wavelength operation. *IEEE Photonics Technology Letters*, Vol.10, June 1998, pp842 – 844

[30] Peh Chiong Teh, P. Petropoulos, M. Ibsen, and D. J. Richardson: A Comparative Study of the Performance of Sevenand 63-chip Optical Code-Division Multiple-Access Encoders and Decoders Based on Superstructured Fiber Bragg Gratings. *IEEE/OSA Journal of Lightwave Technology*, Vol.19, No.9, September 2001, pp1352 – 1365

[31] H.Geiger, A. Fu, P. Petropoulos, M. Ibsen, D. J. Richardson and R. I. Laming: Demonstration of a simple CDMA transmitter and receiver using sampled fiber gratings. in Tech. Proc. ECOC' 98, vol. 1, 1998, pp337 – 338

[32] A. Grunnet-Jepsen, A. E. Johnson, E. S. Maniloff, T. W. Mossberg, M. J. Munroe, and J. N. Sweetser: Demonstration of All-Fiber Sparse Lightwave CDMA Based on Temporal Phase Encoding. *IEEE Photonics Technology Letter*s, Vol.11, No.10, October 1999, pp1283 – 1285

[33] P. C. Teh, M. Ibsen, J. H. Lee, P. Petropoulos, and D. J. Richardson: Demonstration of a Four-Channel WDM/OCDMA System Using 255-Chip 320-Gchip/s Quarternary Phase Coding Gratings. *IEEE Photonics Technology Letters*, Vol.14, No.2, February 2002, pp227 – 229

[34] Xu Wang, Koji Matsushima and Ken-ichi Kitayama, Akihiko Nishiki, Naoya Wada, Fumito Kubota: High-performance optical code generation and recognition by use of a 511-chip, 640-Gchip/s phase-shifted superstructured fiber Bragg grating. *Optics Letters*, Vol. 30, No. 4, 2005, pp355 – 357

[35] M. R.Mokhtar, M. Ibsen, P. C. Teh, and D. J. Richardson: Simple dynamically reconfigurable OCDMA encoder/decoder based on a uniform fiber Bragg grating. OFC'2002, paper ThGG54

[36] M. R.Mokhtar, M. Ibsen, P. C. Teh, and D. J. Richardson: 16-bit multilevel reconfigurable phase encoder foe all optical header generation/recognition based on a Uniform Fiber Bragg Grating. In Proc. Optoelectronics and Communications Conference (OECC), 2002, PD-2-2

[37] C. Tian, Z. Zhang, M. Ibsen, M. R. Mokhtar, P. Petropoulos, D.J. Richardson: Reconfigurable All-Optical Packet Switching Based on Fiber Bragg Gratings. OFC'2005, OFJ4

[38] A. Othonos, K. Kalli: Fiber Bragg grating: Fundamentals and applications in telecommunications and sensing. Artech House Inc., 1999

[39] V. J. Hernandez, W. Cong, R. P. Scott, C. Yang, N. K. Fontaine, B. H. Kolner, J. P. Heritage, S. J. B. Yoo: 320 Gb/s Capacity (32 Users×10 Gb/s) SPECTS O-CDMA Local Area Network Testbed. OFC'2006, PDP45

[40] Xu Wang, Naoya Wada, Gabriella Cincotti, Tetsuya Miyazaki, and Ken-ichi Kitayama: Demonstration of Over 128 Gb/s Capacity (12-User 10.71 Gb/s/User) Asynchronous OCDMA Using FEC and AWG-Based Multiport Optical Encoder/Decoders. *IEEE Photonics Technology Letters*, Vol.18, No.15, 2006, pp1603 – 1605

[41] P.C. Teh, M. Ibsen, J.H. Lee, P. Petropoulos, and D. J. Richardson: A 4-channel WDM/OCDMA system incorporating 255-chip, 320 Gchip/s quaternary phase coding and decoding gratings. OFC'2001, PD37-1

5 Performance Analysis of OCDMA Communication Systems

5.1 Introduction

From the previous chapters we have learned that a typical OCDMA communication system can be shown as in Fig. 5.1. We assume that there are totally M subscribers implementing full duplex communication in an OCDMA network and N users are active and share the common channels at the same time. (In a practical network, all subscribers connected to a network are not always activated, especially in a subscriber access network and, as a matter of fact, the number of subscribers activated at the same time accounts for about 10% of the total number[1].) We suppose that if the j^{th} subscriber wants to send data information to the k^{th} user, the address code for receiver k is impressed upon the data by the encoder at the j^{th} node. One of the primary goals of OCDMA is to extract data with the desired optical pulse sequence in the presence of all other users' optical pulse sequences.

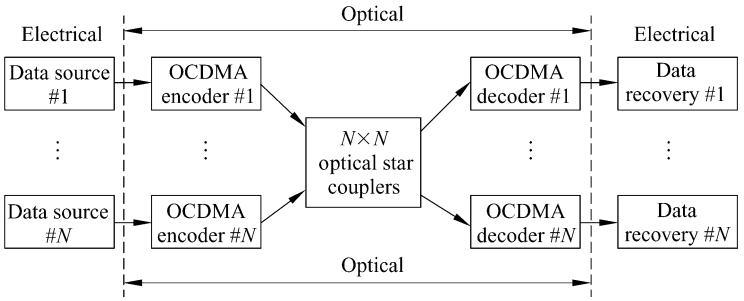

Figure 5.1 Schematic diagram of an OCDMA communication system with a star architecture

At the transmitting end, the periodic short light pulses emitted by light source are modulated by data source and each user in a network is allocated an unique address codeword. OCDMA encoder employing the address code encodes the optical pulse signal output from the electric-optical modulator, i.e., each data bit of output information is mapped into a time and/or wavelength, or spectral phase, or temporal phase sequence. Then, it is coupled into the fiber-optic channel.

At the receiving end, the SUM (correlation) or AND (chip-level) operation is carried out between the optical pulse sequence and the local address code, which has been stored in the optical decoder. After the optical-to-electrical conversion, sampling and threshold-decision of the output from the decoder, the data are retrieved. The main predominance of OCDMA is random and asynchronous communication access. Meanwhile, we expect that the number of simultaneous access subscribers in an OCDMA network is as large as possible under the condition that the requirement of user communication quality, i.e. the highest data rate and the lowest bit error rate (BER), is satisfied. Because the subscribers in a typical OCDMA network are confronted with the broadcast channels the signals transmitted from all subscribers in the network will arrive at every active receiver connected to the network. Therefore, the task for each receiver is how to effectively distinguish its targeted signal from the received signals, which blend with other untargeted signals, that is, the receiver should has strong capability to suppress multiple access interferences (MAIs) and beat noise. This ability depends on the properties of the subscriber address-code set chosen for the construction of network and the processing techniques of optical encoding/ decoding.

As far as the incoherent OCDMA network, the number of subscribers in a network and the quality of communication (BER) rely mainly on the performance of a set of address codes for users and the MAI is the restricted factor for improving system performance. With regard to the coherent OCDMA system, its performance lies on the beat noise besides MAIs. It has been shown by investigation[2] that if the address code with good properties is deployed, the beat noise is the primary factor to confine the performance of coherent OCDMA system. The BER of an OCDMA system is a function of data rate, the probability density function of any two interfering codes from a set of address codes for subscribers, the number of users in the system and the receiver decision-threshold and so on. The probability density function of any two interfering codes from a set of address codes chosen also depends on code length, code weight and code-constructed algorithm, which embodies the characteristic of distribution for “1” chip in the codes.

According to optical encoding based on the power or the field amplitude of optical signal, OCDMA systems are categorized into incoherent OCDMA and coherent OCDMA. From the viewpoint of employing one-dimensional or two-dimensional code for encoding, they are classified into one-dimensional OCDMA and two-dimensional OCDMA. OCDMA receivers are divided into the correlation (SUM) receiver and the chip-level (AND) receiver. The performances of systems with different encoding schemes and different constitution of receivers are very different. Because OCDMA theory and technology has been investigated for more than twenty years, various systems and performance analysis have been proposed in a great many references. Due to the limitation of length of the context, we can not introduce them one by one. In this chapter, we

only introduce the analyzing methods of the performance of five typical OCDMA systems, which are one-dimensional incoherent time-spreading OCDMA system, two-dimensional wavelength-hopping/time-spreading incoherent OCDMA system, spectral amplitude encoding incoherent OCDMA system with balanced detection, spectral phase encoding coherent OCDMA system and temporal phase encoding coherent OCDMA system.

This chapter is organized as follows. The performance analysis of one-dimensional incoherent OCDMA system is introduced in Section 5.2. The operational principle and performance of chip-level receiver is discussed in Section 5.3. Section 5.4 is devoted to the performance analysis of two-dimensional incoherent OCDMA communication system. The performance of spectral amplitude encoding incoherent OCDMA based on fiber-optic Bragg grating is analyzed in Section 5.5. Section 5.6 presents the performance analysis of spectral phase encoding coherent OCDMA. The performance of temporal phase encoding coherent OCDMA is studied in Section 5.7. At last, a brief summary is given in Section 5.8.

5.2 Performance Analysis of One-dimensional Time-spreading Incoherent OCDMA Communication System

An OCDMA network is expected to be able to accommodate many subscribers and simultaneous access users, and to have high data rate for each user and low bit error rate. However, since they are strongly associated with each other, the performance analysis of network becomes an issue of multiple target function description, which is very complex. For example, the numbers of subscribers and simultaneous access users allowed are related to a set of address codes chosen and the requirement of system bit error rate. Meanwhile, the performance of the address-code set again influences the user's data rate and system BER. Furthermore, the BER is associated with the user's data rate as well. In the following, we commence with the system performance analysis from the viewpoint of the system BER as a function of data rate, the address-code parameters, such as code length and code weight, the number of subscribers and the decision-threshold of receiver. The inherent relationship among these parameters will be revealed, which acts as a theoretical basis for the optimized design of the practical network. At the same time, two approaches to effectively reduce MAIs will be introduced here: one approach is to place an optical hard-limiter (OHL) before the desired correlator and another approach is to put one OHL before and after the optical decoder respectively. In this section, we firstly take one-dimensional $(n, w, \lambda) = (n, w, 1)$ optical orthogonal codes (OOC)[3] as an example to present the performance analysis method of one-dimensional incoherent OCDMA communication system based on Reference [4]. In the

analysis, we also assume that the on-off keying modulation is employed, which means that when data bit is "1" the encoded pulse sequence is transmitted and otherwise, when data bit is "0", no signal is sent. Meanwhile, it is assumed that the binary data bits "0" and "1" occur with equal-probability. Secondly, we will give the performance analysis of OCDMA system with double OHLs using photon count method based on Reference [5].

5.2.1 Modeling of One-dimensional Time-spreading Incoherent OCDMA System

In a typical OCDMA network where N transmitter and receiver pairs are simultaneously activated, for the sake of simplified analysis, we firstly assume as follows[4].

- The communication between the transmitters and receivers is pairwise and communications between the j^{th} transmitter and the j^{th} receiver is continuous for $1 \leqslant j \leqslant N$.
- For the sake of simplified analysis, the effects of quantum noise and thermal noise in the system are neglected and consequently, the performance degradation is caused by the presence of other user's interferences.
- The light sources in the network are all incoherent and therefore, the intensities of light signals that occur simultaneously are additive.
- All subscribers have the same effective average power at any receiver, identical bit rate and signal format.

Under such assumption, the output signal from optical encoder of the j^{th} user's transmitter is

$$s_j(t) = P_j \cdot b_j(t) c_j(t) \tag{5.1}$$

where P_j, $b_j(t)$ and $c_j(t)$ represent the j^{th} subscriber's transmitted optical signal intensity, binary data signal and OOC address codewords for $1 \leqslant j \leqslant N$.

The binary data signal $b_j(t)$ transmitted in succession by the j^{th} subscriber is

$$b_j(t) = \sum_{i=-\infty}^{\infty} b_{i,j} p_{T_b}(t - iT_b) \tag{5.2}$$

where $b_{i,j}$ denotes the i^{th} data bit in the data stream, which takes equiprobably on 0 or 1 for on-off keying and $p_{T_b}(t)$ indicates the rectangular pulse of duration T_b, which starts at $t = 0$. The data rate is $R_b = 1/T_b$.

$c_j(t)$ represents the j^{th} subscriber's address codeword, i.e., OOC (or called

signature sequence), which is given by

$$c_j(t) = \sum_{l=-\infty}^{\infty} c_{l,j}\, p_{T_c}(t - lT_c) \tag{5.3}$$

where $c_{l,j} \in \{0,1\}$ indicates the l^{th} chip of the address codeword, which satisfies $c_{l+n,j} = c_{l,j}$. It consists of n chips (or called slots) and the temporal width for each chip is $T_c = T_b / n$. $p_{T_c}(t)$ represents the rectangular pulse of duration T_c. The schematic diagram of generated $s_j(t)$ is shown in Fig. 5.2.

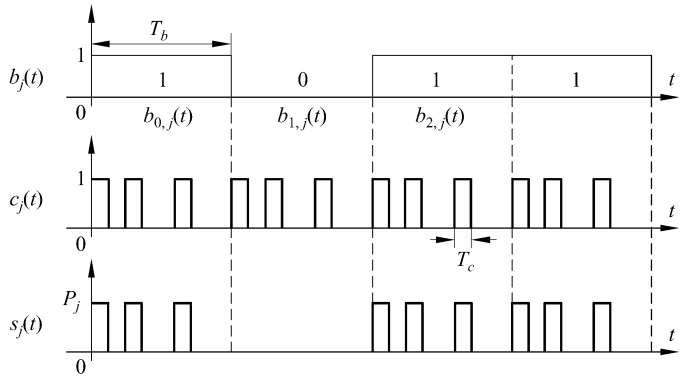

Figure 5.2 Binary data signal $b_j(t)$, signature signal $c_j(t)$ and OCDMA output signal $s_j(t)$ for j^{th} user

The received signal at the front end of each receiver, $r(t)$, is directly superimposing of N signals transmitted by subscribers, which is given by[4]

$$r(t) = \sum_{j=1}^{N} s_j(t - \tau_j) = \sum_{j=1}^{N} b_j(t - \tau_j) c_j(t - \tau_j) \tag{5.4}$$

where τ_j denotes the relative transmission time-delay of the j^{th} subscriber's signal, which is an uniformly distributed random variable on $[0, T_b]$. Because of the assumption mentioned previously, for the sake of simplicity, we have presumed $P_j = 1$ in (5.4) for $1 \leqslant j \leqslant N$. $\tau_j = 0$ can be assumed in the analysis of the receiver that is matched to the j^{th} user's signal. For notation simplicity and with no loss in generality, we suppose the desired subscriber's signal is expressed by $j = 1$ in (5.4). Then, Fig. 5.3 shows the receiver block diagram for subscriber 1, where z_1 is the sampling output of the receiver at time $t = T_b$. The resultant of the j^{th} subscriber's signal on the first receiver is indicated by $I_{j,1}$.

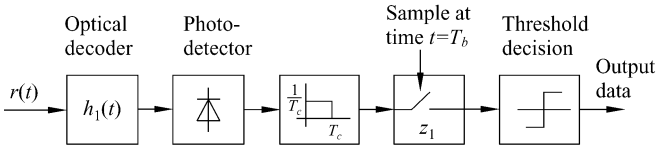

Figure 5.3 Block diagram of the receiver for the j^{th} transmitter in OCDMA (After Ref. [4])

Thus, the output of the first subscriber's correlator at time T_b, z_1, can be expressed by[4]

$$z_1 = \frac{1}{T_c}\int_0^{T_b} r(t)c_1(t)\mathrm{d}t = b_{0,1}w + \sum_{j=2}^{N} I_{j,1} = b_{0,1}w + I_1 \tag{5.5}$$

where $b_{0,1}$ indicates the 0^{th} data of the 1^{th} subscriber, which takes equiprobaly 0 or 1. The first term $b_{0,1}w$ in (5.5) is the desired signal term and the second term $I_1 = \sum_{j=2}^{N} I_{j,1}$ denotes the total interference signal that is the undesired signal term, which consists of $(N-1)$ interfering signals $I_{j,1}$, where each $I_{j,1}$ is a random variable and its mean and variance are $m_{I_{j,1}}$ and $\sigma^2_{I_{j,1}}$ respectively. If $I_{j,1}$ is independent and identically distributed random variables, then the mean and variance of the total interference signal I_1 are represented respectively as

$$m_{I_1} = (N-1)m \tag{5.6a}$$

$$\sigma^2_{I_1} = (N-1)\sigma^2 \tag{5.6b}$$

where for $2 \leqslant j \leqslant N$, there exist $m = m_{I_{j,1}}$ and $\sigma^2 = \sigma^2_{I_{j,1}}$.

5.2.2 Performance analysis of OCDMA System Using One-dimensional OOC

5.2.2.1 Probability Density Functions of Interference Signal I_1 for Cases of Chip Synchronization and Ideal Chip Asynchronization

In order to obtain the bit error rate for the first receiver, we need to find out the probability density function for the interference signal I_1. However, before doing so, we are required to get the probability density function for each $I_{j,1}$ for $2 \leqslant j \leqslant N$ first of all, whose total number is $(N-1)$. For an $N \times N$ network

where there are N transmitters and N receivers, $N(N-1)/2$ probability density functions need to be found out, which is lengthy and tedious especially for large N. Hence, for the sake of analysis simplicity, we give the upper bound and the lower bound on BER based on two extreme cases that are chip synchronous case and ideal chip asynchronous case[3]. The chip synchronization refers to the case of two interfering OOC's with shifts that are integer multiples of T_c, where the chip synchronous interference is a pessimistic approximation to the actual interference. The ideal chip asynchronization refers to the case that two OOC's have no adjacent pulses with respect to each other, i.e., the case that the random shifts of two interfering OOC's are not integer multiples of T_c, where the ideal chip asynchronous interference is an optimistic approximation to the actual interference. The actual inference of two OOC's should be between them. For mathematical convenience, we will employ the probability density functions associated with the chip synchronous, (A), and ideal chip asynchronous, (B), as the basis for evaluating the probability density function for $(N-1)$ interfering OOC's, that is,

$$P_{\mathrm{b}}(\text{Chip synchronous}) \leqslant P_{\mathrm{b}}(\text{Exact}) < P_{\mathrm{b}}(\text{Ideal chip asynchronous})$$

Since the interference signal I_1 is the sum of $(N-1)$ independent identically distributed random variable $I_{j,1}$, the probability density function of I_1, $P_{I_1}(I_1)$, should be the convolution of the probability density functions of random variables $I_{j,1}$, $P_{I_{j,1}}(I_{j,1})$, for $2 \leqslant j \leqslant N$.

(1) Chip Synchronous Case

For the chip synchronous case, the probability density function (PDF) of the interfering signal $I_{j,1}$ can be given by[3, 4]

$$P_{I_{j,1}}(I_{j,1}) = \left(1 - \frac{w^2}{2n}\right)\delta(I_{j,1}) + \frac{w^2}{2n}\delta(I_{j,1} - 1) \tag{5.7}$$

where n and w are code length and code weight of OOC respectively, and $\delta(\cdot)$ represents Dirac's delta function. From the convolution of (5.7), the resulting probability density function of interference signal I_1 from the first receiver is given by [4]

$$P_{I_1}(I_1) = \sum_{i=0}^{N-1} \binom{N-1}{i} \left(\frac{w^2}{2n}\right)^i \left(1 - \frac{w^2}{2n}\right)^{N-1-i} \delta(I_1 - i) \tag{5.8}$$

(2) Ideal chip asynchronous case

For the ideal chip asynchronous case, the probability density function of two interfering OOC's can be given by[3, 4]

$$P_{I_{j,1}}(I_{j,1}) = \left(1 - \frac{w^2}{2n}\right)\delta(I_{j,1}) + \frac{w^2}{n}|\overline{I_{j,1}}| \tag{5.9}$$

where

$$|\overline{I_{j,1}}| = \begin{cases} 1 & 0 < I_{j,1} < 1 \\ 0 & \text{elsewhere} \end{cases} \tag{5.10}$$

then, the resulting probability density function of interfering signal I_1 from the first receiver is given by[4]

$$P_{I_1}(I_1) = q^{N-1}\delta(I_1) + (N-1)pq^{N-2}\left|\overline{I_1}\right| + \binom{N-1}{2}p^2q^{N-3}f(I_1)$$

$$+\sum_{i=3}^{N-1}\binom{N-1}{i}p^i q^{N-1-i}G\left(\frac{i}{2},\frac{i}{12}\right) \tag{5.11}$$

where $p = w^2/2n$, $q = 1 - w^2/2n$,

$$\left|\overline{I_1}\right| = \begin{cases} 1 & 0 < I_1 < 1 \\ 0 & \text{elsewhere} \end{cases} \tag{5.12}$$

$$f(I_1) = \begin{cases} 1 - |I_1 - 1| & 0 \leqslant I_1 \leqslant 2 \\ 0 & \text{elsewhere} \end{cases} \tag{5.13}$$

and $G\left(\frac{i}{2},\frac{i}{12}\right)$ indicates the Gaussian probability density function with mean $i/2$ and variance $i/12$, which is

$$G\left(\frac{i}{2},\frac{i}{12}\right) = \frac{1}{\sqrt{2\pi}\sqrt{\frac{i}{12}}}\exp\left[-\left(I_1 - \frac{i}{2}\right)^2 \Big/ \left(\frac{i}{6}\right)\right] \tag{5.14}$$

5.2.2.2 Upper and Lower Bound on BER of One-dimensional Time-spreading Incoherent OCDMA System

The exact expression of probability of error bit for the binary data communication system is

$$P_{\mathrm{b}} = P_r\left(Z_1 \geqslant Th / b_{0,1} = 0\right) \cdot P_r\left(b_{0,1} = 0\right) + P_r\left(Z_1 < Th / b_{0,1} = 1\right) \cdot P_r\left(b_{0,1} = 1\right) \tag{5.15}$$

where Th indicates the decision-threshold for the detector. If the decision-threshold is set as $0 \leqslant Th \leqslant w$, the second term in (5.15) is zero because

$P_r\left(Z_1 < Th / b_{0,1} = 1\right) = P_r(w - Th + I_1 < 0) = P_r(\eta < 0)$, where $\eta = w - Th + I_1$ is a random variable defined to be nonnegative, which cannot take on any negative value. Therefore, when $b_{0,1} = 1$, the probability of error is zero. In this way, the only remaining from (5.15) is the first term, which corresponds to the probability of error of $b_{0,1} = 0$. Hence, the probability of error bit is given by[4]

$$P_{\mathrm{b}} = \frac{1}{2}\int_{Th}^{\infty} P_{I_1}(I_1)\mathrm{d}I_1 \tag{5.16}$$

(1) Upper bound on Probability of Error Bit for the System

From the chip synchronous case, the upper bound on system BER can be obtained. Substituting (5.8) into (5.16), we have

$$P_{\mathrm{b}} = \frac{1}{2}\int_{Th}^{\infty} P_{I_1}(I_1)\mathrm{d}I_1 = \frac{1}{2}\int_{Th}^{\infty}\sum_{i=0}^{N-1}\binom{N-1}{i}\left(\frac{w^2}{2n}\right)^i\left(1-\frac{w^2}{2n}\right)^{N-1-i}\delta(I_1 - i)\mathrm{d}I_1$$

After the orders of integral and sum operations are exchanged, the resulting upper bound on system BER is given by[4]

$$P_{\mathrm{b}}^{\mathrm{upper}} = \frac{1}{2}\sum_{i=Th}^{N-1}\binom{N-1}{i}\left(\frac{w^2}{2n}\right)^i\left(1-\frac{w^2}{2n}\right)^{N-1-i} \tag{5.17}$$

It can be seen that the BER, P_{b}, is a function of the number of simultaneous communication subscribers, code length n and code weight w of address code, and decision-threshold of receiver. Figure 5.4(a) shows the curves of system BER versus the decision-threshold Th and code weight w for a fixed number of subscribers ($N = 10$) and code length ($n = 1000$). It reveals that ① the BER P_{b} degrades obviously as the Th increases and when $Th = w$, P_{b} achieves its least value, and therefore, the optimal decision-threshold is $Th = w$; ② with the increasing of code weight w, the system BER performance is improved a lot. For example, when $Th = w = 6$, BER is 1.36×10^{-9}, and when $Th = w = 8$, BER is 4.81×10^{-12}. Thus, the BER is improved for about three orders of magnitude. Theoretically, when the code weight w is greater than or equal to the number of subscribers N, the BER is zero if the quantum noise and thermal noise of a receiver are not considered. Figure 5.4(b) gives the curves of system BER versus the number of simultaneous subscribers N and code length n when the receiver employs the optimal decision-threshold $Th = w = 7$. It can be observed from this figure that ① with the increasing of the number of simultaneous subscribers N, P_{b} increases, i.e., the system BER performance decreases, and this is because the MAIs in the system increases as the number of users augments; ② the system

BER decreases as the code length n increases. This is because for a fixed code weight w, when the code length n increases the likelihood of mutual hits among the pulses (i.e., "1"chip) in codewords, would decrease. For instance, when the number of simultaneous subscribers in the system is $N=20$, the corresponding BER of the system for $n=1000$ is 1.03×10^{-7}. Moreover, the system BER for $n=1500$ is 6.57×10^{-9} and the system BER with $n=2000$ is 9.16×10^{-10}.

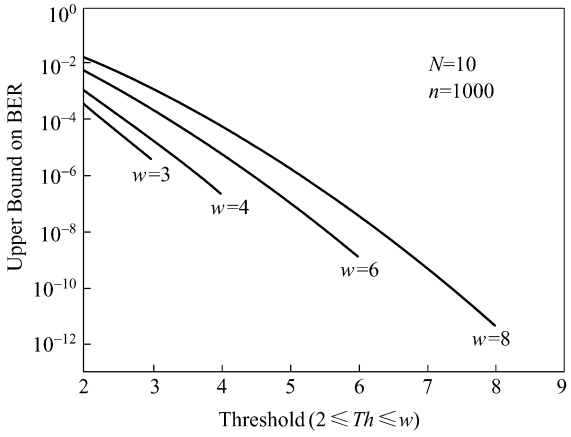

(a) N =10 and n =1000,w =3,4,6 and 8

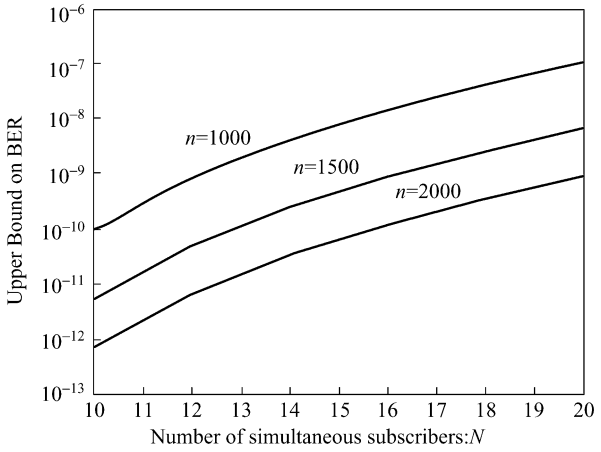

(b) the optimum decision threshold $Th = w$ =7, n =1000, 1500 and 2000

Figure 5.4 Upper bound curves on bit error rate performance

(2) Lower Bound on System BER

From the ideal asynchronous case, the lower bound on the system BER can be obtained. Substituting (5.11) into (5.16), we have[4]

$$
\begin{aligned}
P_{\mathrm{b}}^{\mathrm{lower}} &= \frac{1}{2}\int_{Th}^{\infty} P_{I_1}(I_1)\mathrm{d}I_1 \\
&= \frac{1}{2}\Bigg[q^{N-1}\int_{Th}^{\infty}\delta(I_1)\mathrm{d}I_1 + (N-1)pq^{N-2}\int_{Th}^{\infty}\left|\bar{I}_1\right|\mathrm{d}I_1 + \binom{N-1}{2}p^2q^{N-3}\int_{Th}^{\infty} f(I_1)\mathrm{d}I_1 \\
&\quad + \sum_{i=3}^{N-1}\binom{N-1}{i}p^i q^{M-1-i}\int_{Th}^{\infty} G\left(\frac{i}{2},\frac{i}{12}\right)\mathrm{d}I_1 \Bigg] \\
&= \frac{1}{2}\Bigg[q^{N-1}\int_{Th}^{\infty}\delta(I_1)\mathrm{d}I_1 + (N-1)pq^{N-2}\int_{Th}^{\infty}\left|\bar{I}_1\right|\mathrm{d}I_1 + \binom{N-1}{2}p^2q^{N-3}\int_{Th}^{\infty} f(I_1)\mathrm{d}I_1 \\
&\quad + \sum_{i=3}^{N-1}\binom{N-1}{i}p^i q^{M-1-i}\cdot \mathrm{erfc}\left(\frac{Th-\frac{i}{2}}{\sqrt{\frac{i}{12}}}\right)\Bigg]
\end{aligned}
\tag{5.18}
$$

where $\mathrm{erfc}(x)$ indicates the Error Function that is defined as

$$
\mathrm{erfc}(x) \equiv \frac{1}{\sqrt{2\pi}}\int_{x}^{\infty}\exp\left(-\frac{y^2}{2}\right)\mathrm{d}y \tag{5.19}
$$

Figure 5.5 shows the comparative curves of the upper and lower bounds of system BER for the chip synchronous and the ideal chip asynchronous cases. It can be observed that in comparison with the BER for the chip synchronous case, the system BER for the ideal chip asynchronous case has been improved for two

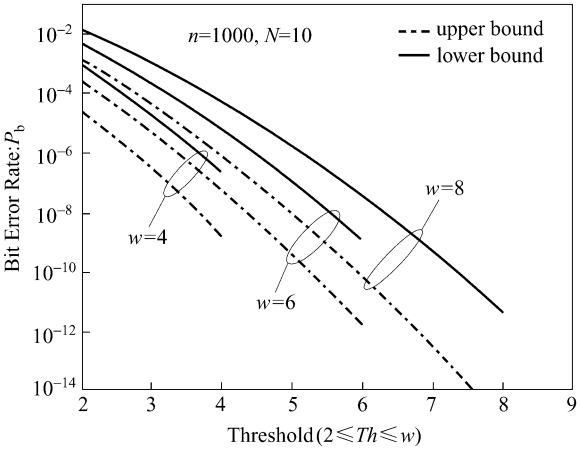

Figure 5.5 Comparison between the lower bound and the upper bound on bit error rate performance versus threshold for $N = 10$, $n = 1000$, and $w = 4, 6, 8$

to three orders of magnitude. For instance, when the code weight is $Th = w = 6$, the BER's for these two cases are 1.36×10^{-9} and 1.78×10^{-12} respectively, and the difference is about three orders of magnitude. The BER performance for the practical system should be between those for these two cases. Therefore, if an OCDMA system is designed based on the requirement of BER for the chip synchronous case then it will be too conservative.

5.2.2.3 System BER Using Optical Hard-limiter for Chip Synchronous and Ideal Chip Asynchronous Cases

The approach to improve the system performance is to degrade the intensity of interference signal, which can be implemented by placing an optical hard-limiter (OHL) before the optical decoder of OCDMA receiver[4], shown in Fig. 5.6. For an ideal OHL, when the intensity of input optical signal is x, its output response $g(x)$ is given by[4]

$$g(x)=\begin{cases}1 & x\geqslant 1\\ 0 & 0\leqslant x<1\end{cases} \tag{5.20}$$

The action of this device is that when the intensity of input optical signal x is greater than or equal to 1 (normalized value), the optical hard-limiter would clip the intensity back to 1. When the intensity of input optical signal is less than 1, its response is zero. In doing so, some combinations of interference patterns that cause errors can be excluded before the optical decoder carries out correlation operation to the signal so that the system performance will be improved significantly.

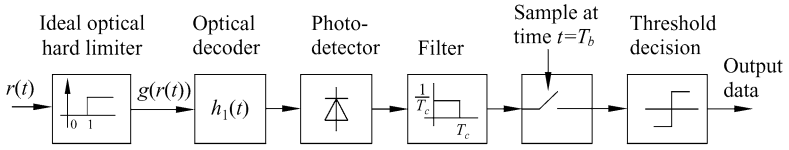

Figure 5.6 OCDMA receiver with an ideal optical hard limiter (After Ref.[4])

After the optical hard-limiter is employed, the interference I_1 at the output of the optical decoder of the first subscriber is given by[4]

$$I_1=\frac{1}{T_c}\int_0^{T_b} g(I_1(t))c_1(t)\mathrm{d}t=\sum_{l=0}^{n-1}V_{l,1}c_{l,1} \tag{5.21}$$

where $I_1(t)\equiv\sum_{j=2}^{N}s_j(t-\tau_j)$ and the random variable $V_{j,1}$ is defined as[4]

$$V_{j,1}=\frac{1}{T_c}\int_{jT_c}^{(j+1)T_c} g(I_1(t))\mathrm{d}t \tag{5.22}$$

(1) Chip Synchronous Case

For the chip synchronous case, the random variable $V_{j,1}$ is[4]

$$V_{j,1} \equiv \begin{cases} 1 & \text{if } I_1(t) \geqslant 1 \text{ for } jT_c \leqslant t \leqslant (j+1)T_c \\ 0 & \text{if } I_1(t) = 0 \text{ for } jT_c \leqslant t \leqslant (j+1)T_c \end{cases} \tag{5.23}$$

Then, the probability density function of the random variable $V_{j,1}$ is given by[4]

$$P_{V_{j,1}}(V_{j,1}) = q'\delta(V_{j,1}) + p'\delta(V_{j,1} - 1) \tag{5.24}$$

where $q' \equiv P_r[I_1(t) = 0 \text{ for } jT_c \leqslant t \leqslant (j+1)T_c] = 1 - q^{N-1}$,

$$\begin{aligned} p' &\equiv P_r[I_1(t) \geqslant 1 \text{ for } jT_c \leqslant t \leqslant (j+1)T_c] \\ &= 1 - P_r[I_1(t) = 0 \text{ for } jT_c \leqslant t \leqslant (j+1)T_c] = 1 - q', \\ q &= 1 - \frac{w}{2n}, \quad p = \frac{w}{2n}. \end{aligned}$$

Employing the method similar to that in the Subsection above, the resulting BER of the system with an optical hard-limiter is[4]

$$P_{\mathrm{b}}^{\mathrm{upper}} \leqslant \frac{1}{2}\binom{w}{Th}\prod_{m=0}^{Th-1}(1 - q^{N-1-m}) \tag{5.25}$$

Figure 5.7 gives the comparative curves of upper bounds on BERs of systems with and without an ideal OHL versus the decision-threshold *Th* and code

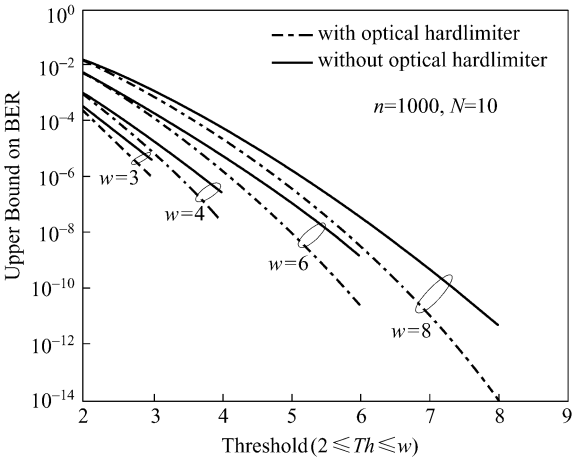

Figure 5.7 Upper bound curves on bit error rate performance for the two cases with and without an ideal optical hard-limiter versus the decision threshold *Th* and code weight *w* when $n = 1000$ and $N = 10$

weight w under chip synchronous case while the number of simultaneous subscribers in the network and the code length of address code used are $N = 10$ and $n = 1000$ respectively. It can be seen that the BER performance has been improved greatly after an ideal OHL is employed. For instance, when $Th = w = 6$, the BER for the system without an ideal OHL is 1.36×10^{-9}, and however, the BER for the system using an ideal OHL is 2.10×10^{-11}. As a result, the BER for the latter has been improved for two orders of magnitude.

(2) Ideal Chip Asynchronous Case

For the ideal chip asynchronous case, the random variable $V_{j,1}$ is defined as[4]

$$V_{j,1} \equiv \begin{cases} 0 < V_{j,1} \leqslant 1 & \text{if } I_1(t) > 0 \text{ for } jT_c \leqslant t \leqslant (j+1)T_c \\ 0 & \text{if } I_1(t) = 0 \text{ for } jT_c \leqslant t \leqslant (j+1)T_c \end{cases} \tag{5.26}$$

Then, the probability density function of the random variable $V_{j,1}$ is[4]

$$P_{V_{j,1}}(V_{j,1}) = q'\delta(V_{j,1}) + p' \mid \overline{V_{j,1}} \mid \tag{5.27}$$

where $q' \equiv P_r[I_1(t) = 0 \text{ within a chip time}] = q^{N-1}$,

$$p' \equiv P_r[I_1(t) > 0 \text{ within a chip time}] = 1 - q^{N-1},$$

$$q = 1 - \frac{w}{n} = 1 - p.$$

Hence, the BER for the system with an optical hard-limiter is given by[4]

$$P_{\mathrm{b}}^{\mathrm{lower}} \leqslant \frac{1}{2}\binom{w}{Th}\prod_{m=0}^{Th-1}\left\{1 - \left[q^{N-1-m} + (N-1-m)pq^{N-2-m} + \sum_{i=2}^{N-1-m}\binom{N-1-m}{i} p^i q^{N-1-i-m}\left(1 - Q\left(\frac{1-\frac{i}{2}}{\sqrt{\frac{i}{12}}}\right)\right)\right]\right\} \tag{5.28}$$

Figure 5.8 gives the curves of lower bound on BERs of systems with and without an ideal OHL versus the decision-threshold Th and the number of simultaneous subscribers N for the ideal chip asynchronous case, where $n = 1000$ and $w = 5$. It can be observed that the performance of system with an ideal OHL has been improved significantly. For example, when $Th = w = 5$ and $N = 40$, the BER for a system without an ideal OHL is 1.28×10^{-6} and otherwise,

the BER for a system with an ideal OHL is 1.35×10^{-11}. Therefore, the system BER has been improved for about five orders of magnitude.

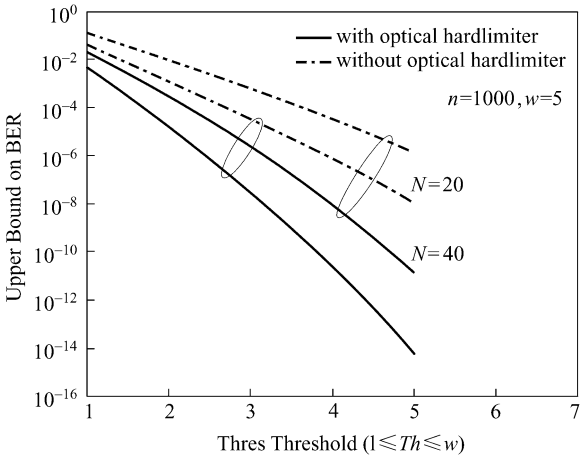

Figure 5.8 Lower bound curves on bit error rate performance for the two cases with and without an ideal optical hard-limiter versus the decision threshold *Th* and the number of simultaneous subscribers *N* when $n = 1000$ and $w = 5$

5.2.2.4 Upper Bound on BER of System Employing Double Optical Hard-limiters

When a desired subscriber sends data bit "0", some interference patterns cannot be completely removed by only placing single optical hard-limiter before the optical correlator. In order to improve system performance further, double optical hard-limiters can be employed, that is, we can place one optical hard-limiter before the correlater and another after it. In the following, let's analyze the BER performance of one-dimensional time-spreading incoherent OCDMA system with double optical hard-limiter by using photon-count technique in this section. In addition, the quantum noise and thermal noise are neglected in the analysis of the above two subsections. In this section, Poisson shot noise model will be employed for the receiver photodetector noise caused by photodetector dark current. Because it is assumed that it is a chip synchronous case, the obtained result is the upper bound on the system BER.

One-dimensional time-spreading correlation OCDMA system with double optical hard-limiter is shown in Fig. 5.9. For optical hard-limiter, when the intensity of its input optical signal is bigger than or equal to its threshold level, its output would be clipped to a fixed value. When its input optical signal is less than its threshold level, its output would be zero. The first optical hard-limiter would clip the received optical signal intensity back to a fixed value so that it can reduce the channel interference by other undesired interferer's pulses. The second optical hard-limiter would clip the optical intensity of output from the

optical decoder. If the optical intensity of the optical decoder output is less than OHL's threshold level it would be clipped back to zero. In doing so, the system BER will be further reduced.

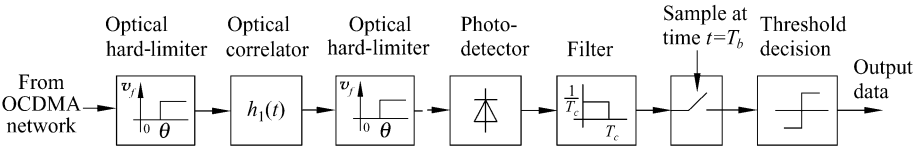

Figure 5.9 Receiver schematic diagram of a direct-detection OCDMA system with double hard-limiters (After Ref. [5])

Under the assumption of Poisson shot noise model for the receiver photodetector where the noise due to the detector dark currents exists, the photon-count over the last chip of the first subscriber's receiver is modeled as a conditional Poisson random variable, Y_1, which is[5]

$$Y_1 = Z_1 + X_1 + W_1 \tag{5.29}$$

where Z_1 and X_1 indicate conditional independent Poisson photon-counts due to the desired signal and the multiple access interference. W_1 represents a Poisson photon-count due to the detector dark current noise. Since the direct detection is employed, the optical signal and the optical noise are additive in the intensity. Let λ_0 be the noise photon rate so that the statistical mean of W_1 is[5]

$$E[W_1] = \lambda_0 T_c$$

where T_c is the chip time. The Poisson random variable Z_1 for the first subscriber relies only on the data $b_{j,1} \in \{0,1\}$ and its conditional mean, which are[5]

$$E[Z_1 \mid b_{j,1} = 1] = w\lambda_s T_c$$
$$E[Z_1 \mid b_{j,1} = 0] = 0$$

where $w\lambda_s$ is the signal photon rate from the output of optical decoder.

The output of the optical hard-limiter is defined as[5]

$$g(x) = \begin{cases} v_f = w\lambda_s T_c & x \geqslant Th \\ 0 & 0 \leqslant x < Th \end{cases} \tag{5.30}$$

where $Th = w\lambda_s T_c$. κ_i is employed to denote the number of hits between the i^{th} "1" chip of the desired subscriber signal and $(N-1)$ undesired interferers' "1" chips for $i = 1, 2, \cdots, w$. And let

$$\boldsymbol{\kappa} \equiv (\kappa_1, \kappa_2, \cdots, \kappa_w)$$

indicate the interference state pattern, $|\boldsymbol{\kappa}|$ denote the number of nonzero elements in $\boldsymbol{\kappa}$ and I_1 represent the total sum of κ_i. Also let

$$\boldsymbol{\xi} \equiv (\xi_1, \xi_2, \cdots, \xi_w)$$

be the normalized interference state pattern, where

$$\xi_i = \begin{cases} 1 & \text{if } \kappa_i \neq 0 \\ 0 & \text{otherwise} \end{cases}$$

and they satisfy $\sum_{i}^{w} \xi_i = |\boldsymbol{\kappa}|$.

The performances of the systems with single optical hard-limiter and double optical hard-limiters rely on $|\boldsymbol{\kappa}|$ and I_1 while the performance of the system without optical hard-limiter depends only on I_1.

For the chip synchronous case, the probability density function of I_1 before the first optical hard-limiter is given by [3]

$$p_{I_1}(I_1) = \sum_{i=0}^{N-1} \binom{N-1}{i} p^i q^{N-1-i} \delta(I_1 - i) \tag{5.31}$$

where $p = w^2/2n$, $q = 1 - w^2/2n$ and $\delta(\cdot)$ is Dirac's delta function.

Each subscriber is equally likely to incur interference at any one of the w "1" chip positions, which is independent of all other users. The interference state pattern vector $\boldsymbol{\kappa}$ obeys a multinomial distribution. The probability that it has $|\boldsymbol{\kappa}|$ nonzero elements, $|\boldsymbol{\kappa}| = 0,1,\cdots,\min(w, I_1)$, can be expressed as[5]

$$P_r(|\boldsymbol{\kappa}| = \alpha \mid I_1) = \sum_{\substack{\boldsymbol{\kappa} \in G_{I_1} \\ |\boldsymbol{\kappa}| = \alpha}} \mathrm{NDP}(\boldsymbol{\kappa}) P_r(\boldsymbol{\kappa}, F_{I_1}) \tag{5.32}$$

where F_{I_1} indicates the set of all interference pattern vectors with total weight equal to I_1, G_{I_1} is the set of representative interference vectors in F_{I_1} with elements in decreasing order and $\mathrm{NDP}(\boldsymbol{\kappa})$ denotes the number of distinct permutations of vector $\boldsymbol{\kappa}$ in G_{I_1}, which is given by[5]

$$\mathrm{NDP}(\boldsymbol{\kappa}) = \frac{w!}{\prod_i R(\kappa_i)!} \tag{5.33}$$

where $R(\kappa_i)!$ is the number of repetition times of an element κ_i in the vector $\boldsymbol{\kappa}$, the product is taken over i for which κ_i are different and $P(\boldsymbol{\kappa}; F_{I_1})$ is the multinomial distribution for the interference pattern vector $\boldsymbol{\kappa}$ in F_{I_1}, which is

represented as[5]

$$P(\boldsymbol{\kappa};F_{I_1})=\frac{I_1!}{w^{I_1}\times\prod_{i=1}^{w}(\kappa_i!)} \tag{5.34}$$

Example 5.1[5] Assume that $I_1=6$, $w=3$ and $|\boldsymbol{\kappa}|=3$. The set G_6 consists of seven distinct vectors, which are (6,0,0),(5,1,0),(4,2,0),(4,1,1),(3,3,0),(3,2,1),(2,2,2). Among these vectors, three vectors have $|\boldsymbol{\kappa}|=3$ nonzero elements, which are (4,1,1),(3,2,1),(2,2,2). The number of distinct permutations of these vectors are as follows:

$$\begin{aligned}
\mathrm{NDP}(4,1,1)&=\frac{3!}{1!2!}=3,\\
\mathrm{NDP}(3,2,1)&=\frac{3!}{1!1!1!}=6,\\
\mathrm{NDP}(2,2,2)&=\frac{3!}{3!}=1.
\end{aligned}$$

Therefore, the multinomial probability distributions for these vectors are

$$\begin{aligned}
P((4,1,1);F_6)&=\frac{6!}{3^6\times 4!1!1!},\\
P((3,2,1);F_6)&=\frac{6!}{3^6\times 3!2!1!},\\
P((2,2,2);F_6)&=\frac{6!}{3^6\times 2!2!2!}.
\end{aligned}$$

Hence, the probability that an interference pattern has $|\boldsymbol{\kappa}|=3$ nonzero elements, $P_r(|\boldsymbol{\kappa}|=3;I_1=6)$, is expressed as

$$\begin{aligned}
P_r(|\boldsymbol{\kappa}|=3;I_1=6)&=\mathrm{NDP}(4,1,1)P((4,1,1);F_6)\\
&\quad+\mathrm{NDP}(3,2,1)P((3,2,1);F_6)+\mathrm{NDP}(2,2,2)P((2,2,2);F_6)\\
&=3\times\frac{6!}{3^6\times 4!1!1!}+6\times\frac{6!}{3^6\times 3!2!1!}+1\times\frac{6!}{3^6\times 2!2!2!}\\
&\approx 0.741
\end{aligned}$$

When the first subscriber sends data bit "1", the output of the first optical hard-limiter at every "1" chip position of the first user is clipped back to $w\lambda_s T_c$. When the first subscriber sends "0", the output of the first optical hard-limiter at the i^{th} "1" chip position of the first user is clipped back to $\xi_i w\lambda_s T_c$. When the first subscriber sends "1", the second optical hard-limiter would clip the optical intensity back to $w\lambda_s T_c$ after the correlation. When the first subscriber sends "0",

the second optical hard-limiter would clip the optical intensity back to $|\boldsymbol{\kappa}|\lambda_s T_c = w\lambda_s T_c$ after the correlation if $|\boldsymbol{\kappa}| = w$; otherwise back to zero.

Since the sum of two Poisson independent random variables with means m_a and m_b respectively is also a Poisson random variable with mean $m_a + m_b$. Thus, the conditional means of Y_1 is given by[5]

$$m_1 = E[Y_1 \mid b_{j,1} = 1] = K_s + K_b \tag{5.35a}$$

$$m_0 = E[Y_1 \mid b_{j,1} = 0] = \begin{cases} K_s + K_b & \text{if } |\boldsymbol{\kappa}| = w \\ K_b & \text{otherwise} \end{cases} \tag{5.35b}$$

where K_s indicates the average signal photon-count in the last chip of the pulse slot and K_b denotes the average noise photon-count in the last chip of each slot. They are expressed as[5]

$$K_s \equiv w\lambda_s T_c \tag{5.36a}$$

$$K_b \equiv \lambda_0 T_c = \frac{\lambda_0}{nR_b} \tag{5.36b}$$

where R_b is the throughput with the unit of bit/s.

If the photon-count received by the first user's receiver satisfies $Y_1 \leqslant Th$, then $b_{j,1} = 0$, and if the received photon-count satisfies $Y_1 > Th$, then $b_{j,1} = 1$, where Th is the threshold level of the optical decoder.

From the analysis above, the BER of this kind of OCDMA system with double optical hard-limiters is given by[5]

$$P_{\mathrm{b}} = \frac{1}{2}[P_r(Y_1 > Th \mid b_{j,1} = 0) + P_r(Y_1 \leqslant Th \mid b_{j,1} = 1)] \tag{5.37}$$

where $P_r(Y_1 > Th \mid b_{j,1} = 0) = P_r(Y_1 > Th \mid I_1 = 0, b_{j,1} = 0)p_{I_1}(0)$

$$+ \sum_{j=1}^{N-1} P_r(Y_1 > Th \mid I_1 = j, b_{j,1} = 0)p_{I_1}(j)$$

$$= P_r(Y_1 > Th \mid I_1 = 0, b_{j,1} = 0)p_{I_1}(0)$$

$$+ \sum_{j=1}^{N-1} \sum_{\alpha=1}^{\min(w, I_1 = j)} P_r(Y_1 > Th \mid I_1 = j, |\boldsymbol{\kappa}| = \alpha, b_{j,1} = 0)p_{I_1}(j)P_r(|\boldsymbol{\kappa}| = \alpha \mid I_1 = j)$$

$$= \sum_{k=\lfloor Th \rfloor + 1}^{\infty} \mathrm{Pos}(k, m_0)p_{I_1}(0)$$

$$+ \sum_{j=1}^{N-1} \sum_{\alpha=1}^{\min(w, I_1 = j)} \sum_{k=\lfloor Th \rfloor + 1}^{\infty} \mathrm{Pos}(k, m_0)p_{I_1}(j)P_r(|\boldsymbol{\kappa}| = \alpha \mid I_1 = j)$$

$$= \sum_{k=\lfloor Th \rfloor+1}^{\infty} \mathrm{Pos}(k, K_b) p_{I_1}(0) + \sum_{j=1}^{N-1} \sum_{\alpha=1}^{\min(w, I_1=j)} \sum_{k=\lfloor Th \rfloor+1}^{\infty} \mathrm{Pos}(k, K_b) p_{I_1}(j) P_r(|\boldsymbol{\kappa}| = \alpha \mid I_1 = j) \tag{5.38}$$

$$\begin{aligned} P_r(Y_1 \leqslant Th \mid b_{j,1} = 1) &= \sum_{j=0}^{N-1} P_r(Y_1 \leqslant Th \mid I_1 = j, b_{j,1} = 1) p_{I_1}(j) \\ &= \sum_{j=0}^{N-1} \sum_{k=0}^{\lfloor Th \rfloor} \mathrm{Pos}(k, m_1) p_{I_1}(j) \\ &= \sum_{j=0}^{N-1} \sum_{k=0}^{\lfloor Th \rfloor} \mathrm{Pos}(k, K_s + K_b) p_{I_1}(j) \end{aligned} \tag{5.39}$$

where $\lfloor Th \rfloor$ indicates the largest integer less than or equal to Th and Poisson function is defined as

$$\mathrm{Pos}(x, \lambda) \equiv \frac{\mathrm{e}^{-\lambda} \lambda^x}{x!} \tag{5.40}$$

In Reference [5], the BER performance of the OCDMA system with double optical hard-limiters is evaluated for the chip synchronous case under the constraint on the average received photon-count and the assumption of Poisson noise model for the dark current noise of photondetector and the upper bound on BER is obtained in this way. Notice that the optimal value of Th must be firstly obtained by numerical calculation. Figure 5.10[5] shows the curves of BER versus

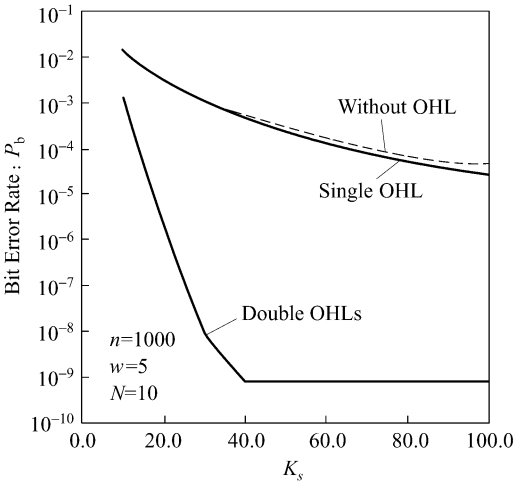

Figure 5.10 Bit error rate versus K_s for OCDMA systems without the optical hard-limiter, with the single optical hard-limiter, and with double optical hard-limiters: $n = 1000$; $w = 5$; $N = 10$; and $\lambda_0 / R_b = 100.00$ (Adapted from Ref.[5], with permission from IEEE © 2007)

K_s for the OCDMA systems without and with single optical hard-limiter, and with double optical hard-limiters. It can be seen from this figure that the BER performance of the system with single optical hard-limiter is a little bit better than that of the system without optical hard-limiter and otherwise, the performance of the system with double optical hard-limiters is much better than those of the other two cases. Figure 5.11[5] gives the curves of the BER versus the number of simultaneous subscribers for these three cases. It can be seen that the performance of the system with double optical hard-limiters is several orders of magnitude better than those of the other two cases under the condition that they have the same number of simultaneous subscribers.

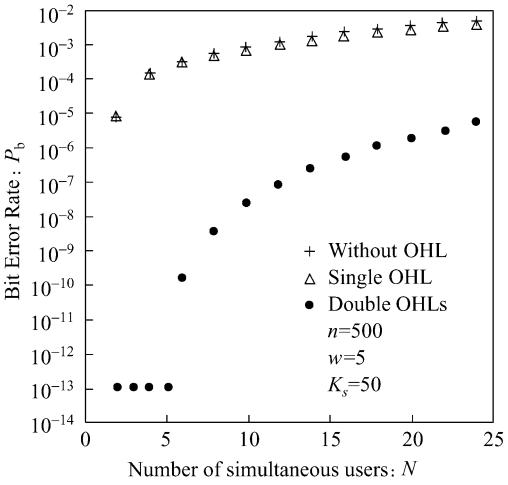

Figure 5.11 Bit error rate versus the number of simultaneous users N for OCDMA systems without the optical hard-limiter, with the single optical hard-limiter, and with double optical hard-limiters: $n = 500$; $w = 5$; $K_s = 50$; and $\lambda_0 / R_b = 100.00$ (Adapted from Ref.[5], with permission from IEEE © 2007)

5.3 Performance Analysis of One-dimensional Time-spreading Incoherent OCDMA System with Chip-level Receiver

Except for the correlation-detection receivers introduced in the previous section, there is another type of receivers for OCDMA communication system, called chip-level receivers[6], which are in turn categorized into the on-off keying (OOK) OCDMA chip-level receiver and the pulse-position modulation (PPM) OCDMA chip-level receiver. Since the multiple access interference received by the receiver increases with the increasing of the number of simultaneous subscribers,

the performance of the correlation-detection receiver degrades with the increasing of the number of users. The performance of the chip-level receiver that will be introduced in this section can be improved a lot at the expense of implementing complexity of receiver. The performance of the chip-level receiver is asymptotically optimal and nevertheless the complexity of the receiver is independent of the number of subscribers.

The block diagram of OOK/PPM OCDMA system is shown in Fig. 5.12. At the transmitting end, the narrow optical pulse signal from light source is firstly modulated by data information through OOK/PPM optical modulator. The output signal of the optical modulator is transmitted to the optical network after encoded by the optical encoder. Figure 5.13 shows the schematic diagram of OOK/PPM OCDMA signal corresponding to data bit. As to the OOK modulation manner, there are only two binary symbols and each symbol corresponds to one data bit. When data bit is "1", the optical encoder sends an optical pulse code sequence to the network. Otherwise, when data bit is "0", the optical encoder doesn't send any optical signal. In *M*-ary PPM signaling format, there are *M* symbols possible. Therefore, each symbol represents $\log_2 M$ bits of data information. The circumstance of $M=4$ is shown in this figure where each symbol represents two bits of data information. In PPM modulation format, the different symbol is expressed by the distinct position where the pulse locates. For example, the pulse at the first slot represents the first symbol, the pulse at the second slot represents the second symbol, etc. Then, an optical encoder encodes the optical pulse and there would be an optical pulse code sequence within the corresponding slot. The temporal sequence corresponding to each symbol is called one frame whose length is represented by T_s. Each frame is divided into *M* slots and the length of each slot is denoted by τ. Furthermore, each slot is composed of n chips and the time width of a chip is indicated by T_c where n corresponds to the code length of the optical orthogonal code. Thus, there exists $T_s = M\tau = MnT_c$. For OOK modulation format, the slot length is equal to the length of a frame, i.e., $T_s = \tau = nT_c$. Assuming that both the chip time T_c and throughput are held fixed, the code length is given by[6]

$$n = \begin{cases} \dfrac{1}{R_0} & \text{for OOK} \\ \dfrac{\log_2 M}{MR_0} & \text{for PPM} \end{cases} \tag{5.41}$$

where *M* indicates the number of possible slots within a PPM time frame and R_0 denotes the throughput in bits/chip-time.

At the receiving end, the data are restored by the OOK/PPM chip-level optical receiver. Since the chip-level receivers are dependent on the number of photons

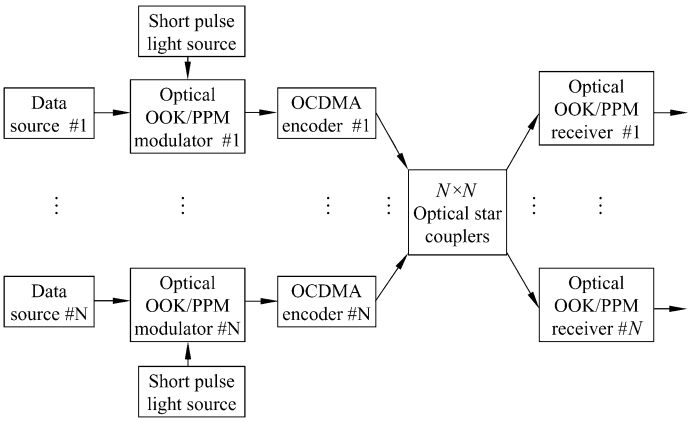

Figure 5.12 Direct-detection OOK/PPM-OCDMA system models (After Ref.[6])

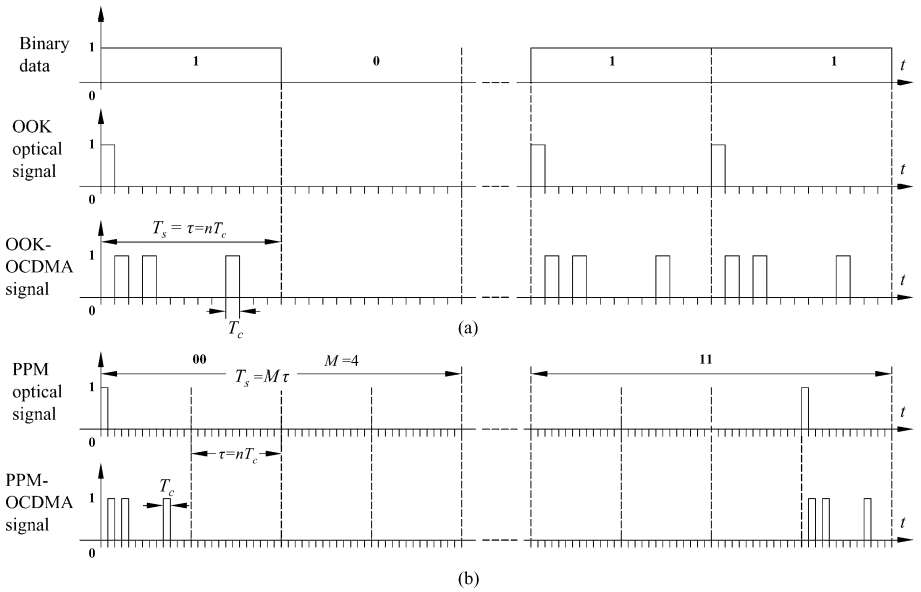

Figure 5.13 Schematic diagram of OOK and PPM OCDMA signals

(optical energy) per chip in the received frame, therefore the multiple access interference can be suppressed effectively.

5.3.1 OOK OCDMA Chip-level Receiver and Its Performance Analysis

In the OOK OCDMA system using the $(n, w, 1)$ OOC as subscriber's address code, the signature with w optical pulse is sent for data bit "1" while nothing is sent

for data bit "0". Assuming that it is the case of chip synchronization, since the constraint of cross-correlation is $\lambda_c = 1$, the contribution of each undesired subscriber to this number of pulses may be only one pulse or none pulse at all.

Let Y_i, $i \in \chi = \{1,2,\cdots,w\}$, denote the photon-count collected from the i^{th} "1" chip of data bit "1", which is a compound Poisson random variable. Again let κ_i ($i \in \chi$) indicate the number of pulses from other subscribers, which cause interference to this chip. κ^j is employed to represent the column vector $(\kappa_1,\kappa_2,\cdots,\kappa_j)^{\mathrm{T}}$, where the superscript T indicates transpose. Therefore, κ^j is a multinomial vector with parameters $w/2n$ and $N-1$, whose probability density function is[6]

$$P_r\{\kappa^j = l^j\} = \frac{(N-1)!}{l_1!l_2!\cdots l_j!s_j!}\left(\frac{w}{2n}\right)^{N-1-s_j}\left(1-j\frac{w}{2n}\right)^{s_j} \tag{5.42}$$

where $l^j = (l_1,l_2,\cdots,l_j)^{\mathrm{T}}$, $s_j = N-1-\sum_{i=1}^{j} l_i \geqslant 0$, $j \in \chi$, and N is the number of simultaneous subscribers.

The block diagram of OOK-OCDMA chip-level receiver[6] is shown in Fig. 5.14, which consists of a photodetector, a chip integrator, a sampler, a pulse counter and a threshold-decider. The received optical signal is firstly converted by optical-to-electrical detector and the resulting signal is integrated over each chip, and then sampled and decided at the end of each "1" chip. If the number of collected photon-count Y_i ($\forall i \in \chi$) within each "1" chip of the receiver address code is greater than or equal to the threshold Th, a data bit "1" is declared to be transmitted. Otherwise, a data bit "0" is declared[6].

Because this receiver is required to employ chip-level electronic integrator, sampler and threshold-decision circuit, the operational speed of receiver is limited. In order to make full use of the tremendous bandwidth from the optical network, an equivalent OOK-OCDMA chip-level receiver[6] is shown in Fig. 5.15. The received optical signal is sampled optically at the correct "1" chip. Then, each sampled signal is photodetected and integrated over the entire time frame $T_s = nT_c$), and is sampled electrically at the end of the frame. If the value of each sampled signal is greater than or equal to Th, a data bit "1" is decided. Otherwise, a zero is declared. For this receiver, the optical signal is processed at the rate $1/T_c = f_c$ and however, the rate of electrical signal processed is only required at $1/T_s = f_c/n$. Thus, the requirement to the speed of electronic circuit is debased significantly.

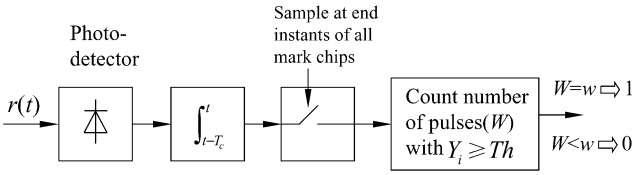

Figure 5.14 Direct-detection OOK-OCDMA chip-level receiver (After Ref. [6])

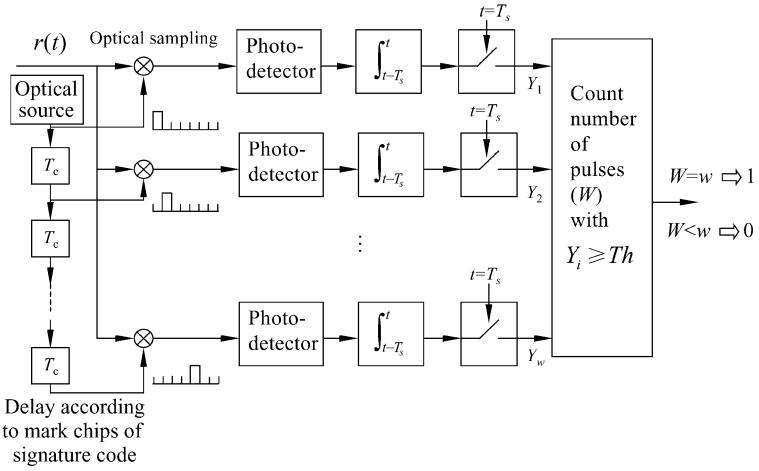

Figure 5.15 All-optical OOK-OCDMA chip-level receiver (After Ref.[6])

In order to simplify the analysis for this receiver, the decision-threshold $Th = 1$ is chosen. (Notice that in doing so, the resulting bit error rate of the chip-level receiver is an upper bound of the optimum chip-level receiver). Therefore, the resulting bit error rate is[6]

$$P_{\mathrm{b}} = \frac{1}{2}(P[E \mid 0] + P[E \mid 1])$$

where $P[E \mid 1] = P_r\{Y_i = 0, \text{some } i \in \chi \mid 1\}$

$$= -\sum_{i=1}^{w} (-1)^i \binom{w}{i} P_r\{Y_1 = Y_2 = \cdots = Y_i = 0 \mid 1\}$$

and $P_r\{Y_1 = Y_2 = \cdots = Y_i = 0 \mid 1\} = \sum_{l^i} P_r\{Y_1 = Y_2 = \cdots = Y_i = 0 \mid 1, \kappa^i = l^i\} P_r\{\kappa^i = l^i\}$

$$= \sum_{l^i} P_r\{\kappa^i = l^i\} \prod_{j=1}^{i} P_r\{Y_j = 0 \mid 1, \kappa_j = l_j\}$$

$$= \sum_{l^i} P_r\{\kappa^i = l^i\} \prod_{j=1}^{i} \exp[-Q(1 + l_j)]$$

$$= \exp(-Qi) \cdot E\left\{\exp\left[-Q\sum_{j=1}^{i}\kappa_j\right]\right\}$$
$$= \left[1 - i\frac{w}{2n} + i\frac{w}{2n}\exp(-Q)\right] \cdot \exp(-Qi)$$

where the second equality holds because the random variables $Y_1, Y_2, \cdots, Y_i$ are independent of the given κ^i. $E\{\cdot\}$ indicates the expected value over the random vector κ^i. Q is the average transmitted photons per chip pulse, which is $Q = \mu / w$. μ is the average transmitted photons per bit.

Similarly, $P[E \mid 0]$ can be evaluated as[6]

$$P[E \mid 0] = P_r\{Y_i \geqslant 1, \forall i \in \chi \mid 0\} = 1 - P_r\{Y_i = 0, \text{some } i \in \chi \mid 0\}$$
$$= 1 + \sum_{i=1}^{w}(-1)^i \binom{w}{i} P_r\{Y_1 = Y_2 = \cdots = Y_i = 0 \mid 0\}$$

and $P_r\{Y_1 = Y_2 = \cdots = Y_i = 0 \mid 0\} = \sum_{l^i} P_r\{Y_1 = Y_2 = \cdots = Y_i = 0 \mid 0, \kappa^i = l^i\} P_r\{\kappa^i = l^i\}$

$$= \sum_{l^i} P_r\{\kappa^i = l^i\} \prod_{j=1}^{i} P_r\{Y_j = 0 \mid 0, \kappa_j = l_j\}$$
$$= \sum_{l^i} P_r\{\kappa^i = l^i\} \prod_{j=1}^{i} \exp[-Ql_j]$$
$$= -E\left\{\exp\left[-Q\sum_{j=1}^{i}\kappa_j\right]\right\}$$
$$= \left[1 - i\frac{w}{2n} + i\frac{w}{2n}\exp(-Q)\right]^{N-1}$$

Therefore, the resulting bit error rate in all is [6]

$$P_{\mathrm{b}} = \frac{1}{2}\left[1 + \sum_{i=1}^{w}(-1)^i \binom{w}{i}\left(1 - \exp(-Qi)\right)\left(1 - i\frac{w}{2n} + i\frac{w}{2n}\exp(-Q)\right)^{N-1}\right] \tag{5.43}$$

When $Q \to \infty$, this expression becomes

$$P_{\mathrm{b}} = \frac{1}{2}\left[1 + \sum_{i=1}^{w}(-1)^i \binom{w}{i}\left(1 - i\frac{w}{2n}\right)^{N-1}\right] \tag{5.44}$$

This is the bit error rate for the ideal optimum receiver, which corresponds to the circumstance without shot noise under the assumption of the photodetector to be ideal.

Figure 5.16 shows the comparison between the bit error rate of correlation receiver with and without an optical hard-limiter and that of chip-level receiver for the OOK OCDMA systems. At the same time, the curve of the optimum receiver is also given in this figure for the sake of comparison. It can be seen that the chip-level receiver outperform the correlation receiver, even the correlation receiver with an optical hard-limiter. For example, If the bit error rate is required not to exceed 8.8×10^{-6} we need (at least) $\mu=325$ for the correlation receiver and $\mu=181$ for the correlation receiver with an optical hard-limiter, whereas $\mu=81$ for the chip-level receiver. This means that more than 75% and 44% save in energy are gained when using the chip-level receiver instead of the correlation receiver without and with an optical hard-limiter, respectively. Furthermore, if $\mu=325$ is employed for chip-level detector we obtain a bit error rate of 7.05×10^{-10} which is so close to the lower bound of the optimum bit error rate of 7.05×10^{-10}.

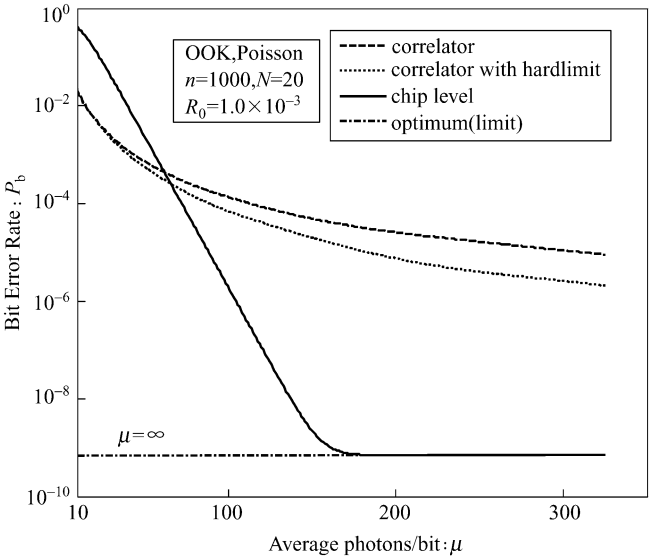

Figure 5.16 A comparison between the bit error rates of correlation receiver (with and without an optical hardlimiter) and chip-level receiver for the case of OOK-OCDMA systems with $n=1000$ and $N=20$

5.3.2 PPM OCDMA Chip-level Receiver and Its Performance Analysis

In M-ary PPM signaling format, the j^{th} symbol, $j\in\mathcal{M}=\{0,1,\cdots,M-1\}$, is represented by transmitting a signature sequence at the j^{th} slot and otherwise,

there is not any pulse within all other slots. Let Y_{ij} ($i \in \chi = \{1,2,\cdots,w\}$, $j \in \mathcal{M} = \{0,1,\cdots,M-1\}$, denote the photon-count collected from the i^{th} "1" chip of the j^{th} slot, which is a compound Poisson random variable. Again let κ_{ij} , $i \in \chi$, $j \in \mathcal{M}$, indicate the number of pulses from other subscribers, which cause interference to the i^{th} chip of the j^{th} slot. Further let κ_j^k represent the vector $(\kappa_{1j},\kappa_{2j},\cdots,\kappa_{kj})^{\text{T}}$, (Notice that the superscript T indicate transpose here.), i.e.,

$$\kappa_j^k \equiv (\kappa_{1j},\kappa_{2j},\cdots,\kappa_{kj})^{\text{T}}$$

The super-vector $(\kappa_0^k,\kappa_1^k,\cdots,\kappa_m^k)^{\text{T}}$, $k \in \chi$, $m \in \mathcal{M}$, is represented by κ^{km} , that is,

$$\kappa^{km} \equiv (\kappa_0^k,\kappa_1^k,\cdots,\kappa_m^k)^{\text{T}}$$

Supposing frame-level synchronization among transmitters, it is not difficult to validate that κ^{km} is a multinomial random vector with parameters w/Mn and $N-1$, whose probability density function is given by[6]

$$P_r\{\kappa^{km} = l^{km}\} = \frac{(N-1)!}{l_{10}!l_{20}!\cdots l_{km}!s_{km}!}\left(\frac{w}{Mn}\right)^{N-1-s_{km}}\left[1-k(m+1)\frac{w}{Mn}\right]^{s_{km}} \tag{5.45}$$

where $l^{km} = (l_0^k,l_1^k,\cdots,l_m^k)^{\text{T}}$, $l_j^k = (l_{1j},l_{2j},\cdots,l_{kj})^{\text{T}}$, and $s_{km} = N-1-\sum_{j=0}^{m}\sum_{i=1}^{k} l_{ij}$, $k \in \chi$, $m \in \mathcal{M}$.

The block diagram of direct-detection PPM-OCDMA chip-level receiver is shown in Fig. 5.17[6], which consists of a photodetector, a chip-level integrator, M chip-level samplers, M counters of pulses and a threshold-decision circuit. The output signal from the photiodetector is integrated over each chip and sampled at the end of each "1" chip of each slot in the time frame. If the sampled value $Y_{ij} \geqslant Th$, the counter of pulses adds one. (For the sake of simplicity, the decision-threshold is set to $Th = 1$.) When the value counted by the counter of the i^{th} slot is $W_i = w$, $\forall i \in \chi$, and the value counted by the counters of all other slots is $W_j < w$ ($j \neq i$), then the symbol m is declared, $m \in \mathcal{M}$. Otherwise, an incorrect decision is declared.

An all-optical PPM-OCDMA chip-level receiver corresponding to Fig. 5.17 is shown in Fig. 5.18. The probability of symbol error of the PPM-OCDMA chip-level receiver is given by[6]

$$P_{\text{s}} = \frac{M/2}{M-1} \cdot P[E \mid 0]$$

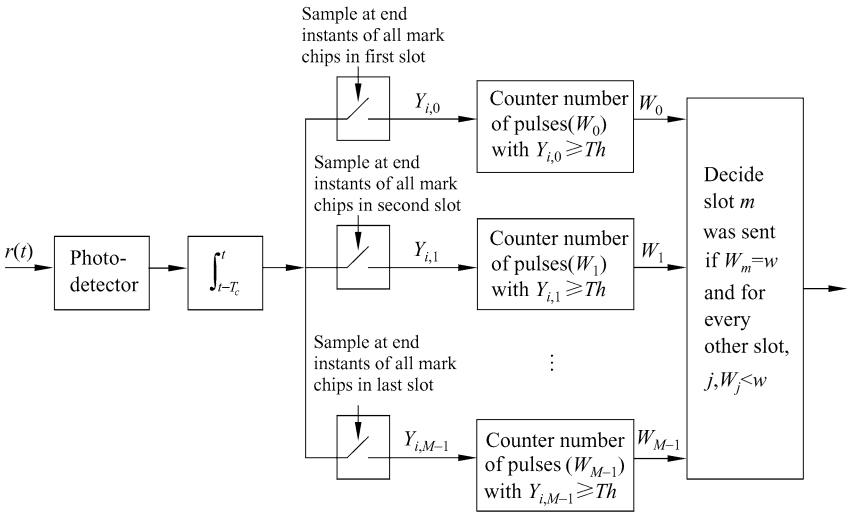

Figure 5.17 Direct-detection PPM-OCDMA chip-level receiver (After Ref.[6])

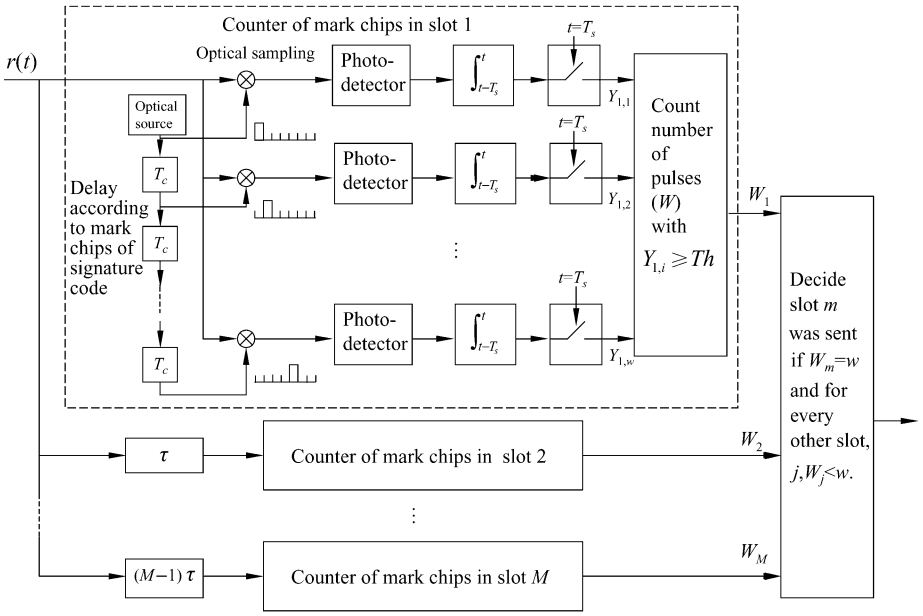

Figure 5.18 All-optical PPM-OCDMA chip-level receiver

where $P[E \mid 0] = P_r\{Y_{i0} = 0, \text{some } i \in \chi \text{ or } Y_{ij} \geqslant 1 \ \forall i \in \chi, \text{some } j \neq 0 \mid 0\}$

$$\leqslant P_r\{Y_{i0} = 0, \text{some } i \in \chi \mid 0\} + (M-1)P_r\{Y_{i1} \geqslant 1 \ \forall i \in \chi \mid 0\}$$

In the similar way to Subsection 5.3.1, the first probability is obtained as[6]

$$P_r\{Y_{i0}=0,\text{some } i\in\chi\mid 0\}=-\sum_{i=1}^{w}(-1)^i\binom{w}{i}P_r\{Y_{10}=Y_{20}=\cdots=Y_{i0}=0\mid 0\}$$
$$=-\sum_{i=1}^{w}(-1)^i\binom{w}{i}\left[1-i\frac{w}{Mn}+i\frac{w}{Mn}\exp(-Q)\right]^{N-1}\cdot\exp(-Qi)$$

The upper bound of the second probability is given by [6]

$$P_r\{Y_{i1}\geqslant 1,\forall i\in\chi\mid 0\}=P_r\{Y_{i1}\geqslant 1,\kappa_{i1}\geqslant 1,\forall i\in\chi\mid 0\}$$
$$+P_r\{Y_{i1}\geqslant 1,\forall i\in\chi,\kappa_{k1}=0,\text{some } k\in\chi\mid 0\}$$
$$\leqslant P_r\{\kappa_{i1}\geqslant 1,\forall i\in\chi\mid 0\}+0$$
$$=1+\sum_{i=1}^{w}(-1)^i\binom{w}{i}\left[1-i\frac{w}{Mn}\right]^{N-1}$$

The zero after the first inequality is because we assume that when a "0" was sent Y_{k1} should also be zero if $\kappa_{k1}=0$. Finally, the resulting upper bound on bit error rate of PPM-OCDMA chip-level receiver is[6]

$$P_{\mathrm{b}}=-\frac{M/2}{M-1}\sum_{i=1}^{w}(-1)^i\binom{w}{i}\left[1-i\frac{w}{Mn}+i\frac{w}{Mn}\mathrm{e}^{-Q}\right]^{N-1}\cdot\mathrm{e}^{-Qi}$$
$$+\frac{M}{2}\left\{1+\sum_{i=1}^{w}(-1)^i\binom{w}{i}\left[1-i\frac{w}{Mn}\right]^{N-1}\right\} \tag{5.46}$$

The upper bound on bit error rate of the ideally optimum PPM-OCDMA chip-level receiver is [6]

$$P_{\mathrm{b}}\geqslant\frac{M/2}{M-1}\left\{(M-1)\sum_{i=0}^{w}(-1)^i\binom{w}{i}\left[1-(i+w)\frac{w}{Mn}\right]^{N-1}-\binom{M-1}{2}\left(\frac{(N-1)w\mathrm{e}}{Mn}\right)^{2w}\right\} \tag{5.47}$$

where $Q=\mu\log_2 M/w$.

The performance comparison between the curves of chip-level receivers and those of correlation receivers for PPM-OCDMA systems is shown in Fig. 5.19. The BER curve of the optimum receiver is also shown in this figure. It can be seen that the performance of chip-level receiver is evidently better than that of correlation receiver. Meanwhile, OCDMA system with PPM receiver can enhance the security of information transmission. However, in the hardware implementation, OCDMA system with PPM chip-level receiver is much more complex than that of OCDMA system with PPM correlation receiver and it is more complex than OOK chip-level receiver system as well.

Optical overlapping pulse-position modulation (OPPM) chip-level receiver was reported in Reference [7], whose difference from PPM chip-level OCDMA

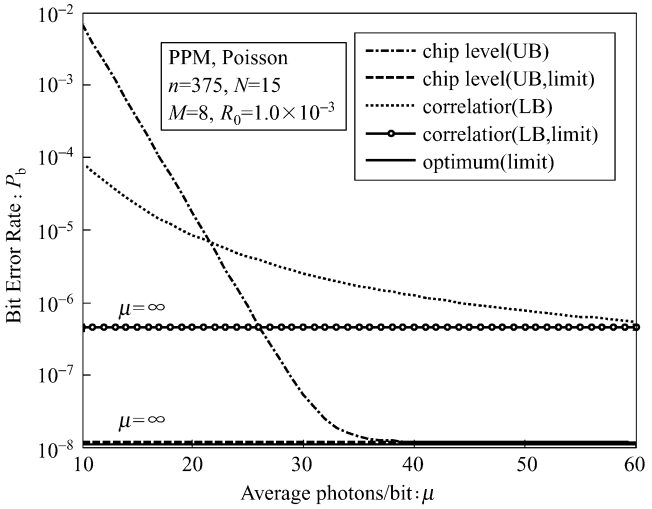

Figure 5.19 A comparison between lower bounds on BER of correlation receiver and upper bounds on BER of chip-level receiver for the case of PPM-OCDMA systems with $M = 8$, $n = 375$, and $N = 15$

is that it allows partial superposition of two adjacent modulated signals on two adjacent slot with width τ and the overlapping depth is $(1-1/\gamma)\tau$, $\gamma \in \{0,1,\cdots, M-1\}$, where γ refers to the overlapping index. Meanwhile, the time frame of OPPM becomes $T_s = M\tau/\gamma = MnT_c/\gamma$, where M/γ is integer. The throughput of OCDMA system with OPPM chip-level receiver is γ multiples as that of PPM OCDMA system and the BER is also improved to some extent. However, its hardware is more complex than that of PPM chip-level OCDMA system.

The performances of various OCDMA receivers employing passive/active and correlation/chip-level structures with and without an optical hard-limiter/double optical hard-limiters have been compared under the consideration of the effect of all major noise sources, i.e., quantum shot-noise, dark current noise, and circuit Gaussian noise in Reference [8] and their applied characteristics and weaknesses are shown in Table 5.1.

Table 5.1 Comparisons of various OCDMA receiver structures and their merits and weaknesses[8]

Receiver structures	Integration time	Electronic bandwidth	Receiver complexity	Notes on overall usability and relative merits/weakness
Passive correlator structure	T_c	Large	Low	Low-speed applications, inefficient power consumption, inexpensive
Active correlator structure	T_s	Low	Moderate	High-speed applications, relative expensive design

Continued

Receiver structures	Integration time	Electronic bandwidth	Receiver complexity	Notes on overall usability and relative merits/weakness
Optical hard-limiter + passive correlator	T_c	Large	Moderate	Low-speed applications, relying on the availability of Optical Hard-Limiter
Optical hard-limiter + active correlator	T_s	Low	Moderate	High-speed applications, relying on the availability of Optical Hard-Limiter
Double optical hard-limiter + passive correlator	T_c	Large	Moderate	Low-speed applications, excellent performance, relatively expensive
Double optical hard-limiter + double correlator	$\geqslant T_c$, $\leqslant T_s$	Medium-large	High	Medium to High-speed applications, inefficient power consumption
High-speed chip-level detector	T_c	Large	Low	Low-speed applications, efficient power consumption
Optical chip-level detector	$\geqslant T_c$, $\leqslant T_s$	Medium-large	High	Unusable

5.4 Performance Analysis of Two-dimensional WH/TS Incoherent OCDMA System

OCDMA receivers are classified into OCDMA correlation receivers and OCDMA chip-level receivers. The former is also called as OCDMA SUM receiver and the latter is called as OCDMA AND receiver. The decisions at the correlation receiver are performed based on threshold value of the total output energy after correlation between the received signal and the desired code. Although this approach benefits from its simplicity it is not optimal with respect to minimizing the error-inducing effects of multiple access interference. Because the correlation receiver model has been employed during introducing the performances of two-dimensional codes in Chapter 3, we will not utilize the correlation receiver model to analyze the performance of 2-D incoherent OCDMA system here. In this section, we will present the analysis method of BER performance of 2-D incoherent OCDMA system with chip-level receiver model[9] and compare the BER performances obtained by employing two distinct models.

5.4.1 Structure of 2-D Incoherent OCDMA Chip-level Receiver

The schematic diagram of chip-level receiver for 2-D WH/TS OCDMA system is shown in Fig. 5.20(a) and (b). Although in these two structures, the optical pulses

at the position of each "1" chip of subscriber address codeword are all taken and decided, their hardware implementations are slightly different. In the structure (a), the optical hard-limiter firstly clips the different optical signals decomposed by the wavelength division demultiplexer (WDM DEMUX) before the optical signal at the position of each "1" chip is taken. After the clipped signals at the positions of "1" chips are taken out, they are multiplexed into a signal by the wavelength division multiplexer (WDM MUX). Then, the signal is processed by the optical-to-electrical conversion of the photodetector, integral of the integrator and sampling of the electrical sampler. At last, the data is restored after threshold-decision. If the signal value at the time of threshold-decision is equal to the threshold level corresponding to code weight, a "1" is declared. If the signal

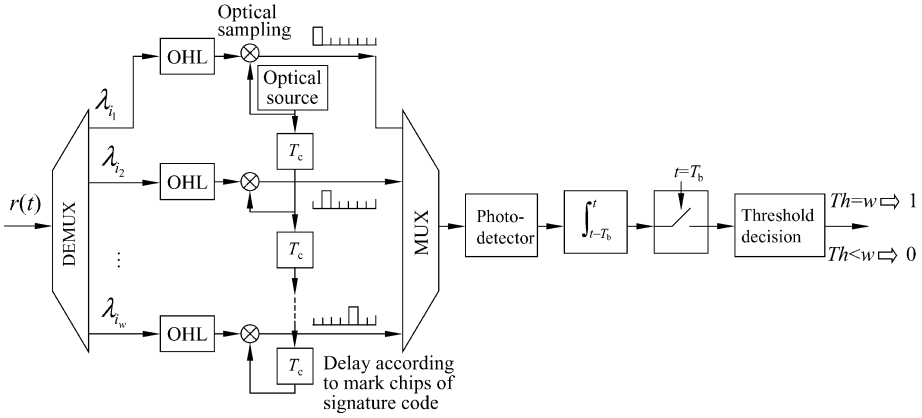

(a) Optical direct-detection chip-level receiver for 2-D WH/TS OCDMA system

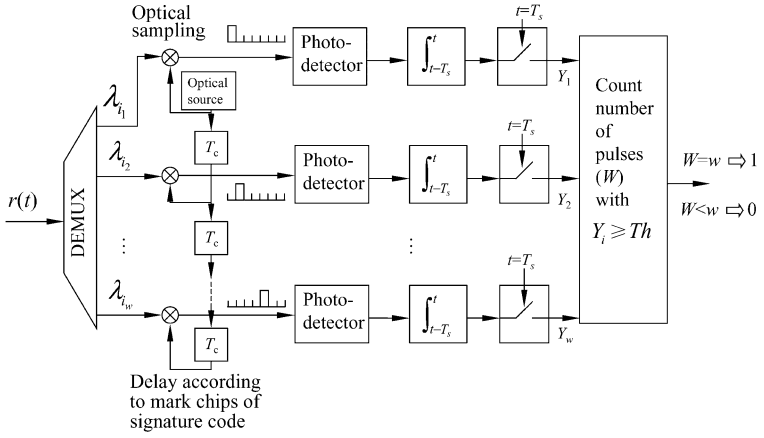

(b) All-optical chip-level receiver for 2-D WH/TS OCDMA system

Figure 5.20 Schematic diagram of chip-level receiver for 2-D WH/TS OCDMA system

value at the time of threshold-decision is less than the threshold level corresponding to code weight, a "0" is output. The advantage of this structure is that the hardware implementation after the wavelength division multiplexer is relatively simple, which only needs one photodetector, one integrator, one sampler and one decision circuit. However, w nonlinear optical threshold hard-limiters before the optical samplers and one more $w\times 1$ wavelength division multiplexer are required. In the structure (b), w nonlinear optical threshold hard-limiters and one $w\times 1$ wavelength division multiplexer can be saved. However, in addition to w electrical-to-optical converters, the integral, sampling and threshold-decision circuit, and the pulse-count circuit are required. Therefore, either of them has its strong point. In practical application, they would be chosen in terms of mature extent of technique and implementing cost. Optical sampler can be implemented by Mach-Zehnder modulator.

5.4.2 Performance Analysis of 2-D Incoherent OCDMA System Based on Chip-level Receiver[9]

For the sake of analytical simplicity, we assume that the case is chip synchronization for subscribers' access so that the upper bound on bit error rate would be obtained. Further we suppose that the subscribers' address code employed is the constant-weight 2-D WH/TS code and each codeword has the number of wavelengths, m, the code length n and the code weight w. When the typical star network topology is employed the signal received by any one of the receivers is a superposition of a subset of the codes transmitted by all of the active transmitters. One of such examples is shown in Fig. 5.21, where the number displayed in each square indicates the intensity of light corresponding to the wavelengths, which is detected by the receiver at each chip. (Notice that although each square is also called a chip for the sake of depiction simplicity it is slightly different from the meaning of chip mentioned previously.)

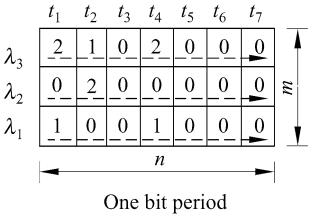

Figure 5.21 Received signal in a 2-D OCDMA system

Any signal received by any subscriber can be expressed by a vector

$$\boldsymbol{r} = [r_1, r_2, \cdots, r_j, \cdots, r_K] \tag{5.48}$$

where $K = m \times n$ is the number of dimensions for signals and r_j indicates the intensity of received optical signal at the j^{th} chip, $1 \leqslant j \leqslant K$.

With the increasing of the optical signal power, multiple access interference becomes the BER-limiting mechanism. Hence, we focus our attention on the impact of MAI on the BER performance for the sake of simplified analysis. At the same time, we assume that the random address code is employed, that is, w pulses occur at random in w positions of K squares in the signal matrix. For on-off keying, a codeword is transmitted for the bit "1" and nothing is sent for the bit "0". Figure 5.22 shows the representations of the bit "1" ($\boldsymbol{s}_1$) and the bit "0" ($\boldsymbol{s}_0$), whose corresponding vectors are

$$\boldsymbol{s}_1 = [0,0,0,1,0,0,0,0,1,0,0,0,0,0,1,0,0,0,0,0,0]$$
$$\boldsymbol{s}_0 = [0,0,0,0,0,0,0,0,0,0,0,0,0,0,0,0,0,0,0,0,0]$$

where the number of dimensions is $K = m \times n = 3 \times 7 = 21$.

	t_1	t_2	t_3	t_4	t_5	t_6	t_7
λ_3	0	0	0	1	0	0	0
λ_2	0	1	0	0	0	0	0
λ_1	1	0	0	0	0	0	0

(a) bit "1"

	t_1	t_2	t_3	t_4	t_5	t_6	t_7
λ_3	0	0	0	0	0	0	0
λ_2	0	0	0	0	0	0	0
λ_1	0	0	0	0	0	0	0

(b) bit "0"

Figure 5.22 The symbol for bit "0" and bit "1"

5.4.2.1 Decision Rule[9]

When bit "1" ($\boldsymbol{s}_1$) and bit "0" ($\boldsymbol{s}_0$) are equiprobable, the maximal-likelihood (ML) criterion for detection will minimize the average probability of error. In on-off keying, the corresponding decision rule is

$$P(\boldsymbol{r} \mid \boldsymbol{s}_1) \underset{\boldsymbol{s}_0}{\overset{\boldsymbol{s}_1}{\gtrless}} P(\boldsymbol{r} \mid \boldsymbol{s}_0) \tag{5.49}$$

If the address codes for subscribers in the network satisfy: (a) the codes employed in the system are at random generated with a uniform distribution, that is, the probability that a "1" chip of a code appears in any of unused chips is the same; or (b) even if the designed codes are deterministic the receiver does not know, or does not take into account the algorithmic constructions of other subscribers' codes in the system. The receiver can only presume that the presence of a pulse at a certain chip does not affect the probability of a pulse at any other chip. Under this circumstance, we can suppose that the received optical signal intensity at any chip is independent of the received optical signal at any other

chips so that the probability in (5.49) can be written as

$$P(\boldsymbol{r} \mid \boldsymbol{s}_l) = \prod_{j=1}^{K} P(r_j \mid s_{lj}), \quad l = 0,1 \tag{5.50}$$

Here, the probability of a pulse from any other active subscriber falling on a particular chip is $w/2K$, where 1/2 comes from the fact that data bits "1" and "0" appear with equiprobability. The detected intensity at a chip is dependent on the number of overlapping pulses from other subscribers. None of optical pulses is transmitted when a user sends data bit "0". Therefore, when data bit "0" is sent the component likelihood functions are

$$P(r_j \mid s_{0,j}) = \binom{N-1}{r_j} \left(\frac{w}{2K}\right)^{r_j} \left(1 - \frac{w}{2K}\right)^{N-1-r_j}, \quad j = 1,2,\cdots,K \tag{5.51}$$

where N is the number of active (simultaneous) subscribers in the network. Similarly, when data bit "1" is transmitted the component likelihood functions for these chips are

$$\begin{aligned} P(r_j \mid s_{1,j}) &= \binom{N-1}{r_j - 1} \left(\frac{w}{2K}\right)^{r_j - 1} \left(1 - \frac{w}{2K}\right)^{N-1-(r_j-1)} \\ &= \binom{N-1}{r_j - 1} \left(\frac{w}{2K}\right)^{r_j} \left(1 - \frac{w}{2K}\right)^{N-1-r_j} \left(\frac{2K}{w} - 1\right), \quad j = 1,2,\cdots,w \end{aligned} \tag{5.52}$$

where j indicates the positions of "1" chips. Since two likelihood functions mentioned previously are

$$P(\boldsymbol{r} \mid \boldsymbol{s}_0) = \prod_{j=1}^{K} P(r_j \mid s_{0j}) \tag{5.53}$$

$$P(\boldsymbol{r} \mid \boldsymbol{s}_1) = \prod_{j=1}^{K-w} P(r_j \mid s_{0j}) \prod_{j=1}^{w} P(r_j \mid s_{1j}) \tag{5.54}$$

thus, (5.49) can be expressed as

$$\prod_{j=1}^{w} P(r_j \mid s_{1j}) \underset{\boldsymbol{s}_0}{\overset{\boldsymbol{s}_1}{\gtrless}} \prod_{j=1}^{w} P(r_j \mid s_{0j}) \tag{5.55}$$

Substituting (5.51) and (5.52) into (5.55), we can obtain

$$\prod_{j=1}^{w} \binom{N-1}{r_j - 1} \left(\frac{2K}{w} - 1\right) \underset{\boldsymbol{s}_0}{\overset{\boldsymbol{s}_1}{\gtrless}} \prod_{j=1}^{w} \binom{N-1}{r_j} \tag{5.56}$$

After mathematical simplification, the decision rule is obtained as

$$\prod_{j=1}^{w}\left(\frac{N-r_j}{r_j}\right)\underset{s_0}{\overset{s_1}{\lessgtr}}\prod_{j=1}^{w}\left(\frac{2K}{w}-1\right) \tag{5.57}$$

After the algorithmic constructions of codes are determined the value of the right-hand side of (5.57) is a fixed value. Hence, (5.57) represents a threshold operation whose threshold is just the value of the right-hand side of this equation. Although all chips are involved in (5.50), the intensities of received optical pulses at the positions of w "1" chips of the code need to be known. Since the component likelihood functions for the rest of the chips are the same regardless of whether a bit "1" or a bit "0" is sent, these probability terms can be cancelled during comparison through (5.49). Thus, these chips do not need to be observed during detection.

Decision rule of (5.55) reveals that if the smaller the left-hand side is the bigger the probability that the received optical signal is a bit "1" is, i.e., if the larger the value of r_j is, which means that the higher the light intensities at the "1" chips of the code are, the more likely it is that the received optical signal is a s_1. On the contrary, the bigger the left-hand side is the larger the probability of a bit "0" of the received optical signal is. However, when there is at least one r_j equal to zero the value of the left-hand side of (5.57) is infinity. In this case, it is decided as s_0. When all values of r_j are equal to 1 the left-hand side of (5.57) attains the largest finite value. In this case, the decision rule becomes

$$(N-1)^w\underset{s_0}{\overset{s_1}{\lessgtr}}\left(\frac{2K}{w}-1\right)^w \tag{5.58}$$

For the deterministic codes, N can not exceed $(2K/w-1)$. This is because the maximal cardinality of any 2-D OOC with the number of available wavelengths $m=w$ and $\lambda_a=\lambda_c=1$ is

$$\begin{aligned}\Phi&=\frac{m(mn-1)}{w(w-1)}=\frac{w(wn-1)}{w(w-1)}=\frac{wn-1}{w-1}\\&=\frac{wn-n+n-1}{w(w-1)}=n+\frac{n-1}{w-1}<2n\end{aligned}$$

and $\dfrac{2K}{w}-1=\dfrac{2mn}{w}-1=\dfrac{2wn}{w}-1=2n-1\approx 2n$.

Therefore, $(2K/w-1)$ is larger than the cardinality of a deterministic 2-D OCDMA. Once the light intensities at the positions of all "1" chips are at least

one the decision is $\boldsymbol{s}_1$ from (5.57). This is equivalent to that the AND logic operation is performed on all "1" chips, which is independent of the number of simultaneous subscribers N in this case. Actually, this is just the decision rule of the chip-level receiver introduced previously. For the random codes, although its cardinality can exceed $\left(2K/w-1\right)$ and thus threshold adjustment is required as N increases, the BER can only be improved a small amount[9].

5.4.2.2 BER Performance Analysis[9]

For OOK format, the symbol error rate is equal to the bit error rate. Assuming that $\boldsymbol{s}_0$ and $\boldsymbol{s}_1$ appear with equiprobability, thus, the BER is given by

$$P_{\mathrm{b}} = \frac{1}{2}\left(P(E \mid \boldsymbol{s}_1) + P(E \mid \boldsymbol{s}_0)\right) \tag{5.59}$$

From the decision rule (5.57) of the chip receiver for 2-D OCDMA, when $\boldsymbol{s}_1$ is transmitted the detected light intensities at w "1" chips are at least one. Thus, the first term of (5.59) is zero. The second term represents the probability that other interfering subscribers make the light intensity at each "1" chip to be at least one when $\boldsymbol{s}_0$ is sent. Hence, we have

$$\begin{aligned} P_{\mathrm{b}} &= \frac{1}{2}\prod_{j=1}^{w}\sum_{i=1}^{N-1}\binom{N-1}{i}\left(\frac{w}{2K}\right)^{i}\left(1-\frac{w}{2K}\right)^{N-1-i} \\ &= \frac{1}{2}\left(\sum_{i=1}^{N-1}\binom{N-1}{i}\left(\frac{w}{2K}\right)^{i}\left(1-\frac{w}{2K}\right)^{N-1-i}\right)^{w} \end{aligned} \tag{5.60}$$

This is the BER of chip-level receiver for 2-D WH/TS OCDMA.

The corresponding decision rule of correlation receiver for 2-D WH/TS OCDMA is

$$\sum_{j=1}^{w} r_j \underset{\boldsymbol{s}_0}{\overset{\boldsymbol{s}_1}{\gtrless}} w \tag{5.61}$$

When a bit "1" is transmitted, the SUM of received light intensities at w "1" chips must be at least w. Similarly, the first term of (5.59) is 0 so that the BER for 2-D WH/TS OCDMA correlation receiver results from the fact that there are at least w pulses from $N-1$ interfering subscribers falling on these w chips. Therefore, we have

$$P_{\mathrm{b}} = \frac{1}{2}\sum_{i=w}^{w(N-1)}\binom{w(N-1)}{i}\left(\frac{w}{2K}\right)^{i}\left(1-\frac{w}{2K}\right)^{w(N-1)-i} \tag{5.62}$$

Figure 5.23 shows the comparison of the BER performances of chip-level receiver and correlation receiver for 2-D WH/TS OCDMA. It can be seen that the BER performance of chip-level receiver is better than that of correlation receiver. For example, when the number of available wavelengths and code weight are all ten, i.e., $m = w = 10$, we assume that the required system BER is 10^{-9}. If the code length is $n = 100$, the network with correlation receivers can only accommodate 14 subscribers and otherwise, 30 subscribers are simultaneously allowed in the network with chip-level receivers. When the code length is $n = 300$ and the requirement of BER is 10^{-9}, the network can only accommodate 41 subscribers with correlation receivers, and otherwise it can implement 88 subscribers with chip-level receivers. If the requirement of BER is 10^{-12}, 20 users with correlation receivers are only allowed in the network and otherwise there can be 43 users with chip-level receivers in the network. It is obvious that the throughput of the network with chip-level receiver doubles.

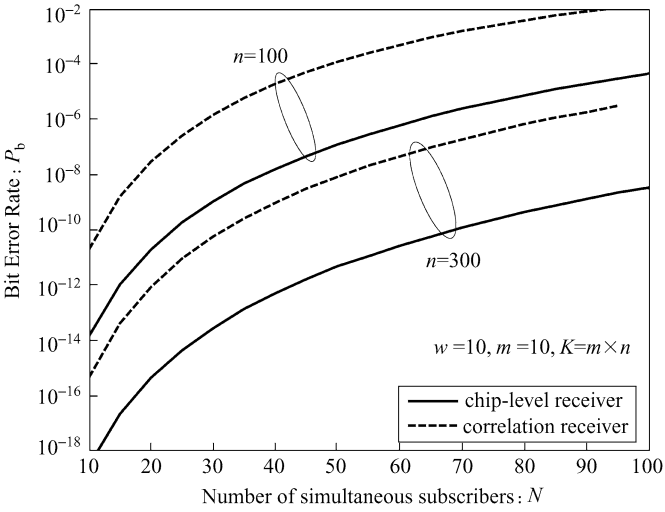

Figure 5.23 Comparison of the BER performances of both chip-level receiver and correlation receiver for 2-D WH/TS OCDMA system

5.5 Performance Analysis of Spectral-amplitude-encoding Incoherent OCDMA System Based on FBGs

Incoherent OCDMA system based on spectral amplitude encoding and balanced detection can employ the broadband incoherent light source with low cost, such as LED, ASE, etc., and suppress MAI effectively. Furthermore, it does not need to utilize the mode-locked laser and the nonlinear optical threshold device. At the receiving end, only a simple direct-detection receiver is required and moreover,

the frequency-spreading gain of the system is independent of the modulation bandwidth. Therefore, these advantages make it possess very big predominance to be applied to optical access network. Meanwhile, because of using incoherent light source, the system is slightly affected by the beat noise. In the earlier days, the proposed spectral amplitude encoding incoherent OCDMA was encoded/decoded by employing bulk-optic components[10, 11] that had big volume and it was difficult to package them and ensure stability for proper operation. At the same time, the components were very expensive, and the implementations were very complicated. With the progress of optical fiber grating technology, the spectral amplitude encoding/decoding can be implemented by employing FBGs. In this section, we introduce the BER performance analysis of incoherent OCDMA system based on FBGs encoding and balanced detection proposed in Reference [12]. The schematic diagram of the incoherent OCDMA network implemented by FBGs is shown in Fig. 5.24.

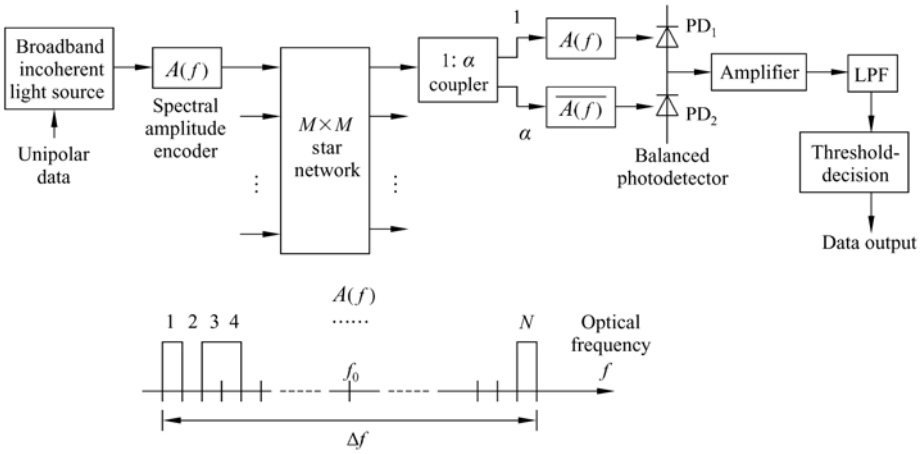

LPF: low pass filter, $\alpha = \lambda/(w-\lambda) = 1/p$

Figure 5.24 Schematic diagram of spectral amplitude encoding OCDMA system (Revised from Ref.[12])

It has been shown by research[12] that the effect of the phase-induced intensity noise (PIIN) on the system performance is proportional to the square of photocurrent in the spectral amplitude encoding incoherent OCDMA system, which results from the intensity fluctuation of broadband light source, and the system performance can not be improved by simply increasing the received optical power. In order to effectively suppress PIIN and not to require too many fiber-optic Bragg gratings, the $(N, w, \lambda) = (p^2 + p, p+1, 1)$ modified quadratic congruence code (MQCC)[12, 13] needs to be employed, where p is a prime number, the code length is $N = p^2 + p$, the code weight is $w = p+1$ and $\lambda = 1$ indicates in-phase cross correlation between any two distinct code sequences. Its

construction is similar to the construction of synchronous quadratic congruence code (SQCC) introduced in Subsection 2.6.3. Firstly choosing an odd prime number p, we construct a quadratic congruence sequence over Galois field, given by[12]

$$\begin{aligned} &\boldsymbol{S}_{\alpha,\beta} = (s_{\alpha,\beta}(0), s_{\alpha,\beta}(1), \cdots, s_{\alpha,\beta}(k), \cdots, s_{\alpha,\beta}(p-1), s_{\alpha,\beta}(p)) \\ &\alpha, \beta \in GF(p) = \{0,1,\cdots,p-1\} \end{aligned} \tag{5.63}$$

The elements of the quadratic congruence sequence are as[12]

$$s_{\alpha,\beta}(k) = \begin{cases} [(k+\alpha)^2 + \beta](\text{mod } p), & k = 0,1,\cdots,p-1 \\ [\alpha + b](\text{mod } p), & k = p \end{cases} \tag{5.64}$$

where $\alpha, \beta \in GF(p) = \{0,1,\cdots,p-1\}$. p^2 quadratic congruence sequences $\boldsymbol{S}_{\alpha,\beta}$ can be designed by varying the parameters α and β.

Then, from the sequences $\boldsymbol{S}_{\alpha,\beta}$ and using the following map[12]

$$c_{a,\alpha,\beta}(i) = \begin{cases} 1 & \text{iff } kp + s_{a,\alpha,\beta}(k) = i; i = 0,1,\cdots,p^2-1; k = \left\lfloor \dfrac{i}{p} \right\rfloor \\ 0 & \text{otherwise} \end{cases} \tag{5.65}$$

thus, the constructed binary (0,1) sequences—modified quadratic congruence codes, are given by[12]

$$\boldsymbol{C}_{\alpha,\beta} = (c_{\alpha,\beta}(0), c_{\alpha,\beta}(1), \cdots, c_{\alpha,\beta}(i), \cdots, c_{\alpha,\beta}(p^2-1)) \tag{5.66}$$

where $\alpha, \beta \in GF(p) = \{0,1,\cdots,p-1\}$ and $\lfloor x \rfloor$ represents taking the integral part of x. Each binary sequence $\boldsymbol{C}_{\alpha,\beta}$ can be divided into $p+1$ subsequences and the length of each subsequence is p. $s_{\alpha,\beta}(k)$ represents the position of the k^{th} "1" in the k^{th} subsequence of the binary sequence $\boldsymbol{C}_{\alpha,\beta}$. For the generated code sequences in this way, the in-phase cross correlation constraint between any two code-sequences is $\lambda = 1$. Let $c_k(i)$ be the i^{th} element of the k^{th} MQCC sequence so that the code sequences have the cross correlation properties as follows[12]

$$\sum_{i=1}^{N} c_k(i) c_l(i) = \begin{cases} p+1 & k = l \\ 1 & k \neq l \end{cases} \tag{5.67a}$$

$$\sum_{i=1}^{N} c_k(i) \overline{c}_l(i) = \begin{cases} 0 & k = l \\ p & k \neq l \end{cases} \tag{5.67b}$$

Because the operational principle of the optical encoder/decoder implemented by FBGs has been introduced in Subsection 4.4.2, we will not say any more than

is needed. In the following, let's introduce the BER performance of the spectral amplitude encoding incoherent OCDMA system with FBG encoder and decoder. In the analysis, the effects of incoherent intensity-induced noise, shot noise of photodetector and thermal noise on the BER performance are taken into account.

Assuming that: (1) each light source is ideally unpolarized and its power spectrum is flat over the bandwidth $\left[f_0-\frac{\Delta f}{2}, f_0+\frac{\Delta f}{2}\right]$ where f_0 is the central frequency of the optical source, Δf is the light source bandwidth in hertz; (2) each power spectrum component has identical spectral width; (3) each subscriber has the same optical power at the receiver; (4) the effect of PIIN, shot noise and thermal noise obeys Gaussian distribution (As a matter of fact, the total effect of PIIN and shot noise obeys negative binomial distribution[12]. However, in order to simplify the analysis, they are assumed to obey Gaussian distribution.), therefore, the power spectrum density (PSD) of received signal is given by[12]

$$r(f)=\frac{P}{\Delta f}\sum_{k=1}^{M}d_k\sum_{i=1}^{N}c_k(i)\left\{u\left[f-f_0-\frac{\Delta f}{2N}(-N+2i-2)\right]-u\left[f-f_0-\frac{\Delta f}{2N}(-N+2i)\right]\right\} \tag{5.68}$$

where P is the effective optical power at the receiver, M is the number of simultaneous subscribers in the network ($\leqslant p^2$), $N=p^2+p$ is the code length of MQCC, $d_k\in\{0,1\}$ indicates the data bit of the k^{th} subscriber and $u(f)$ denotes the unit step function that is given by

$$u(f)=\begin{cases}1 & f\geqslant 0\\ 0 & f<0\end{cases} \tag{5.69}$$

During one bit, the power spectrum densities of PD1 and PD2 of the l^{th} receiver are respectively given by[12]

$$p_1(f)=\frac{P}{\Delta f}\sum_{k=1}^{M}d_k\sum_{i=1}^{N}c_k(i)c_l(i)\left\{u\left[f-f_0-\frac{\Delta f}{2N}(-N+2i-2)\right]-u\left[f-f_0-\frac{\Delta f}{2N}(-N+2i)\right]\right\} \tag{5.70a}$$

$$p_2(f)=\frac{P}{p\Delta f}\sum_{k=1}^{M}d_k\sum_{i=1}^{N}c_k(i)\overline{c}_l(i)\left\{u\left[f-f_0-\frac{\Delta f}{2N}(-N+2i-2)\right]-u\left[f-f_0-\frac{\Delta f}{2N}(-N+2i)\right]\right\} \tag{5.70b}$$

Thus, we have[12]

$$\int_0^{\infty} p_1(f)\mathrm{d}f = \frac{P}{N}(p+1)d_l + \frac{P}{N}\sum_{k=1,k\neq l}^{M} d_k \tag{5.71a}$$

$$\int_0^{\infty} p_2(f)\mathrm{d}f = \frac{P}{N}\sum_{k=1,k\neq l}^{M} d_k \tag{5.71b}$$

The average photocurrent I is the difference of the photocurrents of PD1 and PD2, which is given by[12]

$$I = I_1 - I_2 = \Re\int_0^{\infty} p_1(f)\mathrm{d}f - \Re\int_0^{\infty} p_2(f)\mathrm{d}f = \Re\frac{P}{p}d_l \tag{5.72}$$

where $\Re$ denotes the responsivity of the PD, expressed as $\Re = \dfrac{\eta e}{hf_0}$. Here, η is the quantum efficiency, e is the electron charge equal to 1.602×10^{-19} Coulomb and h is the Plank constant equal to $6.626\times10^{-34}\,\mathrm{J\cdot s}$.

In order to compute the coherent time of the optical signals, expressed as

$$\tau_{ci} = \frac{\int_0^{\infty} p_i^2(f)\mathrm{d}f}{\left[\int_0^{\infty} p_i(f)\mathrm{d}f\right]^2},\quad i = 1,2 \tag{5.73}$$

the integral of $p_i^2(f)$ needs to be calculated firstly, $i = 1,2$. Let's take into account an example of the power spectrum density $p'(f)$ of the received superimposed signal, shown in Fig. 5.25, where $a(i)$ indicates the amplitude of the i^{th} spectrum chip (slot) with width $\Delta f / N$. The integral of $p'^2(f)$ can be expressed as[12]

$$\int_0^{\infty} p'^2(f)\,\mathrm{d}f = \frac{\Delta f}{N}\sum_{i=1}^{N} a^2(i) \tag{5.74}$$

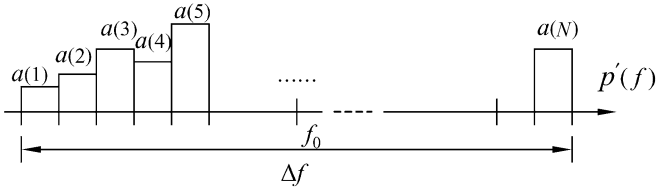

Figure 5.25 Power spectral density of the received signal $r(f)$ (After Ref.[12])

From (5.70), we have[12]

$$\int_0^{\infty} p_1^2(f)\,\mathrm{d}f = \frac{P^2}{N\Delta f}\sum_{i=1}^{N}\left\{c_l(i)\left[\sum_{k=1}^{M} d_k c_k(i)\right]\cdot\left[\sum_{m=1}^{M} d_m c_m(i)\right]\right\} \tag{5.75a}$$

$$\int_0^{\infty} p_2^2(f)\,\mathrm{d}f = \frac{P^2}{p^2 N\Delta f}\sum_{i=1}^{N}\left\{\overline{c}_l(i)\left[\sum_{k=1}^{M} d_k c_k(i)\right]\cdot\left[\sum_{m=1}^{M} d_m c_m(i)\right]\right\} \tag{5.75b}$$

Because the noises of PD1 and PD2 are mutually independent, then the power of noise sources that exist in the photocurrent can be expressed as [12]

$$\begin{aligned}\langle I^2\rangle &= \langle I_1^2\rangle + \langle I_2^2\rangle + \langle I_{th}^2\rangle \\ &= 2eB(I_1+I_2) + B(I_1^2\tau_{c1} + I_2^2\tau_{c2}) + 4k_{\mathrm{B}}T^0 B/Z_L\end{aligned} \tag{5.76}$$

where the first term comes from the shot noise, the second term represents the effect of PIIN, the third term indicates the effect of the thermal noise. Here, B is the noise-equivalent electrical bandwidth of the receiver, k_{B} is Boltzmann constant, which is $k_{\mathrm{B}} = 1.38\times10^{-23}\,\mathrm{J/K}$, T^0 is the absolute noise temperature of the receiver, and Z_L denotes the load impedance of the receiver.

Substituting (5.73) into (5.76), we obtain

$$\begin{aligned}\langle I^2\rangle = {} & 2eB\Re\left[\int_0^{\infty} p_1(f)\mathrm{d}f + \int_0^{\infty} p_2(f)\mathrm{d}f\right] + B\Re^2\left[\int_0^{\infty} p_1^2(f)\mathrm{d}f + \int_0^{\infty} p_2^2(f)\mathrm{d}f\right] \\ & + 4k_{\mathrm{B}}T^0 B/Z_L\end{aligned} \tag{5.77}$$

From (5.71) and (5.75), when all subscribers are sending data bit "1", employing the average value as $\sum_{k=1}^{M} c_k(i) \approx \frac{M}{p}$ and the correlation properties (5.67) of MQCC, then the noise power can be given by[12]

$$\begin{aligned}\langle I^2\rangle &= 2eB\Re\left[\frac{P}{p^2+p}(p+1) + 2\frac{P}{p^2+p}(M-1)\right] \\ &\quad + B\Re^2\frac{P^2}{(p^2+p)\Delta f}\left[(p+1+M-1)\frac{M}{p} + \frac{1}{p^2}p(M-1)\frac{M}{p}\right] + 4k_{\mathrm{B}}T^0 B/Z_L \\ &= 2eB\Re P\frac{p-1+2M}{p^2+p} + \frac{B\Re^2P^2M}{\Delta f(p+1)p^2}\left(\frac{M-1}{p} + p + M\right) + 4k_{\mathrm{B}}T^0 B/Z_L\end{aligned} \tag{5.78}$$

Assuming that all subscribers send equiprobably data bits "0" and "1", then we have[12]

$$\langle I^2 \rangle = \frac{B\Re^2 P^2 M}{2\Delta f(p+1)p^2}\left(\frac{M-1}{p}+p+M\right)+eB\Re P\frac{p-1+2M}{p^2+p}+4k_{\mathrm{B}}T^0 B/Z_L \tag{5.79}$$

where the first term represents the power of PIIN noise, the second term indicates the power of shot noise and the third term denotes the power of thermal noise. From (5.72) and (5.79), the resulting average noise power of the system is given by[12]

$$SNR = \frac{(I_1 - I_2)^2}{\langle I^2 \rangle} = \frac{\frac{1}{p^2}\Re^2 P_{sr}^2}{\frac{B\Re^2 P_{sr}^2 M}{2\Delta f(p+1)p^2}\left(\frac{M-1}{p}+p+M\right)+eB\Re P_{sr}\frac{p-1+2M}{p^2+p}+4k_{\mathrm{B}}T^0 B/Z_L} \tag{5.80}$$

Since Gaussion approximation is employed, the bit error rate of the system is[12]

$$P_{\mathrm{b}} = \frac{1}{2}Q\left[\sqrt{SNR/8}\right] \tag{5.81}$$

where $Q(x) = \frac{1}{\sqrt{2\pi}}\int_x^{\infty}\exp\left(-\frac{y^2}{2}\right)\mathrm{d}y$ is Q function.

Figure 5.26 shows the relationship curves of the system signal-to-noise ratio (SNR) versus the number of simultaneous subscribers for employing MQCC of $p = 5,7,11,13,17$ respectively. The other parameters employed in the simulation are shown in Table 5.2 and we suppose that the effective light power received by every subscriber is $P = -10$ dBm.

Table 5.2 System parameters employed in the calculation

Optical center frequency	f_0 = 194THz (λ_0 = 1550nm)
Light source bandwidth	Δf = 3.75THz
User's bit rate	R_{b} = 500Mb/s
PD quantum efficiency	η = 0.6
Receiver electrical bandwidth	B = 250MHz
Receiver noise temperature	T^0 = 300K
Receiver load impedance	Z_L = 1030Ω

Figure 5.27 gives the curves of the system BER versus the number of simultaneous subscribers for the effective power $P = -10$ dBm from each user. It can be seen that the BER increases as the number of simultaneous subscribers

increases. Under the same BER, the increase of code length can make the number of simultaneous users increase.

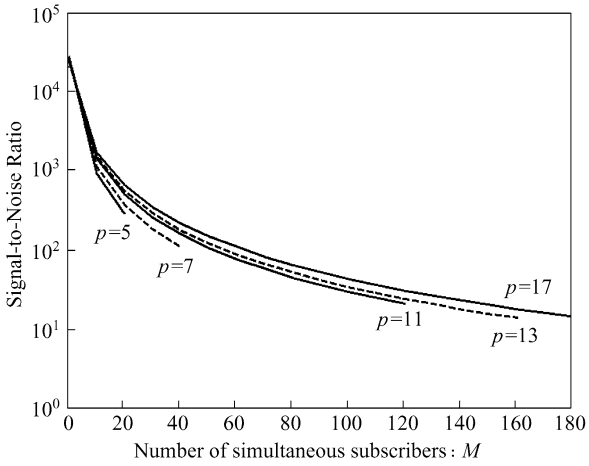

Figure 5.26 SNR versus the number of simultaneous subscribers employing MQCC of $p = 5,7,11,13,17$ respectively when $P = -10$ dBm

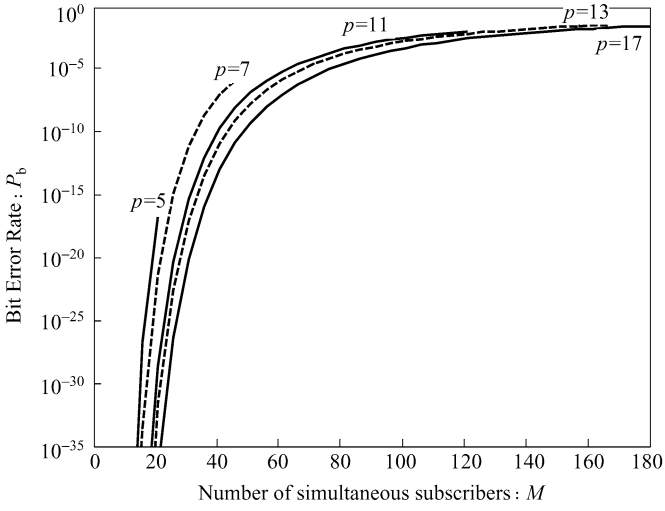

Figure 5.27 BER versus the number of simultaneous subscribers when $P = -10$ dBm

Figure 5.28 gives the variation curves of the BER with the effective light power received by every subscriber for $p = 11$ and the number of simultaneous users 121, where the solid line represents the BER for taking into account the effects of intensity, shot and thermal noises, the dashed line denotes the system BER with the effects of intensity and shot noises and the dotted line indicates the system BER with the effects of intensity and thermal noises. It can be seen that

when the effective power P is big (i.e., > −10dBm), the intensity noise is the main limitation factor of the system performance. When the effective power is not large enough, the thermal and shot noises are the main limitation factors. Furthermore, the effect of thermal noise is much larger than that of shot noise on the BER performance.

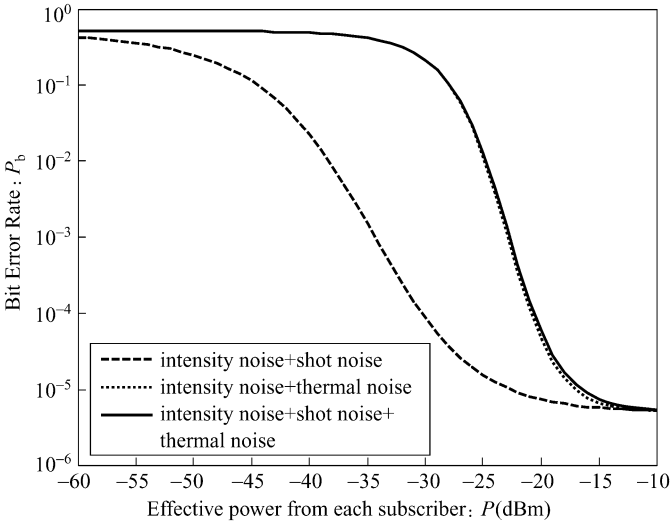

Figure 5.28 BER versus the effective power P when the number of simultaneous subscribers is 49

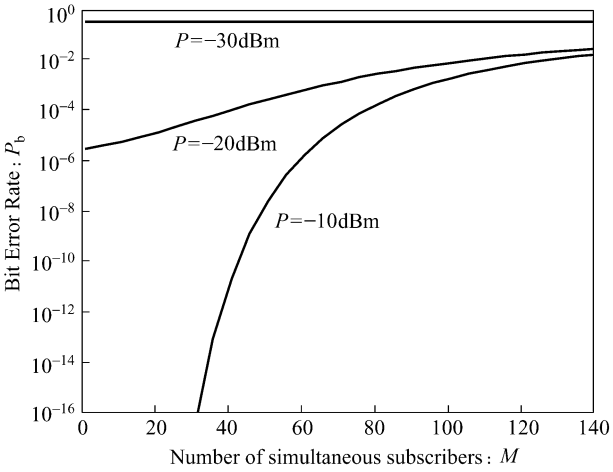

Figure 5.29 BER versus the number of simultaneous subscribers for the different values of P

Figure 5.29 shows the variation traces of the BER versus the effective light power and the number of simultaneous subscribers for taking into account the

PIIN, shot and thermal noises. It can be seen that the system BER increases as the number of simultaneous subscribers increases and the BER decreases as the effective light power received by every user increases. When $p=13$, $P=-10$ dBm and the BER is $P_b=10^{-9}$, the network can accommodates 46 simultaneous subscribers.

5.6 Performance Analysis of Spectral Phase Encoding Coherent OCDMA System

5.6.1 Modeling Spectral Phase Encoding Coherent OCDMA System

The schematic block diagram of the spectral phase encoding coherent OCDMA network employing ultrashort light pulse is shown in Fig. 5.30[14, 15], where the schematic waveforms at some individual points are also given. The transmitter is composed of a coherent ultrashort light pulse source with limited bandwidth, a data source and a spectral phase encoder. The ultrashort light source generates a series of ultrashort light pulses (A) with the duration τ_c and the period T_b, whose broadband spectrum (B) is multiplied by the data produced by the data generator. For the on-off keying format, when the data is "1", the ultrashort pulse is fed into the spectral phase encoder. The spectral phase encoder imposes a specific phase shift on each spectral component of the ultrashort pulse. Otherwise, when the data is "0", the output of the spectral encoder is zero because none optical pulse is fed into the encoder. This encoding process is implemented through a spectral phase code generator multiplying each spectral component of the ultrashort pulse. Since the phase code generated by the spectral phase code generator of each subscriber is unique, the solely spectral phase encoding (C) of the data from each user is implemented. The spectral phase code can employ the binary codes with good properties which are widely applied to the electrical wireless CDMA, such as m-sequences, Gold codes, etc. The optical signal with spectral phase encoded in time domain looks like a low intensity pseudo-noise burst (D), which is fed into the optical fiber communication network. At the receiving end, the spectral phase decoder receives the desired signal with the spectral phase (E) and the multiple-access interference from all other subscribers. When the spectral phase codes for the decoder and encoder are complex conjugate pair the decoder removes the spectral phase shift (F) and reconstructs the original ultrashort pulse (G). Finally, the data is restored through optical-to-electrical conversion and threshold-decision. When the codes for the decoder and encoder do not match the decoder can not remove the spectral phase shift and reconstruct the original pulse. Otherwise, the decoded signal remains the

pseudo-noise burst. Therefore, no data are output after the optical-to-electrical conversion and threshold-decision.

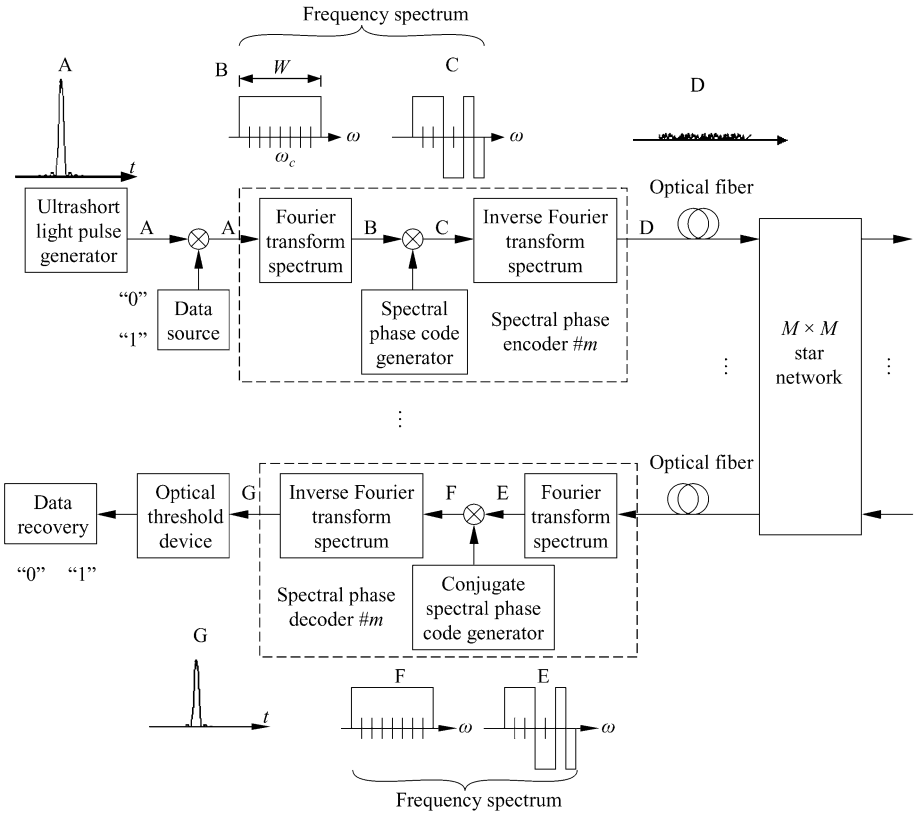

Figure 5.30 Schematic diagram of Spectral phase encoding OCDMA network (After Ref.[14])

Figure 5.31 shows the spectrum of an uncoded signal with limited bandwidth and its corresponding ultrashort light pulse signal in time domain, and an example of spectral phase encoded signal with an m-sequence $(+1,+1,+1,-1,-1,+1,-1)$ of length 7 and its intensity profile after being encoded. The ultrashort pulse from the light source is characterized by the baseband Fourier spectrum at angular frequency ω, $F(\omega)$, expressed as

$$F(\omega)=\begin{cases}\dfrac{\sqrt{P_0}}{W}, & |\omega|\leqslant\dfrac{W}{2}\\ 0, & \text{elsewhere}\end{cases} \tag{5.82}$$

where P_0 indicates the peak power of the ultrshort light pulse and W denotes the

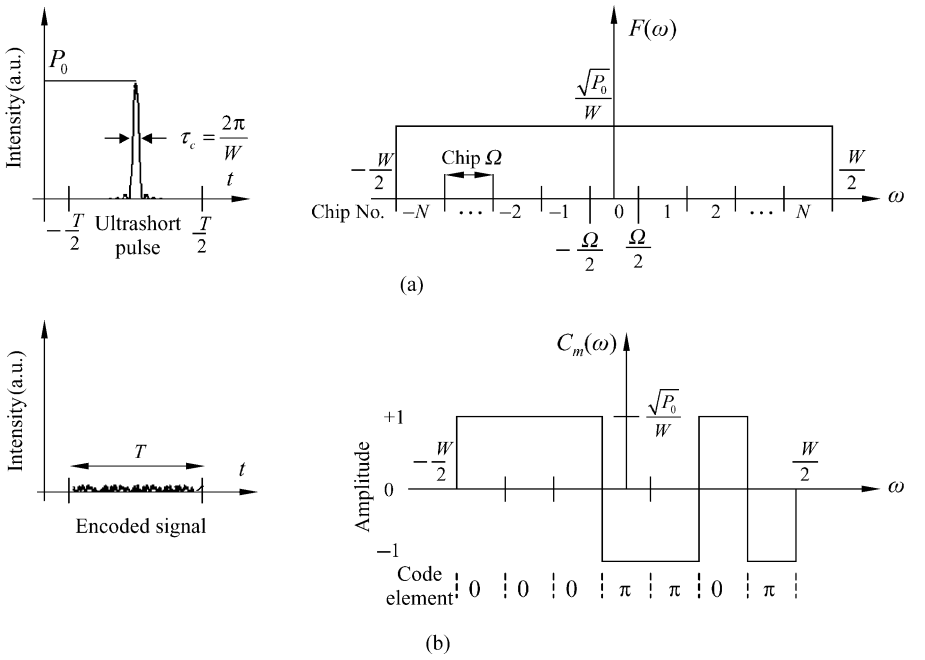

Figure 5.31 (a) Spectrum for an uncoded band-limited signal and its corresponding ultrashort optical pulse; (b) Intensity profile and spectrum of a typically spectral phase encoded signal [14]

total bandwidth of the Fourier spectrum. The temporal waveform of the ultrashort pulse can be expressed as the inverse Fourier transform of $F(\omega)$, given by

$$f(t) = \sqrt{P_0}\,\mathrm{sinc}\left(\frac{W}{2}t\right) \tag{5.83}$$

where $\mathrm{sinc}(x) = \dfrac{\sin x}{x}$. The instantaneous power of the ultrashort light pulse is

$$P(t) = |f(t)|^2 = P_0\,\mathrm{sinc}^2\left(\frac{W}{2}t\right) \tag{5.84}$$

whose full-width at half-maximum (FWHM) duration is $\tau_c \approx 2\pi/W$. In order to encode this light pulse, the phase mask for the encoder is multiplied by $F(\omega)$. This phase mask comprises $N_0 = 2N+1$ distinct chips and the bandwidth of each chip is $\Omega = W/N_0$. The phase of each chip can be adjusted individually. The baseband spectrum of the encoded signal for the m^{th} subscriber can be expressed as[14]

$$C_m(\omega) = \sum_{n=-N}^{N} F(N_0(\omega - n\Omega))\exp(-\mathrm{j}\varphi_n^{(m)}) \tag{5.85}$$

where $\varphi_n^{(m)}$ represents the spectral phase code element of the n^{th} chip for the m^{th} subscriber, which is set to either "0" or "π" randomly with equiprobability, that is, $\exp\left(-\mathrm{j}\varphi_n^{(m)}\right)$ is set to either "+1" or "-1", where j is a unit of imaginary number, equal to $\sqrt{-1}$. The inverse Fourier transform of (5.85) is the electrical field amplitude expression of the encoded signal with the variation of time *t*, given by[14]

$$\begin{aligned} c_m(t) &= \mathrm{sinc}\left(\frac{\Omega}{2}t\right)\frac{\sqrt{P_0}}{N_0}\sum_{n=-N}^{N}\exp[-\mathrm{j}(n\Omega t+\varphi_n^{(m)})] \\ &= G(t)V_m(t) \end{aligned} \tag{5.86}$$

where

$$G(t) = \mathrm{sinc}\left(\frac{\Omega}{2}t\right) \tag{5.87}$$

$$V_m(t) = \frac{\sqrt{P_0}}{N_0}\sum_{n=-N}^{N}\exp[-\mathrm{j}(n\Omega t+\varphi_n^{(m)})],\ \text{for}\ |t|\leqslant\frac{T}{2} \tag{5.88}$$

here, $G(t)$ is a real envelope function, which determines the temporal width of the encoded pulse and is independent of the code elements. $V_m(t)$ is a periodic pseudo-noise signal with the period $T = 2\pi/\Omega$, which is defined by the address code signal of the m^{th} subscriber. The temporal waveform of $V_m(t)$ depends on $\varphi_n^{(m)}$, whose average power is P_0/N_0. When $\varphi_n^{(m)} = 0$ for all n, $V_m(t)$ is simplified as $V_p(t)$, which is[14]

$$V_p(t) = \frac{\sqrt{P_0}}{N_0}\sum_{n=-N}^{N}\exp[-\mathrm{j}(n\Omega t)],\ \text{for}\ |t|\leqslant\frac{T}{2} \tag{5.89}$$

$V_p(t)$ represents the electric field amplitude of the ultrashort pulse with the peak power P_0.

5.6.2 BER Performance of Spectral Phase Encoding Coherent OCDMA System

We assume that all subscribers in the network have identical bit rate and signal format and at the same time, the effects of quantum and thermal noise on the system are neglected for the sake of analysis simplification, that is, the degradation of system performance results completely from the presence of multiple-access interference. Let's take into account the simplest network protocol in which the transmitters and receivers are paired and the communication between the m^{th}

transmitter and receiver pair is consecutive, $0 \leqslant m \leqslant M$, where M denotes the total number of simultaneous subscribers in the network. After the spectral phase encoding, the incident ultrashort light pulse is spread into a pseudo-noise burst with longer duration and lower intensity. For an ideal light source, the electric field expression for the m^{th} transmitted signal is[14]

$$E_m(t) = \sum_{j=-\infty}^{\infty} d_j^{(m)} V_m(t - jT_\text{b}), \text{ for } |t - jT_\text{b}| \leqslant \frac{T}{2} \tag{5.90}$$

where $d^{(m)} = \{d_j^{(m)}\}$ denotes the m^{th} data sequence that takes on "0" or "1" for every j. $V_m(t - jT_\text{b})$ indicates the encoded unit pulse with a duration equal to T for every j, which is defined as shown in (5.88).

For the multiple-access interference in the spectral phase encoding OCDMA system, it can be modeled as Gaussian random processes[14] when the number of simultaneous subscribers is large and the m-sequences or Gold sequences are long enough. The encoded pulse is spread over a characteristic time $T = 2\pi/\Omega$, where Ω is the frequency spacing between adjacent spectral code elements. Since the temporal width of the incident ultrashort light pulse is $\tau_c \approx 2\pi/W = 2\pi/N_0\Omega$, where $W = N_0\Omega$ is the total bandwidth, therefore $T = N_0\tau_c$ is obtained, that is, the original pulse is spread N_0 times by spectral phase encoding. Generally speaking, the duration of data bit, T_b, may be longer than the temporal width of encoded pulse T and let T_b be K times as long as T, i.e., $K = T_\text{b}/T$, where K is a positive integer. The data rate for every subscriber is $1/T_\text{b}$. The relationships among these parameters are shown in Fig. 5.32[14].

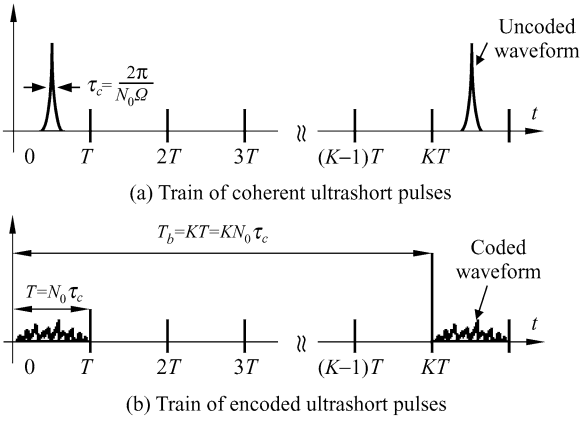

Figure 5.32 A schematic timing diagram for coherent ultrashort pulse OCDMA (After Ref. [14])

Assuming that the m^{th} receiver is a correlation receiver that matches the m^{th} signal, that is, the phase code for the m^{th} optical phase decoder is the complex conjugate of the m^{th} encoder's spectral phase code, then the correct decoding and data restoring can be implemented. The result of the m^{th} encoded signal $E_m(t)$ passing through the k^{th} decoder is expressed as $E_{mk}(t)$. In a spectral phase encoding coherent OCDMA network, where the subscribers send their information asynchronously, the output electric field expression of the k^{th} decoder is given by[14]

$$r(t) = E_{kk}(t) + \sum_{m \neq k} E_{mk}(t - t'_{mk}) \tag{5.91}$$

where $E_{kk}(t)$ denotes the desired signal decoded successfully, which is a replica of the original ultrashort pulse with duration τ_c and peak power P_0. The second term in (5.91) indicates the total multiple-access interference signal at the output of the k^{th} decoder. When $m \neq k$, the unsuccessfully decoded signals $E_{mk}(t)$ remain low intensity pseudo-noise bursts with average power P_0 / N_0 and duration T. Because of assuming random coding, the statistic characteristics of the unsuccessfully decoded signals $E_{mk}(t)$ are identical to the statistic characteristic of the encoded signal $E_m(t)$. t'_{mk} represents the random delay of the signal from the m^{th} encoder to the k^{th} decoder. We assume $t'_{kk} = 0$, that is, the synchronization between the desired transmitter and receiver pair is maintained perfectly.

If the intensity signal is defined as

$$I(t) = r(t) r^*(t) \tag{5.92}$$

where "$*$" represents taking on complex conjugate. For on-off keying format, the decision is performed by the comparison between $I(t)$ and a threshold level I_{th}. The expected sampling instants are at $t = 0$, T_{b}, $2T_{\text{b}}, \cdots, jT_{\text{b}}, \cdots$. At these times ($|T - jT_{\text{b}}| \leqslant \tau_c / 2$), if $d_j^{(k)} =$ "1" the signal E_{kk} is equal to $\sqrt{P_0}$ and if $d_j^{(k)} =$ "0" then the signal E_{kk} is zero. At other times ($|T - jT_{\text{b}}| > \tau_c / 2$), E_{kk} is equal to zero and independent of $d_j^{(k)}$. At any desired sampling times $t = jT_{\text{b}}$, the conditional probability density functions of the intensity are given by[14]

$$P_I(I / d_0^{(1)} = 0, l) = \frac{N_0}{lP_0} \exp\left(-\frac{IN_0}{lP_0} \right) \tag{5.93}$$

$$P_I(I / d_0^{(1)} = 1, l) = \frac{N_0}{lP_0} \exp\left(-\frac{N_0 (I + P_0)}{lP_0} \right) I_0\left(\frac{2N_0 \sqrt{IP_0}}{lP_0} \right) \tag{5.94}$$

where $I_0(x)$ is the modified Bessel function of the first kind zero order, and $l \geqslant 1$. For times that are not coincident with the desired sampling times ($|T - jT_b| > \tau_c / 2$), the conditional probability density function is given by (5.93) and is independent of $d_j^{(k)}$. From (5.93) and (5.94), the conditional probability densities condition on that l other subscribers are transmitting the data "1" at the sampling instant.

It is assumed that if the decoded intensity exceeds the threshold at any time within an interval of duration $\beta\tau_c$ the receiver detects a "1", and otherwise, a "0" is detected by the receiver, $1 \leqslant \beta \leqslant N_0$. The threshold decision is done by employing the nonlinearly optical threshold device or by the electrical threshold circuit after the optical-to-electrical conversion. However, the latter has the electronic "bottle neck" effect at speed. $\beta = 1$ corresponds to the ideal threshold device that is activated at the instant when the desired data are expected. For on-off keying format, the average BER for the spectral phase encoding OCDMA system is[14]

$$P_b = \langle P_b(l) \rangle_l \tag{5.95}$$

where $\langle \cdot \rangle_l$ indicates taking ensemble average with respect to l. l denotes the number of interfering subscribers, which is a random variable and satisfies a binomial distribution, expressed as[14]

$$P(I) = \binom{M-1}{l} \left(\frac{1}{2K}\right)^l \left(1 - \frac{1}{2K}\right)^{M-1-l} \tag{5.96}$$

where $K = T_b / T$ and M is the number of simultaneous subscribers in the network.

$$\begin{aligned} P_b(l) &= P_r(I \geqslant I_{th} / d_0^{(k)} = 0, l) \cdot P_r(d_0^{(k)} = 0) + P_r(I < I_{th} / d_0^{(k)} = 1, l) \cdot P_r(d_0^{(k)} = 1) \\ &= \frac{1}{2}[P_{FA}(l) + P_{MD}(l)] \end{aligned} \tag{5.97}$$

where $P_{FA}(l)$ and $P_{MD}(l)$ represents the probabilities of false alarm and missed detection respectively. They are expressed respectively as[14]

$$P_{FA}(l) = 1 - \gamma^{\beta}(l) \tag{5.98}$$

$$P_{MD}(l) = \gamma^{\beta - 1}(l)\rho(l) \tag{5.99}$$

where

$$\gamma(l) = 1 - \exp\left(-\frac{I_{th} N_0}{l P_0}\right) \tag{5.100}$$

$$\rho(l) = 1 - Q\left(\sqrt{\frac{2N_0}{l}}, \sqrt{\frac{2N_0 I_{\text{th}}}{lP_0}}\right) \tag{5.101}$$

Substituting (5.96) – (5.99) into (5.95), the resulting average BER for the spectral phase encoding OCDMA system are given by[14]

$$\begin{aligned} P_{\text{b}} &= \langle P_{\text{b}}(l)\rangle_l = \left\langle \frac{1}{2} P_{\text{FA}}(l) + P_{\text{MD}}(l) \right\rangle_l \\ &= \frac{1}{2}\sum_{l=1}^{M-1} P(I)[P_{\text{FA}}(l) + P_{\text{MD}}(l)] \\ &= \frac{1}{2}\left[\sum_{l=1}^{M-1}\binom{M-1}{l}\left(\frac{1}{2K}\right)^l \left(1-\frac{1}{2K}\right)^{M-1-l}\left(1-(\gamma(l))^{\beta-1}(\gamma(l)-\rho(l))\right)\right] \end{aligned} \tag{5.102}$$

where $Q(a,b) \equiv \int_b^\infty x \exp\left(\frac{-a^2-x^2}{2}\right) I_0(ax)\mathrm{d}x$. $\gamma(l)$ and $\rho(l)$ are defined respectively as in (5.100) and (5.101). The data bit rate for single subscriber is $R_b = 1/T_b = 1/KT = 1/KN_0\tau_c$.

Figure 5.33 gives the curves of BER versus normalized threshold (I_{th}/P_0) for OCDMA system with code length $N_0 = 127$ and $K = 100$, where $\beta = 1$ (solid lines) and $\beta = 127$ (dashed lines) corresponds to ideal and not ideal but "practical" detection scheme respectively. From this diagram, it can be seen that the optimum normalized thresholds for the numbers of simultaneous subscribers $M = 20$ and

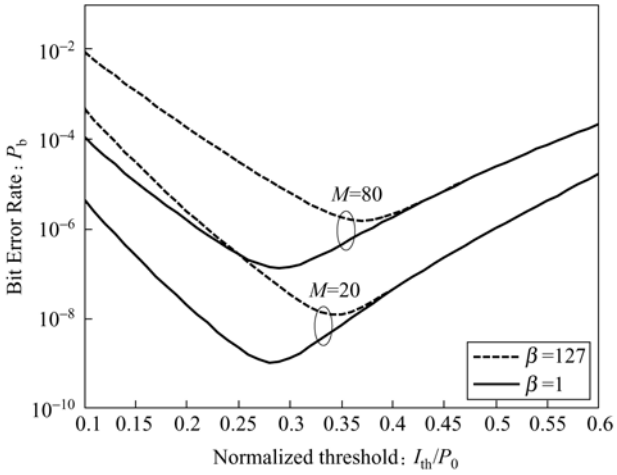

Figure 5.33 Curves of BER versus normalized threshold (I_{th}/P_0) for code length $N_0 = 127$ and $K = 100$[14]

$M = 80$ are approximate 0.28 and the optimum normalized thresholds are slightly dependent on the value of M when $\beta > 1$. The minimum BERs for the systems with optimum thresholds for $M = 20$ and $M = 80$ are around 10^{-9} and 1.4×10^{-7} separately.

The curves of the minimum BERs versus the number of subscribers M for different values of K and N_0 are shown in Fig. 5.34. From these curves, it can be seen that the BER performance degrades as the number of subscribers increases and the BER performance is significantly improved as the code length increases.

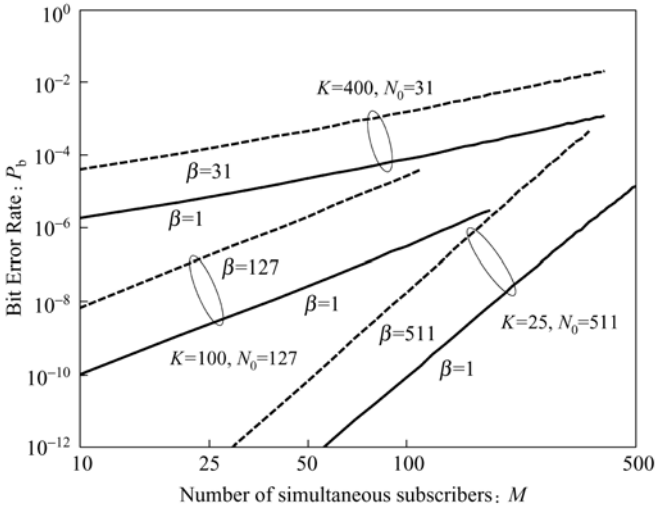

Figure 5.34 BER versus the number of users (M) for different values of K and N_0

5.7 Performance Analysis of Temporal Phase Encoding Coherent OCDMA System

The bipolar or multi-polar codes with good correlation properties, which are widely applied to the wireless CDMA, can be used as the subscribers' address codes in the temporal phase encoding coherent OCDMA systems so that the number of subscribers in such an OCDMA network can increase significantly and the system performance can be improved greatly. Especially, with the progress of technologies of planar lightwave circuits and fiber-optic Bragg grating, the temporal phase encoder and decoder can be implemented by employing PLC and SSFBG, which attracts many researchers' intensive interests. It is at present deemed that it is one of promising technical schemes to implement OCDMA. In this section, we will introduce the BER performance analysis method of the temporal phase encoding coherent OCDMA system.

5.7.1 Modeling Temporal Phase Encoding Coherent OCDMA System

The temporal phase encoding coherent OCDMA system is a type of time-spreading OCDMA, whose system model is shown in Fig. 5.35[2]. Four kinds of noises are represented in this model, which are the MAI noise from the OCDMA network, the multiplied beat noise and additive shot noise from photodetector, and the thermal noise of receiver. In the temporal phase encoding coherent OCDMA, the coherence of the optical signal has to be maintained within the chip duration and thus the coherent beat noise becomes critical. It has been shown from investigation that the BER performance of the incoherent OCDMA system is mainly confined by the MAIs from the network and otherwise the BER performance of the coherent OCDMA system is limited by the beat noise[2]. Therefore, in order to highlight the beat noise, we draw the shot noise behind the photodetector in the system model. The bandwidth of receiver is limited by the chip rate and thus is equivalent to an integrator (over one-chip interval) followed a decision thresholder.

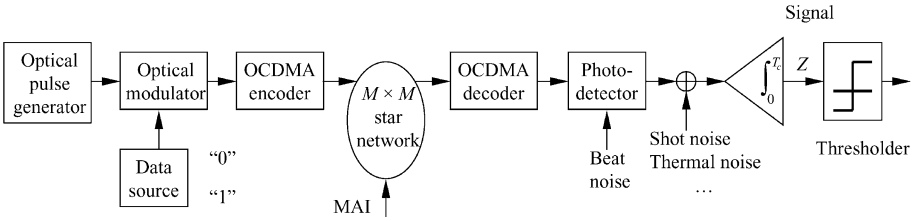

Figure 5.35 Model of temporal phase encoding OCDMA system with various noises[2]

It is supposed that M subscribers are transmitting their signals asynchronously in the network. If there are l interference signals from the undesired active subscribers at a given instant, $1 \leqslant l \leqslant M-1$, then the received autocorrelation optical field at the photodetector of the desired subscriber is expressed as[16]

$$E(t) = \sqrt{P_d}\exp[\mathrm{j}(\omega_d t + \phi_d(t))] + \sum_{i=1}^{l}\sqrt{P_i}\exp[\mathrm{j}(\omega_i(t-\tau_i) + \phi_i(t-\tau_i))] \quad (5.103)$$

where P_d and P_i indicate the optical intensities of the decoded signals from the desired subscriber (data) and the interfering subscribers (undesired) respectively, ω_d and ω_i denote their angular frequencies respectively, ϕ_d and ϕ_i represent the respective phase noise of these signals. It is assumed that ϕ_d and ϕ_i are mutually independent Gaussian distributed Wiener-Levy stochastic processes. τ_i represents the transmission delays of the interferers relative to data through the network and $\mathrm{j} = \sqrt{-1}$ is the unit of imaginary number.

For the temporal phase encoding OCDMA network employing chip-rate square-law photodetector, the output signal Z from the integrator is expressed as[16]

$$\begin{aligned} Z &= \int_0^{T_c} \Re \cdot (E \cdot E^*) \mathrm{d}t + \int_0^{T_c} n_0(t) \mathrm{d}t \\ &= T_c \Re P_d + T_c \Re \sum_{i=1}^{l} P_i + 2\Re \sum_{i=1}^{l} \sqrt{P_d P_i} \int_0^{T_c} \cos[(\omega_i - \omega_d)t - \omega_i \tau_i + \phi_i(t-\tau_i) - \phi_d] \mathrm{d}t \\ &\quad + 2\Re \sum_{i=1}^{l-1} \sum_{k=i+1}^{l} \sqrt{P_i P_k} \int_0^{T_c} \cos[(\omega_i - \omega_k)t - \omega_i \tau_i + \omega_k \tau_k + \phi_i(t-\tau_i) - \phi_k(t-\tau_k)] \mathrm{d}t + \int_0^{T_c} n_0(t) \mathrm{d}t \end{aligned} \tag{5.104}$$

where the symbol $\Re$ indicates the responsivity of the photodetector that is $\Re = \eta e / hf_0$, η is the quantum efficiency, e denotes the electron charge equal to 1.602×10^{-19} coulomb, h is Plank constant equal to $6.626 \times 10^{-34}\,\mathrm{J \cdot s}$, f_0 represents the central frequency of the light source. When the optical center wavelength is $\lambda_0 = 1550\mathrm{nm}$, $f_0 = 194\mathrm{THz}$. T_c denotes the duration of a chip and n_0 indicates the corresponding noise photocurrent of the photodetector shot noise and the receiver thermal noise. In (5.104), it is supposed that the bandwidth of photodetector is larger than the angular frequency differences $(\omega_i - \omega_d)$ between the incoming signals and at the same time, the chip pulse waveform is constant over the chip duration T_c. The first term in (5.104) represents the desired signal term, the second term denotes the MAI noises, the third term indicates the beat noise between data and the interferences, which contains l terms and is the primary composition of the beat noise. The fourth term represents the beat noise between two interferences, which contains $l(l-1)/2$ terms totally, and is the secondary composition of the beat noise. The last term is the shot noise and the thermal noise from the photodetector and the receiver respectively. Here, it is also assumed that the polarization states of the data and interference signals are identical, which corresponds to the worst-case scenario of system BER.

The crosstalk level $\xi \equiv \langle P_i \rangle / P_d$ in the temporal phase encoding OCDMA network is very small, that is, $\xi \ll 1$, where $\langle \cdot \rangle$ represents the assemble average. For instance, $\xi \approx 1/N_{\mathrm{chip}}$ for the temporal phase encoding coherent OCDMA network employing SSFBG encoder and decoder and Gold code as subscriber address code, where N_{chip} is the code length of Gold code. The ratio of the variance of primary and secondary beat noise terms is proximately $2/l\sqrt{\xi}$. When l is not so large that $l\sqrt{\xi} \ll 1$, then the secondary beat noise can be neglected[2]. In this case, we only need to take into account the effect of the primary term on the system performance.

There are three terms within the cosine function of the primary beat noise term, where the first term is $(\omega_i - \omega_d)t \equiv \Delta\omega_{id}t$. Typically, if it is assumed that $\Delta\omega_{id} \leqslant 1\text{GHz}$ and $T_c \approx 10\text{ps}$ in the temporal phase encoding OCDMA network, then there exists $\Delta\omega_{id}t \ll 2\pi$ within the integral duration T_c. Thus, the first term can be ignored. The secondary term $\omega_i\tau_i$ is approximately a constant and can also be neglected. The third term $\phi(t-\tau_i) - \phi_d \equiv \Delta\phi_{id}(t)$ depends strongly on the coherent property of the optical pulse within the integral duration.

Since in the temporal phase encoding coherent OCDMA system, the coherent of light source should be maintained at least within every chip, it must be satisfied that the chip duration T_c is larger than the coherent time τ_c of light source, that is, $\tau_c \geqslant T_c$. In this case, $\Delta\phi_{ik}(t)$ is a small constant within the integral time T_c. Therefore, we have[2]

$$Z \approx T_c\Re\left(P_d + \sum_{i=1}^{l} P_i\right) + \Re T_c\left(2\sum_{i=1}^{l}\sqrt{P_d P_i}\cos(\Delta\Phi_i)\right) + \int_0^{T_c} n_0(t)\,\mathrm{d}t \tag{5.105}$$

where $\Delta\Phi_i \equiv \Delta\omega_{id}T_c + \omega_i\tau_i + \Delta\phi_{id}$ indicates the total phase noise, which is a random process that varies over $[-\pi, \pi]$ from bit to bit and causes the beat noise in the temporal phase encoding coherent OCDMA system. In addition, note that in this expression, the secondary beat noise term has been neglected for the sake of simplicity.

5.7.2 BER Performance Analysis of Temporal Phase Encoding Coherent OCDMA System[2]

The average bit error rate of the temporal phase encoding coherent OCDMA system is given by

$$P_{\mathrm{b}} = \sum_{l=0}^{M-1} p(l)P_{\mathrm{b}}(l) \tag{5.106}$$

where $p(l)$ indicates the probability that l subscribers among $M-1$ interfering subscribers are sending "1"s within the detected chip, which obeys binomial distribution as follows

$$p(l) = \binom{M-1}{l} 2^{-(M-1)} \tag{5.107}$$

$P_{\mathrm{b}}(l)$ is the bit error rate with l interfering subscribers. With the equiprobable

binary data and chip-level detection, $P_{\mathrm{b}}(l)$ is given by

$$\begin{aligned} P_{\mathrm{b}}(l) &= P_r(0)_{\mathrm{chip}} P_e(1\,|\,0)(l) + P_r(1)_{\mathrm{chip}} P_e(0\,|\,1)(l) \\ &= \left[P_r(0)_{\mathrm{data}} + P_r(1)_{\mathrm{data}} \left(1 - \frac{T_c}{T_b} \right) \right] P_e(1\,|\,0)(l) + \left(P_r(1)_{\mathrm{data}} \frac{T_c}{T_b} \right) P_e(0\,|\,1)(l) \\ &= \frac{1}{2} \left[\left(2 - \frac{T_c}{T_b} \right) P_e(1\,|\,0)(l) + \frac{T_c}{T_b} P_e(0\,|\,1)(l) \right] \end{aligned} \tag{5.108}$$

where $P_r(0)_{\mathrm{chip}}$ and $P_r(1)_{\mathrm{chip}}$ indicate the probabilities of chips "0" and "1" respectively, $P_e(1\,|\,0)(l)$ and $P_e(0\,|\,1)(l)$ denote the conditional error probabilities with chip "0" and "1" respectively, and $P_r(0)_{\mathrm{data}}$ and $P_r(1)_{\mathrm{data}}$ represent the probabilities of data bits "0" and "1" respectively. T_b is the period of data bit.

From (5.105), the statistically average of received signals is scaled by $T_c \Re$, we have

$$\frac{\langle z \rangle}{T_c \Re} = (1 + l\xi) P_d \tag{5.109}$$

It is presumed that the MAI, the shot noise from the photodetector and the thermal noise of the receiver have Gaussian distribution. When a chip is "0", $P_d = 0$. For this case, if the secondary beat noise is neglected, we have

$$P_e(1\,|\,0)(l) = \frac{1}{2} \mathrm{erfc} \left[\frac{P_d (Th - l\xi)}{\sqrt{2}\sigma_0} \right] \tag{5.110}$$

where $\mathrm{erfc}(x) = \frac{2}{\sqrt{\pi}} \int_x^{\infty} \mathrm{e}^{-y^2} \mathrm{d}y$ is the complementary error function, $0 < Th < 1 + l\xi$ is the decision-threshold and σ_0^2 is the total noise variance for the chip "0", which is expressed as

$$\sigma_0^2 = \sigma_{\mathrm{MAI}}^2 + \sigma_{\mathrm{th}}^2 + \sigma_{\text{0-sh}}^2 \tag{5.111}$$

where σ_{MAI}^2, σ_{th}^2 and σ_{sh}^2 are the variances of the MAI, thermal noise and shot noise, given respectively by

$$\begin{cases} \sigma_{\mathrm{MAI}}^2 = l\sigma_{\text{MAI-0}}^2 \\ \sigma_{\mathrm{th}}^2 = \dfrac{4k_{\mathrm{B}} T^0 B}{Z_L} = BN_{\mathrm{th}} \\ \sigma_{\text{0-sh}}^2 = 2eB\Re P_d l\xi \end{cases} \tag{5.112}$$

Here, $\sigma^2_{\text{MAI-0}}$ is the variance of a single interference signal. When Gold code with the length $N_{\text{chip}} = 127$ is employed, $\sigma^2_{\text{MAI-0}} \approx 6.5 \times 10^{-5}$. $B = 1/2T_c$ is the bandwidth of the receiver. $N_{\text{th}} = 4k_{\text{B}}T^0 / Z_L$ is the spectral density of the thermal noise, where k_{B} is Boltzmann constant that is equal to $k_{\text{B}} = 1.38 \times 10^{-23}\,\text{J/K}$, T^0 is the absolute receiver noise temperature, Z_L is the equivalent load impedance and e indicates the electron charge. Its typical value is about $N_{\text{th}} = 1\text{pA}^2/\text{Hz}$ that is employed in the following simulation computation.

When the number of secondary beat terms is so large that the secondary beat noise can not be neglected, we can model it as a normal Gaussian distribution in terms of the central limit theorem. In this case, $P_e(1|0)(l)$ still uses (5.110) except for σ_0 of (5.110) in place of the following σ_0'

$$\sigma_0'^2 = \sigma^2_{\text{MAI}} + \sigma^2_{\text{th}} + \sigma^2_{\text{0-sh}} + \sigma^2_{\text{beat-0}} \tag{5.113}$$

where $\sigma^2_{\text{beat-0}}$ is the variance of secondary beat noise, which is equal to

$$\sigma^2_{\text{beat-0}} = l(l-1)\xi^2 P_d^2 \tag{5.114}$$

When a chip is "1", the error probability is expressed as

$$P_e(0|1)(l) = \int_0^{Th \cdot P_d} p_f(x,l)\mathrm{d}x \tag{5.115}$$

Since the beat noise between each interference and the desired signal has a "two-pronged" distribution, the probability density function of the total received signal is given by

$$p_f(x,l) = F[M(\omega)] = \frac{1}{2\pi}\int_{-\infty}^{\infty} M(\omega)\exp(-\mathrm{j}\omega x)\mathrm{d}\omega \tag{5.116}$$

where $M(\omega)$ indicates the characteristic function of the signal, defined by

$$M(\omega) \equiv \int_{-\infty}^{\infty} \exp(-\mathrm{j}\omega x)\mathrm{d}x \tag{5.117}$$

From (5.105) and (5.116), we can obtain

$$M(\omega) = J_0^l\left(2\sqrt{\xi}P_d\omega\right)\exp\left(-\frac{\sigma_1^2\omega^2}{2}\right)\exp\left[\mathrm{j}l\left(\xi+\sqrt{\xi}\right)P_d\omega\right] \tag{5.118}$$

where $J_0(\cdot)$ represents the Bessel function of first kind zero order.

When the Gaussian distribution is employed to approximate the probability density function $p_f(x,l)$ of the total received signal, we can derive

$$P_e(0\,|\,1)(l)=\frac{1}{2}\mathrm{erfc}\left[\frac{P_d(1+l\xi-Th)}{\sqrt{2}\sigma_1}\right] \tag{5.119}$$

where σ_1^2 is given by

$$\sigma_1^2=\sigma_{\mathrm{MAI}}^2+\sigma_{\mathrm{th}}^2+\sigma_{\text{1-sh}}^2+\sigma_{\text{beat-1}}^2 \tag{5.120}$$

σ_{MAI}^2 and σ_{th}^2 have been shown in (5.112), and $\sigma_{\text{1-sh}}^2=2eB\Re P_d(1+l\xi)$. $\sigma_{\text{beat-1}}^2$ is the variance of the beat noise, expressed as

$$\sigma_{\text{beat-1}}^2=2l\xi P_d^2 \tag{5.121}$$

From the central limit theorem, when l is large enough, this approximation is valid.

When the value of l is small the probability density function of the beat noise term between each interferer and the desired signal is two-pronged and bounded within $2\sqrt{\xi}P_d$. Therefore, the Gaussian probability density function needs to be modified by bounding the probability density function of the beat noise within $2l\sqrt{\xi}P_d$ and becomes a case without beat noise. The variance of the resulting modified Gaussian probability function $\sigma_1'^2$ is expressed as

$$\sigma_1'^2=\begin{cases}\sigma_{\mathrm{MAI}}^2+\sigma_{\mathrm{th}}^2+\sigma_{\text{1-sh}}^2+\sigma_{\text{beat-1}}^2 & \text{if } Th>1+l\xi-2l\sqrt{\xi}\\ \sigma_{\mathrm{MAI}}^2+\sigma_{\mathrm{th}}^2+\sigma_{\text{1-sh}}^2 & \text{elsewhere}\end{cases} \tag{5.122}$$

Therefore, after the modified Gaussian probability function is employed, the calculated error probability $P_e(0\,|\,1)(l)$ is given by

$$P_e(0\,|\,1)(l)=\frac{1}{2}\begin{cases}\mathrm{erfc}\left[\dfrac{P_d(1+l\xi-Th)}{\sqrt{2}\sigma_1}\right]+\mathrm{erfc}\left[\dfrac{2l\sqrt{\xi}P_d}{\sqrt{2}\sigma_1'}\right]-\mathrm{erfc}\left[\dfrac{2l\sqrt{\xi}P_d}{\sqrt{2}\sigma_1}\right] & \text{if } Th>1+l\xi-2l\sqrt{\xi}\\ \mathrm{erfc}\left[\dfrac{P_d(1+l\xi-Th)}{\sqrt{2}\sigma_1'}\right] & \text{elsewhere}\end{cases} \tag{5.123}$$

The upper and lower bounds of the BER for the system can be obtained by employing the Gaussian probability density function and the modified Gaussian probability density function. Figure 5.36 shows the curves of upper and lower bounds of BER performance versus the number of simultaneous subscribers for $P_d=-22$ dBm. From the figure, it can be seen that when the number of simultaneous subscribers, *M*, is small, the difference between the upper and

lower of system BER is large and the difference gradually becomes smaller with the increasing of the number of simultaneous users. At the same time, the BER of the OCDMA system increases with increasing of the number of simultaneous subscribers.

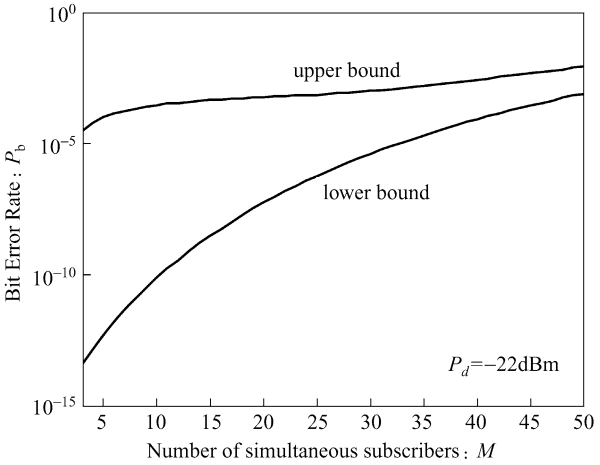

Figure 5.36 BER performance versus the number of simultaneous subscribers

The analysis mentioned above is based on employing the chip-rate detection. In practical application, the photodetector is not fast enough so that the chip-level detection is difficult to be implemented. Hence, we have to employ the photodetector with narrower bandwidth, which would make the integral time become longer so that the BER performance of the system degrades. In addition, the beat noise will limit the system performance significantly in the coherent time-spreading OCDMA network so that the network needs some practical approaches to reduce its effect. In Reference [2], the mechanism and some possible approaches to suppress the effect of the beat noise for the coherent and partially coherent time-spreading OCDMA network have been proposed, where the most feasible and effective approach is to increase the code length, which can reduce the crosstalk level, ξ. However, because of the increase of the code length, the complexity and cost of hardware implementation of the optical encoder/decoder will also increase. At the same time, the data rate will decrease and the bandwidth efficiency will be debased. Due to the progress of FBG technology, SSFBG makes the implementation of longer code possible, for example, the binary code with code length 511 has been implemented by SSFBGs at present. With respect to the BER performance analysis of the temporal phase encoding coherent OCDMA system, there are also other methods proposed, such as the analysis method employing the moment generation function and saddle approximation[17], etc. Readers interested in more details are encouraged to consult the related references.

5.8 Summary

In the research of OCDMA network theories and technologies for about 20 years, the major efforts have been focused on the design of various codes and the physical implementations of optical encoding and decoding. Nevertheless, the performances of the codes designed and the physical implementations of encoding/decoding proposed are evaluated and verified mostly based on their effects on the OCDMA systems (or called networks). Therefore, a large number of OCDMA system performance analysis approaches have come forth, which employ different encoding/decoding schemes, distinct mathematical models, and various approximate approaches. Due to the limited space of this book, it is impossible for us to describe all of them in the references one by one. In this chapter, we only introduce several representational analysis methods for OCDMA systems in detail.

Judging from the optical encoding whether it is based on the power of optical signal or based on the amplitude of optical signal field, the OCDMA systems are classified into the incoherent OCDMA and the coherent OCDMA. In terms of the number of dimensions of the employed codes, the OCDMA systems are categorized into one-dimensional OCDMA and two-dimensional OCDMA. For OCDMA receivers, they are sorted into the correlation (SUM) receivers and the chip-level (AND) receivers. When different encoding formats and different kinds of receivers are employed the system performances have very big differences.

In this chapter, we started from reviewing the BER performance of one-dimensional incoherent time-spreading OCDMA system based on the correlation receiver model, where one-dimensional $(n, w, 1)$ optical orthogonal code with the best correlation property is employed as the subscriber address code. The upper and lower bounds on the system bit error rate are shown for the two extreme cases of the chip synchronization and the ideal chip asynchronization. Because it is affected by the multiple-access interference, the number of subscribers that is allowed to access to the network simultaneously is small and the system bit error rate is high. In order to reduce the effect of the multiple-access interference, an optical nonlinear thresholder can be placed before the optical decoder of the receiver to eliminate some interfering patterns that cause the incorrect decision of the receiver, and thus the system performance can be improved obviously. In the analysis of the system BER performance with and without optical hard-limiter, the shot and thermal noises are not taken into account. In order to further improve the system performance, besides the optical hard-limiter before the optical decoder, another optical hard-limiter is added after the optical decoder, i.e. double hard-limiters are employed. In this case, the system BER performance is analyzed by using the photon-count technique, where the effect of the photodetector shot noise on the system performance is considered and the Poisson noise model is employed in the analysis. For the

correlation receiver the summation of the optical signal intensities at the positions of all "1" chips is employed. When the number of simultaneous subscribers in a network becomes larger the multiple-access interference increases so that the probability of incorrect decision through the sum of optical power would increase. Therefore, the system performance degrades as the number of simultaneous subscribers increases.

The chip-level receiver is one type of AND receivers that determines the data bit "1" or "0" received through detecting whether there does or doesn't exist optical pulse signals at the positions of all "1" chips. The summing of the optical signal intensities is not required so that the probability of incorrect decision decreases significantly. It is shown by the analysis that the system performance using the chip-level receiver is obviously better than that employing the correlation receiver, even better than that employing the correlation receiver with the optical hard-limiter. In this analysis, the shot noise of receiver is also taken into account besides the multiple-access interference. For the chip-level receiver, we consider two modulation formats that are the on-off keying and pulse-position modulation formats. The OCDMA system performance with PPM format is superior to that with OOK format. It is shown by the discussion that the implementation complexity and the cost of the chip-level receiver increases obviously compared with that of the correlation receiver, and the OCDMA system with PPM chip-level receiver is more difficult to be implemented compared with the OCDMA system with OOK chip-level receiver. Although much effort has been done in constructing one-dimensional optical codes with large cardinalities and good correlation properties and improving the system performances for one-dimensional time-spreading incoherent OCDMA systems, it is still difficult for a network to accommodate a large number of users under a certain data rate. This is because the optical signal power is encoded by employing the unipolar code in such a system and it is impossible for the real orthogonality between any two codes to be realized. However, since this part of context is the basis of OCDMA, we have analyzed and discussed these systems in details in this chapter.

In view of the shortcomings of one-dimensional incoherent time-spreading OCDMA network having small capacity, two-dimensional wavelength-hopping/time-spreading incoherent OCDMA system is proposed. Since the correlation receiver model has been employed in most references in the investigation of two-dimensional WH/TS code, in this chapter we only discuss the BER performance analysis method of two-dimensional WH/TS incoherent OCDMA system employing the chip-level receiver model and compare its performance with the performance of two-dimensional WH/TS incoherent OCDMA system using the correlation receiver model. The results show that under the same BER, the former doubles the number of simultaneous subscribers in a network compared with the latter. In this analysis, the beat and shot noises from the photodetector and the thermal noise from the receiver are not taken into account.

The readers interested in this issue can refer to the related references and study them further.

The CDMA technology has been widely applied to the fields of satellite communication, wireless communication and mobile communication. The original idea of OCDMA was to combine the advantages of optical fiber channel having tremendous bandwidth with the predominance of CDMA multiple-access, asynchronously random access and etc., so that the optical fiber communication network with more powerful function could be implemented. The CDMA encoding employs the bipolar code with good performance. Just as the optical unipolar codes and the OCDMA systems employing the unipolar codes have been investigated deeply, the OCDMA encoding and systems using the bipolar codes for CDMA, such as Gold codes, Walsh-Hadamard codes and etc., have also been studied deeply and broadly. First of all, because the subscriber access networks and the local area networks are the sensitive markets to the cost and usage price, the subscribers can not afford it if the cost to access to the network is too high. Meanwhile, the end subscribers do not need to excessively go in for the high data rate. Therefore, the spectral-amplitude-encoding incoherent OCDMA system has been proposed, where the broadband light source with low price, such as LED, ASE and etc., and the balanced (differential) detection at the receiving end can be employed. In the early days, the spectral amplitude encoding employed many bulk-optic components, such as the diffraction grating, lenses, spectral amplitude mask and etc., which had big volume, poor performance stability and so on. Thus it was difficult to be mass-produced and widely applied. Fortunately, with the maturing of optical fiber grating technology, the fiber Bragg gratings can be applied to the spectral amplitude incoherent OCDMA encoding and decoding. Because this scheme has big superiority on cost, we detail the performance analysis of the spectral amplitude encoding incoherent OCDMA system based on fiber Bragg grating. Moreover, in the analysis, the PIIN, shot noises from the photodetector and the thermal noise from the receiver have been taken into account.

The phase encoding coherent OCDMA is realized on the basis of optical field rather than optical intensity. Hence, the bipolar and multi-polar codes can be employed, where the real orthogonality between any two codes can be satisfied, so that the multiple-access interference can be debased significantly. The phase encoding coherent OCDMA is sorted into the spectral phase encoding coherent OCDMA and the temporal phase encoding coherent OCDMA. We detail the performance analysing processes of these systems. In the performance analysis of the spectral phase encoding coherent OCDMA system, for the sake of mathematic simplicity, the beat and quantum noises from the photodetector and the receiver thermal noise are neglected. The readers interested in this system consult the relevant references. In the initial days, the spectral phase encoding was also utilized with bulk-optics, such as diffraction grating, lenses and spectral phase mask. In recent years, with the advancement of planar lightwave circuit, the photonic integrated spectral phase encoder/decoder have appeared. Although

the scale of implementation is still small they represent the trend of development of spectral phase encoding OCDMA.

In recent years, due to the progress and maturing of optical fiber grating technology, the research on the temporal phase encoding coherent OCDMA using superstructured fiber Bragg grating has made great progress. In this chapter, we introduce in detail the BER performance analysis of the temporal phase encoding coherent OCDMA system, in which the beat, shot and thermal noises have been involved. However, in order to simplify the calculation, the Gaussian distribution noise model has been employed in the analysis. So far, the performance analysis of the temporal phase encoding coherent OCDMA system with other noise model and approximation, such as the moment generation function and saddle point approximation, has been reported in the references. The readers can refer to the relevant references. In the phase encoding coherent OCDMA network, high data rate can be implemented, such as single subscriber data rate ~Gb/s. However, it needs the highly coherent mode-locked source with ~ps pulse width, whose price is high. What is more, the light source with broad and flat spectrum for the spectral phase encoding is required. These requirements make the implementing cost for the phase encoding OCDMA network increase enormously. As far as it goes, it is difficult for the subscribers to afford it if the phase encoding OCDMA is applied to the subscriber access network. The lowered cost and extensive application await the progress of technology and the driving force of the market.

Since the OCDMA has been investigated for about twenty years, a large number of OCDMA systems and their performance analysis methods have been proposed in the references. Due to the limited space of context, we cannot introduce them one by one. Therefore, we only detail the representative performance analysis approaches of several systems. The performance analysis of the OCDMA system involves a large amount of mathematic knowledge and a couple of approximate models. Whether these models accord with the practical circumstances or not is to be verified. Thus, the mathematically approximate models in accordance with practice and better performance analysis approaches still need to be studied. Moreover, many new results of the system performance analysis will be reported as the OCDMA theories and technologies are investigated more thoroughly. Therefore, the content of this chapter can be regarded as the basis and primary knowledge for the readers who would like to study and investigate OCDMA theories and technologies in detail.

References

[1] P. Saghari, R. Gholizadeh, P. Kamath, R. Omrani, A. E. Willnar, J. A. Bannister, J. D. Touch, P.V. Kumar: Alalytical model of variable quality of service to increase the number of users in an OCDMA network. ECOC2005, Paper Th1.4.7

[2] X. Wang and K. Kitayama: Analysis of beat noise in coherent and incoherent time-spreading OCDMA. *IEEE/OSA Journal of Lightwave Technology*, Vol.22, No.10, Oct. 2004, pp2226 – 2235

[3] Jawad.A.Salehi: Code division multiple-access techniques in optical fiber networks -part I: Fundamental principles. *IEEE Trans. on Communications,* Vol.37, No.8, Aug. 1989, pp824 – 833

[4] Jawad.A.Salehi and C. A. Brackett: Code division multiple-access techniques in optical fiber networks-part II: Systems performance analysis. *IEEE Trans. on Communications,* Vol.37, No.8, Aug. 1989, pp834 – 842

[5] Tomoaki Ohtsuki: Performance Analysis of Direct-Detection Optical Asynchronous CDMA Systems with Double Optical Hard-Limiters. *IEEE/OSA Journal of Lightwave Technology*, Vol.15, No.3, March 1997, pp452 – 457

[6] Hossam M. H. Shalaby: Chip-Level Detection in Optical Code Division Multiple Access. *IEEE/OSA Journal of Lightwave Technology*, Vol.16, No.6, June 1998, pp1077 – 1087

[7] H. M. H. Shalaby: Optical OPPM-CDMA receivers with chip-level detectors. *IEE Proceedings on Communications*, Vol.148, No.1, Feb. 2001, pp31 – 37

[8] Sina Zahedi, and Jawad A. Salehi: Analytical Comparison of Various Fiber-Optic CDMA Receiver Structures. *IEEE/OSA Journal of Lightwave Technology*, Vol.18, No.12, Dec 2000, pp1718 – 1727

[9] Tung-Wah Frederick Chang and Edward H. Sargent: Optical CDMA Using 2-D Codes: The Optimal Single-User Detector. *IEEE Communications Letters*, Vol.5, No.4, April 2001, pp169 – 171

[10] D. Zaccarin, M. Kavehrad: An Optical CDMA System Based on Spectral Encoding of LED. *IEEE Photonics Technology Letters*, Vol.4, No.4, April 1993, pp479 – 482

[11] M. Kavehrad, D. Zaccarh: Optical Code-Division-Multiplexed Systems Based on Spectral Encoding of Noncoherent Sources. *IEEE/OSA Journal of Lightwave Technology*, Vol.13**,** No.3, March 1995, pp534 – 545

[12] Z. Wei, H. M. H. Shalaby, H. Ghafouri-Shiraz: Modified Quadratic Congruence Codes for Fiber Bragg-Grating-Based Spectral-Amplitude-Coding Optical CDMA Systems. *IEEE/OSA Journal of Lightwave Technology*, Vol.19, No.9, Sept. 2001, pp1274 – 1281

[13] Z. Kostic: The design and performance analysis for several new classes of codes for optical synchronous CDMA and for arbitrary-medium time-hopping synchronous CDMA systems. *IEEE Trans. on Communications*, Vol.42 No.8, 1994, pp2608 – 2617

[14] Jawad A. Salehi, Andrew M. Weiner, and Jonathan P. Heritage: Coherent Ultrashort Light Pulse Code-Division Multiple Access Communication Systems. *IEEE/OSA Journal of Lightwave Technology*, Vol.8, No.3, March 1990, pp478 – 491

[15] Wenhua Ma, Chao Zuo, Hongtu Pu, and Jintong Lin: Performance Analysis on Phase-Encoded OCDMA Communication System. *IEEE/OSA Journal of Lightwave Technology*, Vol.20, No.5, May 2002, pp798 – 803

[16] L. Tancevski, and L. A. Rusch: Impact of the Beat Noise on the Performance of 2-D Optical CDMA Systems. *IEEE Communications Letters*, Vol.4, No.8, August 2000, pp264 – 266

[17] Pu, T., Zhang, H., Guo, Y.; Xu, M., Li, Y.: Evaluation of Beat Noise in OCDMA System With Non-Gaussian Approximated Method. *IEEE/OSA Journal of Lightwave Technology*, Vol 24, No.10, Oct. 2006, pp3574 – 3582

6 Architectures, Protocols and Applications for OCDMA Networks

6.1 Introduction

As various services in telecommunication network increase rapidly, especially the explosively mushrooming of Internet protocol (IP) services, the global telecommunication network infrastructure is required to be upgraded in order to meet the present demands and the future services for the network. The ultrahigh-speed photonic network will play a crucial role in the upgrade of network. Photonic network can provide large capacity, and at the same time, it has the functions of implementing dynamic reconfiguration of network, flexible management of bandwidth, efficient utilization of network resources, securities of network infrastructure and information transmission, etc., so that it can adapt well to the dynamic service variations in the network and the specific demands from different subscribers. These are implemented through the network architectures and protocols, the manners of signal multiplexing and switching, and the formats of signal encoding and decoding. At present, the multiplexing and switching technologies widely used are the electronic time division and optical wavelength division technologies.

In WDM systems, the available optical bandwidth is divided into fixed wavelength channels that are assigned to subscribers simultaneously. As a result, the minimum transmitting and switching granularity of data with WDM is based on wavelength so that the processing traffic capability of WDM technology based on optical channels of the wavelength paths is limited by the fixed number of optical channels and information granularity. Consequently, the flexibility and effectiveness in the utilization of network resources are restricted, which is especially not suitable for IP traffic with the characteristics of burst, self-similarity, imbalance and etc., and furthermore, the wavelength resource provided by pure WDM technology is limited. The predominance of WDM rests with its relatively simple transmission technology, such that it can be applied to long-haul network to support large capacity transmission and circuit-level switching based on wavelength routing.

The performance of TDM systems is limited by the time-serial nature of the technology. Each channel signal must be operated at the total bit rate of the system. Although the electric TDM technology has been well matured, 10Gb/s systems have been used commercially, 40Gb/s systems have been started and the

TDM systems with higher bit rate may be developed in the future, it will be finally confined by the electronic bottleneck effect. In spite of great advancement of optical time-division multiplexing (OTDM) technology developed from many-year research, it still rests on its study stage in laboratory since there is not practically optical logic device. Though TDM/OTDM can employ time-slot multiplexing statistically, the total number of time-slots does not vary dynamically with the traffic status in the network, which is very important for the bursty traffic. Hence, the electrical/optical time-division multiplexing and switching technologies are not suitable for the bursty traffic and the effective utilization of network bandwidth resources.

In view of the shortcomings of WDM and TDM/OTDM, the optical code-division technology that has long remained outside the mainstream of research and development for multiplexing and switching technologies, can support flexible traffic granularity, does not set the bounds on the number of channels and can improve the security of information transmission. Therefore, it is a very promising technology to implement asynchronous multiplexing and switching, and to establish multiple access connections. At the same time, it can make use of network resources effectively. In the long-haul network, optical code-division technology can act as the complementary technology with WDM and OTDM to fill up the shortage of the number of wavelengths and time-slots such that the function of the network can be boosted. In the access networks and local area networks, optical code-division is a multiple-access and label technique with distinctive superiority for the bursty services based on packets. Optical code-division, just as its name implies, differentiates different signals in the network relying on encoding signals orthogonally or quasi-orthogonally. Therefore, it allows signals encoded to overlap both in time and wavelength as shown in Fig. 6.1. It does not need time management and frequency management at the transmitting nodes in the network. It can operate asynchronously and does not suffer from packet collisions such that very low latencies can be implemented.

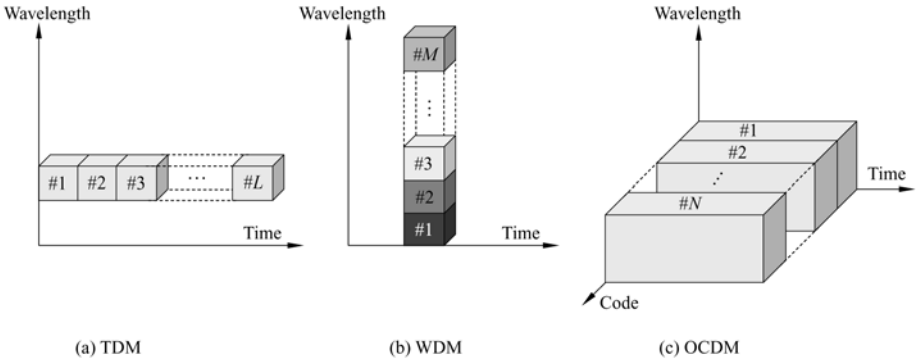

Figure 6.1 Schematic diagrams of three categories of photonic multiplexing techniques

The maximum transmission capacities for TDM and WDM depend on the total numbers of time slots and wavelength channels respectively. Nevertheless, OCDM has soft capacity on demand so that it allows flexible network design. The signal quality for OCDM relies on the number of simultaneously active channels.

In the previous chapters, we have introduced the fundamental knowledge applicable to optical code-division multiple-access network, including one-dimensional and two-dimensional codes, optical encoding and decoding technologies and the performances of representative OCDMA systems. This chapter will be devoted to the networks with optical code-division technologies, protocols for OCDMA local area networks and applications of OCDMA.

This chapter is organized as follows. OCDM/WDM hybrid multiplexing and the interconnections of OCDMA networks with OTDM networks and WDM networks are introduced in Section 6.2. Section 6.3 describes OCDM/WDM hybrid networks. Section 6.4 covers the architectures of OCDMA LANs. Section 6.5 presents the primarily random access protocols of OCDMA LANs. In Section 6.6, optical packet switching network with optical code label is reviewed. Section 6.7 discusses data transmission confidentiality provided by OCDMA networks. Some other applications of OCDMA are introduced in Section 6.8. At last, the conclusion for this chapter is given in Section 6.9.

6.2 OCDM/WDM Hybrid Multiplexing and Interconnections of OCDMA Networks with WDM Networks and OTDM Networks

6.2.1 OCDM/WDM Hybrid Multiplexing

Optical code-division multiplexing (OCDM) can be employed to implement signal multiplexing. Due to the excellent compatibility of OCDM technology with WDM technology, the combination of them can multiple the system capacity and improve the system spectrum efficiency. The operational principle diagram of the system using OCDM/WDM hybrid multiplexing is shown in Fig. 6.2. At the transmitting end, the short light pulse trains generated by a light source is modulated in the optical modulator by the data from each channel, which then are uniquely encoded by an OCDM encoder. Since different codewords are orthogonal with each other, multiple channel data encoded differently can be multiplexed in the same optical fiber. Assuming that an optical code set comprising N codewords with good properties is employed, each wavelength can achieve the multiplexing of N signals through OCDM. In addition, each codeword can be reused in different wavelengths. Again presuming that there are M wavelengths in a system, $N \times M$ signals can be multiplexed together. The

different encoded signals within the same wavelength are combined into the same channel by an optical coupler and the encoded signals with different wavelengths are aggregated into the same fiber-optic by a wavelength division multiplexer (WDM MUX). At the receiving end, the signals with different wavelengths are firstly separated by a wavelength division demultiplexer (WDM DEMUX). The signals on each wavelength are optically decoded uniquely by N optical decoders corresponding to N different codewords. Then, they are photodetected, sampled and threshdd-decided. And finally, data are restored. In this way, the demultiplexing of $N \times M$ signals are achieved.

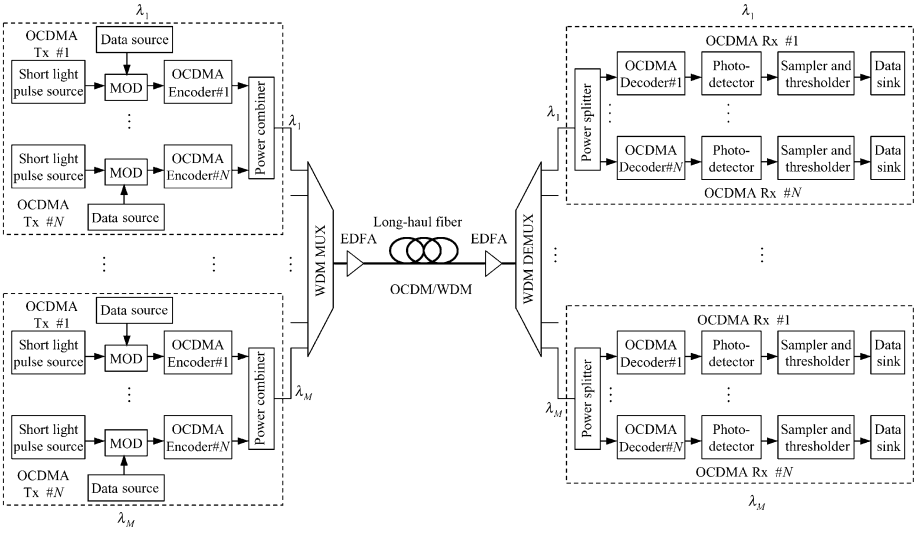

Figure 6.2 Principle of OCDM/WDM hybrid multiplexing

To date, the highest bit rate implemented by OCDM/WDM hybrid multiplexing technology is 6.4 Tb/s and the record spectrum efficiency achieves 1.6 b/(s · Hz). The operational principle diagram for this experiment is shown in Fig. 6.3[1]. An optical pulse train with 10 GHz repetition rate and 1.5 ps pulse width, which was generated by a mode-locked laser diode (MLLD) at wavelength 1532nm, was modulated by a 10 Gb/s Pseudorandom binary sequence (PRSB) of $2^{23}-1$ and then optically multiplexed into 40 Gb/s through OTDM technology. After being amplified to the average power of 0.48W by an EDFA, it was directed to a super-continuum (SC) fiber, which generated 40Gb/s SC signal which is linearly polarized within C-band. Because of using the optical encoder with chip spacing 1.5 ps, the pulse response width of the optical encoder is 200 GHz. When the coherent broadband SC optical pulse served as the chip pulse the simultaneous multi-wavelength optical encoding with WDM channel spacing of 200 GHz could be implemented. The generated 40 Gb/s SC signal became a linearly polarized signal after a polarizer and then split into eight paths, each serving as the light

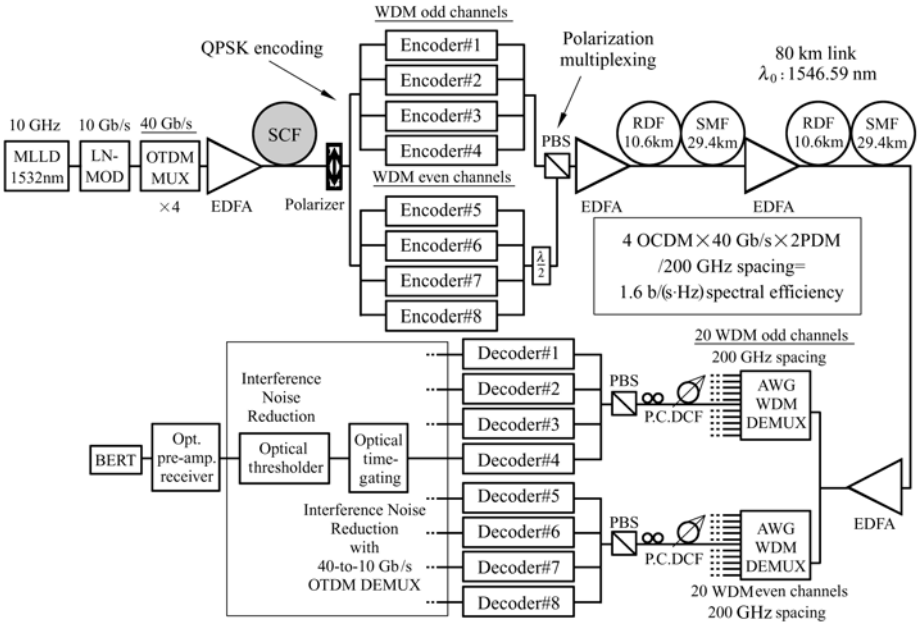

Figure 6.3 Schematic diagram of experimental system of 6.4 Tb/s OCDM/WDM/ Polarization-multiplexing (4 OCDM × 40 WDM × 40 Gb/s) (Adapted from Ref. [1], with permission from IEEE © 2007)

sources for simultaneous multi-wavelength encoding. The optical encoder employed was a temporal phase encoder of monolithic integration, which was composed of three tunable taps, two segments of 5ps delay lines, and three programmable quaternary phase shifters (i.e., quaternary phases: $0, \pi/2, \pi, 3\pi/2$). In the two groups of encoding signals, each group had four differently optical encoding signals, corresponding to optical codes $\#1-4$ ($[0,0,\pi/2]$, $[0,\pi,0]$, $[\pi/2,0,0]$, $[\pi/2,\pi/2,3\pi/2]$) and $\#5-8$ ($[0,0,0]$, $[0,\pi/2,3\pi/2]$, $[0,\pi,\pi/2]$, $[\pi/2,3\pi/2,3\pi/2]$) respectively. The optical codes with even number wavelength are delayed by 2.5 ps relative to the optical codes with odd number wavelength. One group of encoding signals is transformed into orthogonally polarized signals and then these two groups of signals are multiplexed into orthogonal polarized multi-wavelength 2×4 OCDM × 40 Gb/s signals through a polarization beam splitter (PBS). The total bit rate of each group of signals with WDM channel spacing of 200 GHz is 160 Gb/s (4 OCDM×40 Gb/s). The total spectrum efficiency corresponding to the system is 1.6 b/(s · Hz). The 80 km long transmission line consisted of two spans of 10.6 km long reversed dispersion fiber (RDF) and 29.4 km long single-mode fiber. The average zero dispersion wavelength of this line was 1546.6 nm and the dispersion slope was 0.0087 ps/(nm^2 · km) at this wavelength. After 80 km transmission, the multiplexing signal was divided into two parts and each part was demultiplexed by employing a 20-channel AWG

with wavelength spacing of 200 GHz. They corresponded to the odd WDM channels (ch.1: 1532.7 nm – ch.39: 1563.1 nm) and the even WDM channels (ch.2: 1533.5 nm – ch.40: 1563.9 nm) respectively. Each of theses two AWGs had the wavelength spacing of 100 GHz between any two adjacent channels. After WDM demultiplexing, the residual dispersion of signals was compensated and they were again demultiplexed by PBS. Then, every signal was decoded by an optical decoder. Optical time-gating rejected the interference noise outside its time-gating window and optical hard thresholder further reduced the interference noise within the time-gating window. Finally, the data were retrieved by the receiver with an optical preamplifier and the BERs were measured by Bit-Error-Rate Test (BERT) analyzer. For all measured 160-channel × 40 Gb/s signals, the BER were less than 10^{-9}. This experiment revealed that OCDM/WDM hybrid multiplexing with the total capacity of 6.4 Tb/s in single fiber was successfully implemented.

The operational principles of optical time-gating and optical hard thresholding are shown in Fig. 6.4 and Fig. 6.5 respectively[1]. In Fig. 6.4, the nonlinear optical loop mirror (NOLM), which was composed of 100 m long highly nonlinear dispersion-shifted fiber (HNL-DSF), was employed to implement optical time-gating. The control pulse was 10GHz repetition rate, 1.5 ps width pulse train from

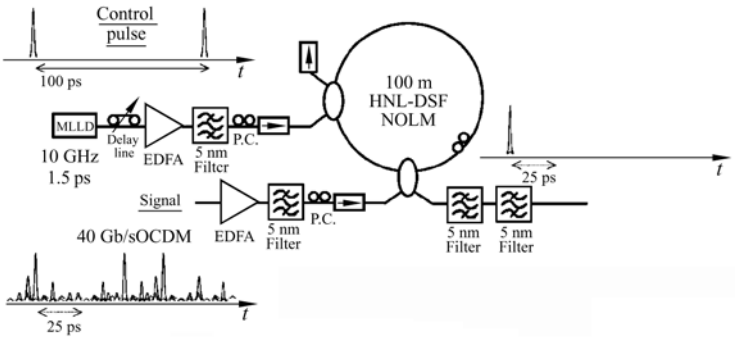

(a) Scheme of operational principle of ultrafast optical time-gating

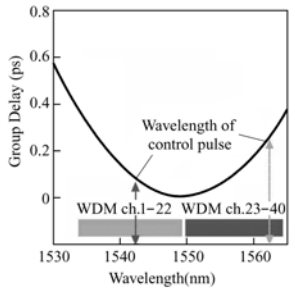

(b) Group delay characteristics of a 100 m long highly nonlinear dispersion-shifted fiber used as optical time-gating device

Figure 6.4 (Adapted from Ref.[1], with permission from IEEE © 2007)

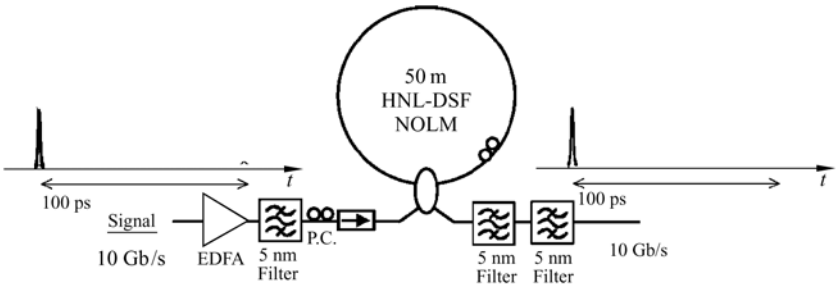

(a) Scheme of operation principle of ultrafast optical hard thresholding

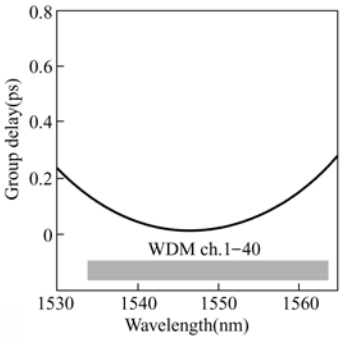

(b) Group delay characteristics of a 50 m long highly nonlinear dispersion-shifted fiber used as optical hard thresholding device

Figure 6.5 (Adapted from Ref.[1], with permission from IEEE © 2007)

the MLLD. When there is no the control pulse, the incoming input signal is reflected. When there is the control pulse, the input signal is output from another output port of the optical coupler in the duration of the control pulse. When the frequency of the control pulse trains and the pulse width are consistent with the occurring frequency and the width of the autocorrelation peaks of the decoded signal respectively, the optical time-gating can suppress the interference noise outside the mainlobe of autocorrelation function, that is, it acts as an optical time-gate. The output filter is to remove the control pulse. In order to improve the operational speed of the optical time-gate, the highly nonlinear dispersion-shifted fiber employed can be shortened to 100m. In this experiment, the wavelength of control pulse was set to 1562.5nm for gating of WDM channel 1 to channel 22 (1533 – 1549nm) and 1542.2nm for gating of WDM channel 23 to channel 40 (1550 – 1564nm). The gating window of optical time-gate is ranged from 1.5 to 1.8ps for all WDM wavelength channels from 1533 to 1564nm.

Although the interference noise outside the window can be rejected by using the optical time-gate, there still exists the interference noise within the optical time-gating window. This interference noise can be alleviated by employing the optical hard thresholder, as shown in Fig. 6.5. It is also implemented by utilizing NOLM. However, in this case, it acts as a pulse shaper through setting the proper

threshold level. It reflects lower intensity signals but only transmits higher intensity signals by limiting its intensity to a proper level. By adjusting the power of input signal, the interference noise within the autocorrelation mainlobe output by the optical time-gate is suppressed in both signal "0" and "1" levels. In order to increase its operational speed, the length of HNL-DSF employed by the optical hard threshoding can be decreased to 50m.

6.2.2 Interconnections of OCDMA Networks with OTDM and WDM Networks

If OCDMA technology can be used practically, it is required to be compatible with the existing technologies, such as OTDM and WDM. OCDMA can be utilized individually to construct the networks and it can also be combined with OTDM or/and WDM to implement networking. When OCDMA is employed to design a network, there exists the issue of interconnections between OCDMA networks and other existing networks. Therefore, the conversion gateways of multiplexing formats between OCDMA networks and the other networks, such as WDM networks and OTDM networks, are crucial components.

The schematic diagram of OCDMA networks interconnecting with WDM networks and OTDM networks, is shown in Fig. 6.6[2]. Photonic gateways are

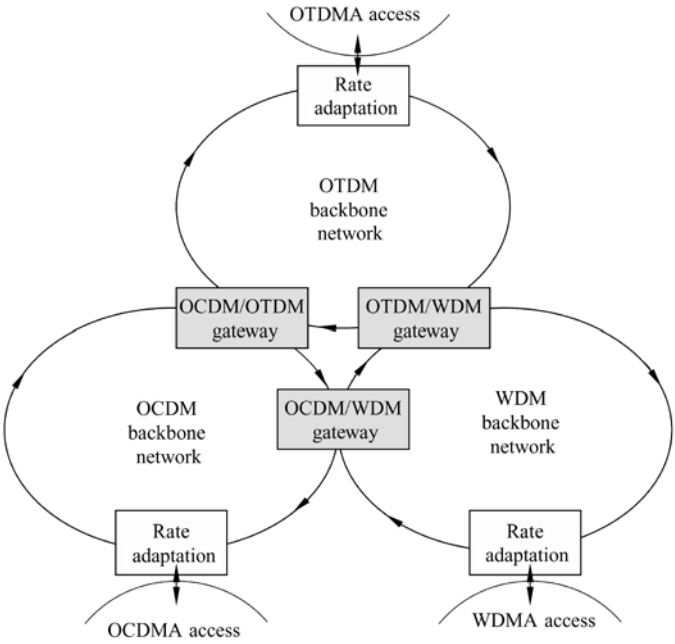

Figure 6.6 Interconnections among OCDM networks, OTDM networks and WDM networks (After Ref. [2])

very important components for interconnections among heterogeneous photonic networks, which offer the bit rate transparency to the photonic network nodes. Photonic gateways execute data format conversion and data rate conversion in the optical layer[2]. The photonic gateways among OTDM networks, WDM networks and OCDM networks implement conversions of multiplexing formats among them.

6.2.2.1 Bidirectional Conversions of OCDM-to-WDM and WDM-to-OCDM

The conversion from OCDM to WDM is shown in Fig. 6.7(a). N OCDM multiplexing signals with wavelength λ_0 from a fiber-optic are firstly split into N paths through an $1\times N$ optical coupler. Each path signal is decoded by a corresponding OCDM-decoder. Then, the autocorrelation peaks are selected by

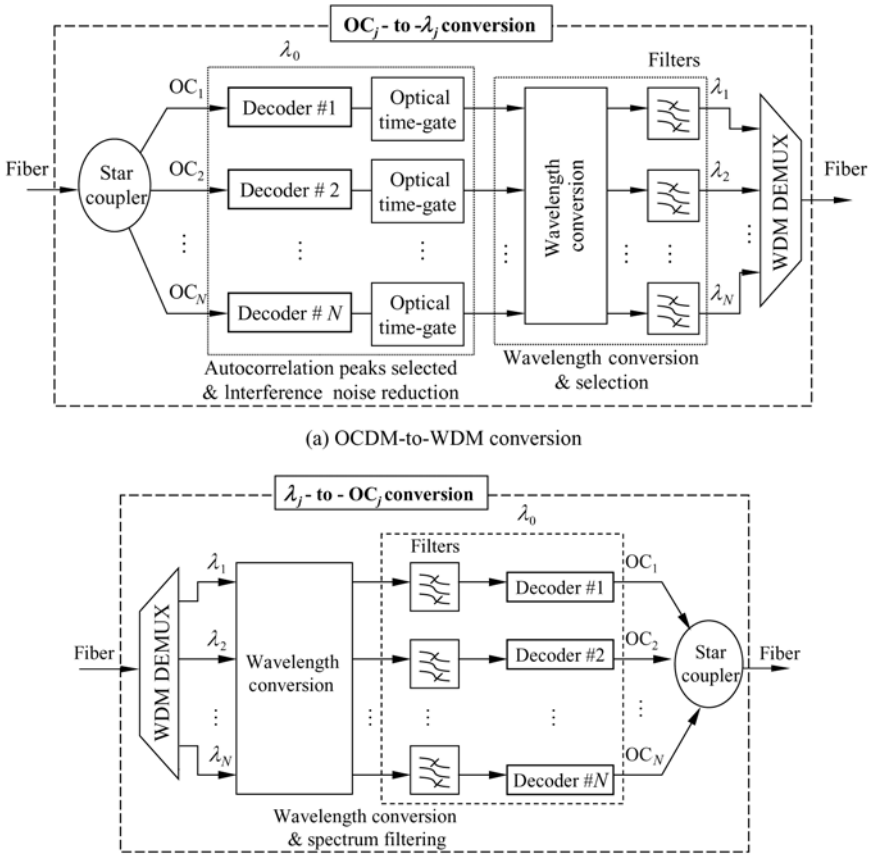

Figure 6.7 Schematic diagrams of bidirectional conversions between OCDM and WDM

an optical time-gating and at the same time, the interference noise is suppressed. Each output signal performs wavelength conversion using wavelength converter and then a wavelength corresponding to each signal is picked out by an optical filter. At last, the signals multiplexed by WDM MUX are output. In this way, the conversion from OCDM signals to WDM signals is achieved, where OC_j corresponds to λ_j, $1 \leqslant j \leqslant N$.

The conversion principle from WDM signals to OCDM signals is shown in Fig. 6.7(b). N signals with wavelength λ_j ($1 \leqslant j \leqslant N$) respectively from a fiber are in the first place separated by a WDM DEMUX and then perform wavelength conversion. Afterwards each signal with wavelength λ_0 is picked out from each path of wavelength-converted signals by the optical filter and is encoded by an OCDM encoder. Finally, these signals are combined into one path of signals to output. In doing so, the conversion from WDM signals to OCDM signals is achieved.

The experimental demonstration[2] based on the operational principle mentioned above is shown in Fig. 6.8. The diagram of the experimental system of conversion from OCDM to WDM is given in Fig. 6.8(a). The mode-locked laser diode with central wavelength $\lambda_0 = 1542.8$ nm, generates an optical pulse train of repetition rate 10 GHz and the pulse train is modulated with a 10 Gb/s pseudorandom binary sequence (PRBS) of $2^{23}-1$ through a Lithium Niobate ($LiNbO_3$) intensity modulator (LN-MOD) and then amplified by EDFA. After being filtered, it is split into four parts. They are uniquely encoded by OCDM encoders respectively and then combined into one 4 OCDM $\times$ 10 Gb/s path of signals. After amplified by EDFA, it transmits 80 km in a fiber-optic line that is composed of a 57.8 km standard single-mode fiber-optic (SMF) and a 22.2 km reversed dispersion fiber-optic (RDF). The latter is to compensate the dispersion in transmission line. The zero-dispersion wavelength of this link is 1546.6 nm and the dispersion slope at this wavelength is $0.0087\,\mathrm{ps}/(\mathrm{nm}^2 \cdot \mathrm{km})$. The optical encoders and decoders employed in this experiment consist of integrated optical transversal filters, as shown in the inset, which implement the bipolar temporal-phase encoding and decoding with chip length of 8 and each chip-width 5 ps. After being transmitted through 80 km line, the OCDM signals arrive at the conversion node of OCDM-to-WDM and each OCDM signal goes through the conversion from an optical code to a wavelength uniquely. The optical time-gate in the conversion node is composed of a high nonlinear dispersion-shifted fiber based nonlinear optical loop mirror and the wavelength conversion is achieved through spectrum broadened by EDFA and supercontinuum generation fiber. Ultimately, the corresponding wavelength is selected by the filtering of AWG WDM-DEMUX. Four codes for OCDM are $OC_1 = (00000000)$, $OC_2 = (0000\pi\pi\pi\pi)$, $OC_3 = (0\pi0\pi0\pi0\pi)$ and $OC_4 = (0\pi0\pi\pi0\pi0)$ respectively and four wavelengths corresponding to them after converted are $\lambda_1 = 1538.6$ nm, $\lambda_2 = 1541.4$nm, $\lambda_3 = 1544.2$ nm and $\lambda_4 =$ 1546.9 nm respectively. The measured eye diagrams and BERs from the signals at

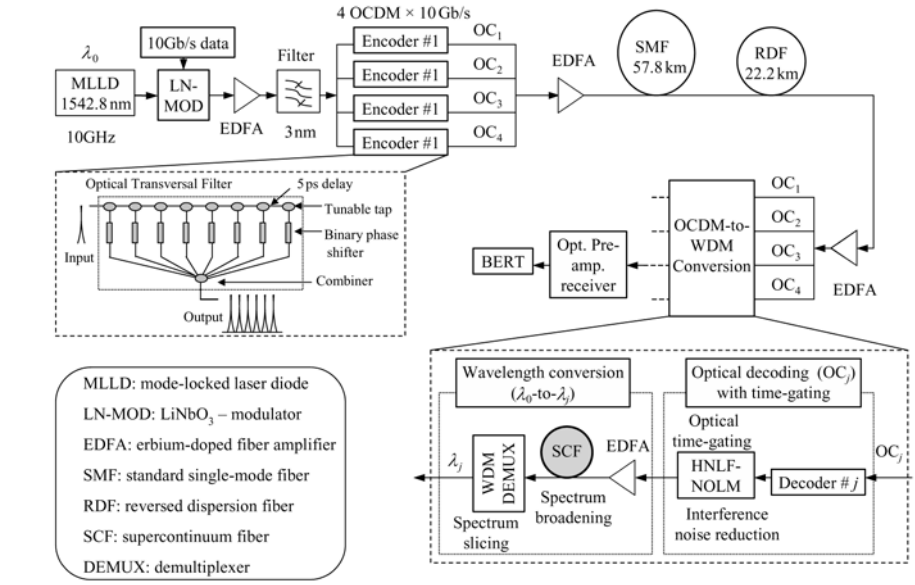

(a) Experimental setup for OCDM-to-WDM conversion

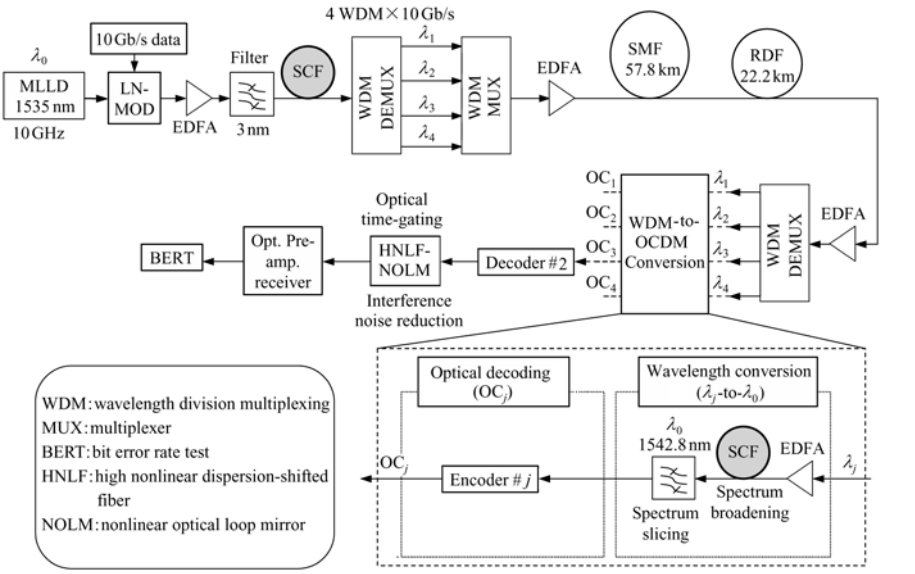

(b) Experiment setup for WDM-to-OCDM conversion

Figure 6.8 Experimental test beds of bidirectional conversions between OCDM and WDM (After Ref.[2])

the receiving end reveal that the error-free 4×10 Gb/s OCDM-to-WDM conversion is successfully demonstrated.

Figure 6.8(b) is a block diagram of the experimental system of 4×10 Gb/s WDM-to-OCDM-conversion. The WDM optical signals of four wavelengths λ_1, λ_2, λ_3 and λ_4 (their concrete values are the same as mentioned above), carry 10Gb/s data signals respectively. After 80 km transmission, they are transformed into four OCDM signals encoded by OC_1 to OC_4 by the photonic gateway of WDM-to-OCDM conversion, which are all at wavelength λ_0. These four codewords are the same as mentioned above.

6.2.2.2 Bidirectional conversions OCDM-to-OTDM and OTDM-to-OCDM

The photonic gateway from OCDM to OTDM is shown in Fig. 6.9(a). *N* OCDM signals multiplexed are firstly split into *N* paths by a $1\times N$ optical coupler and

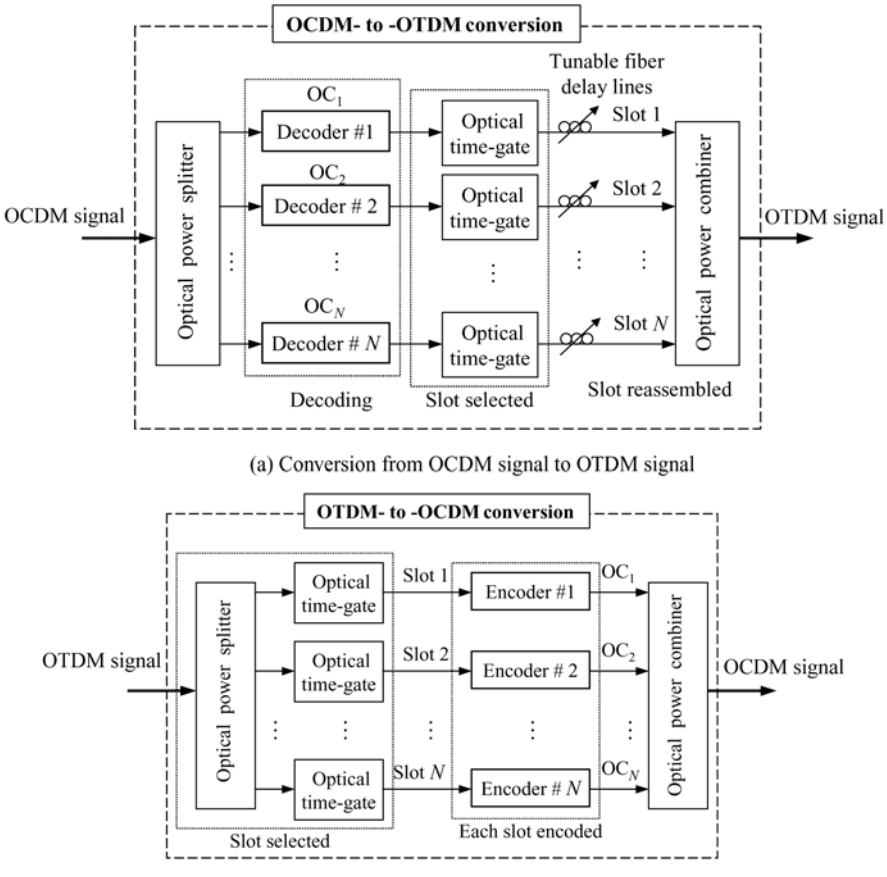

Figure 6.9 Schematic diagrams of bidirectional conversions between OCDM and OTDM signals

each path signal is decoded by a corresponding OCDM-decoder. Then the autocorrelation peaks are picked out by an optical time-gate and at the same time multiple-access interference noise is suppressed. After time alignment adjusted, the time slots are assemble by an optical power combiner at last. In doing so, the conversion from OCDM signal to OTDM signal is achieved.

The block diagram of conversion photonic gateway from OTDM to OCDM in shown in Fig. 6.9 (b). The OTDM signal with N time slots is in the first place divided into N signals by a $1 \times N$ optical coupler. The corresponding time-slots from each signal are extracted from each signal by an optical time-gate and simultaneously the interference noise is suppressed. Then, each data bit at each time-slot is encoded by an optical encoder. At last, these encoded signals are combined by the optical-power combiner to output. In this way, the conversion from OTDM to OCDM is achieved. Notice that when each data at each time-slot is encoded, the length of code employed can not exceed the time-frame length of OTDM. Otherwise, the time synchronization can not be implemented.

As for bi-directional conversion of OTDM-to-WDM, due to the limited space of context, we do not detail it. The readers who are interested in it can refer to the relevant reference [3].

6.3 OCDM/WDM Hybrid Networks

OCDMA technology can be employed not only to construct multiple-access networks, but also to implement optical-code routing networks[4, 5]. Because of very good compatibility of OCDM technology with WDM technology, the virtual optical code path/virtual wavelength path (VOCP/VWP)[5] can be achieved by combining OCDMA technology with WDM technology in the existing WDM wavelength routing network. This is not only a solution to resolve the difficult issues of wavelength resource shortage and complex wavelength allocation strategies in the existing WDM wavelength routing networks, but also results in high flexibility for resource assignment and optimization in the process of network design and management by utilizing OCDM soft capacity. Simultaneously, such a network is capable of increasing network scalability and reconfigurability. It is shown by investigation that the hybrid approach of OCDM/WDM has the tolerance to the wavelength deviation of the light sources in which OCDM is on the basis of spectral spreading/dispreading[5].

Figure 6.10 gives us an example[4] that represents the optical path differences between WDM networking, OCDM networking and OCDM/WDM hybrid networking. When WDM is individually employed to construct a network, large numbers of wavelengths are required. For example, it needs six wavelengths to establish six optical paths among six nodes in the network, shown in Fig. 6.10(a). Similarly, six optical codes in the network topology shown in Fig. 6.10(b) are required when OCDM is individually utilized to build the network.

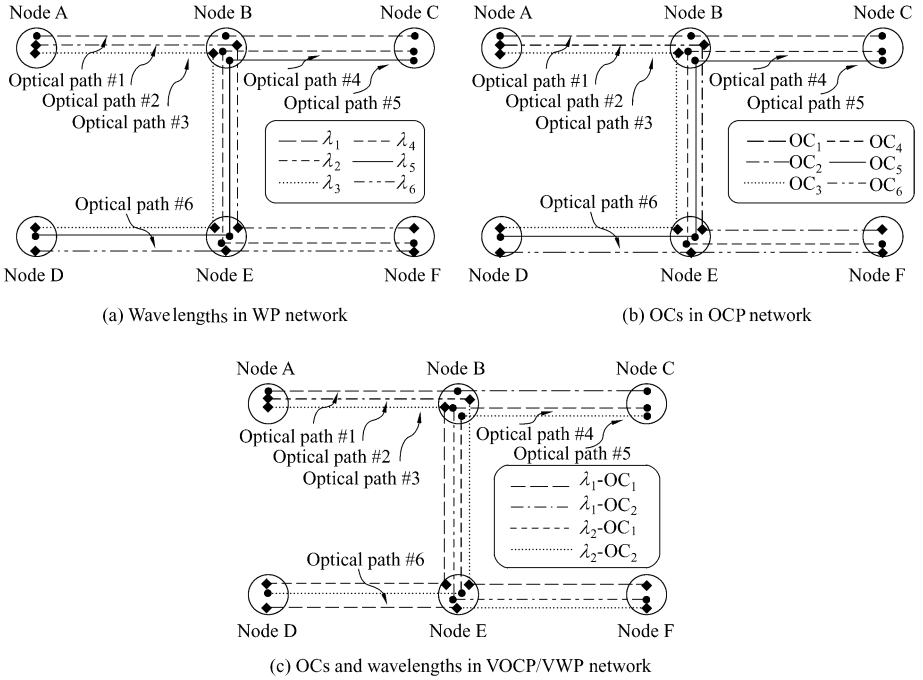

Figure 6.10 (Adapted from Ref. [4], with permission from IEEE © 2007)

Nevertheless, as shown in Fig. 6.10(c), only two optical codes and two wavelengths are required to establish the same number of optical paths by using appropriate VOCP/VWP in the nodes B and E, and allocating the OC and wavelength on a link-by-link basis when the combination of OCDM with WDM is employed. For instance, in order to establish optical path #2, λ_1 is converted to λ_2 in node B while OC_2 is kept invariably and then the wavelength and optical code are transformed into λ_1 and OC_1.

For OCDM/WDM hybrid virtual optical path networks, optical cross-connect (OXC) nodes that can simultaneously implement optical code and wavelength conversions, are crucial. The schematic diagram of OXC node proposed in Reference [4] is shown in Fig. 6.11, which has *K* input optical fibers and *L* output optical fibers. There are *M* wavelengths in each fiber and *N* optical codes on every wavelength. The node can realize the interconnections of $(M \times N \times K) \times (M \times N \times L)$. The output hybrid-optical-signals from each fiber-optic are first separated by WDM DEMUX based on different wavelengths. Then, under the control of signaling, λ_i - OC_k is converted by wavelength converter of λ - conv and optical code converter (OCC) on demand. There are three possible results for this conversion. The first one is that λ_i - OC_k is converted into λ_j - OC_l if the wavelength and the optical code are required to be changed. The second one is that λ_i - OC_k is converted into λ_j - OC_k if only the wavelength is required to be

changed. The last possible result is that λ_i - OC_k is converted into λ_i - OC_l if only the optical code needs to be changed. After wavelength conversion on demand, the signal enters into $M \times L$ optical switch matrix to perform interconnection and outputs from a proper output port. At last, the combination of signals is implemented by the optical coupler. In this way, the VOCP/VWP switching of signals in OCDM/WDM network is achieved. Add/drop multiplexing can also be performed at the selected input (for adding the signal from the node) and output ports (for dropping the signal to the node) of the OXC node.

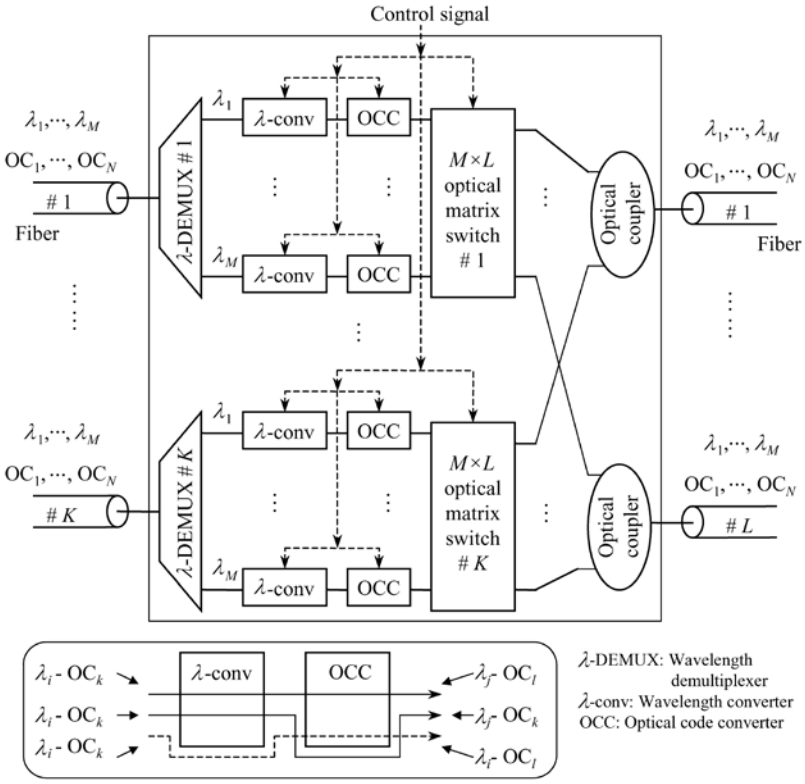

Figure 6.11 Architectures of optical cross-connect switch with the optical code converter (OCC) and the wavelength-to-code converter (After Ref.[5])

In Reference [5], optically bipolar temporal-phase code conversion in the optical-to-electrical (O/E) and electrical-to-optical (E/O) manners was demonstrated experimentally, where 4-chip optical encoder and decoder monolithically integrated by using planar lightwave circuit technology was employed. The data rate is 1.24 Gb/s. Although the O/E and E/O conversion influences the transparency of signal formats, it reveals that the optical code conversion with high bit rate is feasible. In Reference [4], simultaneous optical code and wavelength conversion

was demonstrated by employing all-optical 3R (retiming, reshaping and regenerating) with 8.05 THz ultra-broadband operational bandwidth by supercontinuum generation. At the same time, the transparent VOCP/VWP network was demonstrated through optical code and wavelength conversions in the network nodes, in which there were four nodes in this network and the total link length is 180 km at a channel data rate of 10 Gb/s. The principle diagram of this experiment is shown in Fig. 6.12. Fig. 6.12 (a) shows the layout of nodes and links and gives the structure of node A. Fig. 6.12 (b) presents the architecture of node B with the function of optical code and wavelength conversion. The structure of node C and E is shown in Fig. 6.12 (c). In node B, the signals are first of all separated by AGW DEMUX in terms of different wavelengths and are decoded by different decoders. After the signals are restored by all-optical 3R, wavelength conversions of these signals are performed by SC. Eventually, they are re-encoded by optical encoders. In doing so, simultaneous optical code and wavelength conversions are achieved. The conversion process from λ_2 - OC_2 to λ_1 - OC_1 is shown in Fig. 6.12 (b). The implementation of all-optical 3R is as follows. After λ_2 - OC_2 signal is decoded, it is split into two parts. One part is input to injection mode-locked laser diode (MLLD) for 10 GHz clock recovery. Another part is the data signal to be restored. The central wavelength of the recovered clock signal is λ_c. The clock signal is divided into two parts. The first part is employed as pump pulses of the semiconductor saturable absorber (SA) time gate, which controls the optical time-gate ON/OFF. By optical time-gating of decoded signal, sidelobe of autocorrelation is rejected and interference noise is significantly reduced. Afterwards, the output signal is amplified by EDFA. Two optical filters before and after the EDFA is to remove interference noise outside the passband. The second SA tine-gate is used to gate the clock pulse train under the controlling of the decoded signals acting as pump pulses. Thereby, the signal regeneration is achieved in doing so. After the output signal is amplified and filtered, the all-optical 3R of decoded signal is implemented.

Three demonstrated VOCP/VWPs in the experiment are shown in Fig. 6.13, which represent three different types of optical code and wavelength conversions. For optical path #1, only optical code requires to be converted while wavelength does not need to be changed at the intermediate node B. With regard to optical path #2, only wavelength requires to be converted while optical code does not need to be changed at the intermediate node B. However, concerning optical path #3, both optical code and wavelength are all required to be converted at the intermediate node B. In this experiment, the link length from node A to node B is 80 km, and the link lengths from node B to node C and node B to node E are all 50 km. They are connected by nonzero dispersion-shifted fiber (NZ-DSF) with dispersion compensation fiber (DCF) module. The average zero dispersion wavelength and dispersion slope of these lines are 1550.1 nm and 0.017ps/(nm^2 · km)

respectively. The wavelengths employed are $\lambda_1 = 1549.7$ nm and $\lambda_2 = 1552.5$ nm. Two 8-chip binary temporal-phase codes are $OC_1 = \{00000000\}$ and $OC_2 = \{0\pi0\pi\pi0\pi0\}$ respectively. It is shown by the measured eye diagrams and BERs in node C and E that the expected function of VOCP/VWP network is implemented.

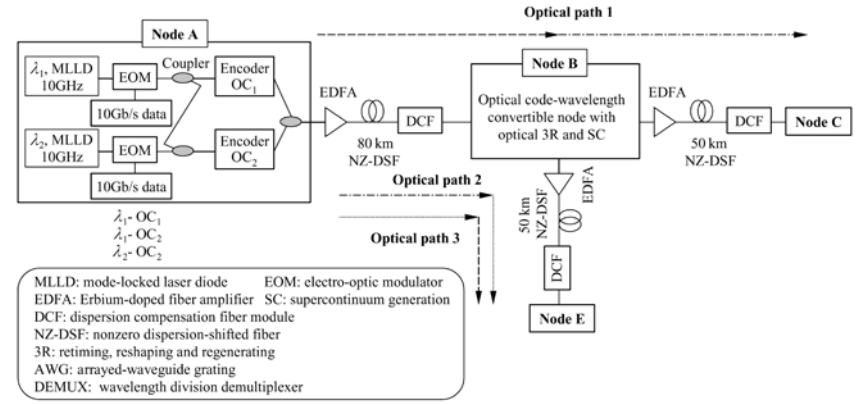

(a) VOCP/VWP network with optical code and wavelength conversions followed by optical 3R

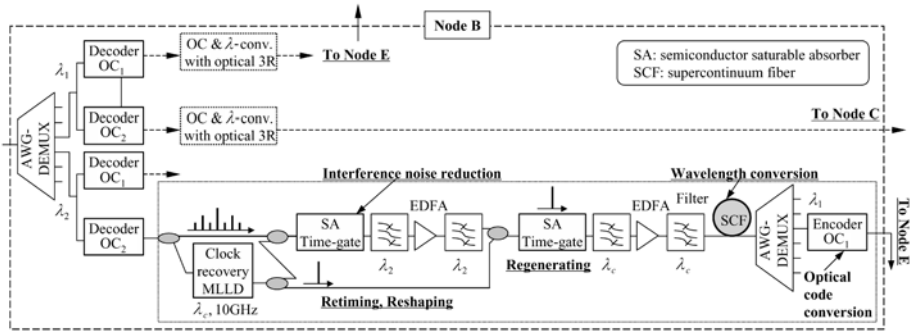

(b) Ultra-broadband both OC and wavelength convertible node by SC generation with optical 3R at Node B

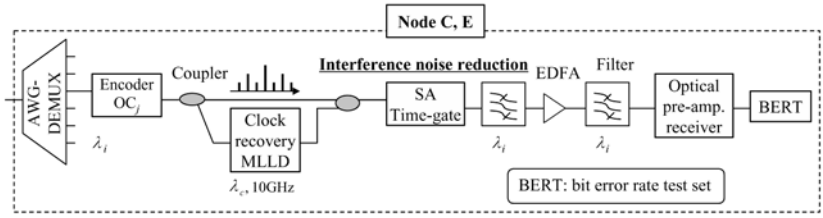

(c) Optical time-gating detection for interference noise reduction at Node C and Node E

Figure 6.12 Schematic diagram of the experimental system and nodes (Revised from Ref.[4])

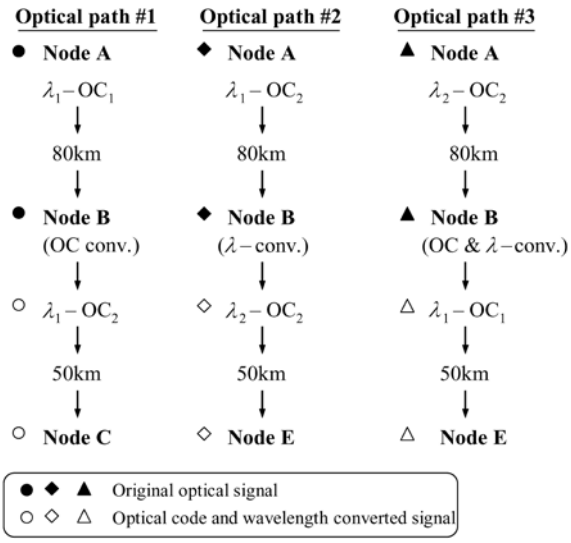

Figure 6.13 Measured three paths in the experiment (After Ref.[4])

6.4 OCDMA Local Area Networks and Access Networks

For the communication protocols of traditional local area networks (LANs), regardless of Carrier Sense Multiple Access with Collision Detection (CSMA/CD) protocol or Token Ring protocol, only one subscriber is allowed to transmit its data packets by using the channel at any given time and another active user is permitted to access the LAN until there is not information collision on the channel (or called channel idle) or it has control of the Token. Thus, they can not support the parallel data communications in real time and multiple access connections. Except that there exists the "bottleneck" effect of electronic component in LANs, there are also processing bottlenecks that result from the complicated communication protocols, the required access controlling/processing and queue buffering, which restrict the network throughput due to long latency. When the network load increases the system performance degrades. In the worst case, the network is totally blocked. In order to meet the demand of increasing bandwidth from current subscribers, Ethernet has to displace its original broadcast architecture into the switch architecture. Gigabit Ethernet clients are connected to the electronic switches by employing optical fibers, which accelerates LAN data rate from 10 and 100Mb/s for legacy Ethernet to 1 and 10Gb/s per subscriber supported by Gigabit Ethernet. However, in the face of the competition of novel and higher speed traffic, upgrading Gigabit Ethernet networks to individual subscriber data rates beyond 10Gb/s will confront big challenge due to the existence of electronic bottleneck in the switching nodes,

which restricts the scalability and flexibility of networks, and simultaneously increases the cost of network implementation.

For some multiple access techniques, such as OTDMA, WDMA and etc., which have the potential to implement high speed LANs, the maximum number of subscribers supported by the network and the bandwidth assignment based on subscriber peak data rates must be determined in the early stage of network design, so that it is very difficult for them to accommodate the dynamic variations of the number of subscribers and the user demands on bandwidth. For example, in an OTDMA network, the maximum number of subscribers depends on the minimum optical time slot width that can be accommodated in a fixed frame, which is relevant to the period of the maximum user data rate. An OTDMA network that can support 25ps time slots can accommodate a maximum of 40 simultaneous subscribers operating at 1Gb/s. WDMA networks require stringent control over the optical wavelength spacing and filter bandwidth to accommodate individual subscribers on uniquely allocated optical channels. A WDMA LAN operating at the C-band (wavelength from 1530 to 1565nm) could accommodate about 44 subscribers employing a wavelength spacing of approximately 0.8nm (corresponding to 100GHz in frequency domain)[6]. For OTDMA or WDMA, any node added to the network must conform to the design tolerance for the initially maximum network capacity no matter how many subscribers are activated on the network. This will not only make the network support a small number of subscribers but also result in the increase of cost and technical complexity to realize optical multiple access LANs. What is more, with respect to the LANs mainly with bursty traffic this will waste a large amount of precious bandwidth resources and abase the efficiency of bandwidth usage.

In the mid-1980s, the earliest proposed and demonstrated OCDMA techniques were based on LAN network architecture[7]. Since OCDMA LAN can allow multiple subscribers to simultaneously employ the same channel, it can support the real-time parallel data communication and multiple access connections on demands. At the same time, because the OCDMA communication implements switching through different address codes, the processing latency of switching is small. For asynchronous OCDMA network, it does not need the global synchronization in the network, and the subscribers can access the network at random with small delay. OCDMA networks are highly flexible and scalable. The various data rates and different types of media can be accommodated in the same network, which meets the requirements of differentiated quality of service (QoS) from different subscribers. OCDMA network provides more flexible and dynamic bandwidth sharing with robustness, which fits the bursty traffic well. In addition, it can support ultrahigh speed data transmitting and networking and it is very easy for the new subscribers to be added to the network through only assigning a remaining optical address codeword. Therefore, OCDMA technology has obvious superiority for constructing the LANs and access networks in contrast to other techniques such as OTDMA, WDMA and so on.

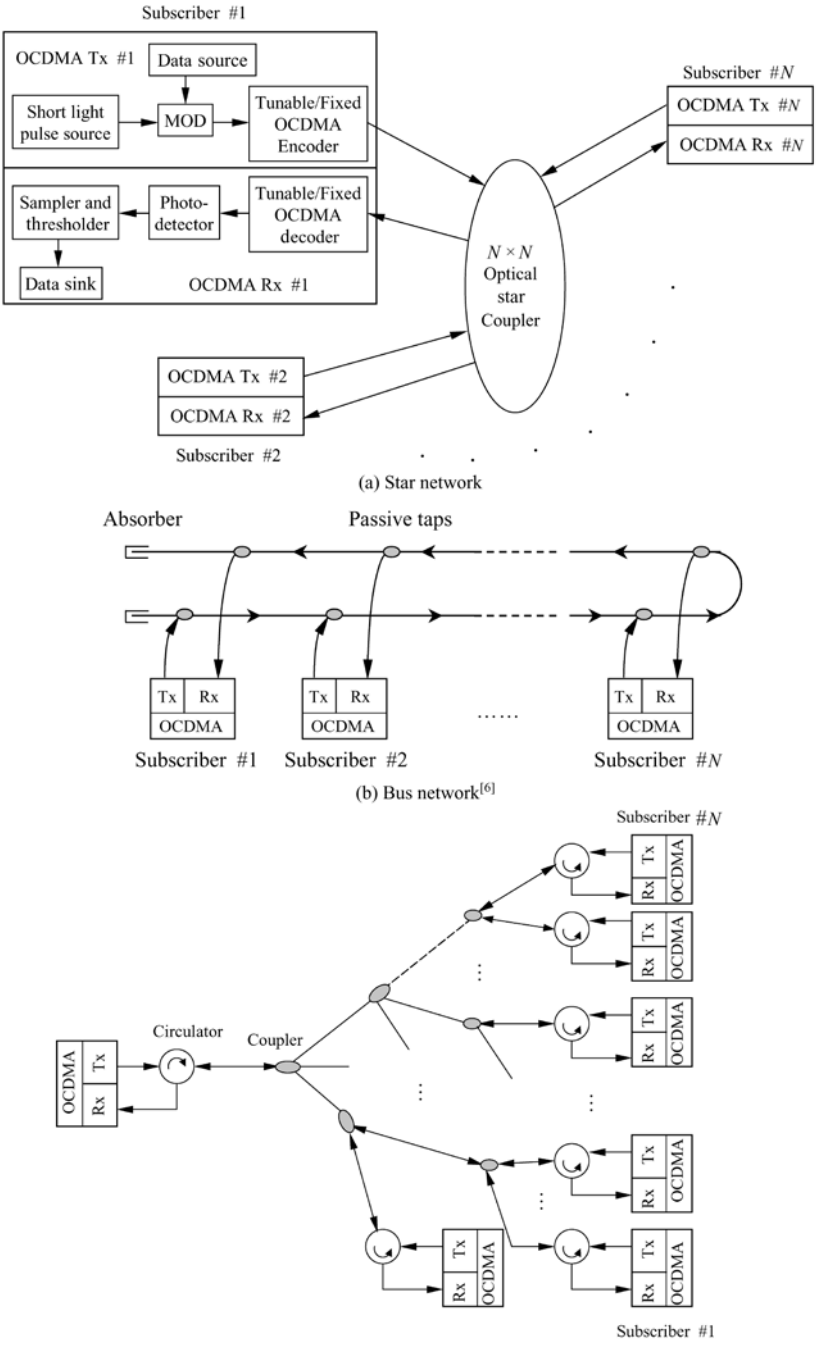

Figure 6.14 Three types of optical network structures implemented by simply passive optical devices

Since OCDMA is well compatible with WDMA, the combination of OCDMA and WDMA can further enlarge the network size and double the number of subscribers in a network. When two or more than two LANs are interconnected, an OCDMA codeset with larger cardinality can be employed to allocate different address codewords to different communication terminals in the interconnected networks. Also, each LAN can be allocated a given wavelength, different LANs employ different wavelengths, which results in that the same codeword can be reused in LANs with different wavelengths. The networks are interconnected by the gateways with the functions of optical code and wavelength conversions. OCDMA supports any network architectures such as star, bus, tree, ring, mesh and so on. For star, bus and tree networks, all nodes/subscribers in a network can be connected by employing simply passive optical components with low cost, such as optical couplers, optical circulators, etc., without requiring a complex active central switching node, as shown in Fig. 6.14[6]. In such a network, any user transmitter can establish a connection with any subscriber receiver, which can implement the point-to-point, multicast and broadcast communications, and bidirectional, full-duplex communications. It is convenient to upgrade the functions of networks to support new services with different data rates without varying the central node. They are well suitable for distributed computer interconnecting in particular[6].

6.4.1 OCDMA Star Networks

In the process of research on OCDMA technology, the star network architecture is employed most frequently. In a star OCDMA network, when the number of subscribers increases and thus the numbers of input ports and outputs of an optical coupler can not meet the demand of the number of users, the number of ports can be extended in the manner as shown in Fig. 6.15. In Fig. 6.15(a), an $M \times 1$ optical combiner is added to each input port of the optical star coupler, and a $1 \times M$ optical splitter is added to each output port so that the network is enlarged into an $MN \times MN$ star network. Taking into account that the optical power of each input signal is required to be split into MN paths and thus the signal power arriving at each receiver may be very small, an EDFA is added to each input port and output port of the $N \times N$ optical star coupler to amplify the signals to a certain power level so that they can be accepted by the receivers. Another method is to employ the wavelength dimension to enlarge the network scale. In this case, an $M \times 1$ wavelength division multiplexer and one $1 \times M$ wavelength division demultiplexer are added to each input and output port of the star coupler respectively, utilizing M wavelengths to implement a communication network with MN pairs of transmitters and receivers, as shown in Fig. 6.15(b). The advantage of the star network is that the network architecture is simple and the nodes in the network have good fairness, which is suitable for local area

network and access network without large geography distances, such as a network with the geography distance less than 10km. However, the star network has poor capability to resist failure. Once a failure occurs in the central node the entire network collapse may be caused. In addition, when the geography distances among the network nodes are far, the signal power will dramatically decline due to the loss in the transmission lines and the splitting of optical signals in the optical coupler. Hence, the signal amplification by multiple stages of EDFAs would be required, which results in the noise accumulation from EDFAs and degrades the quality of signals significantly. Simultaneously, the signal transmission delay between adjacent nodes may be quite large.

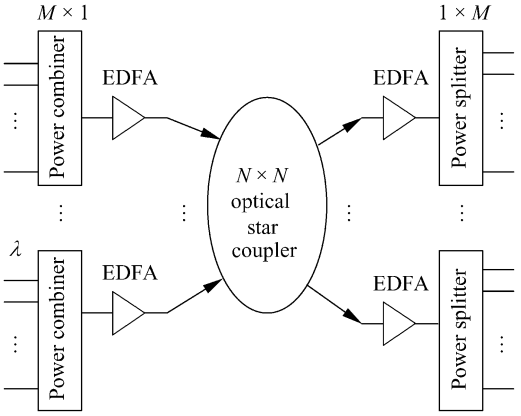

(a) Network extension using optical splitters and combiners[6]

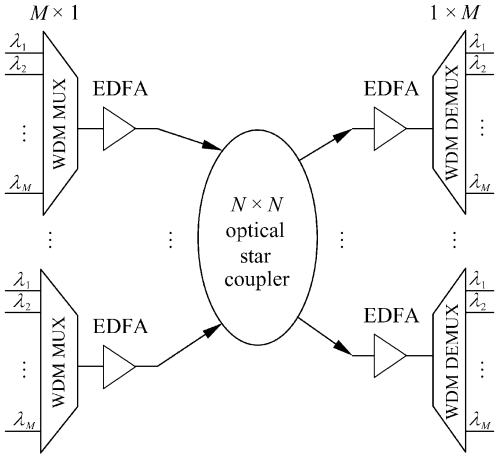

(b) Network extension employing wavelength dimension

Figure 6.15 Star network extended

6.4.2 OCDMA Ring and Bus Networks

Although the research on OCDMA network architecture focuses mainly on the star topology to date, most existing optical fiber networks have the architectures of ring and mesh topologies, as shown in Fig. 6.16. The ring network is suitable for being applied to a wide geographic area, easy to manage and offers redundancy by employing double ring architecture. In addition, it enables protection switching and failure restoration for a node failure or/and optical fiber line broken with simple protocols. Since the ring network is widely adopted and

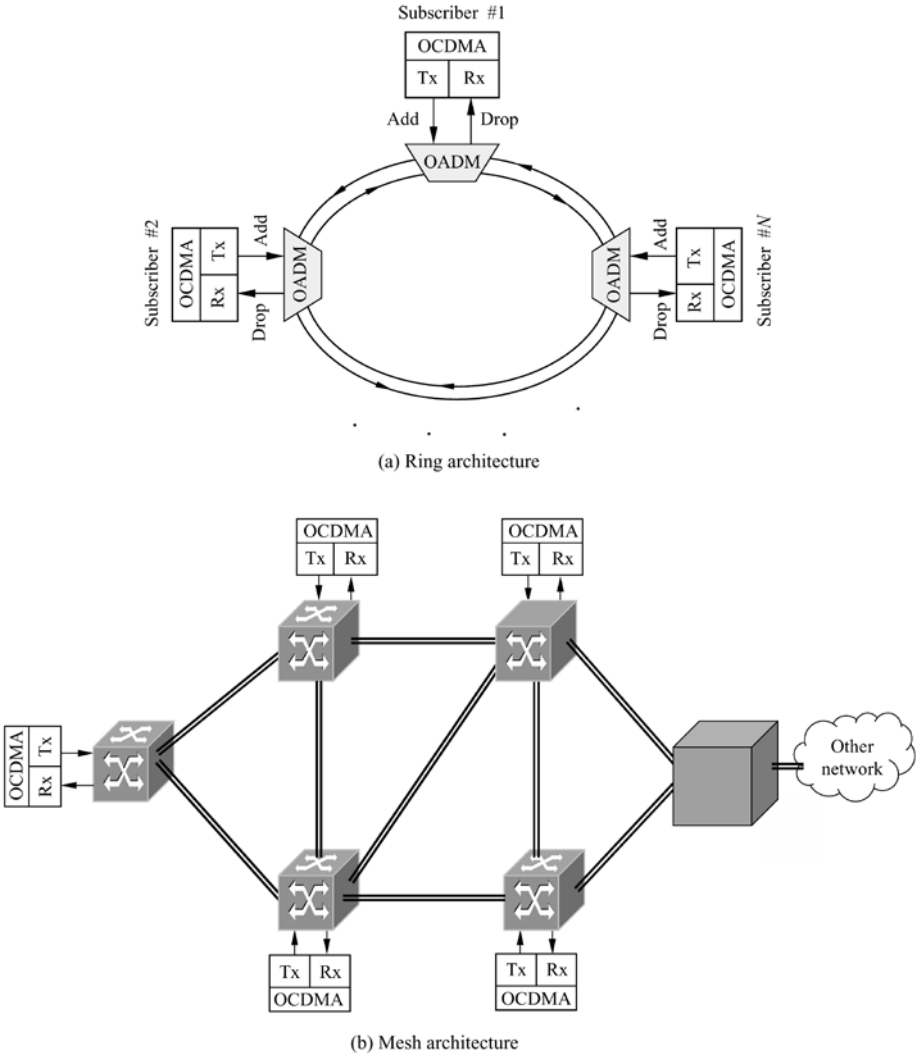

Figure 6.16 Ring and mesh networks[6]

has inherently high reliability it becomes one type of important network architectures. Therefore, OCDMA must be compatible with it. The ring network has the same advantages as the star network. In such a broadcast transmission medium, each node can send its data to any other node on the ring. Thus, the reconfigurable OADM (optical add/drop multiplexer) is a crucial component employed by the ring network. Multiplexing OCDMA code onto a fiber-optic ring can be achieved easily with an optical coupler. However, it is not easy to drop or remove the optical energy of a given code, which is dependent on the system implementation and the encoding technique used by the system. Since the ring networks have closed lightpaths, in general, the codewords are still on the ring and continue to go round along the ring after the drop of the optical signals. Therefore, this will result in the accumulation of noise such that the BER of the system will increase and individual subscriber's performance or the network performance will be deteriorated ultimately. As a result, for the ring network, special encoding/decoding methods and system implementation or filtering are required to reduce or eliminate the accumulation of noise.

With regard to the ring and bus networks, two architectures of OADMs have recently been proposed. One is an OADM employing incoherent spectral amplitude encoding[8], where the code drop demultiplexing deploys the complementary decoding and balanced detection and another is incoherent 2-D WH/TS encoding OADM[9]. These two types of OADMs can effectively reduce the noise accumulating from the remaining codes.

Shown in Fig. 6.17 is an architecture of OADM node with safe protection function. Assuming that the external ring is an operational ring and the inner ring is a spare ring. In the normal operational scenario, under the operation of control signals two 2×2 optical switches are in the bar state. In this case, the outer ring operates. When the line in operational ring has a malfunction the inner ring starts to work. In this case, two optical switches S_1 and S_2 locate at the cross states, which makes the inner ring works in reverse direction. When a failure happens in the local node, S_1 and S_2 are in the cross states and the inner ring starts to work as well, which gets rid of the malfunction equipment in the local node. Hereby, the double ring networks have well safe robustness and high reliability to resist failure.

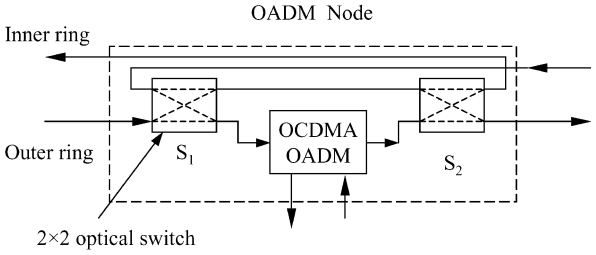

Figure 6.17 Architecture of an OADM node with safe protection function

6.4.2.1 2-D WH/TS OCDMA code add/drop multiplexer

2-D WH/TS OCDMA incoherent code drop demultiplexer based on terahertz optical asymmetric demultiplexer (TOAD) is shown in Fig. 6.18(a)[8], which is composed of a drop code decoder (DCD), a TOAD and a code restorer (CR). The DCD consists of a wavelength division demultiplexer, a wavelength division multiplexer and w fiber-optic delay lines, whose output is a superposition of an autocorrelation and multiple access interferences from other subscribers. DCD output enters Port 1 of the circulator and the signal from its second port is directed to TOAD. TOAD comprises a 50∶50 optical coupler, a semiconductor optical amplifier (SOA) and an optical coupler connected to form a loop. The coupler is to couple a control signal into the loop. The SOA is placed asymmetrically in the loop and provides the basis for the all-optical switching operation. After a control pulse enters the SOA, a switching window is opened for the autocorrelation peak, which makes the autocorrelation peak and the control signal output to a highpass filter (HPF) from the TOAD. The HPF removes the control signal and drops the autocorrelation peak. Since other signals in the TOAD are outside of the switching window they are reflected back to Port 2 and then output from Part 3 of the circulator to the CR. The CR will remove the time shifts of other pulses, which are caused by the DCD, and restore them to their original sequences to be transmitted to downstream nodes on the network. In this way, not only the leftover noise in the network from the dropped code can be eliminated but the dropped code can be reused in downstream nodes as well. After the added data are encoded optically they can directly be added to the network by an optical coupler. The function of the code dropper is demonstrated in Reference [8]. The network is a ring network with four subscribers, where the four codewords of a wavelength-hopping prime code (WHPC) are (1,8,15,22), (1,16,31,46), (1,23,45,67) and (1,31,61,91) with the number of wavelengths 4, code-length 101, auto- and cross-correlation constraints 0 and 1 respectively. The chip rate is 253Gchip/s. Under the control of optical control pulse, the TOAD opens an optical-sampling time window of less than 10ps to let the autocorrelation peak drop. The system supports a 2.5Gb/s bit rate for each subscriber. Note that this architecture of code dropper is not suitable for the formats of broadcast and multicast since the downstream nodes would not receive the data signal after the code dropper. The data broadcast and multicast can be implemented by employing the node shown in Fig. 6.18(b). Nevertheless, there exists the noise accumulation of remaining code in this architecture, which needs to be eliminated by taking some other measures. For instance, after all subscribers receive their data signals the code dropper shown in Fig. 6.18(a) can be employed to remove the leftover codes from the network. For the bus network, although there exist the leftover dropped codes in the network the noises are not accumulated because the lightpath in the bus network is not closed. In this case, the OADM shown in Fig. 6.18(b) can be utilized.

The shortcoming of these two types of code droppers is that they require synchronous control of optical pulse signals.

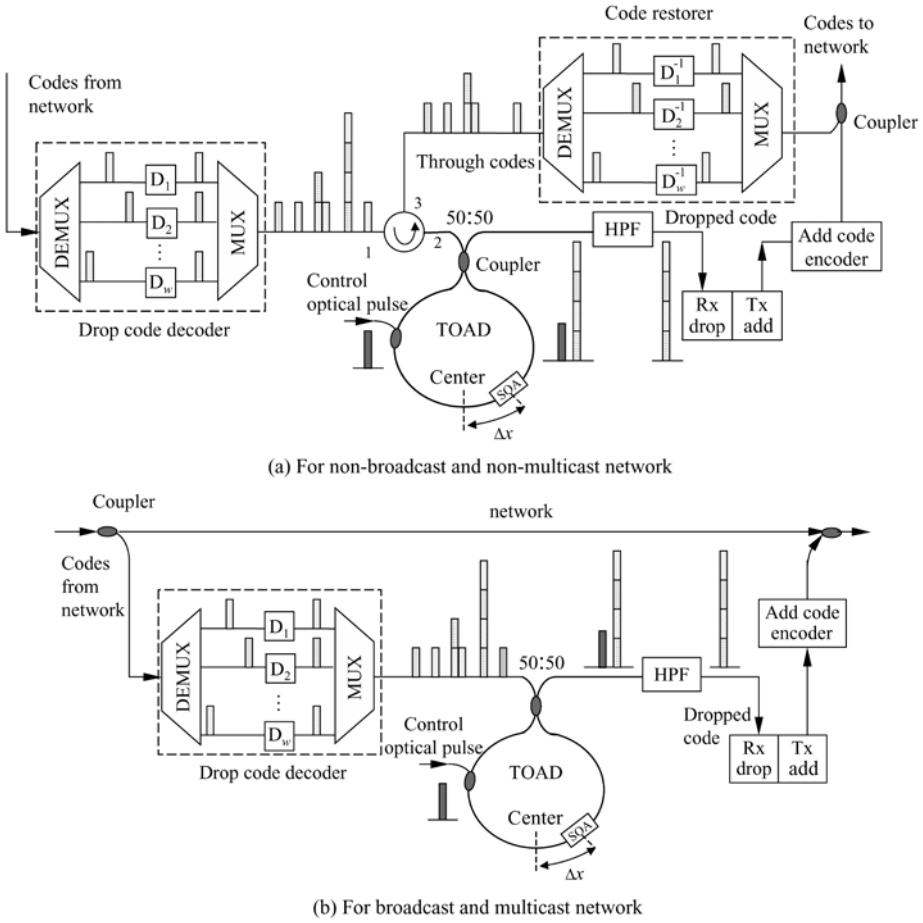

HPF: high pass filter, D: delay, D^{-1}: inverse delay, w: weight of code

Figure 6.18 Schematic of a code add/drop multiplexer for 2-D WH/TS incoherent OCDMA (Revised from Ref.[8])

6.4.2.2 OCD-ADM Employing Incoherent Spectral Phase Encoding

Optical code-division add/drop multiplexer (OCD-ADM) employing incoherent spectral amplitude encoding is shown in Fig. 6.19[9]. A 1×2 optical splitter separates the input optical signal into two branches. In one branch is the signal not to drop in the local node, which is transmitted to the downstream nodes after amplified and delayed, where the leftover signals from the dropped codes are contained. The purpose of delay is to implement time synchronization between the leftover signal of dropped code and the added signal of inverse optical

encoder so that it is convenient for their counteracting. In another branch is the drop signal that is decoded by the drop decoder. Then the receiver recovers it into the drop data. At the same time, in order to counteract the remaining signals of the dropped code in the network, data conversion is performed for the output of the dropped decoder and then the data are added onto the network after reversely encoded by the inverse optical encoder so that they can counteract the inference of leftover code by balanced differential detection in the downstream nodes. Moreover, there may be some signals to be added to the network in the local node. After they are encoded by the optical add encoder, the combining signals and other two signals are transmitted to the downstream nodes. In this way, the OCDMA add/drop multiplexing of incoherent spectral amplitude encoding is implemented.

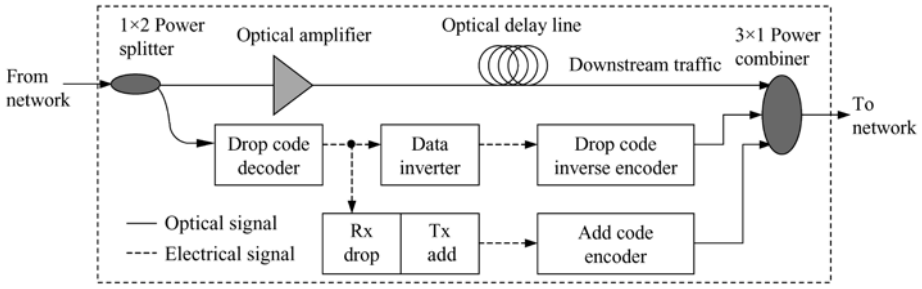

Figure 6.19 Schematic of OADM for incoherent spectrally encoded OCDMA (After Ref.[9])

The encoder and decoder structures for OADM of the incoherent spectrally encoded OCDMA are shown in Fig. 6.20[9]. The decoder employs the balanced differential detection. When data bits are "0" and "1" respectively, the encoder code them to the complementary spectral components. This type of structures needs the balanced address codes, that is, the number of "1" must be equal to that of "0" in each address codeword, such as Walsh-Hadamard code. Since its operational principle has been detailed in Section 4.4.3, therefore we no longer repeat it here. This OADM has two disadvantages. The first one is that the optical switches are required with very high speed, which is at least the same as the data rate. The second one is that when it is employed to construct a ring network, the leftover code in the network makes the noise accumulate, which will lead to the network performance degrading. Thus some other measures must be taken to remove the remaining codes.

Based on the aforementioned OADM structure, the OCDMA network performance analysis with ring and bus topologies was carried out in Reference [9]. $N-1$ rows in an $N\times N$ Walsh-Hadamard matrix are employed as the address codes of the nodes in the network, where the numbers of "0" and "1" in each

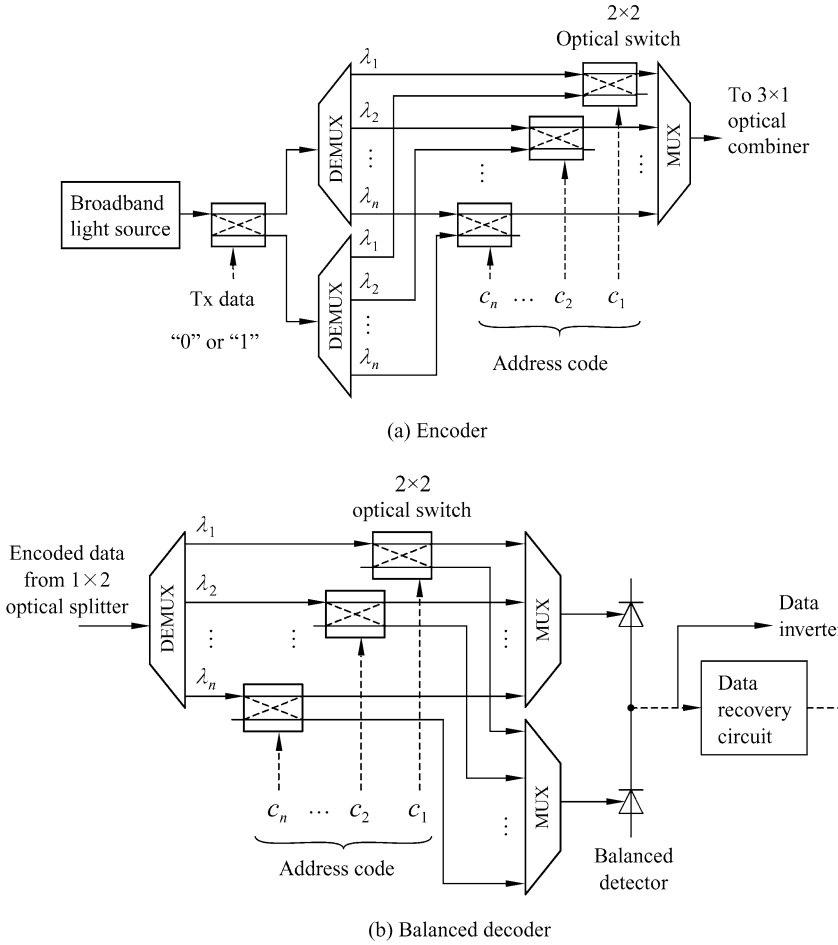

Figure 6.20 Encoder and decoder structures for OADM of the incoherent spectrally encoded OCDMA[9]

code are symmetric. It is shown by comparison of performances between two network topologies that for equivalent encoder output powers, the bus network can support twice as many optical network nodes as the ring network can do under the same system bit error rate. The declining of the ring network performance is caused by the noise which continuously circulates in the closed fiber-optic ring. Although the OADM effectively cancelled out the dropped code from the network it can not eliminate the entire energy of the dropped code. In addition, the inverse optical encoder at each node also results in additional noise to the network, which restricts the scalability of this OADM in the ring topology.

Another type of OADM employing optical fiber Bragg grating (FBG) is shown in Fig. 6.21. The aggregated optical signal from the optical fiber trunk firstly goes to Port 1 of the left-side optical circulator. The output optical signal

from Port 2 enters a FBG optical decoder and the signal reflected by the FBG decoder comes out from Port 3. The transmission signal enters Port 4 of the right-side optical circulator and is output from its Port 5. The transmission and reflection signals perform the differential detection. After the signal output by the balanced detection is sampled and decided, the data is recovered. In doing so, the data drop is implemented. The signal to be multiplexed onto the fiber-optic trunk is inputted from Port 1 of the right-side optical circulator and enters the FBG encoder, whose reflected signal is output from its Port 3 and is sent to the fiber-optic trunk. In this way, the adding of signal is accomplished.

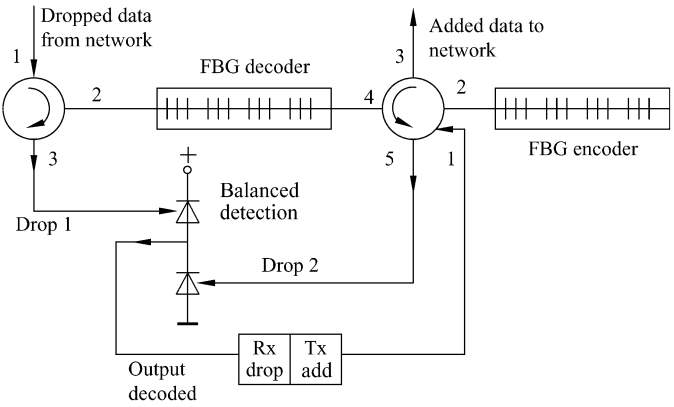

Figure 6.21 Schematic of OADM using FBGs for incoherent spectrally encoded OCDMA

6.4.3 OCDMA Tree Network

In order to actualize the multipoint-to-multipoint communications, the core networks usually employ the ring and mesh network topologies and the local area networks commonly exploit the star, ring and bus network topologies. The access network is a type of service distribution networks, which as a rule utilizes the point-to multipoint tree architecture to form a passive optical network (PON), as shown in Fig. 6.22. The optical line terminal (OLT) in the central office (CO) connects with the end subscriber optical network units (ONUs) by the optical coupler. This structure facilitates low cost and high bandwidth utilization of fiber-to-home (FTTH)/premises (FTTP), fiber-to-building/business (FTTB) and fiber-to-cabinet (FTTCab). The upstream and downstream links can employ different optical fibers to achieve space division or different wavelengths to realize wavelength division, or also optical circulators to implement direction division as shown in Fig. 6.23. With respect to multimedia broadcasting and distribution application, the hybrid network architecture that is formed by the combination of tree and star topologies, is exploited, as shown in Fig. 6.23. Different

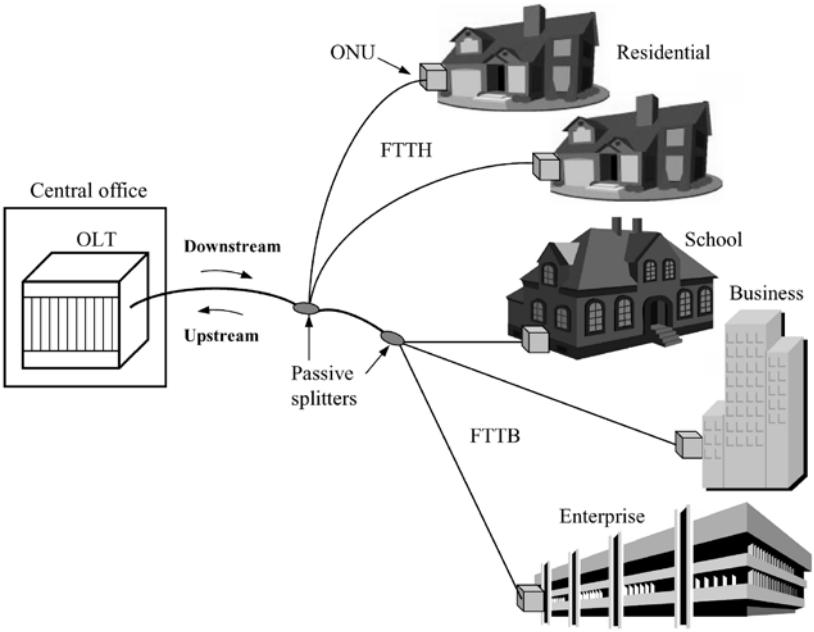

Figure 6.22 Optical passive network based on OCDMA

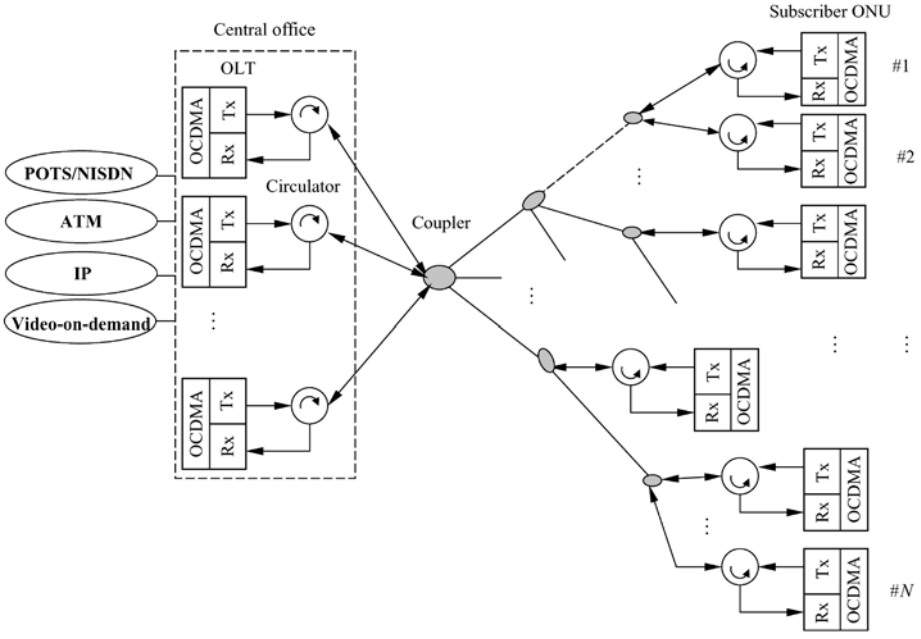

Figure 6.23 Hybrid network architecture of tree incorporating with star

transmitters in OLT convey different real-time media with constant bit rates (CBRs) and variable bit rates (VBRs). Different bit rates and quality of services (QoS) are supported by choosing different OCDMA encoding with different code-length, code-weight and code-performances. The services in such a network may be high-speed data, IP traffic, real-time voice and video, and video on demand with various performance and traffic requirements. The real-time traffic has stringent requirements for time delay while the data traffic has strict specification on bit-error rates (BERs). The conventional FTTH employs the downlinks with high bit rate and the uplinks with low bit rate. With the increasing demands from customers and development of network technologies, a large number of peer-to-peer applications will be emerging, such as exchanging the gigabyte files of uncompressed 1.2Gb/s high-definition class or even higher-definition class digital movies, bi-directional medical applications of telediagnosis and surgery and wide variety of customized service options, for example, different bit rate and QoS requirements. These applications could not be well supported by the asymmetric FTTH with high bit-rate downlinks and low bit-rate uplinks. Thus, the conventional FTTH will eventually be transformed into the gigabit-symmetric systems whose downlinks and uplinks all support ultrahigh bit rates[10]. Figure 6.24 shows a scheme which can support the gigabit-symmetric FTTH by employing OCDMA-over-WDM PON, which was proposed in Reference [10]. In this scheme, an OCDMA codeset with N codewords and M wavelengths are exploited. These codewords can be reused on different wavelengths. The asynchronization, high

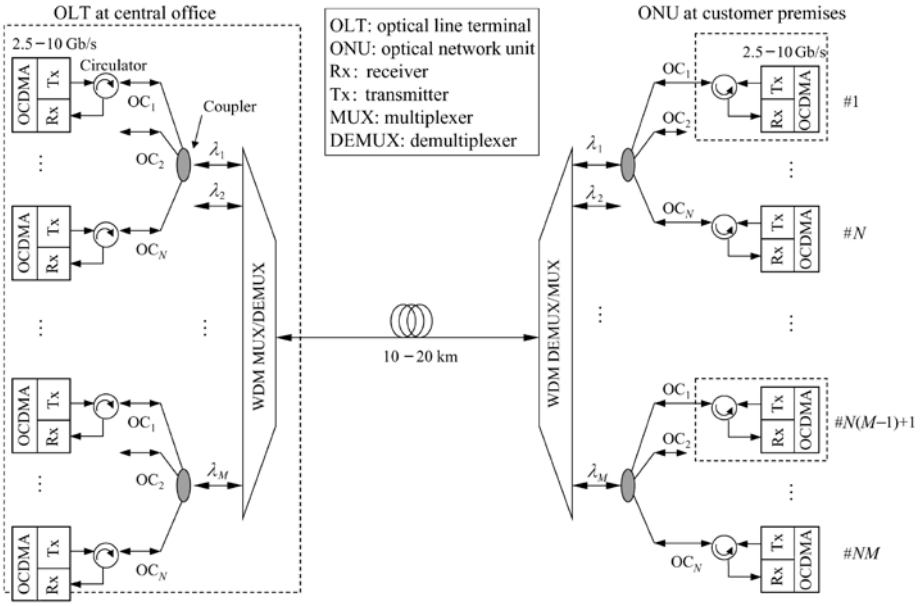

Figure 6.24 Architecture of symmetric FTTH[10]

speed and real-time symmetric traffic can be conveyed between an OLT and NM ONUs by employing such a system.

Concerning the mesh network topology, it is suitable for optical packet data networks. With regard to Mesh network applications, we will detail them in Section 6.6.

6.4.4 Code Translator for Spectral Phase Encoding OCDMA

In an OCDMA network, when the transmitter and receiver are all fixed, it can only implement the point-to-point communication. When the transmitter is fixed and the receiver is tunable the point-to-multipoint broadcast or multicast communication can be accomplished. When the transmitter and receiver are all tunable any mode of communications can be achieved. Since a subscriber needs to communicate with different users in different time at least one of the transmitters and receivers of each subscriber should be tunable. These flexible manners of communications can also be actualized by the code translator in the intermediate node of network under the case of fixed transmitters and receivers. Figure 6.25 gives the configurable principle of establishing connections among subscribers by employing code translators in the spectral-phase-encoding OCDMA star network[11].

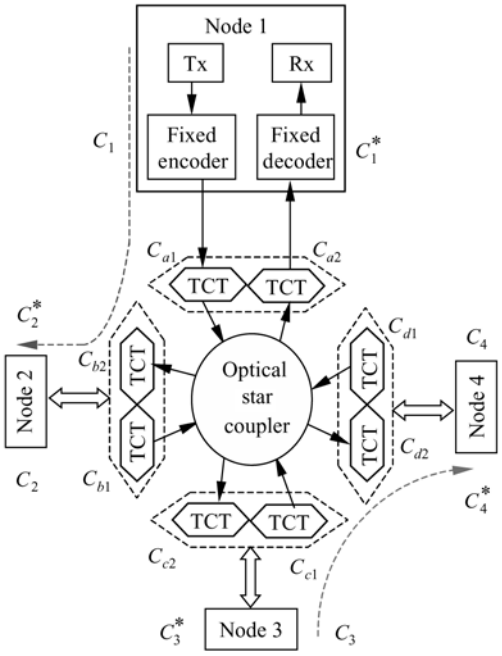

Figure 6.25 Schematic of code translator employed a star network to route connections between subscribers[11]

The function of the code translator is to perform one or more than one times of encoding to an encoded signal. Therefore, a code translator is actually an optical encoder. One time recoding is equivalent to two-encoder cascading, namely, the cascading of the optical encoder in the transmitter and the code translator. The resulting effect is equivalent to the element-by-element multiplication of the spreading sequences (phase codes), which should result in another available codeword. This means that the code used by the optical encoder and code translator should has closed property so that the network performance can be guaranteed and the decoding can be accomplished conveniently at the receiving end. It is shown by investigation[11] that Walsh-Hadamard codeset obtained by viewing each row of a Walsh-Hadamard matrix as a codeword, has such a closed property, that is, the novel codeword obtained by the corresponding element-by-element (chip-by-chip) multiplication of any two codewords is another codeword that still belongs to this codeset. As a matter of fact, many pseudorandom codes possess such a closed property, such as m-sequences, A family sequences[12], etc. For example, all codewords of a Walsh-Hadamard code with the length of 8 are shown in Table 6.1, which are obtained by each row of a 8×8 Walsh-Hadamard matrix. For the convenience of description, each codeword is given a code number according to their orders, as shown in the table. The new codeword (1 −1 1 −1 1 −1 1 −1) obtained through the element-by-element multiplication between code 3, (1 1 −1 −1 1 1 −1 −1), and code 4, (1 −1 −1 1 1 −1 −1 1), is code 2 in the codeset. The translation table among 8 Walsh-Hadamard codewords with the length of 8 based on this method, is shown in Table 6.2.

Table 6.1 All codewords of Walsh-Hadamard code with length 8 and their numbers

Code No.	Codewords of Hadamard code with length 8							
1	1	1	1	1	1	1	1	1
2	1	−1	1	−1	1	−1	1	−1
3	1	1	−1	−1	1	1	−1	−1
4	1	−1	−1	1	1	−1	−1	1
5	1	1	1	1	−1	−1	−1	−1
6	1	−1	1	−1	−1	1	−1	1
7	1	1	−1	−1	−1	−1	1	1
8	1	−1	−1	1	−1	1	1	−1

After the output of a fixed encoder in a network is transformed by one or more tunable code translators (TCT), the connection can be established with any fixed decoder. In this way, multiple communication manners can be implemented. For instance, after the output of a fixed encoder with codeword C_i in a subscriber transmitter is transmitted cross a network, it is decoded by a fixed decoder with codeword C_k^* at the receiving end. Then, a code translator with codeword C_j is

Table 6.2 Code translation table for Walsh-Hadamard code with 8 codewords

Incoming code No.	Coder No.							
	1	**2**	**3**	**4**	**5**	**6**	**7**	**8**
1	1	2	3	4	5	6	7	8
2	2	1	4	3	6	5	8	7
3	3	4	1	2	7	8	5	6
4	4	3	2	1	8	7	6	5
5	5	6	7	8	1	2	3	4
6	6	5	8	7	2	1	4	3
7	7	8	5	6	3	4	1	2
8	8	7	6	5	4	3	2	1

required to transform the encoded signal in the middle of the network. In this case, the relation $C_i \odot C_j = C_k$ must be satisfied, where "$\odot$" indicates the chip-by-chip multiplication between two codewords, "$*$" represents taking complex conjugate. In Fig. 6.25, assuming that node 1 wants to establish a connection with node 2, the signal will go through the encoder C_1 in node 1, two tunable code translators C_{a1} and C_{b2} in the network and the decoder C_2^* in node 2 and arrive at node 2 eventually. These codewords must meet the relation of $C_1 \odot C_{a1} \odot C_{b2} = C_2$. Similarly, when node 3 needs to establish a connection with node 4, the codewords of encoder, tunable code translators and decoder must meet $C_3 \odot C_{c1} \odot C_{d2} = C_4$. Note that if these two connections simultaneously exist $C_1 \odot C_{a1} \neq C_3 \odot C_{c1}$ must be met in order to avoid collision between these two connections. Using such switching patterns, not only the flexible communication connections can be established but also the eavesdropping data among nodes becomes difficult. Consequently, the confidentiality of information transmission in a network will be improved significantly. At the same time, since the network has the capability of flexible choosing address the limitation of codeword continuity will be overcome effectively and the address codewords can be reused in the network, which greatly enlarges the network capacity and reduces the probability of connection collision.

The code translators with this structure can also be applied to the ring and bus network topologies. When they are employed to construct an OADM, the architecture shown in Fig. 6.26 can be utilized. The dropped codeword is firstly transformed into a codeword matching with a fixed decoder by a tunable code translator and then decoded by the fixed decoder. Under the controlling of control signal, TOAD and HPF are utilized to choose the desired data. The data are first of all encoded by a fixed optical encoder and then transformed by a tunable code translator, and finally added to the network by an optical coupler.

This is the process of adding and dropping a signal. The disadvantage of OADM with such an architecture is that there exists the leftover code of dropped code in the network. For bus topology, due to its unclosed lightpath, the remaining codes do not accumulate. However, for ring topology, because of the closed lightpath and the circulation of remaining codes along the ring, the interference noise increases in the network, which will affect the system performance. Hence, some other measures are required to eliminate the leftover noise from the dropped codes.

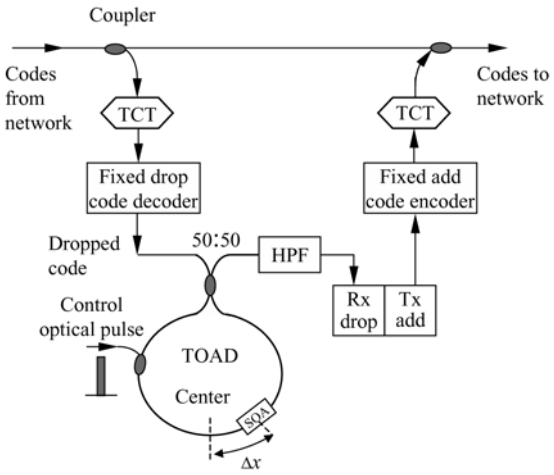

Figure 6.26 OADM based on tunable code translator

The shortcoming of this encoding method is that the network needs synchronous signals. This is because Walsh-Hadamard code is one type of synchronous codes. The operational principle of this passive code translator was experimentally demonstrated in Reference [11]. The experimental principle diagram is shown in Fig. 6.27. The pulsed mode-locked laser (MLL) with repetition frequency 5 GHz was employed and its output optical pulse contained 16 spectral lines (corresponding to code length of 16) spaced at $\Delta f = 5$ GHz in an 80 GHz window. After this signal was modulated by a $2^{31}-1$ PRSB signal at 2.5 Gb/s bit rate it was directed to a cascaded link containing four code translators with codes 9, 12, 14 and 15. These code translators utilized Walsh-Hadamard codes with code length of 16. The code translation table is shown in Table 6.3. The oscilloscope traces at individual points were shown in the upper part of Fig. 6.27. From Table 6.3 we could see that after four stage code translations the signal should be recovered to code 1. In terms of the measured oscilloscope traces and eye diagram at the leftmost side of Fig. 6.27, we would find the code translations were successfully implemented. Note that the double-pulse modulation is employed here, i.e., a pair of pulses from the MLL is used to signify a single data bit.

Table 6.3 Code translation table for Walsh-Hadamard code with 16 codewords[11]

Incoming Code No.	Coder No.															
	1	**2**	**3**	**4**	**5**	**6**	**7**	**8**	**9**	**10**	**11**	**12**	**13**	**14**	**15**	**16**
1	1	2	3	4	5	6	7	8	9	10	11	12	13	14	15	16
2	2	1	4	3	6	5	8	7	10	9	12	11	14	13	16	15
3	3	4	1	2	7	8	5	6	11	12	9	10	15	16	13	14
4	4	3	2	1	8	7	6	5	12	11	10	9	16	15	14	13
5	5	6	7	8	1	2	3	4	13	14	15	16	9	10	11	12
6	6	5	8	7	2	1	4	3	14	13	16	15	10	9	12	11
7	7	8	5	6	3	4	1	2	15	16	13	14	11	12	9	10
8	8	7	6	5	4	3	2	1	16	15	14	13	12	11	10	9
9	9	10	11	12	13	14	15	16	1	2	3	4	5	6	7	8
10	10	9	12	11	14	13	16	15	2	1	4	3	6	5	8	7
11	11	12	9	10	15	16	13	14	3	4	1	2	7	8	5	6
12	12	11	10	9	16	15	14	13	4	3	2	1	8	7	6	5
13	13	14	15	16	9	10	11	12	5	6	7	8	1	2	3	4
14	14	13	16	15	10	9	12	11	6	5	8	7	2	1	4	3
15	15	16	13	14	11	12	9	10	7	8	5	6	3	4	1	2
16	16	15	14	13	12	11	10	9	8	7	6	5	4	3	2	1

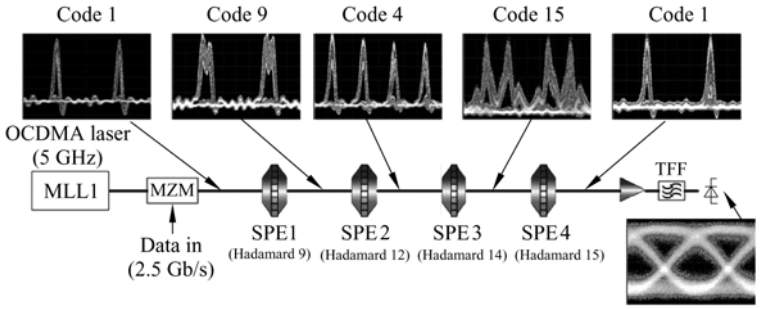

Figure 6.27 Experimental configuration used for four cascaded code translations (bottom), the resulting measured waveforms (top) as the OCDMA signal progresses through a cascade of four spectral phase encoders. The time base in all five figures is identical and the pulse interval in the leftmost and rightmost pair of figures is 200ps (5GHz pulse-repetition rate). The thin film filter (TFF) passband represents a DWDM channel filter. The detected eye diagram is shown at bottom right. In all cases, the optical waveforms correspond to a receiver with a 30GHz bandwidth. (Adapted from Ref.[11], with permission from IEEE © 2007)

6.5 Simple Communication Protocols for OCDMA LANs and Access Networks

From the previous introduction, we can see that OCDMA is a promising scheme to implement ultrahigh bit-rate signal transmission, switching and access networks due to its advantages of subscriber asynchronous access at random, supporting multiple rates and bursting traffic, protocol transparency and so on. However, the research efforts on OCDMA technologies have focused mainly on the network physical layer all along. Until the recent years, the study of network data link layer starts attracting research attention from OCDMA community and some primary research results have appeared[13 – 18]. In this section, we describe the random access protocol and the interference avoidance access protocol.

In a communication network, each subscriber does not always use the network to communicate with other users. For the access network, the ratio of the number of subscribers that simultaneously utilize the network, to the total number of users connected physically to the network is only about 10%. Therefore, in order to improve the efficiency of code utilization, the address codes can be allocated in the manner of statistic multiplexing. For local area network (LAN), the subscribers in a network transmit data in the burst mode under normal situations, that is, they are not simultaneously activated. Thus, the total number of subscribers may be larger than the number of the available codewords.

There are two important performance parameters to evaluate a protocol [13]. The first one is the average system (or network) throughput in packets per slot, which refers to how many packets on the average are received successfully per time slot. Another one is the average packet delay in time slots, which means that a packet will be received successfully after how many slots (from the beginning of transmission) on the average.

6.5.1 OCDMA Random Access Protocols for Packet Networks

Assume that an OCDMA network is a packet network of random access and broadcast and the service of each user arrives randomly but it locates at the start point of some packet and the size of traffic is random, which means that the number of packets to be transmitted by a user is a random number. We further presume that the system possesses the function of automatic retransmission request (ARQ), that is, when an error occurs in a packet transmitted the receiving end will send ARQ to the transmitting end. If the data packet does not arrive at the receiving end yet after being transmitted for L times, then the packet will be discarded and the system will start to transmit next packet. In order to use ARQ mechanism, the receiving end should have the function of packet correction, which can be implemented by using cyclic redundancy correction (CRC). In

addition, for any subscriber in OCDMA network, each subscriber should possess one OCDMA transmitter and one OCDMA receiver and furthermore, either the transmitter or the receiver should be at least tunable. The typical network architecture for OCDMA local area network (LAN) is shown in Fig. 6.28.

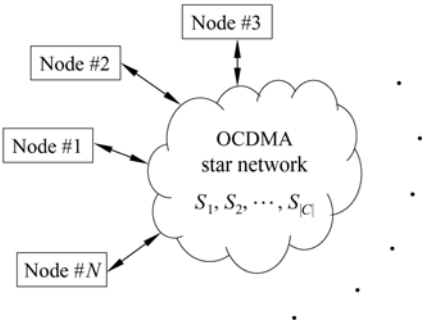

Figure 6.28 OCDMA network architecture

Suppose that there are N nodes (or called subscribers) in the network and the optical address code with cardinality of $|C|$ (the number of codewords contained) and good performance, where N may be greater than the cardinality of $|C|$. The codewords will be assigned to subscribers based on different allocation strategies as follows.

6.5.1.1 Protocol 1[13]

Assuming $N \leqslant |C|$, when a subscriber wants to send a data packet to a receiver, a codeword is randomly allocated from the codeword pool. Then, this codeword is removed from the codeword pool and is no longer available for further allocation during a slot. It is obvious that when the number of active subscribers N is larger than the code cardinality $|C|$ there is no codeword left to be assigned and then the subscriber has no choice but to wait in queue. These subscribers would try to send their packets until there are some idle codewords at subsequent time slots.

6.5.1.2 Protocol 2[13]

Supposing $N < \infty$, when a subscriber wants to transmit its data a codeword is assigned to it at random and this codeword is then removed from the codeword pool. At the same time, the randomly cyclic shift of the codeword is put into the available codeword pool. In this case, the assignment of codeword can be regarded as being random. Although this protocol makes any active subscriber always find a codeword to transmit its data and the network throughput increases significantly, much interference may be produced.

These two protocols need pretransmission coordination. Before the data are

transmitted the transmitter is firstly required to broadcast a control message (or packet) to all receivers to inform them about its address. The control message may be broadcast employing a preamble at the head of each time slot or using another channel with different wavelength. All idle receivers are normally tuned to this control channel to listen to their address codes. Simultaneously, since Protocol 1 randomly assigns a codeword to a subscriber from the residual codewords in the codeword pool and Protocol 2 assigns at random a codeword or its randomly cyclic shift to a subscriber, the transmitter and receiver are all required to be tunable.

For example, an $(n, w, \lambda) = (13,3,1)$ optical orthogonal code (OOC) has two codewords whose codeword blocks are (0,1,4) and (3,5,10) respectively. Their corresponding codewords are (1100100000000) and (0001010000100). Assuming that an OCDMA network is constructed by employing this OOC, then, from Protocol 1, we can be aware of that there are at most two subscribers simultaneously in this network. They employ the two codewords as their address codes to encode their data. Then, their encoded signals are transmitted in the network. Therefore, the network throughput is limited by the code cardinality.

If Protocol 2 is utilized, the situation is different from that of Protocol 1. Suppose that a subscriber in the network has employed the codeword (1100100000000) to start transmitting its data. However, since its randomly cyclic shift is placed into the codeword pool simultaneously, for instance, a randomly cyclic shift is (0110010000000), there are forever two codewords in this codeword pool to be provided to the sequent users. This results in the network to be unblocked but may make the system bit-error rate higher.

6.5.1.3 Protocol 3[13]

This protocol is a modification of Protocol 2. When a subscriber wants to access to the network, it is randomly allocated a codeword from the codeword pool. From now on, the receiver codeword for the subscriber is fixed and the randomly cyclic shift of the codeword is put into the codeword pool. Because a receiver address code is fixed this protocol does not require the pretransmission coordination. However, the transmitters are still required to be tunable.

In Reference [13], employing one-dimensional $(n, w, 1)$ OOC as the subscriber address code, and a discrete-time Markov chain, the three protocols were analyzed quantitatively on their steady-state system throughputs and average packet delays of OCDMA network when the direct-detection correlation receiver and chip-level receiver were used. In the analysis, it was presumed that the control packet was always transmitted successfully and any delay that might cause is ignored, and the effects of thermal and shot noises of the receiver were also neglected. The effect of multiple-access interference was focused on. For Protocol 2 and 3, when the control packets were transmitted successfully they did not have significant difference in performance. Therefore, they were taken into

account as one case in the quantitative analysis. It was shown by the analysis that with correlation receivers, although the throughputs of Protocol 2 and Protocol 3 were slightly better than that of Protocol 1 before the network throughput was unsaturated (less than the code cardinality), Protocol 1 outperformed Protocol 2 and Protocol 3 for most activities. Therefore, from the point of view of network throughput, if the correlation receiver is employed Protocol 1 should be chosen. When the chip-level receiver is utilized the throughputs of Protocol 2 and 3 are always better than that of Protocol 1 and the chip-level receiver with Protocol 2 and 3 outperforms the correlation receiver with any of the proposed protocols. At the same time, the performance of network delay with Protocol 2 and 3 is better than that with Protocol 1. Thus, when the chip-level receiver is employed we should choose Protocol 2 or 3. Furthermore, considering that Protocol 3 does not need pretransmission coordination and the tunable receiver, the performance of Protocol 3 is better than that of Protocol 2 if the control packet has the probability of transmission failure. From the point of network throughput and packet delay, Protocol 3 with the chip-level receiver is the best choice.

6.5.1.4 Protocol 4[14]

Assuming $N_m < \infty$, when a user wants to transmit its data, the system chooses a codeword from the code pool and assigns it to the user, which has been used the least times (including the times of its cyclic shift used.). If there are more than 2 codewords, which have been used for the same amount of times being the smallest, then anyone can be chosen at random among them and assign it to the user. Here the uniform assignment of codewords can be taken into account.

The randomicity of codeword assignment in protocol 3 results in the randomicity of multiple-access interference. Even when the number of users is relatively small the interference may have reached a large value. Here we can consider the uniform assignment of codewords. The code assignment in Protocol 4 is basically uniform, which makes the multiple-access interference reduced. It is obviously that protocol 1 is a special example of protocol 4 at $N_m \leqslant C$. However, Protocol 4 requires that the transmitter and receiver are tunable.

In Reference [14], the steady-state network throughput ratio and the average packet delay under different offered loads were analyzed based on the processor-sharing system model. The results revealed that when $N \leqslant |C|$ the network throughput ratios using protocol 3 and protocol 4 respectively are basically the same. However, when $N > |C|$ the throughput ratios of protocol 4 (uniform assignment scheme) are higher than that of protocol 3 (random assignment scheme). Meanwhile, the average packet delay with Protocol 4 is smaller than that with Protocol 3. Hence, with regard to the total performance, Protocol 4 outperforms Protocol 3.

6.5.2 Interference Avoidance Media Access Control Protocol for OCDMA Packet Networks

In OCDMA random access protocol, once a subscriber obtains a codeword it tries to transmit its data packets. Then, the feedback retransmission mechanism will confirm whether a packet is transmitted successfully or not. If not, the receiving end will ask for re-transmitting the packet until it receives a successful acknowledgement from the destination. In such network architecture there is practically no media access control (MAC) layer protocol besides the choice of the codewords. When the network throughput is saturated, the network performance will fall rapidly as the network load increases. The number of retransmissions asked by the receiving end will increase, which easily results in a vicious circle. In the worst situation, the users who are transmitting data, transmit the same packet repeatedly and the subscribers who try to access the network are required to wait for a long time, which makes the network performance become dramatically vicious and low efficient, even completely collapsed.

This subsection is devoted to describing the media access control layer protocol, namely, Interference Sense/Interference Detection (Is/Id) media access control protocol[15], which is similar to media access mechanism of carrier sense and collision detection in the computer networks. At the expense of reasonable increase of time delay, the network throughput will be effectively improved.

Before a node sends its data, in the first place it performs sensing, i.e., it senses if its transmission will cause interference. If it senses that there is interference on the line it defers transmission. After a certain time delay, it tries to transmit one more time. The conventional carrier-sense multiple-access with collision-detection (CSMA/CD) protocol has a couple of modes to determine how to defer, which are non-persistent mode, p-persistent mode and 1-persistent mode[16]. They can be employed as deferring modes in the interference sensing protocol. The sensing can be divided into the on-demand sensing and the continuous sensing. The former is that when a node wants to transmit its data packets it senses for a window of time. The later is that a node continuously senses the interference state on the line, regardless of whether the node has a packet to transmit.

Three algorithms for interference sensing were proposed in Reference[16], which are selfish sensing, threshold-based sensing and codeword estimation-based sensing algorithms. The selfish sensing algorithm is that the node transmits if the state of the line will not cause interference with the codeword that is being sent, and otherwise the node defers until the state of the line allows transmission. The node does not check whether the transmission of its codeword would interfere with other codewords on the line.

The threshold-based sensing algorithm is to limit the amount of interference caused to other subscribers. The interference can be restricted in two modes. One is to limit the number of overlapping chips, namely, the maximum number of the

overlaps between the codeword allowed and the state of line, where it is signified by the overlap count limit, $Thresh_c$. Another one is to restrict the magnitude of each overlap, that is, the maximum magnitude of a single overlap between the codeword and the state of the line, which is indicated by the overlap magnitude limit $Thresh_m$. A node firstly employs the selfish sensing algorithm to decide whether the line state allows it to transmit without interfering with its own codeword. Then it checks the overlap count and overlap magnitudes between its codeword and the state of the line. If the overlap count and overlap magnitudes are less than their thresholds, the node sends its codeword. Otherwise, the node defers its transmission. Diminishing $Thresh_c$ and $Thresh_m$ would lessen the number of codewords on the line, which results in the decrease of interference. The minimum value of interference may be achieved by tuning the two thresholds. An ideal mechanism is that the number of codewords on the line is maintained to an optimum value and the media access delay is kept within the bound allowed by adjusting the thresholds.

The codeword estimation-based sensing algorithm is to determine which codewords are on the line and what their relative phase shifts are through the codeword estimation in order to decide when the node can transmit and which codeword can be employed by the node without causing interference. The efficiency of this algorithm is dependent on the accuracy of codewords to be estimated. Among the aforementioned three algorithms, the threshold-based sensing algorithm has the maximum throughput. The first two algorithms are suitable for on-demand sensing. Since the code estimation-based sensing algorithm needs a big sensing window it is suitable for the continuous sensing mode.

After interference sensing, a node determines whether and when to transmit its codeword based on the sensing results. There are two issues to be taken into account, which are: (1) will the current state of the line impact its transmission? (2) will the node transmission impact other codewords on the line? The node senses how the transmission on the line will influence its transmission by comparing the chips on the line with its codeword. The interference sensing operation takes a finite amount of time. If 4B/5B encoding is employed five data bit times will be sufficient to receive information about all the codes currently being transmitted on the line[15].

After starting transmission, a node still needs to keep sensing the interference on the line. Because of the finite propagation delay of transmission medium, the packet is still vulnerable by the transmission from other nodes that may have been started in the interval between the beginning of transmission and the packet reaching them. However, other nodes may not have sensed the transmission from the node yet. The interval during which this could happen is called the vulnerable period [16]. If the diameter of the network is approximate 1000m the vulnerable period is about 5μs for a codeword with length of 10 chips. During the transmission, if the transmitting node makes sure that the interference has happen,

it can choose to cease transmitting, back off and retransmit. This process is termed Interference Detection[16]. A dedicated receiver is employed for interference detection. The receiver is tuned to the codeword of the packet being transmitted and verifies that the codeword being transmitted is received correctly. Therefore, there are at least two receivers in each node, one is utilized to receive its data packets and another is employed for the interference detection.

The media access delay does not certainly mean that packets suffer queuing delays. In addition, it is noted that packets can be transmitted out of order. For example, a node may have to transmit two adjacent packets on two different codewords. Interference on the line may prevent the first packet from being transmitted, but may allow the sending of the second packet. Thus, at the receiving end, theses packets are required to be reassembled.

In References [15] and [16], OCDMA network performance with Is/Id media access control mechanism was analyzed by simulating. The result revealed that it could provide up to 30% improvement in throughput with low delays. Otherwise, for OCDMA network employing random access protocol (called Aloha-CDMA protocol in literature), its performance of throughput does not have significant improvement only relying on varying the codeset design parameters. In Reference [17], the experimental demonstration of a WH/TS 2-D OCDMA network with Interference Avoidance protocol was performed. In the network, there were six subscribers and each user employed a PC/EQCC codeword with code-length of 16, weight of 6 and wavelengths of 8. The code can at most support 16 subscribers. FBG is utilized to implement 2-D WH/TS optical encoding. The chip rate is 10Gchip/s and the corresponding data rate is 625Mb/s. Scheduling through delaying each subscriber's traffic, the transmission has the least interference with the traffic on the line. The result revealed that the performance of the system was improved by orders of magnitude.

A media access control protocol for OCDMA packet networks with variable length data traffic was proposed in Reference [18], namely, a variable-size sliding window protocol. The average system throughput and delay with this protocol are analyzed in Reference [18], and in the analysis, the correlation and chip-level receiver models are employed respectively and meanwhile both multiple access interference (MAI) and photodetector shot noise are taken into account. It is shown by the analysis that the system performance with the chip-level receiver is much higher than that with the correlation receiver and MAI is the main factor to degrade the signal performance. In addition, the analysis reveals that performance of system with error control codes (ECC) can be improved.

The protocol is one of the key issues for OCDMA network to be applied practically. Some primary results studied currently have introduced in this section. We are still required to pay tremendous efforts in order to research and develop practical and perfect OCDMA network protocols and standardize them.

6.6 Optical Packet Switching Based on Optical Code Label

The explosive increase of IP traffic requires that the future optical network is a data-centric network. WDM technology makes the optical fiber lines possess massive capacity to transmit data. However, for every data packet the traditional router performs the optical-to-electrical (O/E) and electrical-to-optical (E/O) conversions and processing, even for those packets whose source and destination addresses do not belong to the local router. The tremendous processing burden and electronic bottlenecks make the router not be able to bear the deadweight and, at the same time, the electronic processing capability of router is badly unmatched with the transmission capacity of WDM lines. On the electronic level, the capacity limit of packet routers can be alleviated by multi-protocol label switching (MPLS) technology, which makes use of packet forwarding decision and decouples switching and forwarding capabilities, while the end destination is processed only at the edges of the MPLS domain. The core routers employ high-speed packet switching capabilities to achieve faster data throughputs. However, MPLS-based forwarding is still an electronic solution[19] and can not eliminate the electronic processing bottlenecks.

MPλS has emerged by incorporating MPLS with optical WDM technology, which has the potential to resolve the electronic routing bottlenecks utilizing wavelength routing capability. However, it still poses several challenges. For example, the unit of bandwidth between edge node pairs of the MPLS domain is a full wavelength channel, while in many cases the granularity with wavelength switching is too large to accommodate the majority of traffic between routing node pairs. It is shown by research that up to 50% of IP traffic consists of packets smaller than 522 bytes and 50% of these packets are in the 40 – 44 bytes range[20]. Because the granularity of optical lightpath routing employed by multiprotocol lambda switching (MPλS) may be too large in many cases, and the algorithm to establish topology and assign wavelength is too complex, needs long computing time and has poor flexibility[19], thus packet data switching bottlenecks still can not be solved radically. The most efficient solution to resolve the issue of switching capacity granularity is to utilize photonic routers based on the generalized MPLS (GMPLS) to implement photonic packet label switching.

At present, photonic router employs wavelength band, wavelength, microwave subcarrier (SC)[20] and OCDM optical code[19, 21, 27 – 31] as photonic packet labels. However, due to the drawbacks of wavelength switching mentioned above and insufficient label space that results from the limited number of wavelengths, the packet label using wavelengths is very limited, which restricts the fully utilization of optical network resources.

When the subcarrier label is employed[21], the baseband signal carries the payload data and the low-bit-rate subcarrier multiplexing signals is utilized to carry label information. Subcarrier header recovery is performed employing direct optical and microwave detection components. The SCM header replacement

techniques have been restricted by the optical-to-electrical conversion of the entire packet followed by electronic filtering, modulation and retransmission on a new laser. Although the SCM header recovery can be carried out in optical domain by employing a very precise optical filter, this technique is difficult and expensive[21]. In addition, the SCM technique still needs some microwave components such as local oscillators, mixers and filters. In spite of that the cost of these components is not too high, the microwave detection and electronic processing of header may restrict the applications to moderate and relatively low bit rates. The optical code labels allow reusing the same set of optical codes on different wavelengths and have large label space. Simultaneously, the optical-code-label optical-packet switching does not need to look up the complicated routing table like the traditional electronic routers. The label recognition can be implemented by only employing passive optical components without utilizing optical logic devices. Thus optical-code-label optical-packet switching attracts comprehensive attention from research community of optical packet switching.

The backbone network architecture of optical packet switching (OPS) with optical-code label (OC-label) and optical packet format based on OC-label are shown in Fig. 6.29. At the edge node of OPS network, OC-label OPS switch imprints an OC-label to each data packet. In the intermediate node, the OPS switch determines the packet routing only by recognizing the header information without requiring processing the entire packet. Because the recognizing packet header and selecting routing need a certain amount of time, a guard band is required between OC-label and the packet load.

A general OPS network architecture is shown in Fig. 6.29(a)[32]. The source node A generates IP packets, which are routed by conventional electronic routers to an OPS edge switch in OPS network where labels are added onto the IP packets. The optical core switches perform routing and forwarding by label swapping. When packets leave the OPS network at an OPS edge switch, the labels are removed and the packets are forwarded to their destination. Figure 6.29(b) indicates the physical layer network elements connected by fiber-optic links and the packet routing and forwarding hierarchy[32]. IP packets are generated at the electronic routing layer (IP routers) and processed in an adaptation layer that encapsulates IP packets with an optical label without modifying the original packet structure. The optical label originates from mapping of original IP address. The adaptation layer also converts the packet and label to a new wavelength specified by local routing tables. An optical multiplexing layer directly multiplexes labeled packets onto a shared fiber-optic medium through WDM technology. In the OPS network, the OPS core switch is composed of two main units: control component and forward component, which perform routing and forwarding functions respectively. In the control component, the routing algorithm computes a new label and wavelength from an internal routing table giving the current label and optical interface (including current wavelength and fiber-optic port). The routing tables are generated by mapping IP address into the

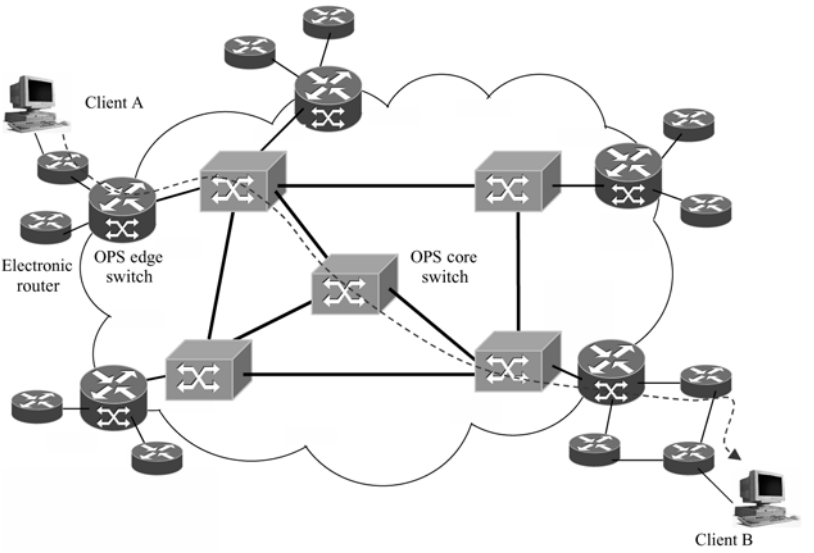

(a) A generic OPS network. The dashed line represents the label switched path(LSP) that routes data from the source, through the router, edge switch, and core switch, to the destination

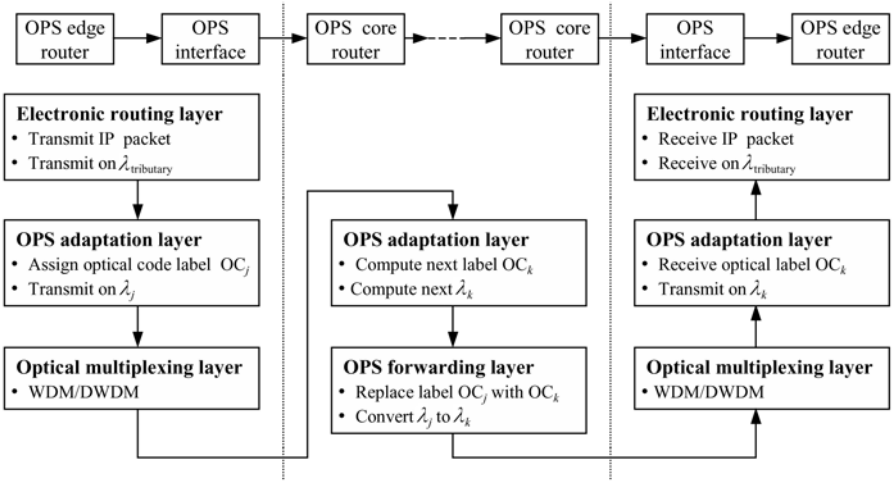

(b) Layered routing and forwarding hierarchy and related network element connection diagram for a generic OPS network

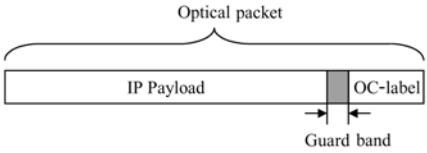

(c) Optical packet format with OC-label

Figure 6.29 Schematic diagram of optical packet switching backbone network based on OC-label and the representation of optical packet (revised from Ref. [32])

optical labels and wavelengths and allocating them across the network based on routing protocols. The forwarding component plays a role in swapping the original label with the new label and physically converting the labeled packet to the new wavelength. The reverse process of optical demultiplexing, adaptation and electronic routing are performed at the egress node. The schematic diagram of optical packet structure is shown in Fig. 6.29(c), where the optical-code label is embedded in the optical packet, which generally represents the crucial label-switched-path information such as the source and destination, etc.

The architecture of OC-label OPS node is shown in Fig. 6.30(a). (For the sake of simplicity, wavelengths are not utilized in the node.) It has K input optical fibers and K output optical fibers and there are M wavelengths in each optical fiber, which are $\lambda_1, \lambda_2, \cdots, \lambda_M$. The input optical signals from every optical fiber are separated by a $1 \times M$ WDM DEMUX based on M different wavelengths. The signals with the same wavelength from different optical fibers are directed to the same OC-label OPS switch router and the routings are selected based on their OC-labels. Any codeword from an OCDM codeset $\{\mathrm{OC}_1, \mathrm{OC}_2, \cdots, \mathrm{OC}_N\}$ can be employed as the label of a packet in a wavelength. The outputs of OC-label OPS router are connected to K $(M \times 1)$-WDM-MUXs. After the packets are routed by OC-label OPS routers they are output to L optical fibers through L wavelength division mutilplexers. The architecture of each OC-label OPS router is shown in Fig. 6.30(b), which is composed of an optical switch matrix, an optical buffer, a photonic label processor and a controller, as well as a photonic label swapper (optionally) if required. Because the processing and recognition of the label of optical packet, and the action of optical switch matrix need a certain amount of time, the delay is performed by adding optical fiber delay line to each input. After the packet label is processed the packet routing is determined. Then, the output port of the packet is chosen by controlling optical switch matrix. When two or more than two packets want to output from the same output port, i.e., when the confliction happens, only one packet is allowed to pass. Other packets enter optical buffer to wait until the output port is idle. In addition, while the packet is switched at the node its OC-label may need to be modified, that is, to remove its old OC-label and to add a new OC-label onto it. This can be achieved by the photonic label swapper. Fig. 6.31 gives a representative case for OC-label processing and swapping. (For the sake of simplicity, the optical buffering part is not given in this figure.) In Fig. 6.31(a), for each optical packet from any wavelength, a small part of optical signal is taken out by an optical coupler, amplified by an EDFA and then split into N paths by an optical splitter, where N is the number of codewords in the chosen codeset. The N optical signals are decoded by N optical decoders corresponding to codewords $\{\mathrm{OC}_1, \mathrm{OC}_2, \cdots, \mathrm{OC}_N\}$, photodetected, threshold-decided. At last, a group of control signals are generated to control a $1 \times N$ optical switch to choose the output of the packet. Meanwhile, the optical signals outputted by the optical decoders are re-encoded

to add onto the packet as the new OC-labels. Note that the old OC-labels need to be erased before the new OC-labels are added. This can be performed by the optical switch matrix simultaneously when the optical switch matrix routes these packets. For example, the optical switch matrix composed by Lithium Niobate ($LiNbO_3$) optical switch can implement this function[10]. The OPS node that employs the fixed optical encoders and decoders to perform the OC-label processing and swapping has a complex hard ware architecture. Since the tapped optical signals need to be in parallel divided into N paths in order to process and swap the labels the loss of signals is large. Thus, N EDFAs are required to amplify the tapped signals.

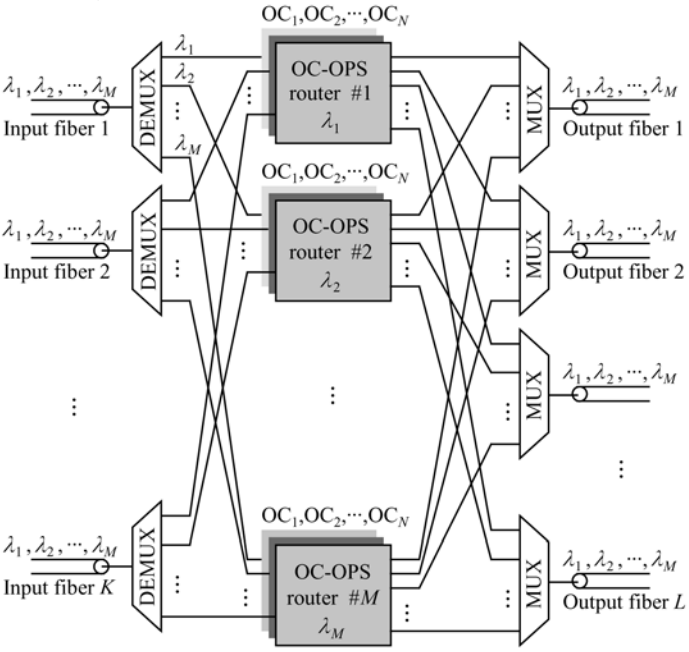

(a) Node architecture of optical packet switching

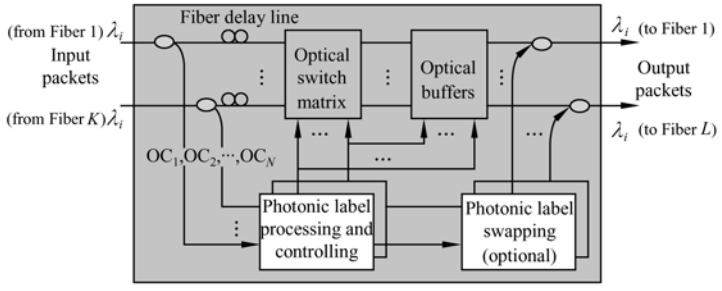

(b) Architecture of optical packet switching router

Figure 6.30 Node architecture of optical packet switching network employing OC-label[19]

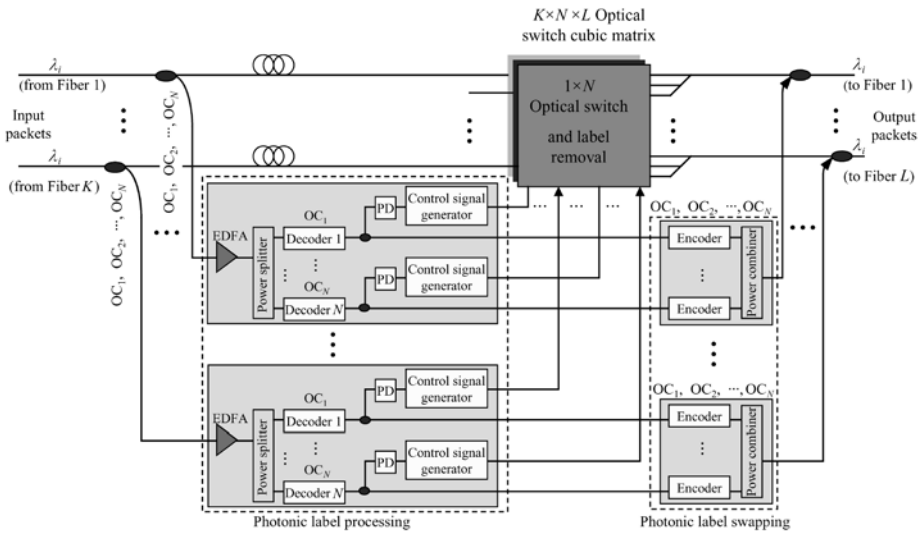

(a) Photonic label processing and label swapping with fixed decoders and encoders

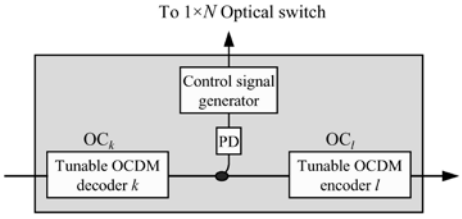

(b) Photonic label processing and label swapping with tunable decoders and encoders

Figure 6.31 An example of photonic label processing and label swapping (without buffers)

With regard to OC-label processing and swapping, it can also be achieved by employing a tunable optical decoder and a tunable optical encoder, as shown in Fig. 6.31(b). However, in this case, the speed of tuning must be fast enough so that the tuning is accomplished before the next packet arrives.

Since one optical code can only be employed to label an optical packet a codeset with N codewords can only label N packets. When the scale of packet switching is big the number of codewords may be insufficient. This issue can be resolved by using the combination of codewords. For instance, one codeset with two codewords can but label two packets originally. However, if their combinations, $\{OC_1OC_1, OC_1OC_2, OC_2OC_1, OC_2OC_2\}$, are employed then four optical packet can be labeled. As a result, a codeset with N codewords can be utilized to label 2^N optical packets. In this way, the label space can enormously be enlarged.

When the OC-label is applied to optical packet switching, the label space is independent of wavelength used to transmit traffic. Since the label space is large

and the switching granularity is flexible, OC-label OPS can effectively make use of the tremendous bandwidth of optical network. However, there also exist a lot of challenges. For example, when multiple packets that will perform switching compete for the same output port, the packet contention is required to be solved in order to prevent packet loss. With regard to oprical packet contention issues, different solutions to resolve packet contention make the network performances very different. The well-known solutions for packet contention are optical packet buffering, deflection routing and wavelength conversion.

The deflection routing method is as follows. When two or more packets want to occupy the same output link with the shortest path only one packet is allowed to be transmitted along the expected path. Other packets are forwarded along the other paths. Hence, for each pair of source and destination, the number of packet hopping is no longer fixed. It is shown[22] by research that with respect to the deflection routing method, the congestion of asynchronous network is severe as the offered load of network increases. After the offered load of network exceeds a certain thresholding value, the network throughput will completely collapse. In order to resolve the congestion the limited optical buffers are still required. In the wavelength conversion method to resolve the contention, one packet is allowed to pass while other packets are converted into other different wavelengths. This solution requires the technique of fast wavelength conversion. Unfortunately, the current wavelength conversion technique has not achieved the practicality. Even though it had attained the practical application level this method would have made the design and control algorithm of optical packet switching node too cmplicated.

Because there does not exist the practically optical random memory (RAM) yet for the purpose of optical packet buffering we have no choice but to buffer optical packets with the combination of fiber-optic delay lines with other optical components such as semiconductor optical amplifier (SOA) switch gates, optical couplers, optical amplifiers, etc., where the amount of delay for optical fiber delay line must be equal to integer multiple of the optical packet slot. In general, the type of optical packet buffers can be classified according to two methods [23]. One is based on the number of the stages of the delay line in the buffers. In this case, they are categorized into single stage delay type[24] and multi-stage delay type[25]. The former is easy to be controlled and the latter can save the amount of hardware for large buffering depth. Another one is on the basis of whether the number of delay lines that a packet passes through is constant. They are in turn classified into the feed-forward structure and the feedback structure[23]. The former represents that the packet is transmitted from one delay line to next delay line and the number of delay lines traversed by a packet is a constant. The latter means that a packet is sent back to this stage by the delay line, that is, the numbers of delay lines traversed by different packets are different. When the optical packet buffers are designed it needs to be taken into account that the

packet loss propability, the network latency, the cost of hardware, the complexity of control circuit, the packet rearrangement, the network scale, the offered load and type of traffic, etc. With respect to optical packet buffering issue, the practical technologies and schemes with big buffering depth, small volume and convenient use still awaits to be studied such as the packet buffering technique with electromagnetically induced transparency (EIT)[26] and so on.

In the schemes of OC-label for optical packet, which are implemented by employing OCDM technology, the schemes of temporal-phase encoding and spectral-phase encoding coherent OCDM using bipolar and multipolar codes are the most promising candidates. This is because the coherent OCDM encoding has the best correlation property and its cardinality is larger than that of incoherent OCDM encoding. Especially, the optical encoders/decoders using PLC technology have very good reconfigurable capability and the optical encoders/decoders employing superstructured fiber Bragg grating (SSFBG) have the advantages of high compactness, polarization-independent performance, low cost for mass production, and most importantly, the potential to generate ultralong OC with very low insertion loss[28]. Up to now, there exist several papers that have reported the experimental demonstrations of OC-label OPS[21, 27 – 30]. For example, the demonstrated experiment was reported in ECOC2002[27], where the optical packets based on OC identifications traversed two OPS network nodes. The OC-labels employed the cascade of two optical codes. The SSFBG optical encoders/decoders and 16-chip quaternary phase codes with chip rate of 20 Gb/s were used for read-in and read-out OC-labels. The total time length of each packet was 25 ns and the ratio of the length of packet header and guard band to the total packet length was 20%. The experimental principle diagram and measured results are shown in Fig. 6.32, where the OC-labels for three packets P_1, P_2 and P_3 are $Q_{11}Q_{21}$, $Q_{12}Q_{22}$ and $Q_{11}Q_{22}$. In the first node, the optical decoder Q_{12}^* identifies optical packet P_2 and a generated control signal controls a 1×2 optical switch to shift to the underside. In this case, P_2 drops down. Then, the optical decoder Q_{11}^* recognizes P_1 and P_3, and knows that they will go across this node and destine for the next node. A generated control signal drives another 1×2 optical switch to move to the upside to let P_1 and P_3 pass. When these two packets arrive at the second node, P_1 and P_3 are recognized by optical decoders Q_{21}^* and Q_{22}^*. P_1 and P_3 will be output from O_{21} and O_{22} ports respectively.

Another representative experimental demonstrating system of OPS network was reported in J. Lightw. Technol.24(8), 2006, which employed hybrid planar lightwave circuit (PLC) and SSFBG en/decoders, as shown in Fig. 6.33. The inset at the right side represents the theoretical autocorrelation of Label A and cross-correlations between Code 1 and Code 2. The measured waveforms at individual points are shown in Fig. 6.34. The 10 GHz optical pulse train generated by the MLLD at wavelength of 1554.13 nm is split into two parts that are utilized to produce OC-label and traffic load. The OC-label encoder is based on a 16-chip,

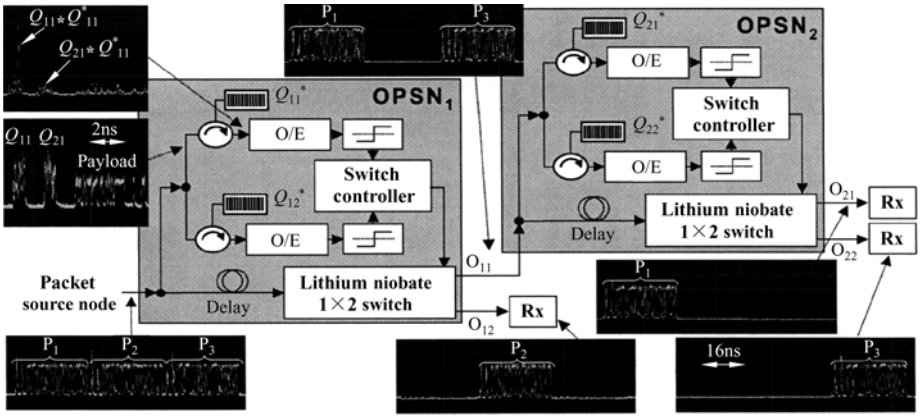

Figure 6.32 Self-routing optical packet switching experimental demonstration for two OPS nodes (Adapted from Ref. [27])

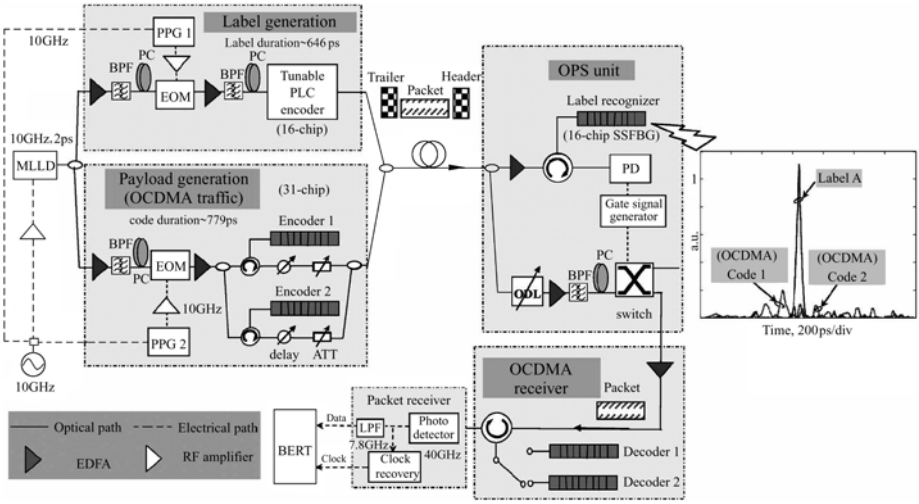

Figure 6.33 Block diagram of experimental system for OC-label OPS network with hybrid PLC and SSFBG en/decoder (Adapted from Ref.[28], with permission from IEEE © 2007)

25 Gchip/s PLC. OCDMA traffic encoding employs two 31-chip, 40 Gchip/s SSFBG optical encoders. The OC-label encoder and the traffic encoders have different chip length and different data rates. The packet is composed of OC-label and OCDMA-payload traffic. Employing the tunable characteristic of PLC optical encoder/decoder, two OC-labels, A (0000001110011010) and B (0100000100110110), are generated by tuning PLC optical encoder in the experiment. The duration of OC-label is about 643 ps and its waveform and spectrum are shown in Fig. 6.34(a). The payload packets with 500 data bits and 1.25 Gb/s bit rate are encoded by SSFBG encoder 1 and encoder 2 respectively,

where two Gold codes with length of 31 are employed. The waveform and spectrum of signal output by encoder 1 is shown in Fig. 6.34 (b). The duration of encoded signal for each bit is about 779ps and the duration of entire packet payload encoded is approximate 400ns. The optical packet is generated by combining the OC-label OCDMA encoding payload through an optical coupler. The guard band between the OC-label and the packet payload is about 10ns. The produced waveform and spectrum of the optical packet is shown in Fig. 6.34 (c). In the OPS node, the packet switching is implemented by recognizing Label A. At last, the payload is restored by an OCDMA receiver and the BER performance

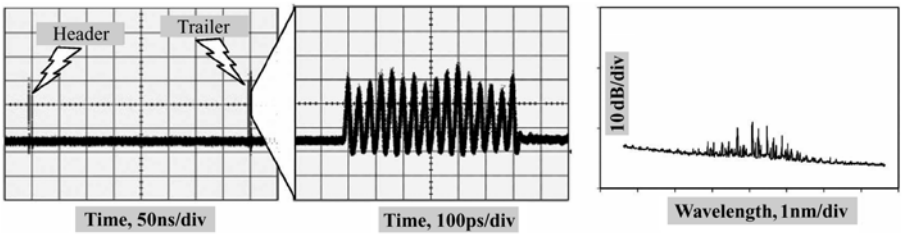

(a) Waveforms and spectrum of encoded Label A

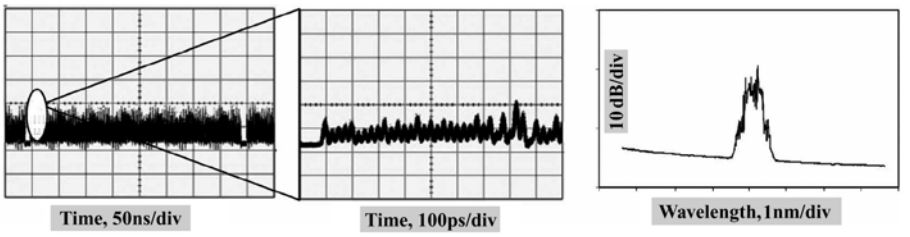

(b) Waveforms and spectrum of encoded OCDMA signal from encoder 1

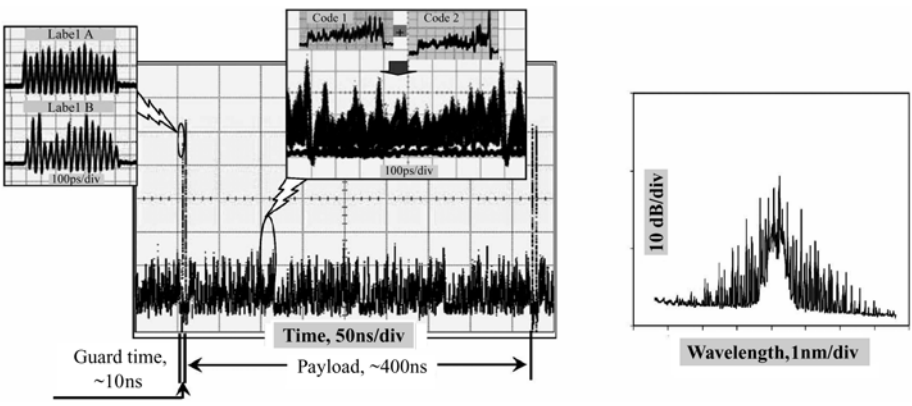

(c) Waveforms and spectrum of the generated optical packet

Figure 6.34 Waveforms of individual points of the experimental system (Adapted from Ref. [28], with permission from IEEE © 2007)

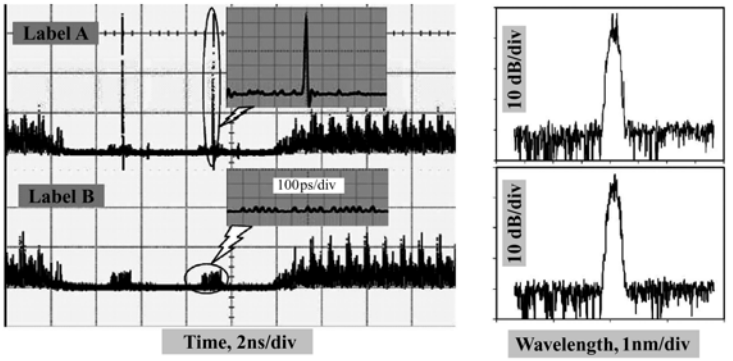

(d) Waveforms and spectra after label decoder

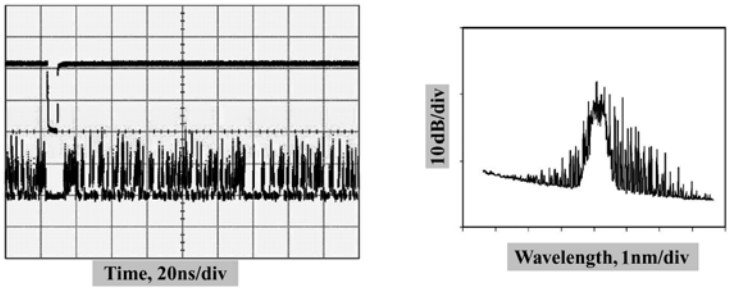

(e) Waveforms and spectra of gating signal and routed data

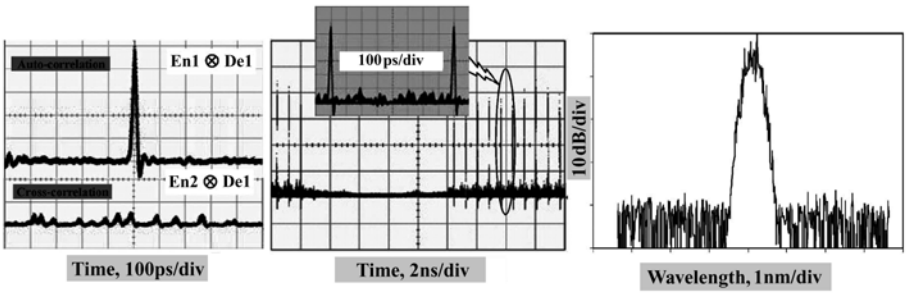

(f) Waveforms and spectra of after OCDMA decoder

Figure 6.34(Continued)

is measured by the BER test system. Figure 6.34(d) gives the temporal waveforms and spectrums of output packet after OC-label being decoded. The upper and lower traces correspond to the packets with Labels A and B respectively. The upper and lower insets are respectively the autocorrelation of Label A, and the cross-correlation between Labels A and B. The decoded label is employed to generate the gate signal and drive the Lithium Niobate optical switch for the packet routing as well as label erasing. Figure 6.34(e) shows the temporal waveform (the left-lower figure) and spectrum (the right figure) of payload after passing the switching node. The left-upper figure in Fig. 6.34(e) is the gating signal trace. In order to recover the payload, the OCDMA decoding is required. The auto- and

cross-correlation traces (the leftmost figure) outputted by decoder 1, and the temporal waveform and spectrum of the decoded payload data after OCDMA decoder are shown in Fig. 6.34(f), where the inset in the middle figure is the eye diagram. The measured BERs of the payload data are less than 10^{-12}.

An OPS system experimental demonstration based on OC-label and chip rate of 160Gchip/s[29] was also reported in ECOC2005. It has been shown by these research results that the OPS based on OC-label have a very bright application perspective. However, there exist a lot of challenges for the applications of OC-label based OPS, such as the packet buffering strategies, practical buffering components, network control and so on. At the same time, the switching scale implemented in the current tests is still small. When the network scale becomes large, what is the performance of the OC-label based OPS network? How does the OC-labels influence the payload data, and etc.? These issues await us to further study intensively.

6.7 Discussion about Information Transmission Confidentiality of OCDMA Networks

In a great deal of literature where OCDMA technologies and theories are studied and introduced, enhanced security and confidentiality on information transmissions is viewed as one of inherent advantages for OCDMA networks[33 – 37]. Generally, the information security is often divided into branches of confidentiality, integrity, availability and authentication[6]. Confidentiality guarantees that only the desired receivers of information can practically receive the information. Integrity means that the information received is the same as that transmitted. Availability means that information transmitted is not “lost” or destroyed en route. Authentication allows the receiver to ascertain the identity of the transmitter and vice versa. Confidentiality is one of the most important and widely required types of security.

It is shown by research that certain representative types of OCDMA signaling only offer a much lower degree of data confidentiality and availability than does the conventional source cryptography and possess the capability of jamming resistance and obscuring data[38, 39]. In these references which argue that OCDMA can provide inherent security and confidentiality on information transmissions[33 – 37], the most rudimentary types of attack on security, such as brute-force code-searching, are taken into account, while the more sophisticated attacks that are typically more effectively, are neglected[38]. In this section, we review the results of research on OCDMA confidentiality currently reported in some references and discuss about OCDMA security. At the same time, some suggestions about improving OCDMA data transmission confidentiality are given.

Actually, OCDMA security mentioned in current literature, is very distinct from the information security meant in encoding cryptography. In cryptography, security means that without some secret information (e.g., a key), decoding data

encoded in some manner is difficult or impossible, even if the encoded or encrypted form of the data is easily read. The eavesdropper or interceptor generally takes tens to hundreds of years to break the real meaning of information with finite computation resources, which makes the information lose its real-time property. The more resources are required and the longer time it takes to break the information, the higher the security (or degree of confidentiality) of this means of encoding or encrypting, or algorithm is. In comparison with standard encryption techniques, the degree of confidentiality provided by OCDMA techniques is much lower. What is more, the degree of confidentiality provided is highly dependent on system design and implementation parameters[38, 39], such as code space size, mode of data modulation, system signal-to-interference ratio, fraction of total available system capacity and so on.

6.7.1 Code Space Size

In an OCDMA network, the communication between each pair of transmitter and receiver is implemented by encoding/decoding data with a unique codeword. Under the situation of multiple users being activated simultaneously, for some data modulation modes and encoding forms, if the number of codewords in the codeset is large enough, in other words, the code space size is big enough and a eavesdropper does not know the codeword employed by a subscriber it is relatively difficult for the eavesdropper to eavesdrop data. An eavesdropper would have to perform a brute-force search through half number of codes, on average, before finding the proper code to attack a given subscriber's data [38]. When different encoding types of OCDMA and code parameters are utilized the size of code space obtained is very distinct. Table 6.4 gives the size and the order of magnitude of code space for four common types of OCDMA coding[38].

Table 6.4 code space size for four types of OCDMA coding[38]

Code types	Representative code type example	Parameters for code space calculation	Potential code space size
Time-spreading	OOCs Prime codes EQCC	Prime code 10,201 time slots	101 codes
Wavelength-hopping/ time-spreading	PC/PC code Multi-wavelength OOCs	PC/PC code 32 wavelengths and 961 time slots	$\sim 10^{35}$ codes [35]
Spectral amplitude	Hadamard codes m-sequences	m-sequences codes 511 mask elements	$\sim 10^{4}$ codes
Spectral phase	Hadamard codes Random codes	Random codes 511 mask elements	$\sim 10^{153}$ codes [40]

The first category is one-dimensional (1-D) time-spreading codes that are introduced in Chapter 2, which have very small cardinalities for a given code length dependent on feasible implementations at ~Gb/s bit rate or above. Therefore, it is impossible for them to deter brute-force searching from the eavesdroppers.

The third category is spectral amplitude encoding. Due to the limitation of spectral partition technique and data rate, the feasible implemented codes cannot be long enough. Thus, although the number of codewords has increased a lot comparing with 1-D time-spreading codes, their code spaces are still small from the point of view of anti-brutal-force code-searching. For example, from Chapter 2 we can see that the number of primitive polynomials to generate m-sequence with length 511 is only 48. As far as the current state-of-the-art, it is not easy to realize the spectral partition for 511 spectral elements. These polynomials produce totally 48 different pseudorandom sequences. Each sequence is cyclically shifted 510 times, produces 510 sequences. Adding the original sequences, the total number of sequences is only $48 \times 511 = 24528$.

The second category is two-dimensional wavelength-hopping/time-spreading (2-D WH/TS) codes. After the wavelength dimension being added, the cardinalities of codes increase dramatically. In particular, when the number of wavelengths, N_w, exceeds code weight p, the code cardinalities become $|C| = N_w!/(N_w - p)!$. For instance, assume that code weight is $p = 31$, the cardinality of PC/PC code is approximately equal to 2.6×10^{35}. The resulting code space size is large enough to prevent a brute-force code searching for any reasonable amount of time.

The forth category is spectral phase encoding. Although the spectral phase encoding is limited by the spectral partition technique and it is difficult to implement relatively long codes, the largest code spaces can be achieved in these categories of codes because the random encoding employed makes phases be randomly distributed in codes with equiprobability[40]. For the binary phase code, its code space size is about $2^{511} = 6.7 \times 10^{153}$. The code size of quadruple phase code is approximately $4^{511} = 4.5 \times 10^{307}$. Note that the number of codewords allowed to simultaneously utilize in a network still does not exceed 10^4 because of the requirement of the network performance. However, since there exists the likelihood that a subscriber may use any one of codewords, an eavesdropper still needs to search half number of the codes, on average, in order to find the correct code employed by the subscriber.

From the above discussion, it can be seen that 2-D WH/TS codes and spectral phase codes can generate very large code space to prevent the attack of brute-force searching to a subscriber code from an eavesdropper. However, as far as data confidentiality, a large code space is a necessary but not sufficient condition for a good information transmission security.

6.7.2 Most Advantageous Intercepting Signal Strategies for An Eavesdropper

When the code space is large enough, the brute-force searching for an individual subscriber's code is not an efficient attack strategy. For a broadcast star optical network, if an eavesdropper is able to detect a subscriber's code through some parts which are most easily attacked in the network, it will feel free to access to the subscriber's data until the subscriber changes its code. An OCDMA encoder can be modeled as a linear time-invariant system for at least some finite time that is large compared with the code duration [38, 39]. If an eavesdropper can detect the output waveform of the encoder and further it also knows the input waveform of the encoder, it can obtain the impulse response of the encoder, corresponding to the subscriber's codeword. There are two approaches to make an eavesdropper be difficult to break a subscriber's codeword. One approach is to increase the complexity of encoding and reduce the eavesdropper's signal-to-interference ratio (SNR) for each code element. Another approach is that each transmitter changes its codeword more frequently than an eavesdropper could detect the channel waveform and find the codeword, which makes the encoder become a time-variant system. As a matter of fact, these variables are dependent on each other in turn. For instance, the time it takes for an eavesdropper to break a codeword, also relies on SNR of the eavesdropper and the complexity of encoding.

For an OCDMA network, an eavesdropper can tap signals from any locations within the network. For example, it can directly tap signals from a fiber of the network by optical couplers or commandeer an authorized subscriber's terminal. However, from the point of view of intercepting codes, the most advantageous method is to tap isolated subscriber signals and to avoid the multiple access interference simultaneously. Eavesdropper 1, shown in Fig. 6.35, is the case.

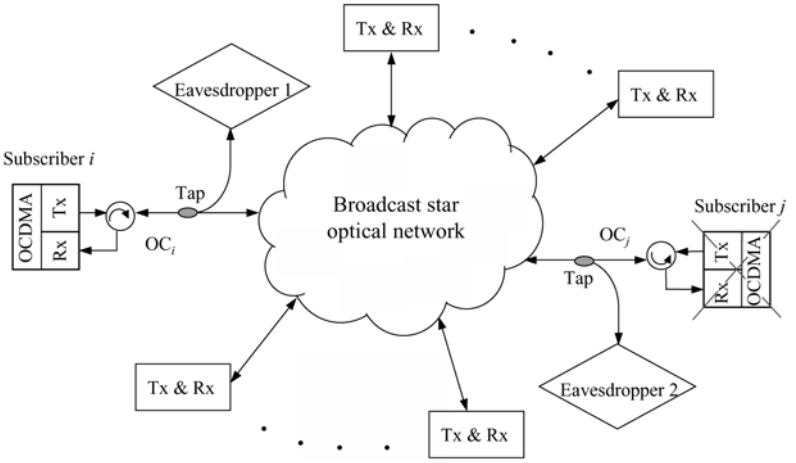

Figure 6.35 Two positions of eavesdropping/intercepting data in the broadcasting optical network including star network [38]

For an OCDMA system with OOK (on-off keying for data modulation format), an encoded signal is sent to represent a data bit "1", and a null is used to represent a data bit "0". The schematic diagrams of output waveforms of 2-D WH/TS encoding incoherent and spectral phase encoding coherent OCDMA transmitters with OOK, are shown in Fig. 6.36(a) and (b) respectively. It can be seen from the waveforms that no energy is transmitted for data bit "0". In this case, if the signal is tapped as shown in Eavesdropper 1, all data transmitted by the subscriber can be read out by a simple energy detector which integrates the energy in a bit period. It is not necessary at all for the eavesdropper to "break" the encoding scheme or steal the code. Thus, any OCDMA encoding scheme with OOK data modulation format does not have any security of information transmission. The probability of eavesdropping for an eavesdropper is independent of the size of code space.

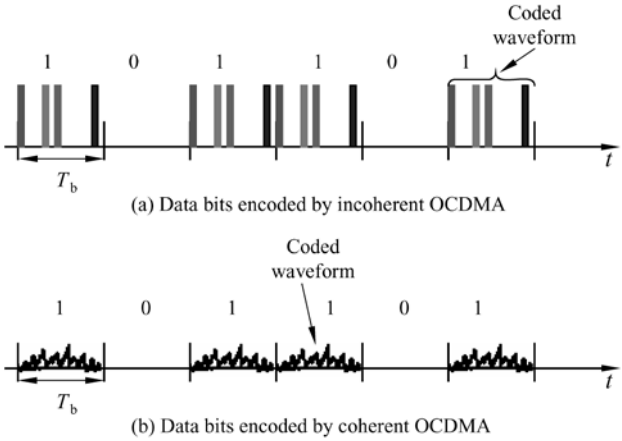

Figure 6.36 Schematic waveforms of encoded data bits for incoherent and coherent OCDMA with OOK modulation format

In order to make an eavesdropper not so easy to eavesdrop a subscriber' data, we should encode data such that it is not easy for an eavesdropper to distinguish data bit "0" and "1". This can be implemented by transmitting different encoded signals for data bits "0" and "1", such as 2-code keying signals[38] or multiple-code keying signals. For example, employing 2-code keying, a codeword OC_1 is transmitted to represent data bit "0" and a codeword OC_2 to indicate "1". If 4-code keying is utilized, OC_1 is sent to signify data bits "00", OC_2 to denote "01", OC_3 to represent "10", and OC_4 to represent "11". However, note that in this way, while it is not easy for an eavesdropper to eavesdrop subscriber's data the number of simultaneous subscribers in a network will be reduced. The network bandwidth is sacrificed and the interference in the network will increase. In other words, the enhanced security of information transmission in the network is obtained at the expense of sacrificing network resources. Shown in Fig. 6.37 is

the schematic diagrams of output waveforms of 2-D WH/TS encoding incoherent and spectral phase encoding coherent OCDMA transmitters with 2-code keying format.

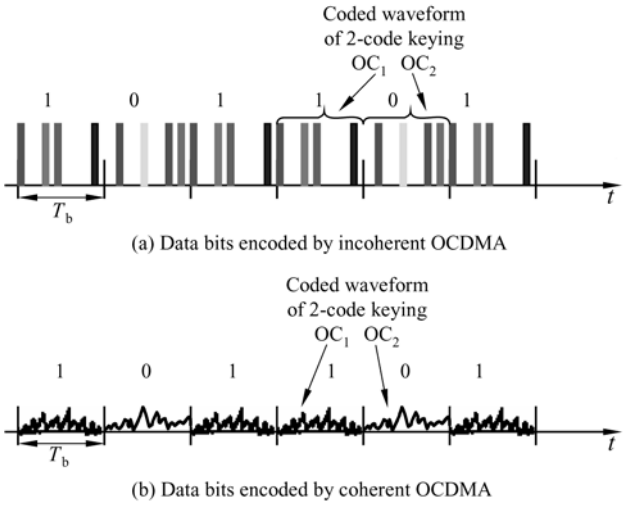

Figure 6.37 Schematic waveforms of encoded data bits for incoherent and coherent OCDMA with 2-code keying

Another approach to tap signals is shown in Eavesdropper 2 of Fig. 6.35, which corresponds to the case that an eavesdropper commandeers an authorized subscriber's terminal. In this situation, the eavesdropper will receive the signals transmitted by all active OCDMA subscribers. At first glance it seems that the transmission security will increase in this case. However, if at any time there is only one subscriber transmitting, which happens to be the transmission eavesdropped by an interceptor, this case is similar to Eavesdropper 1. Therefore, only if the number of subscribers in the network is greater than two at any time, it is different from Eavesdropper 1. The advantage of this signal-tapped approach is that an eavesdropper can intercept any subscriber's signal without tapping into individual users' optical signals.

6.7.3 Data Confidentialities of OCDMA Systems with Two Largest Code Spaces

From the above discussion, we can see that 2-D WH/TS codes and spectral phase codes appear to be two of the most promising code types for generating OCDMA code spaces that are large enough to prevent successful brute-force code-searching attack under the premise of non-OOK data modulation mode. The quantitative analysis of data confidentiality has been for the first time performed for OCDMA

techniques that employ 2-D wavelength-hopping/time-spreading encoding and spectral phase encoding in References [38] and [39]. When employing non-OOK data modulation mode in an OCDMA system, the space size of codes used is so large that brute-force searching for subscriber's codeword takes very long time, the eavesdropper needs to take other more efficient attack measures such as code detection, from the point of view of breaking data confidentiality.

With respect to incoherent 2-D WH/TS encoding OCDMA, the eavesdropper, shown in Fig. 6.38, can be employed to intercept subscriber's codeword. Firstly, a small fraction of the isolated subscriber signals is tapped by an optical tap and amplified by EDFA. Then, the detection is performed by a 2-D WH/TS chip-level receiver described in Section 5.4. For the case of isolated subscriber signals, the quantitatively analyzing results reveal[38] that the probability of correctly detecting the codeword for an eavesdropper is dependent on the SNR at the eavesdropper and the eavesdropping detector's performance in noise. Further, the eavesdropper's effective SNR per code chip is a function of a number of system design and operation parameters, which are the eavesdropper's fiber tapping efficiency, the number of taps in the broadcast star coupler that distributes user signals, the ratio of the eavesdropper's receiver noise density to the authorized user's receiver noise density, the authorized user receiver's multi-chip energy combining efficiency, code weight, the maximum theoretical number of simultaneous users at a specified maximum BER, the required user SNR (per data bit) to maintain the specified BER, the actual number of simultaneous users supported. Adjusting these parameters makes the eavesdropper's SNR decrease so that the probability of correctly detecting the codeword for an eavesdropper reduces. When 2-code keying or multiple-code keying is employed, the probability of correctly detecting the codeword for an eavesdropper can become very small. However, if the combining code transmission from multiple data bits is utilized, the probability of correctly detecting the codeword for an eavesdropper will increase significantly. For 2-code keying, by combining the energy from less than 100 bits, a probability of correctly intercepting codeword for the eavesdropper can attain 100%[38]. If the transmitter changes its codeword more frequently than the eavesdropper correctly detected the codeword, then the confidentiality could be significantly increased.

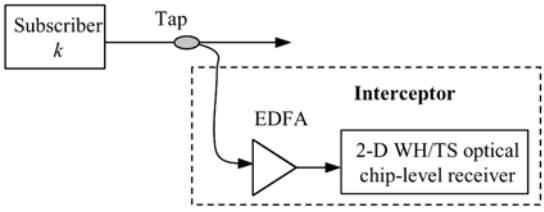

Figure 6.38 2-D WH/TS incoherent receiver for code intercepting detector

For OOK modulation mode, the quantitative analysis in Reference [38] revealed that the confidentiality of OCDMA with transmitting signals tapped in the manner of Eavesdropper 2 was not higher than that with the isolated user signals. The eavesdropper looks for the period of time that a single user is transmitting data bit 1 and at the same time, all other subscribers are transmitting 0's through monitoring the overall power level received on each bit so that the signal of the subscriber transmitting can be effectively isolated.

The schematic diagram of detecting codeword for the coherent spectral phase encoding OCDMA eavesdropper[39] is shown in Fig. 6.39. The isolated subscriber signal obtained is firstly amplified by EDFA and then split into $(L-3)$ channels by a $1\times(L-3)$ optical coupler. The optical signal for each is further divided into two parts by an optical splitter, each of which goes through a grating/filter assembly that passes only selected frequency components. Assume that f_n be the central frequency of the frequency component determined by the n^{th} code element of the encoder phase mask, which has bandwidth f_Δ. The optical filter in the upper half of the n^{th} detector can be an amplitude mask chosen to pass only two components of the input signal f_n and f_{n+2}. Similarly, the lower half only allows to pass two components f_{n+1} and f_{n+3}. These signals are separately photodetected, bandpass-filtered around the beat frequency of $2f_\Delta$, and then beat together to produce a baseband signal that contains information about the relative phase values in bins n through $n+3$ of the transmitted signal. This information can be combined with similar signals from other frequency bins. There are totally $L-3$ signals combined. Assume that the original values ϕ_0, ϕ_1 and ϕ_2 are given. By solving $L-3$ equations, the values of other $L-3$ code element for the transmitting signal can be obtained. In order to determine the subscriber codeword eventually, eight combinations of ϕ_0, ϕ_1 and ϕ_2 need to be tried, which are 000, $00\pi,\cdots,\pi\pi\pi$. Or, another detection channel is employed to resolve this uncertainty. This is the parallel structure of the codeword eavesdropper. Also, the $L-3$ frequency bins of the sequential scanning of a single channel are utilized to eavesdrop the subscriber codeword. However, the sequential scanning approach will require the central frequency of the spectral amplitude mask to be fast tunable. The sequential scans could either be performed on multiple successive transmitted bits from the user or on successive samples of a single-bit transmission captured in an optical re-circulating loop[39].

In Reference [39], the confidentiality performance of the coherent spectral phase encoding OCDMA was analyzed, and the obtained conclusion was analogous to the one of the confidentiality performance of incoherent 2-D WH/TS OCDMA, that is, the spectral-phase encoding OCDMA can only provide a much lower degree of confidentiality than the standard cryptography does. However, the degree of confidentiality provided by spectral-phase encoding is certainly much greater than that provided by an unencoded signaling technique such as the OOK

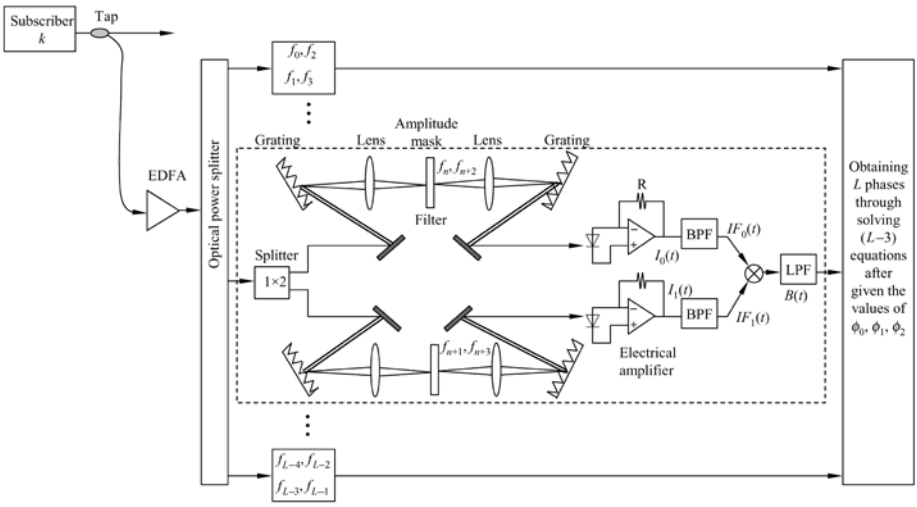

Figure 6.39 An optical beat detector for code interception (Revised from Ref.[39])

WDM signaling used widely since the eavesdropper is required to employ an expensive detector implemented with very complicated technology, even to date there is not such commercial-of-the-shelf components. What is more, if the codeword employed by a subscriber can be changed very frequently, (e.g., at rates approaching to the data rate of the subscriber), the eavesdropper's capability to take advantage of multiple-bit combining techniques may be very restricted. The frequently varied codeword can be implemented by the rapid tunable spectral phase encoder, or by the cascaded code translators described in subsection 6.4.4.

An experimental demonstration of 2-D WH/TS OCDMA confidentiality was reported in Reference [41]. A couple of codewords are assigned to each subscriber and simultaneously employed so that the eavesdropper is always confronted with severe MAI in the scheme. It is verified by the experiment that how many codewords need to be allocated to each subscriber to provide some degree of data confidentiality. The chip rate is 10 Gb/s and the data rate for a single subscriber is 1.25 Gb/s in the experiment. The system can at most support 32 subscribers. More than 16 simultaneously "lit" codes per user are required to degrade the eavesdropping BER to worst than 10^{-2}. Members of a code set can eavesdrop on each other by means of MAI, however, this capability is negligible when the number of concurrent subscribers exceeds four.

In Reference [42], two vulnerabilities that allowed an eavesdropper to extract data from an isolated user in a 2-code keying spectrally phase encoded O-CDMA system were experimentally demonstrated. One of these vulnerabilities was based on spectral bins that resulted from phase-to-amplitude conversion in the encoding process, which allowed eavesdropping by employing a narrowband tunable optical filter and a simple energy detector. Another especially serious

vulnerability employed a differential-phase-shift-keying receiver for eavesdropping. Both of them are all based on a structure of encoding and signaling schemes without requiring knowledge of the codes.

6.7.4 Discussion about OCDMA Confidentiality and Its Applications

The confidentiality of OCDMA with non-OOK modulation format has the following characteristics:

(1) Although compared with WDM and TDM, it has some degree of data transmission confidentiality, its confidentiality is much lower than that of the standard source cryptography.

(2) The degree of OCDMA confidentiality is dependent of an eavesdropper SNR and the eavesdropper SNR relies in turn on the parameters of a system design and implementation. Thus, the confidentiality degree of an OCDMA system may be controlled by the system parameters.

(3) The implementation of eavesdropping needs complicated technologies and components with high cost, and some components are still difficult to be employed to date.

(4) When the network SNR is relatively low, the probability of an eavesdropper intercepting the codeword is very small. Nevertheless, if the eavesdropper makes use of combining multiple-bit energy, the probability of correctly intercepting the codeword would be significantly improved.

(5) If the subscriber codeword can be changed rapidly, for instance, at the rate approaching to the subscriber data rate, the capability of the eavesdropper combining multiple-bit would be seriously limited.

(6) In contrast to the standard cryptography, the confidentiality of OCDMA does not need the special encryption and decryption processing to data and a tremendous memory for the data intercepted, and has a very good real-time characteristic. For the confidentiality of transmitting ultrahigh data, e.g., at the rate of 10Gb/s and above, this is its prominent predominance.

Due to the characteristics mentioned above, OCDMA encoding with non-OOK modulation format may be applied to the transmission confidentiality of information that has the requirements of moderate and low degree of confidentiality and high real-time characteristic. For example, it can be applied to resisting simple interception from the malicious eavesdroppers or the intended eavesdroppers who will not be willing to expend the resources necessary to read the information, taking into account the importance of the information to be eavesdropped. It may be suitable for the applications such as the current Internet and the military environments where the information has high requirement of real-time. In addition, since the degree of OCDMA confidentiality is dependent of the system

design parameters the degree of information confidentiality may be controlled by the system design such that the different confidentiality service for different subscribers and different traffic may be provided by the system design. And OCDMA encoding can combine with the conventional source cryptography to serve different applications as well. For the information with high requirement of confidentiality degree, if the standard cryptography and OCDMA technology are combined together the degree of the standard cryptography may be lowered and the complexity and processing time of encrypting/decrypting algorithms may be reduced.

Since OCDMA optical encoding/decoding methods and technologies contain extensive content, so far, the evaluation and experimental verification of OCDMA confidentiality are still at the early stage, which awaits further study. Especially, whether OCDMA can be applied to the networks and services with different security requirements or not, the quantitative evaluation of security requirements for concrete networks and services remains an open topic for the future research.

6.8 Other Applications for OCDMA

Since OCDMA technology has numerous advantages that we have introduced in Chapter 1, it has comprehensively potential applications. Besides that OCDMA technology can be employed to construct local area networks (LANs) and subscriber access networks individually, and to implement optical-code-label optical-packet-switching network, OCDMA can also incorporate with WDM/OTDM for networking. OCDMA networks can interconnect with OTDM and WDM networks, and OCDMA technology can provide the confidentiality for the transmitted data in some extent, which we have described previously. OCDMA also has many other applications. For example, OCDMA is applied to wireless OCDMA communications, transmission of multimedia information, radio over fiber (RoF) networks, LANs and interconnects in hostile environments, optical sensor networks, etc.

6.8.1 Wireless Optical Communication Based on OCDMA

Although radio frequency (RF) wireless systems have been widely applied to personal mobile communications, the transmission of high-speed data services directly to residential areas employing wireless techniques is still in an early stage of development. Free space optics (FSO) is an emerging technology that can support high-speed access services to residential areas and business subscribers. Deploying existing RF towers or line of site positions on rooftops, the point-to-point communication links can be founded in a metropolitan area to

support the high-speed services with ~Gb/s data rate. Meanwhile, the construction for this engineering is quick and easy and the cost is low. OCDMA technology is applied to FSO[43] by employing its addressing capability for networking such that numerous advantages of wireless optical communication and OCDMA are made use of. This system can be implemented easily and flexibly. It has strong capability to resist the atmospheric effect and its cost is low[44]. At the same time, OCDMA can also be used to wireless infrared communications to establish local area networks (LANs) indoor[45]. Uplink communications between the portable stations and the access points can be implemented by employing low cost LED transmitters at each portable station. The access point broadcasts data in the downlink and the portable stations detect the address of the broadcast to select data destined for the local node, which does not need the complicated system synchronization so that the cost of implementation is low[6].

6.8.2 Multimedia Transmission Employing OCDMA

Since OCDMA technology can implement multiple access, asynchronous access at random and flexible diversity of encoding, in addition to effectively supporting data network, many types of media such as voice, data, image and video, can be sustained in a communication network by the flexible network design and variety of choices of OCDMA systems. At the same time, this kind of network provides appropriate quality of services (QoS) for different subscribers. For example, different service demands from different subscribers can be satisfied by encoding high-rate services with short code and low-rate services with long code, services with high QoS by codes with high performance and low QoS by codes with low performance[46]. Reference [47] has proposed Integrated Services Digital Broadcasting (ISDN) systems employing a multi-rate optical code-division multiplexing technique, which employ one-dimensional optical orthogonal codes (OOCs). The analytic and experimental results reveals that the systems can support Fast Ethernet (125Mb/s), FDDI (125Mb/s), ATM (155Mb/s) and ESCON (200Mb/s) protocol data.

In addition, the spatially spread OCDMA technique has been proposed in References [48] and [49]. This technique can be employed to encode and multiplex images carried by multicore optical fiber over a common fiber path[50]. A magnified two-dimensional (2-D) $N \times N$ bit plane, comprising individual pixels of an image, is encoded employing a 2-D optical orthogonal signature pattern with dimension $M \times M$, where the CDMA spreading factor is M^2. The encoded image has $MN \times MN$ pixels such that the $MN \times MN$ core imaging fiber is required to transmit the encoded images[6]. 2-D image multiplexing has many applications such as transmission of medical images, parallel optical interconnections between processors and memory in high performance computing, etc.

6.8.3 Radio over Fiber Network Based on OCDMA

The fixed or mobile wireless access is regarded as a good way to achieve broadband services in some areas. Due to the unavailability of low microwave frequencies and the insufficient bandwidth of lower frequency ranges, next generation wireless access systems for both mobile and fixed systems will operate in the upper microwave/millimeter wave frequency band. In a cellular system small cells are required in order to increase the traffic capacity and improve the propagation properties of millimeter-wave[51]. Therefore, next generation cellular systems will employ microcellular or picocellular architectures so that a large number of potential subscribers can be accommodated in a metropolitan system. Meanwhile, because millimeter-wave circuits are expensive, the cost of radio base stations (RBSs) will be a decisive factor. One emerging technology applicable in high capacity broadband millimeter-wave access systems is radio over fiber (RoF). In such a system, in order to reduce the cost of RBSs, most of signal processing, including coding, multiplexing, RF generation and modulation, etc., is performed in remote control stations (RCSs) rather than in the RBSs. The signals between RCSs and RBSs are transmitted through an optical fiber network. The design of RBSs would be simple employing this architecture. In the simplest case, there are only optical-to-electrical (O/E) and electrical-to-optical (E/O) converters, an antenna and some microwave circuit.

In an access network, there are three types of photonic multiplexing schemes to distinguish different modulation signals from individual RBSs such as digital voice, data, and legacy RF analog services from multiple service providers, i.e., subcarrier multiplexing (SCM), time-division multiple access, optical code-division multiple access. However, there exist severely optical signal beat noises in SCM format and TDMA method needs the time synchronization of the whole system. Meanwhile, OCDMA with asynchronous access, flexibility, and transparency for various radio air interfaces is a more attractive technique rather than SCM and TDMA. Simultaneously, OCDMA has a significantly larger code space than the number of subcarriers that coexist on the same wavelength. A RoF system based on OCDMA multiplexing method was proposed in Reference [51], in which the theoretical analysis and experimental demonstration were conducted. The unipolar prime code was employed in this system and the results reveal that the proposed scheme is effective. Also it was shown in theory that the number of maximum connected RBSs could be further improved by employing bipolar peseudonoise (PN) codes.

6.8.4 LANs and LAN Interconnections for Hostile Environments

Because OCDMA is one type of spread spectrum technology, it has an anti-jamming capability. Therefore, it can be applied to hostile environments to communicate,

such as the mobile environments for civil and military applications (e.g., aircraft, ship and battlefield). In such cases, large mechanical stresses and thermal gradients across the system would significantly impact the performance of fiber-optic lines, optical components and systems in a LAN or LAN interconnections. In traditional WDMA or TDMA optical access architecture, strict wavelength control and time slot alignment are required in order to maintain the normal communication system performance, which will result in the complexity and the cost increase of system implementation. Nevertheless, OCDMA technology is not sensitive to the drifts of some physical parameters such as wavelength [52]. The flexible design LAN using OCDMA technology enables capacity in the hostile environments and is not as expensive as the LANs employing WDMA and TDMA. At the same time, OCDMA LAN also supports the real-time information confidentiality to some extent, which is advantageous for military applications.

In addition, OCDMA technology can also be applied to the sensor networks to realize the sensor signal multiplexing transmission and routing [53, 54] so that it has enormously potential application foreground in many areas such as military, industry, transportation, environment protection and so on.

6.9 Summary

OCDMA is a technology of multiplexing and networking for optical communication systems and networks. The multiplexing and routing of optical signals are performed by encoding/decoding data employing passively optical components with low cost, not requiring any optical logic components, and it is simple to be implemented. OCDMA has many advantages such as asynchronous access at random, simple management, flexible networking, very good compatibility with WDM and TDM, etc., so that it is a very promising technology to eliminate the last/first mile telecommunication bottleneck in the communication network and to implement high-speed optical LAN and access network. Although it has twenty-year history from its first proposal and its first experimental demonstration in principle, OCDMA has remained outside the mainstream of optical communication research for a long time. This is because the demands on information were not so strong and the development scale of communication network was limited in the past so that the contradiction between the transmitting capabilities of transport network and access network was not highlighted. However, at present, with the coming of knowledge economy that makes everybody strongly depend on information and the widely overspreading of Internet, the disharmony between the service provisions of transport network and access network is becoming from bad to worse. Hence, it is an urgent affair to solve the communication bottleneck of local area network and access network. Among the existing technologies to mitigate the bottleneck of access network, it seems that the ability of WDM and TDM technologies is not equal to its ambition. Therefore,

the high networking flexibility of OCDMA and the very good complementary properties of OCDMA with WDM and TDM have been recognized again. At the same time, due to the advancement of optical component technologies at very fast speed, all aspects of OCDMA technology have become the hotspots of research, which would speed up the progress of OCDMA towards its practicality.

On the basis of OCDMA encoding/decoding theories, optical encoding/decoding technologies and performance analyses of several typical systems introduced in previous chapters, this chapter is devoted to introduce the architectures of OCDMA networks, simple access protocols for local area network and applications of OCDMA technologies. OCDMA is well-suited for any network architectures and has tremendous predominance in the networking of high-speed local area network and access network. The networking through the combination of OCDMA with WDM/OTDM can further upgrade the service provisions of the network and exert the network efficiency fully, which has the effect of holding the balance to support data backbone network and extend the capability of data backbone network, for instance, implementing optical packet switching with optical-code label. Meanwhile, OCDMA can offer the transmitted data confidentiality to some extent so that the confidential requirements of routine and business services from different subscribers can be satisfied. In addition, OCDMA has very good application foreground in many areas such as wireless optical communication, multimedia transmission, Radio over Fiber, LAN for hostile environments and so on.

Although great progresses on the research of OCDMA technologies have been made through hard efforts from OCDMA research community, OCDMA technologies are still immature and can not be applied in practical use for the time being. Therefore, the strong support from business enterprises, research institutes and organizations, and the consecutive efforts from researchers are still required to push the progress of OCDMA technologies towards its practicality. With the advancement of OCDMA optical encoding/decoding theory and component technology, especially the photonic integrated technology, the development of OCDMA network technology, and the study of protocols of access, management and control, OCDMA network technologies will certainly have larger and wider application spaces in the near future.

References

[1] Hideyuki Sotobayashi, Wataru Chujo, Ken-ichi Kitayama: Highly Spectral-Efficient Optical Code-Division Multiplexing Transmission System. *IEEE Journal of Selected Topics in Quantum Electronics*, Vol.10, No.2, Mar./Apr. 2004, pp250 – 258

[2] Hideyuki Sotobayashi, Wataru Chujo, Ken-ichi Kitayama: Photonic gateway: Multiplexing Format Conversions of OCDM-to-WDM and WDM-to-OCDM at 40 Gb/s (4 × 10 Gb/s). *IEEE/OSA Journal of Lightwave Technology*, Vol.20, No.12, Dec. 2002, pp2022 – 2028

[3] Hideyuki Sotobayashi and Wataru Chujo, Ken-ichi Kitayama: Photonic gateway: TDM-to-WDM-to-TDM conversion and reconversion at 40 Gbit/s (4 channels × 10 Gbits/s). OSA J. Opt. Soc. Am. B/Vol. 19, No. 11/Nov. 2002, pp2810 – 2816

[4] Hideyuki Sotobayashi, Wataru Chujo, Ken-ichi Kitayama: Transparent Virtual Optical Code/Wavelength Path Network. *IEEE Journal of Selected Topics in Quantum Electronics*, Vol.8, No.3, May/June 2002, pp699 – 704

[5] Ken-ichi Kitayama: Code Division Multiplexing Lightwave Networks Based upon Optical Code Conversion. *IEEE Journal on Selected Areas in Communications*, Vol.16, No.7, Sept. 1998, pp1309 – 1319

[6] Paul R. Prucnal, et. al.: Optical code division multiple access: fundamentals and applications. CRC Press,Taylor & Francis, 2006

[7] Prucnal, P. R., Santoro, M. A., Fan, T. R.: Spread Spectrum Fiber-optic Local Area Network Using Optical Processing. *IEEE/OSA Journal of Lightwave Technology*, Vol. 4, No. 5, May 1986, pp547 – 554

[8] Camille-Sophie Brès, Ivan Glesk, Robert J. Runser, Paul R. Prucnal: All-Optical OCDMA Code-Drop Unit for Transparent Ring Networks. *IEEE Photonics Technology Letters*, Vol.17, No.5, May 2005, pp1088 – 1090

[9] Jingshown Wu, Che-Li Lin: Fiber-Optic Code Division Add–Drop Multiplexers, *IEEE/OSA Journal of Lightwave Technology*, Vol.18, No.6, June 2000, pp819 – 824

[10] Ken-ichi Kitayama, Xu Wang, Naoya Wada: OCDMA Over WDM PON—Solution Path to Gigabit-Symmetric FTTH. *IEEE/OSA Journal of Lightwave Technology*, Vol.24, No.4, 2006, pp1654 – 1662

[11] Ronald C. Menendez, Paul Toliver, Stefano Galli, Anjali Agarwal, Thomas Banwell, Janet Jackel, Jeffrey Young, and Shahab Etemad: Network Applications of Cascaded Passive Code Translation for WDM-Compatible Spectrally Phase-Encoded Optical CDMA. *IEEE/OSA Journal of Lghtwave Technology*, Vol.23, No.10, October 2005, pp3219 – 3231

[12] Z. Jiang, D. S. Seo, D. E. Leaird, R. V. Roussev, C. Langrock, M. M. Fejer, A. M. Weiner: Reconfigurable All-Optical Code Translation in Spectrally Phase-Coded O-CDMA. *IEEE/OSA Journal of Lightwave Technology*, Vol.23, No.6, June 2005, pp1979 – 1990

[13] Hossam M. H. Shalaby: Optical CDMA random access protocols. in Proc. IEEE 8th International Symposium on Computers and Communication, 2003

[14] Shurong Sun, Hongxi, Yin, Ziyu Wang, Anshi Xu: Performance analysis of a new random access protocol for OCDMA networks. Photonic Network Communications, Vol.14, Feb. 2007, pp89 – 95

[15] P. Kamath, J. D. Touch and J. A. Bannister: The Need for Media Access Control in Optical CDMA Networks. INFOCOM 2004, Vol.4, 7 – 11 March 2004, pp2208 – 2219

[16] Kamath, P., Touch, J.D., Bannister, J.A: Algorithms for interference sensing in optical CDMA networks. IEEE International Conference on Communications, Vol.3, 20 – 24 June 2004, pp1720 – 1724

[17] P. Saghari, P. Kamath, V. Arbab, M. Haghi, A. E., Willner, J. A. Bannister, J. D. Touch: Experimental demonstration of an interference-avoidance-based protocol for O-CDMA networks. OFC 2006, 5 – 10, March 2006, pp1 – 3

[18] Mohamed Aly A. Mohamed, Hossam M. H. Shalaby, El-Sayed Abdel-Moety El-Badawy: Performance Analysis of an Optical CDMA MAC Protocol with Variable-Size Sliding Window. *IEEE/OSA Journal of Lightwave Technology*, Vol.24, No.10, Oct. 2006, pp3590 – 3596

[19] Masayuki Murata and Ken-ichi Kitayama: A Perspective on photonic multi-protocol label switching. *IEEE Network Magazine*, Vol.15, Issue 4, July/August 2001, pp56 – 63

[20] Daniel J. Blumenthal, Bengt-Erik Olsson, Giammarco Rossi, Timothy E. Dimmick, Lavanya Rau, Milan Mašanvić, Olga Lavrova, Roopesh Doshi, Olivier Jerphagnon, John E. Bowers, Volkan Kaman, Larry A. Coldren: All-optical label swapping networks and technologies. *IEEE/OSA Journal of Lightwave Technology*, Vol.18, No.12, Dec. 2000, pp2058 – 2075

[21] Dar-Zu Hsu: A novel photonic label switching based on optical code division multiplexing. ICT2003, Vol.1, 23 Feb.-1 March 2003, pp634 – 640

[22] A. S. Acampora, et al.: Multihop lightwave networks: a comparison of store-and-forward and Hot-Potato routing. *IEEE Trans. on Communications*, Vol.40, 1992, pp1082 – 1090

[23] David K. Hunter, et al.: Buffering in optical packet switches. *IEEE/OSA Journal of Lightwave Technology*, Vol.16, No.12, 1998, pp2081 – 2084

[24] Christian Guillemot, et al.: Transparent optical packet switching: the European ACTS KEOPS project approach. *IEEE/OSA Journal of Lightwave Technology*, Vol.16, No.12, 1998, pp2117 – 2232

[25] David K. Hunter, et al.: SLOB: A Switch with Large Optical Buffers for Packet Switching. *IEEE/OSA Journal of Lightwave Technology*, Vol.16, No.10, 1998, pp1725 – 1736

[26] Shuguang Zhu, Anshi Xu, Hongxi Yin, Deming Wu, Xuzong Chen: Scheme of a WDM Time-Limited RAM for OPS. OECC2003, Shanghai, China, Oct. 2003

[27] B. C. Thomsen, P. C. Teh, M. Ibsen, and D. J. Richardson: Self-routing edge-to-edge optical packet switching network based on superstructured fiber Bragg grating. ECOC2002, PD2.3, 8 – 12 Sept. 2002, Copenhagen

[28] Xu Wang, Naoya Wada: Experimental Demonstration of OCDMA Traffic Over Optical Packet Switching Network With Hybrid PLC and SSFBG En/Decoders. *IEEE/OSA Journal of Lightwave Technology*, Vol.24, No.8 Aug. 2006, pp3012 – 3020

[29] N. Wada, H. Furukawa, K. Fujinuma, T. Wada, and T. Miyazaki: 160 Gb/s/port optical packet switch prototype with variable-length packet BER and loss real-time measurement (invited). ECOC2005, Glasgow, U.K., Sep. 2005, Wednesday 1.4.1

[30] Ken-ichi Kitayama, Naoya Wada: Photonic IP routing. *IEEE Photonics Technology Letters*, Vol.11, No. 12, Dec. 1999, pp1689 – 1691

[31] Ken-ichi Kitayama, Naoya Wada, Hideyuki Sotobayashi: Architectural Considerations for Photonic IP Router Based upon Optical Code Correlation. *IEEE/OSA Journal of Lightwave Technology*, Vol.18, No.12, Dec. 2000, pp1834 – 1844

[32] Y. G. Wen, Y. Zhang, and L. K. Chen: On Architecture and Limitation of Optical Multiprotocol Label Switching (MPLS) Networks Using Optical-Orthogonal-Code (OOC)/Wavelength Label. *Optical Fiber Technology*, Vol.8, Elsevier Science (USA), 2002, pp43 – 70

[33] N. Karafolas and D. Uttamcandani: Optical fiber code division multiple access networks: A review. Optical Fiber Technology, Vol.2, Elsevier Science (USA), 1996, pp149 – 168

[34] K. Iverson and D. Hampicke: Comparison and classification of all-optical CDMA systems for future telecommunication networks. in Proc. SPIE, Vol. 2614, 1995, pp110 – 121

[35] L. Tancevski, I. Andonovic, and J. Budin: Secure optical network architectures utilizing wavelength hopping/time spreading codes. *IEEE Photonics Technology Letters*, Vol.7, No.5, May 1995, pp573 – 575

[36] P. Torres, L. C. G. Valente, and M. C. R. Carvalho: Security system for optical communication signals with fiber Bragg gratings. *IEEE Transactions on Microwave Theory Technology*, Vol.50, No.1, Jan. 2002, pp13 – 16

[37] D. D. Sampson, G. J. Pendock, and R. A. Griffin: Photonic code-division multiple-access communications. Fiber Int. Opt., Vol. 16, 1997, pp129 – 157

[38] Thomas H. Shake*:* Security Performance of Optical CDMA against Eavesdropping. *IEEE/OSA Journal of Lightwave Technology*, Vol.23, No.2, Feb. 2005, pp655 – 670

[39] Thomas H. Shake: Confidentiality Performance of Spectral-Phase-Encoded Optical CDMA. *IEEE/OSA Journal of Lightwave Technology*, Vol.23, No.4, April 2005, pp1652 – 1663

[40] J. A. Salehi, A. M. Weiner, and J. P. Heritage: Coherent ultrashort pulse code-division multiple access communication systems. *IEEE/OSA Journal of Lightwave Technology*, Vol.8, No.3, Mar. 1990, pp478 – 491

[41] A. J. Mendez, V. J. Hernandez, C. V. Bennett, R. M. Gagliardi, and W. J. Lennon: Measurements of Eavesdropping in a Wavelength/Time Optical CDMA (O-CDMA) System, with Data Confidentiality Implications. OFC'2006, WW3

[42] Zhi Jiang, Daniel E. Leaird, Andrew M. Weiner: Experimental Investigation of Security Issues in O-CDMA. *IEEE/OSA Journal of Lightwave Technology*, Vol.24, No.11, Nov. 2006, pp4228 – 4234

[43] Gagliardi, R. M.: Pulse-coded multiple access in space optical communications. *IEEE Journal on Selected Areas in Communications*, Vol.13, No.3, 1995, pp603 – 608

[44] Ohtsuki, T.: Performance analysis of atmospheric optical PPM CDMA systems. *IEEE/OSA Journal of Lightwave Technology*, Vol.21, No.2, 2003, pp406 – 411

[45] Elmirghani, J. M. H., Cryan, R. A.: New PPM-CDMA hybrid for indoor diffuse infrared channels. *IEE Electronics Letters*, Vol.30, No.20, 1994, pp1646 – 1647

[46] G.-C. Yang and W. C. Kwong: Design of multilength optical orthogonal codes for optical code-division multiple-access multimedia networks. *IEEE Trans. on Communications*, Vol. 50, No. 8, Aug. 2002, pp1258 – 1265

[47] Jian-Guo Zhang: Design of Integrated Services Digital Broadcasting Systems Using Multirate Optical Fiber Code-Division Multiplexing. *IEEE Trans. on Broadcasting*, Vol.45, No.1, Sept. 1999, pp283 – 293

[48] E. Park, A. Mendez, and E. Garmire: Temporal/spatial optical CDMA networks-design, demonstration, and comparison with temporal networks. *IEEE Photonics Technology Letters*, Vol.4, No.10, 1992, pp1160 – 1162

[49] E. S. Shivaleela, Kumar N. Sivarajan, A. Selvarajan: Design of a New Family of Two-Dimensional Codes for Fiber-Optic CDMA Networks. *IEEE/OSA Journal of Lightwave Technology*, Vol.16, No.4, Apr. 1998, pp501 – 508

[50] Ken-ichi Kitayama, Moriya Nakamura, Yasunori Igasaki, Keiji Kaneda: Image Fiber-Optic Two-Dimensional Parallel Links Based Upon Optical Space-CDMA: Experiment. *IEEE/OSA Journal of Lightwave Technology*, Vol.15, No.2, Feb. 1997, pp202 – 212

[51] Katsutoshi Tsukamoto, Takeshi Higashino, Takashi Nakanishi, Shozo Komaki: Direct Optical Switching Code-Division Multiple-Access System for Fiber-Optic Radio Highway Networks. *IEEE/OSA Journal of Lightwave Technology*, Vol.21, No.12, Dec. 2003, pp3209 – 3220

[52] Habib Fathallah, Leslie A. Rusch: Robust Optical FFH-CDMA Communications: Coding in Place of Frequency and Temperature Controls. *IEEE/OSA Journal of Lightwave Technolog*y, Vol.17, No.8, Aug. 1999, pp1284 – 1293

[53] Benjamin J. Vakoc, Michel J. F. Digonnet, Gordon S. Kino: A Novel Fiber-Optic Sensor Array Based on the Sagnac Interferometer. *IEEE/OSA Journal of Lightwave Technology*, Vol.17, No.11, Nov. 1999, pp2316 – 2326

[54] Akyildiz, I. F., Weilian Su: A survey on sensor networks. *IEEE Communication Magazine*, Vol.40, No.8, 2002, pp102 – 114

Index

C

D

Q

R

S

T

U

V

W